NANOSTRUCTURES AS ANALYTICAL TOOLS IN BIOASSAYS

M.P. Aguilar-Caballos, J.M. Fernández-Romero, A. Gómez-Hens
Department of Analytical Chemistry. University of Córdoba, Annex to Marie Curie Building, Campus of Rabanales, 14071-Córdoba, Spain
qa1agcam@uco.es

The integration of nanotechnology into bioassays is having a great impact with the development of new nanostructures, nanodevices, nanomaterials or, in general, nanoparticles (NPs), such as nanoshells, nanowires, nanotubes and nanobarcodes, of a variety of shapes, sizes and composition [1-4]. These NPs, which exhibit new properties that are not shown by the bulk matter, are being considered as an alternative to conventional reagents, such as enzymes or organic molecules, often used in bioassays. The main reasons of this success can be ascribed to their ability to improve the features of these assays, allowing their miniaturization and expeditiousness, reducing reagent and sample consumption, and facilitating the performance of heterogeneous formats. NPs present a larger surface area for the display of receptors than flat surfaces and the reactions are faster and more sensitive.

A critical evaluation of the real usefulness of different nanostructures described as labels, nanoscaffolds or separation media in immunoassays and nucleic acid hybridization assays is presented. In spite of the great number of publications, there is a relatively high percentage of them that only describe theoretical aspects related with the use of these nanostructures or nanoparticles, but do not verify their applicability in the presence of potential interferent agents that can be present in the sample matrix. This work attempts to carry out a systematic study of the advantages and limitations of the use of these new reagents in bioassays, the different assay formats described for the individual and multiplexed detection, and the capability of these assays to analyze real samples.

References:

[1] M. Magliulo, E. Michelini, P. Simoni, M. Guardigli, A. Roda, Anal. Bioanal. Chem. **384** (2006) 27.

[2] M. Seydack, Biosens. Bioelectron. **20** (2005) 2454.

[3] N.C. Tansil, Z. Gao, Nanotoday **1** (2006) 28.

[4] A. Merkoçi, FEBS J. **274** (2007) 310.

Poster

THE INFLUENCE OF Ag_2S PERCENTAGE ON THE PHOTOACTIVITY OF TiO_2/Ag_2S NANOCOMPOSITES

Rita Albuquerque[1], Maria Helena Mendonça, Olinda C. Monteiro
University of Lisbon, Department of Chemistry and Biochemistry, CCMM, Campo Grande, Ed. C8, 1749 – 016 Lisboa, Portugal
Contact: ritasba@gmail.com

In the past decades there has been a growing interest in heterogeneous photocatalysis for wastewater treatment and water purification.[1] For such heterogeneous chemical reactions the use of nanocrystalline semiconductors as photocatalysts, to initiate interfacial redox reactions, generally results in higher activities than the corresponding bulk semiconductors.

Nanocrystalline TiO_2 has been intensely investigated as a photocatalyst for environmental remediation processes. Due to its wide band gap TiO_2 only absorbs a small portion of the solar spectrum consequently several studies have been made in order to enhance light absorption. One method that has proven to be very effective is the conjugation of TiO_2 particles with light sensitizers such as dyes or other semiconducting phases.[2]

The TiO_2/Ag_2S nanocomposites were obtained by a single source method using silver dithiocarbamate as metal sulphide precursor.[3] The photocatalytic properties of the TiO_2/Ag_2S nanocomposites were tested on the photodegradation of two distinct dyes, methylene blue and orange II. The influence of Ag_2S percentage on the photocatalytic properties of the TiO_2/Ag_2S nanocomposites was studied and will be discussed.

References:

[1] S. K. Kansal, M. Singh, D. Sud, J. Hazd. Mat. **141** (2007) 581.
[2] P. V. Kamat, D. Meisel, C. R. Chimie **6** (2003) 999.
[3] O. C. Monteiro, A. C. C. Esteves, T. Trindade, Chem. Mater. **14** (2002) 2900.

Acknowledgments

O.C. Monteiro thanks Fundação para a Ciência e Tecnologia (FCT) for a pos-doc grant (SFRH/BPD/14554/2003). This work is supported by FCT, POCI and co-financed by FEDER (POCI/QUI/59615/2004).

1 – Present Address: INL, International Iberian Nanotechnology Laboratory, Av. Central - Edifício dos Congregados, 100, 4710-229 Braga, Portugal

UNDERSTANDING THE SUPRAMOLECULAR SELF-ASSEMBLY OF THE FULLERENE DERIVATIVE PCBM ON Au(111) SURFACE

M. Alcamí[1], D. Écija[2], R. Otero[2], L. Sánchez[3], J. M. Gallego[4], Y. Wang[1], F. Martín[1], N. Martín[3], R. Miranda[2,5]

[1]*Departamento de Química, C-9, Universidad Autónoma de Madrid, 28049, Madrid, Spain*

[2]*Departamento de Física de la Materia Condensada, Universidad Autónoma de Madrid,28049, Madrid, Spain*

[3]*Departamento de Química Orgánica, Facultad de C.C. Químicas,Universidad Complutense de Madrid, 28040, Madrid, Spain*

[4]*Instituto de Ciencia de Materiales de Madrid, Consejo Superior de Investigaciones Científicas, 28049, Madrid, Spain*

[5]*Instituto Madrileño de Estudios Avanzados en Nanociencia (IMDEA-Nanociencia), Madrid 28049, Spain*

manuel.alcami@uam.es

Recent variable-temperature STM experiments[1] have observed a crossover of the site-selectivity in the adsorption and self-assembly of PCBM (Phenyl-C_{61}-Butyric acid Methyl ester), a C_{60} derivative, on the herringbone-reconstructed Au(111) surface as a function of the coverage. At low coverages, PCBM self-assembles to create long, parallel, isolated 1D wires, or 2D extended networks, as dictated almost exclusively by the substrate-controlled preference for nucleating at the fcc sites of the reconstruction. However, at higher coverages, intermolecular interactions take over, bypassing the substrate influence, giving islands composed of laterally ordered parallel, 1D double rows of PCBM molecules (Fig. 1a). In order to understand this last step in the self-assembly of PCBM molecules on the gold surface, theoretical calculations were performed based on density functional theory (DFT).

The geometries of the PCBM monomer and 10 possible dimers were fully optimized at the B3LYP/3-21G and B3LYP/6-31G(d) levels. The calculations show that the binding of the two PCBM molecules is due mainly to the formation of weak hydrogen bonds (C–H···O) between the two PCBM tails (Fig. 1b and c). Then, four low-energy dimers with reasonable C_{60}–C_{60} distances were considered to form PCBM tetramers. By treating the PCBM dimer as a fixed unit, the conformation for a tetramer was optimized as a function of their separation and relative position at the B3LYP/3-21G level. The final geometry is due to the formation of two additional hydrogen bonds between adjacent dimers (Fig. 1d). The comparison with the experimental data is quite good (Fig. 1a), since the estimated values of distances (23.7 and 10.4 Å) and angle (68^o) for the arrangement of the C_{60} balls are in good agreement with experiment (21 and 10 Å and 70^o, respectively). These hydrogen bonds lie well above the surface due to the large size of the C_{60} cages, thus implying that the surface has little influence on them. This is why calculated arrangements of PCBM in the gas phase are in good agreement with the STM images at high coverage. Additionally, the lack of interaction between the tails and the surface also explains the site-insensitive adsorption of PCBM.

At low coverage, the PCBM molecules must approach each other by putting their “bald” sides face to face. This is due to the relatively strong van der Waals interaction between C60 cages. In this arrangement, the tails point in opposite directions (see Figure 2). This should be the dominant mechanism until the fcc areas of the Au(111) reconstruction are completely filled.

To study possible effects due to the surface, we carry out model calculations in which the tails of two interacting PCBM molecules are placed as in the dimer, but replacing the C60 cages and phenyl rings by hydrogen atoms. This simplified structure is placed over two layers of gold atoms representing the Au(111) surface (figure 3) Even though all the atoms are allowed

to move from their initial positions, the tails do not approach the surface after geometry optimization. This is because the tails are so far away from the surface that the gold–oxygen interaction barely affects the weak hydrogen bonds formed between the two tails. Thus, our model calculations support the fact that the surface plays a very minor role in the self-assembly of PCBM at high coverage

References:

[1] D. Écija, R. Otero, L. Sánchez, J. M. Gallego, Y. Wang, M. Alcamí. F.Martín, N. Martín, R. Miranda, Angew. Chem., **119** (2007), 8020–8023.
[2] Y. Wang, M. Alcamí and F.Martín. Chem. Phys. Chem (in press)

Figures:

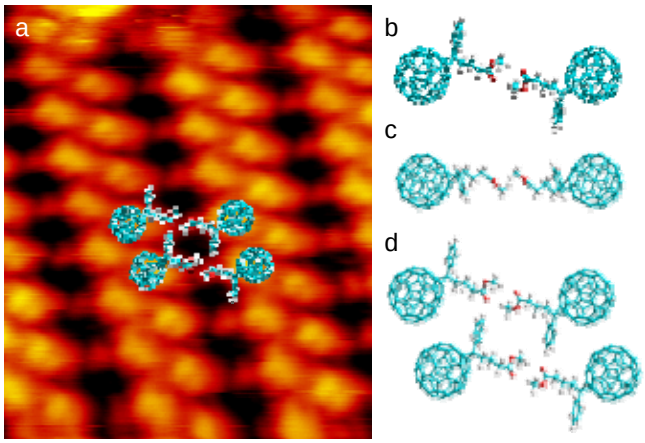

Figure 1 a) STM image of the Au(111) surface after depositing ~0.6 ML of PCBM. b) Top and c) side views showing the optimized calculated structure for a PCBM dimer. d) Optimized structure for a PCBM tetramer. The dotted lines mark the weak hydrogen bonds responsible for this conformation.

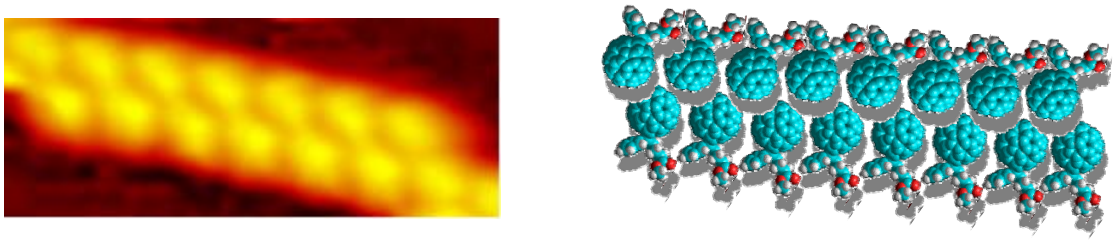

Figure 2. The 1D arrangement of the PCBM twin chain at low coverage

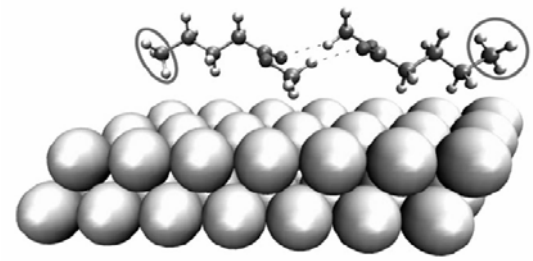

Figure 3. The optimized geometry of a supercell of the model dimer on Au-(111) surface by VASP. At the two ends of the model dimer, the circles indicate the methyl groups with fixed positions during the geometry optimization.

PROPERTIES OF SINGLE-CRYSTALLINE ZnO NANODOTS AND HIGHLY-TEXTURED ZNO FILMS GROWN BY ELECTROCHEMISTRY

D. Alegre, M.S. Martín-Gonzalez, B.Alen, J.L. Costa-Krämer
Instituto de Microelectrónica de Madrid, c/ Isaac newton, 8, Tres Cantos (Madrid), Spain
daniel.alegre@imm.cnm.csic.es

ZnO is a n-type semiconductor with a large band gap in the UV range, and has attractive electronic, mechanical, thermal and acoustical properties. Thin films have been used as piezoelectric transducers, short wavelength optical devices, UV light emitters, and photovoltaic cells [1-6]. Single crystal nanowire arrays can be easily obtained developing a new generation of devices in optoelectronic, photovoltaic cells, gas sensor, field emission and piezoelectrics [7-11]. Most of the films and nanowire arrays are grown by vapor phase techniques, requiring high temperature and vacuum.

In this work self assembled ZnO nanodots and films are grown by one step electrodeposition without further thermal treatment on a large area on Au/Si substrates. This process works at low temperatures (<100ºC), ambient pressure, and is easily implemented in large scale. The basic ZnO formation reaction is the generation of hydroxide ions at the electrode surface (cathode) by a reduction of an oxygen precursor. The results presented in this work have used hydrogen peroxide and nitride ions according to the following reaction:

$NO_3^- + H_2O + 2e^- \rightarrow NO_2^- + 2OH^-$

$H_2O_2 + 2e^- \rightarrow 2OH^-$

Zn^{2+} reacts with OH^- for temperatures above 50ºC following:

$Zn^{2+} + 2OH^- \rightarrow ZnO + H_2O$

The nanodots obtained have an hexagonal shape with a diameter between 150 and 400nm and a height between 50 and 200nm, as determined by SEM and AFM measurements. Characterization by SEM and X-ray diffraction of the nanoparticles showed a single crystal structure oriented with the c-axis perpendicular to the substrate (see figure 1 and 2). Their spatial and size distributions, crystallinity and photoluminescence behavior depends on the deposition parameters such as substrate type, electrochemical potential and intensity, oxygen source, deposition time, bath temperature and composition.

A comparison with highly-textured ZnO films also obtained by electrodeposition will be shown. These have been grown at a constant potential, and at different electrochemical conditions and baths. Figure 3 shows SEM images that demonstrate that the film forms by the coalescence of vertical hexagonal grains. The films have a (002) preferred orientation (XRD in figure 4), suggesting that the nanodots are nucleation points for the film growth

References:

[1] S. Peulon, D. Lincot, Adv. Mater, **8**, (1996) 168.
[2] D. Gal , G. Hodes, D. Lincot, HW. Schock , Thin Solid Films, **79**, (2000) 361.
[3] M. Izaki, T. Omi, Appl. Phys. Lett., **68**, (1996) 2439.
[4] Th Pauporte, D. Lincot, Appl. Phys. Lett, **75**, (1999) 3817.
[5] L. Stott, J. Hedström, M. Rückh, J. Kessler, KO. Velthaus, HW. Schock, Appl. Phys. Lett, **62**, (1993) 597.

[6] Th. Pauporte, T. Yoshida, R. Cortes, M Froment, D. Lincot, J. Phys. Chem. B, **107**, (2003) 10077.
[7] W.I. Park, G.C. Yi, Adv. Mater., **16**, (2004) 87.
[8] C. Levy-Clement, R. Tena-Zaera, M.A. Ryan, A. Katty, G. Hodes, Adv. Mater., **17**, (2005) 1512.
[9] L.C. Tien, P.W. Sadik, D.P. Norton, L.F. Voss, S.J. Pearton, H.T. Wang, B.S. Kang, F. Ren, J. Jun, J. Lin, Appl. Phys. Lett., **87**, (2005) 222106.
[10] Y.K. Tseng, C.J. Huang, H.M. Cheng, I.N. Lin, K.S. Liu, I.C. Chen, Adv. Funct. Mater. **13**, (2003) 811.
[11] Z.L. Wang, J. Song, Science, **312**, (2006) 242.

Figures:

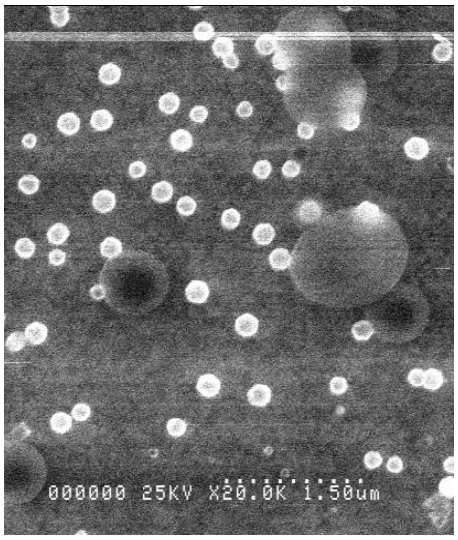

Figure 1. SEM top view of ZnO nanodots grown by a low scan voltammetry from -1,5V to +0,9V at 80ºC

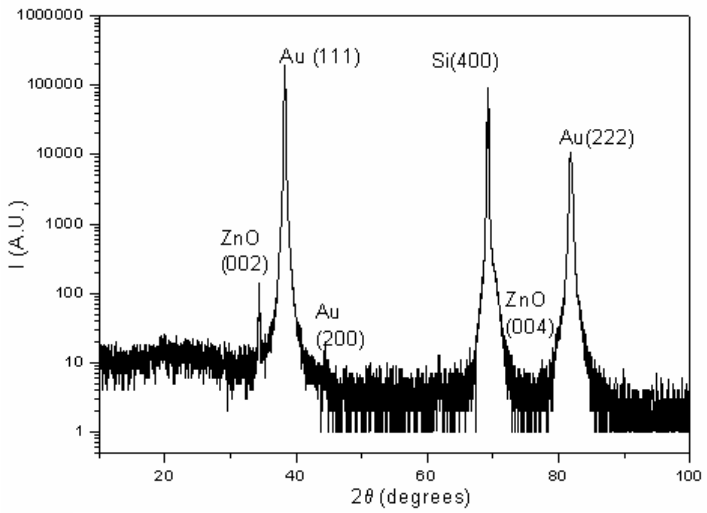

Figure 2. XRD diagram of ZnO nanodots grown by a low voltammetry scan from -1,5V to +0,9V at 80ºC.

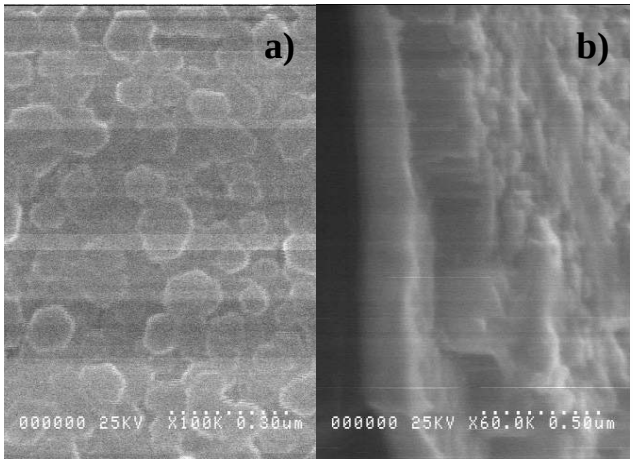

Figure 3. a) SEM top and b) cross sectional view of ZnO film grown at a constant potential of -0,9V for 1h at 80ºC

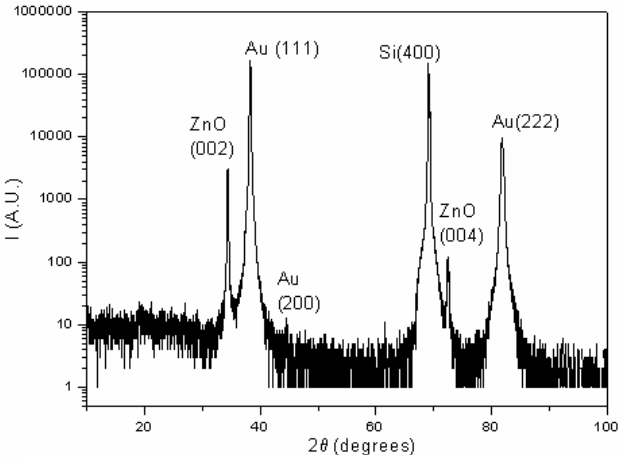

Figure 4. XRD diagram of a ZnO film grown at a constant potential of -0,9V for 1h at 80ºC

Ratchet effects on domain wall motion in Co-Si amorphous films with arrays of asymmetric holes: experiments and theoretical simulations

Alejandro Alija,[1] A. Pérez-Junquera,[1] G. Rodríguez-Rodríguez,[1] V.I. Marconi,[2] A.B. Kolton,[2] L.M. Álvarez-Prado,[1] M. Vélez,[1] J.V. Anguita,[3] Y. Souche,[4] J.M. Alameda,[1] J.M.R.Parrondo,[2] J.I. Martín[1]

1. Depto. Física, Universidad de Oviedo - CINN, Oviedo, Asturias, Spain.
2. Depto. Física Atómica, Molecular y Nuclear, and GISC, Universidad Complutense de Madrid, Madrid, Comunidad de Madrid, Spain.
3. Depto. Dispositivos, Sensores y Biosensores, Instituto de Microlectrónica de Madrid (CNM-CSIC), Madrid, Comunidad de Madrid, Spain.
4.NANO, Institut Néel, CNRS and Universite Joseph Fourier, Grenoble, Grenoble, France.

alija@condmat.uniovi.es

The study of domain wall (DW) movement in magnetic films has long attracted a great interest since it provides both the basis for a wide number of magnetic devices [1] and a good experimental system to analyze the basic physics of an elastic interface in the presence of either ordered or random pinning defects [2,3]. When the pinning potential is asymmetric it can behave as a ratchet, so that DW propagation is favored in one direction. One of the first ratchet potentials used in the field magnetism were “angelfish” patterns that control the sense of propagation of bubble domains in shift registers [4]. Also, asymmetric motion of domain walls (DWs) in nanowires with triangular [5] or notched [6] shapes has been reported recently. However, up to now, in order to ensure a good control of the DW nucleation/propagation process, in all these cases DW motion has been confined to an essentially 1D path, so that its transverse wandering can be neglected. On the other hand, in a thin extended film with a 2D array of asymmetric pinning centers, novel ratchet phenomena can appear since a DW behaves as an elastic line that can distort all along its length in response to the 2D pinning potential.

In this work, the propagation of DWs in extended uniaxial Co-Si amorphous films patterned with a periodic array of asymmetric holes (see Fig.1) has been studied. For the first time, we have experimentally observed and theoretically simulated the existence of two crossed ratchet effects of opposite sign that change the preferred sense for DW motion depending on whether a flat or a kinked wall is moving.

When a magnetic field is applied to push a flat DW across the asymmetric holes, the DW moves more easily (i.e. with lower coercivity) in the direction in which the length of the pinned wall between two antidots increases smoothly. This asymmetric pinning has been experimentally observed [7] and confirmed by both numerical [7] and micromagnetic simulations with the OOMMF code [8] (see Fig.2). The novel ratchet behavior appears as the pinned wall inside the array develops kinks. This provides an extra mechanism for DW motion only possible in a 2D geometry through upward/downward kink propagation. This novel ratchet mechanism has an opposite sign in comparison to the flat DW ratchet and dominates the low field behavior. The interplay between both ratchets implies that the system keeps memory of the sign of the magnetization before a DW enters the array of asymmetric holes.

Work supported by Spanish CICYT (grants NAN2004-09087, MOSAICO and FIS2005-07392)

References:

[1] C.D. Mee and E.D. Daniel, Magnetic Storage Hand-book(1996) (New York: McGraw-Hill); G. Prinz, J.Magn. Magn. Mater. 200, 57 (1999).
[2] S. Lemerle et al., Phys. Rev. Lett. 80 849 (1998).
[3] E. Martínez et al., Phys. Rev. Lett. 98, 267202 (2007).
[4] N. Hayashi et al., IEEE Trans. on Magn. 8 370 (1972).
[5] D.A. Allwood et al., Appl. Phys. Lett. 85, 2849 (2004).
[6] A. Himeno et al., J. Appl. Phys. 97, 066101 (2005); M.Hayashi et al., Phys. Rev. Lett. 97, 207205, (2006); S.Savel'ev et al., New J. Phys. 7, 82(2005).
[7] A. Pérez-Junquera et al Phys. Rev. Lett. 100, 037203 (2008)
[8] OOMMF available at http://math.nist.gov/oommf

Figures:

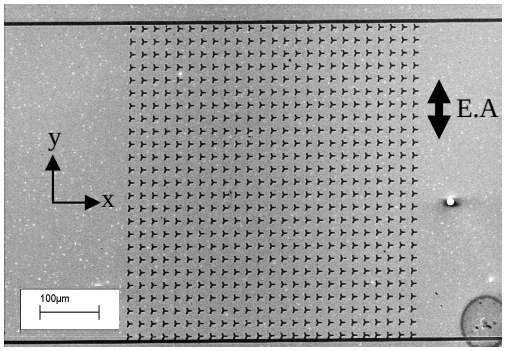

Fig.1 Scanning electron microscopy image of an array of asymmetric holes on an uniaxial Co-Si film. EA direction is indicated.

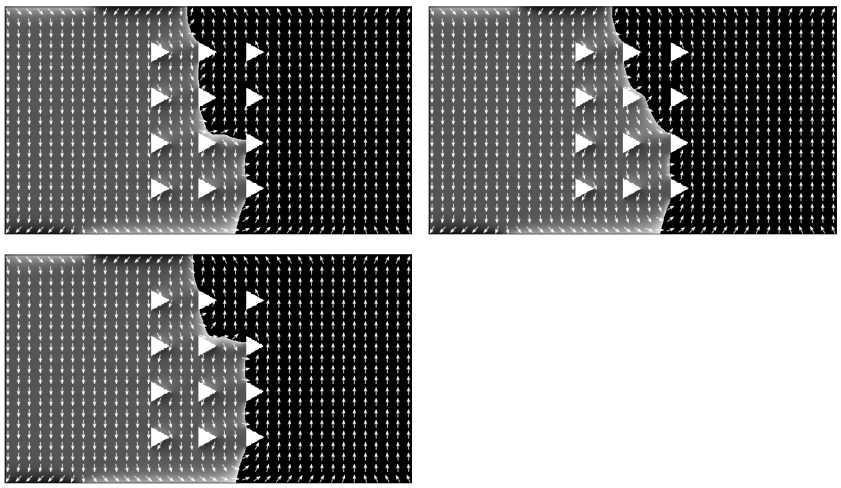

Fig2 OOMMF micromagnetic simulation of the propagation of a DW with a kink over the array of asymmetric holes.

Study of the influence of the interactions in the magnetic behaviour of Fe-Ag thin films above the percolation limit

J. Alonso[1], M.L. Fdez-Gubieda[1], J.M. Barandiaran[1], L. Fernández-Barquín[3], I. Orue[2], A. Svalov[1]

[1]Dpto. Electricidad y Electrónica, Universidad del País Vasco, Bilbao, Spain.

[2]SGIKER, Servicios Generales de medidas magnéticas, Universidad del País Vasco, Bilbao, Spain.

[3]CITIMAC, Universidad de Cantabria, Santander, Spain.

jalonsomasa@gmail.com

The physical properties of nanostructures can be markedly different from those of bulk materials. This is of particular interest in the case of granular alloys composed of magnetic clusters in a metallic nonmagnetic matrix, such as the Fe-Ag systems. Depending on the Fe content, interactions can play a very important role in their magnetic behaviour mainly in the case of samples with high concentrations. In our case, we have focused on the study of the role of the interactions in Fe-Ag granular thin films with Fe contents above the percolation limit (~ 28% at.), for which Binns et al. [1] predicted an interacting-superparamagnet behaviour at high temperatures, and a progressive collective blocking as temperature decreases. Both pulsed laser deposition (PLD) and sputtering techniques have been used for comparison.

We have prepared Fe-Ag thin films (~100-200 nm) in the range of 30-55%. Their composition was determined by energy dispersive X-ray analysis (EDX). Both PLD and sputtered films were coated with ~ 10 nm silver and gold capping layers, respectively. They were deposited at room temperature onto Si(100) substrate with a native oxide layer. The microstructure was studied by X-ray diffraction (XRD), and DC and AC magnetic characterization was performed using a SQUID magnetometer as a function of temperature (5-350 K) and with frequencies in the range 1-100 Hz.

The hysteresis loops measured at 300 K and 5 K reflect that all the samples behave like soft ferromagnets with a coercive field smaller than 50 Oe. Samples deposited by PLD show an increase of the susceptibility up to ~50 K, followed by a smooth variation characteristic of a ferromagnetic state up to 150-200 K, where the susceptibility decreases in a Curie-Weiss type decay. As the volume fraction changes, these phases evolve and even new phases as a spin-glass like state at low temperatures emerge (see Fig 1, bottom). On the other hand, for the sputtered sample a clear Curie transition at 310 K, with the susceptibility dropping to zero, has been found for the lowest composition studied (30%). A slight increase of the composition makes this transition disappear (see Fig 1, top).

In order to get deeper insight of the previous collective magnetic behaviours, we have also performed zero field cooled AC magnetization measurements. Figure 2 shows the thermal evolution of the real, χ', and the complex, χ'', components of the susceptibility data measured between $1 \leq f \leq 1000$ Hz for a PLD thin film (51 % of Fe) and with an AC amplitude of 1 Oe. Above ~150 K a clear dispersionless Curie-Weiss type decay of χ' is observed, and at the same temperature range, the thermal evolution of χ'' is also independent with the frequency and it becomes completely zero at 200 K. This behaviour corroborates the presence of a magnetic phase transition with a Curie temperature due to the magnetic interactions at 150-160 K. Below the transition temperature, χ' presents a smooth variation characteristic of a ferromagnet freezing. A similar magnetic behaviour has been found in discontinuous metal-insulators multilayers [2].

In summary, the susceptibility data indicate the existence of exchange interactions between the magnetic particles besides the dipolar ones, in both both sputterd and PLD thin films. PLD samples behave like a superferromagnet with a Curie-Weiss type transition triggered by interactions (probably meditated by the Fe-Ag interface) and a reentrance into a superspinglass phase at low temperature, while for sputtered sample no decrease of the magnetization is observed until very low temperatures (~20 K), being ZFC and FC curves very similar, what indicates that even at low temperatures, most of the nanoparticles are strongly correlated.

References:

[1] C. Binns, K.N. Trohidou, J. Bansmann, S.H. Baker, J.A. Blackman, J-P. Bucher, D. Kechrakos, A. Kleibert, S. Louch, K-H. Meiwes-Broer, G.M. Pastor, A.Perez, and Y. Xie, J. Phys. D: Appl. Phys. **38**, (2005) R375-R379

[2] W. Kleemann, O. Petracic, Ch. Binek, G. N. Kakazei, Yu. G. Pogorelov, J. B. Sousa, S. Cardoso and P. P. Freitas**,** Phys. Rev. B **63**, (2001) 134423

Figures:

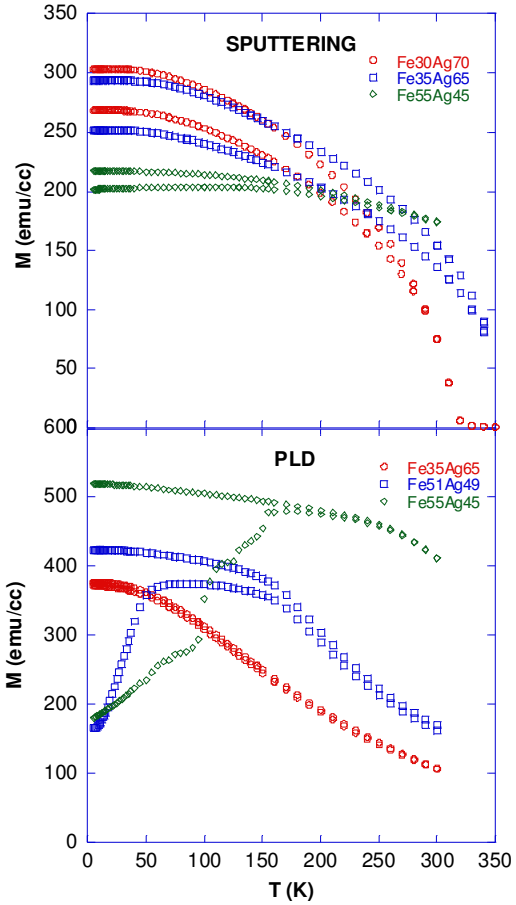

Fig1: ZFC-FC curves for (*top*) sputtered Fe_xAg_{100-x} (x = 30, 35, 55, h = 1 Oe) and (*bottom*) PLD Fe_xAg_{100-x} (x = 51, 53, 55, h = 5 Oe) samples.

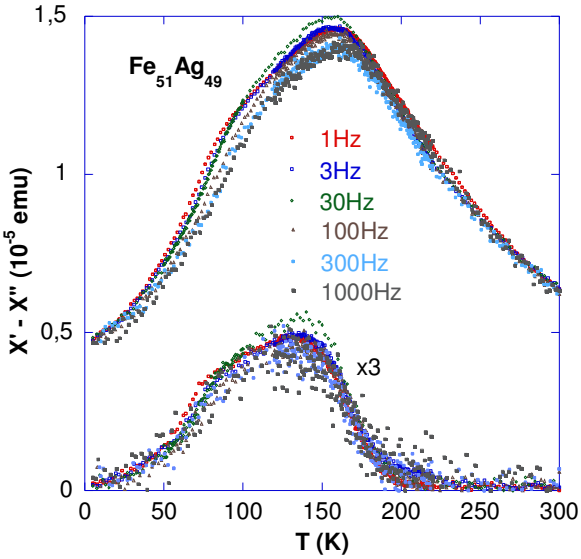

Fig2: real χ' and complex χ'' components of the susceptibility (h = 1 Oe) as a function of temperature measured at different frequencies, 1 ≤ f ≤ 100 Hz, for a PLD $Fe_{51}Ag_{49}$ thin film.

ULTRA-SENSITIVE SHAPE SENSOR TEST STRUCTURES BASED ON PIEZO-RESISTIVE DOPED NANOCRYSTALLINE SILICON

P. Alpuim[1], P.F. Rocha[2], S. Lanceros-Mendez[1], E.S. Marins[1], I.G. Trindade[3], J.G. Rocha[2], M.A. Carvalho[4], A. M. Deus[5], R. Soares[6]

1 Department of Physics, Universidade do Minho, Campus de Azurém, 4800-058 Guimarães, Portugal
2 Department of Industrial Electronics, Universidade do Minho, Campus de Azurém, 4800-058 Guimarães, Portugal
3 Department of Physics, Faculty of Sciences, Universidade do Porto, Rua do Campo Alegre, 687, 4169-007, Portugal
4 Department of Textile Engineering, Universidade do Minho, Campus de Azurém, 4800-058 Guimarães, Portugal
5 Department of Materials Engineering, Instituto Superior Técnico, Av. Rovisco Pais 1049-001 Lisboa, Portugal
6 Department of Biochemistry, Faculdade de Medicina, Universidade do Porto, Al. Prof Hernâni Monteiro, 4200-319 Porto, Portugal
palpuim@fisica.uminho.pt

This paper describes the miniaturization of dense piezoresistive sensor arrays based on doped hydrogenated nanocrystalline silicon deposited on flexible substrates. The substrates are 125 μm-thick polymide (PI) or polyethylene naphthalate (PEN) foils that are rugged, flexible and bendable. The nc-Si:H films, with a thickness of the order of 100 nm are prepared by radio-frequency plasma-enhanced chemical vapor deposition under high-vacuum conditions. The doping level and crystalline fraction were optimized for maximal gauge factor (GF) values. Longitudinal gauge factors GF = -30 and +26 were obtained for n- and p-type nc-Si:H films, respectively.

A piezoresistive flexible sensor for later incorporation in sensing devices for medical applications has been fabricated and its strain sensing potential under laboratory working conditions was demonstrated. The outcome of the first biocompatibility tests shows that the material is not harmful for the tested cells (osteoblasts) but, more important, it favors cell proliferation. This could be exploited in future clinical devices. The sensors, used in a Wheatstone quarter-bridge configuration, show similar sensitivity (output voltage amplitude ~30 μV/nm) when used either in the parallel and transverse relative directions of current and strain, as shown in Fig. 1. This high sensitivity achieved indicates that bi-dimensional mapping of a growing biological tissue or analogous may be accomplished using piezoresistive sensing. Hence, the scale down limits to achieve such high spatial resolution is being developed.

In this paper we describe, in a first approach, the fabrication of test structures, by the use of optical lithographic processes. The test structures consist of piezoresistive rectangularly shaped elements, having lateral dimensions in the range 50 to 100 microns, defined by a reactive ion etching process on nc-Si:H. At the end of each element, two metallic pads, forming ohmic contacts to the sensing elements, are defined by a lift-off process. Electrically conductive leads connect to the electrical pads, allowing wiring to be done in a region far away from the sensors active region. In this way, and using a parallel voltage divider configuration, the piezoresistive sensors periodically distributed in a row, are addressed and read in real-time.

Since the sensing action of the elements consists of a change in their resistance, it is possible to perform their readout without switching elements (e.g. MOSFETs) inside the array, which

simplifies the fabrication process. The readout technique is based on a two-port network, where either a current is applied to the device and the voltage at its terminals is measured, or a voltage is applied and the current is measured. Fig. 2 shows the readout circuit for a 4 × 4 sensor array, with the switches connected to read R11. Notice that since the impedance of the ammeter is very low, sensors R12, R13 and R14 are shunted and their currents are null.

The piezoresistive response of the test structures is analyzed in terms of reliability, sensitivity and linearity. Similar test structures being protected by an optimized encapsulating layer will have wear resistance and fracture toughness tested.

The spatial resolution of the sensors is addressed by bringing them into contact to surfaces having specific topographic feature distributions. The electromechanical experimental tests of the sensor assembly are described by theoretical Finite Element Modeling and compared to the experimental results.

Acknowledgements

This work was partly funded by Fundação para a Ciência e a Tecnologia (FCT) under project grant PTDC-CTM-66558-2006.

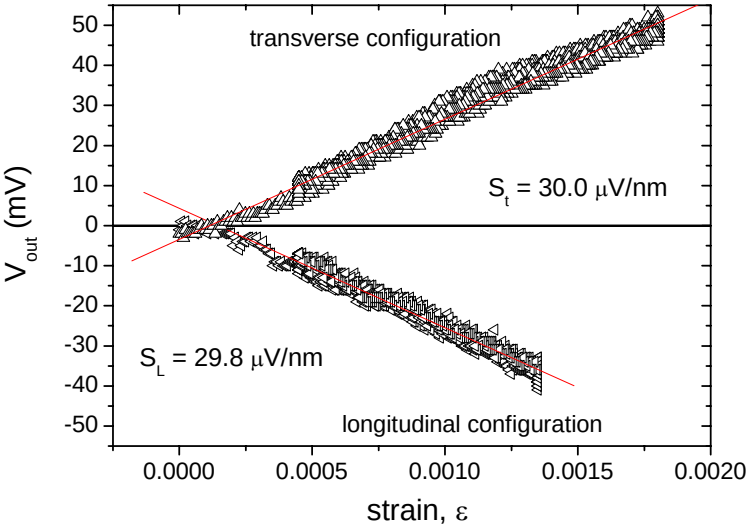

Fig.1 – Wheatstone bridge output voltage, V_{out}, (sensors in a quarter-bridge configuration) as a function of applied axial strain, ε, for two sensor orientations: (bottom) placed parallel to the strain axis, and (top) placed orthogonal to the strain axis.

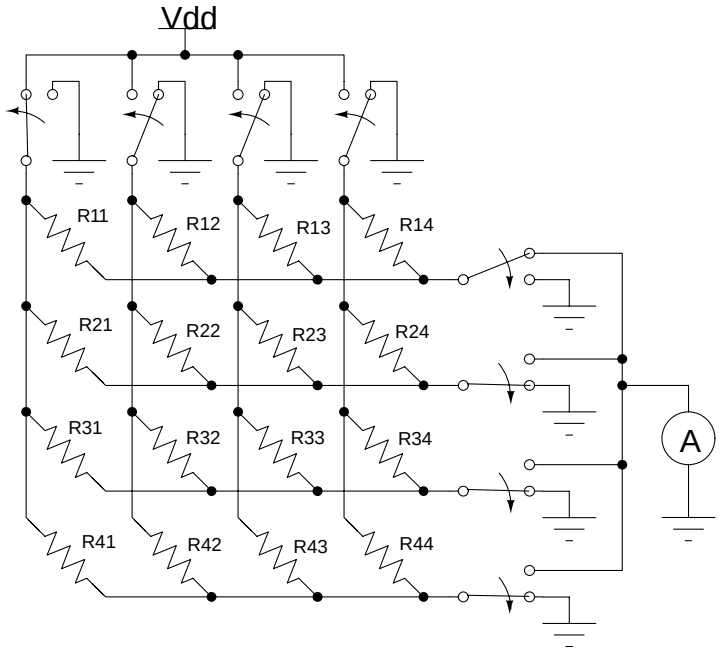

Fig. 2 - Readout circuit for a 4 × 4 sensor array, with the switches connected in the position to read R11. In this case, a voltage is applied to R11 and its current is measured. R12, R13 and R14 are shunted, so their currents are null.

Poster

Study of InAs/GaAs self-assembled QD heterostructures

E. Alves [1,2], S. Magalhães[1], N. P. Barradas[1,2], M. I. Vasilevskiy [3], N. V. Baidus [3, 4], A. Chahboun [3], B.N. Zvonkov [4]

[1] Instituto Técnico Nuclear ITN, EN10, 2686-953 Sacavèm, Portugal
[2] CFN da Universidade de Lisboa, Av. Gama Pinto 2, 1649-003 Lisboa, Portugal
[3] Centro de Física, Universidade do Minho, 4170-057 Braga, Portugal
[4] Faculty of Physics, N. I. Lobachevskii State University, Nihznii Novgorod, Russia

Quantum dot (QD) structures are being developed to build active region of low threshold lasers and light emitting diodes. Self-assembled InAs/GaAs emit in the 1.3-1.55 μm wavelength range, an important region in optical communications. However the luminescence quenching at room temperature (and even below) due to point defects in the GaAs matrix, which open non-radiative recombination paths for photocarriers that otherwise would recombine radiatively in the QDs,is still a problem.

In this study we combined Rutherford backscattering/Channelling (RBS-C), High resolution X-ray diffraction (HRXRD), Atomic force microscopy (AFM) and Photoluminescence (PL) techniques in order to correlate the structural and optical properties of InAs/GaAs QD heterostructures grown by Atmospheric Pressure Metal Organic Vapour Phase Epitaxy. Channelling measurements reveal a good crystalline quality along the main axial directions with minimum yields in the range of 4 to 6% through the entire capping layer. An increase on the dechannelling rate was observed in the region where the InAs quantum dots were buried. The channelling results also give evidence for the presence of defects preferentially oriented on the (110) planes. Detailed angular scans in a structure with a 25 nm cap allowed the study of the In orientation with respect to the GaAs matrix and a perfect alignment was found. Growth interruption during the deposition of the capping layer, with a short surface treatment using tetrachloromethane (CCl_4), has been shown to improve the overall quality of the heterostructures. The improvement has been accounted for by the decrease of the point defect concentration in the capping layer and now is confirmed by the channelling results. Detailed PL studies have shown that such a technological treatment help eliminating the PL quenching at room temperature. This conclusion is confirmed by our modelling of the statistics of the photocarrier distribution between the different states in the QDs and the barriers out of equilibrium.

Magnetic studies of mechanically alloyed metastable fcc $Fe_{23}Cu_{77}$: superferromagnetism with bimodal cluster size distribution.

J. S. Amaral[1*], N. J. O. Silva[1**], V. S. Amaral[1]

[1]Departamento de Física and CICECO, Universidade de Aveiro, P-3810-193 Aveiro, Portugal;

B.F. O. Costa[2]

[2] CEMDRX, Physics Department, University of Coimbra, P-3004-516 Coimbra, Portugal;

G. Le Caër[3]

[3] IPR, UMR UR1-CNRS 6251, Université de Rennes I, F-35042 Rennes Cedex, France

[*]email : jamaral@ua.pt

Abstract

Nanocrystalline materials can be prepared using specific synthesis processes that stabilize non-equilibrium structures, which may present enhanced physical properties. According to the Fe-Cu phase diagram, Fe and Cu are essentially immiscible at room temperature. High Energy Ball-milling of Fe and Cu powder mixtures induces the formation of nanostructured solid solutions, either bcc for Fe-rich Fe(Cu) alloys (Fe>~80 at%) or fcc for Cu-rich (Fe<~40-50 at%) Cu(Fe) alloys while two phases (bcc+fcc) coexist in the intermediate range. The magnetic and Mössbauer spectroscopy properties of a nanostructured fcc Fe23Cu77 at % alloy are presented. The use of a magnetic mean-field method [1] reveals that the system is a bimodal size distribution of magnetic Fe-rich nanoclusters, where the smaller ones are close to the stable 13 atom icosahedral/cuboctahedral arrangement with magnetic moment $30\mu_B$, and the large clusters present a magnetic moment 860 μ_B containing ~400 Fe atoms. The inter-cluster ferromagnetic interactions that lead to super-ferromagnetism with a Curie temperature Tc~220K are determined by the smaller clusters only, which account for 90% of the magnetization.

[1] J. S. Amaral, N. J. O. Silva and V. S. Amaral, Appl. Phys. Lett. 91, 172503 (2007).

[**] *Present address*: Instituto de Ciencia de Materiales de Aragón, CSIC_Universidad de Zaragoza, 50009 Zaragoza, Spain

GOLD NANOPARTICLES AS VERSATILE LABELS FOR ENHANCED PROTEIN DETECTION

Adriano Ambrosi, Alfredo de la Escosura and Arben Merkoçi[*]

Nanobioelectronics & Biosensors Group, Institut Català de Nanotecnologia
&
Departament de Química, Universitat Autònoma de Barcelona
Barcelona, Catalonia, Spain

*E-mail: Arben.Merkoci.icn@uab.cat

Immunoassay represents a promising tool for selective and sensitive analysis and has recently gained increasing attention in different fields including environmental monitoring, food safety, and clinical diagnosis[1]. Despite many advances in this field, it is still a challenge to find new approaches that could improve the simplicity, selectivity, and sensitivity of immunoanalysis.
Analytical signal amplification and background signal reduction are crucial points for obtaining low detection limits in immunoassays[2]. Sandwich-type immunoassays are the most widely used because of the higher specificity and sensitivity achievable by means of a couple of match antibodies[3]. In these platforms the secondary antibody is combined with targeting labels able to generate optical or electrochemical analyte-related signals.

Gold nanoparticles (AuNPs) represent an ideal tool for signal transduction in immunoanalytical systems due to their optical, electrochemical and catalytic features as well as the simplicity of synthesis and the efficient bioconjugation procedures that allow the biomolecules conjugated to retain their functionality and interact with their counterparts[4]. The complex biomolecule/AuNP provides interesting solutions for direct signal transduction of biorecognition events[5], but also for enzyme-mediated signal amplification.

The optical and electrochemical properties of AuNPs with the catalytic activity of the HRP enzyme will be combined and showed in this work with the aim to present a novel versatile label for protein analyses. AuNPs modified with a model anti-human IgG peroxidase-conjugated antibody (anti-human IgG-HRP) offers several analytical routes for immunodetection. Spectrophotometric analyses based on either AuNP absorption or HRP enzymatic activity and the electrochemical detection based on the direct detection of AuNP (without any dissolution step) will be presented and compared. Optical sensitivity enhancement attributable to the use of AuNP as a multi-IgG-HRP carrier which therefore amplify the enzymatic signal, as well as the high sensitivity in the direct electrochemical detection, represent important achievements of this method which could be adopted for several bioanalytical applications.

References:

[1] F. Tsagkogeorgas, M. Ochsenkuhn-Petropoulou, R. Niessner, D. Knopp. *Anal. Chim. Acta,* **573-574,** (2006), 133-137.
[2] Z. Fu, H. Liu, H. Ju. *Anal. Chem.* **78**, (2006), 6999-7005.
[3] D. Knopp. *Anal. Bioanal. Chem.* **385**, (2006), 425-427.
[4] I. Willner, R. Baron, B. Willner. *Biosens.Bioelectron.* **22**, (2007), 1841-1852.

[5] E. Katz, I. Willner, J. Wang. *Electroanal.* **16,** (2004), 19-44.

Figures:

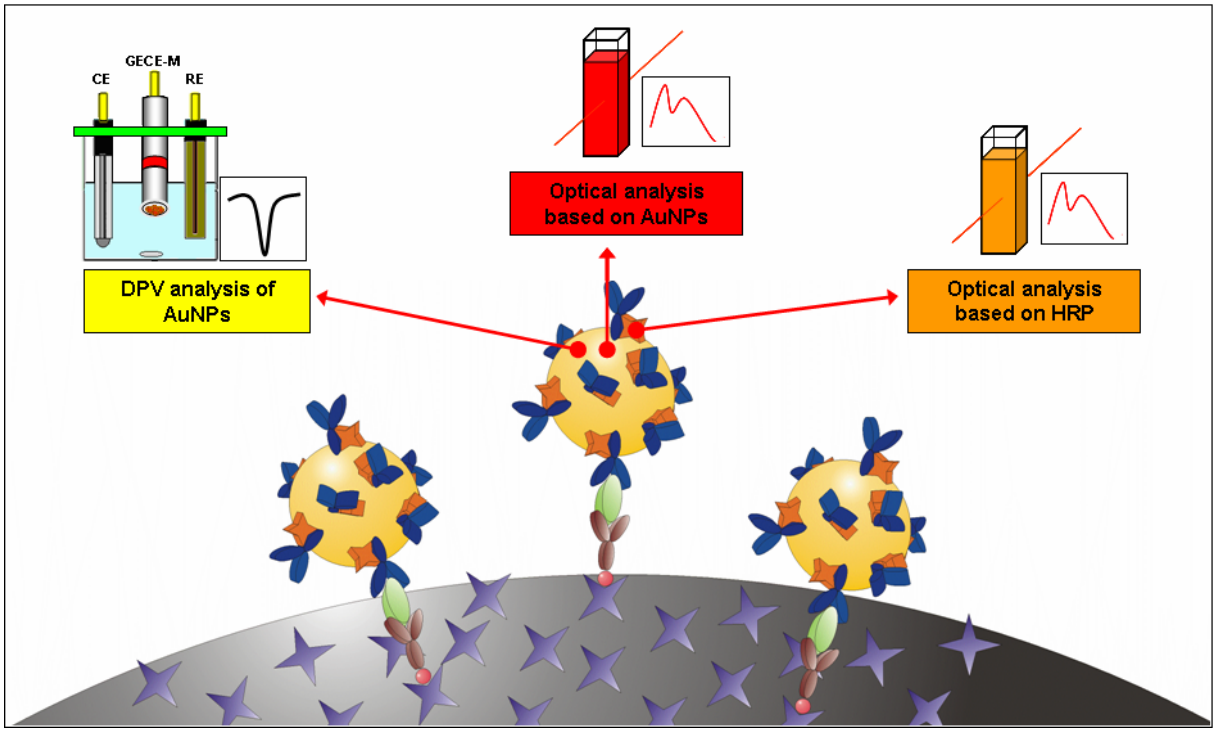

Nanometric aggregates of a covalent porphyrin dimer followed by Fluorescence Correlation Spectroscopy in aqueous buffered solution

Suzana M. Andrade,[a] *V. Vaz Serra*,[b] *M.A.F. Faustino*,[b] *M.G.P.M.S. Neves*,[b] *J.A.S. Cavaleiro*[b], *S.M.B. Costa*,[a]

[a]*Centro de Química Estrutural, Complexo I, Instituto Superior Técnico, Av. Rovisco Pais, 1049-001 Lisboa, PORTUGAL*

[b]*Departamento de Química, Universidade de Aveiro, Campus Universitário de Santiago, 3810-193 Aveiro, PORTUGAL*

suzana.andrade@ist.utl.pt

The design of covalently linked porphyrins envisages the goal of applying it to molecular photonic devices and artificial biomimetic light-harvesting arrays. Porphyrins are well-known for their tendency to self-aggregate in aqueous solution. The type of self-aggregation can be controlled by a series of factors that include the structure of the porphyrin (substituent groups and coordinated metal ion) and environmental conditions (pH, ionic strength, temperature, cosolvents, etc).

We have recently dealt with the aggregation properties of the anionic water-soluble porphyrin, *meso*-tetrakis(p-sulfonatophenyl)porphyrin sodium salt – TSPP induced at aqueous interfaces. It was shown that under suitable conditions of pH and ionic strength this molecule forms highly ordered molecular J and H aggregates. Interestingly, these aggregates were found to be promoted by interaction with proteins (HSA and BSA) [1], dendrimers [2] and surfactants/lipids [3, 4]. Moreover, it was possible to tune the photophysical properties of the nano-aggregates formed, within these organized systems.

The present work reports the study of the covalent dimer 5-(4-carboxyphenyl)-10,15,20-tris(3-methoxyphenyl)porphyrin with a tyrosine spacer – Dim C (Fig. 1) in aqueous solution, at controlled pH and ionic strength using fluorescence techniques. Fluorescence decays obtained in water point to the existence of small undefined porphyrin aggregates which become more organized upon salt addition (5 – 25 mM) and fluorescent particles are detected (τ_f~200 ps, Fig. 2a).

The characterization of these aggregates was further attempted making use of techniques combining both spatial (imaging) and temporal resolution. In particular, Fluorescence Correlation Spectroscopy (FCS) is a highly sensitive tool to measure concentration and diffusion coefficients from which we may determine binding/dissociation equilibria in the nanomolar range [5]. Based on the latter, a diffusion coefficient of D=6±1 $\mu m^2 s^{-1}$ (Fig. 3) could be retrieved pointing to nano-aggregates of Dim C in aqueous buffered solution. A decrease in the fluorescence lifetime of Dim C in the presence of cytochrome c occurs indicating a quenching process, possibly due to electron transfer upon binding the dimer to the protein, as the decrease in the difusional time obtained by FCS suggests (D~120 $\mu m^2 s^{-1}$).

The presence of Brij 35 nonionic micelles clearly destabilizes the porphyrin aggregates by competing hydrophobic interactions leading to incorporation of the porpyrin into the micellar moitie. This is well supported by the increase in the porphyrin lifetime (τ_f~ 12 ns; Fig. 2b) similar to that obtained in neat DMSO and the diffusion coefficient calculated agrees well with that of diffusing Brij 35 micelles (D~70 $\mu m^2 s^{-1}$).

Acknowledgements: This work was supported by POCTI/QUI//57387/2004. S.M. Andrade thanks FCT for the award of Post-Doc grant BPD/24367/2005.

References:

[1] S.M. Andrade, S.M.B. Costa, Biophys. J., **82** (2002) 1607; *ibid*. J. Fluoresc. **12** (2002) 77.
[2] P.M.R. Paulo, R. Gronheid, F.C. De Schryver, S.M.B. Costa, Macromolecules **36** (2003) 9135
[3] S.M. Andrade, S.M.B. Costa, Chem. Eur. J. **12** (2006) 1046.
[4] S.M. Andrade, R. Teixeira, S.M.B. Costa, A.J.F.N. Sobral, Biophys. Chem. **133** (2008) 1.
[5] S.M. Andrade, S.M.B. Costa, J.W. Borst, A. van Hoek, A.J.W.G. Visser, J. Fluoresc. (2008) 000.

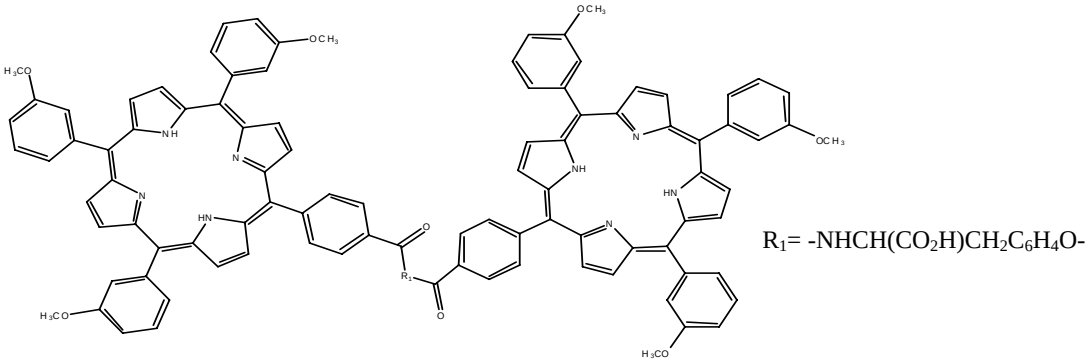

Figure 1 – Scheme of Dim C.

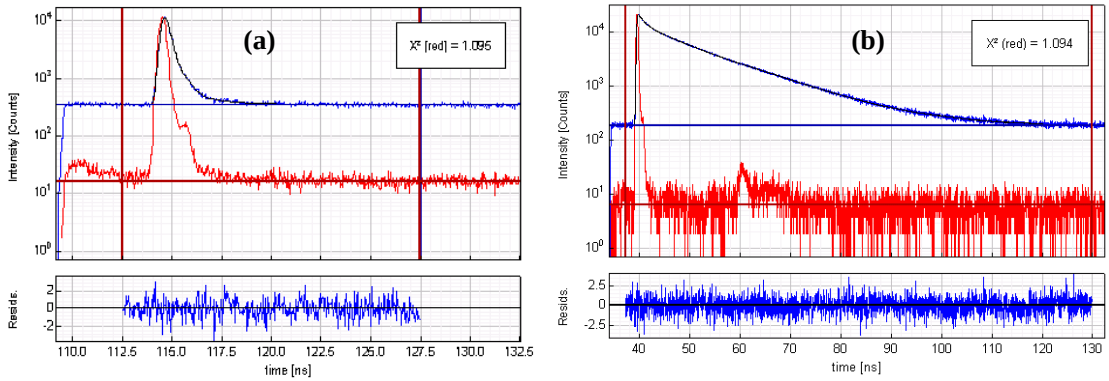

Figure 2 – Fluorescence decays of Dim C in aqueous buffer solution (a) and in the presence of Brij 35 micelles (b).

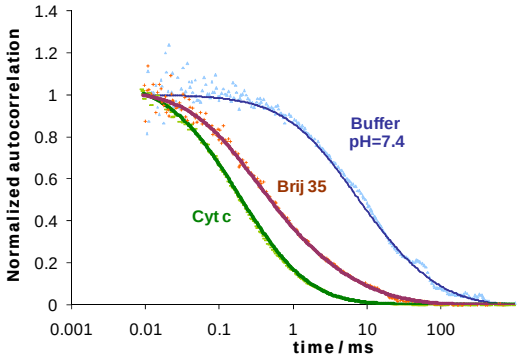

Figure 3 - Normalized autocorrelation traces (experimental – dotted lines; fitting – solid lines) of Dim C (70 nM) in aqueous solution (blue) and in the presence of Cyt c (5 μM, green) and Brij 35 micelles (1 mM; red).

SEPARATION OF ARGON AND OXYGEN BY ADSORPTION ON A TITANOSILICATE MOLECULAR SIEVE

A. Ansón[1], *S.M. Kuznicki*[2], *T. Haastrup*[2], *T. Kuznicki*[2], *C.C.H. Lin*[2], *G. Konya*[3], *B.C. Dunn*[3], *E.M. Eyring*[3], *D.B. Hunter*[4]

[1]*Instituto de Carboquímica, CSIC, Miguel Luesma Castán 4, 50018 Zaragoza, Spain*

[2]*Department of Chemical and Materials Engineering, University of Alberta, Edmonton, AB T6G 2G6, Canada*

[3]*Department of Chemistry, University of Utah, Salt Lake City, UT 84112, USA*

[4]*Savannah River National Laboratory, Aiken, SC* 29808, USA

alanson@icb.csic.es

The separation of argon and oxygen is one of the important processes in the industrial purification of the constituents of air, and is also one of the most difficult. The basic methods used to effect this separation include cryogenic distillation and selective adsorption.

Several titanosilicates, including ETS-4 [1], ETS-10 [2], and other structures based on octahedral titanium units [3], have been recognized for their adsorptive and molecular sieving properties. ETS-4, in particular, has been noted for its ability to differentiate molecules by size, including the commercial separation of N_2 from methane at high pressure.

In the present communication, we examine the separation of O_2 and Ar at room temperature using Ba-RPZ, a new synthetic titanosilicate molecular sieve. RPZ is synthesized by mixing sodium silicate, NaOH and $TiCl_3$ with potassium chloride. From X-ray powder diffraction analysis, it is clear that, like ETS-4 [4], RPZ (Reduced Pore Zorite) is structurally related to the mineral zorite [5].

A clean resolution of O_2 and Ar was achieved in pulse chromatographic experiments using Ba-RPZ standard columns (0.25" OD, 3.5 grams of adsorbent), even when the argon content was only 10% of the mixture (Figure 1). The argon and oxygen retention times were almost identical regardless of the composition of the O_2-Ar mixture. In another experiment, using a column containing 30 grams of adsorbent and a continuous O_2+Ar feed at 10 cm^3/min, argon breakthrough was detected more than 5 minutes before oxygen breakthrough, even in the case of mixtures with low argon content (95% O_2).

Equilibrium adsorption isotherms and isosteric heats of adsorption for oxygen and argon were found to be almost identical at room temperature. The thermodynamic selectivity was found to be mildly in favor of oxygen (~ 1.1 – 1.2). However, the adsorption of oxygen was observed to be much faster than argon (Figure 2), indicating that the separation of the O_2+Ar mixtures was based on the sieving properties of the adsorbent and the difference in sizes of O_2 molecules and Ar atoms. This indicates that a suitably oriented oxygen is physically smaller than argon, despite the fact that many references assume oxygen is larger than argon.

References:

[1] S.M. Kuznicki, V.A. Bell, S. Nair, H.W. Hillhouse, R.M. Jacubinas, C.M. Braunbarth, B.H. Toby, M. Tsapatsis, Nature, **412** (2001) 720.
[2] S.M. Kuznicki, US Patent 5,011,591 (1991).
[3] V. Sebastián, Z. Lin, J. Rocha, C. Téllez, J. Santamaría, J. Coronas, Chem. Mater., **18** (2006) 2472.
[4] S.M. Kuznicki, U.S. Patent 4,938,939 (1990).
[5] G. Cruciani, P. De Luca, A. Nastro, P. Pattison, Micropor. Mesopor. Mater., **21** (1998) 143.

Figures:

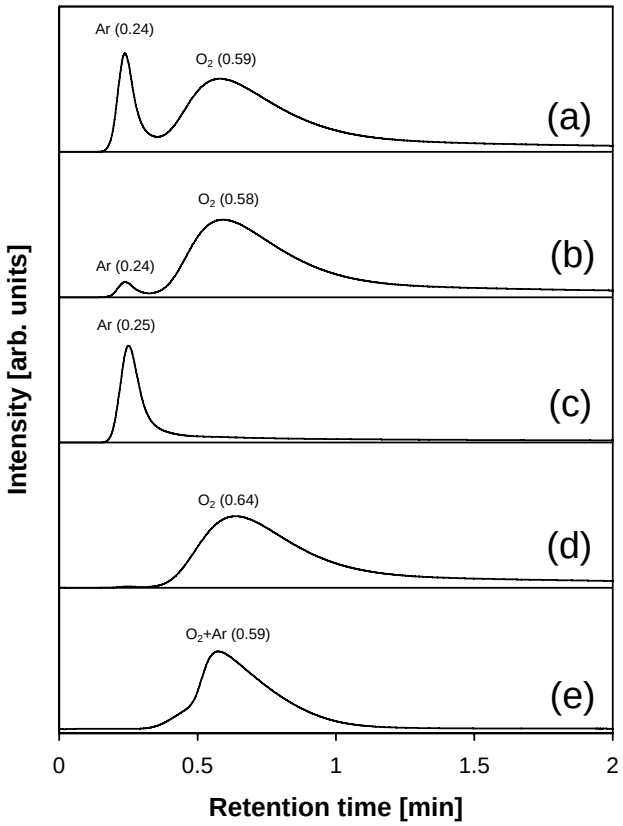

Figure 1. Chromatographic profiles at 30ºC under 30 cm^3/min carrier gas helium obtained by injecting: a) 50-50% O_2-Ar; b) 90-10% O_2-Ar; c) pure argon; d) pure oxygen in a column of Ba-RPZ, and e) 50-50% O_2-Ar in a column of Ba-ETS-4.

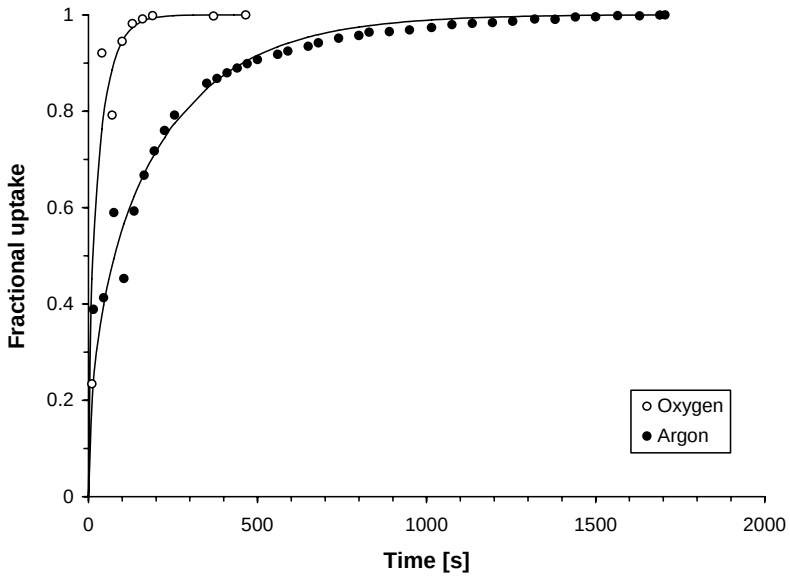

Figure 2. Adsorption uptake curves for oxygen and argon on Ba-RPZ at 30ºC in the pressure step 70-100 kPa.

SusChem – ESPAÑA – DRIVING FORCE FOR INNOVATION

Mª Eugenia Anta
Innovation and Technology Development Manager
FEIQUE- Spanish Federation of Chemical Industry
C/ Hermosilla 31 1ºD
28001 Madrid -SPAIN
Web: http://www.pte-quimicasostenible.org
http://www.suschem.org
Email: info@pte-quimicasostenbile.org

Sustainable chemistry is the driving force for global sustainable development. Closer to home sustaining chemistry and molecular science and engineering in Europe is at the heart of improving industrial competitiveness, maintaining and improving further our quality of life.

It forms a significant basis for the future knowledge-based European economy. Sustainable chemistry means that chemical technologies and products have to improve directly or indirectly through their use the following areas: human and environmental health, meeting consumer requests regarding their function, quality of life for all of society, energy efficiency and resource consumption.

The Spanish Technology Platform for Sustainable Chemistry (SusChem- ESPAÑA) is leading a initiative to boost chemistry, chemical engineering and industrial biotechnology research activities and enhance collaborative R&D. SusChem was jointly initiated by FEIQUE (the Spanish Federation of the Chemical Industry) and ASEBIO (the Spanish Association for Bioindustries) in 2005. It is an open multi-stakeholder forum with additional organisational support from FEDIT (Spanish Federation of Technology Centres) and OTRI - net of Universities and financial support from the Education Minister.

SusChem- ESPAÑa participates in the projects of SUSCHEM for a sustainable European chemical industry with enhanced global competitiveness and minimal environmental impact powered by a world leading, technological innovative drive.

SusChem- ESPAÑA has also developed a web platform where you can find the services developed in the last three years to enhance innovation and sustainability.
One of our last services is the International Innovation Unit, for giving assistance in the 7FP proposals of our members.

You can find our in our web: www.pte-quimicasostenible.org, many other services, as well as the SusChem's Strategic Research Agenda (published in December 2005), and its detailed Implementation Action Plan (completed in December 2006) represented and will continue to represent a significant contribution to the formulation of the European Commission's FP7, future European R&D Framework Programmes and other major collaborative European research initiatives.

SusChem will help to build bridges between the different disciplines of chemistry and biotechnology with other molecular sciences, technologies and engineering as well as between stakeholders.

SusChem also provides an invaluable opportunity to improve the public perception of chemistry. The programme clearly shows the chemical sciences and the chemical industry as *the* drivers of beneficial change for society and finding the solutions to the tremendous challenges facing humanity today.

Poster

GOLD NANOPARTICLES MODIFICATION WITH INTRAMOLECULAR COORDINATION LIGANDS WITH INTEREST FOR SENSING APPLICATIONS

Gemma Aragay[1,2], *Josefina Pons*[1], *Josep Ros*[1], *Arben Merkoçi**[1,2]

[1]*Departament de Química, Universitat Autònoma de Barcelona*

[2]*Nanobielectronics and biosensors group, Institut Català de Nanotecnologia*

Bellaterra, Catalonia, Spain

*Corresponding author: arben.merkoci.icn@uab.cat

Noble metal nanoparticles, especially copper, silver and gold ones, have been known since antiquity for their interesting optical properties due to the so-called surface plasmon band, a physical property of nanometric clusters which involves absorption and scattering phenomenon.

Specially, gold nanoparticles (AuNP) have unique optical and chemical properties that make them ideally suited for a number of applications including optical or electrochemical probes, targeted drug delivery as well as other applications.

AuNPs can be synthesized by different ways. One of the most reported is the *Turkevich* method which involves the reduction of $HAuCl_4$ with citrate in water. Another alternative is the reduction of water solutions of Au(III) with $NaBH_4$ in the presence of a proper ligand that confines the AuNP size. The synthesis of modified AuNPs by complexation with a ligand that acts as reducing agent and subsequently stabilizes the gold particles seems to be an interesting alternative. (REF).

The synthesis and characterization of AuNPs modified with home-made intramolecular coordination ligands (i.e. from *N*-alkylaminopyrazole family) using amine chemistry for reduction as well as for the surface modification will be shown. Herein, the optical and chemical properties of the synthesized gold nanoparticles including some applications with interest for future optical and electrochemical sensing systems will be reviewed.

Acknowledgement. This work has been done under the WARMER research project, FP6-034472.

INCREASING THE SENSITIVITY OF MAGNETORESISTIVE-BASED BIOCHIPS

F. A. Cardoso[1,2], S. Cardoso[1,2], V. C. Martins[1,3], P. P. Freitas[1,2]

[1] INESC Microsistemas e Nanotecnologias (INESC MN), Rua Alves Redol 9, 1000-029 Lisbon, Portugal
[2] Instituto Superior Técnico (IST), Av. Rovisco Pais, 1000-029 Lisbon, Portugal
[3] Center for Biological and Chemical Engineering (CEBQ), Instituto Superior Técnico Av. Rovisco Pais, 1000-029 Lisbon, Portugal

In the last few years, biochips based in magnetoresistive sensors have been used for biomolecular recognition assays [1-3]. In these assays biological probes are immobilized on the chip surface and complementary target biomolecules can be detected using a magnetic label. The detection of the magnetic label fringe fields is accomplished by a magnetoresistive sensor. Because of its sensitivity, its reliability and its easiness of fabrication, spin valve sensors are the most commonly used sensor. Several groups reported the detection of tens and hundreds nanometer sized particles [4],[5]. In order to increase the sensitivity of this technique, an emerging interest in using magnetic tunnel junctions (MTJ) as magnetoresistive sensors is arising due to its higher magnetoresistance (up to 70% with AlOx barrier and 350% with MgO barrier) and its potential increase in sensitivity. However, due to its current-perpendicular-to-plane (CPP) configuration which increases the distance between the sensing layer and the particles, in similar sensor architectures, MTJs show lower particle sensitivity when compared to spin valves sensors (with current-in-plane configuration) [4].

MgO-barrier MTJs with linear response were successfully fabricated. The linear response observed in figure 1 was obtained by shape anisotropy (30x2 μm^2). The MTJ shows a tunneling magnetoresistance (TMR) of 78%, a sensitivity of 1.89%/Oe and a resistance of 2000 kΩ. In order to reduce the distance between the sensing layer and the particles, an Au contact was used for the MTJ top contact. In this way, if a thiol-based chemistry is used the biological probes can be directly immobilized on top of the contact and no passivation layer is needed. [6]

Figure 2 shows the MTJ voltage variation due to the presence of magnetic particles. The detection was made applying an external in-plane transverse 30 Oe + 15 Oerms magnetic field and acquiring the signal using a lockin technique. A volume of 10µl of 250nm superparamagnetic particles (~10^{11} particles/ml) was put over the chip and let to settle down during 10 minutes. A saturation signal of 860 µV was obtain. After washing, the signal came back to the baseline value meaning that all the particles were removed from the sensor (see fig. 2). It is important to note that these experiments with particles demonstrated that neither the Au contacts nor the MTJs are damaged by the corrosion due to liquid used in the experiments. Further experiments with different particles concentrations and with biological probes immobilized over the Au contact will be performed.

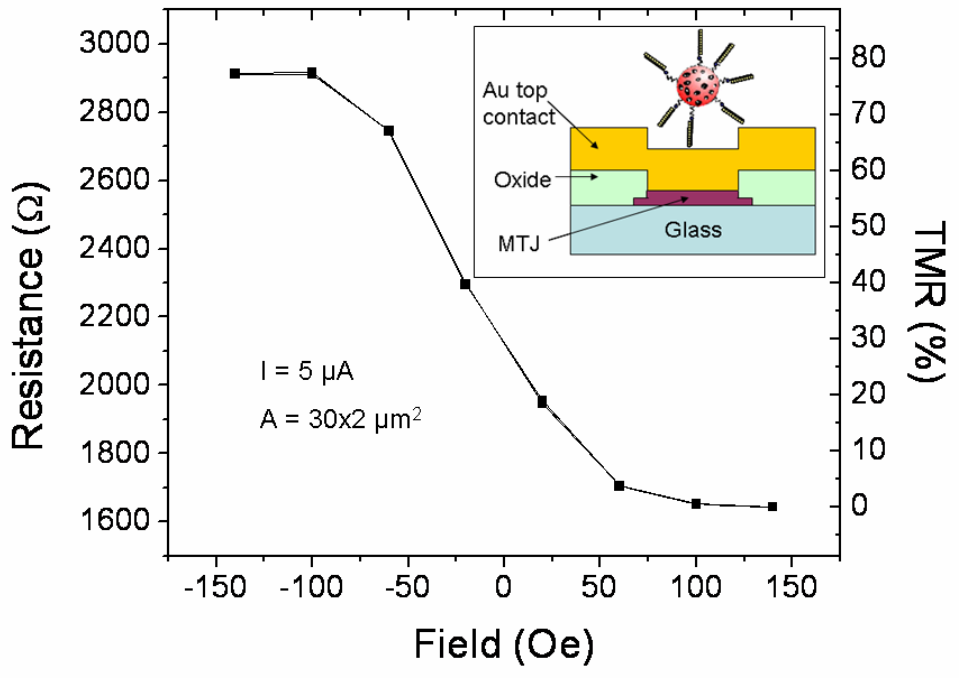

Figure 1: MTJ transfer curve measured for a current bias of 5 µA. The area of the MTJ is 30x2 µm^2. **Inset:** Cross section of the magnetic tunnel junction chip. The probes biomolecules are immobilized on top of the Au contact.

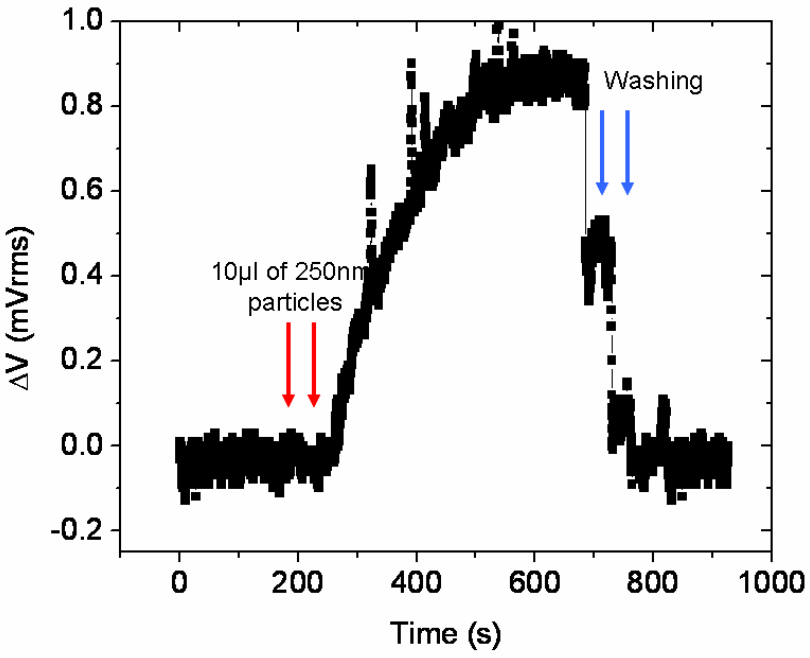

Figure 2: 10 µl of 250nm particles (~10^{11} particles/ml) detection using an MTJ. An in-plane external 30 Oe + 15 Oerms magnetic field was applied to magnetize the particles.

[1] “Detection of cystic fibrosis related DNA targets using AC field focusing of magnetic labels and spin-valve sensors”, H. A. Ferreira et al. (2005), IEEE Trans. Magn, vol. 41, no. 10, pp 4140-4142.
[2] “Detection of a micron-sized magnetic sphere using a ring-shaped anisotropic magnetoresistance-based sensor: a model for a magnetoresistance-based biosensor.”, Miller, M.M. et al. (2002) , Appl. Phys. Lett. 81, 2211–2213
[3] “Design and performance of GMR sensors in the detection of magnetic microbeads in biosensors.”, Rife, J.C. et al. (2003), Sens. Actuat. 107, 209–218
[4] “Detection of 130 nm magnetic particles by a portable electronic platform using spin valve and magnetic tunnel junction sensors”, F. A. Cardoso et al. (2008), J. Appl. Phys., (in press).
[5] “Spin valve sensors for ultrasensitive detection of superparamagnetic nanoparticles for biological applications”, G. Li, et al. (2006), Sensors and Actuators A , 126, 98-106.
[6] “Toward a magnetic microarray for sensitive diagnostics”, S. X. Wang, et al. (2005), J. Mag. Mag. Mat., 293, 731-736.

DEVELOPMENT AND APPLICATION OF PEPTIDE NUCLEIC ACIDS (PNA) FOR THE RAPID IDENTIFICATION OF MICROORGANISMS BY FLUORESCENCE *IN SITU* HYBRIDIZATION (FISH)

N. F. AZEVEDO[1,2]; C. ALMEIDA[1,2]; L. CERQUEIRA[1]; T. JARDIM[1]; N. GUIMARÃES[1,3]; C. FIGUEIREDO[3,4]; C. W. KEEVIL[2] AND M. J. VIEIRA[1]

[1]IBB - Institute for Biotechnology and Bioengineering, Centre of Biological Engineering, Universidade do Minho, Campus de Gualtar 4710-057, Braga, Portugal; [2]Environmental Healthcare Unit, School of Biological Sciences, University of Southampton, Bassett Crescent East, Southampton SO16 7PX, United Kingdom; [3]IPATIMUP – Institute of Molecular Pathology and Immunology of the University of Porto, Porto, Portugal and [4]Medical Faculty of Porto, Porto, Portugal.

nunoazevedo@deb.uminho.pt

Fluorescence *in situ* hybridization (FISH) is a well-established technique that is used for a variety of purposes, ranging from pathogen detection in clinical diagnostics to the determination of chromosomal stability in stem cell research. The key step of FISH involves the detection of a nucleic acid region and as such, DNA molecules have typically been used to probe for the sequences of interest. However, since the turn of the century, an increasing number of laboratories have started to move on to the more robust DNA mimics methods, most notably to peptide nucleic acids (PNA). In this work, we report the development of four new probes that target well-known human pathogens [e.g. 1]. The method has been optimized for the detection of these pathogens in less than 5 hours by epifluorescence microscopy with high specificity and sensitivity. Additionally, counter-staining with 4′,6-diamidino-2-phenylindole (DAPI) allowed discrimination of the pathogens in mixed populations of contaminants in a variety of microenvironments.

These new probes will act both at the level of population well-being, by providing faster and more efficient methods for the detection of infectious agents and at the level of worldwide economy, by bringing down patient care associated costs (mainly those related with less-than-optimum antibiotic usage and median length of hospital stay for each patient)

References:

[1] Guimaraes N, Azevedo NF, Figueiredo C, Keevil CW, Vieira MJ. Development and application of a novel peptide nucleic acid probe for the specific detection of *Helicobacter pylori* in gastric biopsy specimens. J Clin Microbiol **45(9)** (2007) 3089-3094.

Poster

NANOPARTICLES FOR BIOSENSING APPLICATIONS

Raul Baltazar, Guilherme N. M. Ferreira
IBB-Institute for Biotechnology and Bioengineering
Centre for Molecular and Structural Biomedicine
University of Algarve, Campus Gambelas, 8005-139 Faro, Portugal
rbaltazar@ualg.pt

The development of detection systems is a key issue in Nanomedicine. In particular the establishment of novel methodologies to link biomolecules to metallic and semiconductor materials to generate biologically active semiconductor nanocrystals and nanoparticles constitutes an important issue to generate optical nanosensors for the detection of molecular interactions both in vivo and in vitro.

A number of interesting colorimetric methods have been recently developed for molecular recognition and detection, many of them using noble metal nanoparticles has sensing elements. Gold nanoparticles are well known for their strong interactions with light that result on surface plasmon resonances, with frequencies that depend on the nanoparticles shape, size, material properties and surrounding medium. Given the fact that both experimental and theoretical studies show that the surface plasmon resonance peak of two closely-coupled nanoparticles is significantly red-shifted from that of the un-aggregated ones and that these nanoparticles are amenable to the attachement of biomolecules, the controlled aggregation of GNPs has become an interesting application of nanoparticles in biosensing, where the inter-particle interactions can be simply characterized by optical absorption spectroscopy.

Three types of sensing strategies are in development in our laboratory, using gold nanoparticles as biosensor elements. (1) A biomolecule-mediated template assay for antibody-antigene recognition was developed based on the controlled aggregation of biotinylated gold nanoparticles induced by addition of streptavidin molecules to solution; (2) Detection of DNA sequences based on the different electrostatic attraction properties towards unmodified gold nanoparticles of single- and double-stranded oligonucleotide sequences, resulting in differentiation of plasmon resonance signals due to particle aggregation ; and (3) Use of aptamers adsorbed to gold nanoparticles unmodified surfaces to detect specific targets. In the last two cases, the detection is made through the colorimetric changes associated with the gold nanoparticles aggregation when exposed to determined salt concentrations.

Futher work will focus on the approach of direct probe questioning for molecular recognition using RET between quantum dots (QDs) and gold nanoparticles (AuNPs). The general objective is to use QDs and AuNPs in biorecognition analysis and identification. As such, the fundamental understanding of the QDs and AuNPs interaction is pursued, namely the impact of the interparticle distance on fluorescence quenching/enhancement pathway. Synthetic oligonucleotides, PCR amplicons, and antibody/antigen pairs are used as model biosystems to develop the generic QDs/AuNPs sensing methodology and to settle-up prototype nanosensors with potential biomedical applications.

Acknowledgments:
The authors thank to Portuguese Foundation for Science and Technology (FCT) the financial support through the research project POCI/BIO/61912/2004 and grant SFRH/BD/17286/2004.

Z-AXIS (DEPTH) CONTROL OF CELL SPREADING ON MICROPATTERNED SURFACES

E. T. Baran[1,2], *R. Pirraco*[1,2], *A. P. Marques*[1,2], *S. Merino*[3], *N. Neves*[1,2], *R. L. Reis*[1,2]

[1] *3B's Research Group-Biomaterials, Biodegradables and Biomimetics. Dept. of Polymer Engineering, University of Minho, Campus de Gualtar, 4710-057 Braga, Portugal, www.3bs.uminho.pt*

[2] *IBB-Institute for Biotechnology and Bioengineering, PT Government Associated Laboratory, Braga, Portugal*

[3] *Fundación Tekniker, Micro y Nanotecnologías, Spain*

turkerbaran@dep.uminho.pt

The control of the proliferation and differentiation by the cell reaction to a surface was reported recently [1]. However, the mechanisms involved in the cell contact to micro- and nano-topographies have not been fully understood. Also the study of cell morphology when seeded in surface micropatterns with different depths was not yet quantitatively analysed. In this study, the response in terms of cell morphology and alignment to micro-scale topographical structures was evaluated. A range of parallel grooved surfaces with equidistant spaces (3.38-11.36 μm) and various depths (1.35-4.95 μm) were prepared in poly(caprolactone) (PCL) membranes using the hot embossing technique. The response of osteoblastic cells to those patterns after fluorescence labeling of the cytoskeletons was evaluated. The results were quantitatively analyzed by image analysis.

As shown in Figure 1 (a) and (b), it was found that the cell area and maximum length were marginally affected by the pattern dimension varying from 3.35 to 11.36 μm. In contrast, the cell area and length changed significantly when the pattern depth was varied between 1.35 to 4.95 μm, being the effect more pronounced in terms of cell length.

Figure 2 (a) shows the compiled data from the previous parameters, where a very distinct transition in the cell morphology parameter is shown with depth. The cell area/cell length ratio was significantly more affected by the smaller in-plane dimensions and by the deepest patterns. In addition, at the lowest depth, the ratio decreased directly with the pattern dimension from 3.35 to 11.36 μm. As the pattern depth increase, the ratio dropped drastically and the differences caused by the in-plane dimension variation were not so clear. The decrease in the ratio cell area/cell length indicates that the cell behavior changed from round spread shape into highly aligned morphology, which could be confirmed by the microscopical analysis (Fig 2 (b)). The effect of the pattern depth over the cell morphology was 2-4 times larger than that caused by the variation of pattern size in the plane, thus being strongly effective in controlling the cell alignment.

References:

[1] D. M. Pirone, W. F. Liu, S. A. Ruiz, L. Gao, S. Ragdavan, C. A. Lemmon, L. H. Romer, C. S. Chen. J Cell Biol, (2006) 277-287.

Acknowledgements:
E.T. Baran thanks the Portuguese Foundation for Science and Technology for providing him a PostDoc scholarship (SFRH/BPD/30768/2006), European Union Funded STREP Project HIPPOCRATES (NMP3-CT-2003-505758) and the European NoE EXPERTISSUES (NMP3-CT-2004-500283).

Figures:

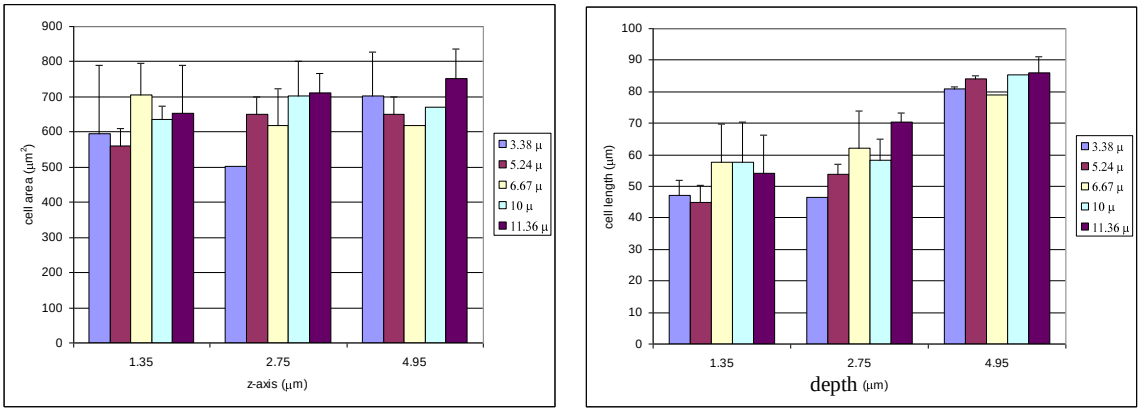

(a) (b)

Figure 1. In-plane pattern dimensions and pattern depth effect over the average cell area (a) and cell length (b).

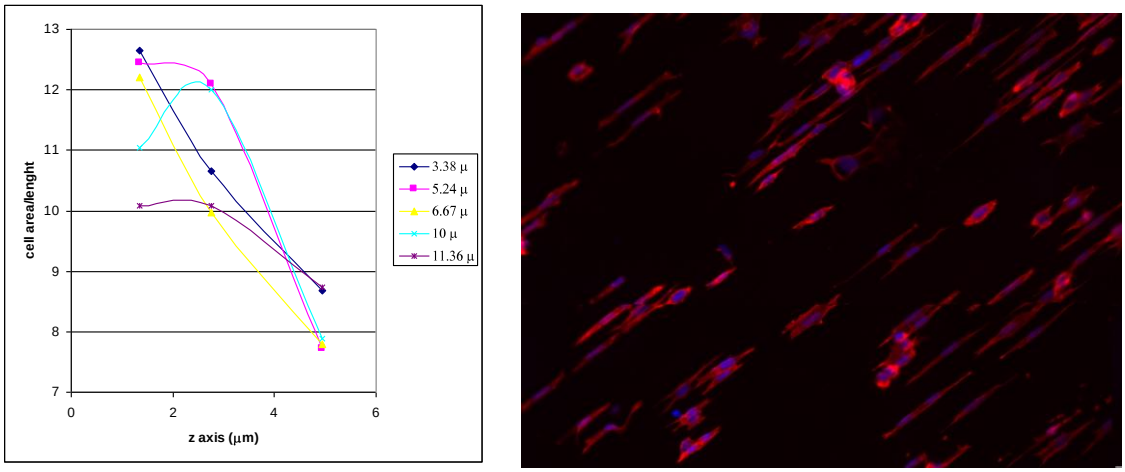

(a) (b)

Figure 2. Variation of morphology parameters (cell area/cell length ratio) with depth for each pattern dimension (a). Fluorescence light microscope image of highly elongated and aligned SeOs-2 cells on PCL surface with 11.36 µm ridge and 4.95 µm deepness (b).

SIMULATION IN ORGANIC NANOELECTRONICS: FROM SINGLE MOLECULE TO THIN FILM

Hélder M. C. Barbosa, Marta M. D. Ramos and Helena M. G. Correia
Department of Physics, University of Minho, Campus de Gualtar, 4710-057 Braga Portugal
helder@fisica.uminho.pt, marta@fisica.uminho.pt, hcorreia@fisica.uminho.pt

During the last decades, the organic electronic field has suffered a tremendous development due to the potential of using organic materials as active components in electronic devices that result from the possibility of tuning their electronic properties by changing the molecular structure of the organic molecules or the experimental conditions in which they are prepared. Most of the knowledge reached so far on the electronic properties of these materials occurred at the experimental level; nevertheless that research is not able to provide a deep understanding of the effect of their properties at molecular scale or the influence of the nanostructure in device performance, among other factors, separately. It is in this context that theoretical modelling reveals to be the ideal approach to understand these effects separately as well as get inside in the physics underlying the electronic processes involved. In this talk we will present some results of our work on nanoelectronic thin film and molecular devices that use small conjugated molecules and conjugated polymers. [1]

By using a quantum molecular dynamics method we study the electron transfer in a molecular device (see Fig. 1) made of a single conjugated molecule (with and without spatial symmetry) bound to two metal electrodes separated by a distance approximately 2 nm. To perform the electronic calculations we used molecular dynamics in parallel with a self-consistent quantum mechanical method since organic molecules are flexible and have strong coupling between the electronic and atomic motion. A significant difference in electron transfer through symmetric and asymmetric conjugated molecules was found to be due to molecular distortion and molecular vibrations along their axis.

To study the influence of the nanostructure, namely the molecular arrangements relative to the electrodes surface, on optoelectronic devices that uses poly(p-phenylene venylene) derivatives as the active component, we developed a nanoscale model for polymer light emitting diodes (see Fig. 2) that uses a dynamical Monte Carlo method for charge injection and transport [2,3]. Our model considers the electronic processes involved in the device functioning, namely charge injection, that depends on the barrier height at electrode/polymer interfaces, two processes for charge transport (e.g. intra-molecular charge transport along a polymer chain and inter-molecular charge transport between polymer chains), charge collection by the electrode opposite to the injection, charge trapping within the polymer layer and charge recombination. Our simulations show that by controlling the nanostructure of the polymer and the type of electrodes used it is possible to increase the performance of the device.

References:

[1] H.M.G. Correia, PhD Thesis, University of Minho, 2007.

[2] M.M.D. Ramos, H.M.G. Correia, J. Phys.: Condens. Matter, **18** (2006) S429.

[3] H.M.C. Barbosa, M.M.D. Ramos, Plasma Process. Polym., **4** (2007) S104.

Figures:

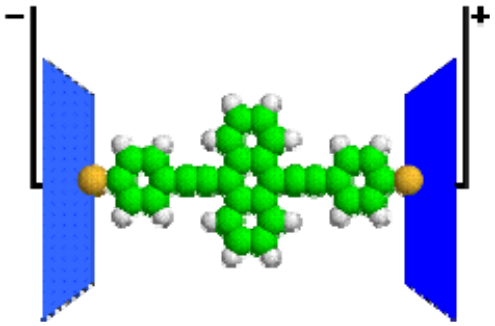

Figure 1 - Scheme of a molecular device made of a symmetric conjugated molecule bond to two gold electrodes.

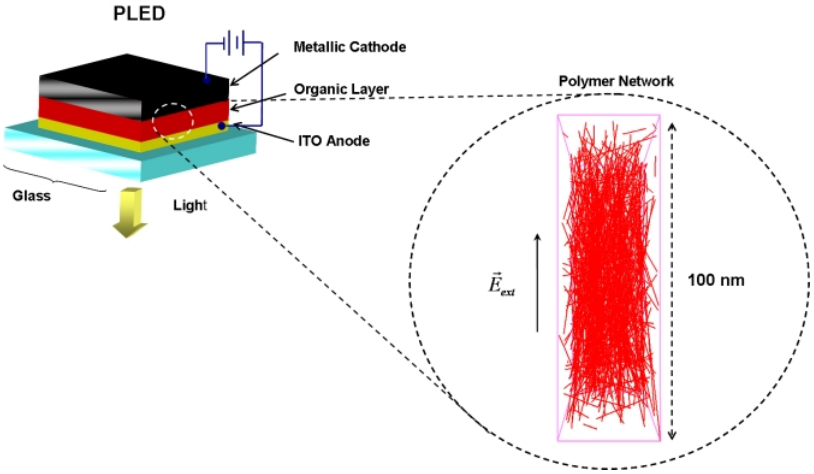

Figure 2 – Scheme of a polymer light emitting diode (PLED) where the sticks represent the different arrangements of the polymer conjugated segments relative to the electrodes surface.

GALLIUM-INDIUM-ZINC OXIDE BASED THIN-FILM TRANSISTORS PRODUCED AT ROOM TEMPERATURE

Pedro Barquinha, Gonçalo Gonçalves, Luís Pereira, Rodrigo Martins and Elvira Fortunato
CENIMAT/I3N, Materials Science Department, Campus de Caparica, 2829-516 Caparica, Portugal
Tel: +351212948562; Fax: +351212948558
pmcb@fct.unl.pt

During the last years oxide semiconductors have shown that they will have a key role on the future of electronics [1,2]. In fact, several research groups have already presented working devices with remarkable electrical and optical properties based on these materials, mainly thin-film transistors (TFTs). Most of these TFTs use indium-tin oxide (ITO) as the material for source/drain electrodes. This work is focused on the investigation of different materials to replace ITO in inverted-staggered TFTs based on gallium-indium-zinc oxide (GIZO) semiconductor. The analyzed electrode materials were indium-zinc oxide (IZO), Ti, Al, Mo and Ti/Au, being each one of these materials used in two different kinds of devices: one was annealed after GIZO channel deposition but prior the source/drain deposition; the other was annealed at the end of device production. The results show an improvement on the electrical properties when the annealing is performed at the end (for instance, with Ti/Au electrodes, mobility rises from 19 to 25 cm^2/Vs and turn-on voltage drops from 4 to 2 V). Using Time-Of-Flight Secondary Ion Mass Spectrometry (TOF-SIMS) we could confirm that some diffusion exists in the source/drain electrodes/semiconductor interface, which is in close agreement with the obtained electrical properties. Besides TOF-SIMS results for relevant elements, electrical characterization is presented for each kind of device, including the extraction of source/drain series resistances and TFTs intrinsic parameters, such as μi (intrinsic mobility) and V_{Ti} (intrinsic threshold voltage).

TABLE I – COMPARISON OF THE ELECTRICAL PROPERTIES OF GIZO-BASED TFTS WITH DIFFERENT SOURCE/DRAIN ELECTRODES. DEVICES WITH W/L=50/50 μm

Source/Drain material	μ_{FE} (cm^2/Vs)	μ_{sat} (cm^2/Vs)	On/Off @ V_{DS}=15V	V_{on} @ V_{DS}=15V (V)	V_T @ V_{DS}=15V (V)
IZO	20.7	15.7	2.1×10^8	1.0	12.7
Ti	21.1	16.9	1.3×10^8	2.0	13.7
Mo	22.6	17.4	6.0×10^7	-2.0	12.5
Ti/Au	24.5	18.7	6.1×10^7	2.0	12.9

[1] E. M. C. FORTUNATO, P. M. C. BARQUINHA, A. PIMENTEL, A. M. F. GONCALVES, A. J. S. MARQUES, L. M. N. PEREIRA, AND R. F. P. MARTINS, "Fully transparent ZnO thin-film transistor produced at room temperature," Advanced Materials, VOL. 17, PP. 590-+, MAR 2005.

[2] P. BARQUINHA, A. PIMENTEL, A. MARQUES, L. PEREIRA, R. MARTINS, AND E. FORTUNATO, "Influence of the semiconductor thickness on the electrical properties of transparent tfts based on indium zinc oxide," JOURNAL OF NON-CRYSTALLINE SOLIDS, VOL. 352, PP. 1749-1752, JUN 2006.

NANOTUBE BASED THERMAL MOTORS: SUB-NANOMETER MOTION OF CARGOES DRIVEN BY THERMAL GRADIENTS

Amelia Barreiro[1], *Riccardo Rurali*[2], *Eduardo R. Hernández*[3], *Joel Moser*[1], *Thomas Pichler*[4], *Laszlo Forro*[5], *Adrian Bachtold*[1]

[1]*CIN2 Barcelona and CNM-CSIC, Campus UAB, E-08913 Bellaterra, Spain*
[2]*Departament d´Enginyeria Electronica, Campus UAB, E-08913 Bellaterra, Spain*
[3]Institut de Ciencia de Materials de Barcelona, Campus UAB, E-08913 Bellaterra, Spain
[4]*Faculty of Physics, University of Viena, Strudlhofgasse 4, 01090 Wien, Austria*
[5]*EPFL, CH-1015 Lausanne, Switzerland*
amelia.barreiro.icn@uab.es

There is a growing effort in the scientific community to design and fabricate ever more versatile nanoelectromechanical systems (NEMS). Because carbon nanotubes are very small, mechanically robust and chemically inert, they have attracted considerable interest as NEMS components. In addition, their one-dimensional tubular shape offers a natural track for motion. This tubular shape restricts the motion to only a few degrees of freedom (typically translation or rotation), much as bearings do in every-day machines.

A new generation of nanotube based motors has been envisaged that takes advantage of the atomic corrugation for a new class of tracks [1]. For example, the motion of two coaxial nanotubes relative to one another is given by the track that results from the mutual atomic interaction between the nanotubes. In some cases, the track follows energy minima that can consist of helical orbits ranging from pure rotation to pure translation. In some others, the energy barrier for motion contains local minima and maxima, arranged e.g. as a twisted chess-board like pattern (see some examples in Fig. 1 C-E) [1].

Here we report on an artificial nanofabricated motor (Fig. 1 A,B) in which one short nanotube moves relative to another coaxial nanotube and we present two major advances. First, the atomic interaction between the nanotubes is shown to generate distinct kinds of motion for different devices, namely rotation and/or translation along the nanotube axis. Figure 2 shows an example of a translational motion. Second, we show that the motion is actuated by imposing a thermal gradient along the nanotube, allowing for sub-nanometer displacements. More specifically, the thermal gradient generates a phononic current in one nanotube that hits and drags the second tube. This is, to our knowledge, the first experimental demonstration of displacive actuation at the nanoscale by means of a thermal gradient; we believe that thermal gradient actuation offers many possibilities in the design of novel nanoelectromechanical systems.

References:

[1] R. Saito, R. Matsuo, T. Kimura, G. Dresselhaus, M.S. Dresselhaus, Chem. Phys. Lett. **348** (2001) 187.

Figures:

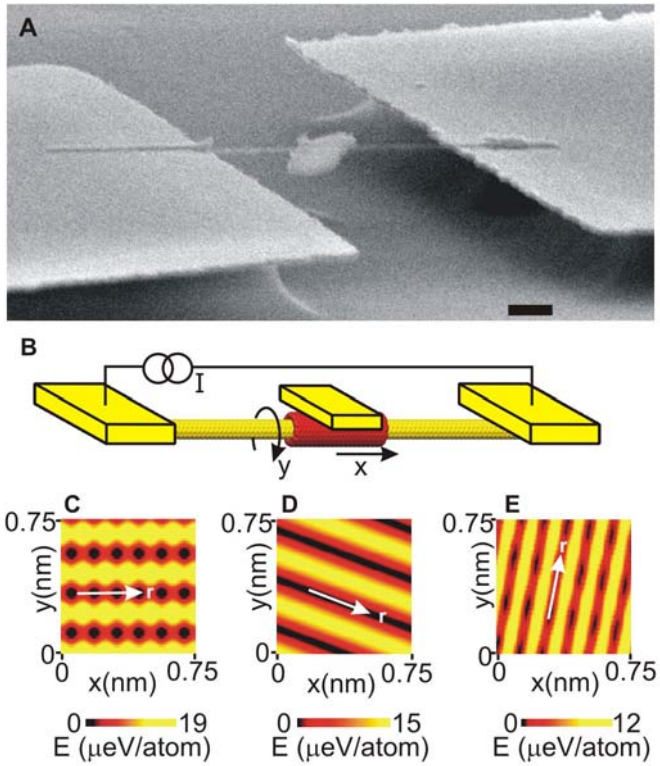

Fig. 1. Experimental setup. (A) Scanning electron microscope (SEM) image of one device. The scale bar is 300 nm. (B) Schematic of the nanotube motor and its degrees of freedom. The outer (red) nanotube moves with respect to the inner (yellow) nanotube. (C, D, E) Shape of the energy barrier for the relative motion between two coaxial nanotubes, namely (5,5)/(10,10), (29,9)/(38,8) and (27,12)/(32,17), respectively. The diameters of the inner tubes are 0.67, 2.7, and 2.7 nm, respectively. The white arrow indicates the easy axis of motion. The motion is modulated by a series of small periodic barriers in C and E, while vanishingly small friction is expected in D.

Fig. 2. Translational motion. Top down SEM images where the gold cargo is moving along the nanotube. The motion is actuated by passing a large electrical current through the nanotubes. Note that the driving mechanism for the motion is not due to electromigration, but comes from the thermal gradient along the nanotubes (induced by the electrical current). The metal plate, which initially had a rectangular shape, melted through Joule heating, and became a ball. The scale bar is 400 nm.

Poly(L-lactic)acid as stimulator of bone growth: Piezo-force microscopy study of the local piezoelectric properties.

N. B. Barroca [a], *A. Wu* [a], *A. L. Daniel-da-Silva* [a], *M. H. Fernandes* [a], *P. M. Vilarinho* [a]
[a] *Department of Ceramics and Glass Engineering, CICECO, University of Aveiro, Aveiro, Portugal*
nbarroca@ua.pt

Poly-L-lactic acid (PLLA) is a biodegradable semi-crystalline polymer, widely investigated in biomedical field because it is also biocompatible and its properties can be tailored to match the properties of living tissues. For instance, PLLA degradability and mechanical performance can be altered by varying the content and the characteristics of the crystalline phase through the processing conditions [1]. More recently, PLLA has attracted attention due to one of its less-known properties: the piezoelectricity, which is also related to the crystalline phase characteristics. When implanted in bone, piezoelectric active PLLA has shown to promote bone growth [2].

As piezoelectricity and poling phenomena have been implicated in physiological mechanisms of bone growth and remodelling [3], there is the need to investigate the piezoelectric properties of PLLA at a local scale. These studies will allow to understand how to manipulate the piezoelectric activity of PLLA in order to control the physiological phenomena that take place at a local scale, such as protein adsorption. Indeed our previous studies, using scanning probe microscopy, clearly indicated the superior affinity of poled PLLA samples to human fibronectin compared to non-poled samples [4].

The present study aims to systematically investigate the local piezoelectric properties of PLLA thin films with different crystallinity degrees using piezoresponse force microscopy. With this purpose, spin-coated PLLA thin films were submitted to different post-melting heat treatments near the glass transition temperature and crystallization temperature (as indicated by DSC) to induce both nucleation and crystallization to obtain different microstructures.

The possibility to manipulate dipoles at micro and nanoscale by the application of a dc field through the tip was demonstrated. Piezoelectric activity was detected in the different films. Different piezoelectric hysteresis curves were measured locally on crystalline (Figure 1) and amorphous regions. The effect of poling on piezoelectric behaviour was also studied and the possible correlation between local and macroscopic properties is presented and discussed.

References:

[1] K. Rezwan, Q. Z. Chen, J. J. Blaker, Aldo Boccaccini, Biomaterials, **27** (2006) 3413-3431
[2] E. Fukada, Jpn. J. Appl. Phys., **37** (1998) 2775-2780
[3] A.A. Marino, R.O. Becker, Nature, **228(5270)** (1970) 473-474
[4] N. Barroca, A.L. Daniel-da-Silva, A.Wu, M.H.V. Fernandes, P.M.Vilarinho, A. Gruverman, Poly (L-lactic) acid for biomedical application - assessment of polarization phenomena and their effect on human protein adsorption by scanning probe microscopy, to be submitted

Figures:

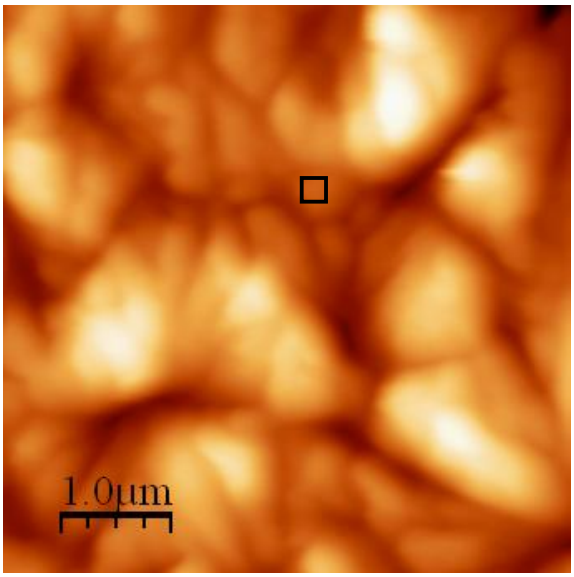

Figure 1a. Morphology of 500 nm x 500 nm area of semi-crystalline PLLA thin film observed with AFM contact mode in air

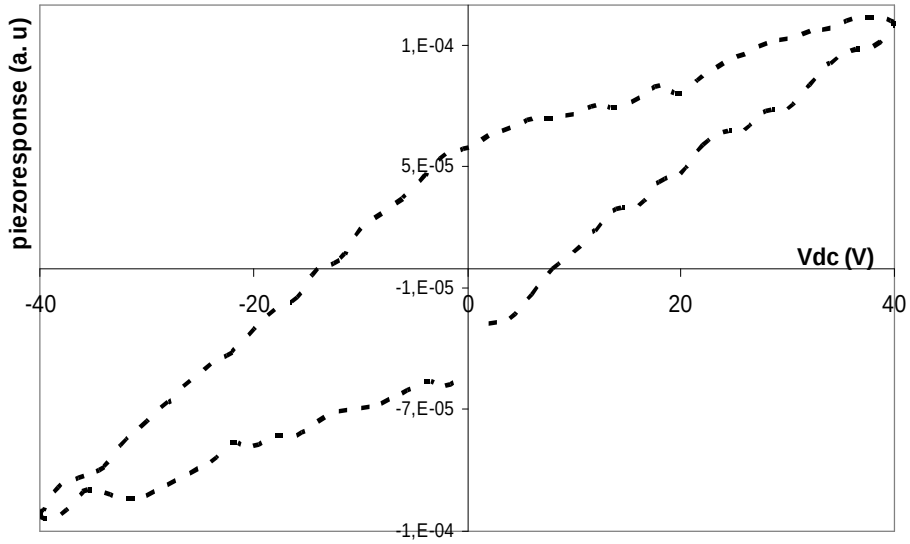

Figure 1b. Piezoelectric hysteresis curve measured on 25 nm x 25 nm area (black square in Figure 1a.) in semi-crystalline PLLA

VO_2-Based Thermochromic Thin Films for Energy Efficient Windows

Carlos Batista, Vasco Teixeira
University of Minho, Department of Physics, Campus de Gualtar, 4710-057 Braga, Portugal
cbatista@fisica.uminho.pt

Abstract

The latest approach on the improvement the energy efficiency of buildings is based on the use of thermochromic coatings on so-called "smart" windows. These coatings possess the ability of changing their optical properties as a consequence of a reversible structural transformation when going through a critical temperature. Vanadium dioxide is an example of a transparent thermochromic material which is a promising candidate for this kind of application. The change on its optical and also electrical properties takes place at 68ºC as a result of a first-order structural transition, known as Mott transition [1], going from a monoclinic to a tetragonal phase on heating. The low temperature semiconducting phase which is transparent to radiation in the visible and infrared wavelength range maximizes the heating due to blackbody radiation, while the metallic high temperature phase blocks the infrared radiation and maintains at the same time the transparency required, in the visible range, to keep an environment of natural light. A transition temperature of 68ºC is too high for this application and must therefore be reduced. Tungsten-doping of VO_2 has demonstrated to decrease the transition temperature in the greatest extent, when compared with other metals, and has therefore been the focus of most of the research [2].

In the current study, VO_2 thin films doped with different W at.% and consequent dissimilar switching temperatures, were successfully deposited onto SiO_2-coated float-glass substrates by reactive direct current (DC) magnetron sputtering. The doping methodology associated with optimized processing conditions allowed the production of W-doped VO_2 films with reduced switching temperatures and maximum transmittances at the visible region ranging 40%. Structural analyses have shown, for undoped films, single phase VO_2(M) films with (002) as the preferred crystal orientation plane. The addition of W favors the crystallization in the (011) direction which becomes dominant above a critical level of dopant concentration. The surface morphology of pure VO_2 films revealed elongated grains oriented within the film plane, and the doped ones have shown an increased tendency to be oriented out of the film plane as well as increased roughness. The relationship between W contents in the film and consequent transition temperature presented a linear behavior.

References:

[1] A. Zylbersztejn and N.F. Mott, Physical Review B 11 (1975) 4383-4395.
[2] I.P. Parkin and T.D. Manning, Journal of Chemical Education 83 (2006) 393-400.

Poster

LOCAL ELECTRIC FIELD INDUCED POLAR STATE IN MANGANITE SINGLE CRYSTALS

I. K. Bdikin, A. L. Kholkin
Department of Ceramics and Glass Engineering & CICECO, University of Aveiro, 3810-193 Aveiro, Portugal
Yu. G. Pogorelov
Departament of Physics, University of Porto, Rua Campo Alegre 687, 4169-007 Porto, Portugal
R. F. Mamin
Zavoisky Physical-Technical Institute, Russian Academy of Science, Kazan, Russia
Contact@E-mail: kholkin@ua.pt

Many materials for sensor and data storage technology use the effects of alignment of atomic moments, either electric or magnetic. However certain materials, called multiferroics, show both effects, resulting in rather intriguing properties. Thus, ferromagnetic order can be controlled by an electric field, or ferroelectric order can be controlled with a magnetic field. This could have a revolutionary effect on sensors and data storage applications, but multiferroics are still poorly understood. Magnetoelectric effect (induction of magnetization by an electric field or of polarization by a magnetic field) is present in several single-phase materials: $BiFeO_3$, $TbMnO_3$, $BiMnO_3$, and in two-phase composite systems, as PZT ($Pb(Zr,Ti)O_3$) or $BaTiO_3$ (piezoelectric) combined with manganites ($La_{1-x}Sr_xMnO_3$ or $La_{1-x}Ca_xMnO_3$) [1,2]. Manganites, primarily known for their colossal magnetoresistance effect, also possess a variety of useful multifunctional properties including high dielectric constant and magnetocapacitance [3]. The $La_{1-x}Sr_xMnO_3$ (LSMO) compound has perovskite structure and competing ferro- and antiferromagnetic phases under low temperatures. At low Sr doping level, the model compound (LSMO) is in insulating state where the localized carriers (polarons) give rise to space charge/magnetization fluctuations and local Jan-Teller effect.

In this work, the local electrical properties of manganites are assessed via several Scanning Probe Microscopy (SPM) techniques including Kelvin Force Microscopy and Piezoresponse Force Microscopy (PFM) [4].

The original state of the samples does not reveal piezoresponse contrast of images (Fig.1a). Weak variations of intensity are correlated with surface sample topography by electrostatic tip-sample interaction. After scanning in the central part of a separated sample area under electric field, as shown in Fig. 1b, the PFM signal appears directly and only in the poling scanning spot. The electric-field-induced contrast was also observed in the Kelvin mode images, confirming a local modification/redistribution of space charges (Fig.2b). Electric field induced polar state in 100 orientated LSMO crystals is shown too. Magnitudes of the effect in 111 and 100 orientated LSMO crystals are similar (Fig.2c).

The found electric-field-induced state is not absolutely stable and eventually disappears with time. But the relaxation time is very long, of ~100 h. After several days, both PFM and Kelvin signals are still present. Using the measured conductivity of these samples, the Maxwell relaxation time is estimated as only $t_r = 5 \cdot 10^{-9}$ s. Thus, the induced charge should disappear under the SPM measurement conditions. Very long relaxation time for the charge state after poling in these experiments may be explained by the occurrence of a polar state in the samples. On the basis that the charge compensating ferroelectric polarization is much more stable than the injected charge itself, the stability of the polar state and charge compensation state are mutually dependent, which defines the actual long relaxation times of these states. We assume that two processes are realized under the voltage in the AFM experiments. The first process is the creation of polar phase. This process may

be promoted by the ordering of Mn^{3+} and Mn^{4+} ions and by the lattice instability in manganite. The second process is the injection of additional charges, changing the balance between Mn^{3+} and Mn^{4+}. In this material, a distortion of LSMO lattice is due to the Jahn-Teller effect which is also sensitive to charge concentration. Effectively, injection of charges that changes the hole concentration results in a local shift of the phase diagram boundary in the system [5].

References:

[1] M. Fiebig, J. Phys. D: Appl. Phys. **38** (2005) R123.
[2] G. Srinivasan, E. T. Rasmussen, B. J. Levin, and R. Hayes**,** Phys. Rev. B **65** (2002) 134402.
[3] T. Kimura et al., Nature (London) **426** (2003) 55.
[4] Scanning Probe Microscopy: Electrical and Electromechanical Phenomena at the Nanoscale, Eds. S. Kalinin, A. Gruverman, Springer, 2006.
[5] J. Hemberger, A. Krimmel, T. Kurz, H.-A. Krug von Nidda, V. Yu. Ivanov, A. A. Mukhin, A. M. Balbashov, and A. Loidl, Phys. Rev. B **66** (2002) 094410.

Figures:

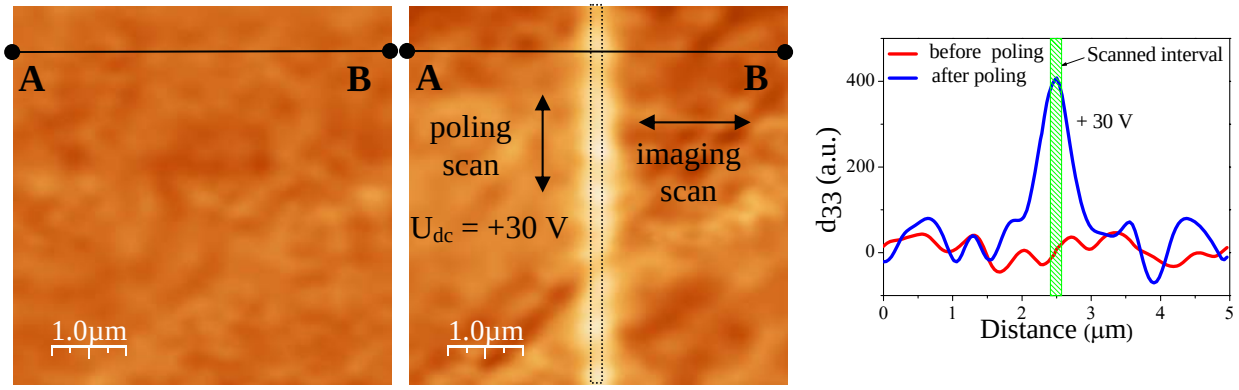

(a) (b) (c)

Fig. 1. PFM images of the electric-field-induced contrast in a 111-oriented LSMO single crystal: (a) before poling; (b) after poling. The lines are written with V_{dc}= +30 V applied to the tip during scanning 10 s (poling area is 100 nm * 5 μm^2). (c) Cross section along the PFM images before and after poling along the AB line.

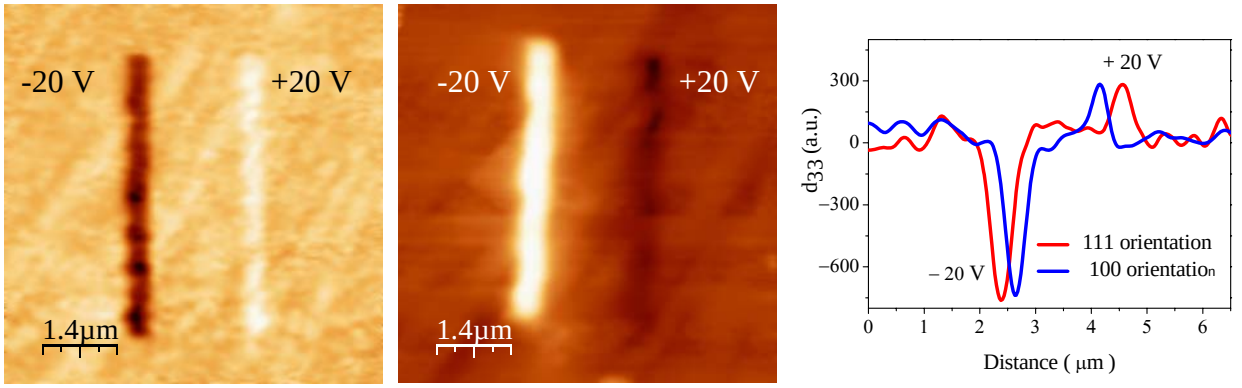

(a) (b) (c)

Fig. 2. SPM images of the electric-field-induced contrast in 111-oriented LSMO single crystal on the same place: (a) piezoresponse image; (b) image of the potential contrast in the Kelvin mode. The lines are written with V= ± 20 V applied to the tip. (c) Cross section along the PFM images after poling in 100-oriented and 111-oriented LSMO single crystals.

BIOTECHNOLOGIES FOR OBTAINING NEW PHARMACEUTICAL FORMULATIONS BASED ON MIXTURES OF TYPE I NON-DENATURED FIBRILLAR COLLAGEN GELS AND EXTRACTS FROM MARINE ALGAE WITH APPLICATIONS IN NANOMEDICINE

RODICA SIRBU*, ANAMARIA BECHIR* ,
MARIS MARIA *, MINODORA LECA, DAN ARTENIE MARIS***

**"Ovidius" University of Constanta, Faculty of Pharmacy, Romania*
*** University of Bucharest Romania*

Diseases of the oro-dental tissues are of great interest in dental medicine. On these lines, the interest shown for the parodontal diseases has increased since it has been scientifically proved that there is a connection between cutaneous-mucous diseases and the paradontopathies, with different degrees of severity, within systemic morbidity: arteriosclerosis, myocardial infarction and cerebral haemorrhages, [1]. Anti-inflammatory ingredients can be used in regenerative therapy for tissues affected by the parodonthal disease; these ingredients are obtained from natural resources such as marine algae, which have proved to have an anti-inflammatory action on some negative gram and positive gram germs. The extracts from marine algae are incorporated in type I non-denatured fibrillar collagen matrixes.

Structural modifications of the marine biomass performed by extraction biotechnological processes, the production of type I fibrillar collagen hydrolysate (de-reticulation) by **lyophilization** techniques **in order to obtain hydrogels and porous matrixes or by free drying in order to obtain membranes and atomization in the production of powders, [2,3]** as well as the actions of the active ingredients at the bio-cellular level are **considered to be nanomaterials** acting at trans-dermal and trans-mucous levels.

Based on certain previous rheological measurements performed with type I non-denatured fibrillar collagen gels [4,5], containing ethyl alcohol with a pH of 3 or not, the concentrations selected for preparing gels with hydro-alcoholic extracts of marine algae were 0.6% for collagen and 5 and 10% for extracts from algae, in mass percentages. We have not used higher concentrations for extracts from algae nor for ethyl alcohol when extracting the components thereof, since ethyl alcohol can cause a decrease in the viscosity of the collagen-based gel, large quantities of it being likely to actually lead to its destruction (dissociation into two phases, one rich in water, the other rich in collagen).

Hydroalcoholic extracts from marine algae have been used as they have been obtained, without being previously diluted or concentrated in order to be brought to the same concentration, which means that the gels which contain prepared algae extracts do not have the same concentration of dry ingredients.

The gels with collagen concentrations of 0.6 and hydroalcoholic extract concentrations of 5%, 10% respectively in mass percentages have been prepared at room temperature for the initial gel with a collagen concentration of 1.64% (g collagen per 100 g of gel) by adding the relevant quantities of distilled water and hydroalcoholic extracts from marine algae while shaking.

In order to state, subsequent to rheological measurements, whether there are interactions between the components of the three hydroalcoholic extracts from algae and Type I

fibrillar collagen, we have prepared gels with the same collagen concentration and which also contain a concentration of 5, 10% respectively, of 70% ethyl alcohol solution, which represents the dispersing medium for the collagen gels which contain extracts (the quantities of ingredients introduced together with the extracts are very small in the final gels and can therefore be neglected), and which have been used in order to perform the relevant comparison.
The collagen gels into which a concentration of 5% of 70% ethyl alcohol solution has been introduced contain a concentration of ethyl alcohol of 3.5% in mass percentages and of 4.03% in volume percentages, and the ones with ethyl alcohol concentration of 10% contain double quantities of ingredients, ethyl alcohol concentration of 7% respectively in mass percentages and 8.06% in volume percentages. Ethyl alcohol is also present in the same mass or volume percentages in the collagen gels which contain the relevant quantities of extracts from algae. Both acid (3) and neutral pH gels have been prepared.
The concentrations of 70% ethyl alcohol solution, of extracts from algae with the same concentration of ethyl alcohol solution respectively, of 0.6% collagen gels with a pH of 3 and their appearance are presented in table 1.

Table 1. Collagen gels without/with prepared extracts from algae,

Alga extract	The extract's concentration, %	The gel's aspect
Without alga extract	0 5% of 70% alcohol solution 10% of 70% alcohol solution	Colourless, clear Colourless, clear Colourless, barely opalescent
CYSTOSEIRA BARBATA	5 10	Opalescent, yellowish green More opalescent, brownish yellow
ULVAE LACTUCA	5 10	Clear, barely green Barely opaque, barely green
CERAMIUM RUBRUM	5 10	Barely opalescent, yellowish green A degree more opalescent, brownish yellow

All gels have been introduced in the refrigerator, at a 4^{o}C temperature, for maturation. They have been shaken from time to time during the first four hours, after which they have been left to rest for 12 hours minimum and then subjected to shearing.

References

[1] Löe H. Oral hygiene in the prevention of caries and periodontal disease. *International Dental Journal*, **50** (3): 129-139,(2000)
[2]J. B. Parks, Biomaterials: Principle and Applications, CRC Press, Boca Raton, (2002).
[3 S. Yunoki, T. Suzuki and M. Takai, J. Biosci. Bioeng. **96**, 575 (2003).
[4] K. S. Weadock, E. J. Miller, I. D. Bellincampi, J. P. Zawadsky and M. G. Duna, J. Biomed. Mater. Res. **29**, 1373 (1995).
[5] S. D. Gorham, N. D. Light, A. M. Diamond, M. J. Williams, A. J. Bailey, T. J. Wess and N. J. Leslie, Int. J. Biol. Macromol. **14**, 129 (1992).

INTERFERO-DIFRACTIVE LINEAR OPTICAL ENCODER WITH NANOMETRIC RESOLUTION

Luis Miguel Sanchez-Brea, Francisco José Torcal-Milla, Eusebio Bernabeu
Universidad Complutense de Madrid,
Departamento de Óptica, Grupo Complutense de Óptica Aplicada,
Facultad de Ciencias Físicas, Ciudad Universitaria s.n., 28040, Madrid, Spain
sanchezbrea@fis.ucm.es

Tomás Morlanes
Aotek S. Coop., Bº. San Andrés, 19,
20500, Mondragón, Guipúzcoa, Spain

In this work we develop a device for determining the linear displacement between a linear grating and a scanning head. Then, the standard technique used for generating the optical signals is double grating imaging: Moiré, Talbot or Generalized grating imaging configurations. The accuracy and resolution of optical encoders improves when the period of the diffraction gratings decreases. When the period of the grating is smaller than 10 um, double grating configuration is not valid since the mechanical tolerances are too restrictive. In our case, we use a diffraction grating of 4 um and then the Talbot distance is about 30 um for visible light.

As a consequence, we have used an interfero-diffractive configuration where one diffraction grating is used. The light coming from a laser-diode impinges the diffraction grating. The diffracted orders are redirected using a retro-reflector and then they interfere. As a consequence, an optical sinusoidal signal is obtained. This optical signal varies with the relative linear displacement between the scanning head and the diffraction grating. The displacement of the optical signal is 4 times the real displacement. Nanometric resolution is obtained using additional interpolation electronics (+50). An analysis of the technique and an experimental verification are performed.

References:

[1] K. Patorski, “The self-imaging phenomenon and its applications”, in E. Wolf (Ed.), *Progress in Optics*, Vol. **27**, North Holland, Amsterdam, 1989.

[2] K. Patorski, “Moirè Metrology”, Pergamon, New York, 1998.

[3] E.G. Loewen, E. Popov, *Diffraction gratings and applications* (Marcel Dekker, New York, 1997)

[4] C. Palmer, *Diffraction Grating Handbook* (Richardson Grating Laboratory, New York, 2000)

[5] D. Crespo, J. Alonso, T. Morlanes, E. Bernabeu, "Optical encoder based on the Lau effect", Opt. Eng., **39**, (2000), 817-824.

[6] G. J. Swanson and E. N. Leith, "Analysis of the Lau effect and generalized grating imaging" J. Soc. Opt. Am. A, **2** (1985) 789-793.

[7] D. Crespo, J. Alonso, E. Bernabeu "Generalized grating imaging using an extended monochromatic light source", J. Soc. Opt. Am. A, **17** (2000) 1231-1240.

[8] D. Crespo, J. Alonso, E. Bernabeu "Experimental measurements of generalized grating images", Appl. Opt., **41** (2002) 1223-1228.

[9] F.J. Torcal-Milla, L.M. SanchezBrea, E. Bernabeu "Talbot effect with rough reflection gratings", Appl. Opt., 46 (2007) 3668-3673.

[10] M. Dobosz "Application of a focused laser beam in a grating interferometer for high-resolution displacement measurements", Opt. Eng., 38 (1999) 958-967

[11] C.K. Lee et al. "Design and construction of linear laser encoders that possess high tolerance of mechanical runout" Appl. Opt. 43 (2004) 5754-5762

[12] J.D. Lin and H.B. Kuo "Development of a new optical scale system by the diffractive phase interference method" Meas. Sci. Technol. **6** (1995) 293-296

Poster

NANOSTRUCTURAL SEMICONDUCTING PHOTOCATALYSTS FOR MEDICAL APPLICATIONS

I. Bernacka-Wójcik[1, 2], P. Łabuz[1], G. Stochel[1] , W. Macyk[1]
1 - Faculty of Chemistry, Jagiellonian University, Ingardena 3, 30-060 Krakow, Poland
2 - CEMOP/UNINOVA, Campus de Caparica,2829-516 Caparica, Portugal
iwonabernacka@gmail.com

The photocatalysis, according to IUPAC, is a catalytic reaction involving light absorption by a catalyst or by a substrate. This work considers a special type of the photocatalysis – photosensitization. The photosensitization is the process by which an alteration occurs in one molecular entity as a result of initial light absorption by another molecular entity.

Ultrabandgap illumination of the semiconducting photocatalyst can produce the reactive oxygen species (ROS, for example $OH^{\bullet}$, $O_2^{\bullet-}$, $^1O_2$), which are incredibly powerful oxidants [1]. ROS can cause a lot of damages in an organism, however by a proper targeting of their toxic effect can be applied in many fields, for example in inactivation or killing of cancer cells in the photodynamic therapy (PDT). Unfortunately, the ROS attack is not specific – beside cancer cells also a number of healthy cells is destructed. A possible solution of this problem is based on the connection of the photocatalyst particles with biomolecules (e.g. monoclonal antibodies), which enable a molecular recognition of the cancer cells [2].

The main goal of this project was a modification of heterogeneous photocatalysts (namely TiO_2) in order to enable its connection with antibodies, retaining the photocatalytic activity. TiO_2 particles could be connected with antibodies through the avidin-biotin bridge, because biotin can be easily linked to antibodies, while avidin – a positively charged protein – can be bound electrostatically to the negatively charged oxide surface. A similar methodology was successfully applied for CdS quantum dots [3]. In order to build the antibody-biotin-avidin-TiO_2 system the surface of TiO_2 has to be negatively charged. Moreover, the dimensions of the photocatalyst particles have to be comparable with the dimension of the antibodies (a few nanometers) in order to retain molecular recognition properties of the applied antibody.

The TiO_2 nanoparticles (q-TiO_2) synthesized by hydrolysis of titanium isopropoxide [4] were modified with selected organic molecules. The determined band gap energy of the obtained TiO_2 nanoparticles was close to 3.45 eV, *i.e.* the value by 0.3 eV higher than the band gap energy of microcrystalline TiO_2. This increase confirms the nanometric dimension of obtained TiO_2 particles.

Stable sols were obtained in the case of 4-amino-2-hydroxybenzoic acid, however the surface charge was positive in this case.

The photocatalytic properties were tested by monitoring the photodegradation of the standard compounds – methylene blue and cyanuric acid. Photodegradation of methylene blue requires hydroxyl radicals which are generated in the processes of charge transfer, while the photodegradation of cyanuric acid undergoes in the presence of singlet oxygen which is formed in the energy transfer processes.

The results show that unmodified q-TiO_2 exhibits a significant photocatalytic activity in the charge transfer processes. Only q-TiO_2 modified with 4-amino-2-hydroxybenzoic acid exhibits a significant photoactivity in analogous processes. Photodegradation of the cyanuric acid was not observed upon ultraviolet light illumination neither in the presence of unmodified nor modified q-TiO_2. These results reflect a negligible efficiency of the energy transfer processes.

References:

[1] Jańczyk, A.; Krakowska, E.; Stochel, G.; Macyk, W., J. Am. Chem. Soc., **2006**, *128*, 15574-15575.
[2] Barber, P.; Barr, H.; George, J.; Krasner, N.; Morris, A., I.; Sutedja, T., G., Clinical Oncology, **2002**, *14*, 110-116.
[3] Goldman, E. R.; Balighian, E. D., Mattoussi, H.; Kuno, M.; Mauro, J. M.; Phan, T. T.; Anderson, G. P., J. Am. Chem. Soc., **2002**, *124*, 6378-6382.
[4] Weng, Y.-X.; Wang, Y.-Q.; Absury, J. B.; Ghosh, H. N.; Lian, T., J. Phys. Chem. B, **2000**, *104*, 93-104.

Figures:

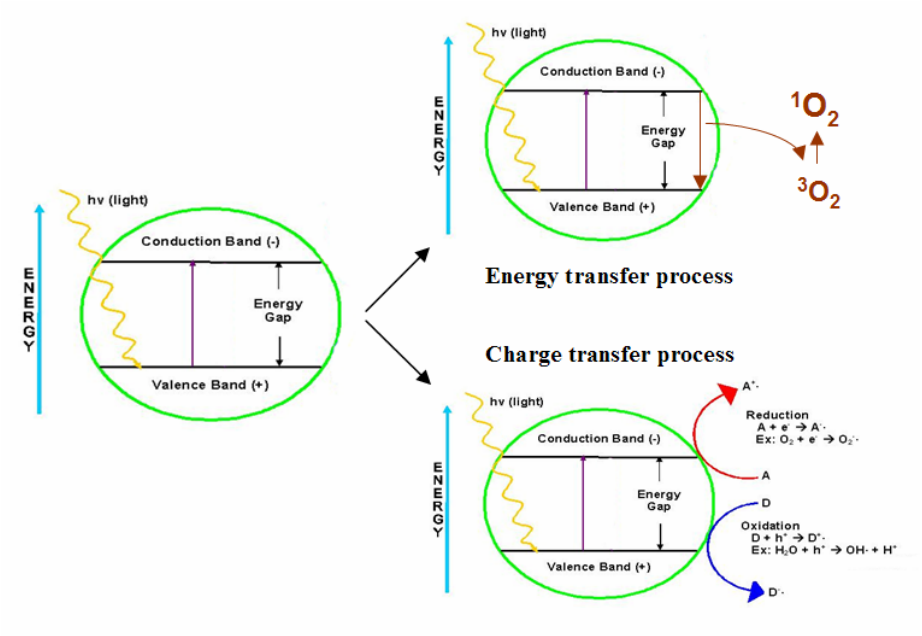

Fig. 1 Mechanism of TiO_2 photocatalysis.

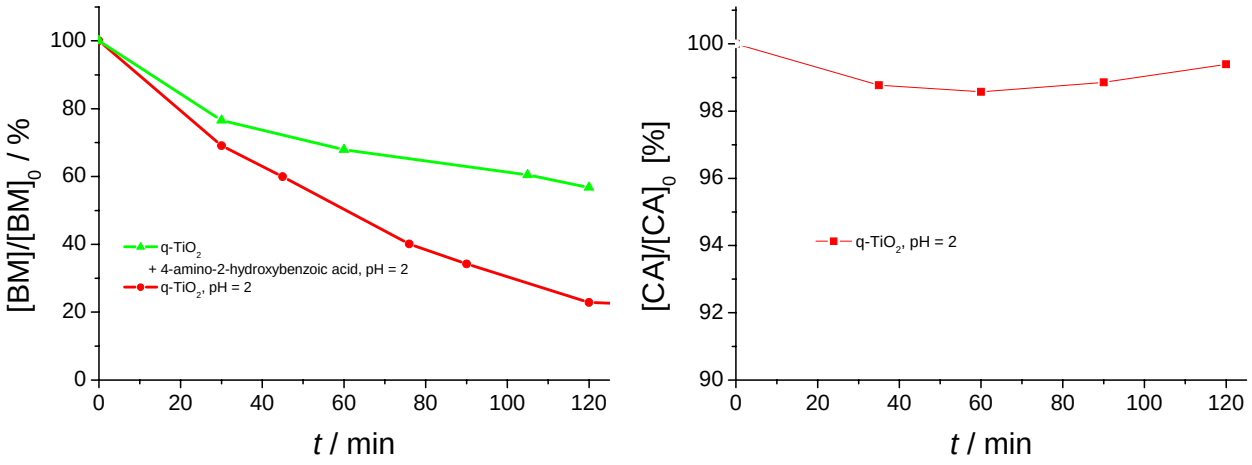

a) b)

Fig. 2 Photocatalytic properties of obtained materials in the:
a) charge transfer processes; b) energy transfer processes.

GOLD NANOPARTICLES USED IN IMPEDIMETRIC GENOSENSING OF DOUBLE-TAGGED PCR SAMPLES

A. Bonanni, M.I. Pividori, S. Alegret, M. del Valle

Grupo de Sensores y Biosensores, Departamento de Quimica, Universitat Autònoma de Barcelona, Edifici Cn, 08193 Bellaterra, Barcelona, SPAIN

alessandra.bonanni@uab.cat

Double stranded DNA sequences coming from polymerase chain reaction (PCR) amplification of real samples were detected by the use of an electrochemical impedimetric genosensor previously developed in our laboratories [1]. Electrochemical Impedance Spectroscopy is a rapid developing technique for the transduction of biosensing events at the surface of an electrode [2]. Transduction principle exploits changes in interfacial resistance of charge transfer after modification of the genosensing transducer with DNA [3]. Many different protocols have been recently used in DNA detection by this technique. Some of them employ different types of nanoparticles as a way to increase the sensitivity of the method [4-6].

In the present work, an avidin bulk-modified graphite-epoxy biocomposite (Av-GEB) was employed to immobilize –onto the electrode surface– the double-tagged DNA, modified in each end with biotin and digoxigenin, respectively. Impedance spectra were recorded to detect the change in interfacial charge transfer resistance (R_{ct}), experimented by the redox marker ferri/ferrocyanide at the applied potential. A further step in the genosensing procedure was the amplification of impedimetric signal by the use of gold nanoparticles modified with Anti-Mouse IgG (whole molecule)–Gold antibody. The latter were immobilized to the digoxigenin-modified end of the amplicon by a monoclonal IgG1kappa anti-Digoxigenin antibody from mouse.

Results obtained by the comparison of R_{ct} values after each further modification of the electrode surface show a significant difference in the impedimetric signal variation between experiments and negative controls. Moreover, this difference results thoroughly amplified thanks to the procedure used for signal enhancement (see results shown in Figure 1).

The attained sensitivity plus the improved reproducibility of results confirm the validity of this method based on a universal affinity biocomposite platform coupled with the use of gold nanoparticles for signal amplification. The described strategy was used for the rapid and sensitive detection of PCR amplified samples of Salmonella spp, the most important pathogen affecting food safety.

References:

[1] A. Bonanni, M.I. Pividori, M. del Valle, Anal. Bioanal.Chem, **389** (2007) 851.
[2] C. Berggren, P. Stålhandske, J. Brundell, G. Johansson, Electroanal. **11** (1999) 156.
[3] E. Katz, I. Willner, Electroanal. **15** (2003) 927.
[4] A. Bonanni, M. J. Esplandiu, M. del Valle, Electrochim. Acta (2007), *in press*.
[5] Y. Xu, H. Cai, , P.G. He, Y.Z. Fang, Electroanal. **16** (2004) 150.
[6] J. Wang, Anal Chim Acta, **500** (2003) 247.

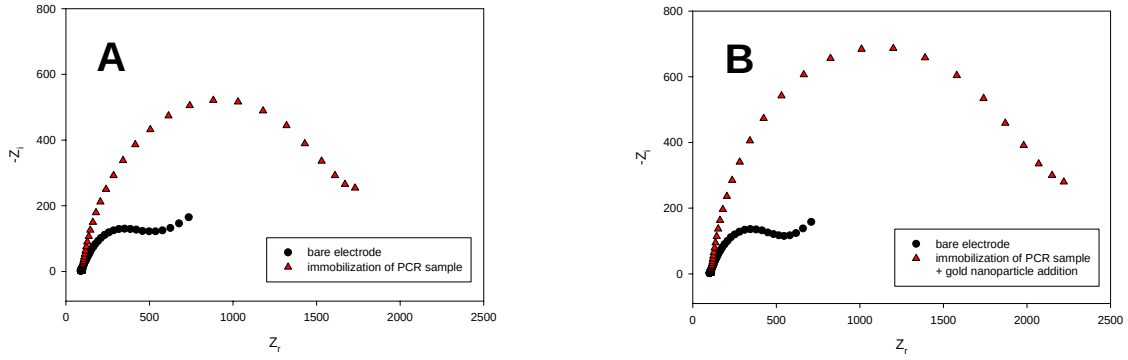

Figure 1: Comparison between Nyquist plots obtained in: A, experiment without signal amplification. B, experiment with signal amplification.

REACTIVITY OF PERIODICALLY RIPPLED GRAPHENE GROWN ON RU(0001)

B. Borca[1], F. Calleja[1], J.J. Hinarejos[1], A.L. Vázquez de Parga[1] and R. Miranda[1,2]

[1] Dep. Física de la Materia Condensada, Universidad Autónoma de Madrid, Cantoblanco 28049, Madrid, Spain

[2] Insituto Madrileño de Estudios Avanzados en Nanociencia (IMDEA Nanociencia), Cantoblanco 28049, Madrid, Spain

bogdana.borca@uam.es

The recent discovery of an experimental method to prepare graphene [1] enforced the research field, stimulating new discoveries [2-4] and potential application [5-7] based principally in the exceptional electronic properties [8] of the graphene layer.

We present here the study of the growth of epitaxial graphene islands and complete monolayers on a Ru(0001) substrate and its reactivity towards oxygen and air. The graphene is prepared by thermal decomposition at 1000 K of ethylene molecules pre-adsorbed at 300 K on a Ru(0001) surface on an ultra high vacuum chamber. The difference in lattice parameter between graphene and ruthenium induce a rippled structure in grapehene with a triangular periodicity of 2.4 nm. The periodic ripples produce spatial charge redistribution in the graphene. This have been measured with spatially resolved dI/dV scanning tunnelling maps and confirmed with a theoretical model [9].

The growth method described here can be used to produce nanometer wide islands on terraces or a complete monolayer of graphene. The islands are truncated hexagons with straight edges of a single structural type (fig1a). The apparent step height of the island in these imaging conditions is 0.15 nm (from the Ru surface to the lower part of the ripples) showing that the graphene layer is indeed only one monolayer. The relative orientation of the graphene layer with respect to the underlying Ru lattice can be determined by resolving simultaneously both atomic lattices. A complete monolayer can be produce by repetitive procedures of thermal decomposition. The monoatomic steps and dislocations of the substrate are faithfully reproduced by the epitaxial graphene, but there are also upper parts of the ripples that are weaker or even missing completely.

In order to investigate the reactivity of graphene we expose graphene islands grown on Ru(0001) to a partial pressure of oxygen and following the evolution of the surface by STM in real time. It is well known that exposure of clean Ru(0001) surface to partial pressures of oxygen lead to the formation of a 2x2 superstructure of oxygen atoms on the Ru(0001) surface. For a exposure during 3 minutes to a pressure of $5x10^{-8}$ Torr the 2x2 oxygen superstructure is already form [10] but the graphene structure, even the borders of the islands, remain intact as can be seen in the fig1b. There is no change in this behaviour upon increasing the oxygen partial pressure or the exposure time. A similar study was performed by exposure to air. STM images were recorded before and after exposing the sample during 12 hours to 1 atmosphere of air. The surface areas not covered by the graphene islands present a dramatic change, before the exposure to air the surface was flat and atomically clean and after the exposure the ruthenium surface is completely covered by irregular bumps due to contamination. On the contrary the graphene islands presented on the surface did not change after the air exposure. In the case of a complete graphene monolayer the exposure to oxygen or to air does not affect or destroy the rippled structure of the graphene monolayer.

References:

[1] K.S. Novoselov *et al.,* Science **306** (2004) 666
[2] K.S. Novoselov *et al.,* Nature **438** (2005) 197
[3] Y. Zhang *et al*., Nature **438** (2005) 201
[4] T. Nikolaos *et al*., Nature **448** (2007) 571
[5] J.S. Bunch *et al.,* Science **315** (2007) 490
[6] J.R. Williams *et al.,* Science **317** (2007) 638
[7] F. Schedin et al., Nature **6** (2007) 652
[8] A.K. Geim and K.S. Novoselov, Nature Mater. **6**, 183 (2007)
[9] A. L. Vázquez de Parga *et al.*, Phys Rev. Lett. **100** (2008) 056807
[10] F. Calleja et al.,. Phys. Rev. Lett. **92** (2004) 206101

Figures1: 18 nm x 18 nm STM images showing the edge of a graphene nanoisland on Ru(0001), taken in the constant current mode with a bias voltage of -0.9V and tunnel current of 0.1 nA, before (a) and after 4 minutes of exposure to a partial pressure of $5x10^{-8}$Torr of oxygen (b)

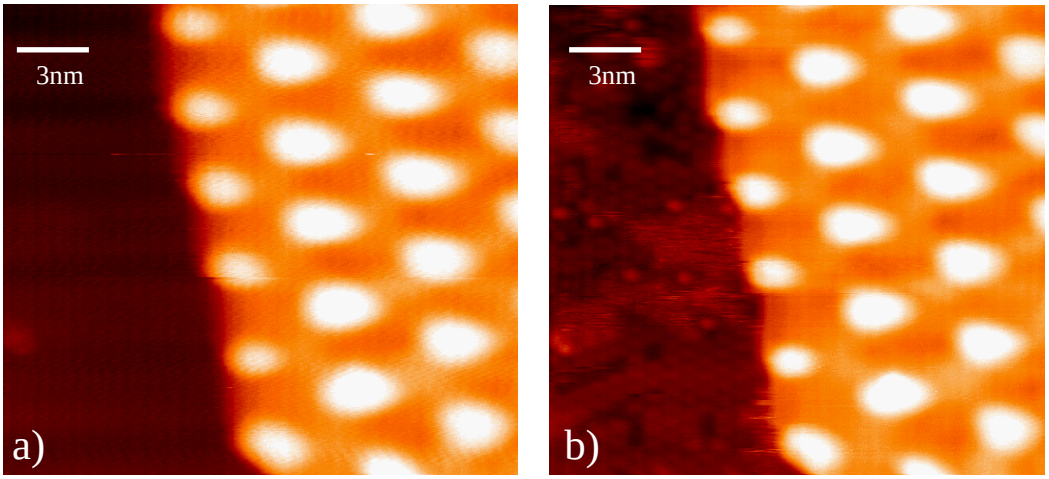

Poster

HOW DOES PENTAGONAL MOLECULES SELF-ASSEMBLE ON A SIX-FOLD SYMMETRY SURFACE? THE CASE OF PENTA-TERT-BUTYL-CORANNULENE MOLECULE ON CU(111)

E. Niemi, O. Guillermet, S. Nagarajan, D. Martrou,
A. Gourdon, S. Gauthier and X. Bouju

CEMES - CNRS, 29, rue Jeanne Marvig, 31055 Toulouse cedex, FRANCE

bouju@cemes.fr

Among point group symmetries, five-fold rotational symmetry plays a special role because of its incompatibility with translational symmetry. Our focus is on tiling of penta-tert-butyl-corannulene molecules (PTBC, $C_{40}H_{50}$) on a hexagonal Cu(111) surface. Corannulene buckybowl is the smallest separable fullerene C_{60} fragment, and in the study it is functionalized with five tert-butyl legs in order to enhance the five-fold symmetrical properties.

We have investigated the deposition of PTBC submonolayer on Cu(111) surface by means of low temperature STM and adsorption simulations. In these experiments, annealing at 100°C for one hour leads to the formation of two coexisting island structures. The first ressembles a slightly disordered hexagonal phase, while the second one forms rosette structures consisting of units of seven molecules.

The adsorption simulations were performed with ASED+ approach. In the simulations for few molecules, PTBC molecules tend to form rigid dimer and trimer structures, which adapt to the hexagonal surface symmetry. The interplay between the adsorption of one molecule and the interaction between the tertbutyl legs leads to the formation of observed rosette superstructure.

Figures:

PTBC molecules on Cu(111). Top, STM image presents the observed rosette superstructure, and, bottom, the optimized adsorption geometry of six trimers PTBC molecules adapts to the hexagonal surface symmetry.

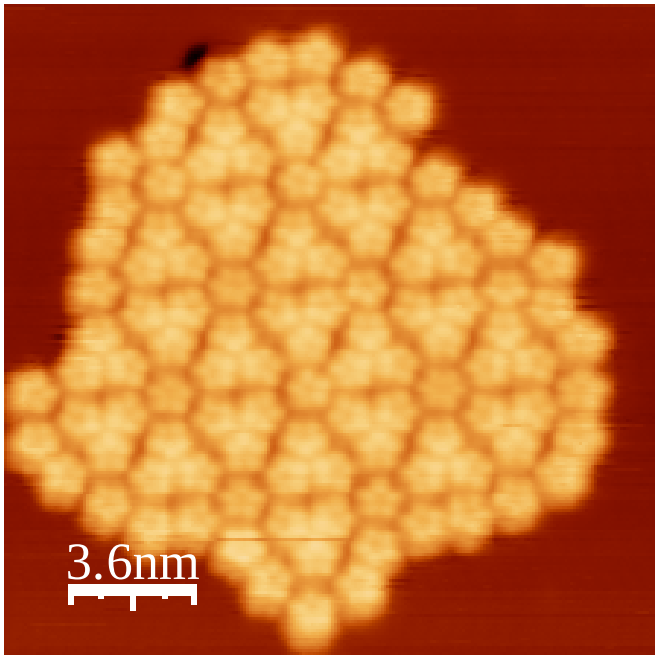

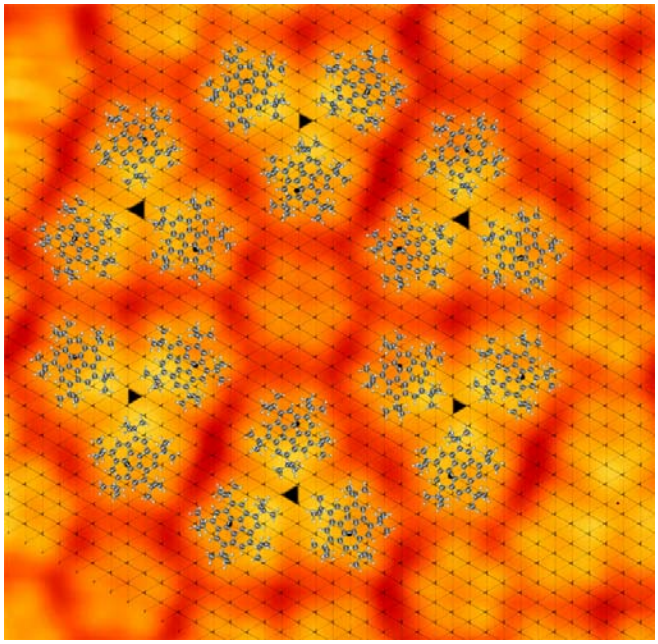

The Role of Porous Materials in the Efficient Storage of Hydrogen

Ernesto Brunet, Carlos Cerro, Olga Juanes and Juan Carlos Rodriguez-Ubis
Department of Organic Chemistry, Faculty of Sciences C-I-207, Universidad Autónoma de Madrid, 28049-Madrid (Spain)
ernesto.brunet@uam.es

Hydrogen is a very appealing energy vector: the release of its energy does not involve the noxious carbon dioxide. Yet, it is becoming a well known fact by our society that two problems must be solved if hydrogen is to be efficient and safely used as the clean energy carrier of the future: *i*) its environmental-friendly production and *ii*) its safe storage and transportation. Although there are already many reasonably useful technical approaches, neither of the two problems is nowadays at a level of resolution which would make the use of hydrogen routinely possible. Besides, the technical solutions to these problems must be quite robust in order to make a smooth transition to the "hydrogen culture" from the actual fossil-fuel civilization, whose economic moguls are far too powerful to be convincingly counterfeited. Therefore, a lot of research is being performed and even new institutions are being created to accomplish the aforementioned double task. Concerning the second one, hydrogen storage (**HS**) may be attained by at least four main methods: *i*) in high-pressure cylinders, *ii*) as a liquid in cryogenic tanks, *iii*) in ionic or covalent compounds (chemisorption), and *iv*) by *physisorption* in porous matrices.[1] This communication will give a critical quick view of the visible state-of-the art of the latter method (*physisorption*) and report our approach and progress in the use of porous organic-inorganic solids based in Al and Zr and various phosphonates.

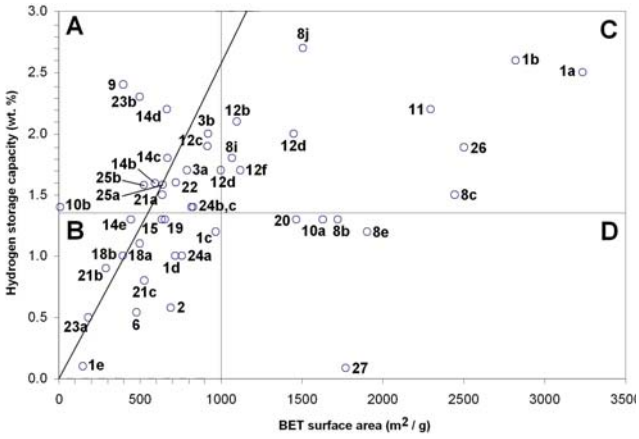

Figure 1

A thorough revision of the literature (Figure 1) shows that the materials with very large specific surface areas (the record is well above 3000 m^2/g) are not suitable for efficient HS at room temperature and low pressures, as common sense would have been anticipated. The free energy of interaction among the hydrogen molecules and the scarce matter of these systems is very low similarly as it is in an empty cylinder. Therefore, to increase that interaction energy, closer contact H_2-material and thus much smaller pores are needed. It is now considered that a material bearing micropores or even ultramicropores would be more efficient for HS.[2] Many reported materials fall within this category. However, the average HS capacity (A and B in Figure 1) is around 2 wt% (77K and 1 atm) and a barrier of 3-4 wt% appears to be by far insurmountable. The average enthalpy of interaction H_2-material is around 6-7 KJ/mol. It seems clear that higher enthalpies are needed (15-20 KJ/mol) to achive HS at room temperature and atmospheric pressure. It should be noted that a record enthalpy of interaction (17.5 KJ/mol) was reported in faujasite-type (Mg,Na)-Y zeolite[3] but, unfortunately, the HS was low due to a strong entropic compensation. The existence of ions, specially Li^+, and/or the presence of metals with open coordination sites in microporous organic-inorganic scaffolds are considered quite favourable features to increase HS.[4] Also, the presence of aromatic moieties in these scaffolds, probably with the idea of building kin

structures to superactivated carbon, graphenes and carbon nanotubes, is also a coveted architectural characteristic.

We are investigating the possibilities that organic-inorganic scaffolds based in phosphonates and Al and Zr have in this field. Although our preliminary results have been only quite modest,[5] we believe that we have a set-up of conceptual and material tools,[6] similar to that reigning organic chemistry, which could lead to the design of an endless number of structures and interesting results. For instance, the use of $Al_2(HPO_3)_x$ $(C_{12}H_8P_2O_6)_{1.5-x/2}$ allows the easy control of the HPO_3/diphenyl-phosphonate ($C_{12}H_8P_2O_6$) ratio. The resulting materials displayed a good correlation between wt% HS and the HPO_3 content (UAM-150 $\rightarrow$ 152: *cf.* Figure 2), probably due to the increasing internal area caused by the increment of latter.[7]

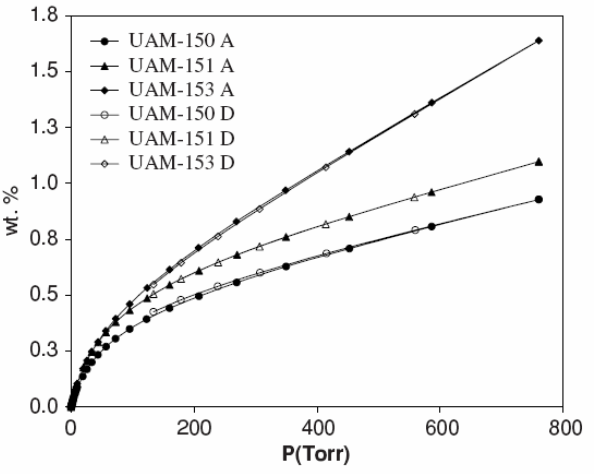

Figure 2

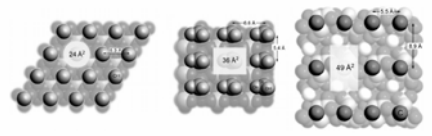

Figure 3

The Zr derivatives, in which we have a larger experience, seem to be even much more flexible. Three phases (α, γ and λ; Figure 3) of quite different structures are known for Zr phosphates which easily allow the inclusion of a variety of species, comprising various organic components (carboxylic acids, amines, phosphonates, etc), various phosphorous acids and metal ions. Preliminary results in the building of these structures with the phosphonates of Scheme 1 will be reported in this communication.

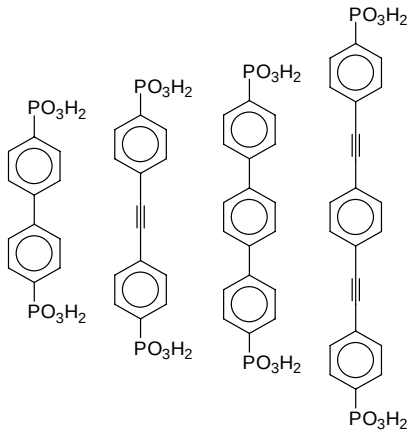

Scheme 1

References

[1] See for example: Zuettel, A. *Naturwissenschaften* **2004**, *91*, 157-172.

[2] Bhatia, S. K.; Myers, A. L**.** *Langmuir* **2006**, *22*, 1688-1700.

[3] Turnés, G.; Llop, M. R.; Otero, C. *J. Mater. Chem.*, **2006**, *16*, 2884–2885.

[4] Sun, Q.; Jena, P.; Wang, Q.; Marquez, M. J. Amer. Chem. Soc. **2006**, *128*, 9741-9745.

[5] Brunet, E.; Alhendawi, H. M. H.; Cerro, C.; de la Mata, M.J.; Juanes, O.; Rodríguez-Ubis, J.C. *Angew. Chem. Int. Ed.* **2006**, *45*, 6918-6920.

[6] Brunet, E.; de la Mata, M.J.; Alhendawi, H. M. H.; Cerro, C.; Alonso, M.; Juanes, O.; Rodríguez-Ubis, J.C. *Chem. Mater*. **2005**, *17*, 1424-1433.

[7] Brunet, E.; Cerro, C.; Juanes, O.; Rodríguez-Ubis, J.C.; Clearfield, A. *J. Mater Sci.* **2008**, *43*, 1155-1158

Poster

HOW WELL ALIGNED ARE THE MAGNETIC ANISOTROPY AXES IN CRYSTALS OF MN_{12} MOLECULAR NANOMAGNETS? AN ANGLE-DEPENDENT AC SUSCEPTIBILITY STUDY

E. Burzuri[a], C. Carbonera[a], F. Luis[a], D. Ruiz-Molina[b], C. Lampropoulos[c], and G. Christou[c]
[a]Instituto de Ciencia de Materiales de Aragón, CSIC-Universidad de Zaragoza, 50009 Zaragoza, Spain

[b]Centro de Investigación en Nanociencia y Nanotecnología (ICN-CSIC) , Campus UAB-Edifici CM7, 08193 Bellaterra, Spain.

[c]Department of Chemistry, University of Florida,Gainesville FL32606, USA.

fluis@unizar.es

Molecular clusters like Mn_{12} and Fe_8 are seen as the lowest limit of miniaturization of magnetic nanoparticles. Indeed, these clusters have a large ground-state spin (S = 10 in Mn_{12}) and they show magnetic hysteresis below liquid Helium temperatures, much as larger nanoparticles do [1]. The hysteresis phenomenon is a property of the isolated molecule (it is preserved in solution). It is caused by the large magnetic anisotropy energy barriers that separate spin-up and spin-down states of the whole molecule. In contrast to other nanostructured magnetic materials, single molecule magnets (SMM) are monodisperse and tend to form crystals in which the magnetic anisotropy axes are very well aligned. They offer then the possibility of investigating the Physics of *individual* molecules with conventional experimental techniques. These studies reveal the existence of quantum phenomena, like quantum tunnelling [2], which are typical of the atomic world.

Despite the intense research activity devoted to investigate these phenomena, the origin of quantum tunnelling in Mn_{12} and other SMM remains obscure. In recent years, it has been suggested that the *off-diagonal* energy terms that induce quantum spin tunnelling are caused by small distortions of the molecular core from its perfect structure [3]. In some compounds, like Mn_{12} acetate, the origin of these distortions has been associated with an intrinsic disorder in the position of solvent molecules [4]. The disorder would then tend to tilt the anisotropy axes of the molecules from their perfect alignment.

In the present contribution, we report a careful study of the degree of alignment of the magnetic anisotropy axes in crystals of Mn_{12} SMM. For this, we have made use of the extreme sensitivity that the linear susceptibility has on the angle that the applied ac magnetic field makes with the anisotropy axis. We have measured the frequency-dependent linear susceptibility (see Fig. 1) of high-quality single crystals of two Mn_{12} derivatives: Mn_{12} acetate and Mn_{12}-tBu. In the latter, the position of solvent molecules is extremely well ordered [5], which therefore makes for an interesting comparison with the acetate derivative. By adequately selecting the temperature, we have also been able to separately estimate the degree of orientation for the so-called “fast-relaxing” Mn_{12} species, a fraction of the SMM in the crystal that show faster spin tunnelling than the standard clusters.

Our results (see Figs 1 and 2) show: a) that the tunnelling rate is faster for the better ordered Mn12-tBu compound, and b) that the angular variation of is very similar in the two compounds investigated. The susceptibility data are in fact compatible with a perfect alignment of the anisotropy axes of the two molecular species within each crystal, with a maximum possible misalignment smaller than 3 degrees. These results therefore question the importance of solvent disorder in determining the tunnelling rates of Mn_{12} molecular nanomagnets.

References:

[1] R. Sessoli, D. Gatteschi, A. Caneschi and M. A. Novak, Nature, **365** (1993) 141; R. Sessoli, H. -K. Tsai, A. R. Schake, S. Wang, J. B. Vincent, K. Folting, D. Gatteschi, G. Christou and D. N. Hendrickson, J. Am. Chem. Soc. **115** (1993) 1804.

[2] J. R. Friedman, M. P. Sarachik, J. Tejada, and R. Ziolo, Phys. Rev. Lett. **76**, 3830 (1996); J. M. Hernández, X. X. Zhang, F. Luis, J. Bartolomé, J. Tejada, and R. Ziolo, Europhys. Lett. **35**, 301 (1996); L. Thomas, F. Lionti, R. Ballou, D. Gatteschi, R. Sessoli, and B. Barbara, Nature (London) **383**, 145 (1996).

[3] E. M. Chudnovsky and D. A. Garanin, Phys. Rev. Lett. **87**, 187203 (2001).

[4] A. Cornia, R. Sessoli, L. Sorace, D. Gatteschi, A. L. Barra, C. Daiguebonne, Phys. Rev. Lett. **89**, 257201 (2002).

[5] W. Wernsdorfer, M. Muguresc u, and G. Christou, Phys. Rev. Lett. **96**, 057208 (2006).

Figures:

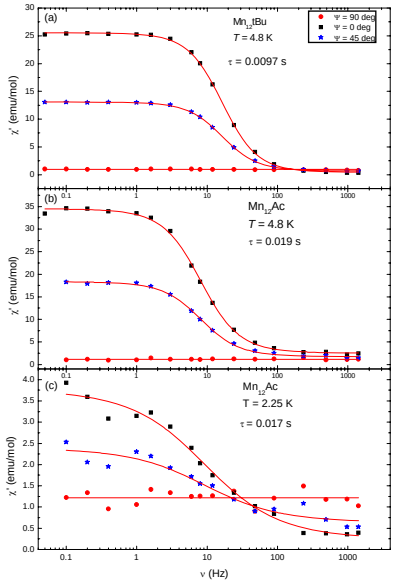

Figure 1: Frequency-dependent ac susceptibility of a single crystals of Mn_{12}-tBu (a) and Mn_{12} acetate (b and c). Solid lines are fits to a Cole-Cole function from which the tunneling time τ and the susceptibility drop $\Delta\chi$ between the low and high frequency limits are estimated.

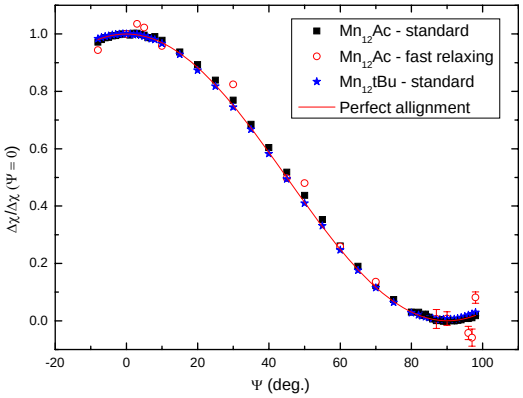

Figure 2: Angular dependence of $\Delta\chi$ (normalized by its value at $\Psi = 0$) for the slow and fast relaxing species in the two Mn_{12} derivatives investigated. Solid lines represent the predictions for different degrees of misalignment in the relative orientations of the magnetic anisotropy axes.

COMPOSITE NANO-BIOMATERIALS BASED ON POLYVINYLIDENE FLUORIDE COPOLYMERS

Vladimir Bystrov[1], Natalia Bystrova[2,3], Ekaterina Paramonova[2], Herbert Kliem[4], Sergei Yudin[5], Vladimir Fridkin[5], Dmitry Kiselev[1], Igor Bdikin[1], M. Machado[6], I. Delgadillo[6], and Andrei Kholkin[2]

[1]*DECV & CICECO, University of Aveiro, Aveiro, Portugal*

[2] *Institute of Mathematical Problems of Biology, RAS, Pushchino, Russia*

[3]*Institute of Theoretical and Experimental Biophysics, RAS, Pushchino, Russia*

[4]*Saarland University, Institute of Electrical Engineering Physics, Saarbruecken, Germany*

[5] *Institute of Crystallography RAS, Moscow, Russia*

[6]*Dept. of Chemistry, University of Aveiro, Aveiro, Portugal*

E-mail: bystrov@ua.pt

Development of the composite nano-biomaterials is very much needed for nanobioelectronics, nanomedicine and other nanobiotechnological applications. Polymer ferroelectrics, such as polyvinylidene fluoride (PVDF) and its copolymers prepared in the form of ultrathin films by Langmuir-Blodgett (LB) technique are suitable objects for these applications owing to their unique physical properties (high polarization and dielectric constant, low acoustic impedance) and compatibility with many organic and biomolecules. It has been recently shown [1, 2] that the nanoscale polarization patterning of these films opens up new opportunities for self-assembly of organic and biomoilecules on the polarized surface. Thus the interaction of polarized patterns with bioactive materials (such as lipids and proteins, human tissues) is of primary importance.

In this work, the PVDF-based composites are studied to understand the interaction between the PVDF chains, layers and adhered biomolecules. Lipid molecules were used as a model for PVDF-based nanocomposites. First, the computational modelling of the PVDF-lipid interaction was done using the HyperChem 7.52 program. Second, the Atomic Force Microcopy (AFM) and Piezoresponse Force microscopy (PFM) were used for experimental studies of this interaction. The results show that the composite nanostructures lead to the modification of PVDF surface charges (changes in dipole moment) and the deformation of adhered lipid molecule to incorporate the polarized PVDF layer. The structure-property relationships of such composites are discussed.

This work is supported by EU-funded project INTAS (Nº 05-1000008-8091) and by FCT project PTDC/CTM/73030/2006. V. Bystrov acknowledges FCT (Portugal) and DFG (Germany) for individual grants SFRH/BPD/22230/2005 and KL654/25-1 AOBJ:539404, respectively.

[1] V. Bystrov et al., J. Phys. D: Appl. Phys. 40, 4571 (2007).

[2] Ch. Rankin et al., ACS Nano; (Article); 2007; 1(3); 234-238.

CONDUCTIVE POLYMERS WITH EMBEDDED MAGNETITE NANOPARTICLES: SYNTHESIS AND CHARACTERIZATION.

L. Cabrera[1,2], M.P. Morales[3], N. Menéndez[1], S. Gutiérrez[2], P. Herrasti[1]
[1]Universidad Autónoma de Madrid, Ciudad Universitaria Cantoblanco s/n 28049, Madrid, Spain
[2]IIC, Universidad de Guanajuato, Cerro de la Venada s/n 36040, Guanajuato, Mexico
[3]Instituto de Ciencia de Materiales de Madrid, CSIC, Sor Juana Inés de la Cruz, 3, 28049, Madrid, Spain
lourdes.cabrera@uam.es

Composites of intrinsic conductive polymers containing magnetic nanoparticles have caught the attention because of their physical and chemical unique properties. This kind of composites are composed by polymeric materials and magnetic inorganic materials in the nanometric scale, such as magnetite (Fe_3O_4)[1]. This material exhibits characteristics from both components, and since composites are non-invasive systems, selective and magnetically controlled, they have a great demand. They have many applications in batteries, electrochemical digital instrumentation, electronics, electrochromic instruments, non-linear optic systems, among many other instrumental uses, like information recording[2]. Their use is not limited to the electronic area, they have great application in the areas of bioscience and medicine in the separation of proteins and biomolecules, transport for drug delivery, and hyperthermia treatment[3].

A lot of effort is being focused to the development of methodologies and processes for the incorporation of Fe_3O_4 nanoparticles into the intrinsic conducting polymeric matrixes, such as polyaniline or polypyrrole (Ppy). The efforts to prepare these composites have had limited success[4]. One of the synthetic problems is the use of strong acids for the generation of the polymeric matrix, since they can promote the decomposition of the magnetic material. In the case of Fe_3O_4 magnetic nanoparticles, the formation of aggregates must be avoided in order to allow the iron oxide to disperse in the polymeric matrix homogeneously[2].

The synthesis of nanometric Fe_3O_4 can be achieved by several methods, being the co-precipitation method the most used[5]. However, in this preparative route, there is a limited control over the particle size and usually wide particle size distributions are obtained. In addition, the aggregation phenomenon is difficult to avoid unless surfactants are used in the reaction media[6-9].

In this work, an electrochemical synthesis allowed the preparation of Fe_3O_4 with a control over the particle size distribution, and when generated in the presence of cationic surfactants, the phenomenon of aggregation of nanoparticles was avoided. The obtained product was mixed with the monomer pyrrole, followed by its chemical oxidation in order to obtain the magnetite-polypyrrole (Fe_3O_4/Ppy) composites.

Two iron electrodes were used as anode and cathode for the electrolysis. The Fe_3O_4 nanoparticles were obtained by oxidation of iron in the presence of tetraalkyl ammonium salts. For its synthesis, chronopotentiometric techniques were employed, where the conditions were optimized in order to generate nanoparticles of 20 nm. The iron oxide was then mixed with a solution of the pyrrole, which was oxidized with $FeCl_3$ in order to polymerize the monomer and obtain Ppy with Fe_3O_4 nanoparticles embedded in its matrix.

The characterization of the generated composite Fe_3O_4/Ppy was carried out by different techniques. The spectroscopic techniques involved X-ray diffraction, X-ray fluorescence, Mössbauer, and FT-IR. Analyses by thermogravimetry (TG), transmission electron microscopy (TEM), and magnetization curves were also performed. Figure 1 shows the Fe_3O_4/Ppy morphology, were it can be observed that the dispersion of the iron oxide nanoparticles is

homogeneous within the polymer. Magnetization curves are also presented (figure 2), which show that properties such as coercive field, depend of the synthetic conditions.

Acknowledgements:

The authors acknowledge the Comunidad de Madrid project S-0505/MAT/019, as well as CONACyT (Mexico), for financial support, and Nanospain2008 Conference for the assistantship granted to the author.

References:

[1] Y. Lee, J. Rho, B. Jung. J. Appl. Polym. Sci., **89** (2003) 2058

[2] A. Chen, H. Wang, B. Zhao, X. Li. Synth. Met., **139** (2003) 411

[3] C. Bergemann, D. Müller-Schulte, J. Oster, L. a Brassad, A.S. Lübbe. J. Magn. Magn. Mater., **194** (1999) 45

[4] R. Gangopadhyay and A. De. Chem. Mater., **12** (2000) 608

[5] K.V.P.M. Shafi, A. Ulman, A. Dyal, X. Yan, N.-L. Yang, C. Estournes, L. Fournes, A. Wattiaux, H. White, M. Rafailovich. Chem. Mater., **14** (2002) 1778

[6] C. Pascal, J.L. Pascal, F. Favier, M.L.E. Moubtassim, C. Payen. Chem. Mater., **11** (1999) 141

[7] C. Tsouris, D.W. DePaoli, J.T. Shor, US 6,179,987 B1, 2001

[8] T.-Y. Ying, S. Yiacoumi, C. Tsouris. J. Dispersion Sci. Tech., **23** (2002) 569

[9] S. Franger, P. Berthet, J. Berthon. J. Solid State Electrochem., **8** (2004) 218

Figures:

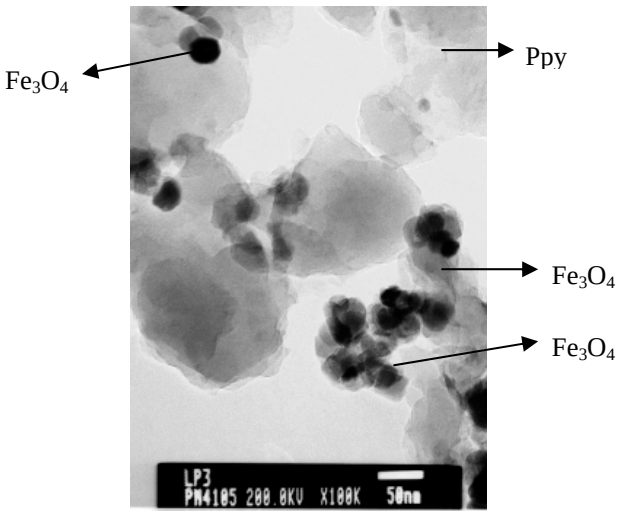

Figure 1. Fe_3O_4/Ppy composite, where Fe_3O_4 was obtained with $(CH_3)_4NCl$ as surfactant

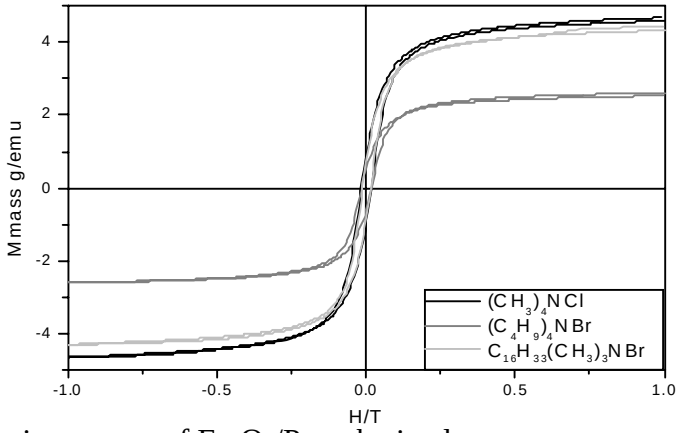

Figure 2. Magnetization curves of Fe_3O_4/Ppy obtained at room temperature, where Fe_3O_4 was prepared in each case with different tetraalkylammonium surfactants.

INTRODUCTION OF OF POLYPYRROL NANOPARTICLES IN CEMENT PASTE TO IMPROVE THE PHYSICAL PROPERTIES

Luís Cadillon Costa, François Henry
[1]*I3N, Departamento de Física, Universidade de Aveiro, Aveiro, Portugal*
[2]*CNRS, Thiais, France*
kady@ua.ptl

The introduction of different nanofillers in cements is frequently used to give mechanic reinforcement or flexibility and to hydrophobe the material.

In this work we introduced polypyrrol (PPy) nanoparticles at low concentrations in the cement paste, and we studied their influence in the physical properties of the cement.

The cement powder (CEM I 52.5N) and the desired concentrations of PPy in an aqueous emulsion, were introduced in a reactor and mixed during 5 minutes at 300 r.p.m. The initial water/cement ratio of 0.4 was maintained constant for all the samples.

The complex impedance and admittance was measured during the hardening of the cement, as a function of frequency between 1 Hz and 5 MHz, in order to follow the evolution of electrical properties with the hydration time as well as the effect of the nanoparticles.

Dielectric measurements were carried out using an 850 Stanford Research lock-in amplifier. The method consists in the measuring of the 'in phase' and the 'out of phase' components of the output signal, and these quantities were then used to calculate the values of effective resistance and capacitance in a parallel RC model of the sample. All the measurements were carried out at constant temperature of 23 ^{o}C.

Using the Cole-Cole model of dielectric relaxation [1],

$$Z^*(\omega) = Z_\infty + \frac{Z_0 - Z_\infty}{1 + (i\omega\tau)^\beta}, \tag{1}$$

$$Y^* = i\omega\left[C_\infty + \frac{C_0 - C_\infty}{1 + (C_0 - C_\infty)/A_0 (i\omega)^\beta}\right] \tag{2}$$

we calculated the relaxation parameters.

In these expressions, which are empirical modifications of the Debye equation [2], Z_∞ is the high frequency impedance, Z_0 the low frequency impedance, τ the relaxation time, β a parameter between 0 and 1 that reflects the homogeneity of the system, C_∞ the high frequency capacitance and C_0 the low frequency capacitance. An angle of depression can be defined as

$$\alpha = (1-\beta)\frac{\pi}{2}. \tag{3}$$

and is a measurement of the heterogeneity of the material.

The calculated parameters of the dielectric response had given information about the porosity of the material [3], which was confirmed by the measurement of the contact angle at water.

Figure 1 shows the evolution of the depression angle, during the hardening process, for the cement with several concentrations of PPy nanoparticles. For the higher concentration of nanofillers, the homogeneity, measured by this angle, increases.

References:

[1] K. S. Cole, R. H. Cole, J. Chem. Phys., **9** (1941), 341.
[2] P. Debye, *Polar molecules*, Chemical Catalog Company, New York, 1929.
[3] F. Henry, M. Reis, L. C. Costa, C. Freire, Mater. Sci. For. (submitted).

Figures:

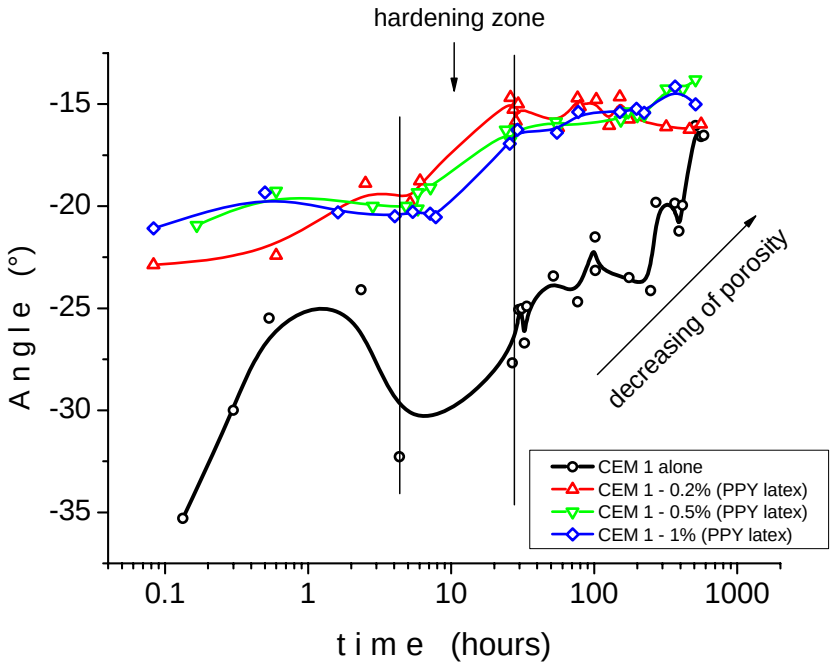

Fig. 1- Depression angle, during the hardening process, for the cement with several concentrations of PPy nanoparticles.

Nanoparticle based One-Dimensional Photonic Crystals

Mauricio E. Calvo,Silvia Colodrero, Manuel Ocaña, Hernán Míguez
Instituto de Ciencias de Materiales de Sevilla, Américo Vespucio 49 41092 ,Sevilla, España
hernan@icmse.csic.es

Herein we present a synthetic route to build 1D films of TiO_2/TiO_2 and SiO_2/TiO_2 nanoparticles that display bright structural color, which arises as a result of the periodic modulation of the refractive index. This is achieved by controlling the degree of porosity of each alternate layer through the particle size distribution of the precursor suspensions, which were cast in the shape of a film by spin coating. This method allows tailoring the lattice parameter of the periodic multilayer, thus tuning the Bragg peak spectral position (i.e., its color) over the entire visible region, as it can be seen in the figure 1. In addition, the SiO_2/TiO_2 multilayer can be doped optically leading to photonic crystals in which the opening of transmission windows due to the creation of defect states in the gap is demonstrated. The potential of this new type of structures as sensing materials is illustrated by analyzing their specific color changes induced by infiltration of solvents of different refractive index. Moreover, photoelectrochemical measurements show that the TiO_2/TiO_2 Bragg mirrors films are conductive and distort the photocurrent response as a result of the interplay between photon and electron transport through them.

Figures:

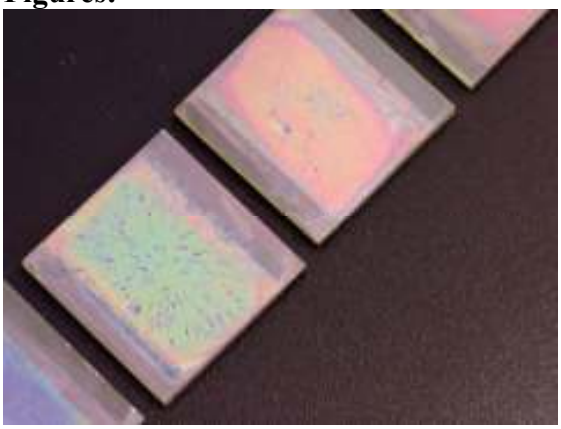

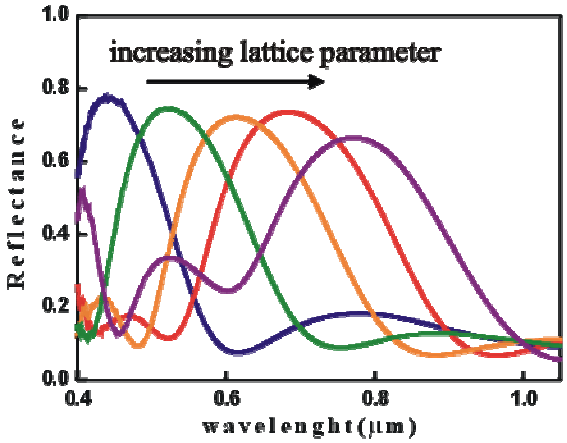

PREPARATION OF GOLD NANOPARTICLES ON SEVERAL SUPPORTS AND THEIR USE FOR THE OXIDATION OF CARBON MONOXIDE

Sónia A. Carabineiro[1], Philippe Serp[2], José L. Figueiredo[1]
[1] Laboratório de Catálise e Materiais, Departamento de Engenharia Química, Faculdade de Engenharia, Universidade do Porto, 4200-465 Porto, Portugal
[2]Laboratoire de Chimie de Coordination UPR CNRS 8241, composante ENSIACET, Toulouse University, 31077 Toulouse, France
Email: sonia.carabineiro@fe.up.pt

The oxidation of carbon monoxide is a simple reaction that although intensively studied in the literature is still poorly understood, as the mechanistic pathways are still uncertain. It is however a reaction of outstanding importance in pollution control (CO removal), fuel cells, and gas sensing [1].

Gold catalysts, in particular, have advantages in this reaction which arise from their improved activity at low temperatures and stability in the presence of water [2,3]. However, for gold to be active as a catalyst, use of a careful preparation procedure is crucial in order to obtain it as nanoparticles well dispersed on the support. The most common methods are Deposition Precipitation (gold precursor is precipitated onto a suspension of the preformed support by raising the pH either by the addition of alkali or urea) Co-Precipitation (support and gold precursors are brought out of solution, perhaps most likely as hydroxides, by adding a base such as sodium carbonate), and the use of colloids (prepared by reduction of chloroauric acid by citric acid and other reducing agents) [1].

In the present work, several gold catalysts were prepared by less usual methods, namely incipient wetness impregnation (variation of the traditional impregnation method in which the pores of the support are filled with a solution of $HAuCl_4$, using ultrasonication), double impregnation (similar to the previous one but with a second step of impregnation of Na_2CO_3) [4] and liquid phase reductive deposition (the gold precursor $HAuCl_4$ is mixed with NaOH and aged for 24h in the dark before it is impregnated onto the support) [5]. The main advantage of the latter two methods is that chloride is removed from the catalyst sample, which is well known to cause sintering of Au nanoparticles, thus turning them inactive [1].

Different supports were also tested, such as functionalised activated carbons, carbon xerogels and multi-walled carbon nanotubes [6], as well as oxides such as TiO_2, ZnO, among others. Samples were characterised by TEM and XRD. Catalysts were used as prepared or subjected to different surface pre-treatments. Activities for CO oxidation are compared and results are discussed.

References:

[1] S.A.C. Carabineiro, D.T. Thompson, "Catalytic Applications for Gold Nanotechnology", In: Nanocatalysis, Eds. U. Heiz and U. Landman, Springer-Verlag, Berlin, Heidelberg, New York (2007) pp. 377-489 (ISBN-13 978-3-540-32645-8).
[2] M. Haruta CATTECH, **6** (2002) 102.
[3] M. Haruta Chem. Record **3** (2003) 75.
[4] M. Bowker, A. Nuhu, J. Soares, Catal. Today, **122** (2007) 245.
[5] Y. Sunagawa, K. Yamamoto, H. Takahashi, A. Muramatsu, Catal. Today, **132** (2008) 81.
[6] J.L. Figueiredo, M.F.R. Pereira, M.M.A. Freitas, J.J.M. Orfão, Carbon, **37** (1999) 1379.

Poster

FABRICATION OF NANOSPHERES FROM Mn12 ACETATE SMM: DO THE CHEMICAL PROPERTIES OF THE ORIGINAL CLUSTER SHOW CHANGES?

C. Carbonera[a], *I. Imaz*[b], *D. Ruiz-Molina*[b], *D. Maspoch*[b], *F. Luis*[a]

[a]*Instituto de Ciencia de Materiales de Aragón, CSIC-Universidad de Zaragoza, 50009 Zaragoza, Spain*

[b]*Institut Català de Nanotecnologia, Centre d'Investigació en Nanociència i Nanotecnologia, Campus UAB-Edifici CM7, 08193 Bellaterra, Spain*

carboner@unizar.es

Micro- and nanoparticles have recently shown prosperous fields of application in diverse technological areas ranging from data storage, catalysis, and lithography to biosensors.[1] Considering the interest on these materials, a current goal in this area is the fabrication of particles with novel compositions that can offer interesting properties for new applications. In this field, we have recently published a precipitation-based methodology for fabricating sub-50 nm metal-organic spheres from macroscopic crystalline Mn_{12} acetate SMM of formula $[Mn_{12}O_{12}(CH_3COO)_{16}(H_2O)_4]\cdot 2CH_3COOH\cdot 4H_2O$ (see Figure 1).[2]

The magnetic properties of the synthesized Mn_{12}-based nanoparticles clearly indicate that particle formation does not affect the molecular composition of $Mn_{12}O_{12}$ clusters, although some interesting differences appear when the magnetic behaviour exhibited by such nanoparticles is compared with a polycrystalline sample of $[Mn_{12}O_{12}(CH_3COO)_{16}(H_2O)_4]$ (see Figure 2) [3].

In this contribution, a general overview of the magnetic properties of these novel Mn_{12}-based nanospheres will be shown. The comparison of the magnetic behavior of these nanoparticles and the starting crystalline Mn_{12} acetate will give important information about how changes in the environment influence the resulting magnetic properties of SMMs. This fundamental knowledge can prove useful in order to control the behaviour of these clusters when we try to build useful devices for quantum computation and data storage since the degree of decoherence as well as the lifetime of the data stored strongly depend on the magnetic relaxation.

References:

[1] (a) A. T. Bell, Science, **299** (2003) 1688; (b) M. J. Bruchez, M. Moronne, P. Gin, S. Weiss and A. P. Alivisatos, Science, **281** (1998) 2031; (c) T. A. Taton, C. A. Mirkin and R. L. Letsinger, Science, **289** (2000) 1757; (d) J. Wang, M. S. Gudksen, X. Duan, Y. Cui and C. M. Lieber, Science, **293** (2001) 1455; (e) M.-H. Wu and G. M. Whitesides, Appl. Phys. Lett., **78** (2001) 2273; (f) J. Ramos, A. Millan and F. Palacio, Polymer, **41** (2000), 8461.

[2] I. Imaz, F. Luis, C. Carbonera, D. Ruiz-Molina, D. Maspoch, Chem. Commun., (2008) 1202.

[3] C. Carbonera, I. Imaz, D. Ruiz-Molina, D. Maspoch, F. Luis, Inorg. Chim. Acta, in press.

Figures:

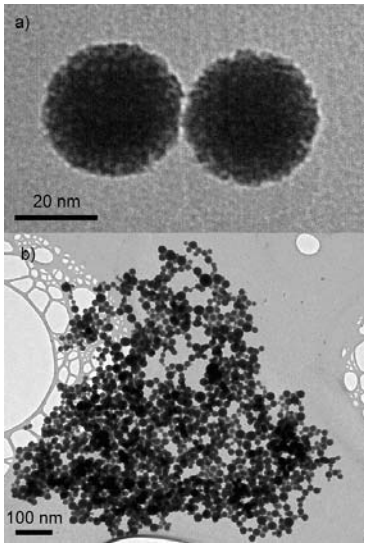

Figure 1. TEM images of nanospheres of Mn_{12} acetate.

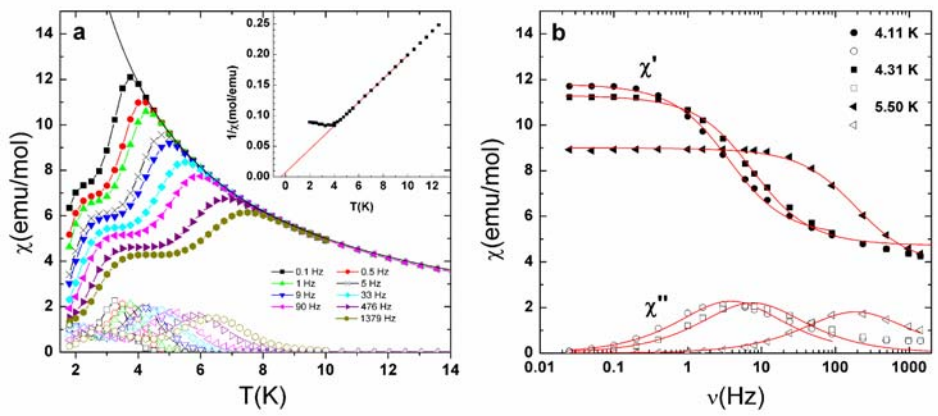

Figure 2. Magnetic ac-susceptibility data (real and imaginary parts) for the Mn_{12}Ac-based nanospheres: (a) as a function of the temperature, inset: $1/\chi$ *vs.* T; (b) as a function of the frequency. Three selected temperatures have been represented. The red line corresponds to the Cole-Cole fit.

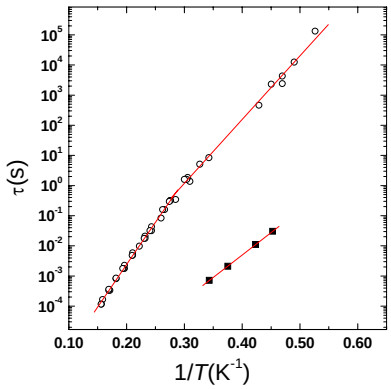

Figure 3. This plot resumes the relaxation times obtained from ac ($0.1 < T^{-1} < 0.3$ K^{-1} range) and magnetic relaxation ($T^{-1} > 0.3$ K^{-1}) measurements. Square symbols represent the data obtained for the fast relaxing species.

Single-Crystalline $La_{0.7}Sr_{0.3}MnO_3$ Nanowires Grown by Template Directed Chemical Solution Synthesis*

A. Carretero-Genevrier[1] *N. Mestres*[1], *T. Puig*[1], *A. Hassini*[1], *A. Pomar*[1], *J. Oró*[1], *J. Gázquez*[1], *F. Sandiumenge*[1], *X. Obradors*[1], *E. Ferain*[2]

[1] *Institut de Ciència de Materials de Barcelona ICMAB-CSIC, E-08193 Bellaterra, Catalonia, Spain*

[2] *Université Catholique de Louvain (UCL), B-1340 Louvain la Neuve; Belgium*

Organization, Address, City, Country

Acarretero@icamb.es

One dimensional (1D) nanostructures offer a means of tuning the strong interactions that exist between magnetic, electronic and crystal structures of manganites. The development of facile, mild an effective approaches for generating size controllable 1D manganite structures remains a significant challenge. In this report, we demonstrate that self standing single crystalline $La_{0.7}Sr_{0.3}MnO_3$ (LSMO) nanowires several microns long with controllable morphology can be successfully synthesized by template assisted chemical solution deposition (CSD) using track-etched polymer membranes of varying pore size. Nanowires were synthesized using a sol-gel based polymer precursor route allowing a good control of the viscosity and stability of the precursor solution, which are crucial parameters for template aided synthesis. The pores of the membrane were filled with the precursor solution by capillarity and subsequently heated at high temperature for polymer elimination and phase formation. Extensive characterization has been performed using XRD, SEM and TEM microscopy and SQUID magnetometry. We prove that these nanowires exhibit a monoclinic crystallographic structure not known up to now for manganite that seems to modify its electronic and magnetic properties.

Moreover, we have nanostructured single crystalline substrates with vertically aligned magnetic LSMO nanopillars and nanopyramids combining CSD with supported track-etched polymer templates, this opens the possibility to study new phenomena and interactions in nanomagnet systems embedded into magnetic/non magnetic matrices.

*This work has been financed by the EU (Hiperchem NMP4-CT2005-516858), MEC (NANOFUNCIONA, NAN2004-09133-CO3-01, NANOSELECT and FPI) and the CSIC (PIF project CANNAMUS).

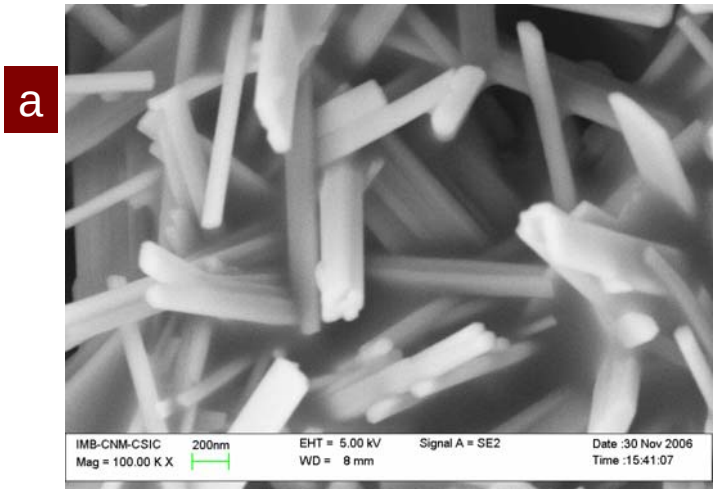

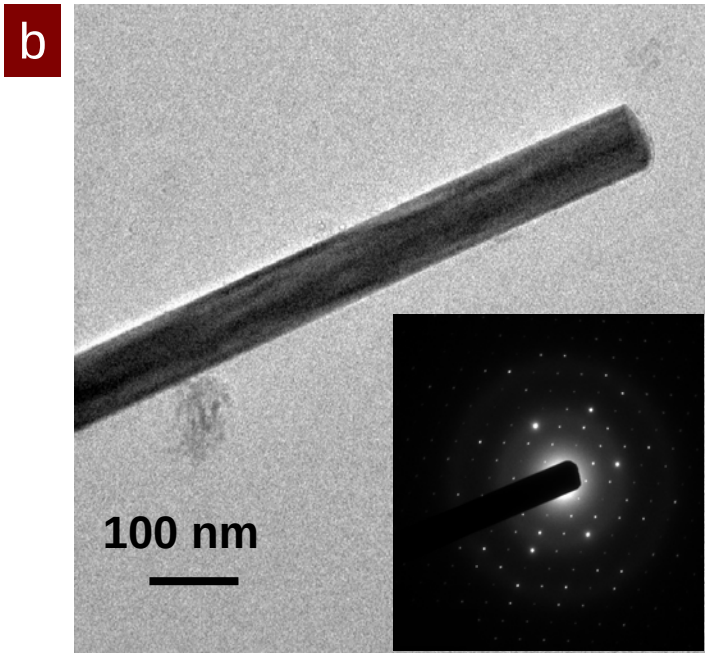

Figure 1: a) Typical field emission SEM image of LSMO nanowires prepared using polyimide membranes with 100 nm pore size, (b) Transmission electron microscopy (TEM) image of a single LSMO nanowire. The inset shows the corresponding SAED pattern indicating the single crystalline nature of the nanowires.

MECHANICAL AND FATIGUE PROPERTIES OF SINTERED NANOTUBE-BASED FUNCTIONALLY GRADED MATERIALS

Oscar Samuel Novais Carvalhor,
Departamento de Engenharia Mecânica,
Campus de Azurem
4800 – 058 Guimarães, Portugal
oscar.carvalho@gmail.com

Summary

This PhD project is concerned with development and assessment of metallurgical, mechanical and fatigue properties of nanotubes functionally graded metal matrix composites obtained by powder metallurgy.
The gradient will be obtained by a variation on nanotubes volume fraction from bulk part to surface of the specimen, where the volume fraction is lighter.
This work will focus on processing conditions as well as on its influence over the material metallurgical properties and mechanical and fatigue mechanisms (crack nucleation and propagation). This study results are intended to be used in fatigue theories in order to predict fatigue initiation life of automotive components. The research consists on experimental work with specimens obtained from different processing routes.

STRATEGIES FOR THE SELECTIVE CONFINEMENT OF NANOPARTICLES IN THE INNER CAVITY OF MULTI-WALLED CARBON NANOTUBES

Eva Castillejos-López, Abderrahim Sohly, Victor Martinez, Karine Philippot, Bruno Chaudret , and Philippe Serp

Laboratoire de Chimie de Coordination, CNRS UPR 8241, 205 Route de Narbonne, Toulouse University, 31077 Toulouse France

Philippe.Serp@ensiacet.fr

Carbons nanotubes (CNTs) have a well-defined hollow structure and exhibit unusual chemical, mechanical and thermal properties as well as high electron conductivity. They can be employed as catalyst supports since they present a very open macrostructure with large mesoporosity allowing to avoid mass transfer limitations [1].
The shape of these carbons nano-objects allows to explore the effect of confinement on the catalytic activity and selectivity of CNT based catalysts. The introduction of foreign elements inside CNTs may modify the physical and chemical properties of the encapsulated material and also of the support itself, thanks to the electron transfer between the graphite structure and the metal particles [2]**.** The presence of relatively well-defined inner cavities can also induce differences of reactivity between the external and internal surfaces. It is expected that specific properties will be observed with these encapsulated nanomaterials, particulalry in the heterogeneous catalysis field, compared to those usually encountered with traditional catalysts [3,4]. Up to date, the selective confinement of discrete nanoparticles (NPs) in the inner cavity of CNTs is a rather difficult task and unexplored field [5,6].
We have developed an effective strategy to selectively deposit PtRu NPs either on the whole surface of multi-walled carbon nanotubes, either in their inner cavity (Figure 1).

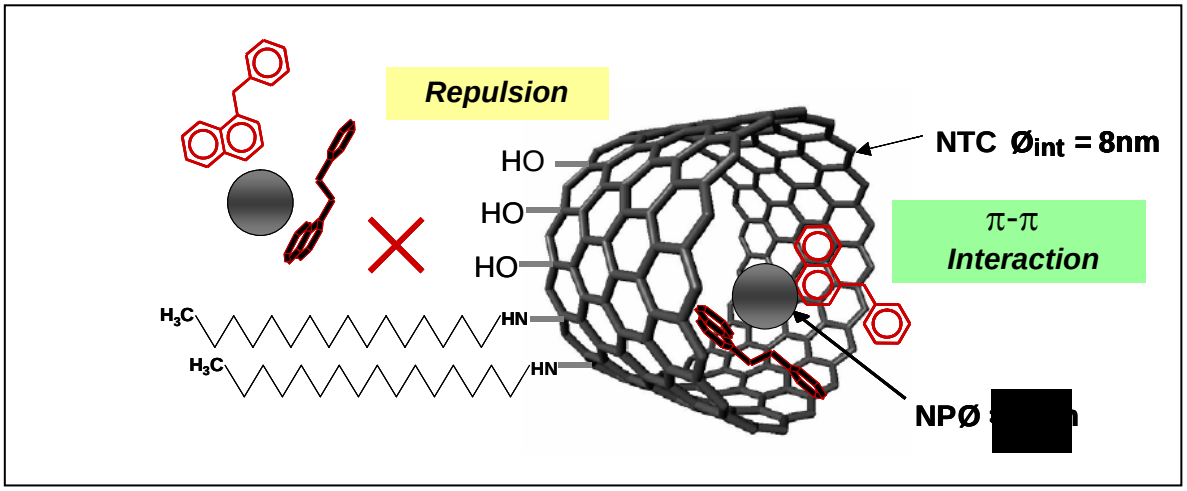

Figure 1. Strategy to confine NP in the inner cavity of CNTs.

The first step consists in the controlled preparation (chimie douce approach) of NPs stabilized by a ligand presenting two functionalities: one having an affinity for the surface of the NP and the other presenting an affinity for the grapheme layers (π-π interaction). The second step

requires the external surface functionalization of CNTs to introduce for example long chain amine groups, which should induce repulsion between the NPs and CNT external surface.
In this contribution we will present results on NP preparation, CNT functionalization and NP deposition in (NP@CNT) or onto CNTs (NP/CNT). The different materials (Figure 2) have been characterized by Transmission electronic microscopy, EDX, infrared spectroscopy, X-ray photoelectron spectroscopy, acid-base titrations and elemental micro-analyze.

References:

[1] P. Serp, M. Corrias, P. Kalck, Appl. Catal. A: Gen. 253 (2003) 337.
[2] J.Tessonnier, L. Pesant, G Ehret, M.J. Ledoux, C. Pham-Huu, Appl. Catal. A, 288 (2005) 203.
[3] D. Ugarte, A. Châtelain, W.A. de Heer, Science 274 (1996) 1897.
[4] S. C. Tsang, Y. K. Chen, P.J.F. Harris, M.L.H. Green, Nature 372 (1994) 159.
[5] F. Winter, G. Leendert Bezemer, C. van der Spek, J.D. Meeldijk, A. Jos van Dillen, J.W. Geus, K.P. de Jong, Carbon, 43 (2005), 327.
[6] X. Pan, Z. Fan, W. Chen, Y. Ding, H. Luo, X. Bao, Nature Materials 6 (2007) 507.

Figures:

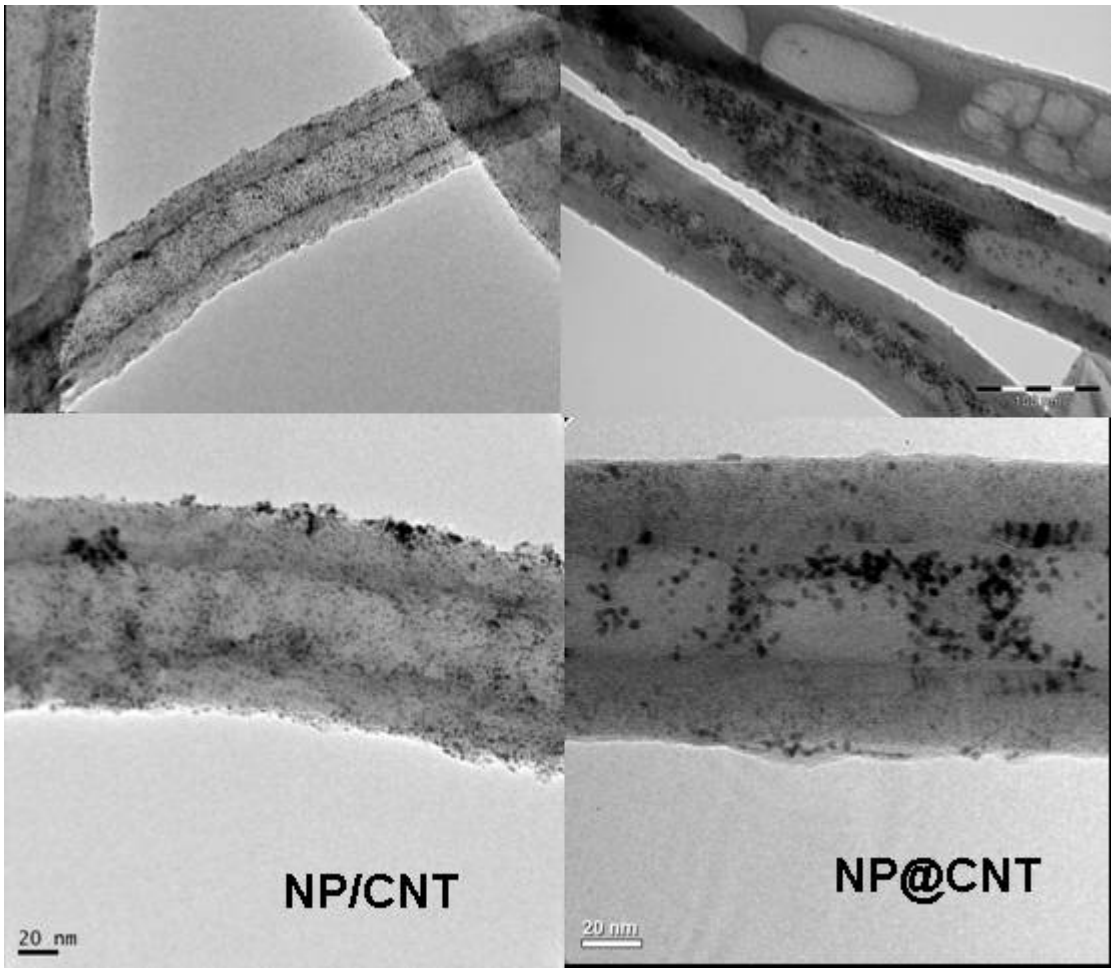

Figure 2. TEM micrographs of NP/CNT and NP@CNT.

Adiabatic magnetothermal setup for accurate Specific Absorption Rate measurements.

Eva Natividad[1], Miguel Castro[1], Arturo Mediano[2]
[1]Instituto de Ciencia de Materiales de Aragón, CSIC-Universidad de Zaragoza, María de Luna, 3, 50018 Zaragoza, Spain
[2]Instituto de Investigación en Ingeniería de Aragón, Universidad de Zaragoza, María de Luna, 3, 50018 Zaragoza, Spain

mcastro@unizar.es

In magnetic fluid hyperthermia for cancer treatment [1] a biocompatible fluid based on magnetic nanoparticles is introduced into tumours, so that the heat generated by the nanoparticles under a alternating magnetic field destroys cancerous tissue. The minimization of the invasive character of this technique requires the use of magnetic nanoparticles with large heating power, that allowing the clinical dose to be reduced.

The heating efficiency of these fluids is determined by the specific absorption rate (SAR), defined as $SAR = (1/m)\cdot C\cdot(\Delta T/\Delta t)$, where m is the mass of dissipating material , C, the heat capacity of the whole sample, and ΔT, the sample temperature increase during the ac-field application interval, Δt. Current SAR installations reported in literature [2,3] do not allow to use the above expression to evaluate the SAR since heat losses (conduction, radiation, convection) are not minimized. Then an approximate procedure is followed, based on the temperature-versus-time exponential curve according to the expression $SAR = C\cdot\beta/m$, where $\beta = (dT/dt)|_{t0}$ is the initial slope. This method can lead to unknown errors in the determination of β and, therefore, to incorrect SAR values because initial thermal losses and a non-homogenous temperature distribution across the sample can be present.

In order to overcome these limitations, we have developed the first adiabatic magnetothermal setup [4], in which the sample undergoes only a weak net heat exchange with the surroundings. In such conditions, the generated heat can be considered to be entirely invested in the sample temperature raise, allowing direct measurement of ΔT, and providing more precise SAR values.

The measurements performed on a commercial magnetite aqueous ferrofluid from Chemicell GmbH, namely the fluidMAG-UC/A, showed clearly the typical step-like behaviour of the adiabatic processes (see Figure). By averaging seven heating steps in the same conditions, a SAR value of 0.217 W/g was obtained with good reproducibility (4%). On the other hand, the measurements performed on a copper sample provided comparison between experimental and theoretical values: adiabatic conditions gave SAR values only 3% higher than the theoretical ones, while the typical non-adiabatic method underestimated SAR by 21%. These results have allowed, on the one hand, to evaluate for the first time the accuracy in SAR determination by calorimetric methods and, on the other hand, to point the improvement of the adiabatic over the non-adiabatic method, by using the same setup.

In conclusion, the adiabatic magnetothermal setup has provided accurate and reproducible SAR measurements of solid and liquid samples. This improved characterization will be of great importance in the studies on correlation between the SAR and nanoparticle properties like size polydispersity, shape, crystallinity or coatings, in simulations of temperature distributions in tissues or phantoms and in the optimization of hyperthermia therapies.

References:

[1] M. Johannsen, U. Gneueckow, B. Thiesen, K. Taymoorian, C.H. Cho, N. Waldofner, R. Scholz, A. Jordan, S.A. Loening and P. Wust, European Urology **52** (2007) 1653.
[2] G. Glockl, R. Hergt, M. Zeisberger, S. Dutz, S. Nagel and W. Weitschies, Journal of Physics-Condensed Matter **18** (2006)
[3] J.P. Fortin JP, C. Wilhelm, J. Servais, C. Menager, J.C. Bacri and F. Gazeau, Journal of the American Chemical Society **129** (2007) 2628.
[4] M. Castro, A. Mediano, E. Natividad and F. Palacio "Equipo adiabático para medida del coeficiente de absorción específico de un material sometido a un campo magnético alterno", Spanish Patent Application, 2007. Filed 24 Dec. 2007, Application No. P200703426.

Figure:

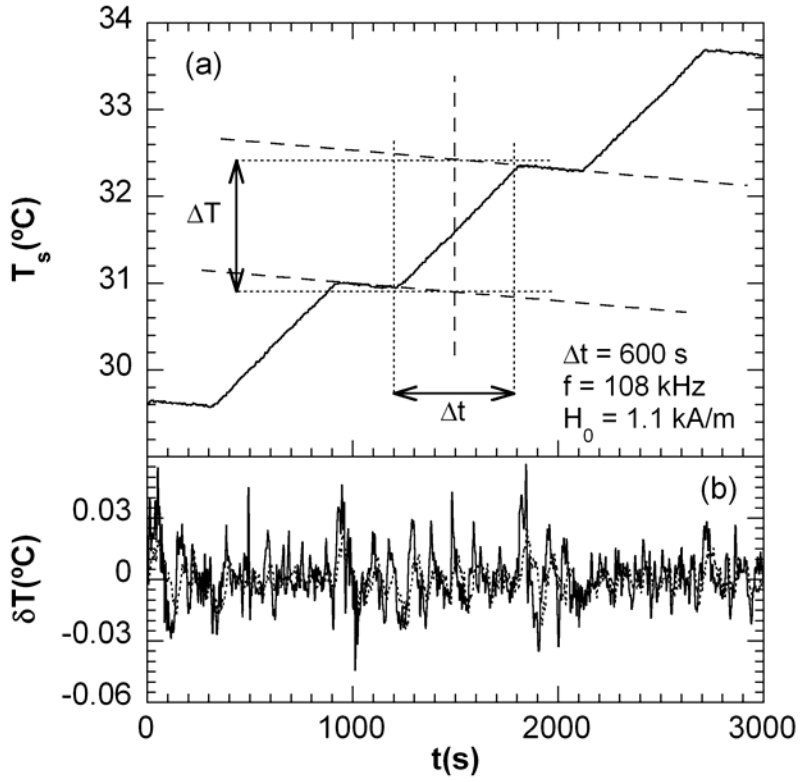

Three consecutive heating steps of the ferrofluid sample.

Magnetocapacitive response in Fe_3O_4 nanoparticles

S. Castro-Garcia, S. Yáñez-Vilar, M. Sánchez-Andújar, M. A. Señarís-Rodríguez
Dept. Química Fundamental, Univ. da Coruña, A Zapateira s/n, 15071 A Coruña, España
suqui@udc.es

There is a renewed interest in materials in which their dielectric constant can be modified by the application of a magnetic field [1]. Unluckily, relatively few compounds display such a magnetocapacitive (MC) behavior and many efforts have been devoted in the last years to search for new alternatives.

Recently, several authors have reported magnetocapacitive response in magnetic nanoparticle systems such as ε-Fe_2O_3 [2], $MnFe_2O_4$ and γ-Fe_2O_3 [3], and ferroelectric and magnetic nanocomposites [4]. Therefore, nanoparticle technologies open a new route to obtain materials with such a behavior.

In this contribution, we report the dielectric and magnetocapacitive response of the magnetic nanoparticles of magnetite, Fe_3O_4. This compound is a very well known material that shows a ferrimagnetic transition around $T_C \sim 850$ K and a charge localization around $T_v \approx 120$ K (the so-called Verwey transition). Also, it shows magnetoresistance at room temperature [4].

The Fe_3O_4 nanoparticles (ϕ~30 nm) were synthesized following the solvothermal method described by Pinne et al. [5]. The obtained sample was morphologically and structurally characterized by means of X-ray powder diffraction, scanning electron microscopy and transmission electron microscopy. Its complex dielectric permittivity, $\varepsilon_r = \varepsilon_r' - i\varepsilon_r''$, was measured as a function of frequency ($20 \leq \nu(\text{Hz}) \leq 10^6$) and temperature ($90 \leq T(\text{K}) \leq 300$). Dielectric measurements as a function of a magnetic field, $H_{max} = 0.5$ T, were additionally performed in the temperature range $200 \leq T(\text{K}) \leq 300$.

The variation of the dielectric constant (ε'_r) and the dielectric loss (tanδ) as a function of temperature reveal interesting features as the Verwey transition takes place (see Figure 1): the dielectric constant drops abruptly while a peak appears in tanδ, results that suggest a coupling between the charge condensation and the dielectric response.

In addition, we have found a magnetocapative response at room temperature and under a relative moderate magnetic field, $MC = [\varepsilon'_{r(H=0.5T)} - \varepsilon'_{r(H=0T)}] / \varepsilon'_{r(H=0T)} \approx 6\%$ under $H = 0.5$ T (Figure 2).

References:

[1] G. Catalan, *Appl. Phys. Lett*. **88** (2006) 102902.
[2] M. Gith, C. Frontera, A.Roig, J. Fontcuberta, E. Molins, *Nanotechnology* **17** (2006) 687.
[3] G. Lawes, R. Tackett, O. Masala, B. Adhikary, R. Naik, R. Seshadri, *Appl. Phys. Lett*. **88** (2006) 687.
[4] J. M. D. Coey, A. E. Berkowitz, Ll. Balcells, F. F. Putris, F. T. Parker, *Appl. Phys. Lett.* 72 (1998) 734.
[5] N. Pinna, S. Grancharow, P. Beato, P. Bonville, M. Antonetti, M. Niederberger, *Chem. Mater*. **17** (2005) 3044.

Figures:

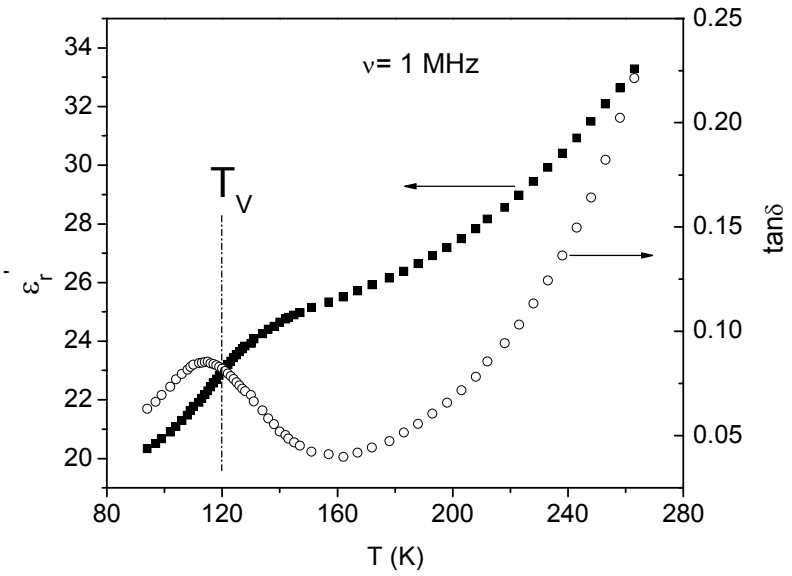

Figure 1. Temperature dependence of the dielectric constant (ε'_r) and dielectric loss (tanδ) measured at ν = 1 MHz.

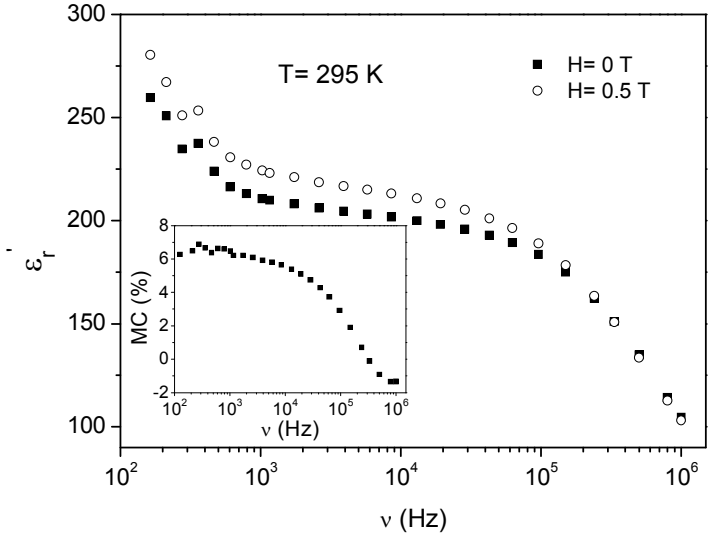

Figure 2. Influence of the magnetic field (H) in the frequency (ν) dependence of the dielectric constant (ε'_r) measured at T = 295 K. Inset: Magnetocapacitive effect, where $MC = [\varepsilon'_{r(H=0.5T)} - \varepsilon'_{r(H=0T)}] / \varepsilon'_{r(H=0T)}$.

Acknowledgements
The authors are grateful for financial support from Xunta de Galicia under PGIDIT06PXB103298PR project.

FORMATION OF NANOPLATELETS IN TMD-C SPUTTERED COATINGS

T. Polcar[1,2], M. Evaristo[1], R. Colaço[3], C. Sandu[1,4], A. Cavaleiro[1]
1)SEG-CEMUC - Department of Mechanical Engineering, University of Coimbra, Polo II, 3030-788 Coimbra, Portugal
2)Department of Control Engineering, Faculty of Electrical Engineering, Czech Technical University in Prague, Technická 2, Prague 6, Czech Republic
3)Instituto Superior Tecnico, Technical University of Lisbon, Department of Materials Engineering, Av. Rovisco Pais, 1049-001 Lisbon, Portugal
4) EPFL – Ecole Polytechnique Federale de Lausanne, CH-1015 Lausanne, Switzerland

corresponding author: albano.cavaleiro@dem.uc.pt

Abstract.

Transition metal dichalcogenides (TMD) exhibits unique sandwich lamellar structure with weak inter-layer bonding. TMD family covers disulphides, diselenides and ditellurides of molybdenum, tungsten or niobium. The physical and tribological properties of TMD's, particularly MoS_2 and WS_2, have been intensively studied for more than five decades. Nowadays, they are mainly used as oil additives or thin films in the low-frictional role. Fullerene-like[i,ii,iii] and nanotubes[iv,v] TMD structures have been considered as a very promising material for tribology applications; however, their industrial applicability is still very limited. In spite of the fact that the mechanism supporting the low friction was not fully understood, it has been suggested that one possibility would be the opening of the closed structure that would promote to the formation of platelets which, when disposed parallel to the sliding movement, would lead to low friction coefficients[i].
In late nineties, a new concept of coatings based on the alloying of transition metal dichalcogenides (TMD) with carbon started to attract the attention of various scientific groups[vi]. The original idea was to join the excellent frictional behavior of TMD in vacuum and dry air with the tribological properties of DLC coatings. The frictional performance of the deposited W-S-C coatings during environmental cycling could be regarded as a friction coefficient alternating between 0.02 and 0.15 values. The low friction in dry air increased in the presence of humidity and fell down when the atmosphere was dried again. These values were interpreted by successive changes in the sliding mechanisms based on the modification of the chemical composition of the contact layers.
Recently, the authors deposited W-S-C coatings by magnetron sputtering from a carbon target with embedded WS_2 pellets[vii,viii]. Very interesting tribological results could be found having been suggested that the sliding mechanism was similar whatever the testing environment was: the modification of the top contact surface of the worn track which was enriched in TMD material. However, the same cyclic change of the air humidity led to an alternating low / high friction as described above. One of the few research works on other members of the TMD family, molybdenum diselenide, showed that low friction could be achieved almost independently of the air humidity[ix]. Thus, in this work the mechanical and tribological properties of Mo-Se-C coatings prepared by non-reactive magnetron sputtering from a carbon target with $MoSe_2$ pellets were studied.
The results allowed concluding that, with increasing C content, there was a decrease of the size of the crystalline features, particularly in relation to the perpendicular direction of the basal TMD planes. For C contents close to 50 at.%, a nanocomposite structure consisting of an arrangement of platelets (a couple of tens of nanometers planar dimension with only a small thickness consisting in a few basal planes) immersed in a C-matrix could be detected (see figure 1). Furthermore, when tested in tribological sliding, there was a progressive

alignment of the platelets parallel to the sliding movement when going from the bulk to the surface (see figure 2). In the top layers there are exclusively basal planes of the TMD phase.

References:

[i] L. Rapoport, Y. Bilik, Y. Feldman, M. Homyonfer, S.R. Cohen, R. Tenne, Nature, 387 (1997) 791-793
[ii] M. Chhowalla, G.A.J. Amaratunga, Natura, 407 (2000) 164-167
[iii] Y. Golan, C. Drummond, M. Homyonfer, Y. Feldman, R. Tenne, J. Israelachvili, Advanced Materials, 11 (1999) 934
[iv] M. Remskar, A. Mrzel, Z. Skraba, A. Jesih, M. Ceh, J. Demsar, P. Stadelmann, F. Levy, D. Mihailovic, Science, 292 (2001) 479-481
[v] M. Remskar, Advanced Materials, 16 (2004) 1497-1504
[vi] A.A. Voevodin, J.S. Zabinski, Thin Solid Films 370 (2000) 223
[vii] T. Polcar, M. Evaristo and A. Cavaleiro, Plasma Processes & Polymers, 4 (2007) S541
[viii] T. Polcar, M. Evaristo, A. Cavaleiro, Vacuum, 81 (2007) 1439
[ix] T. Kubart, T. Polcar, L. Kopecký, R. Novák and D. Nováková, Surf. Coat. Technol. 193 (2005) 230

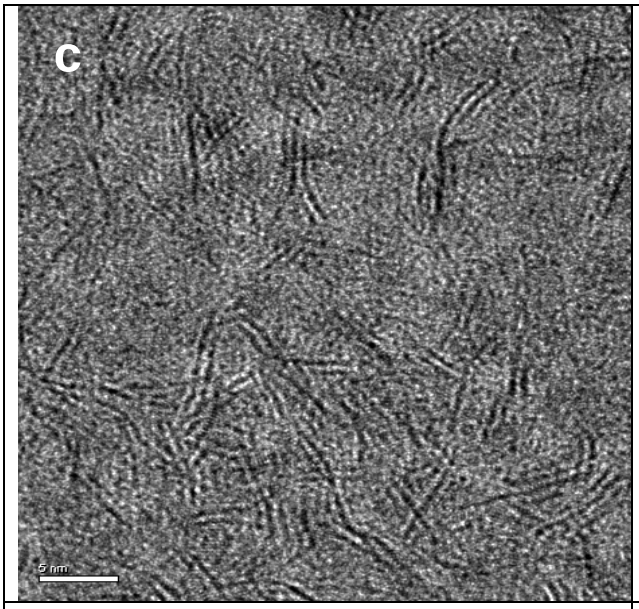

Figure 1 TEM micrograph of the cross section of a sputtered Mo-Se-C film deposited with 50 at.% C.

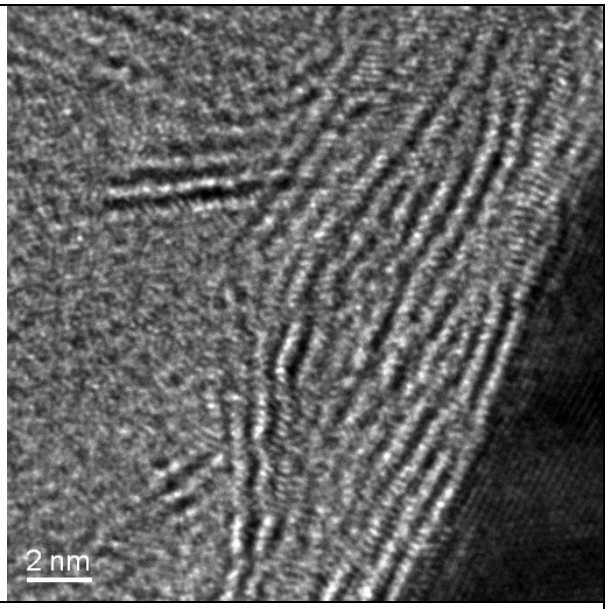

Figure 2 Top surface layers of the wear track of a Mo-Se-C sputtered coating after having been submitted to a sliding test.

.

Influence of Patterned Electrospun Nanofiber Meshes on Human Dermal Fibroblasts, Keratinocytes and Adipose Stem Cells Behaviour

M. T. Cerqueira [1,2], *A. Martins* [1,2], *T. Rada*[1,2], *M. E. Gomes*[1,2], *A. P. Marques*[1,2], *N. M. Neves*[1,2], *R. L. Reis*[1,2]

[1] *3B's Research Group – Biomaterials, Biodegradables and Biomimetics; Dept. of Polymer Engineering, University of Minho, Campus de Gualtar, 4710-057 Braga, Portugal, www.3bs.uminho.pt*

[2] *IBB – Institute for Biotechnology and Bioengineering, PT Government Associated Laboratory, Braga, Portugal*

mariana.cerqueira@dep.uminho.pt

Natural extracellular Matrix (ECM) creates a unique cellular microenvironment. It acts as a support to organize cells in tissues, maintains their structure and works also as a reservoir for cytokines, thus controlling cell growth and differentiation. A well-defined biomaterial surface topography is believed to be adequate to mimic native ECM for guiding cell growth or tissue regeneration. This structure can be achieved by using an electrospinning technique, which allows producing a non-woven nanofibrous structure with topographic features mimicking the natural ECM [1].

This study evaluates the influence of micro-topography of patterned Polycaprolactone (PCL) nanofiber meshes, aimed at being used in skin regeneration approaches. The morphology, adhesion and proliferation of primary cultures of human keratinocytes (hKC), dermal fibroblasts (hDFs), and adipose-derived stem cells (hASCs), isolated from the abdominal region, was evaluated after seeding in those structures .

In vitro studies showed that the characteristic morphology of each cell type and respective phenotype was maintained on the patterned electrospun nanofiber meshes during the culture period. SEM micrographs demonstrated that these cells adhered better on the randomly distributed areas (Fig. 1B) of the nanofibers than in the aligned ones. Furthermore, DNA quantification and metabolic activity analysis confirmed the enhanced performance of the cells adhered on the random structures. Additionally, the patterned areas were able to induce cell alignment along the nanofibers (Fig. 2).

The combination of the organized and random structures into patterned nanofiber meshes, being able to control cell distribution and proliferation, showed promising characteristics for upcoming studies regarding skin tissue engineering applications.

References:

[1] Neves N.M., Campos R., Pedro AJ, Cunha J., Macedo F., Reis RL, Patterning of polymer nanofiber meshes by electrospinning for biomedical applications. International Journal of Nanomedicine, 2007. 2(3): p. 433-48

Figures:

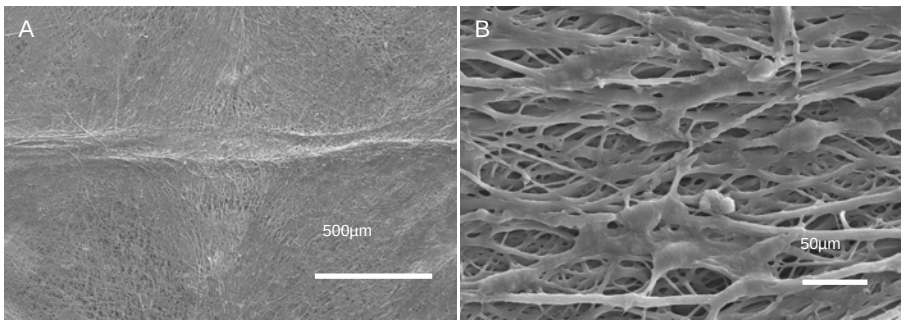

Figure 1- SEM micrograph of A) random and aligned electrospun nanofibres and B) HDFs in electrospun PCL patterned nanofiber meshes after 14 days of culture.

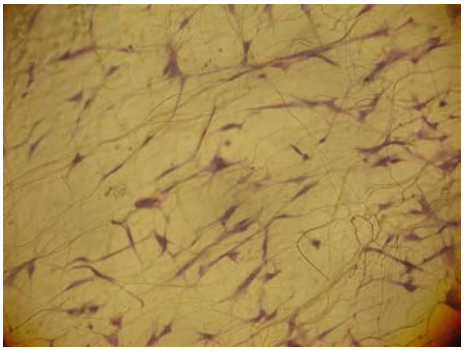

Figure 2- Cell alignment along the nanofibers.

Poster

ERBIUM-DOPED NANOCRYSTALLINE SILICON THIN FILMS GROWN BY R.F. SPUTTERING METHOD. COMPETITION BETWEEN OXYGEN AND SILICON TO GET ERBIUM

M. F. Cerqueira[a], M. Stepikhova[b], E. Malainho[a], M. Losurdo[c], A. Kozanecki[d], T. Monteiro[e]

[a]Departamento de Física, Universidade do Minho, Campus de Gualtar 4710-057 Braga, Portugal,
[b]Institute for Physics of microstructures, RAS, 603600 Nizhnij Novgorod, GPS-105, Russia,
[c]Institute of Inorganic Methodologies and Plasmas, IMIP-CNR, Via Orabona 4-70126 Bari, Italy,
[d] Polish Academy of Sciences, Institute of Physics, PL-02668, Warsaw,
[e]Departamento de Física, Universidade de Aveiro, Campus de Santiago, 3700 Aveiro, Portugal

During the last 15 years, modern growth techniques have shown the ability to fabricate semiconductor nano-structures of typical size<10*nm*, with spatial confinement of electrons in all three dimensions. These systems are of considerable current interest because of the new physics involved and potential device applications. One of these applications can be Si-based optoelectronics. Erbium doped silicon (Si:Er) is a recognised candidate to become the material for emitters and detectors to be used in optical communication systems. However, there is a problem with efficient energy transfer from the Si matrix to the Er centres. The use of Er-doped Si nano-crystallites can help to solve this problem. Studies of the photoluminescence of Er-doped nanocrystalline silicon constitute an important probe for these applications.

Erbium doped nanocrystalline silicon (nc-Si:Er) thin films were grown by r.f. reactive magnetron sputtering in an Ar/H_2 atmosphere on ordinary glass substrates under several different conditions. We have grown 3 groups of samples changing basically the amount of oxygen and hydrogen present in the structure. In particular, we have grown samples without oxygen, samples with more oxygen than hydrogen and in the last series the samples have a little bit more hydrogen than oxygen. For each group we obtain samples with different structural parameters by varying the experimental parameters. The film structure was studied using X-ray diffractometry, Raman spectroscopy and spectroscopy ellipsometry. The chemical composition was determined using RBS technique. Our samples show sharp photoluminescence (PL) spectra of Er centres with the strongest peak positioned at the wavelength 1.536 μm and full width at half maximum (FWHM) of about 8 nm. Our results indicate that the formation of Er-silicide or Er-oxide depending on microstructure, this means that the kind of matrix where the nanocrystals are embedded influences strongly the erbium emission.

Contact and presenting author:
Eva Malainho
Departamento de Física, Universidade do Minho
Campus de Gualtar, 4710-057 Braga, Portugal
phone: +253604332, Fax: +253678981

ANALYTIC MODEL OF QUANTUM ELECTROSTATIC POTENTIAL IN DOUBLE-GATE MOSFETs

Ferney Chaves, David Jiménez, Jordi Suñé*

Departament d'Enginyeria Electrònica, Escola Tècnica Superior d'Enginyeria, Universitat Autònoma de Barcelona, Barcelona, Spain

**ferneyalveiro.chaves@uab.cat*

Double-gate (DG) silicon-on-insulator (SOI) MOSFETs (Fig. 1) with undoped channels is one of the most promising structures for scaling CMOS devices down to nanometer sizes [1]. Among the advantages of DG MOSFET can be distinguished the reduction of the OFF current, a better control of short channel effects, making unnecessary the conventional use of high channel doping densities and gradients, and the undoped channel eliminates intrinsic parameter fluctuations and minimizes impurity scattering.

MOSFET compact modelling for circuit simulation applications requires accurate formulations which are at the same time computationally efficient [2]. Some models that have been proposed for these devices do not take into account quantum effects and lack computational efficiency since they rely on numerical iteration to solve the fundamental equations [3-6]. In Ref. [7] Ge et. al proposed a compact quantum-effect model for DG-MOSFETs using a variational approach which is a good model for the volume inversion description but not for the electrostatic potential of Si-film larger than 5 nm and gate voltages above subthreshold region.

In this work we present an analytic model of the quantum electrostatic potential for DG-MOSFET structure. We extend a previous physics based analytic solution for the electrostatic potential of undoped (or lightly doped) DG-MOSFET [3] by incorporating a minimal number of parameters and without using numerical iterations. We obtain excellent results compared with results obtained from self-consistent numerical solutions from Poisson and Schrödinger equations (Figs. 2,3).

References:

[1] Q. Chen et al., *IEEE Circuits Devices Mag.*, **vol. 19** (2003) 28
[2] J. P. Colinge, *Solid State Electron.*, **vol 48** (2004) 897
[3] Y. Taur, *IEEE Electron Devices Lett.*, **vol 21** (2000) 224
[4] Y. Taur, *IEEE Trans. Electron Devices*. **vol 48** (2001) 2861
[5] X. Shi and M. Wong, *IEEE Trans. Electron Devices*. **vol 50** (2004) 1793
[6] A. Ortiz-Conde, F. J. Garcia and S. Malobabic, *IEEE Trans. Electron Devices*. **vol 52** (2005) 1669
[7] L. Ge and J. G. Fossum, *IEEE Trans. Electron Devices*. **vol 49** (2002) 287

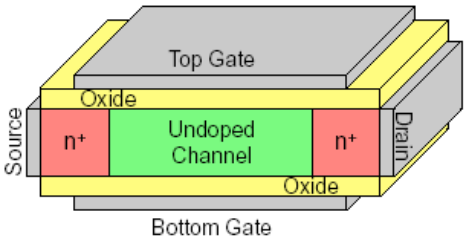

Figure 1. Schematic diagram of a DG-MOSFET

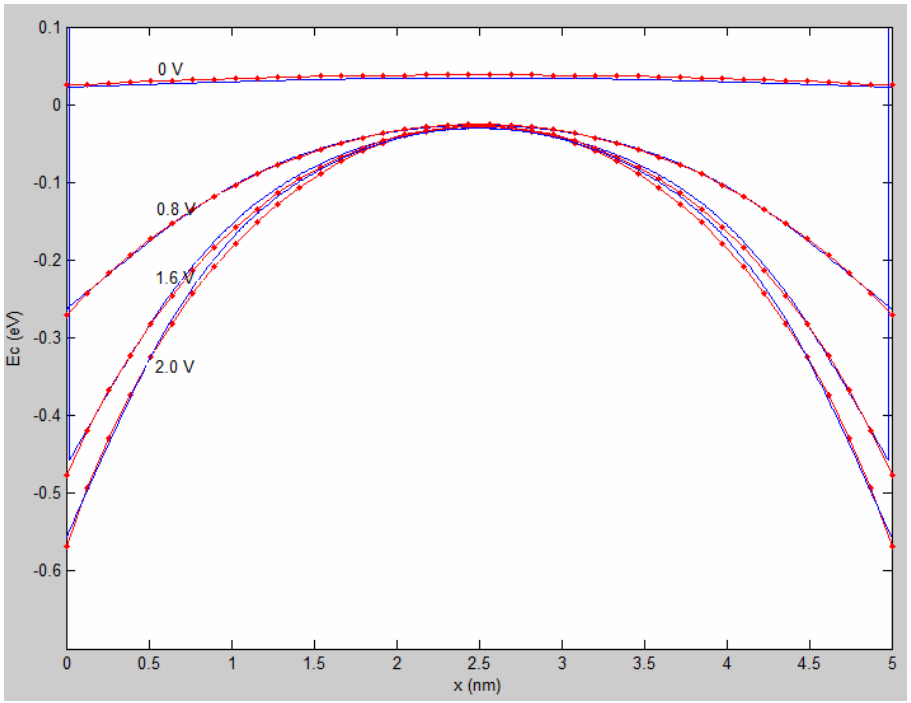

Figure 2. Conduction band profile in a 5 nm silicon film for different applied gate voltages. The continuous lines correspond to self-consistent Poisson-Schrodinger solutions (SHRED) and the dotted lines are derived from our model.

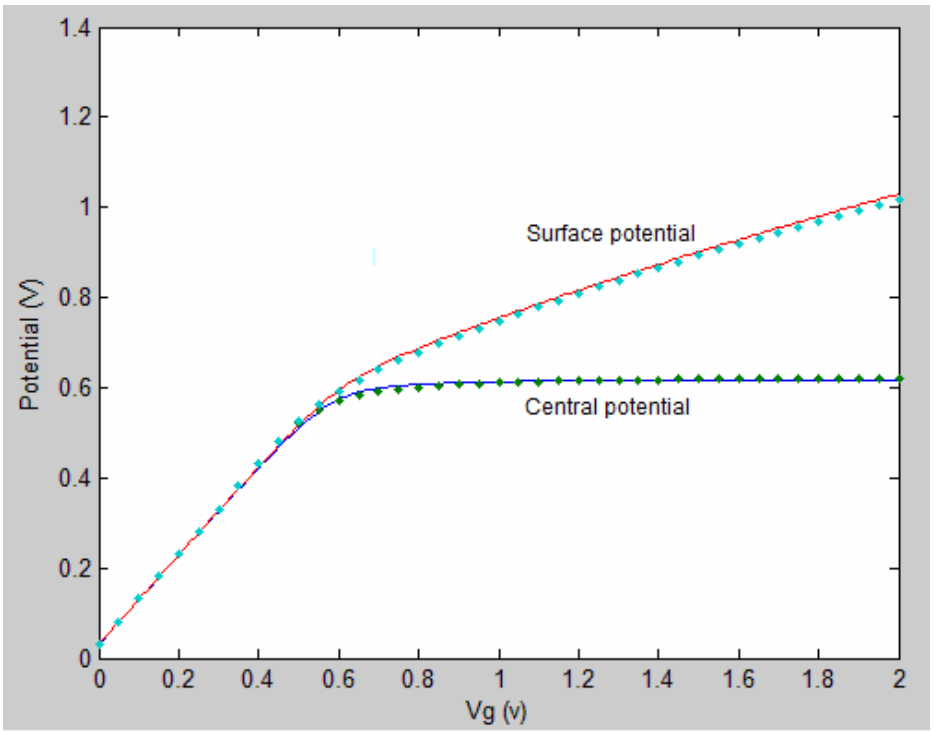

Figure 3. Surface and central potentials as a function of gate voltage. The continuous lines are self-consistent Poisson-Schrodinger solutions (SHRED) and the points are derived from our model.

ATOMIC FORCE MICROSCOPY AND ELECTROCHEMICAL STUDIES OF PALLADIUM NANOPARTICLES AND NANOWIRES ELECTRODEPOSITED ONTO CARBON ELECTRODE SURFACES

*Ana-Maria Chiorcea Paquim, Oana Corduneanu, Victor Constantin Diculescu, Ana Maria Oliveira Brett**
Departamento de Química, Universidade de Coimbra, 3004-535 Coimbra, Portugal
**brett@ci.uc.pt*

In situ and *ex situ* atomic force microscopy (AFM) and voltammetry were used to study nanoparticles and nanowires of palladium electrodeposited on the surface of two carbon electrodes: highly oriented pyrolytic graphite (HOPG) and glassy carbon [1]. The morphology, size, shape and distribution of the palladium nanostructures are influenced by the electrodeposition parameters, the concentration of the precursor solution and the topography of the carbon substrate, with potential applications in nanotechnology.

Reducing the rate of growth of the Pd(0), using underpotential deposition and decreasing the concentration of the palladium plating solution, the dimensions and the shape of the Pd(0) nanowires can be controlled. As a result, the underpotential deposition process is a simple procedure for the production of thick uniform palladium nanowires under ambient conditions of pressure and temperature, Fig. 1A. On the contrary, the formation of small Pd(0) nanoparticles with a uniform distribution over the electrode requires fast electrodeposition that can be achieved by overpotential deposition and high Pd^{2+} concentration in solution, Fig. 1B.

The growth of the Pd oxide layer begins at negative potentials with the formation of a palladium oxide pre-monolayer film. This phenomenon is strongly dependent on the size and morphological characteristics of the Pd(0) nanostructures existent on the surface of the electrode, relevant for palladium electrocatalysis. At high positive potentials, the Pd(0) nanoparticles and nanowires undergo oxidation leading to the formation of a mixed oxide layer, which in turn may act as nucleation points for additional Pd metal growth, increasing the metal electrode surface coverage.

References:

[1] V. C. Diculescu, A.-M. Chiorcea-Paquim, O. Corduneanu, A. M. Oliveira Brett, J. Solid State Electrochem., **11** (2007) 887.

Figures:

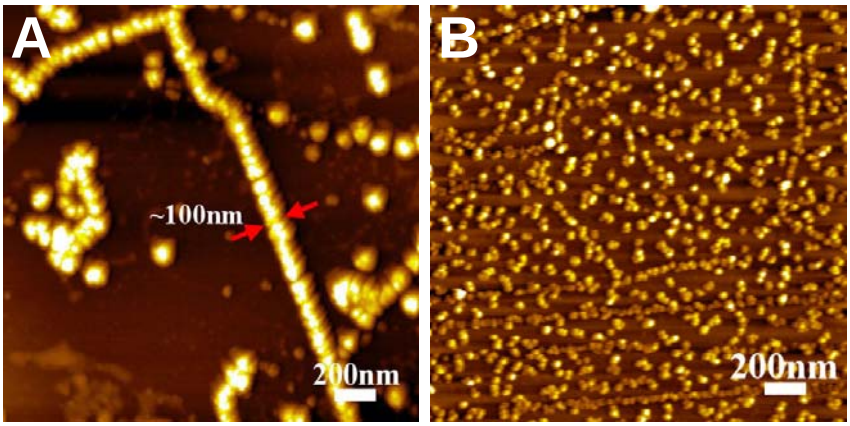

Fig. 1 AFM topographical images of Pd(0) deposited on the HOPG during 30 min, from solutions of **(A)** 0.1 mM $PdSO_4$, at –0.45 V and **(B)** 1.0 mM $PdSO_4$, at –1.00 V.

Single Molecule and Ensemble Fluorescence Lifetime of a Proton Transfer Dye Encapsulated in the Zeolite MCM-41 Nanochannels

Boiko Cohen, Juan Angel Organero, Abderrazzak Douhal
Departamento de Química Física, Sección de Químicas, Facultad del Medio Ambiente, UCLM, 45071 Toledo, Spain
boyko.koen@uclm.es

Studies by our group on the excited state dynamics of guest molecules encapsulated in various nanohosts have contributed to the characterization of the confinement effect.[1-3] Of these the interactions within the zeolite nanocavities are least characterized. Mesoporous silicate networks have many applications ranging from medicine[4] and photonics[5-6] to catalysis. It is of great importance to gather knowledge regarding the behavior of a chromophore encapsulated in zeolite nanocavity on single molecule level. In this presentation, we report on the results of single molecule confocal microscopy studies of fluorescence lifetime of a proton transfer dye absorbed to the inner surface of amorphous silica and mesoporous structured silicate, MCM-41. A representative image, the photobleach fluorescence trace and the derived monoexponential decay of such complex is presented in Figure 1. Its photophysical properties were investigated using single molecule confocal microscopy technique. We compare the results from single molecule emission studies of the dye, chemically bound to the zeolite framework using the ship-in-a-bottle technique, and the same dye encapsulated by free diffusion and interaction with the zeolite nanocavities. We were able to isolate single lifetime distribution arising from single molecule-zeolite complexes prepared by the ship-in-a-bottle technique whereas the system prepared by free diffusion and interaction with the zeolite framework has three individual lifetime distributions. These we assign to three separate single molecule-zeolite complexes. This assignment is confirmed by additional studies on the single molecule behavior of the proton transfer chromophore covalently bound to silica. We further report on the effect of chemical modification to the zeolite framework on the excited state behavior of a single zeolite-encapsulated chromophore.

Acknowledgements: This work was supported by the MEC and JCCM through the projects: CTQ-2005-00114/BQU, UNCM05-23-025 and PCI08-0037-5868. BC acknowledges MEC for the Ramon y Cajal fellowship

References:

[1] A. Douhal, *Chem. Rev.* 2004, 104, 1955.
[2] A. Douhal, *Acc. Chem. Res.* 2004, 6, 349
[3] A. Douhal, Editor, "Cyclodextrin Materials Photochemistry, Photophysics, and Photobiology", Elsevier, Amsterdam, 2006,ISBN-13: 978-0-444-52780-6.
[4] K. Pavelic, M. Hadzija, *Handbook of Zeolite Science and Technology*, 2003,1141
[5] G. Calzaferri, S. Huber, H. Maas, C. Minkowski, *Angewandte Chemie, International Edition* 2003, 42, 3732.
[6] A. Corma, *Journal of Catalysis* 2003, 216, 298.

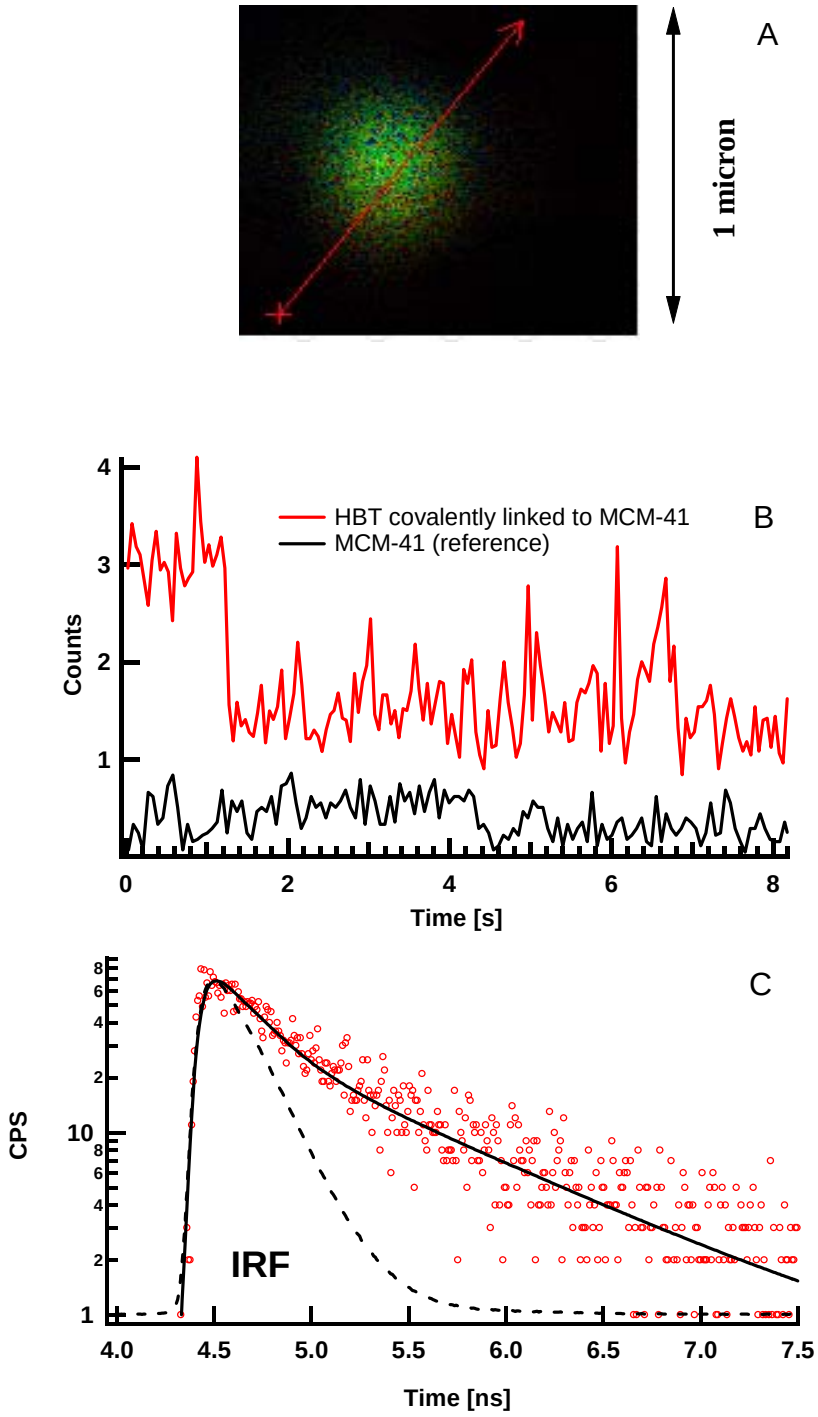

Figure 1. A) Fluorescence image of the studied single molecule dye covalently linked to the MCM-41 framework, B) representative single step fluorescence photobleach transient and C) representative monoexponential TCSPC signal (red circles) derived from the single step fluorescence photobleach trace along with the model fit (full line) and the IRF (dashed line).

ADDRESSING THE IMMUNE SYSTEM: MACROPHAGES RESPONSES TOWARDS AU NANOPARTICLE CONJUGATES.

Neus G.Bastus[2], Ester Sánchez-Tilló[3], Silvia Pujals[4],Consol Farrerra[3], Joan Comenge[1,2]Marcelo Kogan[4], Ernest Giralt[4], Antonio Celada[3], Jorge Lloberas[3] and Victor Puntes[2,5]

[1]International Iberian Nanotechnology Laboratory , Braga, Portugal
[2] Institut Català de Nanotecnologia, Campus UAB, Barcelona, Spain.
[3] Macrophage Biology Group, IRB, Barcelona, Spain.
[4] Design Synthesis and Structure of Peptides and proteins, IRB, Barcelona, Spain.
[5] Institut Català de Recerca i Estudis Avançats

victor.puntes@icrea.es

There has been a rapid proliferation of technologies based on nanoparticle (NP) conjugates for diagnostic and therapeutic uses in biomedicine, and some of them are at different stages of preclinical development. Such advances require an in-depth understanding of NP evolution in biological media as well as of their specific interaction with cells and living systems. This is particularly true for the immune system, which is responsible for maintaining body integrity and preventing external invasion.

The first line of defence, typically triggering a protective inflammatory response within minutes, is carried out by the innate immune system. The key feature of innate immune cells enabling them to detect and categorize infection is their repertoire of pattern-recognition receptors (PRRs), which bind certain general types of molecules expressed by broad classes of pathogens. In fact, what seems to distinguish a pathogen as non-self by the innate immune system cells is the structural conformation and spatial distribution of its molecules and not the recognition of specific protein sequences.

Based on these principles, we used Au NP conjugates as scaffolds for biomolecules to test the response of macrophage cells. These cells play key roles in the innate (phagocytosis) and adaptive immune system (stimulation of lymphocytes). In order to analyze the activation of bone marrow macrophages, production of pro-inflammatory cytokines (TNF-α, IL-1β, and IL-6) as well as the induction of nitric oxide synthase were measured by Real-Time PCR after exposure to Au NP conjugates and controls. In addition, activation of macrophages was also measured analyzing the inhibition of proliferation. Both experiments indicate that Au NP-peptides conjugates induce macrophage activation while neither the peptide nor the citrate-coated nanoparticles do activate macrophages, even at concentrations thousand times higher, showing the biological relevance of conjugation.

The observed macrophage activation occurs concomitantly with that of Toll-like Receptor 4 (TLR 4) which is described to be involved in the recognition of Lipopolysaccharide (LPS) or Heat Shock Protin 60 (HSP60) from bacteria. The activation of macrophages via TLR 4 was confirmed by the absence of activation when macrophages came from a knock-out strain unable to express TLR4. If TLR4 is required for nanoparticle-mediated activation, it is critical to exclude LPS contamination. We discarded the possible presence of LPS by using a Limulus Lysate

assay and polymyxin B. Thus, while LPS-inhibited proliferation is reversed in the presence of PMB, we detected no similar changes in the proliferation of AuNP-peptide conjugates, thus indicating that their effect was not due to LPS contamination.

Moreover, it has been suggested that TLR4 activation results in the onset of phagocytosis and Au NP-peptide conjugated internalization. The presence of Au NP in vesicles within short time frames indicates that they are internalized actively via specific receptors, rather than a passive mechanism such as pinocytosis. No NP were observed when they have not been conjugated to peptides

All in all helps determine a small number of principles that should be taken into account when working with nanomedical devices in vivo.

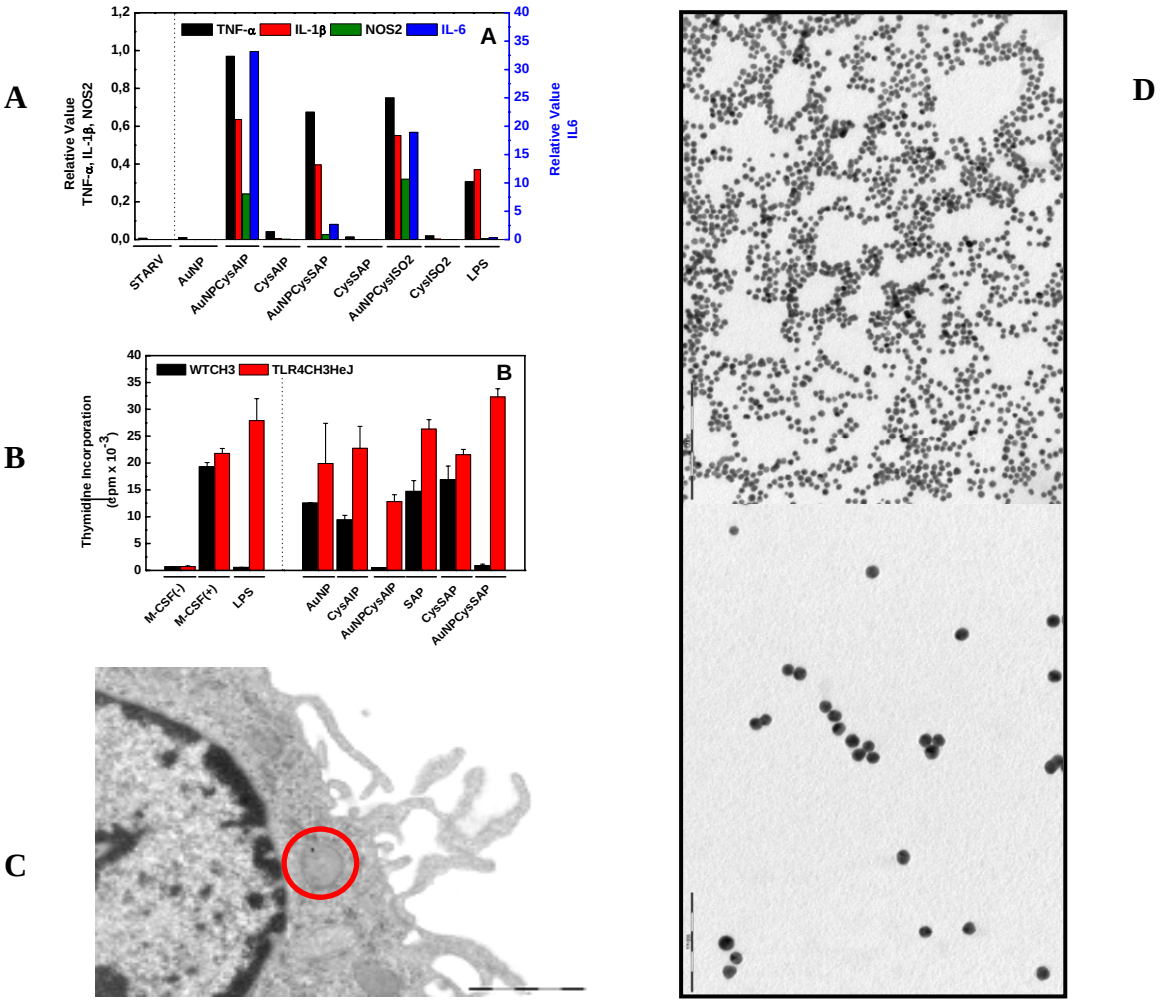

A: mRNA levels (as measured by real-time PCR) of TNF-α, IL-1β, IL-6 and NOS2 in relation to β-actin of macrophages stimulated for 6 hours with LPS.
B: Macrophages from WT C3H and mutant TLR4 C3H/HeJ mice were stimulated with different substances, and proliferation was determined
C: TEM image of macrophage revealing internalization at 6 hours
D: TEM images of citrate-coated gold nanoparticles. The bar indicates 200 nm (up) and 100nm (down).

Cellular Automata Model for Controlling Supercooling: NanoBioTechnology Perspective into CryoPreservation of Living Tissues

R.C. Martins[1,2,a], V.V. Lopes[1,3], A.C.F. Ferreira[1,4], A.A. Vicente[1,5], J.A. Teixeira[1,5]

[1] Portuguese Complexity and NanoBioTechnology Research Network
[2] Molecular Biology Research Centre - University of Minho
[3] Institute for Systems and Robotics - Technical Institute of Lisbon
[4] Biotechnology Research Center - Interface A4 - Catholic University
[5] Institute for Biotechnology and BioEngineering - University of Minho

[a]email: rui.martins@deb.uminho.pt

Abstract

Cryopreservation of biological materials is essential for BioTechnology. The ability of stopping the metabolic activity in living tissues is an important step forward which opens new frontiers to biotechnology, from nano-agriculture to nano-medicine. Traditional cryopreservation systems enhance vitrification using cryoprotectants, which in most cases are detrimental and toxic, not allowing the full potential of the technology in susceptible areas such as in food, tissue engineering and biomedical applications. Recent discoveries of the Mpemba effect and its mechanics at the nano-scale level lead to new possibilities for controlling the structure of water inside biological materials without cryo-preservatives. Once controlling the supercooling of water, Nano-biotechnology can shut down biochemical networks and preserve living tissues for long storage periods without the damage provoked by ice crystals growth or the chemical toxicity of cryoprotectants. In this research paper we present the theoretical foundations of supercooling control and some results obtained with food systems.

1. Introduction

Cryopreservation pretends to preserve living tissues by shutting down the biological machinery, without damaging the same molecular devices. Traditional technology fails due to: i) ice crystals growth and recrystallization; ii) dehydration; and iii) toxicity from cryoprotectants (e.g. dimethyl sulfoxide). The hope for cryogenics in BioTechnology is that somehow future NanoBiotechnology repairs the biological machinery (e.g. tissue reconstruction). Nevertheless, a new insight is gained when is possible to understand how to manipulate the structure of water by its non-linear and complex intrinsic properties [1]. The structure of liquid water affects significantly the nucleation process. Liquid water is formed mainly by clusters of molecules in equilibrium between an expanded structure (ES) and a collapsed structure (CS) [2], presenting a density peak at $+3.984^oC$. Below, ES is predominant and the free volume is reduced. At higher temperatures, free volume expands and CS predominates [3]. The expansion of ES cluster is only thought possible until the homogeneous nucleation temperature (-45^oC), due to an expansion limit which induces the breaking of hydrogen bounds [4]. Therefore, thermodynamic conditions that allow the predominance of the ES structure enhances large supercoolings, and more ES clusters need to be broken, larger SC are obtained [5]. In this research paper, we show how to maximize the ES cluster structure by maximizing the supercooling effect in frozen strawberries and modelling the Mpemba effect by a cellular automata.

2. Results and Discussion

Thermal energy propagation by lattice vibrations, molecular motion and orbital interactions is considerably faster than the establishment and disaggregation of the hydrogen bounds involved during liquid-solid phase change. Thus, it is possible to remove heat from liquid water in foods at a faster rate, than it can nucleate or crystallize, generating supercooling. Therefore, water structure can be manipulated by changing the way heat is transfered, in order to minimize the heat released during nucleation, which contributes to the expansion of the structure of surrounding supercooled water. By increasing the ES clusters number, it is possible to decrease the probability of nucleation, since to form a nucleus, more water molecules are needed, and therefore, one can begin to consider that nucleation occurs at random inside a thermal restriction interval. An important concept is that nucleation at nodes j and k does not occur during thermal compression ($ES \rightarrow CS$) (see Figure 1), but rather by thermal expansion ($CS \rightarrow ES$), which may influence the size and shape of ice crystals, depending upon the obtained nucleation temperature. The minimum nucleation temperature (maximum supercooling) was assumed

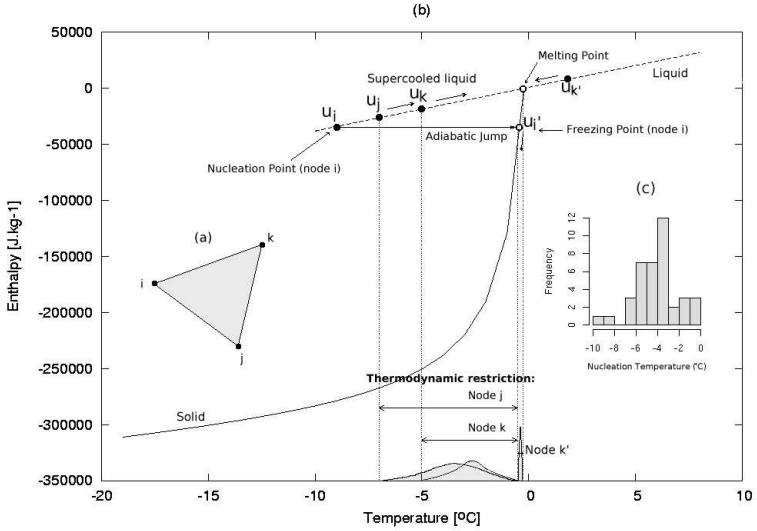

Figure 1: Thermodynamic restriction to nucleation inside a finite space: (a) finite space; (b) enthalpy diagram; and (c) histogram of the surface nucleation temperature

to occur near the surface. The initial nucleation temperature at any point of the physical domain was assumed to depend mostly on the ES and CS distribution, which is directly related to the initial temperature. After the nucleation of a point in space, the temperature at adjacent space tends to increase, where as at node k tends to decrease. As in the last case, node j nucleates by thermal expansion, being its nucleation interval inside $[u_j, u'_i]$. Node k nucleates by thermal compression (see Figure 1).

3. Conclusions

Results show that nucleation across a physical domain is predictable by using a CA with thermodynamic restrictions [1]. Such opens the possibility of maximizing the ES of liquid water cluster, preventing nucleation until a point where vitrification is inevitable. Experimental and simulation results show that the trick is to decrease the temperature of liquid water, maintaining low temperature gradients and stabilizing the expansion of water. Yet, the best results are obtained with initial temperatures just below the water maximum density point [6]. This research work we can already minimize the use of cryoprotectants by maximizing the supercooling effect. In the future, nanotechnology ultimate goal is to stabilize ES water cluster hydrogen bonds in order to inhibit nucleation.

References

[1] R. C. Martins and V. V. Lopes. Modelling supercooling in frozen strawberries: Experimental analysis, cellular automation and inverse problem methodology. *Journal of Food Engineering*, 80(1):126–141, 2007.

[2] H. Tanaka. Simple physical model of liquid water. *Journal of Chemical Physics*, 112:799–809, 2000.

[3] M. F. Chaplin. A proposal for the structuring of water. *Biophysical Chemistry*, 83:211–221, 1999.

[4] C. A. Angell, R. D. Bressel, M. Hemmati, E.J. Sare, and J.C. Tucker. Water and its anomalies in perpective: tetrahedral liquids with and without liquid-liquid phase transitions. *Physical Chemistry Chemical Physics*, 2:1559–1566, 2000.

[5] S. Büchner and A. Heuer. Metastable states as a key to the dynamics of supercooled liquids. *Physical Review Letters*, 84:2168–2171, 2000.

[6] R.C. Martins and V.V. Lopes. Maximising the supercooling effect in frozen strawberries. *Submitted*, 2008.

TiO_2 AND CdS NANOPARTICLES OBTAINED FROM SOFT TEMPLATING METHODS

Paulo J. G. Coutinho , Arlindo Garcia, Teresa V. Reis, Cândido Mendes, Teresa Barbosa
Centro de Fisica, Universidade do Minho, Portugal, 4710-057 Braga
pcoutinho@fisica.uminho.pt

Nanotechnology is a field of very active investigation. There is a wide scope of technological applications ranging from photocatalysis and sensors to fluorescence imaging. In this work, semiconductor nanoparticles are prepared by soft templating methods using the aqueous cavities of microheterogeneous media. We have used two main methods. In the first one (M1), adapted from Pileni et al [1], the spherical cavities of w/o microemulsions (reverse micelles) are used as templates. In the other (M2), a new method based in gel electrophoresis is used in which the metal ions and the corresponding anions, migrate under an electric field in opposite directions until they meet and react within the gel pores [2]. Method M1 was used for CdS and TiO_2 nanoparticles using either negative (AOT - sodium bis(2-ethylhexyl) sulfosuccinate), positive (CTAB – Cetyltrimethylammonium Bromide) or neutral (Brij®56 – polyoxyethylene 10 cetyl ether) surfactants. CdS nanoparticles were passivated with suitable capping agents. TiO_2 and CdS nanoparticles were successfully deposited as Langmuir-Blodgett films in glass slides. The obtained coated slides have photocatalytic properties as shown in figure 1.

The size dependence of CdS electronic states was obtained by a tight binding approximation [3]. Using these theoretical results, in conjunction with a size distribution and a Mie formalism for the scatter/absorption of nanoparticles of a given size, we were able to fit the experimental absorption and excitation spectra of CdS nanoparticles, either in AOT reversed micelles or in dried gels. In the case of AOT templating, the resulting particles should be spherical and the calculated average sizes can be compared to those obtained using empirical relations between first absorption peak and nanoparticle size proposed by Yu et al [4]. In the gel electrophoresis templating experiments, the effect of excess concentration of one of the ions, the presence of SDS surfactant and the type of gel, were found to influence the size distribution of the CdS nanoparticles and the corresponding photoluminescence spectra. (figure 2).

References:

[1] Cizeron, M. P. Pileni, J. Phys. Chem. **99** (1995) 17410.
[2] Paulo J.G. Coutinho, Candido A. G. Mendes, Teresa S. V. Reis, NYAS, in press.
[3] V. A. Fonoberov et al., Phys. Rev. B 66 (2002) 085310.
[4] W. William Yu et.al., Chem. Mater. 15(14) (2003) 2854.

Figures:

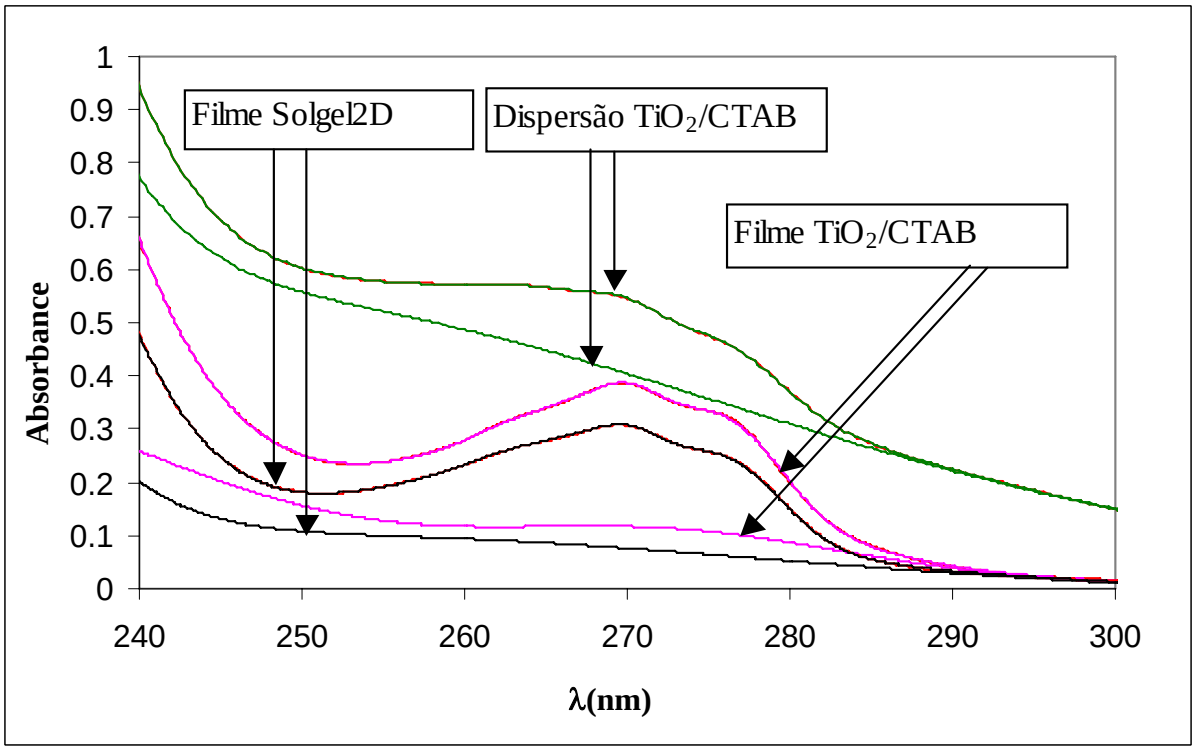

Figure 1: Photodegradation of phenol using TiO_2 nanoparticles.

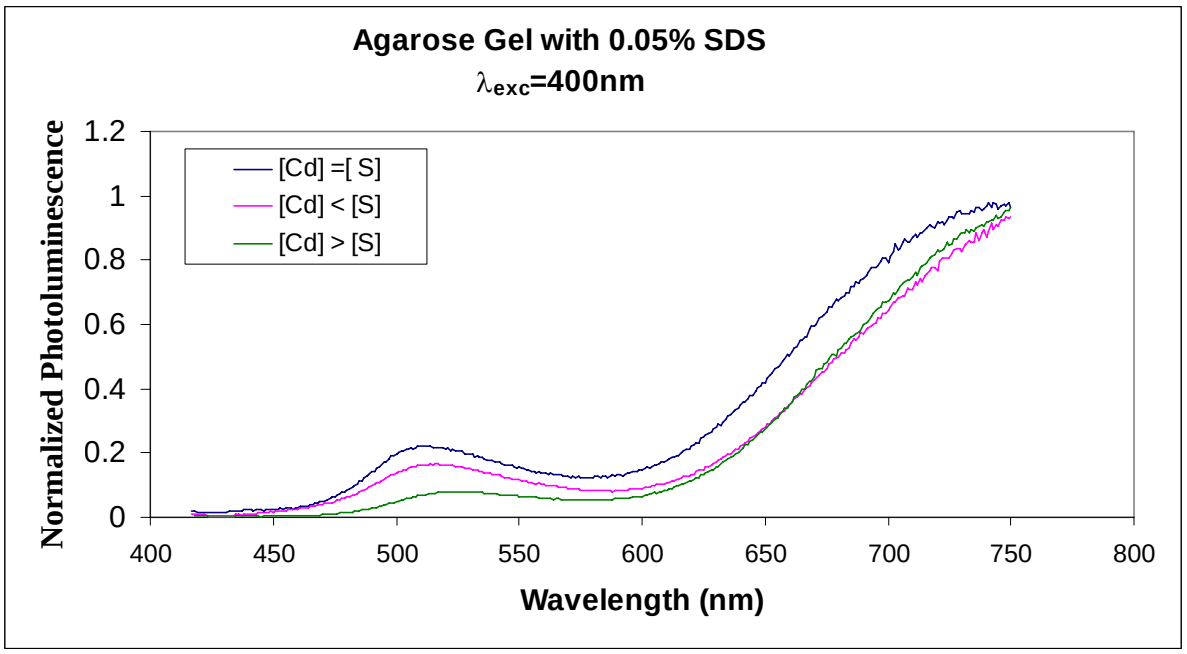

Figure 2: Photoluminescence of CdS nanoparticles obtained from templating with agarose gel electrophoresis.

NANO-COMPOSITE MATERIALS OBTAINED USING NANO-MAGNETIC FLUIDS AND RESINS

Nicolae CRAINIC[1], Doina BICA[2], Antonio TORRES MARQUES[3], Nicolae Calin POPA[2], Paulo J. NOVOA[4], Nuno CORREIA[4], Oana MARINICA[1], Carlos Pinto MOREIRA DE SA[5] and Ladislau VEKAS[2]

[1] "Politehnica" University of Timisoara, National Center for Engineering of Systems with Complex Fluids (NCESCF); e-mail: ncrainic@flumag2.mec.utt.ro
[2]Romanian Academy – Timisoara Branch, Center for Advanced and Fundamental Technical Research (CAFTR);
e-mail: vekas@acad-tim.tm.edu.ro, ncpopa@acad-tim.tm.edu.ro
[3] Universidade do Porto, Faculdade de Engenharia da Universidade do Porto (FEUP),
e-mail: marques@fe.up.pt
[4] Instituto de Engenharia Mecanica e Gestao Industrial (INEGI), Unidade de Materiais Compositos (CEMACOM), Porto, Portugal;
e-mail: prnovoa@inegi.up.pt, nuno.correia@inegi.up.pt
[5] Universidade do Porto, Centro de Materiais da Universidade do Porto (CEMUP), Porto, Portugal; e-mail: cmsa@cemup.up.pt

The paper presents the possibility to create a new category of nano-magnetizable composite materials, using nano-magnetic fluids (ferrofluids) and resins ([1]). The target of these investigations is to obtain new materials having magnetic controllable properties.

The use of MNF as one of the basic components of the nanocomposite manufacturing process enables a simple fabrication procedure. The magnetic nanoparticles are stably dispersed in a resin compatible volatile carrier, such as methyl-ethyl-ketone (MEK) or ethylic ether (EE)([2]). Mixing this MNF with the resin while keeping the colloidal stability of the fluid state composite, the magnetic nanoparticles will be well dispersed in the resin matrix .([1]).

The polymerization process took place with and without magnetic field. The research was focused on the compatibility between the various types of nanomagnetic fluids and resins. Samples were prepared varying the resins, carrier liquids and volume fraction of magnetic nanoparticles.

Results of investigations presented in this paper refer to the microstructure of the samples (optical and/or electronic microscopy), and to the mechanical properties corresponding to different preparation methods (three points bending test, elastic properties, gel time determination). ([3]).

[1] N. Crainic, A. T. Marques, D. Bica, L. Vekas, P. J. Novoa, C. P. Moreira de Sa, **Mol. Cryst. Liq. Cryst.**, Vol. 418 (2004) pp. 29/[757] – 40/[768].
[2] Bica, D., Vékás, L. and Rasa, M. (2002), **Journal of Magnetism and MagneticMaterials**, Vol. 252, pp.10–12.
[3] N. Crainic, Doina Bica, A. Torres Marques, N. C. Popa, P. J. Novoa, N. Correia, Oana Marinica, C. P. Moreira de Sa, L. Vékás, **Proceedings of the 4-th International Symposium on Nanomanufacturing, ISNM2006**, Cambridge, November 1 - 3 (2006) MA USA, pp. 70 – 75.

TARGETING NANOPROBES FOR EARLY INVASIVE CANCER CELLS USING HEREDITARY DIFFUSE GASTRIC CANCER (HDGC) AS A MODEL.

Cristiana Cunha[1,2], Pedro Granja[2], Gianpaolo Suriano[1], Carla Oliveira[1] and Raquel Seruca[1]

[1] IPATIMUP – Instituto de Patologia e Imunologia Molecular da Universidade do Porto, Rua Dr. Roberto Frias s/n, Porto, PORTUGAL

[2] INEB – Insituto de Engenharia Biomédica da Universidade do Porto, Rua do Campo Alegre 823, Porto, PORTUGAL

ccunha@ipatimup.pt / ccunha@ibmc.up.pt

Introduction

The present work aims to improve early detection and disease prognosis in individuals at risk of hereditary diffuse gastric cancer (HDGC). For that purpose, we aim at identifying molecular markers specifically upregulated in invasive cancer cells, which will then be incorporated in nanoparticles designed to target diseased cells to improve disease diagnosis and prognosis.

The emerging field of Nanomedicine has been attracting unprecedented attention since nanostructures provide the means for monitoring cellular and molecular processes in vivo, in real time, with improved sensitivity and resolution. Nanoparticles can reach locations in the body of difficult access due to their reduced size and provide more convenient administration routes. Novel multifunctional nanoparticles can be engineered to target and diagnose a specific tissue or cell, to cross biological barriers, and be additionally combined with a pharmacological agent for applying therapy at early stages of the disease.

Improvements in the treatment of cancer have been slow mainly due to poorly predictable models, and lack of tumor targeting specificity and of effective cellular and intracellular delivery. Methods to increase local drug concentration at the tumor while lowering the systemic dose, coupled with the ability to kill only cancer cells while affecting as few healthy cells as possible, would result in more efficient treatments with fewer side effects..Hereditary Diffuse Gastric Cancer (HDGC) is a rare but devastating cancer susceptibility syndrome. It has been identified E-(epithelial) Cadherin germline mutations in families with HDGC, and pathology studies showed the presence of early invasive (intramucosal) diffuse carcinoma, without the presence of pre-malignant lesions, in all gastrectomy specimens performed to date in those patients. At the moment, prophylactic gastrectomy is still the best (and only) clinical approach, since endoscopic screening techniques are shown to be ineffective for surveillance of E-Cadherin mutant carriers. Therefore, the development of reliable screening methods for early detection, disease prognosis and continuous follow-up of these patients, is urgent.

Experimental

In a first approach we compared the expression profile, by cDNA array analysis, of two non-expressing E-Cadherin cell lines (MDA-MB 231 and MDA-MB 435) transduced with two E-Cadherin missense mutations (T340A and V832M) and with wild-type E-Cadherin, as control, in order to identify differentially expressed membrane proteins in mutant cells that could be used as molecular markers for primary diffuse gastric carcinoma. CD44 emerged as a differentially expressed protein in cells transduced with mutants of E-cadherin.

CD44 undergoes extensive alternative splicing, a process which is commonly dysregulated in neoplasic cells. CD44 gene contains ten variable exons (v1-v10) that can be spliced to generate (theoretically) hundreds of different protein isoforms, some of which have already been shown to be upregulated in neoplasia. If proved to be neoplastic-specific, some of these CD44 isoforms might constitute a potential biomarker as well as a target for therapeutic approaches.We selected a panel of six gastric cancer cell lines (NCI-N87, AGS, MKN45, MKN28, KATO-III and SNU-1) and one breast cancer cell line (MCF7), as well as normal gastric and breast tissue, for comparison. We amplified and cloned the entire variable region of the CD44 gene from all cell lines and normal tissues. We characterized all CD44 transcripts expressed by each one by sequencing. MKN28 cell line was used as a negative control since CD44 expression is silenced by promoter hypermethylation.SNU-1 cell line, also did not present any CD44 expression.

We observed that KATO-III and MKN45 E-Cadherin mutant gastric cancer cell lines harboured common aberrant CD44 transcripts which were absent in all other cell lines and normal tissues.

We hypothesize that this abnormal splicing profile could be used to target specific regions of the CD44 extracellular domain in E-Cadherin mutant cell lines, and to recognize tumor cells of diffuse gastric carcinoma with E-Cadherin mutations. In order to validate the neoplasic specificity of these CD44 transcripts further studies need to be performed.

MAGNETIC POLYSACCHARIDE NANOSPHERES WITH POTENTIAL FOR BIOMEDICAL APPLICATIONS: PREPARATION VIA A REVERSE MINIEMULSION METHOD

A.L. Daniel-da-Silva, T. Trindade, B.J. Goodfellow, A.M. Gil
University of Aveiro, Department of Chemistry, CICECO, Campus Universitario de Santiago, 3810-193 Aveiro, Portugal
ana.luisa@ua.pt

Magnetic polymeric supports such as micro- and nanospheres have attracted increasing interest in the last few years due to their potential for applications in biology and medicine, such as cell isolation, protein immobilization, targeting drug delivery and clinical diagnosis [1]. For use in biomedical applications, magnetic polymer nanospheres need to fulfill some requirements: biocompatibility, narrow size distribution and high density of reactive surface groups for the coupling of active biomolecules. In addition, nanospheres should have high and uniformly dispersed magnetic content with superparamagnetic behavior. In our previous work [2] κ-carrageenan, a non-toxic sulphated polysaccharide has been successfully employed as a colloidal stabilizer in the in-situ synthesis of superparamagnetic magnetite nanoparticles, preventing their spontaneous agglomeration and conferring biocompatibility to the resulting composite. Moreover, the resulting ferrofluid, that contained magnetite nanoparticles prepared by co-precipitation within the κ-carrageenan under alkaline conditions, could undergo gelation under cooling conditions due to the gelling properties of this biopolymer.

In this work, taking advantage of the ability of the ferrofluid to form gels, composite nanospheres consisting of magnetite nanoparticles embedded in a κ-carrageenan matrix have been prepared for the first time, using reverse miniemulsions. The reverse miniemulsions were obtained by sonication of a quaternary system comprising n-heptane as the organic phase, cetyltrimethylammonium bromide (CTAB) as surfactant and 1-butanol as the co-surfactant. The aqueous phase consisted on the ferrofluid containing the biopolymer and magnetite nanoparticles (d~8nm). The stability of the miniemulsion was seen to be affected by the fine composition of the aqueous phase, namely by the concentration of alkali-metal cation added for magnetite precipitation.

Using the method outlined above, stable miniemulsions containing the magnetic polymeric fluid as aqueous phase were successfully obtained. The spherical morphology of the resulting polymer nanocomposites was confirmed by scanning electron microscopy (SEM), with particles showing an average diameter of 75 nm (Fig.1). DLS measurements have shown larger sizes than SEM probably due to some magnetic interaction of the spheres to form aggregates in solution. The control of the average size of the nanospheres was seen to be possible upon the variation of the concentration of surfactant. Furthermore, magnetic measurements have shown that magnetite nanoparticles are superparamagnetic at ambient temperature (Fig. 2).

The resulting composites are, therefore, of potential interest for several biomedical applications. Since κ-carrageenan forms thermoreversible gels, the controlled release of magnetic particles or loaded drugs can be envisaged by both thermal and magnetic stimuli. In addition, carrageenan can be further functionalized for the conjugation of biomolecules on the surface of the nanospheres, which is the subject of ongoing work.

References:

[1] U. Hafeli, W. Schutt, J. Teller, M. Zborowski, Scientific and Clinical Applications of Magnetic Carriers, Plenum, New York, 1997.
[2] A.L.Daniel-da-Silva, T. Trindade, B.J. Goodfellow, B.F.O. Costa, R.N. Correia, A.M. Gil,

Biomacromolecules, **8** (2007), 2350.

Figures:

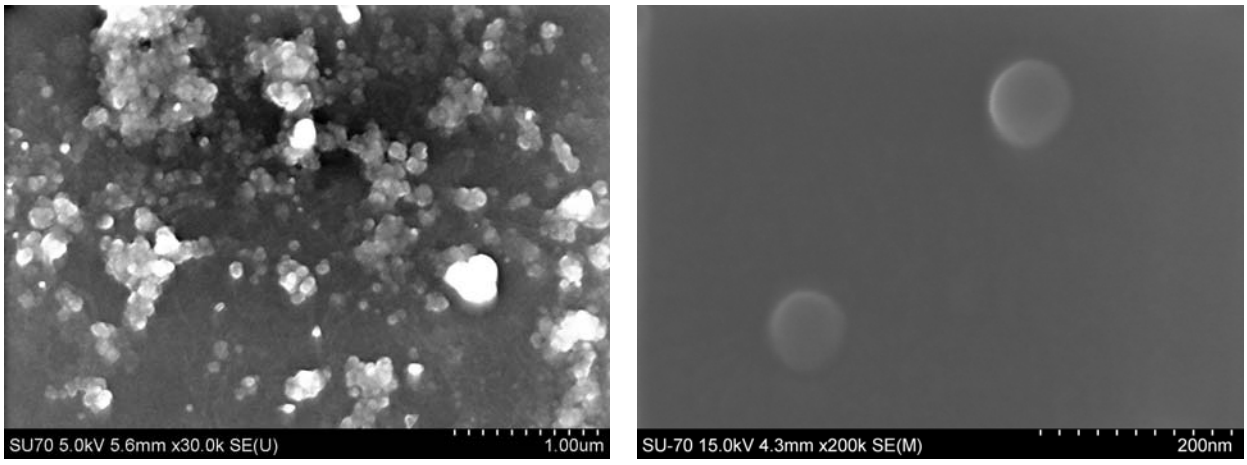

(a) **(b)**

Figure 1. SEM images of magnetic nanospheres at different magnification (a) 30,000×; (b) 200,000×.

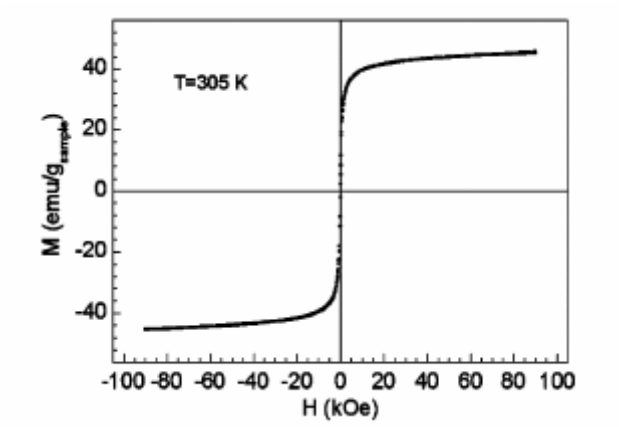

Figure 2. Magnetization as function of magnetic field at 305K.

Nanoscale periodicity in stripe-forming systems at high temperature the Au/W(110) system

J. de la Figuera, F. Léonard, N. C. Bartelt, R. Stumpf, and K. F. McCarty

Insituto de Química-Física "Rocasolano", CSIC, Madrid 28006
Universidad Autónoma de Madrid, Madrid 28049
Sandia National Laboratories, Livermore, CA 94550
juan.delafiguera@iqfr.csic.es

It has been known for many years that self-assembled stress domain patterns can occur on solid surfaces. These patterns arise from the competition between the short-range attractive interaction between atoms, leading to a phase-boundary energy, and a long-range repulsive interaction between boundaries, due to the difference in surface stress between the two phases. This repulsion is mediated by elastic deformations of the substrate. So far, such stress-domain patterns have been observed and quantified in the low-temperature sharp-interface regime, where the interfaces between the two separated phases are abrupt[1, 2]. Theories of pattern formation at crystalline surfaces have focused mainly on this sharp-interface regime[3,4]. These theories predict an exponential dependence of the periodicity of the stress-domain patterns on the strength of the competing interactions. This implies that it should be possible to tune the periodicity over large ranges, but also that the predictive power of the models is limited in the absence of extremely accurate estimates of the interactions. However, as the temperature is increased the amplitude of the modulated pattern decreases. At sufficiently high temperature, the transition to a homogeneous phase occurs. We call this temperature the order-disorder transition (ODT). As the ODT is approached, the interface width is expected to increase, eventually becoming on the order of the stripe periodicity, making the sharp-boundary theory inappropriate. In this paper we present an experimental study of Au on W(110) which shows explicitly this breakdown.We compare the detailed measured temperature dependence with the mean-field theory of the ODT and argue that nanometer-scale periodicities should be much more common than one would expect from the low-T sharp-interface theory.

Experimentally, quantitative observations near the ODT are difficult because thermal fluctuations of boundaries typically destroy the long-range order of the pat-tern. Here we study stripe formation with long-range order in the system of Au on W(110). As first observed by Duden and Bauer[5, 6], submonolayers of Au on W(110) self-assemble into stripe patterns, which consist of monolayer-thick stripes of condensed-phase Au in coexistence with stripes of a Au adatom gas (see Fig. 1a). Because of strong surface anisotropy, the stripes in this system form along a particular crystallographic direction, [110], and we are able to use low-energy electron microscopy (LEEM) to measure the amplitude (related to the Au density[7]) and wavelength of the pattern as it approaches the ODT. We demonstrate that the amplitude decreases steadily with increasing temperature and vanishes at the ODT. The modulation wavelength also decreases with temperature, depends quadratically on the reduced temperature, but has a finite value of 100 nm at the ODT.

The experimental observations serve as evidence that Au stripes observed on W(110) at high temperature are in the diffuse-interface limit of surface stress domains,with a temperature and coverage dependence qualitatively different from the oft-applied sharp-interface limit. By comparing our results with theoretical calculations of the stripe periodicity, we predict that nanometer-scale stripe patterns should be common near two-dimensional critical points.

This research was supported by the Office of Basic Energy Sciences, Division of Materials Sciences, U.S. Department of Energy under Contract No. DE-AC04-94AL85000, by the Spanish Ministry of Science and Technology through Project No. MAT2006-13149-C02-02.

References:

[1] K. Kern et al., Phys. Rev. Lett. **67** (1991) 855 .
[2] R. Plass, J. A. Last, N. C. Bartelt, and G. L. Kellogg, Nature **412** (2001) 875.
[3] O. L. Alerhand, D. Vanderbilt, R. D. Meade, and J. D. Joannopoulos, Phys. Rev. Lett. **61** (1988) 1973.
[4] V. I. Marchenko, Sov. Phys. JETP **54** (1981) 605.
[5] T. Duden, Ph.D. thesis, Technischen Universität Clausthal, 1996.
[6] E. Bauer, in The many facets of metal epitaxy, edited by D. A. King and D. P. Woodruff (Elsevier, Amsterdam,1997), Vol. 3, Chap. 2, p. 46.
[7] J. de la Figuera, N. C. Bartelt, and K. F. McCarty, Surf. Sci. **600** (2006) 4062.

Figures:

The LEEM image shows the W(110) surface with several steps (wavy lines), with monolayer high islands of Au forming a striped pattern on the surface. The field of view is 7 μm.

SiO_2-CeF_3:Eu^{3+} NANO-GLASS-CERAMICS PREPARED BY SOL-GEL METHOD STRUCTURAL AND OPTICAL CHARACTERIZATION

J. del-Castillo[1], A. C. Yanes[1], J. Méndez-Ramos[2], J. J. Velázquez[2] and V. D. Rodríguez[2]

[1]*Dpto. Física Básica, Universidad de La Laguna, 38206 La Laguna, Tenerife, SPAIN*

[2]*Dpto. Física Fundamental y Experimental, Electrónica y Sistemas, Universidad de La Laguna, 38206 La Laguna, Tenerife, SPAIN*

fjvargas@ull.es

A great effort has been devoted in recent years to synthesize inorganic nanocrystals of controlled size and shape by using different methods due to the quantum confinement effects on their properties [1]. Lanthanide compounds have been extensively investigated in diverse applications ranging from high-performance luminescent displays, optical communications and biochemical probes to laser materials [2]. SiO_2 based glasses shows excellent durability and optical quality, although their large phonon energy increases the non radiative decay rate that reduces the luminescence efficiency. On the other hand, cerium fluoride (CeF_3) has been attracting increasing attention due to its technological importance as an inorganic scintillating crystal [3] presenting obvious advantages over other conventional scintillators in their high density, fast response and high radiation resistance. Furthermore, it is also an important fluorescent host material owing to its low vibrational energies and the subsequent minimization of the quenching of the excited state of the rare earth ions [4].

In that effect, oxyfluoride glass-ceramics with composition of $94.9SiO_2$-$5CeF_3$-$0.1Eu^{3+}$ (mol%), were prepared by hydrolysis of tetraethoxysilane (TEOS) in a similar way as Fujihara et al. [5]. The structural analysis has been carried out by means of X-Ray diffraction confirming the precipitation of hexagonal CeF_3 nanocrystals. Luminescent study has confirmed the incorporation of Eu^{3+} ions in the CeF_3 nanocrystals discerning the contribution to the spectra of the Eu^{3+} ions partitioned into the CeF_3 nanocrystals and those remaining in the glassy phase.

References:

[1] A.P. Alivisatos, Science **271** (1996) 933
[2] T. Jüstel, H. Nikol, C. Ronda, Angew. Chem., Int. Ed. Engl. **186**(1998) 3084
[3] K. Shimamura, E.G. Villora, S. Nakakita, M. Nikl, N. Ichinose, J. Cryst. Growth **264** (2004) 208.
[4] Z.L. Wang, Z.W. Quan, P.Y. Jia, C.K. Lin, Y. Luo, Y. Chen, J. Fang, W. Zhou, C.J. O'Connor, J. Lin, Chem. Mater. **18** (2006) 2030.
[5] S. Fujihara, C. Mochizuki and T. Kimura, J. Non Crist. Solids 244, 267 (1999).

Poster

STRUCTURAL CHARACTERIZATION AND LUMINESCENT STUDY OF TRANSPARENT NANOSTRUCTURED Eu^{3+} DOPED SOL-GEL DERIVED SiO_2-PbF_2 GLASS-CERAMICS

J. del-Castillo[1], A. C. Yanes[1], J. Méndez-Ramos[2] , J. J. Velázquez[2] and V. D. Rodríguez[2]

[1]*Dpto. Física Básica, Universidad de La Laguna, 38206 La Laguna, Tenerife, SPAIN*

[2]*Dpto. Física Fundamental y Experimental, Electrónica y Sistemas, Universidad de La Laguna, 38206 La Laguna, Tenerife, SPAIN*

fjvargas@ull.es

Transparent rare-earth-doped glass-ceramics have been widely studied for their promising application in various fields like colour display, optical data storage, sensor, and optical communication [1–2]. Oxyfluoride glass-ceramics have been studied as host materials for active optical ions because they combine the particular optical properties of these ions in fluoride hosts with the elaboration and manipulation advantages, high mechanical and chemical stabilities of oxides glasses [3]. SiO_2 based glasses shows excellent durability and optical quality, although their large phonon energy increases the non radiative decay rate. On the other hand, PbF_2 provides a low phonon energy environment for rare-earth ions that enhances their luminescent efficiency.

Thus, glass-ceramics with an oxyfluoride composition of $89.9SiO_2$-$10PbF_2$-$0.1Eu^{3+}$ (mol%), were prepared by hydrolysis of tetraethoxysilane (TEOS) in a similar way as Fujihara et al. [4]. Structural analysis has been carried out by means of X-Ray diffraction confirming the precipitation of cubic β-PbF_2 nanocrystals. Finally, luminescent study has confirmed the partition of Eu^{3+} ions in the PbF_2 nanocrystals.

References:

[1] M. Takahashi, M. Shojiya, R. Kanno, Y. Kawamoto, K. Kadono, T. Ohtsuki, N. Peyghambarian, J. Appl. Phys. 81 (1997) 2940.
[2] S.Q. Man, E.Y.B. Pun, P.S. Chung, Appl. Phys. Lett. 77 (2000) 483. [5] S.Q. Xu, Z.M. Yang, J.J. Zhang, G.N. Wang.
[3] M.J. Dejneka, J. Non-Cryst. Solids 239 (1998) 149.
[4] S. Fujihara, C. Mochizuki and T. Kimura, J. Non Crist. Solids 244, 267 (1999).

HIGHLY ORDERED CO NANOESTRUCTURES ARRAYS

W. O. Rosa, M. Jaafar, A. Jacas, A. Asenjo and M. Vázquez
ICMM-CSIC, Cantoblanco, 28049 Madrid, Spain

Different techniques have been used to obtain ordered magnetic nanostructures some of them based on self-organization process. In particular, our group has long experience in the fabrication of arrays of magnetic nanowires embedded in AAM (Anodic Alumina Membrane) [1] In addition, the AAM have been used to translate the ordering degree into different material following replica-antireplica process [2]. In this work, PMMA (poly (methyl methacrylate)) patterned surfaces has been prepared. The nanostructured samples present hexagonal symmetry following the geometry of the Aluminium substrate used as a precursor. Notice that many works have been reported using the PMMA (poly (methyl methacrylate)) as a base material to perform replications for submicrometric and nanometric structures for a variety of applications [3] [4].

The aim of this work has been to use the PMMA polymer as a substrate for the deposition of magnetic materials creating a nanostructured array of magnetic nanoparticles. The morphology of the PMMA surface is controlled by the geometry of the Al precursor. The Al template used for this purpose suffered an anodization process that induces the hexagonal pattern on its surface, after 24h. In particular, hexagonal arrays of PMMA nanostructures with a lattice parameter of 105nm and 180nm have been fabricated. Magnetic thin films have been deposited by sputtering onto the polymer at different angles.

We have studied the magnetic properties of these samples by using Vibrating Sample Magnetometer (VSM) and Magnetic Force Microscope (MFM). Figure 1 shows the topography and the domain structure of two samples with different lattice parameter. Figure 1 (a) and (b) corresponds to the sample with a lattice parameter of 105nm. In this case, the bright and dark magnetic contrast corresponds to the out-of-plane component of every nanoparticle. The dependence of the domain configuration with the previous magnetic history has also been observed by MFM. The samples with higher lattice parameter (180nm) present weak out-of-plane magnetization component, which oscillates in up and down direction as shown in Fig 1(d).

In the VSM we have measured successive hysteresis cycles varying the angle from in plane (0º) to out of plane (90º) and extracted their coercivities from each one (fig. 2). Theses measurements correspond to the polymer replica with 105 nm of lattice parameter recovered with Co, without a protect layer. In this graphic one can note that the coercivity increases respect with the angle.

In this work we have reported a technique to fabricate magnetic nanostructures on polymeric substrates with controllable magnetic behaviour. This procedure can be reproducible many times without damage the Al template used for it, and this suppose a great advantage in economic terms.

Referencias

[1] M. Vázquez *et al.* , *European Journal of Physics, B*, **40** (4) 489-497 (2004)

[2] M. Jaafar *et al. J. Apply. Phys*. 101, 09F513 (2007)

[3] Li M. *et al.*, *Appl. Phys. Lett*., 76, 673-675 (2000).

[4] Scheer H.C. and Schulz H., *Microelectronic Engineering*, 56, 311–332 (2001).

Figures:

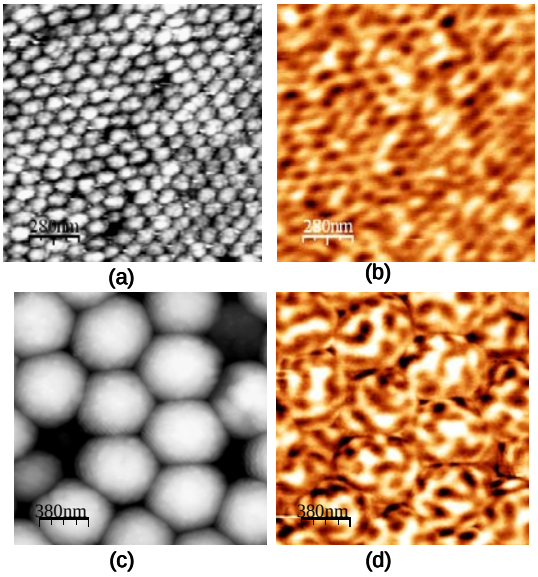

Figure 1: (a) AFM and (b) MFM image of the sample with a lattice parameter of 105nm. The Co thin film thickness is Co 30 nm. (c) AFM and (d) MFM image of the sample with a lattice parameter of 180nm. The Co thin film thickness is Co 30 nm.

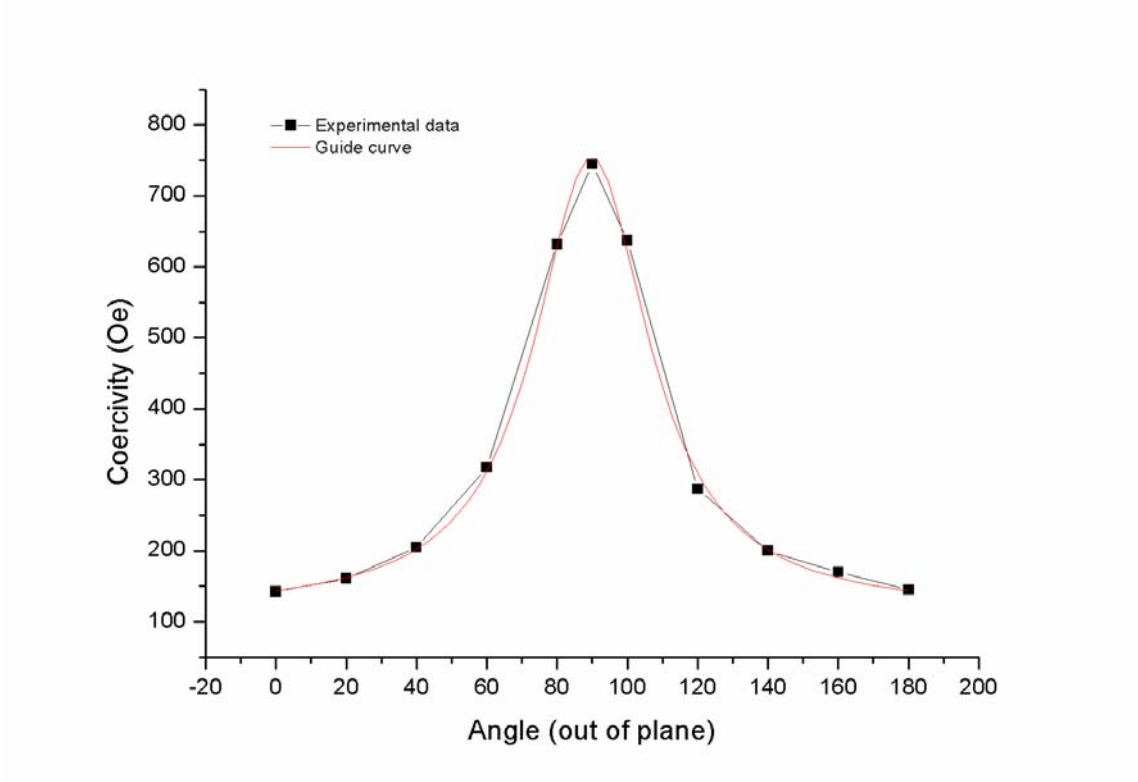

Fig 2 – Coercivity as function of the out of plane angle.

In-situ STEM investigation of thin films in a dual-beam equipment

J. M. De Teresa [a], *R. Córdoba* [b], *P. Strichovanec* [b], *N. Marcano* [b], *M.R. Ibarra* [b]

[a] *Instituto de Ciencia de los Materiales de Aragón, Universidad de Zaragoza-CSIC, Facultad de Ciencias, Zaragoza, 50009, Spain*
[b] *Instituto de Nanociencia de Aragón, Universidad de Zaragoza, Zaragoza 50009, Spain*

deteresa@unizar.es

We use a dual-beam equipment (Nova 200 NanoLab from FEI) that integrates a 30 kV field-emission electron column and a Ga-based 30 kV ion column to prepare electron-transparent lamellae (<100 nm) out of thin films for subsequent cross-section transmission electron microscopy studies. An Omniprobe nanomanipulator is used to place the lamellae on suitable Cu TEM grids for in-situ STEM imaging under 30 keV. The STEM detector is retractable and allows bright-field, dark-field, and high-angle-annular-dark-field STEM imaging. In general, resolution below 5 nm can be obtained in these conditions. If further resolution is required, the same lamellae, already placed on TEM grids, can be straightforwardly used for HRTEM, where we have regularly obtained atomic resolution under 200 keV.

In this contribution we report, as an example, the successful fabrication of lamellae out of three different types of thin films and their in-situ STEM imaging under 30 keV. The first example is a multilayer grown by MOCVD that consists of 50 repetitions of (AsGa/$Al_{0.3}Ga_{0.7}As$) bilayers covered by a GaAs layer. This kind of multilayer, grown in Bratislava (Slovakia), is being investigated for their optical properties arising from the formed quantum-well structure [1]. As can be observed in the STEM image (figure 1), the basic AsGa and $Al_{0.3}Ga_{0.7}As$ layers have typical thicknesses of 5.6 nm and 36 nm respectively and the cover layer is much thicker, 440 nm. The images indicate that all the layers are flat and continuous in lateral distances of 1 μm. The second example is a Bi thin film grown on a Si_3N_4//Si substrate by thermal evaporation in UCM (Madrid), which we are studying for their outstanding magnetransport properties [2]. The STEM images (figure 2) indicate that the average film thickness is about 150 nm and the microstructure of the films consists of grains with lateral size of the order of 100 nm that extend from the substrate up to the film surface. The third example is an ion-beam-induced Pt deposit on a Si_3N_4//Si substrate grown in-situ by injecting the precursor gas $(CH_3)_3Pt(CpCH_3)$ in the proximity of the substrate. The Ga ion column in the voltage/current conditions 30 kV/10 pA is used to break the precursor gas and produce the local deposition of Pt. This kind of deposits is useful in several applications in Nanotechnology such as for sample protection in lamellae preparation, circuit editing, nanocontacting, etc. [3]. The STEM imaging (figure 3) indicates that a 50 nm damage-region occurs at the interface of the sample and substrate, which matches the stopping range of the Ga ions in this substrate. Also, the microstructure of the deposited film consists of small Pt grains of the order of 5 nm inside a carbonaceous matrix. Subsequent HRTEM investigation indicated the crystalline nature of the Pt grains and the amorphous nature of the matrix [3].

References:

[1] J. Novak, P. Strichovanec, I. Vavra, R. Kudela, M. Kucera, Microelectronics Journal, **37** (2006) 1515.
[2] N. Marcano, S. Sangiao, J.M. De Teresa, L. Morellon, M.R. Ibarra, M. Plaza, L. Pérez, to be published.
[3] J.M. De Teresa, R. Córdoba, A. Fernández-Pacheco, O. Montero, P. Strichovanec, M.R. Ibarra, submitted.

Figures:

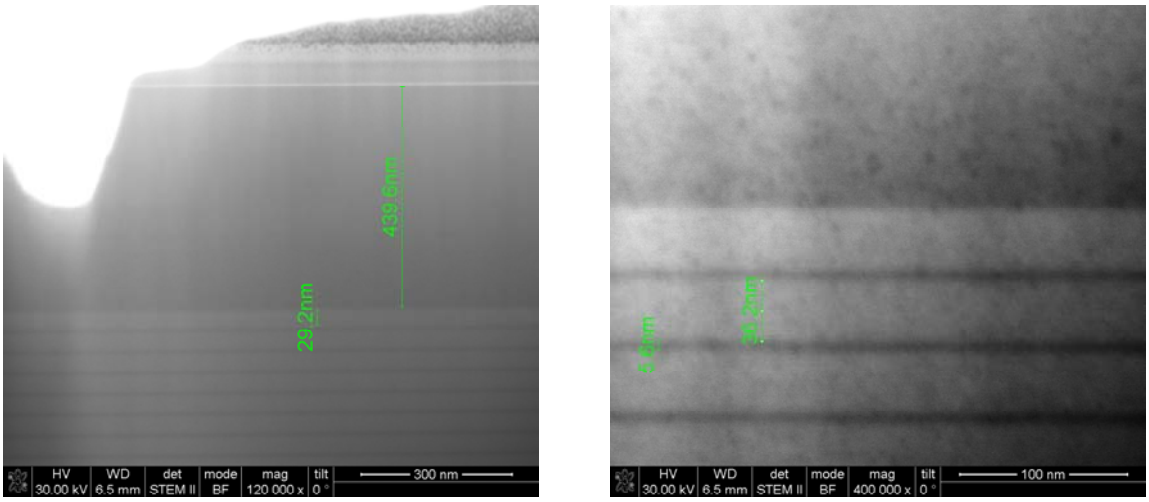

Figure 1. In-situ bright-field STEM images under 30 keV of a lamella prepared inside our dual beam equipment from a GaAs/GaAsAl multilayer grown by MOCVD.

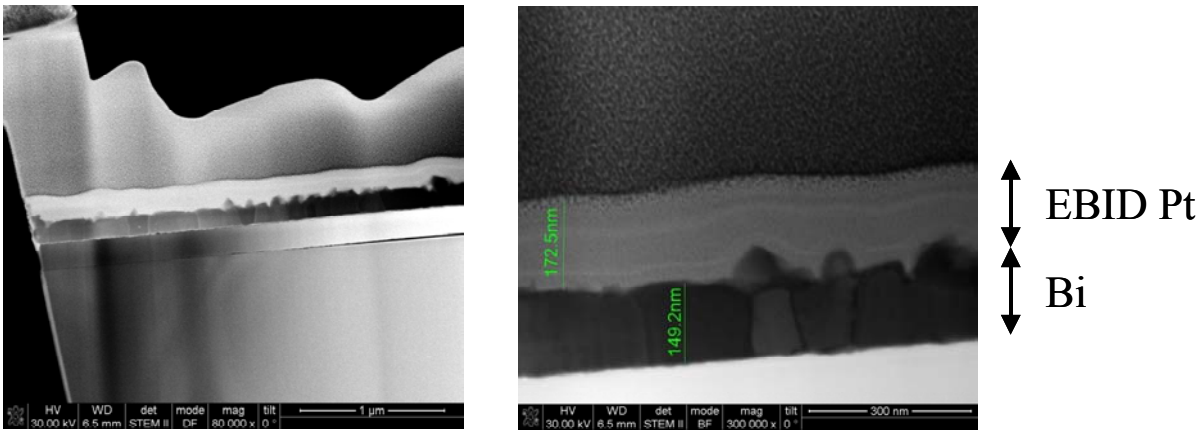

***Figure 2*.** In-situ STEM images under 30 keV of a lamella prepared inside our dual-beam equipment from a Bi thin film grown by thermal evaporation on a Si_3N_4//Si substrate. The left picture is a dark-field STEM whereas the right one is a bright-field image.

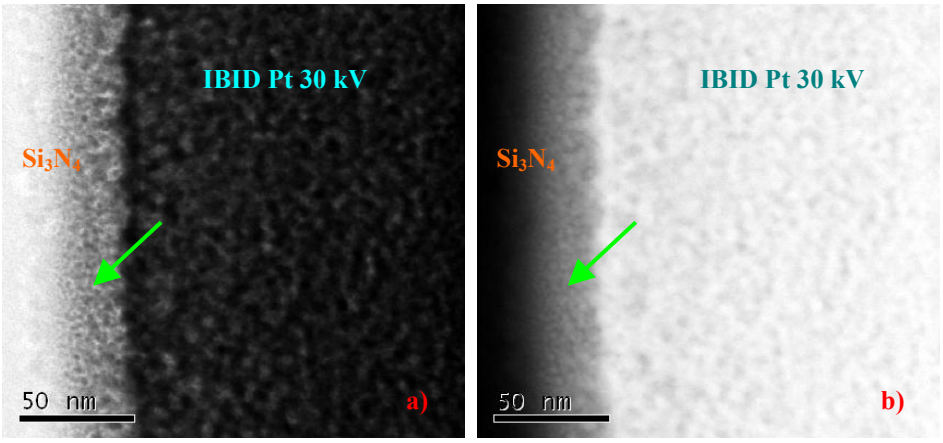

***Figure 3*.** In-situ STEM images under 30 keV of an ion-beam-induced deposit of Pt grown on a Si_3N_4//Si substrate in our dual-beam equipment. The left picture is a bright-field image whereas the right one is a high-angle-annular-dark-field image.

Poster

ROS INDUCTION AND CYTOTOXICITY OF INORGANIC NANOPARTICLES IN HUMAN CELLS

Belén Díaz[a], Christian Sánchez-Espinel[a], Manuel Arruebo[b], Esther Carregal-Romero[c], Isabel Pastoriza-Santos[c], José Faro[a,d], Susana Magadán[f], Clara Yagüe[b], Rodrigo Fernández-Pacheco[b], Ricardo Ibarra[b], Jesús Santamaría[b], Luis Liz-Marzan[c], África González-Fernández[a]

[a]Immunology Section, Experimental Sciences Centre, University of Vigo. Rúa das Abeleiras, Campus As Lagoas Marcosende, 36310 Vigo, Pontevedra, Spain. Email: belendi@uvigo.es

[b]Aragon Nanoscience Institute (INA), Pedro Cerbuna 12, University of Zaragoza, 50009 Zaragoza, Spain.

[c]Department of Physical Chemistry, Faculty of Chemistry; University of Vigo. Rúa das Abeleiras, Campus As Lagoas Marcosende, 36310 Vigo, Pontevedra, Spain.

[d]Estudos Avançados de Oeiras, Instituto Gulbenkian de Ciência, Oeiras, Portugal.

[f]Instituto Superior de Saude do Alto Ave (ISAVE), Quinta de Matos, Geraz do Minho, 4830-31 PVL , Portugal.

In the last few years there has been a large increase of studies on nanoparticles (NPs) showing their great potential for medical applications. These applications are from areas as diverse as diagnosis (e.g., contrast agents for magnetic resonance imaging and biosensing)[1], prevention of infectious diseases (e.g., vaccines)[2], and therapy (e.g., targeted drug delivery, gene therapy, hyperthermia)[3]. In this last area, NPs can offer clear advantages, compared to traditional therapy treatments. However, biocompatibility studies are essential to determine their safety. The biological activity of NPs depends on chemical and physical factors like size and shape, surface area, agglomeration state, chemical composition, surface chemistry (charge and hydrophilicity), surface activity, solubility, dose, etc[4]. The most extensively analyzed biological effects of NPs are those resulting from their interaction with the innate immune system. Among them, the stimulation of phagocytosis and the potential induction of cell stress are considered highly relevant.

Inorganic NPs like silica, gold, carbon-based materials, layered double hydroxides, etc., are a large group among those designed to transport drugs and bioactive molecules (peptides, proteins, enzymes, DNA, etc.) into cells. Our present work describes the interaction *in vitro* of seven of those NPs (magnetic iron/graphite, magnetite/silica, bare and polyethileneglycol(PEG)-ylated silica, magnetite/FAU zeolite, Au@SiO_2 and Au@PSS@PHA@PSS@CHI) with different human peripheral blood cells (lymphocytes, monocytes, granulocytes and erythrocytes), as well as mouse macrophages and several human tumor cell lines. We compare here the kinetics of several functional activities like phagocytosis, cell growth, viability and ROS production[5], at varying doses of NPs, for each of the different combinations of cell types and NPs used. Our results reveal different effects depending on the cell analyzed. For instance, while all NPs are phagocytosed and able to induce ROS by mouse macrophages, they behave differently on distinct human cell lines and in human peripheral blood cells both in respect to internalization and ROS induction. Moreover, contrary to previous reports, we have not always found a positive correlation between toxicity and ROS production induced by NPs.

References:

(1) Lee, J.H.; Huh, Y.M.; Jun, Y.; Seo, J.; Jang, J.; Song, H.T.; Kim, S.; Cho, E.J.; Yoon, H.G.; Suh, J.S.; Cheon, J. *Nature Med.* **2007**, *13*, 95.
(2) Koping-Hoggard, M; Sanchez, A.; Alonso, M.J. *Expert Rev. Vaccines* **2005**, *4*, 185.
(3) Arruebo, M., Fernández-Pacheco, R., Ibarra, M.R., Santamaría, J. *Nano Today* **2007**, *2*, 22.
(4) Nanotechnology White Paper. *U.S. Environmental Protection Agency*. EPA 100/B-07/001. **2007**.
(5) Gao, F.; Yi, J.; Yuan, J.Q.; Shi, G.Y.; Tang, X.M. *Cell Res.* **2004** *14*, 81.

REVEALING THE MECHANISM OF SNP DETECTION WITH GOLD NANOPROBES BY NON-CROSS-LINKING AGGREGATION

Gonçalo Doria[1,2], Ricardo Franco[2], Nuno Santos[3] and Pedro Baptista[1]
[1]CIGMH/DCV – FCT/UNL, Campus de Caparica, Caparica, Portugal
[2]REQUIMTE/DQ – FCT/UNL, Campus de Caparica, Caparica, Portugal
[3]UBM/IMM – FM/UL, Avenida Professor Egas Moniz, Lisboa, Portugal
doria_go@fct.unl.pt

The impact of advances in nanotechnology has been particularly relevant in molecular diagnostics where gold nanoparticle based assays have been developed for specific detection of bioanalytes of clinical interest[1]. Recently, we presented a colorimetric method for the detection of single base mutations/single nucleotide polymorphisms (SNP) based on the differential non-cross-linking aggregation of gold nanoparticles derivatized with thiol-modified oligonucleotides - Au-nanoprobes - upon hybridization with complementary DNA target[2]. The detection is based on the color difference upon salt addition between solutions containing the Au-nanoprobe and either complementary or mismatched/non-complementary target. These color differences are induced by shifts of the surface plasmon resonance (SPR) band of the gold nanoparticles, and are directly related to the level of Au-nanoprobes aggregation - red color of dispersed Au-nanoprobes turns blue upon aggregation.
Here, we try to elucidate the underlying mechanism that allows for single base mismatch resolution detection of DNA targets at room temperature. Using fluorescent spectroscopy and zeta potential measurements, we determined more DNA molecules binding to the Au-nanoprobe for fully complementary targets than for those harboring a mismatch. Non-complementary targets showed only residual binding, hardly distinguishable from background noise. The higher number of negatively charged DNA molecules bound provides a greater repulsive force between Au-nanoprobes, thus higher stability against salt induced aggregation.

Acknowledgments: Work supported by FCT/MCTES (CIGMH); PTDC/BIO/66514/2006, PTDC/SAU-BEB/66511/2006 and PTDC/QUI/64484/2006; SFRH/BDE/15544/2005 and STAB Vida, Lda. for G. Doria.

References:

[1] Baptista *et al.*, Anal Bioanal Chem, ***Epub ahead of print*** (2007).
[2] Doria *et al.*, IET Nanobiotech, **1** (2007) 53-57.

Figures:

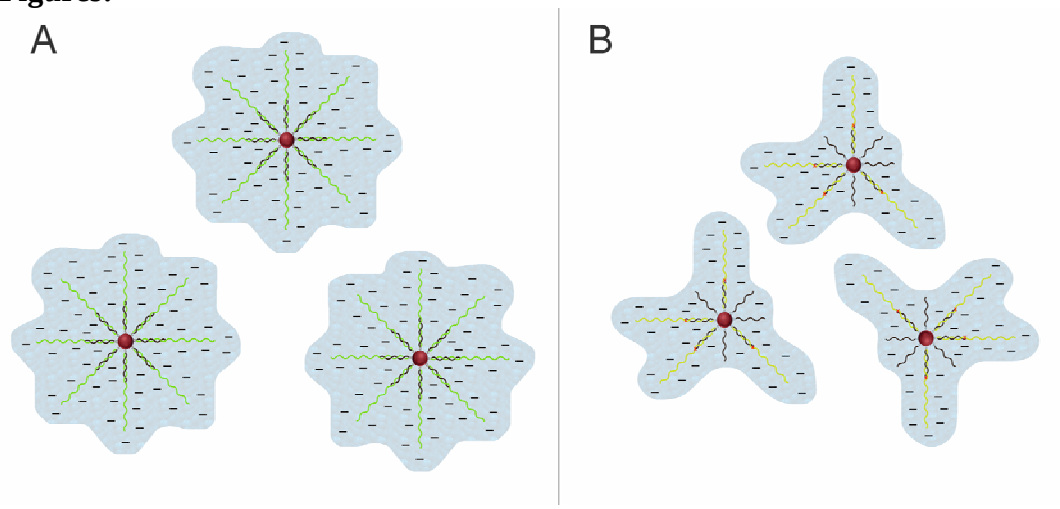

Figure 1- Model of the electrostatic field of targets hybridized with Au-nanoprobe - (A) fully complementary and (B) single base mismatch

ATOMIC FORCE MICROSCOPY AND FLUORESCENCE MICROSCOPY OF MALARIAL HEPATOCYTES

Peter Eaton[1], Miguel Prudêncio[2], Vanessa Zuzarte-Luis[2] and Maria Manuel Mota[2]
REQUIMTE, Dept. Química, Fac. Ciências, Universidade do Porto, Rua do Campo Alegre, 4169-007 Porto, Portugal
Unidade de Malária - Instituto de Medicina Molecular. Edifício Egas Moniz, Av. Prof. Egas Moniz, 1649-028 Lisboa, Portugal
peter.eaton@fc.up.pt

Malaria is a devastating disease which kills millions of people around the world each year. The disease is caused by one of several parasites of the genus *Plasmodium*. The parasite enters the human host in the form of sporozoites, delivered by a mosquito bite and reaches the liver through the bloodstream. In the liver, the parasite undergoes a development and multiplication process, after which thousands of merozoites, a second form of the parasite, are released into the blood stream, where the characteristic fevers of the disease occur. Because the liver stage of infection is asymptomatic, and samples are more difficult to extract, it has been studied much less than the blood infection stage, but is vital for the lifecycle of *Plasmodium*, and for the progression and severity of the disease[1].

We have used simultaneous atomic force microscopy (AFM) and optical microscopy to study a human hepatoma cell line, Huh7, infected by *Plasmodium berghei*. Exposure of liver cells to the parasites causes a low percentage of infection (ca. 1%) of the cells, and so we used *P. berghei* genetically modified to express green fluorescence protein (GFP). This allowed fluorescence microscopy to be used to identify and locate infected cells. Having identified which cells were infected, we studied both infected and uninfected cells using AFM to identify any morphological differences upon malaria infection.

We studied both fixed cells and living cells under physiological conditions, in order to ensure the results were not artefacts of the drying procedure. The results show considerable and significant differences between infected and uninfected hepatocytes. The AFM could clearly differentiate the infected from the uninfected cells, and the infected cells showed characteristic features which suggest interesting possibilities about the occupation of host hepatocytes by the *Plasmodium* parasites.

A further batch of cells was subjected to a proteolysis treatment. This process removes the surface proteins on the membrane of the cells, enabling us to eliminate morphological features associated with these proteins. These results show how the presence of these proteins affectthe cell-surface features observed in the infected hepatocytes.

References:

1. Prudencio, M.; Rodriguez, A.; Mota, M. M.,. *Nature Reviews Microbiology **11*** (**2006)**, 849.

Figures:

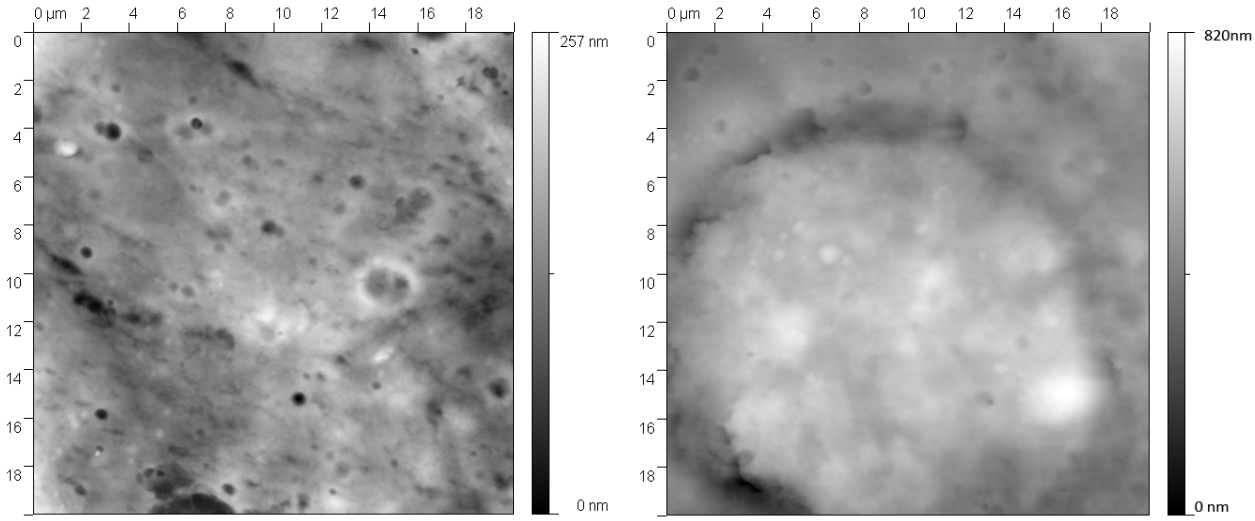

Figure 1: Tapping mode AFM images of an uninfected hepatocyte (left), and a hepatocyte infected with malaria (right).

Acknowledgements: We would like to thank Drs Miguel Castanho and Nuno Santos of the IMM for the use of the AFM.

MOLECULAR CONFORMATION, ORGANIZATIONAL CHIRALITY, AND Fe METALLATION OF MESO-TETRAMESITYLPORPHYRINS ON Cu(100)

David Écija [1], *Marta Trelka* [1], *Christian Urban* [1], *Roberto Otero* [1,2], *Rodolfo Miranda* [1,2], *Paula de Mendoza* [3], *Antonio M. Echavarren* [3], *Eva Mateo-Martí* [4], *Celia Rogero* [4], *José A. Martín-Gago* [4,5], *José M. Gallego* [5]

[1] *Dpto. de Física de la Materia Condensada, Universidad Autónoma de Madrid, 28049 Madrid, Spain*

[2] *Instituto Madrileño de Estudios Avanzados en Nanociencia (IMDEA-Nanociencia), Madrid 28049, Spain*

[3] *Institut Català d'Investigació Química, 43007 - Tarragona, Spain*

[4] *Centro de Astrobiología (CSIC-INTA), 28850 Madrid, Spain*

[5] *Instituto de Ciencia de Materiales de Madrid - CSIC, 28049 Madrid, Spain*

josemaria.gallego@uam.es

The controlled study of biomimetic systems is of paramount importance in order to understand the fundamental processes that govern biological systems. In this sense, ordered layers of organic compounds on solid surfaces can be used as model systems to study chemical reactivity or energy transfer mechanisms. Specifically, porphyrins and metalloporphyrins are key components in many biological processes, and Fe porphyrins in particular are of special interest as they are at the core of haemoglobin, the protein in the red blood cells responsible for the transport of oxygen. Morever, porphyrin derivatives have been used in chemical sensors, molecular wires, information storage memory devices, catalysts, solar cells, etc. The behaviour of different metalloporphyrin systems may be significantly altered by adsorption on metal surfaces. Therefore the observation of their surface structures is of fundamental importance to fully understand the effect of structural and conformational changes on their reactivity.

In this work we report on the self-assembly of meso-tetramesitylporphyrin (TMP, Fig. 1) when vapour-deposited in UHV conditions on Cu(100). Although at room temperature the molecules are very mobile, for low coverages they remain isolated or forming small clusters on the surface (Fig. 2a), indicating a rather low intermolecular interaction. Intramolecular resolution (Fig. 3), in combination with photoemission experiments and theoretical calculations, allows to determine their conformation and thus the effect of the copper surface. The molecular orientation comes dictated by the substrate, with the porphyrin main axis parallel to the Cu[110] directions.

Only for higher coverages do the porphyrins nucleate into islands (Fig. 2b) forming a square lattice with a $\begin{pmatrix} 6 & 2 \\ 2 & 6 \end{pmatrix}$ structure. Interestingly, our calculation reveal that the intermolecular distance and relative orientation are almost independent of the substrate, indicating that the assembly process comes mainly dictated by the intermolecular forces. The STM images show the existence of two types of molecules within the islands, probably corresponding to two different conformations (Fig. 4). In addition, the porphyrins can be Fe metallated by sublimation of Fe at room temperature on a porphyrin overlayer deposited on the Cu surface (Fig. 5), which opens the way to the study of the reactivity of Fe-TMP.

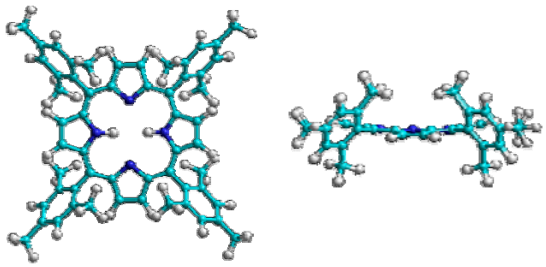

Figure 1: Top and lateral view of the minimum-energy gas-phase conformation of meso-tetramesitylporphyrin (TMP).

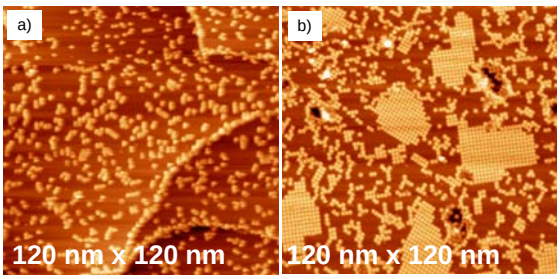

Figure 2: Large scale STM images after depositing a) 0.2 ML, and b) 0.45 ML ML of TMP on the Cu(100) surface.

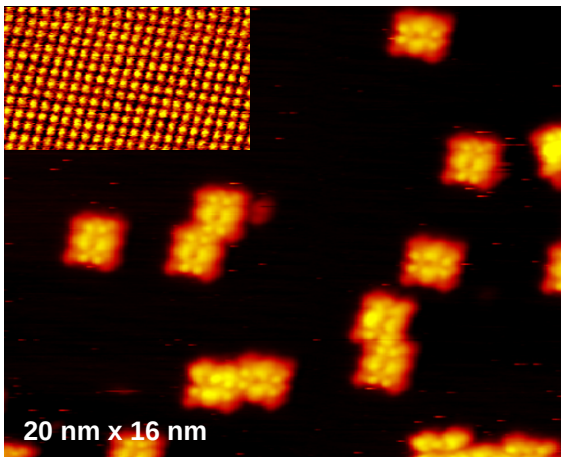

Figure 3: STM images of the Cu(100) surface after depositing ~ 0.2 ML of TMP. The inset shows the atomic lattice of the Cu substrate.

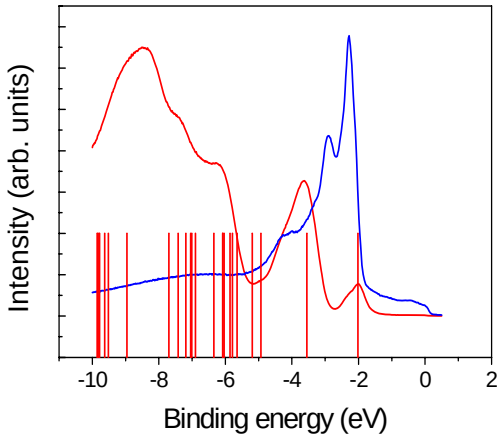

Figure 4: UPS spectra of the clean Cu(100) surface (blue), and after TMP deposition (red).

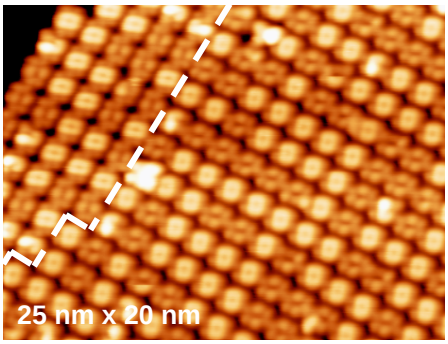

Figure 5: STM image of a porphyrin island showing two types (dark and bright) of molecules,

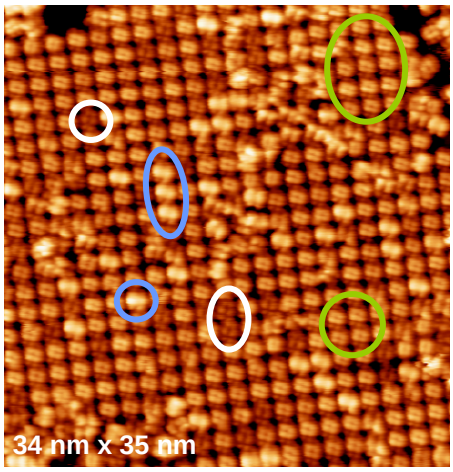

Figure 6: STM image of a porphyrin island after depositing a small amount of Fe.

.

A NOVEL METHOD OF SYNTHESIS OF SILICA NANOPARTICLES IN NON ALCOHOLIC ORGANIC MEDIUM

N. El-Hawi[1], C. Nayral[1], F. Delpech[1] and B. Chaudret[2]
[1]Laboratoire de Physique et Chimie des Nano-Objets, INSA, 135 avenue de Rangueil, 31077 Toulouse Cedex 4, France.
[2] Laboratoire de Chimie de Coordination du CNRS, 205 route de Narbonne, 31077 Toulouse Cedex, France
nel_hawi@insa-toulouse.fr

The synthesis of silica nanoparticles (NPs) has attracted steady interest for several decades because of their wide industrial applications (use in many fields including ceramics, chromatography, catalysis, and chemical mechanical polishing) [1]. In 1968, Stöber introduced a pioneering method for the synthesis, in solution, of spherical and monodisperse silica NPs with a narrow size distribution [2]. This method is based on hydrolysis and condensation of a tetraalkoxysilane (mainly tetraethoxysilane (TEOS)) in the presence of ammonia as a catalyst in an aqueous alcohol solution. However, this method is effective only in an aqueous alcohol solution which narrows the scope of applications requiring a non protic solvent (for example compatibility with some polymers for composite materials, or associations with organometallic compounds or metallic nanoparticles in organic media).

We describe here a novel method of synthesis of silica NPs in a non-alcoholic organic medium [3] via a process derived from the Stöber method. Two main types of reaction are involved: hydrolysis and condensation of TEOS, using water as reactant in the presence of primary amines as catalyst and tetrahydrofuran (THF) or dimethoxyethane (DME) as solvents.

The study of mechanism of silica elaboration revealed that the particles' growth seems to occur inside polysiloxane network, by progressive condensation around seeds included in the network. As a result, the particle size of silica NPs increases with reaction time.

The effect of different parameters (concentration, reaction time, temperature, solvents, nature and concentration of surfactants) on the reaction kinetic has been studied. It appears that the size and the morphology of NPs are closely related to the concentration and to the length of chains of the surfactant used.

This novel method opens new opportunities for the use of silica NPs in an organic medium, whether in biomedical applications or microelectronics by allowing the coating of metallic NPs with silica shell [4].

References:

[1] D. L. Green, J. S. Lin, Yui-Fai Lam, M. Z. -C. Hu, Dale W. Schaefer and M. T. Harris, Journal of Colloid and Interface Science**, 266,** *(2003), 346–358*

[2] W. Stöber, A. Fink and E. Bohn, Journal of colloid and interface science, **26**, (1968), 62-69
[3] N. El-Hawi, F. Delpech, C. Nayral, in preparation
[4] N. El-Hawi, F. Delpech, C. Nayral, submitted patent n° **07/08107**, (2007)

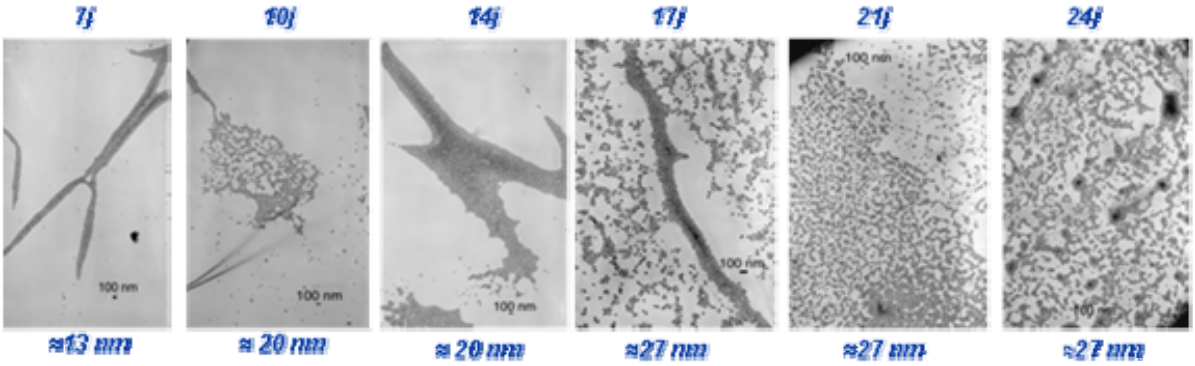

TEM images: Effect of reaction time on the particle size of silica Nps

Compressed Fluid Based Technologies for the Preparation of Drug Delivery Systems

Elizondo E[1], Ventosa N[1], Sala S[1], González D[2], Blanco-Príeto M.J[2], Veciana J[1]**

[1] Molecular Nanoscience and Organic Materials Department. Institut de Ciència de Materials de Barcelona (CSIC)-CIBER-BBN, Campus de la UAB s/n 08193-Bellaterra (Barcelona), SPAIN. Phone: 34 93 580 18 53, Fax: 34 93 580 57 29
[2]Department of Pharmacy and Pharmaceutical Technology , University of Navarra, Irunlarrea s/n, Pamplona 31080, Spain
contact e-mail: vecianaj@icmab.es, ventosa@icmab.es

From an esthetic perspective, it is attractive to build all desirable pharmacological features of a drug- such as solubility, stability, permeability to biological membranes, and targeting to particular tissues, cells and intracellular compartments- into the drug molecule itself. But it would be simpler and perhaps more powerful to obtain these features by decoupling the biological action of the drug from the other biochemical and physicochemical characteristics that determine these key features of its pharmacology [1]. In agreement with this, the obtaining of new micro- and nanostructured molecular materials, and the understanding of how to manipulate existing materials at nanoscopic level, are playing a crucial role in the fields of drug delivery and clinical diagnostics.

However, in order to be able to commercially exploit the enormous potential of these nanomedicines is necessary the development of efficient and environmental respectful technologies for the manufacturing at industrial scale of these nanostructured materials. Technologies using compressed fluids (CFs) – such as CO_2 – have been proved to be very effective for the straightforward preparation of micro- and nanoparticulated materials, with reproducible supramolecular organization (i.e. crystallinity degree, polymorphic form) [2-7]. Therefore, using compressed solvent media it is often possible to prepare materials with unique physico-chemical characteristics (size, porosity, supramolecular organization, morphology, etc…) unachievable with classical liquid media. Therefore, in this work, we have chosen a CO_2 based process for the preparation of a micro and nanoparticulate material for the treatment of Brucellosis.

Brucellosis is a worldwide zoonosis caused by different species of the genus Brucella. The intracellular location of this pathogen, particularly in macrophages, renders treatment difficult since most antibiotics –such as gentamicin- known to be efficient in vitro, do not actively pass through cellular membranes. The enhancement of intracellular penetration by using biodegradable polymers as drug carriers has already been studied [8,9]. Complementary to other conventional methods, compressed fluid techniques have found many useful and sometimes unique applications in the production and processing of such drug delivery systems [10]. In this work, the gentamicin:polymer microparticles were prepared by the method called Precipitation with a Compressed Antisolvent (PCA). In a PCA process a liquid solution is sprayed though a nozzle into a compressed antisolvent, which rapidly diffuses into the sprayed droplets causing the precipitation of the solute. It was proved that by using this PCA process much higher loading factors of the antibiotic were achieved compared to conventional processes for production of nanoparticles. Five different composites were prepared with different proportions between the antibiotic (an inonic complex of gentamicin sulphate and bis(2-ethylhexyl) sulfosuccinate sodium salt (AOT), *GmAOT*) and the biodegradable polymer (poly(methylvinylether/maleic anhydride), *gantrezAN*): 0.09:1, 0.19:1, 0.37:1, 0.67:1, 1:1 (GmAOT:gantrezAN, w:w) [11].
It was observed that by increasing the amount of antibiotic in the composite, both the morphology and the primary particle size of the resulting nanostructured material changed. In vitro studies were performed in order to check the activity of the composites against the

Brucella. All the compositions have shown the same activity as the one observed for the equivalent quantity of gentamicin sulphate. By achieving this high loading factors reduced doses would be needed and therefore, an easier and faster treatment could be provide to the patients.

References:

[1] J.A Hubbel, Science, **300** (2003) 595.
[2] D.W. Matson, J.L. Fulton, R.C. Petersen, R.D. Smith, Ind. Eng. Chem. Res, **26**, (1987) 2298.
[3] (a) N. Ventosa, S. Sala, J. Veciana, J. Llibre, J. Torres, Cryst. Growth & Design, **1** (2001) 299. (b) N. Ventosa, S. Sala, J. Veciana, J. Supercrit. Fluids, **26 (**2003) 33. (c) M. Gimeno, N. Ventosa, S. Sala, J. Veciana, Cristal Growth & Design, **6** (2006) 23.
[4] M. Cano-Sarabia, N. Ventosa, S. Sala, C. Patino, R. Arranz, J. Veciana, Langmuir, DOI: 10.1021/la7032109
[5] E.Weidner, Z. Knez, Z. Novak, PGSS (Particles from gas saturated solutions) a new process for powder generation, in: G. Brunner, M. Perrut, (Ed.), Proceedings of the third International Symposium on Supercritical Fluids, **3** (1994) 229.
[6] P.M. Gallagher, M.P. Coffey, V.J. Krukonis, N. Klasutis, ACS Symp. Ser., **406** (1989) 334.
[7] J. Bleich, B.W. Müller, W. Wabmus, Int. J. Pharm., **97** (1993) 111.
[8] C. Lecaroz, C. Gamazo, M-J. Blanco-Príeto, J. Nanosci. Nanotechno, **6** (2006) 3296.
[9] E. Briones, C.I. Colino, José M. Lanao, J.Controlled Release, **125** (2007) 210.
[10] P. Pathak, M.J. Meziani, Y.-P. Sun, Expert Opin. Drug. Deliv, **2** (2005) 747.
[11] E. Elizondo, N. Ventosa, S. Sala, J. Veciana, E. Imbuluzqueta, D. Gonzalez, M.J. Blanco-Prieto, C. Gamazo, Patents: P200703314, P200703315. Aplication date: 7th of December of 2007.

Figures:

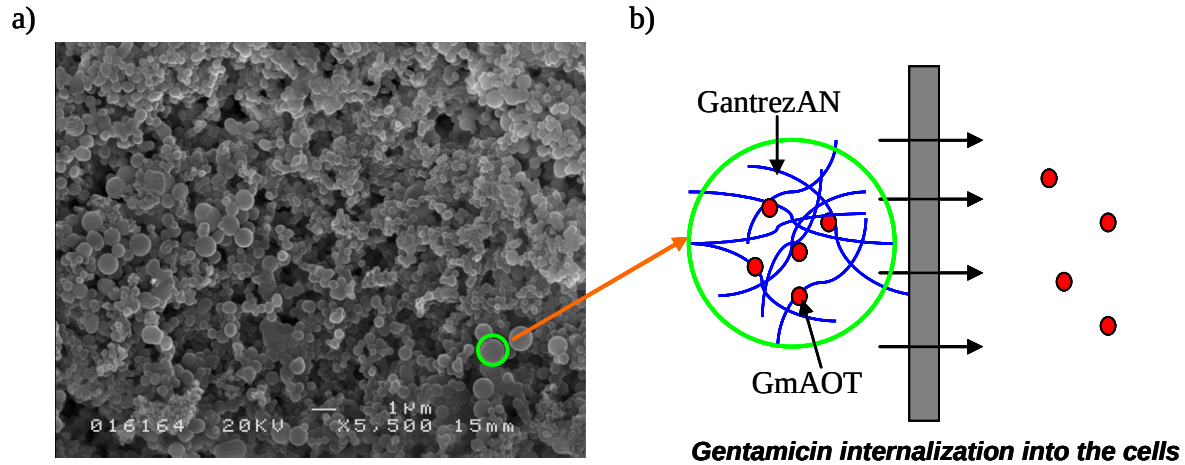

Figure 1. a) SEM image of a GmAOT:GantrezAN composite. b) Squeme of the enhanced permeability of gentamicin through cell membranes by using GantrezAN as a carrier.

FORMATION OF NANOCOMPOSITE STRUCTURES IN TMD COATINGS BY ALLOYING WITH C

M. Evaristo[1], *T. Polcar*[1,2], *A. Cavaleiro*[1]

1) SEG-CEMUC - Department of Mechanical Engineering, University of Coimbra, Polo II, 3030-788 Coimbra, Portugal

2) Department of Control Engineering, Faculty of Electrical Engineering, Czech Technical University in Prague, Technická 2, Prague 6, Czech Republic

manuel.evaristo@dem.uc.pt, tomas.polcar@dem.uc.pt, albano.cavaleiro@dem.uc.pt

Abstract.

Transition metal dichalcogenides (TMD) coatings are well known as self-lubricant materials. However, their drawbacks, such us low load-bearing capacity or environmental sensitivity, reduces the spectrum of application. Alloying the coatings with carbon can lead to significant changes in the coatings structure that can improve significantly the mechanical and tribological properties.

In this work, W-S-C coatings were deposited by sputtering with increasing C contents using 3 different approaches: (1) co-sputtering from two individual targets (WS_2 and C) varying the power applied at each target; (2) sputtering a WS_2 target in a reactive atmosphere with different CH_4 partial pressures; (3) co-sputtering a C target embedded with increasing number of WS_2 pellets. The coatings deposited by procedure (1) presented XRD patterns typical of an amorphous structure, whatever the C content. For the others process (procedures 2 and 3) crystallinity could be observed, which changed progressively with increasing C content (see e.g. the evolution of XRD patterns in figure 1 for reactively sputtered coatings). W-S coatings with low C content presented a main XRD peak placed at $2\theta \sim 40^{\circ}$ with a long tail corresponding to the turbostatic stacking of (10L) planes (L=1, 2, 3,…) which could be interpreted as a 2D organization of the basal planes [1]. With increasing C content, the lateral dimension of the basal planes decreased leading to broader and less intense peaks suggesting a decrease in the grain size down to the nanometer level. This was confirmed by TEM analysis. For C contents higher than 40 at.% small features in the XRD pattern allowed suggesting the presence of other phases such as tungsten carbides. Such a fact was confirmed by X-ray photoelectron spectroscopy (XPS) [2] which clearly showed the presence of different types of bonds such as, W-S, W-C and C-C confirming the formation of a nanocomposite structure where nanocrystals of WS_2 and W-C phases were dispersed in a C-rich amorphous matrix. The differently contrasted zones in the TEM micrograph of one of these coatings (inset in figure 1) and the direct observation of crystalline planes in darker areas support this assessment. Raman analysis of the coatings showed undoubtedly the presence of D and G bands characteristics of low order C phases confirming the presence of the amorphous matrix in the W-S-C coatings.

Figure 2 presents the evolution of the hardness (H) of the coatings with increasing carbon content for all the approaches adopted for deposition. For the W-S-C, as a general trend, the hardness rises with increasing C content, up to ~45 at.%, and decreases thereafter. The first increase should be closely correlated to either the great improvement in the density of coatings (see typical cross section morphologies in the inset figures) or the formation of other harder phases such as W-C or C-based. With the addition of carbon in the coating, there is no more W available to establish W-C bonds and the domination of carbon phases takes place. As the deposition conditions used in this work leads to only 7 GPa for the hardness of pure C coatings, the growing influence of C in the W-S-C coatings justify the observed decrease in hardness values.

References:

[1] G. Wise, N. Mattern, H. Herman, A. Teresiak, I. Bascher, W. Bruckner, H.-D. Bauer, H. Vinzelberg, G. Reiss, U. Kreissig and M. Mader, P. Markschlager, Thin Solid Films **298** (1997) 98.
[2] A. Nossa and A. Cavaleiro, J. Mater. Res. **19** (2004) 2356.

Figures:

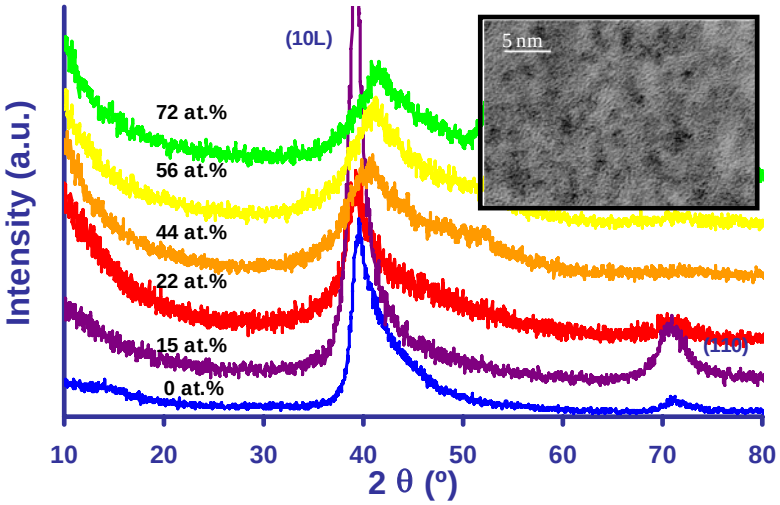

Figure 1 XRD patterns of reactively deposited W-S-C coatings with increasing C content. A TEM micrograph of the cross section of a high C content coating (64 at.%) is shown inset.

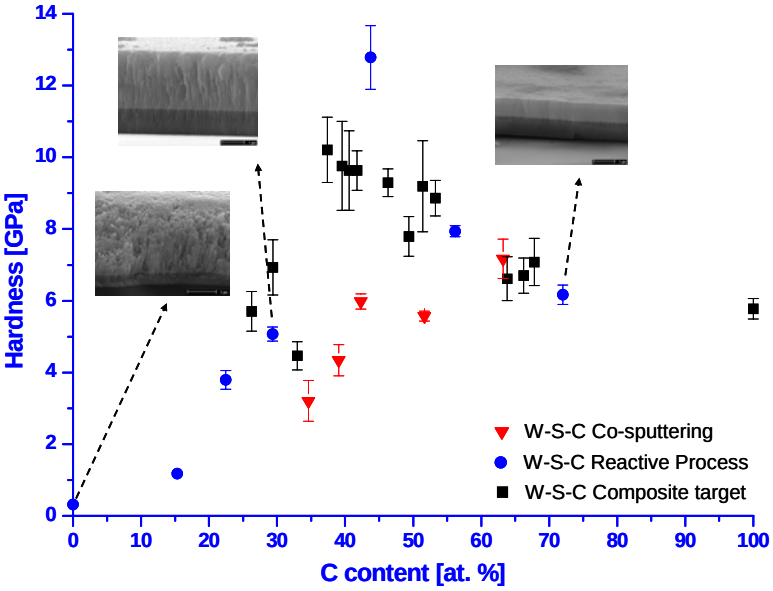

Figure 2 Hardness of W-S-C sputtered coatings as a function of the C content. SEM micrographs of the cross section of selected coatings are shown inset.

Restricted epitaxial growth during thermal crystallization of nanocrystalline silicon: experiments and modeling

J.Farjas[1], P.Roura[1], F. Kail[1] and P.Roca i Cabarrocas[2]
[1]GRMT, Campus Montilivi, Department of Physics, University of Girona, E-17071-Girona, Catalonia, Spain.
[2]LPICM, Ecole Polytechnique, 91128 Palaiseau, France.
jordi.farjas@udg.cat

Hydrogenated nanocrystalline silicon (nc-Si:H) has attracted greater attention because of its improved transport properties with respect to hydrogenated amorphous silicon (a-Si:H) [1]. In addition, its deposition conditions are compatible with amorphous silicon technology which makes it possible to use both materials in the same device. In this sense, it has been proposed as a candidate for the circuits connecting amorphous thin film transistors (TFTs) in active matrix liquid crystal displays [2] and has been used as a part of a-Si:H photovoltaic solar cells and other devices [3]. Essentially, the high crystalline fraction (up to 90%) of nc-Si:H results in high carrier mobility and electrical conductivity. However, in contrast with polycrystalline silicon obtained by crystallization of a-Si:H [4], the conductivity of nc-Si:H cannot be described by a simple law of mixtures between the values for its amorphous and crystalline phases [5]. Deviations from this simple behaviour are explained by the important role of grain boundaries between crystallites and the amorphous phase [6]. They act as potential barriers to charge transport. Important changes in conductivity are observed when the grain boundaries are modified by thermal annealing [7, 8].

In the present work, we study the thermal crystallization of nc-Si:H by means of differential scanning calorimetry (DSC). Experiments reveal that the amorphous phase crystallizes by solid phase epitaxy around the pre-existing crystallites. However, and in contrast with the usual crystallization of wafers partially amorphized by ion implantation, only a small fraction of the interface contributes to the epitaxial growth. This conclusion relies on two main results: a) the crystallization temperature is much higher and b) the crystallization peak is sharper than expected. Both features result in the characteristic dependence of the interface area active for epitaxy versus the epitaxial distance plotted in Fig.1.

To test the correctness of our conclusion, we have modelled the restricted epitaxial growth of nc-Si [9]. The model assumes that all pre-existing crystallites are identical squares randomly distributed inside the amorphous phase (Fig. 2). This 2D model successfully describes the dependence of the active interface area on the epitaxial distance and delivers a fraction of the interface area coherent with the experimental results. Furthermore, the numerical simulation provides information about the spatial distribution of the active a-c interface sites and about the grain morphology development during crystallization. A calculated microstructure cross section corresponding to a transformed fraction of 84% relative to the initial amorphous volume fraction is given in Fig 2.

The restricted epitaxial growth revealed by our study can be useful for undertanding the microscopic mechanisms of carrier transport in nc-Si:H.

References:

[1] See the critical reviews in Solar Energy Mater. Solar Cells **78** (2003) and C.Rath, Solar Energy Mater. Solar Cells, **76**, 431 (2003).
[2] S.Kasouit, P.Roca i Cabarrocas, R.Vanderhaghen, Y.Bonaissieux, M.Elyaakoubi, I.French, J.Rocha, B.Vitoux, Thin Solid Films **427**, 67 (2003).

[3] J.Meier, R.Flückiger, H.Keppner, A.Shah, Appl.Phys.Lett. **65**, 860 (1994).
[4] C.S.Pai, S.S.Lau, Thin Solid Films **109**, 263 (1983).
[5] S.K. Ram, S. Kumar, P. Roca i Cabarrocas, Phys. Rev. B **77**, 045212 (2008).
[6] J.Kocka, A.Flejfar, H.Stuchlikova, J.Stuchlik, P.Fojtik, T.Mates, B.Rezek, K.Luterova, V.Svrcek, I.Pelant, Sol.Energy Mater.Sol.Cells **78**, 493 (2003).
[7] C.-H.Lee, D.J.Grant, A.Sazonov, A.Nathan, J.Appl.Phys. **98**, 034305 (2005).
[8] J.H.Yoon, J.Mater.Res. **16**, 1531 (2001).
[9] The numerical algorithm is based on the one reported in: J. Farjas, P. Roura, Phys. Rev B. **75**, 184112-1 (2007).

Figures:

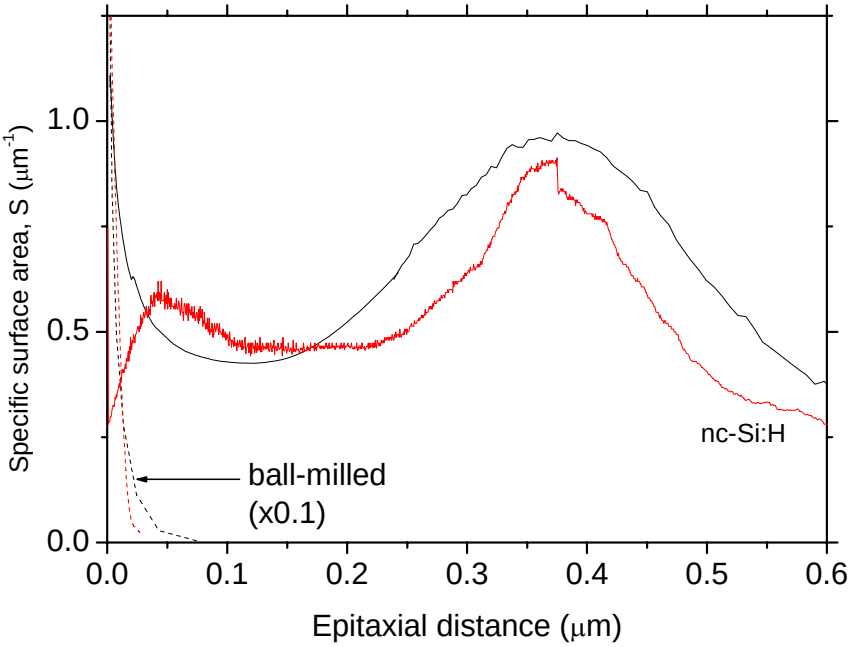

Fig 1. Specific surface area of the crystallization front vs epitaxial distance for the nc-Si:H (solid line) and ball-milled Si (dashed line). Black lines correspond to experimental data while red lines are numerical results.

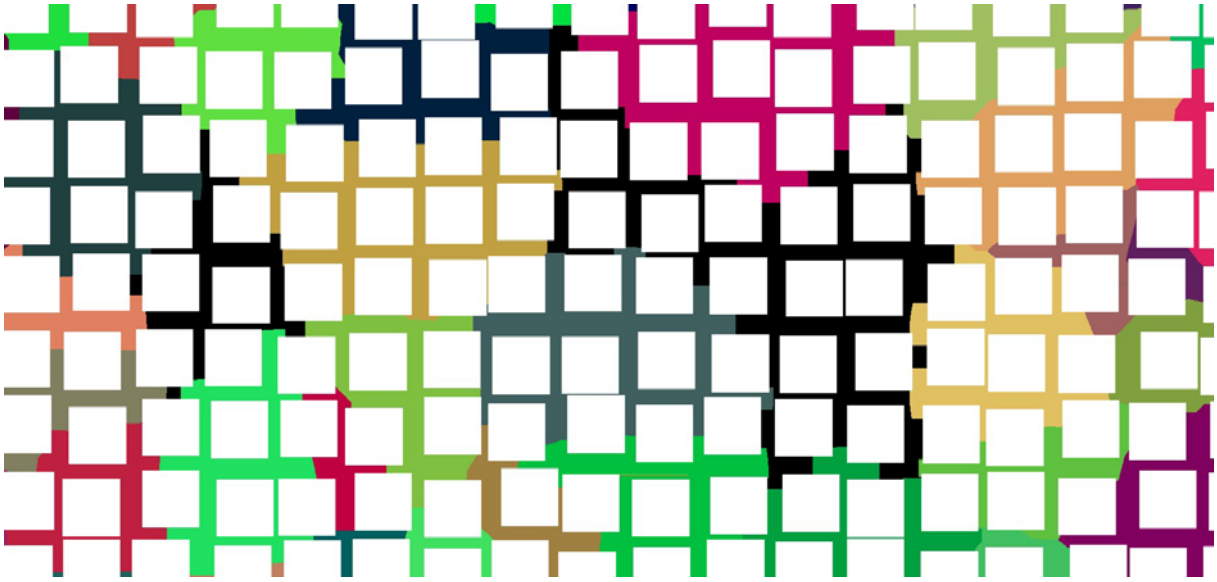

Fig 2. Calculated microstructure cross section; transformed fraction of 84%. White squares are pre-existing crystallites, black regions are untransformed amorphous phase and colored regions correspond to thermally crystallized regions.

ATOMIC FORCE MICROSCOPY OF THE ANTIBACTERIAL EFFECTS OF CHITOSANS ON *BACILLUS CEREUS* (AND ITS SPORES)

João C. Fernandes[1], Peter Eaton[2], Manuela E. Pintado[1] & F. Xavier Malcata[1]

[1]Escola Superior de Biotecnologia, Universidade Católica Portuguesa,
Rua Dr. António Bernardino de Almeida, P-4200-072 Porto, Portugal

[2]REQUIMTE, Departamento de Química, Faculdade de Ciências da Universidade do Porto,
Rua do Campo Alegre, P-4169-007 Porto, Portugal

Chitosan is known to be a non-toxic, biocompatible and antibacterial agent – with an associated potential for several applications[1]. The aim of this work was to elucidate the relationship between the molecular weight (MW) of chitosan and its antimicrobial activity upon both vegetative and resistance forms of *Bacillus cereus*. Atomic Force Microscopy (AFM) imaging was used to obtain high resolution images of the effect of the chitosans on the bacterial morphology. The results of the antibacterial assays showed that antimicrobial effect is strongly dependent on the cell stage and on the MW of the chitosan: it increased with MW for the vegetative form, and the opposite for the spores. The images obtained reveal that higher MW chitosans (i.e. 610 and 100 kDa) formed a slimy layer around both forms of *B. cereus.* Chitosan oligomers (<3 kDa) images also disclosed survival strategies used by *B. cereus* such as clustering formation, on the other hand no clear changes were observed over spores morphology. However, nanoindentation experiments with the AFM revealed mechanical changes in the cell wall caused by the aforementioned oligomers, correlated to damage caused by the polymers. The antibacterial assays and AFM results are correlated and help us to understand the mechanism of action and efficacy of chitosans against this food spoilage microorganism.

References:

[1] R. Jayakumar, N. Nwe, S. Tokura and H. Tamura, *International Journal of Biological Macromolecules* **40** (2007) 175-181.

Figures:

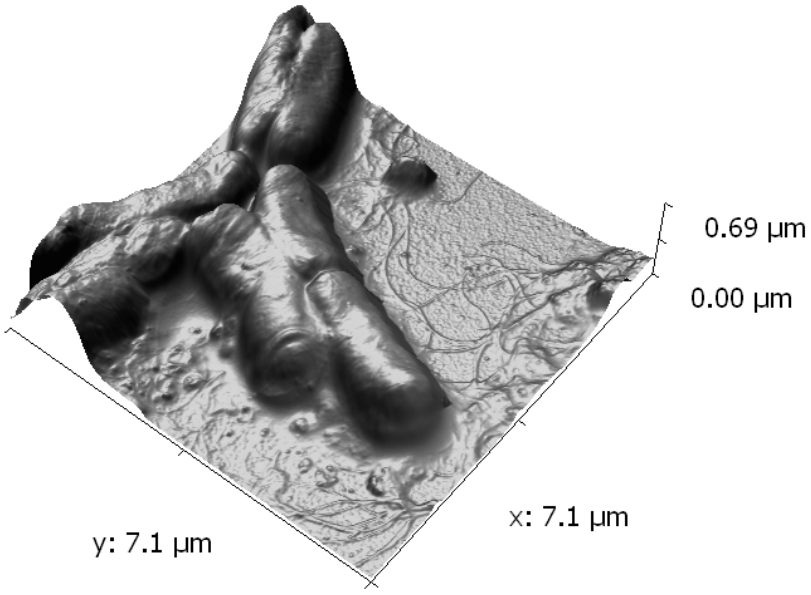

Figure 1 – 3D AFM image of *B. cereus* control in the vegetative form.

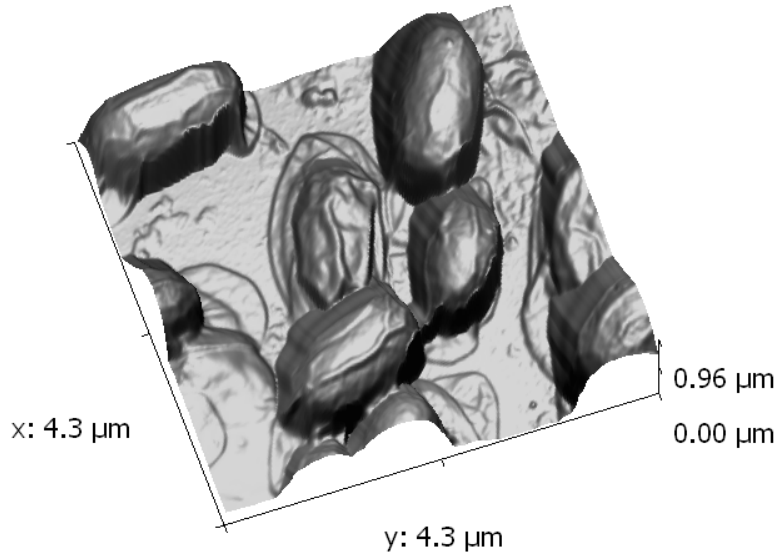

Figure 2 – 3D AFM image of *B. cereus* spores control.

STRUCTURAL AND FUNCTIONAL PROPERTIES OF GELATIN-CLAY NANOCOMPOSITES

Francisco M. Fernandes, Ana I. Ruiz, Margarita Darder, Pilar Aranda, and Eduardo Ruiz-Hitzky
Materials Science Institute of Madrid, CSIC, Campus de Cantoblanco, 28049 Madrid, Spain
ffernandes@icmm.csic.es

Polymer-clay nanocomposites are a well known class of hybrid materials with enhanced functional and structural properties[1]. In particular bio-nanocomposites, which result from the interactions of biopolymers and inorganic solids with dimensions in the nanometric scale, are receiving increasing attention due to their potential as ecological, biocompatible and economically viable high performance materials[2-4].

Gelatin, which exhibits a transition temperature between coiled coil conformation and triple helix around 37 ºC, is a widely used biocompatible polymer whose molecular structure resembles that of collagen. Although the main uses of this polypeptide regard textural modification in the food industry, it has recently been subject of research to develop materials that present enhanced structural properties. This approach consists on the reinforcement of the polymeric matrix with layered expandable silicates such as montmorillonite to obtain gelatin-clay nanocomposites with improved tensile properties[5].

The present work reports the use layered silicates montmorillonite and vermiculite, fibrous clay sepiolite, and a layered double hydroxide ([Zn2Al(OH)6]Cl·nH2O) to develop functional and structural nanocomposites and micro-composites. Although gelatin could be intercalated into the layered solids through interactions at the nanometric scale, only montmorillonite displays clear evidence of this feature. Also sepiolite shows high affinity towards the gelatin matrix, originating homogeneous films similar to those obtained with montmorillonite. The Young's modulus of gelatin-sepiolite nanocomposites was increased by a factor of 2.5 with respect to neat gelatin without severe loss of elongation at break. The incorporation of methyl red pH indicator dye into the montmorillonite galleries, allowed the formation of an optical pH sensing nanocomposite film.

Results confirm sepiolite and montmorillonite as high performance fillers in gelatin nanocomposite films, enhancing structural and functional properties respectively.

References:

[1] Sinha Ray, S. and Bousmina, M., Progress in Materials Science, **50**, 8 (2005) 962-1079.

[2] Darder, M., Aranda, P., and Ruiz-Hitzky, E., Advanced Materials, **19**, 10 (2007) 1309-1319.

[3] Fernandes, F.M., Ruiz, A.I., Darder, M., Aranda, P., and Ruiz-Hitzky, E., Journal of Nanoscience and Nanotechnology, (2008), in press.

[4] Ruiz-Hitzky, E., Ariga, K., and Lvov, Y.M., eds. *Bio-inorganic Hybrid Nanomaterials, Strategies, Syntheses, Characterization and Applications*. Vol.18. 2007, Wiley-VCH: Weinheim.

[5] Darder, M., Ruiz, A.I., Aranda, P., Van Damme, H., and Ruiz-Hitzky, E., Current Nanoscience, **2**, 3 (2006) 231-241.

Figures:

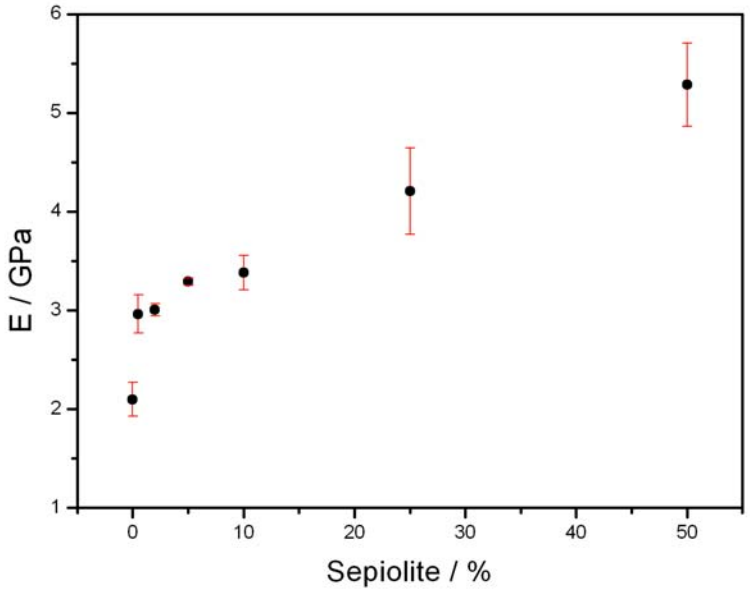

Figure 1 – Young's modulus of the gelatin-sepiolite nanocomposite as a function of clay content.

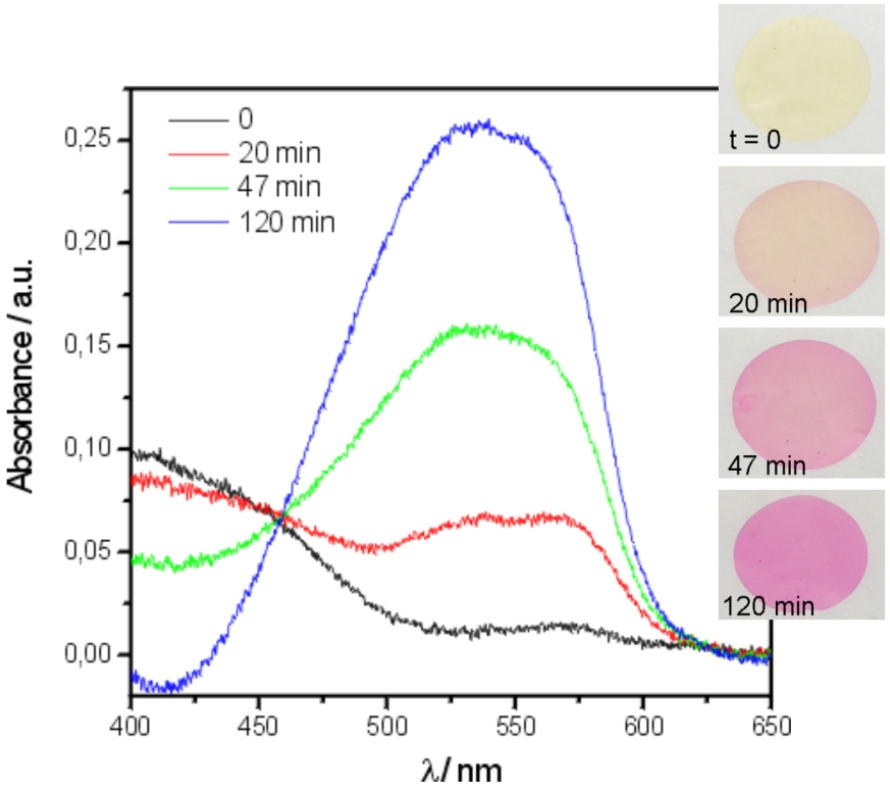

Figure 2 – Self-supported hybrid films of gelatin incorporating 50% of methyl red intercalated montmorillonite for optical pH sensing. Absorbance spectra and photographs at different time periods under acidic atmosphere.

Interdigitated nanoelectrodes for sensing: fabrication and characterization

Irene Fernandez-Cuesta, Jesús García, Jahir Orozco, César Fernández-Sánchez, Antoni Baldi, Xavier Borrisé and Francesc Pérez-Murano
Centro Nacional de Microelectrónica - Barcelona (CNM-IMB, CSIC)
Irene.Fernandez@cnm.es

Interdigitated nanoelectrodes (nIDEs) consist on two arrays of electrodes with comb shape which, under proper bias polarization, can be used for (bio)chemical sensing by measuring the change of impedance or electrochemical current.

In this work we present the fabrication of a complete device, and the first results of its characterization. The device can be used in different configurations: (i) measurement of the electrochemical current generated by chemical reactions occurring in the solution [1], and (ii) study of the impedimetric response of the system when the nature of the solution changes [2] or even further, with the inclusion of nanoparticles in between the digits [3].

Fabrication.

In order to combine micro and nanometer size features, the connection pads and lines are first fabricated by UV lithography, metallization (Ti/Au, 7nm/60nm) and lift-off. Aligning marks have been included in the design of the UV mask for a second lithography level which consist of electron beam lithography to define the digits, followed by metal evaporation and lift off. Figure 1 shows results of the fabrication process: the whole chip, fabricated in gold onto a SiO_2/Si substrate (a), and a detail of the digits (b), which are 180 nm wide and with a pitch of 230 nm. These devices can be used already for sensing or as the master to fabricate stamps for nanoimprint lithography (NIL). In the second case, a reactive ion etching (RIE) process is performed. Then, the fabrication of subsequent samples is easier and faster, since the two lithography levels (UV and e-beam lithography) are substituted by one single NIL step.
Once the electrodes have been fabricated, they are passivated with PMMA, leaving open only the large pads for external connections and the areas with the digits. Then, they are bounded to a printed circuit board (PCB), and encapsulated with *epotec*®. At this point, the sensor is ready to be connected to an external electronic system and the electrodes can be immersed in a liquid media (Figure 1 (c)).

Characterization.

Figure 2(a) shows the first results of electrochemical current measurements. The nIDE was immersed in a solution 1mM of $[Fe(CN)^{3-}]_6$ in KNO_3 (red line). A stabilization potential was applied during the first 30seconds, and then changed to 0V (*). After the stabilization of the system when V = 0V, the current is due to the reduction processes occurring in the solution. The black line corresponds to the same measure, but in a KNO_3 solution. No electrochemical current is observed after the stabilization in this case. The sensors are being calibrated by adding known concentrations of $[Fe(CN)^{3-}]_6$, so subsequently can be used to determine the concentration of unknown solutions.
Figure 2(b) corresponds to results of the impedimetric response of the electrodes (total impedance of the media measured as a function of frequency). The electrode was immersed in DI water and then in solutions of NaCl with different concentrations (i.e., the resistivity of the media changes). The figure shows that the change from the low frequency capacity to the high frequency capacity depends on the concentration of Na^+ Cl^- ions in the aqueous media. Thus, the device can be also calibrated, to be used for sensing. Additional tests performed in liquids

* $Fe(CN)_6^{3-} + e^- \rightarrow Fe(CN)_6^{4-}$, E_0=+0.35V

with different permitivities (ε_r) have been performed, showing that the higher ε_r is, the lower the high frequency capacity.

Once the proper response of the sensors has been demonstrated, the devices are being currently used to detect and quantify the presence of insulating nanoparticles (Figure 3). The final goal is to functionalize the nanoparticles to perform specific detection of bioentities: an increase of sensitivity is expected since nIDES would allow the detection of a single nanoparticle. The results will be presented at the conference.

Proyects NILSIS and Consolider NanoBioMed are gratefully acknowledged.

References:

[1] K. Aoki et al., *J. Electroanal. Chem*, **256** (1988) 269
[2] R. de la Rica et. al., *Appl. Phys. Lett*. **90**, 174104 (2007)
[3] L. Malaquin et al. *Nanotechnology*, **16**, (2005) S240–S245

Figures:

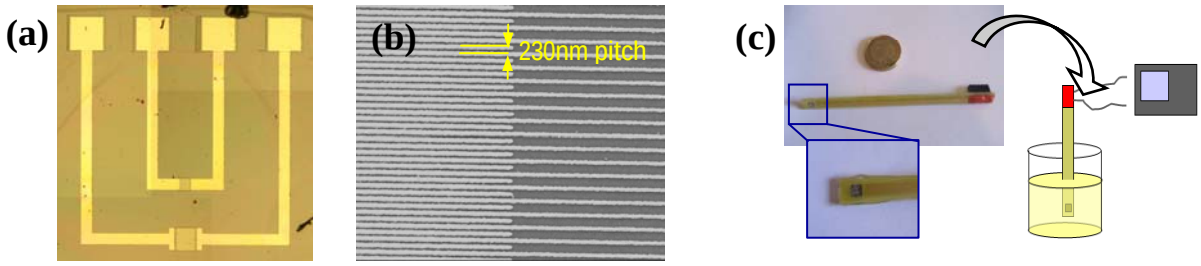

Figure 1. (a), optical image of a sensor, fabricated in gold on a SiO_2/Si substrate. The pads are defined by optical lithography, metallization and lift off, and the digits are fabricated in a second step, by e-beam lithography, metallization and lift off. A detail can be seen in the SEM image in (b). (c) once the electrode is fabricated, it is bounded to a PCB and encapsulated, so it can be connected to an external electronic system and the electrodes immersed in a solution, for characterization.

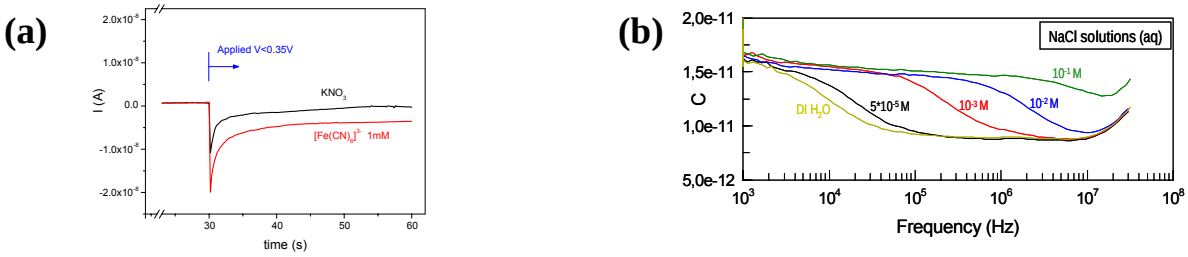

Figure 2. (a) Electrochemical current measurements**,** for an applied potential similar to the reduction potential of $[Fe(CN)_6]^{3-}$. When the electrode is immersed in a FeCN63- 1mM solution, a current due to the electrochemical reaction is measured (red line). For a non-active solution (KNO3), no current is observed (black line). **(b) Impedimetric characterization:** Dependence of the capacity of the system on the frequency when the electrode is immersed in solutions with different resistivity (i.e., aqueous solutions of NaCl at different concentrations). In this case, the transition from the high frequency capacity to the low frequency one depends on the concentration of ions in the solution.

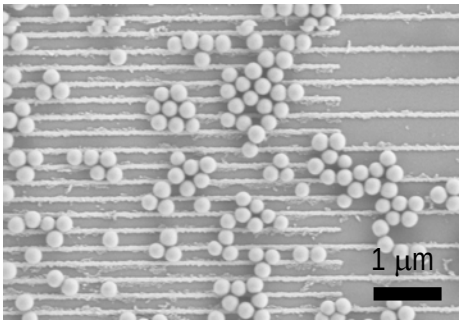

Figure 3. SEM image of one of the electrodes (140nm width, 400 nm pitch), where silica nanoparticles (300nm diameter) have been precipitated.

Poster

PARALLEL NANOGAP FABRICATION WITH NANOMETER SIZE CONTROL USING III-V SEMICONDUCTOR EPITAXIAL TECHNOLOGY

Iván Fernández-Martínez, Yolanda González, Jose L. Costa-Krämer and Fernando Briones.

Instituto de Microelectrónica de Madrid, IMM-CNM-CSIC, Isaac Newton 8 PTM, 28760 Tres Cantos, Madrid, Spain.

Contact@E-mail ivan@imm.cnm.csic.es

A reproducible and full-wafer compatible fabrication process for adjustable contact electrodes separated several nanometers is a major technological challenge. Until now, several approaches have been developed [1-6] to achieve a controlled parallel process for patterning multiple nanogaps with controlled sizes. In this letter a novel method for parallel nanogap fabrication using strained epitaxial III-V beams is presented. The process is highly reproducible, allows parallel fabrication and highly accurate gap size control. The beams are fabricated from MBE grown (GaAs/GaP)/AlGaAs strained heterostructures, standard e-beam lithography, and wet etching. During the wet etching process, the relaxation of the accumulated stress at the epitaxial heterostructure produces a controlled beam breakage at the previously defined beam notch. After the breakage, the relaxed strain is proportional to the beam length, allowing nanogap size control. The starting structure is similar to a mechanically adjustable break junction but the stress causing the breakage is, in this case, built-in the beam. This novel technique should be useful for molecular-scale electronics devices.

An array of four beams with different lengths (from 4 to 10 μm) has been designed and fabricated and it is shown in Fig. 1.a). The formed nanogaps for different cantilever lengths are shown in Fig. 1.b). Fig. 1.c) shows the nanogap size d as a function of the cantilever length L. A linear relation is obtained. These results clearly show that the nanogap formation mechanism developed in this work allows us to control the nanogap size by changing the III-V heteroepitaxial beam length, getting nanogap sizes as low as 5 nm.

References:

[1] Champagne, A. R.; Pasupathy, A. N; Ralph, D. C. NanoLetters, **5** (2005) 305.
[2] Park, H.; Lim, A. K. L.; Park, J.; Alivisatos, A. P.; McEuen, P. L. Appl. Phys. Lett., **75** (1999) 301.
[3] Reed, M.A.; Zhou, C.; Muller, C. J.; Burgin, T.P.; Tour, J.M. Science **278** (1997) 252.
[4] Qin, L.; Park, S.; Huang, L.; Mirkin, C. A. Science **309** (2005) 113.
[5] Krahne, R.; Yacoby, A.; Shtrikman, H.; Bar-Joseph, I.; Dadosh, T.; Sperling, J. Appl. Phys. Lett**. 81** (2002) 730. Maruccio, G.; Marzo, P.; Krahne, R.; Passaseo, A.; Cingolani, R.; Rinaldi, R. Small **3 (**2007) 1184.
[6] Johnston, D. E.; Strachan, D. R.; Johnson, A. T. *NanoLetters* **7** (2007) 2774.

Figures:

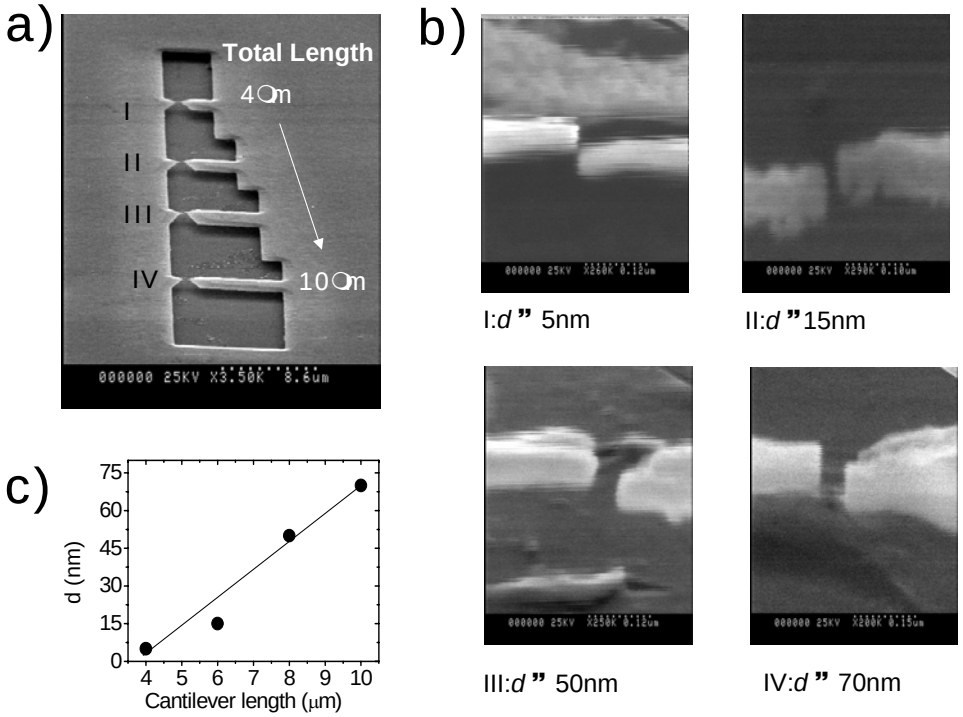

Figure 1) a) Scanning electron microscope image of a four-junction array in which the length of the beam is designed from 4 to 10 μm. The device is tilted 45 degrees during the image acquisition. b) Side view of the different nanogaps that correspond to different beam lengths. The device is tilted 90 degrees during the image acquisition. c) Nanogap size *d* as a function of the beam length *L*.

SELF-PHOTOPATERNABLE DI-UREASIL-ZIRCONIUM OXO-CLUSTERS ORGANIC-INORGANIC HYBRIDS FOR LOW COST INTEGRATED OPTICAL SUBSTRATES

R. A. S. Ferreira[1], D. C. Oliveira[2], A. G. Macedo[1], N. J. O. Silva[1], C. Molina1[2], P. S. André[3], K. Dahmouche[4], V. de Zea Bermudez[5], Y. Messaddeq[2], S. J.L. Ribeiro[2], L. D. Carlos[1]

[1]*Departamento de Física and CICECO, Universidade de Aveiro, 3810 -193 Aveiro, Portugal*
[2]*Instituto de Química, UNESP C.P. 355, 14801-970, Araraquara-SP, Brazil*
[3]*Departamento de Física and Instituto de Telecomunicações, Universidade de Aveiro, 3810 - 193 Aveiro, Portugal*
[4]*Universidade Estadual da Zona Oeste (UEZO), Campo Grande 23070-200, Rio de Janeiro-RJ, Brazil*
[5]*Departamento de Química and CQ-VR, Universidade de Trás-os-Montes e Alto Douro, 5000-801 Vila Real, Portugal*
rferreira@ua.pt

The exploitation of the potential applications of the so-called organic/inorganic hybrids in many different areas, including integrated optics (IO), has been presented during the last years [1]. The simplicity and low cost of the sol-gel process make this method very suitable for the development of organic/inorganic hybrid materials for the production of functional IO devices [2]. Among the various organic/inorganic hosts that have been developed in the last years, those containing amine functionalities, namely urea cross-linked hybrids classed as di-ureasils (Fig. 1) present acceptable transparency, mechanical flexibility and thermal stability to be processed as IO substrates [3-5]. In particular, distributed feedback lasers (DFB) by using dynamic gratings have been demonstrated for di-ureasil thin films incorporating rodhamine 6G [3]. Diffraction gratings, channel and monomode planar waveguides with low propagation losses, both in the infrared (0.6-1.1 dB/cm) and in the visible (0.4-1.5 dB/cm), were fabricated using the synergism between two hybrid precursors (di-ureasil and methacryloxypropyltrimethoxysilane) and methacrylic acid (McOH, CH_2=C(CH_3)COOH)) modified zirconium tetrapropoxide, $Zr(OPr^n)_4$ [4,5].

New perspectives for the development of innovative IO devices, such as low-cost optical power splitters for the general use spreading of all optical access networks, for instance, are therefore envisaged. The requirement of larger bandwidth may be attained by the development of access networks based on optical technology, such as passive all-optical networks (PONs) operating at high bit rate optical signals (40 Gbits/s). This will require low cost components to operate in the infrared spectral region, typically at 1550 nm. Examples of applications being narrow band optical filters (used as demultiplexers to access the desirable wavelengths in a multi-wavelength system), low losses optical power splitters, and optical cavities (for the optical clock extraction function). A window of opportunity for sol-gel derived components is therefore opened.

In this work, di-ureasil hybrids containing McOH modified $Zr(OPr^n)_4$ are prepared and structurally characterized by X-ray diffraction (XRD), small angle X-ray scattering (SAXS), Fourier transform infrared (FT-IR) and Raman spectroscopies, ^{29}Si and ^{13}C nuclear magnetic resonance (NMR), and atomic force microscopy (AFM). XRD and SAXS results point out the presence of Si- and Zr-based nanobuilding blocks (NBBs) dispersed into the organic phase [5]. Furthermore, monomode waveguides, diffractions gratings, and Fabry-Perot cavities are written through the exposure of the hybrid monolith to UV light [5]. The guidance region in patterned channels is determined as a Gaussian section located below the exposed surface. The number of propagating modes, the refractive index gradient and the maximum index contrast are analyzed. Moreover, the reflection coeficient the of the Fabry-Perot cavity (formed

by a grating patterned into a 0.278 cm channel) and its free spectral range value will be estimated [5].

[1] C. Sanchez, B. Julian, O. Belleville, M. Popall, J. Mater. Chem. **15** (2005) 3559.
[2] *Functional Hybrid Materials*, P. Gomez-Romero, C. Sanchez, Eds.; Wiley Interscience: New York, 2003.
[3] D. C. Oliveira, Y. Messaddeq, K. Dahmouche, S. J. L. Ribeiro, R. R. Gonçalves, A. Vesperini, D. Gindre, J.-M. Nunzi, J. Sol-Gel Sci. Techn. **40** (2006) 359.
[4] C. Molina, P. J. Moreira, R. R. Gonçalves, R. A. S. Ferreira, Y. Messaddeq, S. J. L. Ribeiro, O. Soppera, A. P. Leite, P. V. S. Marques, V. de Zea Bermudez, L. D. Carlos J Mater Chem **15** (2005) 3937.
[5] D. C. Oliveira, A. G. Macedo, N. J. O. Silva, C. Molina, R. A. S. Ferreira, P. S. André, K. Dahmouche, V. de Zea Bermudez, Y. Messaddeq, S. J. L. Ribeiro, L. D. Carlos, submitted.

Figures:

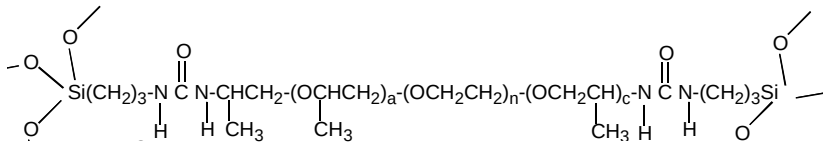

Figure 1. Molecular Structure of the di-ureasil hybrid (a+c=4.5, n=8.5).

FUNCTIONALIZED NANO-MICROSTRUCTURES TO COMBAT BIOFOULING OF INDUSTRIAL SURFACES

Ferreira C., Rosmaninho R., Pereira M. C., Bastos M.M.S.M., Nunes O.C., Coelho M. and Melo L. F.
LEPAE, Departamento de Engenharia Química, Universidade do Porto, Rua Dr. Roberto Frias, 4200-465 Porto, Portugal

carlaf@fe.up.pt

Biofilm formation is a strategy that bacteria use in order to survive in hostile environments, causing serious problems in the food industry, cooling water systems, medical equipment, etc. [1]. The control and destruction of undesirable biofilms often includes the use of chemical products with antimicrobial properties like biocides and surfactants. However, these substances can be considered harmful for the environment and consequently should be used in as small quantities as possible.

The goal of the work is to develop a novel procedure for biofilm control based on the transport of antimicrobial compounds on nano-microparticles or capsules. In this study, the efficacy of the method against suspended cells of *Pseudomonas fluorescens* was assessed, using benzyldimethyldodecylammonium chloride (BDMDAC), which is a surfactant belonging to the family of benzalkonium chloride, as a biocide carried on microparticles (diameter: 4 μm). The latter were prepared using the layer-by-layer self-assembly (LBL) technique [2]. The oppositely charged polyethyleneimine (PEI), sodium polystyrene sulfonate (PSS) and BDMDAC were assembled on polystyrene (PS) cores (Figure 1).

The BDMDAC coated particles were observed by CryoSEM and their composition by X-ray microanalysis (Figure 2). Their size distribution (Coulter Particle Size Analyzer) and zeta potential (Nano Zetameter) were also determined. The evaluation of the minimum amount of surfactant/biocide needed for effective microbial reduction was carried out through the determination of the survival ratio of the microbial population after different periods of exposure to BDMDAC coated particles (Figure 3). The assays were performed with a cell suspension in sterile saline solution (0.85% NaCl) containing $1.1\times10^{3}\pm150$ UFC/ml. After exposure to BDMDAC coated particles, the enumeration of viable cells was done spreading on Plate Count Agar, and incubation for 24h at 30ºC. A cell suspension without contact with the biocide was used as control. The possibility of reusing the BDMDAC coated microparticles to increase their life time and save biocide was also studied in order to optimize the industrial cleaning procedures (Figure 4).

References:

[1] Melo, L.F., Vieira, M.J., Bioprocess Engineering, **Physical stability and biological activity of biofilms under turbulent flow and low substrate concentration (**1999) 20, 363-368

[2] Cordeiro, A. L., Coelho, M., Sukhorukov, B. G., Dubreuil, F., Möhwald, H., Journal of Colloids and Interface Science, **Effect of shear stress on adhering polyelectrolyte capsules**, (2004) 280, 68-72

Figures:

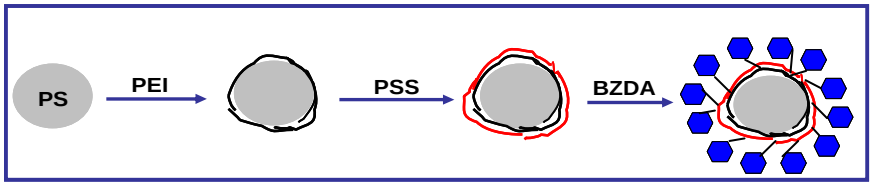

Figure 1: Schematic sequence of the formation process of the microparticles.

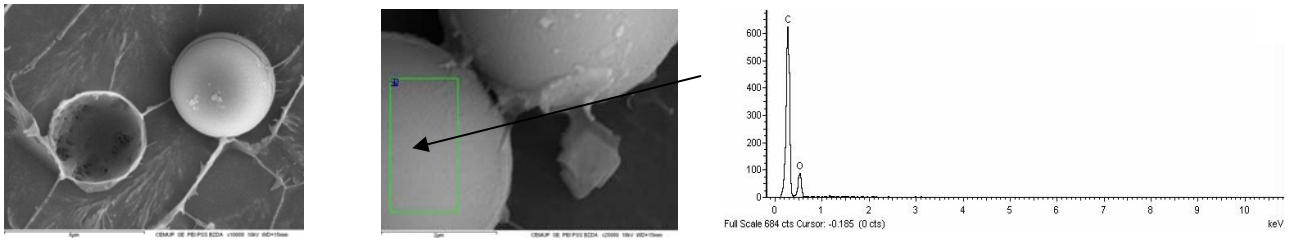

Figure 2: CryoSEM image of the coated particles and X-ray Microanalysis of the coating layer.

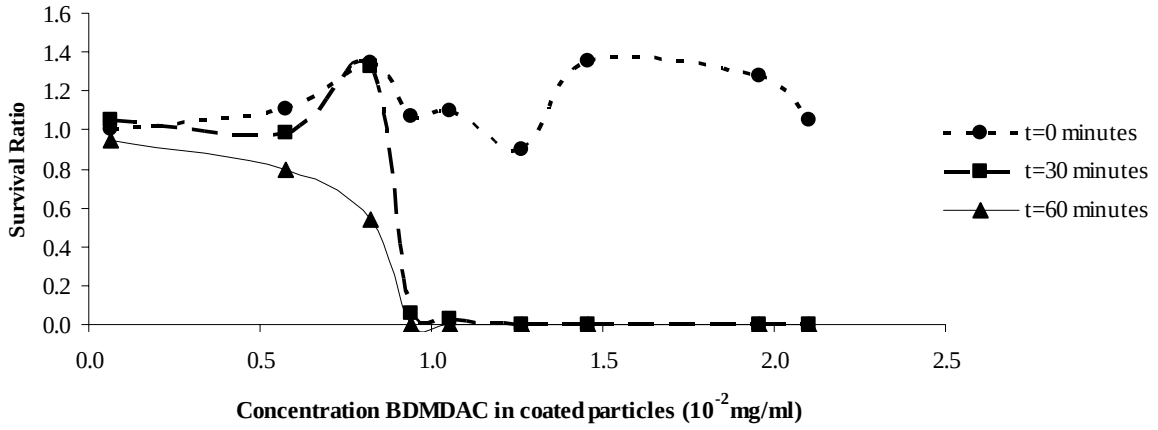

Figure 3: Determination of the minimum concentration of adsorbed biocide needed for effective biocidal action.

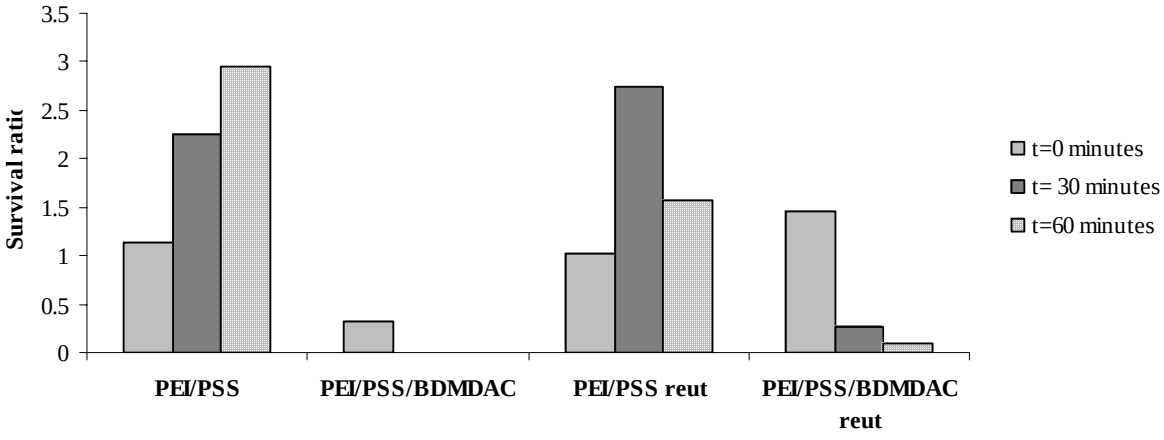

Figure 4: Reutilization test for the biocide coated particles at the minimum biocide concentration. Microparticles without biocide (PEI/PSS) were used as control.

Synthesis and electric properties of nanoporous $BaTiO_3$

Paula Ferreira, Ru Zhong Hou, Paula M. Vilarinho
University of Aveiro, Department of Ceramics and Glass Engineering, CICECO, 3810-193 Aveiro, Portugal

pcferreira@ua.pt

Ferroelectrics are a very important class of functional materials, particularly in the area of electronics and microelectronics industry. They are used in bulk and film forms and find applications in a huge range of devices from multilayer capacitors, piezoelectric generators, motors, actuators, positive temperature coefficient sensors, integrated optics and memories.[1] Controlling the morphology of ferroelectrics in the nano-scale inputs new energy into the research and development of ferroelectric materials. For example, various 1-dimensional nano-rods, nano-wires and nano-tubes as well as self-assembly of 0-dimensional nano-islands of ferroelectrics have been achieved, providing candidates for both fundamental studies and novel applications of ferroelectricity in nano-scale.[2]

A common thought is that porosity is adverse to both ferroelectric and dielectric materials. Perfect single crystals or dense ceramics are desired in most cases. But actually, porosity may also have good impacts on materials properties of ferroelectrics. A typical example could be porous pyroelectric films which exhibit higher figure of merits over their dense counterparts.[3] Porous piezoelectric ceramics are known to have higher hydrostatic figure of merit and better acoustic impedance matching with ambient medium in applications of low frequency hydrophones and sensors. These effects come from the lowering of dielectric constant of materials due to the introduction of porosity. By manipulating the volume ratio of porosity, dielectric constant can be adjusted in a wide range. Taking advantage of it, materials with highly anisotropic dielectric constant were fabricated with the introduction of aligned pores.[4] In the above cases, pores are usually formed by incomplete sintering or using sacrificial pore formers and exist in between the grains. The negative influence of porosity in these applications is known as the decrease of mechanical stiffness of the materials. If pores reside inside the grains, this would not be a problem any more.

In this work, the synthesis of nanoporous barium titanate prepared by template assisted methodology using cationic cetyltrimethylammonium chloride surfactant[5] or non-ionic block copolymer Pluronic PE 10300 ($EO_{15}PO_{70}EO_{15}$) is reported. The materials were characterized by powder X-ray diffraction, scanning and transmission electron microscopy, low temperature nitrogen adsortion-desorption isotherms and Raman spectroscopy. Well crystallized nanoporous $BaTiO_3$ crystallites were directly synthesized from solution via a simple sol-precipitation process with both types of templates. The nanoporous structures were disordered and wormhole-like with thick single-crystalline framework (Figure 1). The ferroelectric properties of the materials were evaluated by measuring the variation of the dielectric permittivity with the temperature (Figure 2). Using Landauer-Bruggeman effective medium aproximation (EMA) and Spherical Inclusion model (SI), the effective dielectric constants of BaTiO3 porous materials were estimated to be around 2500 for 10 kHz which are similar to those of nano-grain $BaTiO_3$ ceramics (Figure 2).

References:

[1] P. M. Vilarinho, Functional materials: properties, processing and applications, in Scanning Probe Microscopy: Characterization, Nanofabrication and Device Application of

Functional Materials, pag 3 – 33, NATO Science Series, II. Mathematics, Physics and Chemistry – Vol. 186, Kluwer Academic Publishers, 2005.

[2] F. D. Morrison, Y. Luo, I. Szafraniak, V. Nagarajan, R. B. Wehrspohn, M. Steinhart, J. H. Wendorff, N. D. Zakharov, E. D. Mishina, K. A. Vorotilov, A. S. Sigov, S. Nakabayashi, M. Alexe, R. Ramesh, J. F. Scott, *Rev. Adv. Mater. Sci.* **4** (2003) 114.

[3] G. Suyal, A. Seifert, N. Setter, Appl. Phys. Lett. **89** (2002) 1059.

[4] Z.N. Wing, B. Wang,J. W. Halloran et al. J. Am. Ceram. Soc. **89** (2006) 3696.

[5] R.Z. Hou, P. Ferreira, P. M. Vilarinho, Micropor. Mesopor. Mater. (2007) doi:10.1016/j.micromeso.2007.06.051

Figures:

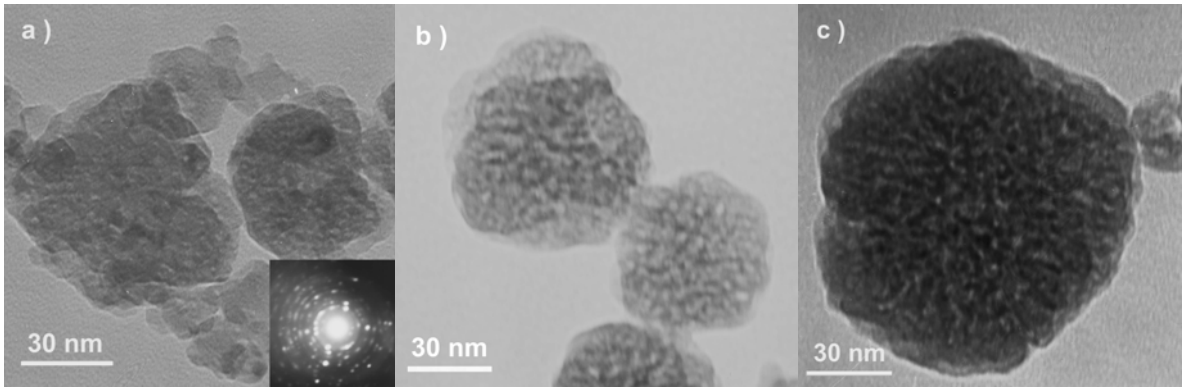

Figure 1. TEM images of nanoporous $BaTiO_3$ prepared with PE 10300: a) as-synthesized crystallites (selected area electron diffraction is shown as inset); b) calcined at 573 K and c) calcined at 673 K.

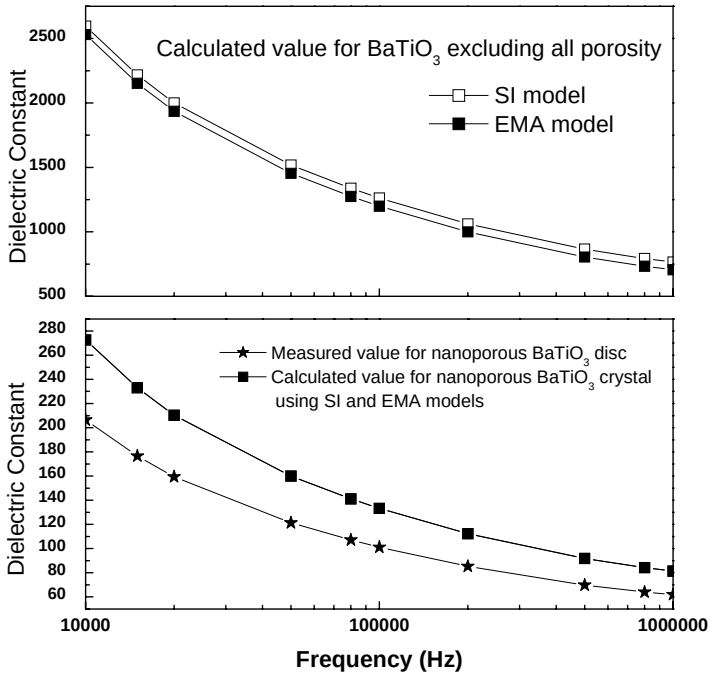

Figure 2. Dielectric characterization on isostatic pressed discs composed of nanoporous $BaTiO_3$, based on which, the apparent dielectric constants of nanoporous $BaTiO_3$ crystallites and $BaTiO_3$ without any porosity are estimated using both SI and EMA models. For nanoporous $BaTiO_3$ crystallites, using SI and EMA results in very close values.

Enzymatic Synthesis of Amorphous Calcium Phosphate-Chitosan Nanocomposites and its Processing into Hierarchical Structures

Mª Luisa Ferrer, Mª Jesus Hortigüela, M. C. Gutierrez, I. Aranaz, F. del Monte
Instituto de Ciencia de Materiales de Madrid, Campus de Cantoblanco 28049
mferrer@icmm.csic.es

The requirements for the production of suitable supports for the growth of cells and tissues involve the use of biocompatible and/or biodegradable materials and the processing of the components into a porous matrix of adequate morphology. The use of organic and inorganic materials has been widely explored, but lately, the use of organic-inorganic composite materials is attracting even increased attention. Controlling the length scale at the organic-inorganic interface within the nanometer range produces a wealth of both novel structural features and enhanced properties arising from the synergistic interaction of the individual constituents; i.e., consequence of the strong mechanical interface between mineral substrate and polymer matrix [1]. Biomineralization offers the opportunity to produce highly organized nanocomposite structures, controlling specific architectures over extended length scales for a wide range of compositions [2]. Here in, we have applied an enzymatically assisted route (e.g., the urease assisted hydrolysis of urea) for the preparation of nanocomposites. The base generated by urea hydrolysis promoted both CHI gelation and calcium phosphate precipitation at biological temperatures (~37 ºC) [3]. Macroporous hierarchical structures were thereafter obtained by a cryogenic process (named ISISA, ice segregation induced self-assembly) that simply consist on the unidirectional freezing (at -196 ºC) of the hydrogel nanocomposite [4, 5]. Upon freezing, the ice formation (hexagonal form) causes every solute originally dissolved/dispersed in the hydrogel to be segregated from the ice phase. After freeze-drying, the resulting hierarchical structures consists on well aligned micrometer-sized pores in the freezing direction corresponding to the empty areas where ice crystals originally resided, being the macrostructure supported by the matter (e.g., calcium phosphate nanoparticles dispersed within CHI matrix) accumulated between adjacent ice crystals [6].

References:

1] (a) Mann, S. *Angew. Chem. Int. Ed., 39*, (2000) 3392-406. (b) Sanchez, C.; Arribart, H.; Giraud-Guille, M. M. *Nat. Mater., 4*, (2005)277.

[2] (a) Sanchez, C.; Julián, B.; Belleville, P.; Popall, M. *J. Mater. Chem. 15 (*2003)*,* , 3559-3592. (b) Tai, K.; Ulm, F.-J.; Ortiz, C. *Nano Lett. (6)*,2006, 2520-2525.

[3] (a) Sondi, I.; Matijević, E. J. Coll. Inter. Sci. 238, (2001), 208-214. (c) Chenite, A.; Gori, S.; Shive, M.; Desrosiers, E.; Buschmann, M. D. *Carbohyd. Polym. 64, (* 2006), 419-424.

[4] For a recent review see: Gutierrez, M. C.; Ferrer, M. L.; del Monte, F. *Chem. Mater. 20,(4), (*2008), 634-648.

[5] See also: (a) Mukai, S. R.; Nishihara, H.; Tamon, H. *Chem. Commun.* 874, (2004). (b) Gutierrez, M. C.; Hortigüela, M. J.; Amarilla, J. M.; Jimenez, R.; *Ferrer, M. L.*; del Monte, F. *J. Phys. Chem. C*, *111*, (2007) 5557, and references there in. (c) Gutierrez, M. C.; Garcia-Carvajal, Z.; Hortigüela, M. J.; Yuste, L.; Rojo, F.; *Ferrer, M. L.*; del Monte, F. *J. Mater.*

Chem. 17(29), (2007), 2992-2995. (d) Gutierrez, M. C.; Garcia-Carvajal, Z.; Yuste, L.; Rojo, F.; *Ferrer, M. L.*; del Monte, F. *Adv. Funct. Mater.* 2007 (DOI: 10.1002/adfm200700093) (e) Abarrategui, A.; Gutierrez, M. C.; Moreno-Vicente, C.; Hortigüela, M. J.; Ramos, V.; López-Lacomba, J. L.; *Ferrer, M. L.*; del Monte, F. *Biomaterials 29, (*2008), 94-102.

[6] Gutierrez, M. C.; Jobbagy, M.; *Ferrer, M. L.;* del Monte, F. *Chem. Mater.,20 (* 2008), 11-13.

Figures:

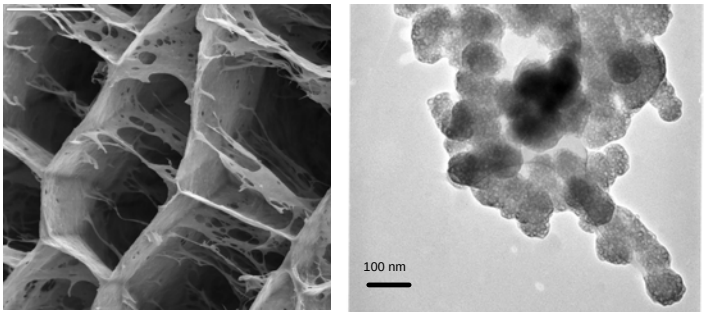

Figure 1: SEM micrograph of hierarchically structured amorphous calcium phosphate-chitosan nanocomposites (left, bar is 50 μm). TEM micrograph of amorphous calcium phosphate aggregates entrapped within the chitosan network gel (right, bar is 100 nm).

MODIFIED ELECTRODE BASED ON ZEOLITE-ENCAPSULATED Cr(III) COMPLEX

Sara Gonçalves[1], Hugo Figueiredo[2], Bruna Silva[2], Teresa Tavares[2], Pier Parpot[1], Isabel C. Neves[1], António M. Fonseca[1], Anna E. Lewandowska[3], Miguel A. Bañares[3]

[1]Departamento de Química, Universidade do Minho, Campus de Gualtar, 4170-057 Braga, Portugal - Email:ineves@quimica.uminho.pt
[2]IBB – Instituto de Biotecnologia e Bioengenharia, Centro de Engenharia Biológica, Universidade do Minho, Campus de Gualtar, 4710-057, Braga, Portugal - Email:ttavares@deb.uminho.pt
[3]Instituto de Catálisis y Petroleoquímica, Instituto de Catálisis y Petroleoquímca, CSIC Universidad Autónoma de Madrid, E-28049-Madrid, Spain – Email: banares@icp.csic.es

Zeolites are very important in materials science for the development of functional materials as well as in nanotechnology and these solids are very attractive in heterogeneous catalysis [1, 2]. For these applications, zeolites provide a rigid structure in which some active compounds can be included. In addition to the space constraints imposed by the zeolite, the negative charge of the zeolite framework and the distribution of the positive charges of the cations can lead to specific interactions with the zeolite framework which in turn induce structural and functional modifications as compared to solution activities [2].
The first syntheses of encapsulated complexes within zeolites generated much interest due to effects of site isolation and steric confinement on the physical properties and chemical reactivity of the molecules trapped within supercages of the crystalline microporous zeolite lattice [3]. Zeolite-encapsulated transition metal complexes are generally characterized by spectroscopic techniques and elemental analyses [4].
This work reports the studies of the electrochemical behaviour of Cr(III)-PAN complexes encapsulated in NaY zeolite. The redox properties of these zeolite-encapsulated complexes were investigated by cyclic voltammetry with a new method for the preparation of carbon toray-zeolite-modified electrode.
The synthesis of Cr(III) complexes encapsulated in supercages of Y zeolite was carried out by free diffusion of the PAN (1-(2-pyridylazo)-2-naphtol) ligand (Figure 1) through the zeolite pores exchanged with the Cr(III) metal ion, obtained by the previous use of the biosorption process [5].
The resulting materials were characterized via surface analysis (SEM, XRD), chemical analysis, spectroscopic methods (FTIR and Raman) and cyclic voltammetry in aqueous medium with zeolite-modified electrodes.

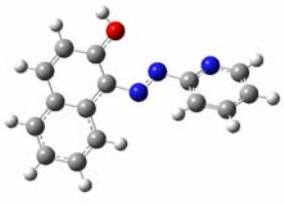

Figure 1 – 1-(2-pyridylazo)-2-naphtol (PAN) ligand

Zeolite-encapsulated Cr(III)-PAN complex was deposited on carbon Toray (CT) in order to determine the electroreactivity by cyclic voltammetry. The cyclic voltammetry studies obtained with a new method for the preparation of zeolite-modified electrodes shows

evidence for electroactivity restricted to boundary associated Cr(III)-PAN complexes (Figure 2).

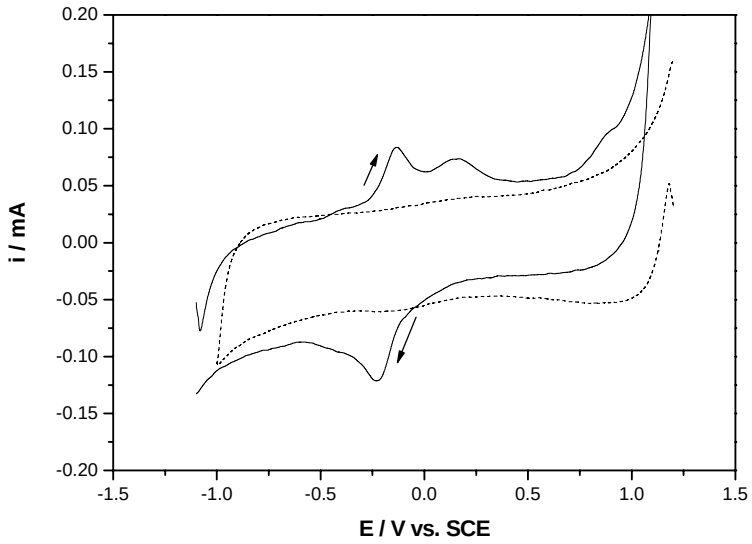

Figure 2 - The voltammograms of Cr(III)PAN-NaY/Carbon (…..) and Cr(III)PAN-NaY/Carbon (—) in 0.1 M NaCl at ambient temperature (scan rate: 50 mV s^{-1})

The combination of the spectroscopic techniques and elemental analysis with electrochemical methods provide a powerful tool to reveal the unequivocal evidence for the encapsulation of Cr(III)-PAN complex in the supercages of zeolite Y.

The micro Raman spectra underline a non-homogeneous distribution of chromium oxide species. Figure 3a shows the Raman spectrum at spots that exhibit orange color in optical microscopy while Figure 3b, that of the white spots. The Raman bands 1001 and 882 cm^{-1} are related to surface chromium (VI) oxide species (Fig. 3a). A band at 880 cm^{-1} is attributed to the stretching mode of bridging oxygen sites (Cr-O-Cr) in surface polymeric Cr^{VI} species. The 1001 cm^{-1} Raman band is assigned to the terminal Cr=O stretching mode in surface isolated and polymeric Cr^{VI} species. The Raman spectra show no Cr_2O_3 aggregates, which would exhibit an intense band at 550 cm^{-1}.

The bands observed on the Raman spectrum, Figure 3b, are assigned to NaY zeolites vibration modes. The Raman bands observed between 200 and 600 cm^{-1} are assigned to the motion of the oxygen atom in a plane perpendicular to the T-O-T bonds in the zeolite structure.

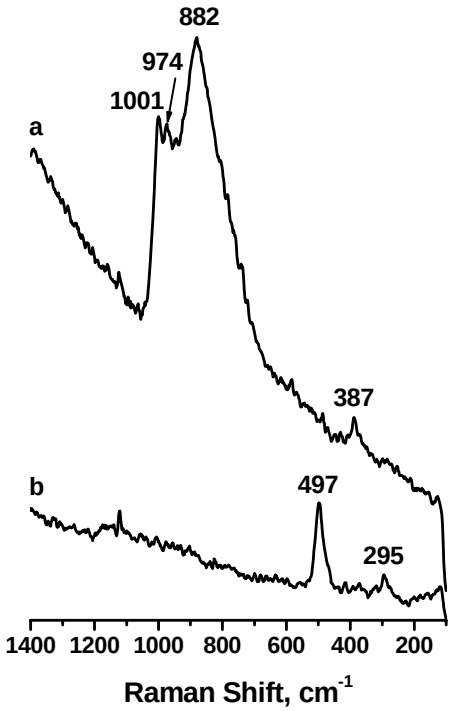

Figure 3 – Raman spectra of dehydrated Cr-NaY catalyst.

References:

[1] M. E. Davis, Nature, **417** (2002) 813-821.
[2] A. Corma, H. Garcia, Eur. J. Inorg. Chem., **6** (2004) 1143-1164.
[3] C.A. Bessel, D. Rolison, J. Phys. Chem. B, **101** (1997) 1148-1157.
[4] F. Costa, C.J.R. Silva, M.M.M. Raposo, A.M. Fonseca, I.C. Neves, A.P. Carvalho, J. Pires, Microporous Mesoporous Mater., **72** (2004) 111-118.
[5] H. Figueiredo, I.C. Neves, C. Quintelas, T. Tavares, M. Taralunga, J. Mijoin, P. Magnoux, Appl. Catal. B: Environmental, **66** (3-4) (2006) 274-280.

RUTHENIUM COMPLEXES ENCAPSULATED IN NANOSTRUCTURED SOL-GEL SILICA MATRICES

Luís Manuel F. Lopes, Ana Rosa Garcia, Alexandra Fidalgo, Laura M. Ilharco
Centro de Química-Física Molecular, Complexo I, Instituto Superior Técnico
Av. Rovisco Pais, 1, 1049-001, Lisboa, Portugal
luis.f.lopes@ist.utl.pt

Ruthenium complexes are very promising as anti-tumoral drugs, due to their selective activity and reduced cytotoxicity when compared to the traditional platinum complexes, widely used in chemotherapy [1]. On the other hand, it is a prime concern to specifically attack the malignant cells causing minimum collateral effects, which is attainable by targeted controlled delivery of the drugs encapsulated in nanoporous materials. The ideal carrier must be bioresorbable, with non-toxic degradation products, and assure a drug release kinetics that meets the treatment requirements.

The sol-gel process emerges as a very promising approach to synthesise those devices, given the fact that it is soft and versatile. The drugs may be encapsulated during the synthesis without risking decomposition and the capability to synthesize nanostructured matrices with tailored properties has been extensively stressed [2]. In the case of silica, an adequate control of the synthesis parameters allows producing materials ranging from dense xerogels to very light aerogels, from hydrophilic to highly hydrophobic, with very different porous structures and dimensions [3]. This potential justifies the recent interest in using sol-gel silica matrices to the encapsulation of catalysts and pharmaceutical drugs, in the first case to enhance the catalytical performance and in the latter to eventually use those devices in controlled drug delivery [4].

The purpose of the present work is to mimetize a controlled drug delivery system by encapsulating Ru complexes in nanoporous sol-gel silica matrices and, in a first stage, to characterize the structural modifications induced by the dopant on the matrix and vice-versa.

The following Ru complexes were rehearsed:

- HexaamineRu(III) chloride $[Ru(NH_3)_6]Cl_3$;
- Triruthenium dodecacarbonyl $[Ru_3(CO)_{12}]$;
- Ruthenium(III) nitrosylnitrate $[RuNO(NO_3)_3]$;
- Ruthenium(III)chloride oxide, ammoniated, or ruthenium red, $[(NH_3)_5RuORu(NH_3)_4ORu(NH_3)_5]Cl_6$.

They are schematized in Figure 1.

The pure Ru complexes were earlier characterized by diffuse reflectance infrared Fourier transform spectroscopy (DRIFTS) and diffuse reflectance UV-Vis spectroscopy. In aqueous solution, infrared attenuated total reflection (ATR) and UV-Vis spectroscopies were used.

The silica matrices with and without complexes were prepared using tetraethylorthosilicate (TEOS) as precursor and iso-propanol as the co-solvent, by a two step process, consisting

of acid hydrolysis and neutral condensation. Given the low solubility of some of the Ru complexes in the initial sol, an important parameter under study was the water/TEOS molar ratio.

Other parameters explored were the catalysis conditions, the complex concentration with respect to silica, the stage of incorporation and the drying velocity.

All the matrices were thoroughly characterized by diffuse reflectance infrared and UV-Vis spectroscopies, and also by nitrogen gas-solid adsorption isotherms and envelope density measurements.

It was possible to conclude that the encapsulation of the Ru complexes, even in small contents, increased the gelation times and induced modifications in the silica structure.

The complexes hexaaminoruthenium and Ru-red undergo redox reactions as the sol-gel process occurs, contrarily to triruthenium dodecacarbonyl and ruthenium(III) nitrosylnitrate, which only interact with the matrix.

In the case of triruthenium dodecacarbonyl a preferential orientation within the matrix pores is proposed .

References:

[1] M. Bouma, B. Nuijen, E. E. Challa, J. Sava, A. Flaibani, A. Bult, J. H. Beijnen, J. Oncol. Pharm. Pract., **10** (2004) 7.
[2] A. Fidalgo, L. M. Ilharco, Chem. Eur. J., **10** (2004) 392.
[3] A. Fidalgo, M. E. Rosa, L. M. Ilharco, Chem. Mater., **15** (2003) 2186.
[4] P. Gancitano, R. Ciriminna, M. L. Testa, A. Fidalgo, L. M. Ilharco, M. Pagliaro, Org. & Biomol. Chem., **3** (2005) 2389.

Figure 1: Schematic structures of the ruthenium complexes under study

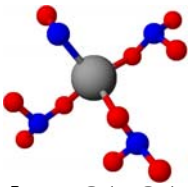

$[RuNO(NO_3)_3]$

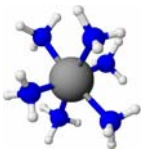

$[Ru(NH_3)_6]^{3+}$

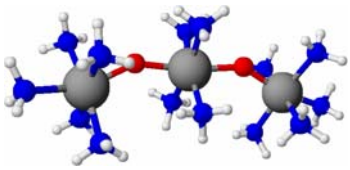

$[(NH_3)_5RuORu(NH_3)_4ORu(NH_3)_5]^{6+}$

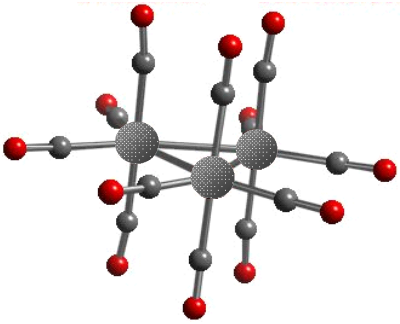

$[Ru_3(CO)_{12}]$

ELECTRICAL, STRUCTURAL AND OPTICAL CHARACTERIZATION OF AMORPHOUS/NANO CUPPER OXIDE BASED SEMICONDUCTORS

V. Figueiredo[1], E. Elangovan[1], G. Gonçalves[1], P. Barquinha[1], L. Pereira[1], N. Franco[2], E. Alves[2] R. Martins[1], E. Fortunato[1]

[1]CENIMAT/I3N, Materials Science Department, Campus de Caparica, 2829-516 Caparica, Portugal

[2]LFI, Dep. Física, Instituto Tecnológico e Nuclear, EN10, 2686-953 Sacavém, Portugal

Tel: +351212948562; Fax: +351212948558

vitor.figueiredo@gmail.com

Thin films of cupper oxide were prepared on glass substrate by thermal evaporation assisted by electron beam at room temperature and post annealed at different temperatures (100-450º C) at atmospheric pressure. It is observed a strong correlation between the electrical and structural properties. The Cu phase is only present at as deposited sample and at the 100º C annealed sample, although with a less amount of Cu. The oxide Cu_2O phase is also observed in this sample, and remains until 300º C, where occurs a phase transition from Cu_2O to CuO. This phase remains in the rest of the samples. The films were electrically characterized by Hall effect and conductivity as a function of temperature. In order to estimate the oxidation rate in-situ dc conductivity has been done as a function of temperature. The films have also been characterized by SEM, AFM and UV-VIS-IR techniques. The possibility to perform electronic devices will be investigated.

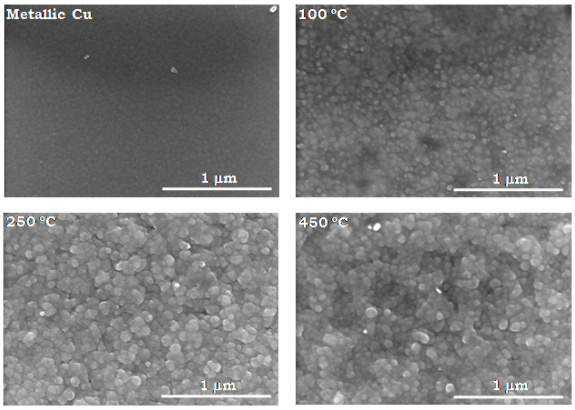

SEM microstructures of the copper oxide films as a function of annealing temperature.

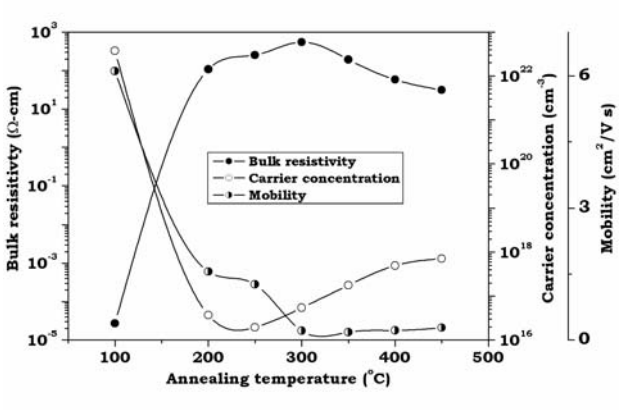

Variation of electrical properties of the copper oxide films as a function of annealing temperature.

DNA DETECTION USING AMORPHOUS SILICON SENSORS WITH GOLD NANOPARTICLES

Leonardo Silva[1], Elvira Fortunato[1], Hugo Águas[1], Gonçalo Doria[2], Pedro Baptista[2], and Rodrigo Martins[1]

[1]CENIMAT/I3N, Materials Science Department,

[2]CIGMH/SABT, Biotechnology Department, Campus de Caparica, 2829-516 Caparica, Portugal

Tel: +351212948562; Fax: +351212948558

elvira.fortunato@fct.unl.pt

Advances in nanosciences are having a significant impact in many areas of research on nearly every industry. The impact of new nanotechnologies has been particularly large in biodiagnostics, where a number of nanoparticle-based assays have been introduced for biomolecules detection extending the limits of molecular diagnostics to the nanoscale. The applications of nanoparticles have largely focused on DNA-functionalised gold nanoparticles used as the target-specific probes. These gold nanoparticle-based systems can be used for the detection of specific sequences of DNA or RNA. Gold nanoparticles derivatised with thiol modified oligonucleotides complementary to DNA targets - Au-nanoprobes - are used to distinguish fully complementary from mismatched sequences. Here a rapid and inexpensive colorimetric nanoparticle-based method for mismatch detection in DNA using an optoelectronic platform samples is reported [1,2]. The device integrates an amorphous/nanocrystalline biosensor and a light emission source with a gold nanoprobe for specific DNA / RNA detection. This low cost, fast and simple optoelectronic platform permits detection of few picomole of nucleic acid without target or signal amplification making it suitable for application in population diagnostics and in point-of-care hand–held devices.

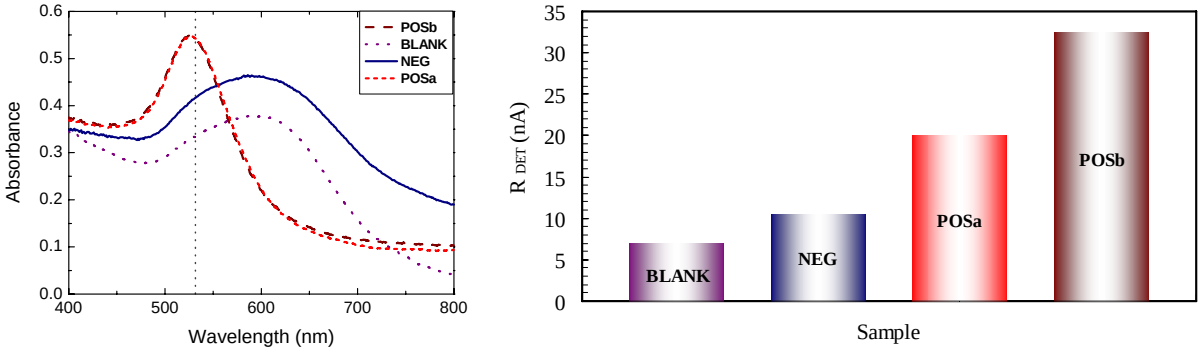

a) b)

Figure – Comparison between the results obtained by using the conventional method (a) with those ones using the new optoelectronic platform (b), using exactly the same biological samples. The new method besides the DNA identification enables also its quantification (see figure b, POSa and POSb).

[1] R. Martins, P. Baptista, L. Raniero, G. Doria, L. Silva, R. Franco, E. Fortunato, Applied Physics Letters 90 (2007) 023903

[2] Patent pending (September 2006, nº 103 561).

Poster

THEORY OF TOPOGRAPHY AND RECOGNITION IMAGING BY DYNAMIC FORCE MICROSCOPY

Martina Fuss[1], *Enrique Sahagún*[2], *Mariana Köber*[1], *Marcos Penedo*[1], *Mónica Luna*[1], *and Juan José Sáenz*[2]

[1]*Instituto de Microelectrónica de Madrid, Consejo Superior de Investigaciones Científicas, E-28760 Tres Cantos, Madrid, Spain;* [2]*Departamento de Física de la Materia Condensada, Universidad Autónoma de Madrid, E-28049 Madrid, Spain*

martina.fuss@imm.cnm.csic.es

Since the beginnings of Atomic Force Microscopy (AFM), measurement techniques have steadily evolved leading to a growing field of successful applications in biology. Although force spectroscopy (consisting in recording force vs. distance curves) represents an excellent method for studying one key issue in biological processes, molecular recognition, until recently it was impossible to record recognition maps at the same resolution and imaging speed as the conventional maps of topography, lateral force, phase, etc. The introduction of simultaneous Topography and RECognition (TREC) imaging [1,2] provided a simple and fast Dynamic Force Microscopy mode capable of simultaneously recording images of topography and specific recognition between the molecules at scanning tip and sample. This is achieved by evaluating the maxima and minima of the cantilever oscillation separately in intermittent contact mode. In this poster, we aim to theoretically confirm the working principle of TREC and identify the experimental conditions needed in order to obtain optimal sensitivity.

To that end, the dynamic response of the cantilever-tip system in water was simulated as a damped, driven harmonic oscillator with additional terms describing the interaction with the sample. The non-specific tip-sample interactions considered were van-der-Waals forces and Derjaguin-Muller-Toporov contact repulsion [3]. Specific recognition forces (F_{rec}) between the ligand tethered to the tip and its epitopes on the sample surface was modelled in different ways. On one hand, interactions depending on the molecular linker were simulated. Therefor, a harmonic potential with

$$F_{\mathrm{rec}}(d) = -k_{\mathrm{l}}(d - L_{\mathrm{opt}})$$

centred at the linker's "optimum extension" L_{opt} (d: instantaneous tip-sample distance, k_{l}: linker's force constant) or the worm-like chain model

$$F_{\mathrm{rec}}(d) = -\frac{k_B T}{L_p}\left[\frac{1}{4\left(1 - d/L_0\right)^2} - \frac{1}{4} + \frac{d}{L_0}\right]$$

(k_B: Boltzmann's constant, T: temperature, L_0: linker's contour length, L_p: linker's persistence length) were used. In both cases, the oscillation amplitude was chosen to be slightly smaller than the tether length [1]. On the other hand, the effect of additional van-der-Waals attraction (intruduced by means of a locally higher Hamaker constant without considering any ligand) was studied. The resulting equations of motion were integrated using a fifth-order Runge-Kutta algorithm.

Our results show that when $Q \approx 1$, indeed variations in sample topography and the presence of binding sites affect different parts of the cantilever's oscillation. The recognition events modelled by a harmonic potential or a worm-like chain lead to qualitatively equal results and give very similar numerical results when reasonable values for a typical PEG linker are chosen for L_{opt}, k_{l}, L_0, and L_p. Whereas recognition sites of all three types cause the upper half of the deflection period to diminish (oscillation maxima decrease), topographic changes

mainly influence the lower half of the cantilever oscillation (deflection minima adapt to topography).

In order to efficiently distinguish contributions from topography and recognition events (and to keep the scanning tip at a constant distance from the sample), a feedback loop based on the deflection minima has to be employed. Only then, the signal provided by the deflection maxima contains the true recognition information and the vertical piezo movement compensating the minima signal accurately represents topography. An example of this situation is given in fig. 1, where the scanning of a sample with mixed topographic and recognition features (modelled as harmonic potential) is simulated. As can be seen, the recognition signal (built from the deflection maxima) is not affected by the substrate topography and vice versa. This insight is not readily available in the experiment since the presence of molecular recognition sites on a sample is always linked to the topographic detection of the respective epitopes.

In view of these findings, from a theoretical point of view we show that Dynamic Force Microscopy employing a low quality factor ($Q \approx 1$) and an oscillation amplitude adequate for the chosen cross-linker can be used in TREC mode to simultaneously map topographic and recognition information. Simulations point out that a feedback loop based on the deflection minima signal succeeds in the optimal separation of both signals. Our results indicate that molecular recognition in TREC can be usefully modelled by both a harmonic potential or a worm-like chain model, and that even other attractive interactions like locally enhanced van-der-Waals forces could be detected by evaluating the cantilever's deflection maxima.

References:

[1] C. Stroh, A. Ebner, M. Geretschläger, G. Freudenthaler, F. Kienberger, A.S.M. Kamruzzahan, S.J. Smith-Gill, H.J. Gruber, and P. Hinterdorfer, Biophys. J. **87** (2004) 1981-1990.
[2] C. Stroh, H. Wang, R. Bash, B. Ashcroft, J. Nelson, H. Gruber, D. Lohr, S.M. Lindsay, and P. Hinterdorfer, Proc. Natl. Acad. Sci., **101** (2004), 12503-12507.
[3] B.V. Derjaguin, V.M. Muller, and Y.P. Toporov, J. Colloid Interface Sci. **53** (1975), 314-326.

Figures:

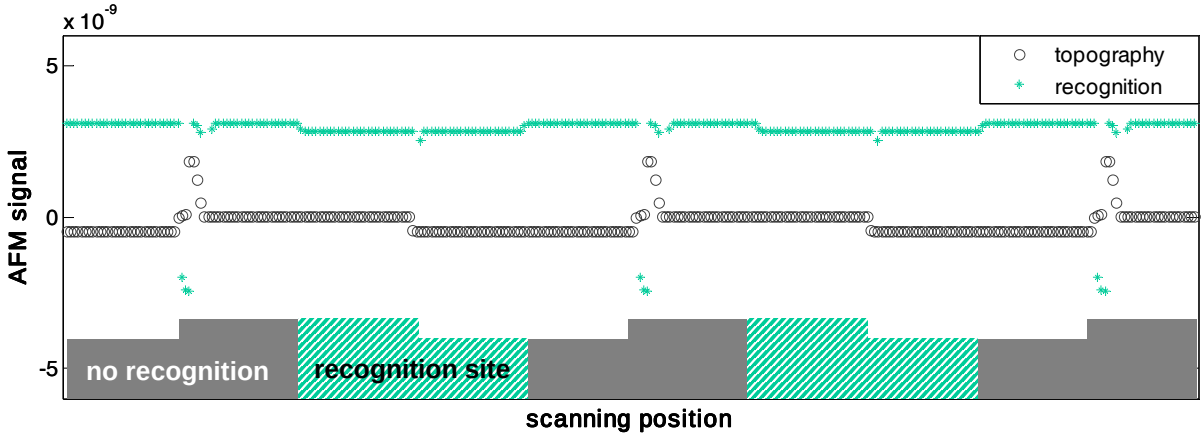

Figure 1. Simulated scan line of an area containing both topographic and recognition features. The sketch at the bottom represents the sample scanned (striped portions are recognition sites). It can be seen that the topography signal represents an accurate measure of the sample's height, whereas the recognition signal identifies the epitopes on the sample.

Preferential nucleation, molecular distortion, charge transfer, and elastic effects in the self-assembly of TCNQ on Cu(100)

Christian Urban [1], Marta Trelka [1], David Écija [1], Roberto Otero [1,2], Rodolfo Miranda [1,2], Luis Sánchez [3], Nazario Martín [2,3], Yang Wang [4], Manuel Alcamí [4], Fernando Martín [4], José M. Gallego [5]

[1] Dpto. de Física de la Materia Condensada, Universidad Autónoma de Madrid, Cantonblanco, 28049-Madrid, Spain

[2] Instituto Madrileño de Estudios Avanzados en Nanociencia (IMDEA-Nanociencia), Cantoblanco, 28049-Madrid, Spain

[3] Departamento de Química. Universidad Autónoma de Madrid. Cantoblanco, 28049 - Madrid. Spain

[4] Departamento de Química Orgánica. Universidad Complutense de Madrid. Cantoblanco, 28040 - Madrid. Spain

[5] Instituto de Ciencia de Materiales de Madrid - CSIC, Cantoblanco, 28049-Madrid, Spain

josemaria.gallego@uam.es

It is well known that the 2D self-assembly of organic molecules on solid surfaces is the result of a combination of molecule-molecule and molecule-substrate interactions. However, due to the large number of factors involved (which can include charge transfer between the molecule and the substrate, changes in the molecular conformation, the combination of weak noncovalent forces, like van der Waals or dispersive forces, with stronger ones, like hydrogen bonding or even covalent bonding), there are few cases where the surface arrangement of the molecule is completely understood. In this work we report on the self-assembly of TCNQ when vapour-deposited in UHV conditions on Cu(100), as studied with a combination of STM experiments and DFT calculations, which has allowed us to get a complete picture of the system, even although TCNQ is a strong electron acceptor, and then it is expected to interact strongly with the Cu surface.

The STM results show that submonolayer amounts of TCNQ grow epitaxially on Cu(100), with an almost rectangular lattice, although forming four different domains on the surface (Fig. 1). Taking into account the size of the molecule, and the angular orientation of the molecular main axis with respect to the substrate, these domains can be explained by assuming that the molecule rotates on the surface until the four N atoms are on bridge positions of the Cu atomic lattice (Fig 2). In addition, the theoretical calculations show that the Cu-N bonding changes the molecular conformation: the N atoms are closer to the Cu surface than the rest of the molecule (Fig. 3), while at the same time the Cu surface is noticeably distorted.

The self-assembly of the molecule is also the result of a combination of forces. Along one direction of the overlayer unit cell, the molecular arrangement comes dictated mainly by dispersive and van der Waals forces, in combination with elastic effects that produce the dislocations visible on the STM images. Along the other direction, on the other hand, the intermolecular interaction is mediated through the substrate, involving charge transfer and surface distortion.

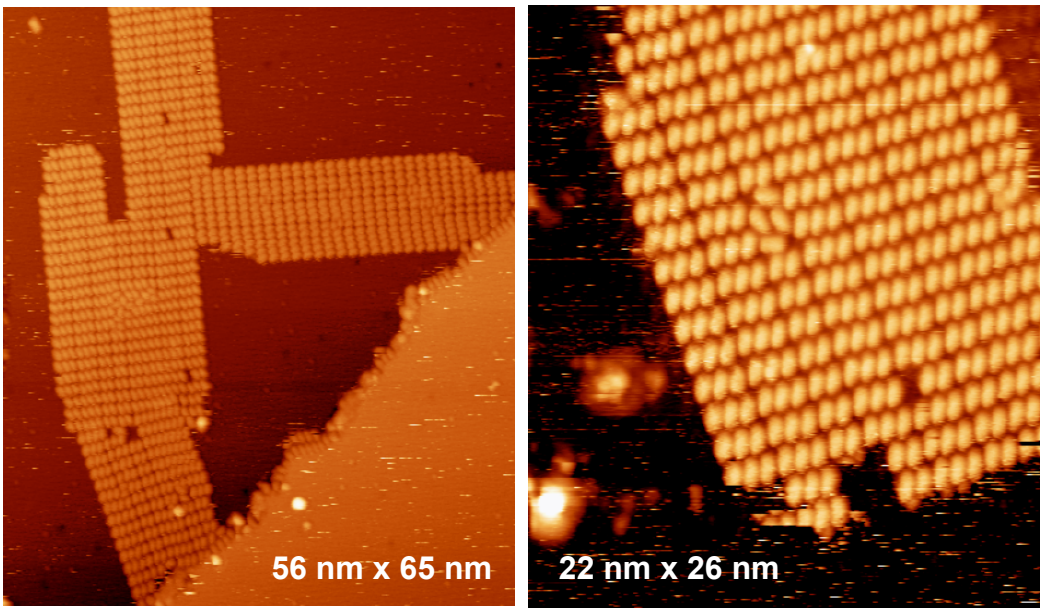

Figure 1: STM image of the Cu(100) surface after depositing ~0.4 ML of TCNQ.

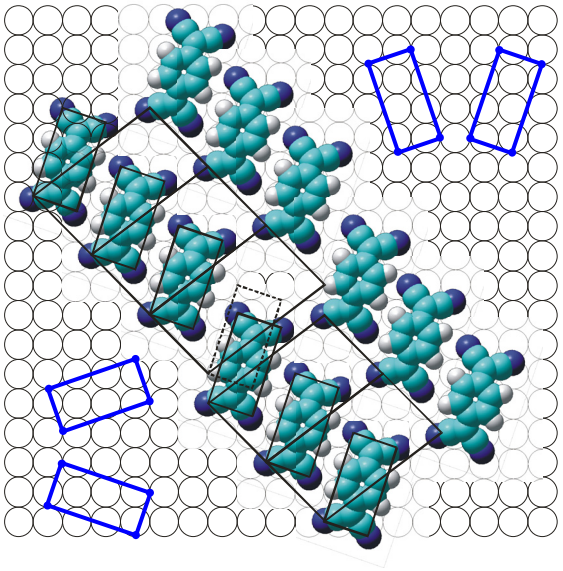

Figure 2: Proposed model of the TCNQ lattice on Cu(100), showing the surface unit cell and the molecular orientation. The blue rectangles show the four different orientations of the molecule with respect to the substrate.

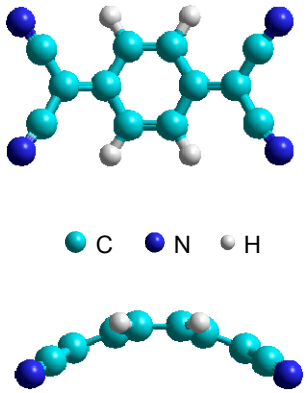

Figure 3: Top and lateral view of the calculated conformation of TCNQ when adsorbed on the Cu(100) surface.

.

Nanomateriales para aplicaciones avanzadas.

Javier García Martínez, Gonzalo Abellán, Adela I. Carrillo, Noemi Linares.

Laboratorio de Nanotecnología Molecular. www.ua.es/grupo/nanolab

Dpto. Química Inorgánica, Universidad de Alicante. Carretera San Vicente s/n, E-03690, Alicante. e-mail: j.garcia@ua.es

Introducción

La síntesis de nanomateriales es actualmente una de las ramas más activas dentro de la nanociencia. La definición de nanomateriales engloba aquellos en los que al menos una de sus dimensiones se encuentra en el rango de la nanoescala, es decir, entre 1 y 100 nanómetros. La cualidad más importante y sorprendente de esta nueva familia de materiales es el desarrollo de importantes propiedades dependientes del tamaño cuando sus dimensiones alcanzan el rango nanométrico.

El auge experimentado por la investigación en el campo de los nanomateriales en los últimos años pone de manifiesto las potenciales aplicaciones de estos materiales en muy diversos sectores tanto de la sociedad como de la industria.

Una de las clasificaciones propuestas más acertada para los nanomateriales los divide en base a sus dimensiones o la de alguno de sus componentes. [1] Se establecen así cuatro categorías: 0D, 1D, 2D y 3D, indicándose con esta nomenclatura cuántas de las dimensiones de la nanoestructura superan el rango de la nanoescala (ver Figura 1). Así, y según la definición de nanomaterial dada con anterioridad, no se deberían incluir en la categoría de nanoestructuras los materiales llamados 3D, ya que todas sus dimensiones serán mayores de 100 nm. Sin embargo, se consideran materiales nanoestructurados 3D a aquellos en los que se utilizan nanoestructuras (0D, 1D o 2D) como bloques de construcción, replicándose en las 3 direcciones del espacio de forma ordenada.

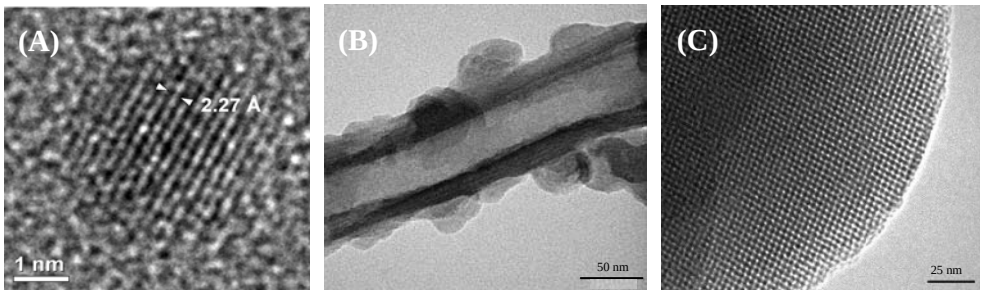

Figura 1. Imágenes de microscopía electrónica de transmisión de diferentes matriales nanoestructurados. (A) Nanopartícula de Pd (nanoestructura 0D), (B) Nanotubo de sílice (nanoestructura 1D) y (C) Sílice con porosidad ordenada de forma cúbica en el rango de los nanómetros conocida como MCM48 (nanoestructura 3D).

La producción de nuevos nanomateriales se puede llevar a cabo mediante dos estrategias diametralmente opuestas, por un lado, técnicas descendentes o "top-down" (reducción del tamaño de materiales másicos hasta límites nanométricos), y por otro, técnicas ascendentes o "botton-up" (síntesis de nanomateriales mediante unidades de construcción más pequeñas). Centrándonos en las técnicas ascendentes, el uso de unidades de construcción de tamaño nanométrico permite la preparación de sólidos organizados a varias escalas con gran precisión. [2]

La organización del sólido se consigue mediante el control preciso de las interacciones existentes entre los bloques de construcción, recurriéndose al autoensamblaje de dichos bloques para formar estructuras más complejas. [2,3] La síntesis, modificación y funcionalización de estas nanounidades, así como el control de sus interacciones, condicionan la arquitectura final del material y con ello, sus propiedades. El desarrollo de nuevas estrategias de síntesis basadas en interacciones débiles, técnicas biomiméticas y la utilización conjunta de precursores inorgánicos y biomateriales han sido determinantes para la construcción y organización de los materiales que aquí se describen.

Nanopartículas de Pd subnanométricas

La síntesis y caracterización de nanopartículas de metales constituye una importante área de investigación en la actualidad. Su uso está especialmente extendido en el ámbito de la catálisis debido a sus características diferenciadas que permiten optimizar tanto la actividad como la selectividad catalítica de las partículas. [4]

Recientemente, hemos desarrollado un método de síntesis de nanopartículas metálicas en el que las nanopartículas se preparan en tolueno por reducción en presencia de un agente inhibidor del crecimiento. [5-7] Si se desea, las nanopartículas pueden transferirse cuantitativamente a fase acuosa sin incremento del tamaño de partícula. [6] En el caso del Pd, la reducción controlada de $[PdCl_4]^{2-}$ con $NaBH_4$ en tolueno, en presencia de bromuro de tetraoctilamonio -utilizado como inhibidor del crecimiento- produce nanopartículas monodispersas de Pd con una distribución de tamaño de partícula comprendido entre 0,4 - 1,6 nm, estando el máximo por debajo de un nanómetro.

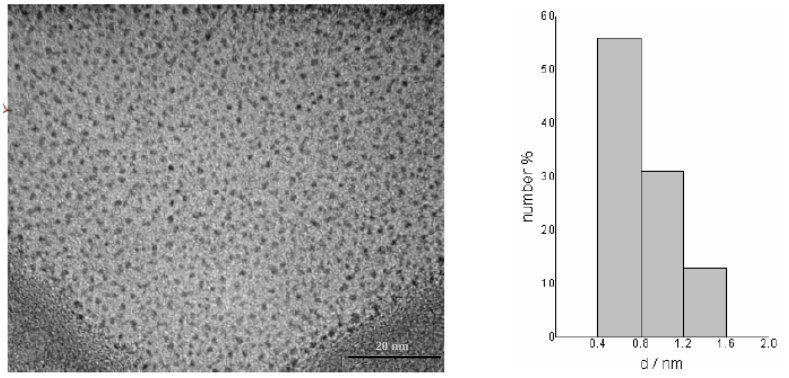

Figura 2. Imagen de TEM. Histograma que muestra la distribución de tamaño de nanopartículas en agua.

Utilizamos dimetilaminopiridina (DMAP) como agente de transferencia de Pd a la fase acuosa y también, como agente inhibidor del crecimiento en agua. Se ha llevado a cabo un estudio sistemático para optimizar el proceso de preparación, variando los parámetros de síntesis de las nanopartículas tales como: concentración de reactivos y agente inhibidor de crecimiento, contenido en agua y velocidad de agitación. [7] La Figura 2 muestra una fotografía obtenida mediante microscopía de transmisión electrónica (TEM) de nanopartículas de Pd (en agua) y su histograma en el que se observa un máximo de tamaño de partícula en torno a 0.5 nm. El interés de este método radica en que se obtienen suspensiones acuosas con alta concentración de nanopartículas (hasta 20 g/L) de Pd subnanométrico con una distribución de tamaños estrecha (0,4 – 1,6 nm) y estables durante meses.

Incorporación de nanopartículas metálicas en sílice mesoestructurada

Los principales inconvenientes que presentan las nanopartículas metálicas durante su uso en catálisis son, por un lado, la tendencia que estas partículas tienen a aglomerar para reducir su tensión superficial y, por otro, la difícil manipulación que conlleva su pequeño tamaño. Tradicionalmente, estos inconvenientes se han resuelto soportando las nanopartículas de metal en materiales porosos.

Hemos desarrollado un método de síntesis que incorpora nanopartículas metálicas en la estructura interna de un soporte poroso, tipo MCM-41, embebiéndolas en el sólido durante la preparación conjunta de ambos. [7] Para llevar a cabo la incorporación de las nanopartículas durante la formación del soporte se han utilizado dos estrategias: i) funcionalizar las nanopartículas de metal con grupos catiónicos, en este caso dimetilaminopiridina, que induzcan la formación de la sílice a su alrededor mediante un mecanismo similar al de la síntesis con surfactantes catiónicos de materiales mesoestructurados (S^+I^-), ó ii) funcionalizar las nanopartículas de metal con un trietoxisilano con tiol terminal que, posteriormente, copolimeriza con un precursor silíceo, normalmente tetraetoxisilano (TEOS). Ambos métodos se llevaron a cabo en presencia de surfactantes, como el bromuro de cetiltrimetilamonio (CTAB), para inducir la formación de mesoporosidad controlada y ordenada. [7] El surfactante y los grupos funcionales se eliminan del sólido mediante calcinación, produciéndose un material compuesto con nanopartículas de Pd homogéneamente dispersas en un soporte con mesoporos ordenados, tal como se muestra en la Figura 3.

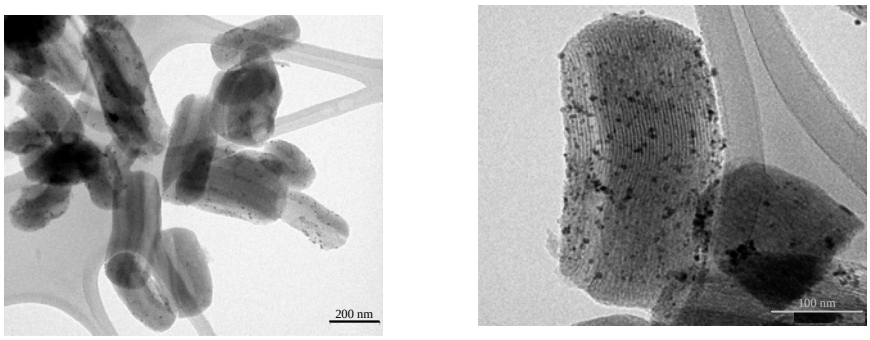

Figura 3. Imágenes de TEM de una muestra preparada por DMAP y CTAB.

Nuevas nanoestructuras mesoporosas mediante surfactantes neutros y catiónicos

La preparación de materiales mesoestructurados mediante el uso de surfactantes es una técnica de síntesis muy extendida. [8] Esta estrategia, basada en el autoensamblaje del surfactante en micelas, permite un control preciso de la arquitectura del poro mediante la variación de los parámetros de síntesis. Mediante esta técnica se han preparado una gran variedad de materiales porosos con atractivas propiedades, tales como alta área superficial y estrecha distribución de tamaño de poro. [9,10]

En este estudio se ha analizado la influencia de la longitud y del grupo polar del surfactante sobre el tamaño del poro en la arquitectura del material. La utilización de surfactantes con diferentes grupos polares (aminas secundarias, terciarias y cuaternarias) permite la obtención de nanomateriales con diferentes arquitecturas, tales como vesículas y nanotubos (ver Figura 4). Los mejores resultados en términos de superficie específica, control de tamaño de poro y rendimiento se han obtenido con surfactantes catiónicos.

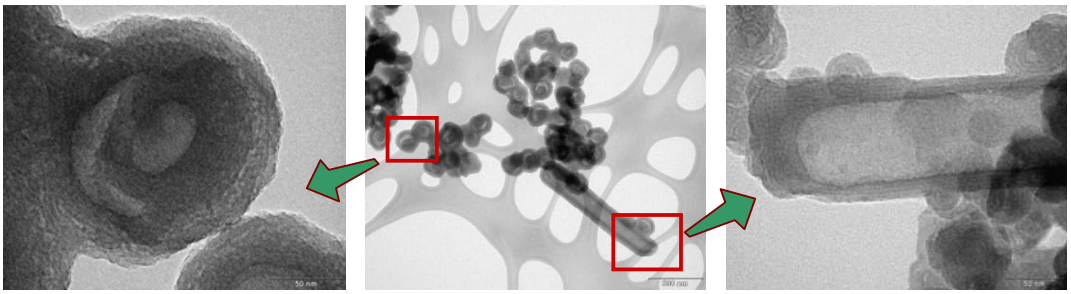

Figura 4. Imágenes de TEM de vesículas y nanotubos de sílice.

Nanoestructuras circulares mediante estrategias biomiméticas

Nuestro grupo de investigación ha desarrollado una estrategia de síntesis híbrida para la producción de nuevas estructuras jerarquizadas por combinación del uso de surfactantes catiónicos, típicamente usados en la síntesis de sílice mesoporosa y fosfolípidos de membrana. [11] Más específicamente, la adición de L-α-fosfatidilcolina (lecitina) a una solución de bromuro de cetiltrimetilamonio (CTAB, usado en la síntesis de MCM-41), nos permitió obtener nuevas estructuras de sílice con mesoporosidad circular ordenada (ver esquema Figura 5 y Figura 6).

Mediante la adición de cantidades cada vez mayores de lecitina se ha podido controlar de forma precisa la curvatura de los poros, obteniendo estructuras hexagonales y laminares para diferentes cantidades de fosfolípido manteniendo en todo momento la porosidad circular.

La organización de esta nueva arquitectura se produce a tres escalas (ver esquema Figura 5a,b,c): (i) los mesoporos adquieren forma circular, (ii) ensamblaje concéntrico, y (iii) ordenamiento hexagonal. A mayores concentraciones de lecitina, el ordenamiento hexagonal se pierde y emerge una nueva estructura laminar. Aplicando ultrasonidos a estas estructuras se obtuvieron anillos circulares huecos (nanotubos circulares).

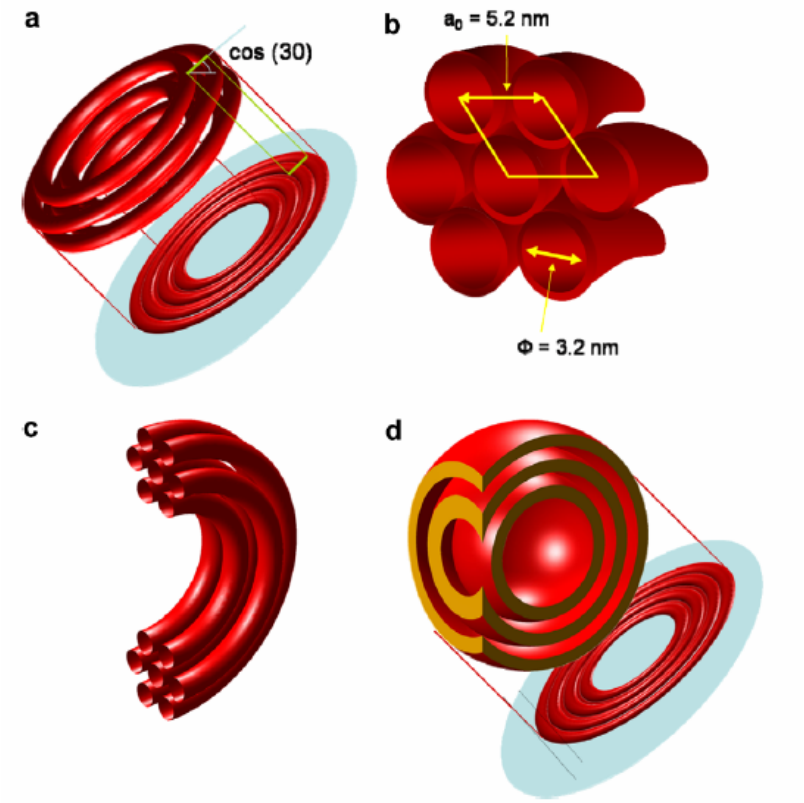

Figura 5. Esquema de una estructura de sílice circular mesoporosa con distintas geometrías.

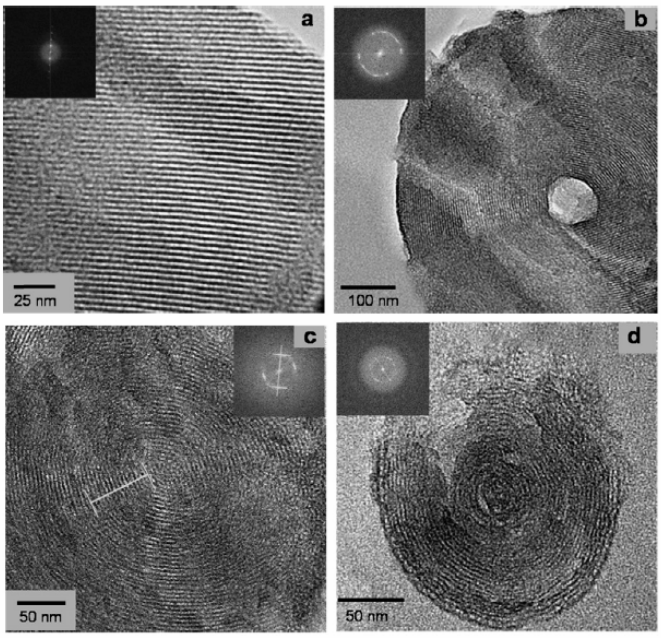

Figura 6. Imágenes de TEM de materiales mesoporosos preparados incrementando la concentración de lecitina.

Las ventajas que presentan estos novedosos materiales son: (i) alta área superficial, (ii) estrecha distribución de tamaño de poro, y (iii) estructuras jerarquizadas que son muy útiles para aplicaciones tales como catálisis, adsorción y separación [9].

Conclusión

En el Laboratorio de Nanotecnología Molecular hemos puesto a punto una serie de técnicas, basadas en interacciones débiles, para la preparación de nanomateriales a partir de componentes más sencillos. Estas técnicas nos han permitido sintetizar nanomateriales funcionales, en condiciones de síntesis suaves. En el futuro estudiaremos la aplicación de estos materiales en campos tan diversos como la catálisis, la separación y el suministro controlado de medicamentos.

Referencias

[1] V.V. Pokropivny et al., *Materials Science and Engineering C* 27 (2007) 990–993

[2] J. García-Martínez in *Highlights of Chemistry. Nanostructured Porous Materials. Building matter from the bottom-up.* Wiley-VCH (Ed. Bruno Pignataro) (2007)

[3] J. García-Martínez, *An. Quim.* 102 (2006) 5-12.

[4] E.Roduner in *Nanoscopic Materials. Size-dependent Phenomena. RSC Publishing, Cambridge* (2006) 239-262.

[5] D.I. Gittins, F. Caruso, *Angew. Chem. Int. Ed.* (2001) 40, 3001.

[6] M.Brust et al., *J. Chem. Soc.Chem. Commun.* (1994**)** 801.

[7] J.García-Martínez, N.Linares, S.Sinibaldi, E.Coronado, A.Ribera, *Micropor. Mesopor. Mater.* (enviado)

[8] T.Linssen, K.Cassiers, P.Cool, E.F.Vansant, *Adv. Colloid Interf. Sci*. (2003) 103, 121.

[9] M.E. Davis, *Nature*, (2002) 417, 813.

[10] J.García-Martínez, et al., *Micropor. Mesopor. Mater*. (2007) 100, 63-69.

[11]G. Øye, et al., *Adv. Colloid Interface Sci*. (2004) 439, 89-90.

[12] F. Fajula, A. Galarneau, F. Di Renzo, *Micropor. Mesopor. Mater.* (2005) 82, 227.

Poster

FORMATION OF STABLE PENTAGONAL NANOWIRES UNDER STRETCHING ON FCC METALS

P. García-Mochales [1,], R. Paredes [2,3], C. Guerrero [4], S. Pelaez [3], P.A. Serena [3]*

[1] *Dept. Física de la Materia Condensada, Facultad de Ciencias, Universidad Autónoma de Madrid, c/ Tomas y Valiente 7, Cantoblanco, E-28049-Madrid, Spain*
[2] *Centro de Física, Instituto Venezolano de Investigaciones Científicas, Apto. 20632, Caracas 1020A, Venezuela*
[3] *Instituto de Ciencia de Materiales de Madrid, Consejo Superior de Investigaciones Científicas, c/ Sor Juana Inés de la Cruz 3, Cantoblanco, E-28049-Madrid, Spain*
[4] *Departamento de Física, Facultad Experimental de Ciencias, La Universidad del Zulia, Maracaibo, Venezuela*

[*] *pedro.garciamochales@uam.es*

Different works during the last decade have showed the formation of staggered pentagonal configurations on breaking nanowires [1-5]. These pentagonal nanowires are formed by subsequent staggered parallel pentagonal rings (with a relative rotation of $\pi/5$) connected with single atoms (Fig. 1). The atomic sequence -1-5-1-5- presents a fivefold symmetry with respect the nanowire axis. This symmetry does not correspond to any crystallographic FCC nor BCC structures. The -1-5-1-5- staggered nanowire configuration may be understood in terms of a sequence of interpenetrated icosahedra. This icosahedral symmetry is very common in very small systems [6].

The formation of staggered pentagonal configurations during the stretching process has been already reported for Cu [1] and Au [2] nanowires using different Molecular Dynamic (MD) approaches. In particular the high stability of the Cu nanowire was confirmed with ab-initio calculations [3]. Pentagonal motives also appear in infinite Al and Pb nanowires obtained from MD simulated annealing methods [4]. More recently such structures have been reported for stretched Ni nanowires with different crystallographic orientations [5]. These pentagonal structures are very stable, with lengths larger of 10 Å and presenting a high plastic deformation under strain.

The aim of the present work is to carry out a statistical study of the structural evolution of FCC nanowires under stretching for a broad range of temperatures and three crystallographic stretching directions. We have carried out hundreds of MD simulations of aluminium, copper and nickel nanowires breaking processes, within the EAM approximation, following the procedure used in previous works [5, 7]. This study will confirm the existence of pentagonal nanowires, and, more important, will present the optimal set of parameters (temperature, size, crystallographic orientation) required for maximizing their occurrence probability.

The formation of pentagonal nanowires is a very anisotropic process. In fact, long pentagonal structures are relatively common for [100] and [110] stretching directions, whereas rarely occur for the [111] case. These preferred configurations have a minimum cross-section of $S_m \sim 5$ and are unveil in computational minimum cross-section histograms $H(S_m)$ as a very large peak at $S_m=5$ (Fig. 2). The configurations that contribute to this peak are mainly staggered pentagonal nanowires. This type of arrangement is not seen at 4K because a larger temperature is required to explore and overcome those energy barriers leading to configurations able to develop these pentagonal chains. The probability of apparition of these structures and its stability it is reflected on the distribution function of time spent into the interval $4.5<S_m<5.5$ (Fig. 3): the long tail of the distribution corresponds to very long stable pentagonal nanowires. Depending on the material, the $S_m=5$ peak in $H(S_m)$ increases with temperature up to certain value ($\sim T_{melting}/3$), at the same time the tail of the pentagonal nanowire length distribution enlarges. At further temperatures there is a decreasing behaviour of both due to melting processes.

The present statistical study shows a protocol helpful to form these long pentagonal nanowires for different materials.

References:

[1] H. Mehrez and S. Ciraci, Phys. Rev. B **56**, 12622 (1997); J. C. González, V. Rodrigues, J. Bettini, L. G. C. Rego, A. R. Rocha, P. Z. Coura, S. O. Dantas, F. Sato, and D. S. Galvao, and D. Ugarte, Phys. Rev. Lett. **92**, 126102 (2004).

[2] H. S. Park and J. A. Zimmerman, Scripta Materialia **54**, 1127 (2006).

[3] O. Gülseren, F. Ercolessi and E. Tosatti, Phys. Rev. Lett. **80**, 2775 (1998).

[4] P. Sen, O. Gülseren, T. Yildirim, I.P. Batra, and S. Ciraci, Phys. Rev. B **65**, 235433 (2002).

[5] P. García-Mochales, R.Paredes, S. Peláez and P.A. Serena, Physica, Stat. Sol. (a) (accepted, 2008) ; P. García-Mochales, R.Paredes, S. Peláez and P.A. Serena, arXiv:0710.0645 [cond-mat.mes-hall].

[6] N.A. Bulienkov and D.L. Tytik, Russ. Chem. Bull. Int. Ed. **50**, 1 (2001).

[7] A. Hasmy, E. Medina, and P. A. Serena, Phys. Rev. Lett. **86**, 5574 (2001); A. Hasmy, A. J. Pérez-Jimenez, J. J. Palacios, P. García-Mochales, J. L. Costa-Krämer, M. Díaz, E. Medina, and P. A. Serena, Phys. Rev. B **72**, 245405 (2005).

Figures:

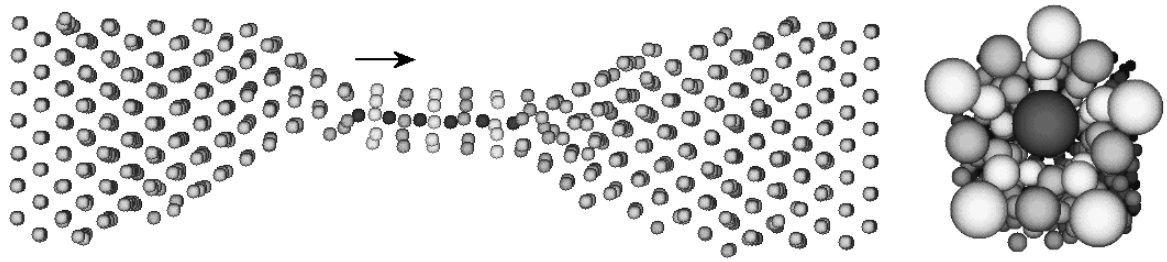

Fig. 1: Longitudinal (left) and cross-section (right) views of a Ni nanowire stretched along the [100] direction at 300K. The cross-section image shows a perspective view of the nanowire as seen from the position indicated on the longitudinal view. This image illustrates the appearance of staggered pentagonal structures -5-1-5-1-.

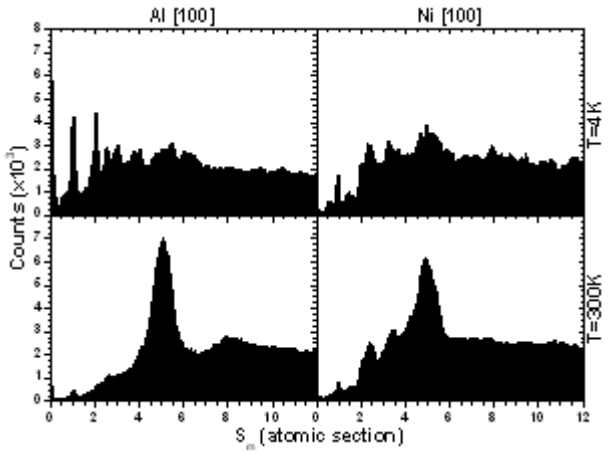

Fig. 2: Minimum cross section histograms $H(S_m)$ of Aluminium and Nickel breaking nanowires stretched along [100] direction at T=4 and 300K.

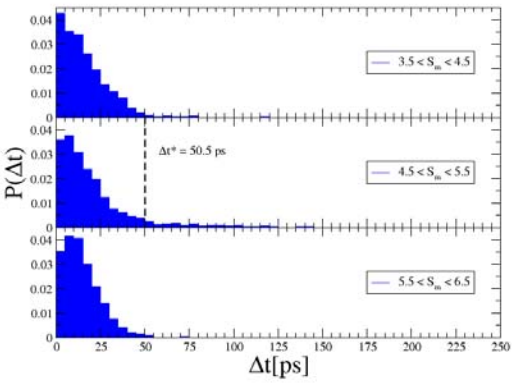

Fig. 3: Distribution function P(Δt) of the time spent by Ni nanowires stretched at 300K along the [110] direction within the minimum cross section interval showed in the figure.

SERS on Functionalized Silver Nanostructures: Towards the Detection of Single Molecules in Hot Spots

José V. García-Ramos, L. Guerrini, C. Domingo and S. Sánchez-Cortes
Instituto de Estructura de la Materia. CSIC, Serrano, 121, Madrid, Spain
jvicentegr@iem.cfmac.csic,.es

The optical properties of metallic Nanoparticles have a big scientific and technological importance. Such properties are determined by the Localized Surface Plasmons (LSP) the nanoparticles (NPs) support, which strongly depend on the NPs size and shape. The resonant excitation of the LSP leads to enormous enhancement of the electromagnetic field in close proximity of the NPs which originates a very important enhancement in the cross sections of SERS technique (Surface Enhanced Raman Scattering). This is the reason of the high sensitivity of this technique which, together with its ability to provide accurate structural information, makes it suitable to be employed as a molecular sensing technique. The possibility of controlling the LSP, tailoring the NPs morphology, pushes ahead the investigation of new methods of production of metallic NPs. Besides, they can be functionalized to improve their properties and increase their selectivity, consequently enlarging their applications.

In general the molecules active in SERS show some affinity for the metal resulting in the necessary approach to the surface. However many other molecules, whose trace detection is of great interest, do not present this affinity and their SERS signal is not detectable. The important environmental contaminants polycyclic aromatic hydrocarbons (PAHs) belong to the last group of molecules. Nonetheless it has been shown that by modifying properly the chemical properties of the metal surface it is possible to augment drastically the approaching of these pollutants to the metallic substrate [1-3], then their SERS sensing being feasible.

At the same time it is generally accepted that the possibility of single molecule detection (SMD) depends on the existence of interparticle gaps where the main part of the electromagnetic field intensification occurs [4,5]. One usually refers to these special regions of the metallic surface as *hot spots* (HS). Aggregated colloids are the main source for SMD [6] but the fabrication of such HS escapes from the experimental control in macro conditions. Thus, the molecules adsorbed on the metal surface may effectively play a crucial role in the formation of these HS [7,8].

We have employed three Viologen Dications (VGD), specifically paraquat (PQ), diquat (DQ) and lucigenin (LG), for the functionalization of silver colloidal nanoparticles (Ag NPs). VGD are able both to form charge transfer (CT) complexes with electron donor species such as PAHs [9] and interact strongly with the metal surface. In particular their bifunctional nature makes them able to induce the formation of HS. Thus VGD act simultaneously as HS builders and as molecular hosts in the detection of analytes to the highly sensitive region of the so-formed HS. The three VGD considered were selected because of their different structure regarding the extension of the aromatic part and the position of N atoms included.

The LG functionalization provided the most powerful VGD-NPs sensor system: we have reported the SERS detection of pyrene (PYR) down to nanomoles through spectra obtained employing the colloidal suspension (macro Raman) and in the zeptomol regime for spectra products of single aggregate of NPs (micro Raman). Furthermore we concluded that the LG-

NPs sensor system presents the ability to improve at the same time its stability (increased CT contribution and tighter bridging between LG and the two silver particle constituting the dimer) when interacting with the target molecule PYR.

Acknowledgements
Authors acknowledge grants FIS2007-63065 from Dirección General de Investigación, Ministerio de Educación y Ciencia (Spain) and Comunidad Autonoma de Madrid project MICROSERES number S-0505/TIC 0191 for financial support. L.G. acknowledges CSIC for the I3P fellowship co-founded by the European Social Fund.

References

[1]. Leyton, P.; Sanchez-Cortes, S.; Garcia-Ramos, J.V.; Domingo, C. ; Campos-Vallette, M.M.; Saitz, C.; Clavijo, R.E. *J. Phys. Chem. B* **2004**, 108**,** 17484.
[2]. Leyton, P.; Sanchez-Cortes, S.; Garcia-Ramos, J.V.; Domingo, C. ; Campos-Vallette, M.M.; Saitz, C. *Appl. Spectrosc.* **2005**, 59, 1009.
[3]. Guerrini, L.; García- Ramos, J.V.; Domingo, C.; Sanchez-Cortes, S. *Langmuir* **2006**, *22,* 10924.
[4]. Otto, A. *J. Raman Spectrosc.* **2006**, *37*, 937.
[5]. Le Ru, E. C.; Etchegoin, P. G.; Meyer, M. *J. Chem. Phys.* **2006**, *125*, 204701.
[6]. Aroca, R. Surface-enhanced Vibrational Spectroscopy, John Wiley & Sons: Chichester, 2006
[7]. Anderson, D. J.; Moskovits, M. *J. Phys. Chem.* **2006**, *110*, 13722.
[8]. Lee, S. J.; Morrill, A. R.; Moskovits, M. *J. Am. Chem. Soc.* **2006**, *128*, 2200.
[9]. Wiley: New York, 1998 Monk, P. The Viologens: Physicochemical Properties, Synthesis and Applications of the Salts of 4,40-Bipyridine.

Mechanical detection of the vibrations of Carbon Nanotube and Graphene Resonators

Daniel Garcia-Sanchez,[1,2] Alvaro San Paulo,[2] Arend M. van der Zande,[3] Maria Jose Esplandiu,[1] Benjamin Lassagne,[1,2] Francesc Perez-Murano,[2] Laszlo Forró,[4] Albert Aguasca,[5] Paul L. McEuen[3] and Adrian Bachtold[1,2]

[1]CIN2 Barcelona Campus UAB, E-08913 Bellaterra, Spain. [2]CNM-CSIC Campus UAB, E-08913 Bellaterra, Spain. [3]Cornell Center for Materials Research, Cornell University, Ithaca, NY 14853, USA. [4]EPFL, CH-1015 Lausanne, Switzerland. [5]Universitat Politecnica de Catalunya, Barcelona, Spain.

daniel.garcia.icn@uab.es

Carbon nanotubes are often recognized as the ultimate material for high-frequency mechanical resonators. For instance, nanotube resonator devices hold promise for ultralow mass detection or quantum electromechanical experiments. However, the detection of the mechanical vibrations remains very challenging. We have developed a novel detection method for nanotube vibrations, which is based on atomic force microscopy [1]. This method enables the detection of resonances up to 3.1 GHz with subnanometer resolution in vibration amplitude as shown in figure 1. Importantly, it allows the imaging of the mode-shape for the first, second and third eigenmodes, as shown in figure 2.

We have also applied this method to study suspended graphene sheets [2]. As shown in figure 3, we have found a new class of exotic nanoscale vibration eigenmodes not predicted by the elastic beam theory, where the amplitude of vibration is maximum at the free edges. The edge modes are frequently, but not always, observed in resonators for which the suspended sheet displays local buckling. To understand the relationship between local buckling and the edge modes, we have calculated the effect of strain with simulations based on the finite element method. Figure 3 shows that the resonance frequencies and shape modes of the model are in reasonable agreement with the measurements.

Simulations based on the finite element method show that these edge eigenmodes are the result of non-uniform stress, which is generated during fabrication. The shape of these exotic eigenmodes and the corresponding stress must be taken into account in future experiments and applications, such as the determination of the Young's modulus[3] and the accurate calibration of mass, force, or charge sensing[4-6]. It may also be possible to manipulate the eigenmode shape by varying the strain during measurements via electrostatic tuning[4].

References:

[1] D. Garcia-Sanchez *et al.,* Phys. Rev. Lett., **99** (2007), 085501.
[2] D. Garcia-Sanchez *et al.,* Submitted.
[3] I.W. Frank *et al.,* J. of Vac. Sci. And Tech. B, **25** (2007) 2558.
[4] Bunch, J.S. et al. Science, **315** (2007) 490.
[5] H. Craighead, Nature Nanotech. **2** (2007), 18.
[6] J. Tamayo, *et al.* Appl. Phys. Lett. **89,** (2006) 224104.

Figures:

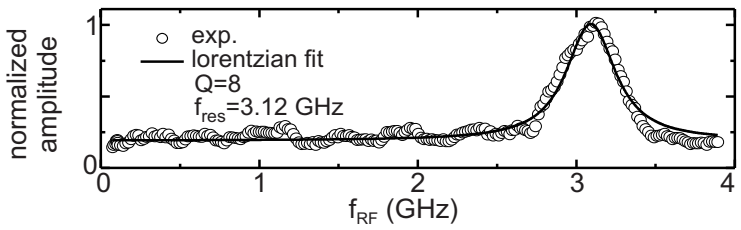

Figure 1. Resonance peak of the fundamental eigenmode for a 265 nm long MWNT resonator.

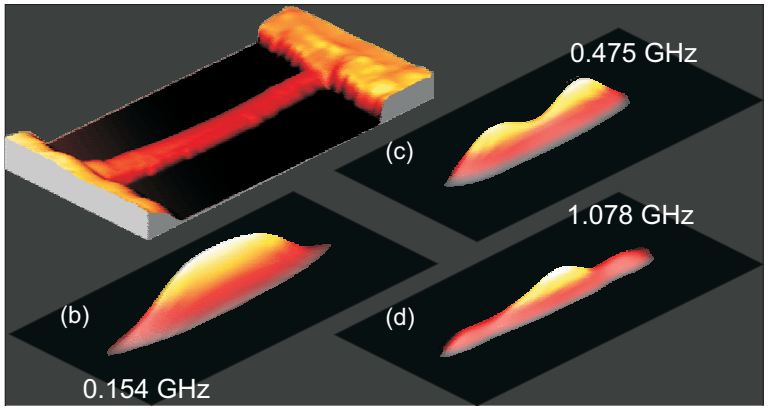

Figure 2. (a) Topography and (b)-(d) vibration images for a 770 nm long MWNT resonator. The images (b), (c), (d) correspond to the first, second and third eigenmodes.

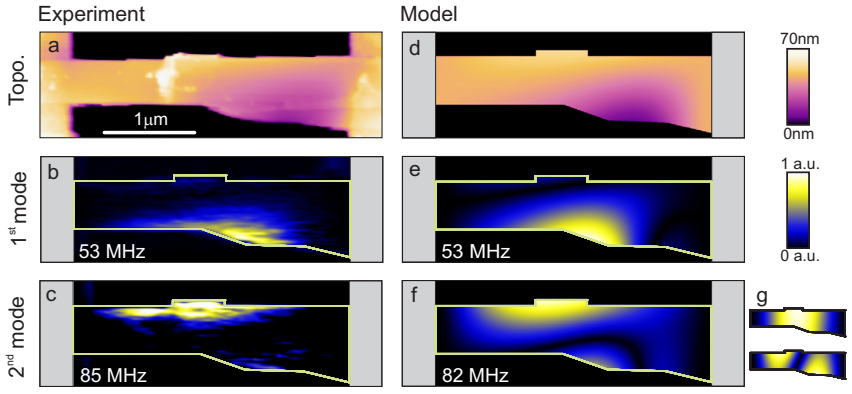

Figure 3. Graphene resonator with local buckling. (a) Measured topography. (b) Shape of the first eigenmode (raw data). (c) Shape of the second eigenmode (raw data). (d) Topography obtained using FEM simulations on a stressed graphene sheet. (e) Shape of the first eigenmode using FEM simulations. (f) Shape of the second eigenmode using FEM simulations. (g) Shape of the two first eigenmodes using FEM simulations without any stress. The resonance frequencies are 17 and 46 MHz.

New strategies of colloidal stabilization of nanoparticles for applications in aqueous media

Fabienne GAUFFRE, Jean-Daniel MARTY, Christophe MINGOTAUD, Nelly PERIGNON, Kamil RAHME, Javier RUBIO GARCIA and Stéphanie SISTACH
Laboratoire des IMRCP, CNRS-Université de Toulouse, Toulouse, France
gauffre@chimie.ups-tlse.fr

Since it was discovered that metallic and semi-conducting nanoparticles have unique optical properties, many biomedical applications have been proposed for these nanomaterials in the fields of imaging, sensing, and therapy. All these biomedical applications require water dispersability and long term stability of the nanoparticles at high ionic strength. In addition, the need to develop "green" catalytic processes also demands new water dispersable nanoparticles. The synthesis of well-defined metallic and semi-conducting nanoparticles are usually achieved in organic solvent, producing particles with a hydrophobic surface. Thus, the obtention of water-dispersible nanoparticles by direct synthesis or transfer is still a challenging task.

Our group develops new strategies to produce various water dispersible metal or semi-conducting nanoparticles (Au; Pt; Ag, ZnO). The nanoparticles can be synthesized *in-situ,* transferred from organic solvent or synthesized in water and stabilized *a posteriori*. We focus on the design of stabilizers. The properties (catalysis, toxicology...) of the so-formed water-dispersable nanoparticles are investigated (Figure 1).

We will particularly describe the use of amphiphilic stabilizers. Indeed, the self-assembling properties of amphiphilic compounds provide (i) enhanced adsorption at the surface of the particles; (ii) stabilization through non-covalent interactions with the surface, that avoids modification of the nanoparticles properties and allows direct generalization to particles made of various materials. We have investigated the stabilizing efficiency of various amphiphilic compounds with a diblock A-B structure (A= hydrophilic, B= hydrophobic), such as surfactants and diblock copolymers, or with a triblock A-B-A structure: bola-amphiphile surfactants, triblock copolymers[3], core-multishell hyperbranched polymers.

Triblock amphiphilic structures act as efficient stabilizers even in conditions where the formation of self-assembled objects (micelles, vesicles...) does not occur in solution (for instance at concentrations lower than the critical agregation concentration). The predominent role of the length of the hydrophobic B segment, for the colloidal stability is clearly evidenced. In addition, the use of bolaamphiphile surfactants (notedwith charged polar head and long alkyl chains (n>12) allows one to precipitate and redisperse the nanoparticles at will[4]. Long term stability in condition of high ionic strength can be achieved by an appropriate choice of non ionic A-B or A-B-A copolymers, for instance made of hydrophilic oxyethylene and hydrophobic oxypropylene segments.

Finally, core-multishell polymeric structures designed with a careful choice of their external groups exhibited a remarkable behaviour, combining extremely long term stability with dispersability of hydrophobic and hydrophilic nanoparticles in a wide range of solvents (from water to chloroform, see Figure 2).

In all cases, water-dispersability and stability are investigated in relation with the chemical structure of the stabilizers in order to optimize the design of efficient stabilizers.

References:

Figures:

Figure 1: Cellular uptake of gold nanoparticles coated by triblock copolymers (PEO-PPO-PEO)

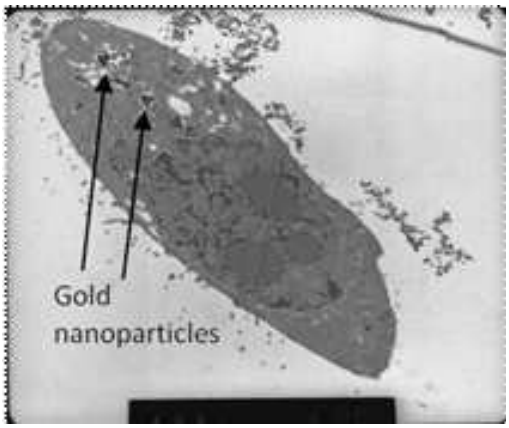

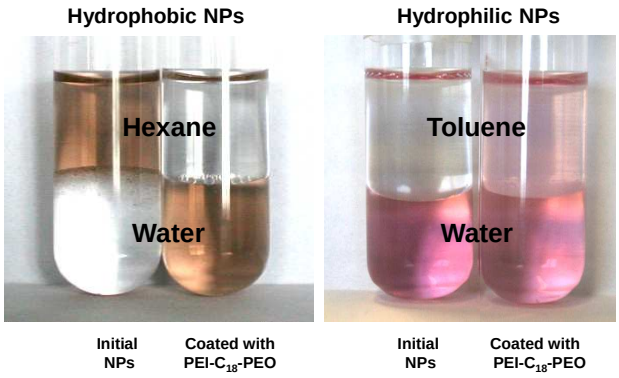

Figure 2: Left: phase transfer of hydrophobic AuNPs from hexane to water before and after capping with a core-multishell polymeric structures (PEI-C_{18}-PEO). Right: partial phase transfer of hydrophilic AuNPs from water to toluene before and after capping with PEI-C_{18}-PEO.

SYNTHESIS AND CHARACTERIZATION OF MODIFIED ORDERED MESOPOROUS MATERIALS

[a]Gil, M., [a]de la Iglesia, O., [a]Mallada, R., [a]Santamaría, J., [a]Serrano, J.L.

[a] *Institute of Nanoscience of Aragón, University of Zaragoza, Pedro Cerbuna 12, 50009 Zaragoza, Spain*

martagil@unizar.es

The family of mesoporous materials called M41S (MCM-41, MCM-48 and MCM-50) is a subject of growing interest since they were discovered by Mobil researchers in 1992 [1]. The synthesis of mesoporous materials is based on the formation of siliceous structures around template micelle assemblies.

The main properties of these materials are: i) very narrow pore size distribution in the mesoporous region, between 2 and 4 nm, ii) high specific surface area (1000-1500 m^2/g), iii) highly ordered structure and iv) active surface chemistry that allows an easy modification of the properties. All of them make these materials very attractive for numerous applications such as catalysis, encapsulation of molecules, sensors and separations.

The MCM-48 powders are synthesized as reported by Kim et al. [2].The aim of this work is the surface modification of the MCM-48 by silane coupling agents (figure 1) in order to obtain specific interactions between the analyte and the surface. The synthesis of modified MCM-48 layers would increase the selectivity to a certain analyte. It is well known that the amine group reacts with CO_2, which makes these devices suitable for sensing purposes on CO_2 controlled atmospheres, for example in the food industry. In this work we report the MCM-48 modification with 3-aminopropyl tri-etoxisilane (APTS).

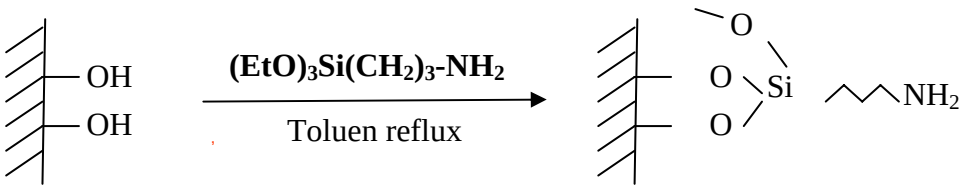

Figure 1. Post-grafting of MCM-48 with APTS

In order to control the loading rate several parameters of this method were studied: APTS concentration vs stoichiometric amount [3]., reaction temperature, reaction time and time of stirring at room temperature.

MCM-48 materials were characterized before and after modification with different techniques: XRD, N_2 adsorption, FTIR, TGA and elemental analysis.

References:

[1] J.S. Beck, J.C. Vartuli, W.J. Roth, M.E. Leonowicz, K.D. Schmitt, C.T-W Chu, D.H. Olson, E.W. Sheppard, S.B. McCullen, J.B. Higgins and J.L. Schlenker, J. Am. Chem. Soc. **114** (1992) 10834-10842.

[2] Kim, Kim y Ryoo, Chem. Commun., 1998, 259-260

[3] H. Landmesser, H. Kosslick, W. Storek and R. Fricke. Solid State Ionics 101-103, (1997) 271-277

CARBON NANOFIBRE- POLY(VINYLIDENE FLUORIDE) NANOCOMPOSITES: EFFECT OF THE CARBON NANOFIBRE CONCENTRATION ON THE α TO β PHASE TRANSFORMATION AND THE DEGREE OF CRYSTALLINITY

V. Sencadas[1], J. Gomes[1,2], P. Costa[1], F. W. J. van Hattum[3], J.G. Rocha[4], S. Lanceros-Mendez[1]

[1]Depto de Física da Universidade do Minho: Campus de Gualtar, 4710-057 Braga, Portugal.
[2]CeNTI - Centre for Nanotechnology and Smart Materials, Rua Fernando Mesquita 2785, 4760-034 Vila Nova de Famalicão, Portugal
[3]IPC-Institute for Polymers and Composites, University of Minho, 4800-058, Guimarães, Portugal
[4]Departamento de Engenharia Electrónica Industrial e Computadores, Universidade do Minho, Campus de Azurém, 4800-058 Guimarães, Portugal
(jgomes@centi.pt)

The present study is based on the use of Carbon Nanofibres (CNF) instead of Carbon Nanotubes (CNT) in order to increase the dielectric constant of polymer materials and/or the electrical conductivity. The main advantage of the CNF with respect to the CNT from the scientific point of view is that their structure and dimensions potentially reduce the Van der Waals forces acting between them, thus facilitating their dispersion during composites preparation. Furthermore, CNFs can be easily functionalised to improve interaction with the surrounding matrix due to a better accessibility to the graphene planes inherent to their 'stacked cup' structure. [1, 2]

In this work CNF/PVDF nanocomposites have been prepared by a solution method with different amounts of CNF (0.1, 0.5, 1, 2, 5%) dispersed in the polymeric matrix. The crystalline phase of the matrix was the apolar α-PVDF. Further, the nanocomposites are uniaxially stretched in order to achieve the phase transformation α to polar β-phase within the polymeric matrix. The influence of the CNF on the amount of the crystalline part of the polymer, morphological properties, mechanical and electrical properties and thermal stability of the composites were studied.

The SEM micrographs of the samples showed that the composites crystallise in a spherulitic structure, similar to the one of pure α-PVDF [3], with a random distribution of the CNF along the surface of the sample.

The insertion of CNF within PVDF increased the elastic modulus with respect to the polymer matrix. The elastic modulus of the composites nearly doubles for a small incorporation of CNF (lower than 1%) and remains almost constant for higher concentrations.

The α to β phase transformation was studied for the pure polymer and for the nanocomposites and it was concluded that the maximum amount of β-phase is obtained by stretching ratios of 5 or more at a temperature of 80 ºC [3, 4] (see Fig. 1).

The DSC thermograms showed that the incorporation of CNF in the polymeric matrix has a direct influence thermal stability of the nanocomposites, increasing the melting temperature (T_m) of the composites. This behaviour is observed for the polar and non-polar polymeric matrix, α and β-phase of PVDF, respectively. The T_m of the nanocomposites appears at higher temperature when compared to the pure samples of PVDF, as the well dispersed CNF within the PVDF matrix promotes heterogeneous nucleation and act has nucleation agents for the polymer crystallites, increasing the crystallinity fraction of the matrix [5].

The electrical response in the polymer/CNF composites was evaluated by measuring the bulk resistivity and the dielectric constant. The bulk resistivity for the α-phase composites changes from 4.35×10^{10} Ωm for the sample with 0.1% CNF to 9.0×10^{6} Ωm for the sample with 5% CNF, the threshold being at CNF concentrations of about 1.5%, where the resistivity undergoes a change of three orders of magnitude (see Fig. 2). When the samples are stretched in order to achieve the β-phase, the resistivity remains for the lower CNF concentrations within the same range.

Dielectric measurements reveal, in general, an increase of the dielectric constant with increasing CNF concentration. The dielectric constant increases further by the stretching process, i.e. by achieving the polar β-phase though the α– to β-phase transformation.

Acknowledgements

Authors want to express their thanks to *Solvay* and *Applied Sciences, Inc.*, for the excellent material provided and to *Portuguese Foundation for Science Technology – FCT* for financial support (Grant POCI/CTM/ 59425/2004). V. Sencadas acknowledges the FCT for the PhD Grant (SFRH/BD/16543/2004).

References:

[1] Tibbetts GG, Lake ML, Strong KL, Rice BP, Composites Science and Technology 67 (2007),1709-1718.
[2] Burton D, Lake P, Tibbetts GG and Lake ML, SAMPE Journal, 43, 4 (2007), 36-41.
[3] Sencadas V, Moreira VM, Lanceros-Mendez S, Pouzada AS, Gregório Filho R, Mat. Sci. Forum Vol. 514-116 (2006), 872-876.
[4] Sencadas V, Lanceros-Mendéz S, Gregorio Jr. R, *submitted* to Acta Materialia, 2008
[5] Nam Y, Kim W, Cho Y, Chae D, Kim G, Hong S, Hwang S, Hong S, Macromolecular Symposium, 249-250 (2007), 478-484.

Figures:

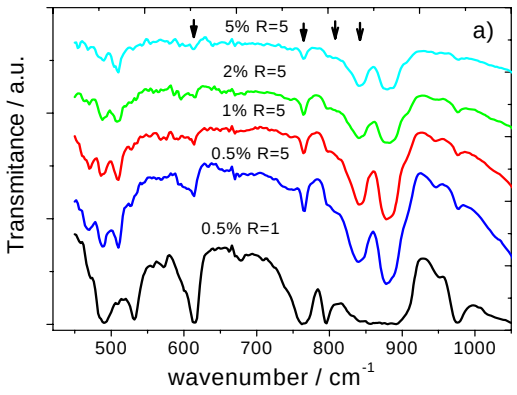

Figure 1. FTIR spectra of PVDF-CNF nanocomposites with different CNF concentrations.

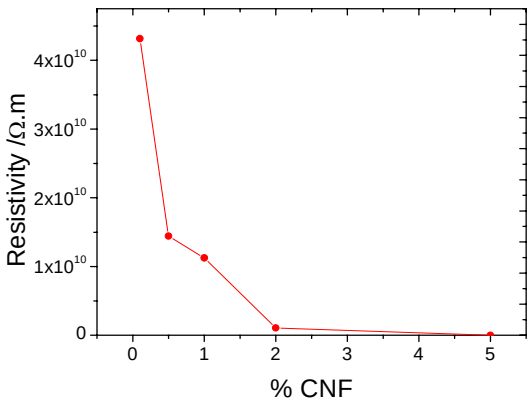

Figure 2. Electrical bulk resistivity of the CNF-PVDF nanocomposites as a function of CNF volume concentration.

PROBING THE SURFACE PROPERTIES OF CYTOCHROMES *C*/GOLD NANOPARTICLES COMPLEXES

Inês Gomes[a], Nuno C. Santos[b], L. M. A. Oliveira[c], A. Quintas[c] and Ricardo Franco[a]

[a] *REQUIMTE, Departamento de Química, Faculdade de Ciências e Tecnologia, Universidade Nova de Lisboa, 2829-516 Caparica, Portugal*
inesgomes@dq.fct.unl.pt
[b] *Unidade de Biopatologia Vascular, Instituto de Medicina Molecular, Faculdade de Medicina da Universidade de Lisboa, Av. Prof. Egas Moniz, 1649-028 Lisboa, Portugal*
[c] *Laboratório de Patologia Molecular, Instituto Superior de Ciências da Saúde Egas Moniz, Campus Universitário, Quinta da Granja, 2829-511 Caparica, Portugal*

Gold nanoparticles (AuNPs) present unique optical, electronic and chemical properties and can be stabilized by proteins, generating bio-nanoprobes with wide applications in bioassays and cell targeting[1]. Spherical gold nanoparticles were prepared and coated with two natural cytochromes of the *c* type, namely, horse heart cytochrome *c* (HHCC) and yeast iso-1-cytochrome *c* (YCC), each at a ratio of 250 proteins per AuNP, assuring complete AuNP surface coverage. According to previously published models, HHCC is bound to the gold surface through electrostatic interactions while YCC is covalently bound to the gold surface *via* the thiol group of its single cystein-102 residue[2]. Upon pH variation of solutions containing the AuNP-protein complexes, a UV/vis-detectable change occurred as the solution shifted from the original color (red) to blue. This shift was sharper for the HHCC-AuNP complex and occurred around pH 6.2, whereas for the YCC-AuNP complex was more gradual and the color change occurred around pH 9.2. The bare gold nanoparticles and the cytochrome *c* solutions alone showed no change from the original color upon pH variation. The conformational changes occurring on the protein secondary structure upon interaction with the gold nanoparticles were investigated by Circular Dichroism (CD) spectroscopy, by monitoring the "far-UV" spectral region (190-250 nm). Preliminary experimental results at several pH values showed conformational changes of little significance in HHCC alone and a gradual increase of β-sheet from pH 6 for the HHCC-AuNP complex. In YCC alone, CD spectrum at pH 11 showed predominance of random coil. Comparing these results with the CD spectrum of the YCC-AuNP complex, an increase of random coil around 10% is observed from pH 10 and a gradual increase of β-sheet is observed from pH 9. ζ-Potential measurements obtained for AuNP-complexes with different protein:nanoparticles ratio, showed that the ζ-potential of the complexes increases as more protein binds to the AuNPs, until a protein:nanoparticles ratio of 250, stabilizing for larger ratios. For YCC-AuNP complexes, the ζ-potential values were more negative than for the HHCC-AuNP complexes. Taken together, the experimental data seem to indicate that the surface charge distribution is very different for both complexes, indicating that natural derivatives of cytochromes can be used to control properties at the nanoscale for these bio-nanoprobes.

Inês Gomes acknowledges Fundação para a Ciência e a Tecnologia for the doctoral fellowship (SFRH/BD/18630/2004).

1. You, C-C. *et al*., *Soft Matter*. **2006**, *2*, 190-204
2. Aubin-Tam, M-E.; Hamad-Schifferli, K. *Langmuir*. **2005**, *21*, 12080-12084.

NANOENCAPSULATION OF BIOACTIVE COMPOUNDS

J. F.P.S. Gomes, I.Ferreira, S. Rocha M. C. Pereira and M. Coelho
LEPAE, Chemical Engineering Department, Faculty of Engineering, University of Porto, Rua Dr. Roberto Frias, 4200-465 Porto, Portugal
joana.gomes@fe.up.pt

Natural extracts are an attractive source of new compounds, not only owing to the diversity and novelty of chemical structures, but also owing to their potential biological action. The potential applications of these extracts include cosmetic and pharmaceutical areas.

The aim of this research is to encapsulate fruit and plant extracts with biological activities such as antioxidants. The need for encapsulation lies in the instability of the bioactive compounds.

Liposomes and polymeric nanocapsules were produced for the protection and maintenance of the bioactive specie properties.

Nanocapsules with a polysaccharide shell matrix were developed by spray-drying technology to encapsulate antioxidants from green tea extracts. Scanning Electron Microscopy (SEM) pictures shows that the carbohydrate nanocapsules are spherical and have a smooth surface. The particle size distribution was determined by Laser Scattering (LS) and Dynamic Light Scattering (DLS). The mean diameter from LS was quantified to be 0.08±0.02 microns. DLS measurements revealed particles with diameters from 5 to 7 nm. The confocal micrograph of nanocapsules in fluorescence mode shows that the active principles are concentrated in the core of the capsules.

Egg-yolk L-a-Phosphatidylcholine (Egg-PC) liposomes were prepared by the thin film hydration method. Extracts from grape skin and seed were encapsulated with 35% efficiency. These extracts exhibit high antioxidant activity as shown by the *2,2-Diphenyl-1-picrylhydrazyl* (DPPH) radical scavenging capacity method. DLS shows narrow size distribution of liposomes containing extracts.

References:

[1] I. Ferreira, S. Rocha, J. Gomes, M. Pereira, M. Coelho. Encapsulation of Antioxidants by Spray Drying, AIDIC Conference Series Vol.8 (REED BUSINESS INTERNATIONAL copyright) (2008) 119.

[2] J. Gomes, A. Sonnen, A. Kronenberger, J.Fritz, M. Coelho, D. Fournier, C. Fournier-Nöel, M. Mauzac, M. Winterhalter, Langmuir, **22(18)** (2006), 7755-7759.

[3] T. Ruysschaert, M. Germain, J. Gomes, D. Fournier, G. Sukhorukov, W. Meier, M. Winterhalter, IEEE Transactions on Nanobioscience, Vol. 3, nº 1. (2004)

Poster

Synthesis of nanoparticles in microfluidic devices based on the LTCC technology

Sara Gómez-de Pedro, Mar Puyol, Julián Alonso
Sensors and Biosensors Group, Department of chemistry, Universidad Autónoma de Barcelona, Bellaterra, España
sara.gomez@uab.cat

The synthesis and characterisation of nanoparticles (NPs) have been widely investigated in recent years due to their great variety of applications. Specifically, metallic NPs are great candidates owing to their tuneable optical and electronic properties. However, conventional synthetic methods are handicapped by the low production of NPs and by the difficulties of controlling their morphology, size distribution and crystalline properties, which makes very difficult achieving a good reproducibility. Some factors such as the injection process, local temperature and concentration fluctuations, rate of stirring and rate of cooling are difficult to control in batch processes but not in microfluidic flow reactors, where the reaction is confined in a small area and all the parameters can be defined.

Herein, we propose the use of ceramic microfluidic devices based on the LTCC (Low-Temperature Co-fired Ceramics) technology for the synthesis and functionalization of metallic NPs. These microfluidic reactors show some very interesting advantages regarding other existing ones, which make them a great alternative.

The LTCC technology enables the construction of multilayered systems, where can be integrated other mechanic, electronic and fluidic components. Moreover, the construction process of the designed prototypes is carried out in a simple and fast way without the need of sophisticated facilities, reducing significantly the cost and production time. The technique also allows the integration of multiple analytical paths in a single device without holding structural problems related to the lack of sealing between layers or components.

Green tape's properties allow working in a wide range of temperatures, while other materials cannot, by the introduction of resistor and thermistor systems inside the microfluidic platform. The manipulation of reagent droplets is controlled by the geometry and size of the channels and the flow rates. Furthermore, a good reagents mixing can be achieved by introducing passive or active mixers, so more uniform particles can be obtained. They also permit the addition of reagents when necessary and the modification of the composition of the reaction mixture is controlled by the injection volumes of each channel.

Figures:

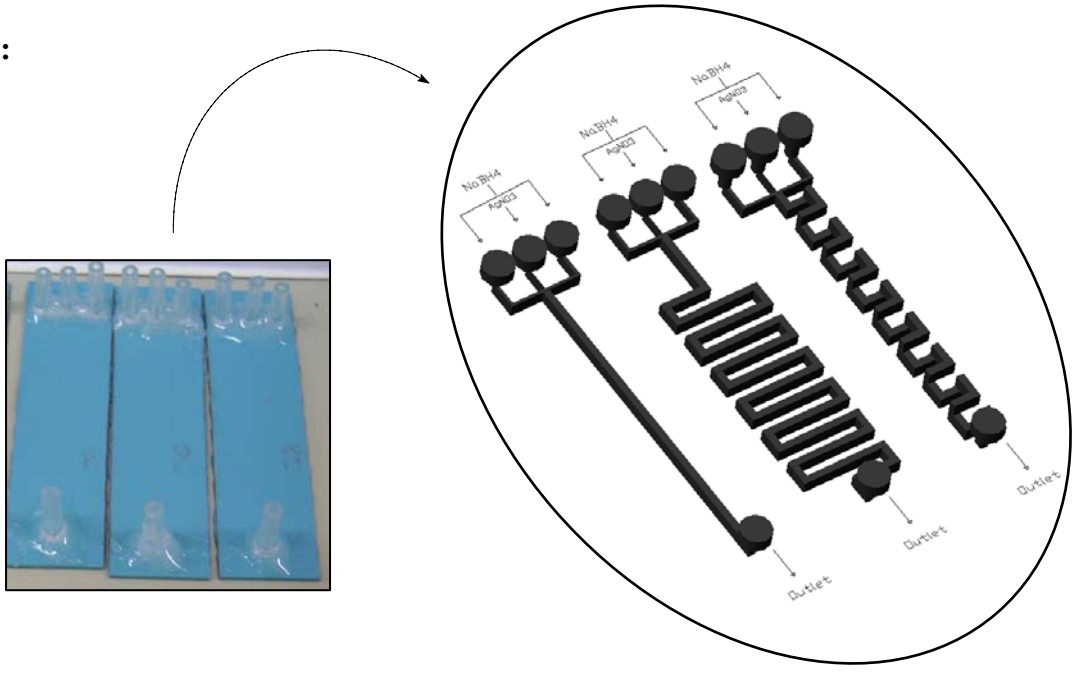

Some of the designed and constructed structures for the metallic NPs synthesis in LTCC.

THERMOELECTRIC THIN-FILMS FOR MICROCOOLERS AND ENERGY SCAVENGING MICROSYSTEMS

L.M. Goncalves [1] H. R. Silva [1], Rui Rocha [1], P. Alpuim [2], J.H. Correia [1]
1 University of Minho, Department of Electronics, 4800-058 Guimarães, Portugal
2 University of Minho, Department of Physics, 4800-058 Guimarães, Portugal

lgoncalves@dei.uminho.pt

The present work reports on the fabrication and characterization of the first planar Peltier microcooler (Fig. 1) on a flexible substrate. The microcooler was fabricated on flexible Kapton© polyimide substrate, 25 μm in thickness, using Bi_2Te_3 and Sb_2Te_3 thermoelectric elements deposited by thermal co-evaporation.

The cold area of the device (4 mm^2) is cooled using four pair of thermoelectric elements, connected in series with aluminum/nickel contacts (Fig. 3). Flexible substrates add uncommon mechanical properties to the composite film-substrate and enable their integration with many novel types of electronic devices. Kapton was chosen as substrate because of its low thermal conductivity (0.16 $W.m^{-1}.K^{-1}$), thus allowing for higher performance of cooler devices. The value of thermal expansion coefficient of Kapton (12×10^{-6} K^{-1}), which closely matches the thermal expansion coefficient of the telluride films, reduces residual stress and increases adhesion of thermoelectric films. Films were deposited by co-evaporation of Bismuth and Tellurium or Antimony and Tellurium to obtain Bi_2Te_3 or Sb_2Te_3 compounds (Fig. 2), respectively. The performance of thermoelectric devices depends on figure of merit (ZT) of the film, given by $ZT = \alpha^2T/(\kappa\rho)$, where α, T, κ and ρ are the Seebeck coefficient, absolute temperature, thermal conductivity and electrical resistivity, respectively. Optimal growing deposition parameters allow the fabrication of films with ZT = 0.9 and ZT = 0.5 for Bi_2Te_3 and Sb_2Te_3, respectively. These values are comparable with the best published results for the same material, under various fabrication methods (thermal co-evaporation [1], sputtering, MO-CVD, flash-evaporation or electrochemical deposition). A layered structure (superlattice) can increase films performance and a figure of merit of 2.4 can be achieved [2] in a layered Bi_2Te_3/Sb_2Te_3. Seebeck coefficient is increased and thermal conductivity reduced, by controlling the transport of phonons and electrons in the superlattice structure.

Thermoelectric devices were fabricated using photolithography and wet-etching techniques [3,4] with HNO_3 / HCl based etchants The performance of a Peltier microcooler was analyzed by infrared image microscopy, on still-air and under vacuum conditions, and 4 ºC temperature difference between the cold side and the hot side of the device was recorded (Fig. 4).

Acknowledgments:
This work was supported by FCT/PTDC/EEA-ENE/66855/2006 and FCT (SFRH/BD/18142/2004).

References:

[1] Luciana Silva,, Massoud Kaviany, "Fabrication and Measured Performance of a First-Generation Microthermoelectric Cooler", *Journal of Microelectromechanical Systems*, vol. 14, 5, pp. 1110 (2005).

[2] Rama Venkatasubramanian, Edward Siivola, Thomas Colpitts & Brooks O'Quinn, "Thin-film thermoelectric devices with high room-temperature figures of merit", Nature vol 413 (2001)

[3] L. M. Goncalves, J. G. Rocha, C. Couto, P. Alpuim, Gao Min, D.M. Rowe J.H. Correia, Fabrication of flexible thermoelectric microcoolers using planar thin-film technologies, J. Micromech. Microeng. 17 (2007)

[4] L.M. Goncalves, J.G. Rocha, C. Couto, P. Alpuim, and J.H. Correia, On-Chip Array of Thermoelectric Peltier Microcoolers, Sensors and Actuators A: Physical, In Press (2008)

Figures:

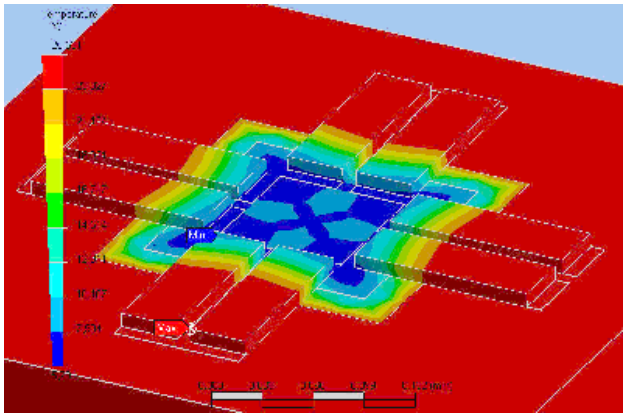

Figure 1: Microcooler simulation shows the possibility to obtain 20ºC of cooling at the center of microcooler.

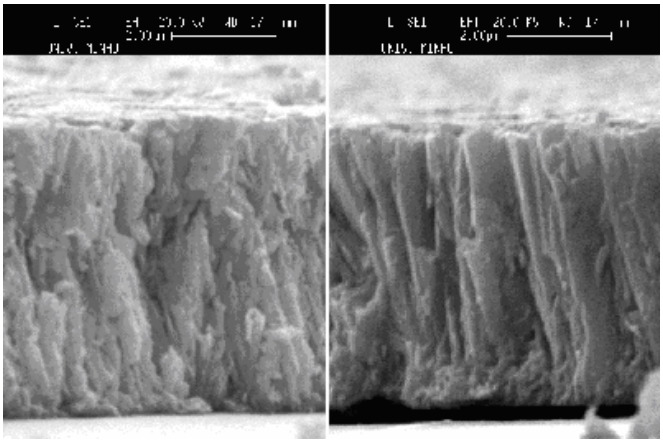

Figure 2: SEM photo of Bi_2Te_3 (left) and Sb_2Te_3 (right) thin films.

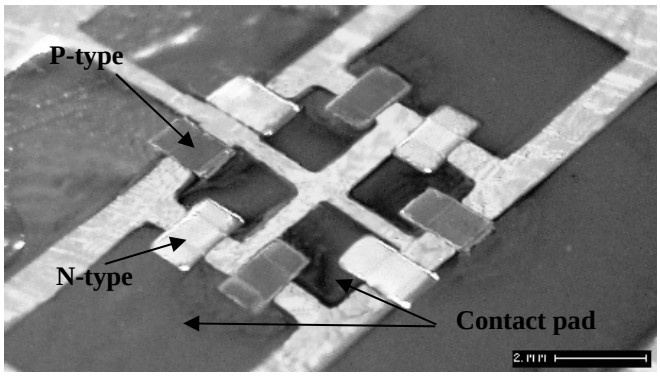

Figure 3: Photo of a microcooler pixel, on top of a polyimide substrate.

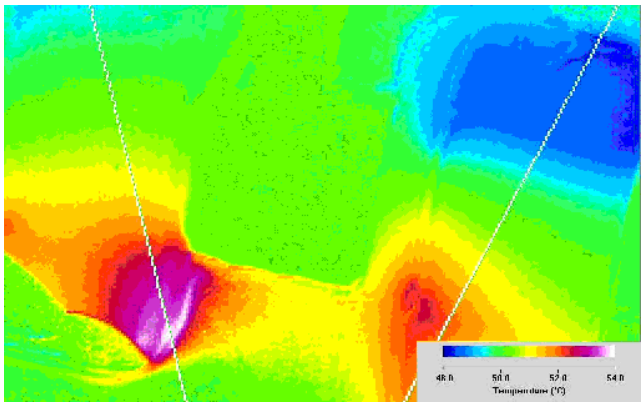

Figure 4: Thermal image of n-type and p-type thermoelectric elements presented on figure 5, powered with 4mA current, under vacuum.

NON- SPECIFIC ADSORPTION OF BIOMOLECULES ON SINGLE WALLED CARBON NANOTUBES

*González Mónica[a]; Benito, Ana Maria[a]; Maser, Wolfgang[a], , Marco, Maria Pilar[b]; Tort, Núria[b], Martínez, Maria Teresa[a]**
[a]*Instituto de Carboquímica, Miguel Luesma Castán,4, Zaragoza, Spain*
[b] *IIQAB-CSIC, Jordi Girona, 18-26, Barcelona, Spain*
mtmartinez@icb.csic.esl

Carbon Nanotubes, CNTs, exhibit a unique combination of excellent mechanical, electrical and electrochemical properties, which has stimulated increasing interest in the application of CNT as components in bio-sensors. Nevertheless, the control of non-specific protein adsorption is important for the use of CNTs in specific protein-binding or biorecognition.. There are several molecules reported in the literature that has been used to prevent the protein adsorption. Among them, polyethylene glycol, PEG, bonded no covalently to CNTs has been reported to be an effective way to achieve the protein resistance [1]. The protein resistant coating usually requires amphiphilic molecules with a hydrophobic backbone that interactions hydrophobically with the CNT and a hydrophilic segment extended in the aqueous solution. In this work we have explored the existence of non specific protein adsorption on single wall nanotubes, SWNTs, using the biotin- streptavidin system. We have modified the hydrophobic character of the SWNTs by surface functionalization with carboxylic groups, amine groups and PEG that renders the SWNTs surface more hydrophilic. The streptavidine adsorption on these modified SWNTs has been determined and compared with the biotin-streptavidine interaction on SWNTs covalently functionalized with biotin.

The specificity of streptavidin adsorption on SWNTs have been determined using a colorimetric method based on the horseradish peroxidase-catalyzed oxidation of 3,3',5,5'-tetramethylbenzidine[2]. The nanotubes were dispersed in PBS buffer by sonication and streptavidina-HRP solution is added. After 30 minutes of reaction time, the solution is filtered and washed with PBST buffer. SWNTs were sonicated, filtered again and dried under vacuum at room temperature. Substrate HRP buffer was then added and blue colour was observed in the presence of streptavidin. The reaction was stopped after 30 minutes by addition of H_2SO_4 4N the colour turning to yellow. For quantitative study, UV detection can be used measuring the absorbance at 450 nm of supernatant.

Single-walled nanotubes were produced by arc discharge method (100A, 20V), using Ni and Y as catalysers (4:1) under 660mb of helium [3,4]. The as-produced SWNTs is a multicomponent material consisting of entangled SWNT bundles associated with metal nanoparticles and carbon phases more or less graphitized. (Figure 1)

Oxidation of as-produced SWNTs was achieved by adding an aqueous solution of nitric acid 1'5M and refluxing during 2 hours. The resulting suspension was then centrifuged, filtered, washed with milliQ water and dried under vacuum.[5,6,7]

To obtain aminated SWNTs, carboxylated carbon nanotubes were first acylated, by addition of thionyl chloride and dimethylformamide and stirred at 120ºC during 24 hours. After filtration and washing with tetrahydrofuran to remove the $SOCl_2$ excess, the SWNT material was dried under vacuum. Afterwards, it was mixed with ethylenediamine and stirred at 60ºC during 4 days. The material was then filtered, washed repeatedly with ethanol and dried under vacuum to obtain the final aminated nanotubes.[6,7]

The aminated nanotubes were then dispersed in dimethylformamide and reacted overnight with N-hydroxysuccinimidyl biotin at room temperature to form biotinated SWNTs. The dispersion was then filtered and dried under vacuum. A scheme of the reaction is shown in Figure 2.

To obtain SWNTs functionalized with polyethylene glycol, Figure 3, the acylated nanotubes were mixed with PEG and pyridine in dimethylformamide, and stirred at 100ºC during 5 days. After filtration, the product was washed with water and dried under vacuum.

References :

[1] Y.Lin, S. Talylor, H. Li, K.A. S. Fernanddo, L. Qu, W. Wang, L. Gu, B. Zhou Y.P. Sun. *J. Mater. Chem.*, 2004, 14, 527-541.

[2] P. David Josephy, Tohomas Eling, Ronald P. Mason, *The Journal of Biological Chemistry,*. 1982, *257*, 7, 3669-3675.

[3] Journet C., Maser WK, Bernier P., Loiseau A., Lamy de la Chapelle M., Lefrant S. ; *Nature,* 1997 ;388 ;756-8

[4] Benito A.M., Maser W.K., Martínez M.T.; *Int. J. Nanotechnology* 2, 71, (2005)

[5] Martínez M.T., Callejas M.A., Benito A.M., Cochet M., Seeger T., Ansón A., Schreiber J., Gordon C., Marhic C., Chauvet O., Maser W.K. ; *Nanotechnology*, 14 (2003) 1-5

[6] Martínez M.T., Callejas M.A., Benito A.M., Cochet M., Seeger T., Ansón A., Schreiber J., Gordon C., Marhic C., Chauvet O., Fierro J.L.G., Maser W.K. ; *Carbon, 41 (2003) 2247-2256*

[7] Montesa I., Muñoz E., Benito A.M., Maser W.K., Martínez M.T.; *Journal of Nanoscience and Nanotechnology*, Vol. 7, Iss. 10, 3473-3476, (2007)

Figures:

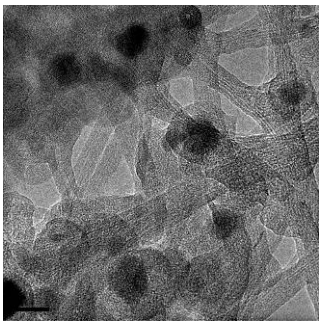

Figure 1. TEM image of as-produced SWNTs.

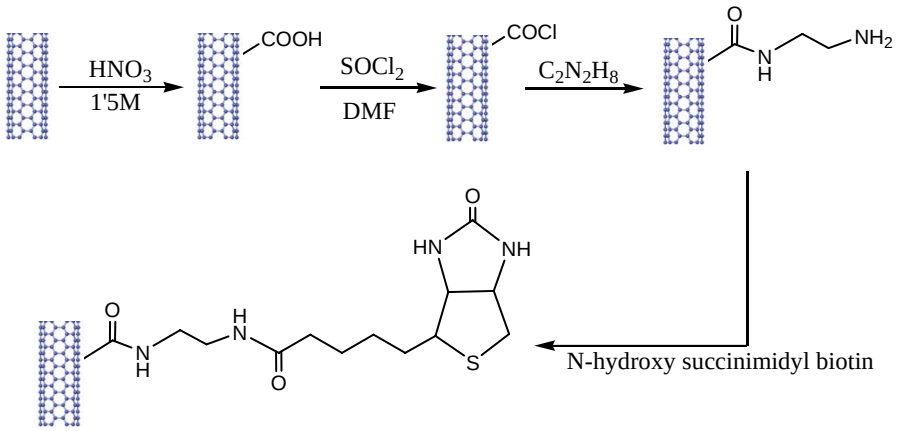

Figure 2. Scheme of biotin functionalization of SWNTs

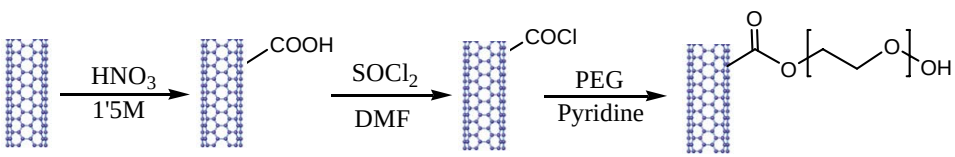

Figure 3. Scheme of PEG functionalization of SWNTs

SURFACE PLASMON RESONANCE EFFECTS ON THE MAGNETO-OPTICAL RESPONSE OF NOBLE METAL-FERROMAGNET NANODISKS.

J.B. González-Díaz, A. García-Martín, J.F. Torrado, J.M. García-Martín, A. Cebollada and G. Armelles
Instituto de Microelectrónica de Madrid, Consejo Superior de Investigaciones Científicas, C\Isaac Newton 8 (PTM) 28760 Tres Cantos, Spain
juanb@imm.cnm.csic.es

B. Sepúlveda and M. Käll
Chalmers University of Technology, Göteborg, 41296, Sweden

In this work, a new kind of active nanostructure combining plasmonic and magneto-optical (MO) properties has been fabricated and analyzed. To date, the excitation of a surface plasmon has already been shown to enhance the MO activity of continuous films composed of Au/Co/Au trilayers [1]. This enhancement can be used to develop new high sensitivity biosensors as pointed out in recent studies [2]. A further step is the use of nanostructures. The advantages that localized surface plasmons (LSP) present in that kind of systems with respect to propagating surface plasmons in continuous films are considerable. A first advantage is that the localization of the electromagnetic field can lead to a larger enhancement in the MO response [3]. Secondly, the enhancement in the MO response found in continuous films can only be achieved via a transversal kerr configuration, in which the magnetic field is applied parallel to the sample's plane and perpendicular to the incidence of the light. On the contrary, nanoparticles can be useful in other configurations as the way to excite the surface plasmon is different to that of continuous layers. Finally, the wide range of parameters that can be modified, such as size and shape of the nanoparticles, or interparticle distance, gives the possibility to freely tune the MO response.

The system analyzed here consists of Au/Co/Au nanodisks prepared using a colloidal lithography procedure from continuous Au/Co/Au films grown onto glass by sputtering. This nanostructuration gives rise to strong changes in the optical absorption properties of the system. Figure 1 shows the absorption spectra of two samples with disk diameters of 60 and 110 nm, exhibiting a characteristic peak around 2 eV. The peak is due to the excitation of the LSP of the Au/Co/Au nanodisks and its energy position depends on the nanodisk aspect ratio that is given by the trilayer thickness and the disk diameter. This excitation in turn affects the MO response of the system. In this work we will study two Kerr MO configurations. In the polar configuration (magnetic field applied perpendicular to the sample plane), the Kerr effect that accounts for the MO response shows an enhancement of this magnitude with respect to that of continuous layers. For example, figure 2 shows the Polar Kerr ellipticity spectra of the nanodisks. The peak observed lies in the same energy region to that observed in the absorption spectra, illustrating the effect of the LSPR on the enhancement of the MO response. Moreover, the peak red-shifts as the diameter of the nanodisk increase, in the same manner the absorption peak does. In the transverse configuration the enhancement of the MO activity is not so obvious (see figure 3). However, the zero crossing lies as well in the same energy region of the absorption peak associated to the plasmon excitation. Similarly, the energetic evolution with the disk diameter of the zero crossing reproduces the observed in the absorption spectra.

References:

[1] J.B. Gonzalez-Diaz et al. Phys. Rev. B. **76**, (2007) 153402.
[2] B. Sepúlveda et al. Oppt Lett.**31**, (2006) 1085.
[3] J.B. Gonzalez-Diaz et al. SMALL, **4**, (2008) 202.

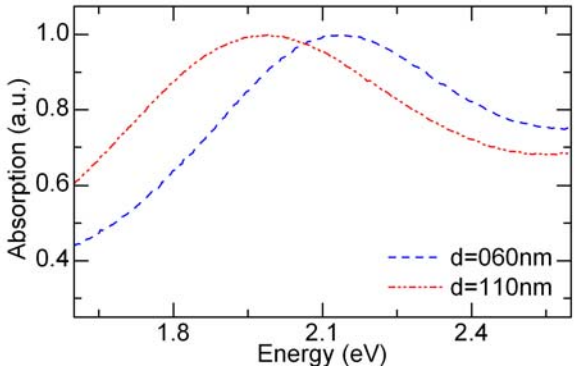

Figure 1.- Absorption spectra for a nanostructured system composed of Au/Co/Au disks. Two diameters are considered: 60nm and 110nm.

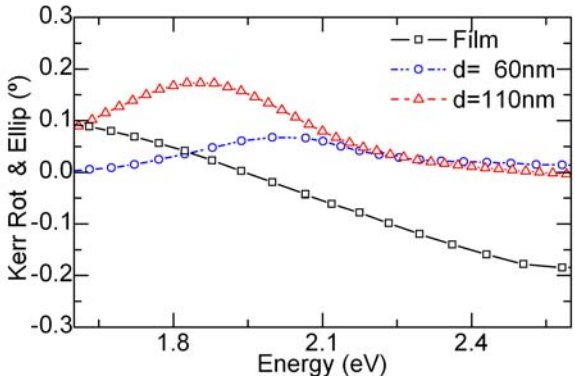

Figure 2.- Kerr ellipticity spectra for a nanostructured system composed of Au/Co/Au disks. Two diameters are considered: 60nm and 110nm. For comparison, it is also depicted the Kerr ellipticity spectra for a continuous Au/Co/Au trilayer.

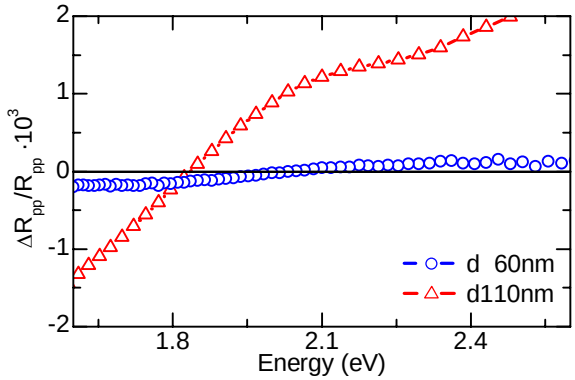

Figure 3.- Kerr transverse spectra for a nanostructured system composed of Au/Co/Au disks. Two diameters are considered: 60nm and 110nm.

CARBON NANOTUBES DISPERSION TOWARDS POLYMER INTEGRATION

J.M. González-Domínguez , W. Maser, A. Benito, P. Castell, A. Ansón, M.T. Martinez*.
Instituto de Carboquímica (CSIC), C/ Miguel Luesma Castán nº4 50018, Zaragoza, Spain
* Corresponding author's e-mail : mtmartinez@icb.csic.es

INTRODUCTION

Single wall carbon nanotubes, SWNTs, are born in their synthesis as bundles of tubes well aligned and packed in a triangular compact lattice entangled in nets due to Van Der Waals interactions. Their applications and excellent performance usually make reference to the individual tube, and the fact of appearing entangled-synthesized, provokes their complete insolubility in both aqueous and organic media, making SWNTs practically unprocessable. Thus, bundles represent the main obstacle in developing SWNTs technological potential, being necessary debundling in individual tubes. Some of the strategies used cause modification of physical properties and electronic structure of nanotubes [1], which could not be desirable for their applications, specially in fabricating composites. The debundling of SWNTs and the possibility of influencing SWNTs' alignment are major goals, specially in the field of nanocomposite materials [2,3].

Polymers could offer a suitable alternative in carbon nanotubes' interfacial union engineering [4]. It is possible to achieve this goal, by making them interact via weak bonding Van der Waals type, resulting in a "polymer–decorated", adsorbed or extreme–connected nanotube. This causes steric repulsions among polymer layers which, because of the system's entropy alteration, leading to a separation of tubes. Typical examples can be observed in block copolymers. They are excellent promoters of wetting and adhesion. Choosing a chemically compatible block copolymer with the target matrix of SWNTs, and codispersing them in the target polymer, it is possible to prepare SWNTs–Polymer nanocomposites.

EXPERIMENTAL AND RESULTS

Attending to what's been said before, and having a future look on integrating SWNTs in epoxy resins, a block copolymer was chosen containing the polyethylenoxide (PEO) block. A suitable homopolymer to the other block is polypropylenoxide (PPO). PEO was used as one of the monomers because of its good affinity to water. The second monomer, PPO, was chosen for being more hydrophobic than PEO in order to reach good interactions with SWNTs surface in aqueous media. A commercial block copolymer containing those blocks has been the one used in the present work, F68 PLURONIC ® with average molecular weight of 6800 g/mol. It is registered by BASF and consists in a triblock copolymer having the sequence PEO-PPO-PEO. At room temperature is a white solid with grain aspect and water soluble (maximum solubility above 20% wt).

Dispersions of Single Walled Carbon Nanotubes (SWNTs) were prepared using PEO-PPO-PEO triblock copolymer as dispersing agent. Thus, several series of polymer's aqueous solutions were made varying both polymer and SWNTs' concentration. They were prepared in the range of 0.4 – 10% wt of PLURONIC ® in water. SWNTs concentrations were also varying from 0.4 to 1% wt. It implies that total load in the solvent moved in the range 0.9 – 11% wt. Optimum ratio (polymer:SWNT) was found to be 5:1. Applying sonication by ultrasonic horn in different conditions of time and oscillation amplitude and controlling experimental conditions, fine and stable dispersions were eventually obtained. The experimental protocol includes optical microscopy and density measurements as a first step to control the SWNTs dispersion. Optical microscopy (50X) showed whether the initial mixture of components was homogeneous. Density measurements were used to check changes in mass/volume ratio of mixtures during sonication which could be attributed to bundle exfoliation.

The dispersed SWNTs were characterized by TEM, Raman Spectroscopy and X-Ray Diffraction. XRD (figure 1) indicated disgregation because of bundle's lattice peaks disappearance [5]. Raman Spectroscopy supported the debundling of SWNTs (figure2) due to the Radial Breathing Mode shift displacement, since the radial character of RBM band is likely to be much influenced by the nanotube packing [6]. It also observed the effect of the polymer presence because the G/D band ratio alteration. TEM micrographies were the ultimate proof as they were clearly showing individual polymer-

decorated nanotubes and small bundles (3-4 tubes) probably also wrapped by the polymer (figure 3). From the characterization data, optimum time of sonication was established at two hours.

References:

[1] M.T. Martínez, M.A. Callejas, A.M. Benito, A. Ansón, W. Maser. *"Sensitivity of SWNTs to oxidative processing: sturctural modification, intercalation and functionalization"*, Carbon, 41 (2003), 2247-2256.
[2] Erik T. Thostenson, Chunyu Li, Tsu-Wei Chou, *"Nanocomposites in Context"*, Composites Science and Technology 65 (2005) 491-516.
[3] R. Andrews, M.C. Weisenberger, "*Carbon nanotube polymer composites"*, Current opinion in Solid State & Material Science, 8 (2004) 31-37.
[4] Pratap Bahadur, "*Block Copolymers, their microdomain formation (in solid state) and surfactant behaviour(in solution)*", Current Science-Soft condensed matter, Vol 80, nº8 (2001), 1002-1007.
[5] Rina Schvartzman-Cohen, Yael Levi-Kalisman, Einat Nativ-Roth, Rachel Yerushalmi-Rozen, "*Generic Approach for dispersing SWNTs: the strength of a weak interaction*", Langmuir 2004, 20, 6085-6088.
[6] L. Alvarez, A. Righi, S. Rols, E. Anglaret, J.L. Sauvajol, "*On the Raman Spectrum of nanobundles of SWNTs*", http://www.geocities.com/CollegePark/3972/MRS_99.pdf

Figures:

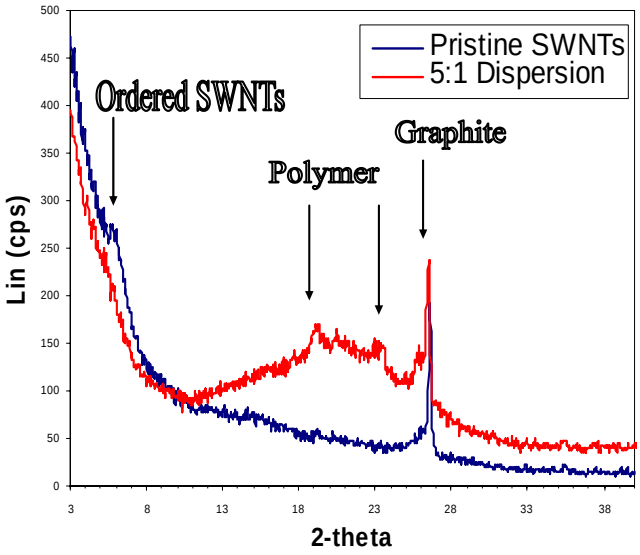

Figure 1: XRD Difractogram

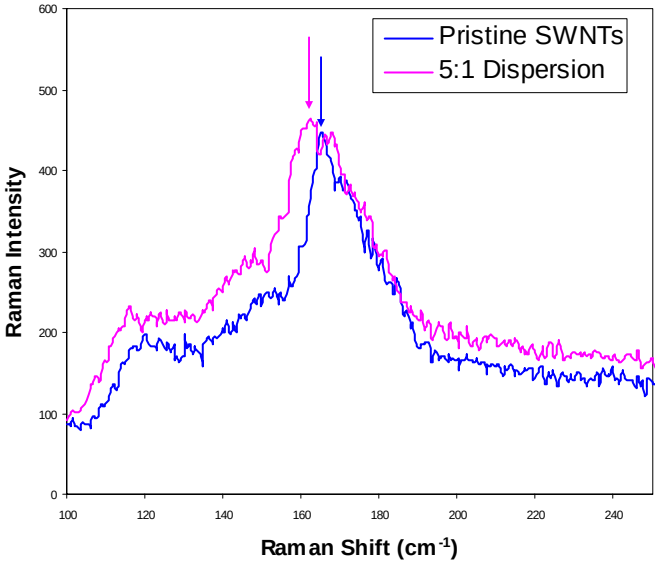

Figure 2: Radial Breathing Mode part of Raman Specter

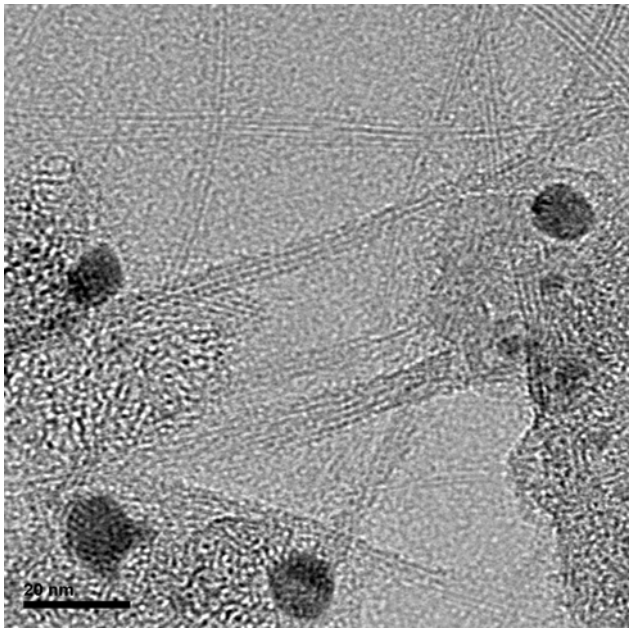

Figure 3: TEM Micrography

DOMAIN WALL PROPAGATION IN THIN FE-RICH GLASS-COATED AMORPHOUS WIRES

V. Zhukova[1*], J.M. Blanco[1], M. Ipatov[2], J. Gonzalez[2] and A. Zhukov[2]

[1] *Física Aplicada, EUPDS, Universidad del Pais Vasco/EHU, 20009, San Sebastián, Spain.*
[2]*Fac. Químicas, Universidad del Pais Vasco /EHU, 20009, San Sebastián, Spain.*

Keywords: amorphous microwires, domain wall propagation
Category: Amorphous, nano-crystalline materials and granular materials

Recently great attention has been paid to studies of thin glass coated microwires consisting of ferromagnetic thin nucleus (typically of the diameter 1 - 30 μm) coated by the glass exhibit excellent soft magnetic properties useful for the technological applications (magnetic bistability, GMI effect, enhanced magnetic softness, ...) [1]. These microwires with positive magnetostriction constant are convenient magnetic materials to study the domain wall propagation because of their peculiar domain structure consisting of single axially magnetized domain surrounded by the outer domain structure with radial magnetization [1].

Such Fe-rich magnetic microwiries exhibit a phenomenon of the magnetic bistability characterized by the appearance of rectangular hysteresis loop at low applied magnetic field. This rectangular hysteresis loop was interpreted in terms of nucleation or depinning of the reversed domains inside the internal single domain and the consequent domain wall propagation [2]. Surprising results such as exiting of the domain wall propagation below the switching field [2] and negative critical propagation field [3] have been reported.

We studied the velocity of domain wall propagation, v, of $Fe_{69}Si_{10}B_{15}C_6$ with different metallic nucleus diameter, *d*, and different total diameter, *D* (*d*=14 μm; *D*=33 μm and *d*=18 μm; *D*=23.4 μm respectively) in the temperature range between 78 and 300 K and at different frequencies of applied magnetic field. It is worth mentioning, that *v(H)* dependence is essentially not linear, showing significantly higher domain wall mobility, *S*=*dv/dH*, at low filed limit. Domain wall mobility, *S*, increases significantly with increasing the temperature. From *v(H)* dependence the critical field, H_{cr}, associated with the change of the slope on *v(H)* dependence is determined. All characteristics, *v(H)* dependence, *S(H)* dependence and H_{cr} are sensitive to the sample geometry, i.e. to the internal stresses. The origin of such dependence on internal stresses is discussed in terms of magnetoelastic energy contribution.

REFERENCE

[1] A. Zhukov et al. J. Mat. Res. 15 (2000) 2107
[2] A. Zhukov Appl. Phys. Let. 78 (2001) 3106
[3] R. Varga et al. Phys. Rev. B 73 (2006) 054408

HIGH MOBILITY INDIUM ZINC OXIDE DEPOSITED BY RF MAGNETRON SPUTTERING AT ROOM TEMPERATURE

G. Gonçalves, E. Elangovan, P. Barquinha, L. Pereira, R. Martins, E. Fortunato
CENIMAT/I3N, Materials Science Department, Campus de Caparica, 2829-516 Caparica, Portugal
Tel: +351212948562; Fax: +351212948558
gpg@fct.unl.pt

Transparent conducting oxide (TCO) with optical transmission exceeding 80 % in the visible region (550 nm) and resistivity less than 10^{-3} Ωcm have been widely used in a variety of applications, for more than a half-century. More recently, they become the subject of intense investigation for applications as transparent electrodes for optoelectronic devices like flat panel displays, solar cells to organic light emitting diodes. Most of the previous research on TCOs has been focused on indium tin oxide (ITO) and fluorine tin oxide (FTO).

The TCOs most widely used for display applications are crystalline indium tin oxide (c-ITO), amorphous indium tin oxide (a-ITO), and amorphous indium zinc oxide (a-IZO). The most common method for the deposition of these TCOs is DC/RF magnetron sputter deposition.

In general, ITO is deposited from sintered ceramic In_2O_3 targets containing between 3 and 10 wt% SnO_2 while IZO targets contain 7-10 wt% ZnO. At present, crystalline ITO deposited onto substrates heated to 250-350 °C offers the lowest resistivity currently available ($1\text{-}3\times10^{-4}$ Ωcm). Two alternatives to c-ITO that may be processed at room temperature are a-ITO and a-IZO. Both of these amorphous materials have slightly inferior electrical transport properties compared to c-ITO but, they are, in some applications, favoured over crystalline ITO because they offer improved lithographic line definition due to the more controllable wet-etch characteristics of the amorphous phase. In addition, a-IZO offers the advantage of not requiring the addition of oxygen to the sputter gas since the optimum resistivity is at or near zero oxygen partial pressure.

In this paper we present some of the the morphological, electrical and optical properties of a-IZO thin films as well as its applications to optoelectronic devices with improved performances like: transparent TFTs, electrochemical devices and PLEDs.

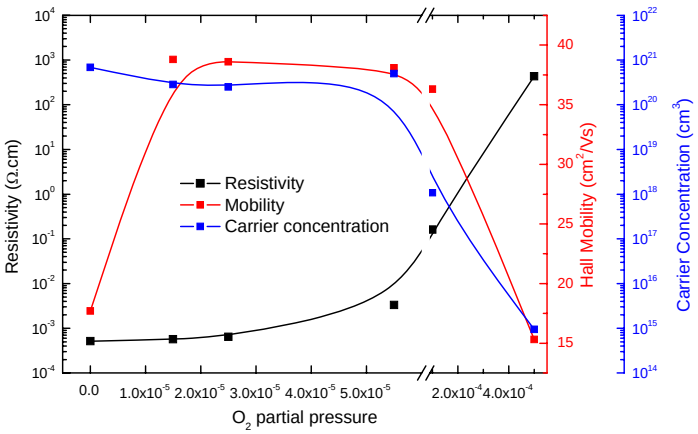

Dependence of the electrical resistivity, carrier concentration and carrier mobility of a-IZO films as a function of oxygen partial pressure.

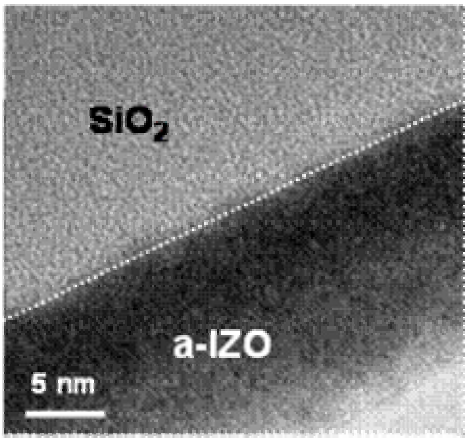

TEM cross section of an amorphous oxide semiconductor (indium zinc oxide) deposited onto SiO_2 by rf magnetron sputtering at room temperature. The electron Hall mobility is 60 cm^2/Vs.

Experimental realization of a high efficient coupling technique for SOI devices based on inverted taper and V-groove integration

A. Griol,[*] J. Hurtado, J. V. Galan, P. Sanchis, G. Sanchez, and J. Marti
G. Petersson[#], B. Nilsson[#] and J. Halonen[#]

Valencia Nanophotonics Technology Center – Universidad Politecnica de Valencia, Camino de Vera s/n 46022 Valencia, Spain
[#] MC2 Nanofabrication Laboratory, Chalmers University of Technology, Gothenburg, Sweden
[*] *Corresponding author: agriol@ntc.upv.es*

Abstract: This paper demonstrates a coupling technique between SOI (*Silicon on insulator*) waveguides and singlemode fibers based on an inverted taper structure integrated with V-groove auto-alignment structures thus allowing an easier passive alignment of the optical fiber and easier packaging**.** Total fiber in-to-fiber out transmission losses around 20dB have been measured experimentally for a wavelength range between 1530nm and 1560nm when coupling the fabricated sample to a 9μm core diameter standard singlemode fiber.

Introduction

Light coupling into SOI devices is a key point in silicon photonics. It is very important to develop efficient coupling techniques which allow high coupling efficiency, so that no Fabry-Perot resonances appear in the measured spectrum power. Different coupling techniques as grating couplers [1] and inverted tapers [2] have been researched to achieve efficient light coupling in SOI devices. However, the fiber-chip alignment in that kind of structures is not an easy task. This approach was designed to allow the integration with V-groove structures for easier passive fiber alignment purposes.

Proposed structure

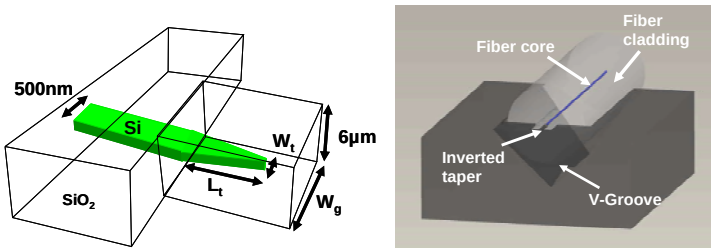

Figure 1: Illustration of the proposed coupling technique. Detail of the integration of the coupling technique with V-Groove structures.

Figure 1 depicts the proposed coupling technique. As it is shown, the singlemode SOI waveguide (which width has to be around 500nm for singlemode condition) is tapered down by the inverted taper, whose main physical parameters are illustrated in the picture. The inverted taper is surrounded by a 6μm height silica (SiO_2) layer. The design parameters of the inverted taper as well as the SOI waveguide and the silica waveguide were optimised with 3D BPM (Beam Propagation Method) simulations in order to achieve the lowest coupling losses between the proposed taper and a 9μm core diameter standard single-mode fibre. The design procedure is similar to the one explained at [3]. Figure 1 also shows the integration of the proposed coupling technique with V-groove auto-alignment structures, thus enabling an easier fiber alignment and an easier packaging.

Fabrication and experimental results

The fabrication process comprises two different steps. The first one consists of the implementation of the SOI waveguide and the inverted taper. To carry out this implementation, a lithography process based on e-beam was employed, obtaining a high resolution HSQ resist mask that is used to transfer

the patter to the Silicon layer of the SOI structure by using a dry etching process. Finally, an upper cladding of silica is deposited over the whole structure by means of a PECVD process. The second fabrication step consists of the physical realisation of the V-grooves. For this purpose, a lift-off process is carried out in order to obtain a window corresponding to the V-groove location in a niquel-chromium mask which aim is to protect the SOI waveguide and inverted-taper from a silica etching process. Finally, the V-groove is created in the silicon substrate by means of a TMAH chemical process. Figure 2 (a) shows a detail of the layout of the fabricated sample which consists in two waveguides ended with the designed coupling structure, which are joined by two curves, so both input and output chip access waveguides are accessible through the same chip facet, thus enabling high compactness of photonic integrated circuits. The separation of the V-Grooves is 250µm. The curves have a radius of 5 µm. It can be also seen a SEM image of the fabricated sample.

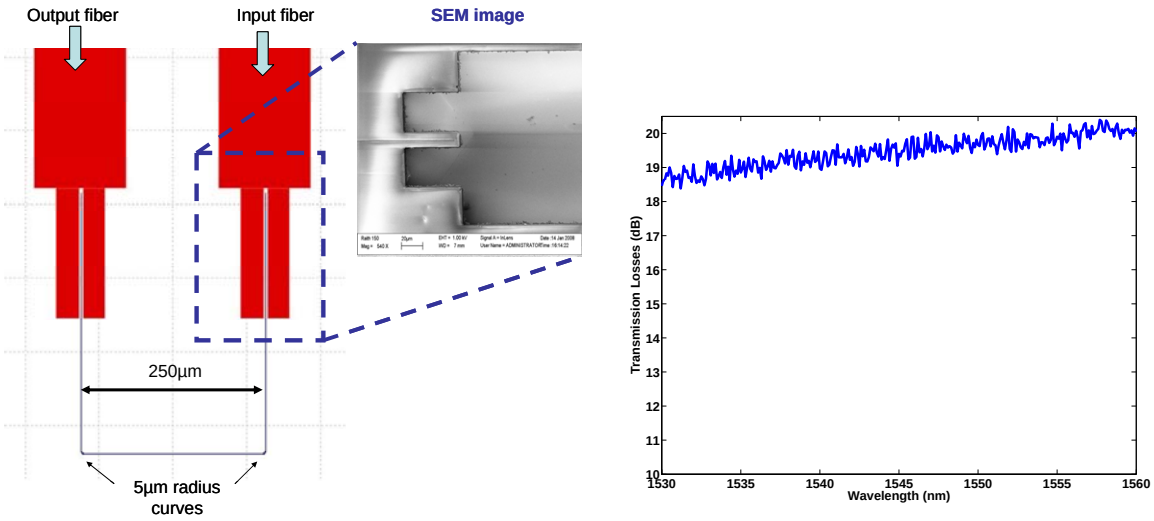

(a) (b)

Figure 2: (a)Layout and SEM image of the fabricated sample. (b) Measured spectrum.

Figure 2(b) shows the measured spectrum of the fabricated sample for TE polarization. It is achieved less that 20dB fiber-to-fiber transmission losses at λ=1550nm. Furthermore, an almost flat optical spectrum has been obtained, so that no resonance effects appear in the spectrum, due to the efficiency of the achieved coupling.

Conclusions

A coupling technique between SOI waveguides and single-mode optical fibres based on optimised inverted tapers have been proposed and experimental realised. Total fiber-to-fiber transmission losses of 20dB have been obtained for the fabricated sample, which allows high compactness of photonic integrated circuits. An almost flat spectral response is also achieved.

Acknowledgments

The work at Chalmers was financed by the FP6-Research Infrastructures program **MC2ACCESS** through **Contract No:** 026029.

References:

[1] F. V. Laere, G. Roelkens, M. Ayre, J. Schrauwen, D. Taillaert, D. V. Thourhout, T. F. Krauss and R. Baets, J. Lightwave Technol., Vol. 25, No. 1 (2007).
[2] V. R. Almeida, R. R. Panepucci and M. Lipson, Opt. Lett. , Vol. 28, No. 15 (2003).
[3] J.V. Galan, P. Sanchis, G.Sanchez and J. Marti, Opt. Express, Vol. 15, No. 11 (2007).

HYBRID MAGNETORESISTIVE/MEMS DEVICE FOR 1/F NOISE REDUCTION

A. Guedes[1,2], S. Patil[1], P. Wisniowski[1], V. Chu[1], J.P. Conde[1,2] P. P. Freitas[1,2]

[1] INESC Microsistemas e Nanotecnologias (INESC MN), Rua Alves Redol 9,
1000-029 Lisbon, Portugal
[2] Instituto Superior Técnico (IST), Av. Rovisco Pais,
1000-029 Lisbon, Portugal
aguedes@inesc-mn.pt

It was previously shown that it is possible to suppress 1/f noise in spin valve (SV) sensors, by modulating an external DC magnetic field at high frequency through the movement of a MEMS cantilever with an incorporated magnetic flux guide[1]. This shifts the operating frequency and enables the detection of DC magnetic fields in the high frequency thermal noise regime, where the 1/f noise is typically 2 orders of magnitude lower.

In this work we present a hybrid magnetoresistive/MEMS device, where MgO based magnetic tunnel junction (MTJ) and MEMS torsionators are used, allowing a DC field detection limit of 27 nT/Hz$^{1/2}$ and improving the MEMS magnetic field modulation efficiency to 20 %.

MgO based MTJ sensors were deposited in an automated sputtering machine with the following structure: Glass/Ta[50] / Ru [180] / Ta [30] / MnPt [200] / CoFe [20] / Ru [9] / CoFeB [30] / MgO [15] / CoFeB [15.5] / Ru [50] / Ta [50] / TiW(N2) [150], (thickness in Å). The TMR ratio was 30 %. The MTJ sensors were patterned down to a dimension of 1.5x15 μm^2. A 4000 Å thick CoZrNb flux guide concentrator was patterned close to it, to convey and focus the external field to the sensor area. Finally, after passivating the sensor with an oxide layer, a 30x20 μm^2 MEMS torsionator was fabricated with a double layer of a-Si:H (4000 Å)/Al (1000 Å) and an additional 2000 Å thick CoZrNb flux guide. The MEMS torsionator is actuated by a gate electrode at frequency *f*, causing it to oscillate at 2*f*. This oscillation produces a 2*f* AC magnetic field, which is read by the MTJ in a spectrum analyzer. Fig.1 shows a SEM micrograph of the integrated device and a cut view diagram.

Noise measurements in the 2 kHz – 500 kHz range were performed in the MTJ sensor. For a bias a current I = 10^{-5} A and at 500 kHz (close to the thermal noise background) the magnetic field detection limit is S_B^{SV}= 4 nT/Hz$^{1/2}$

With this MTJ-MEMS hybrid device the minimum detectable DC field is given by:

$$B_{detect} = S_B / e_{tors} \qquad (1)$$

where S_B is the MTJ noise in T/Hz$^{1/2}$ at the modulation frequency, and e_{tors} the magnetic modulation efficiency of the MEMS torsionator.

Figure 2 shows the MTJ output, when the MEMS gate is actuated by a 20 V_{pp} AC signal at 230 kHz . The MEMS torsionator oscillates at 460 kHz. For a DC external

field B_{ext} = 0.36 mT entering the flux guide, the MTJ sensor detects the generated AC field at 460 kHz, showing a magnetic output of 240 μV/Hz$^{1/2}$.

The MEMS torsionator modulation efficiency (e_{tors}) was calculated and found to be 20 %. Putting this together with the noise of the MTJ sensor at this frequency – S_B^{SV} (4.4 nT/Hz$^{1/2}$ at 460 kHz) we can estimate from Eq. (1) the DC detection limit of this hybrid-device, B_{detect} = 27 nT/Hz$^{1/2}$.

Further work is being developed, mainly to reduce the thermal noise in the MTJ sensors, so that its further integration in this hybrid-device would lead to pT DC field detection.

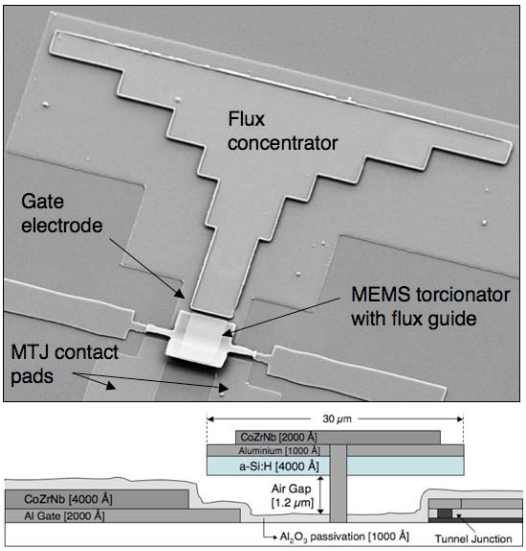

Figure 1

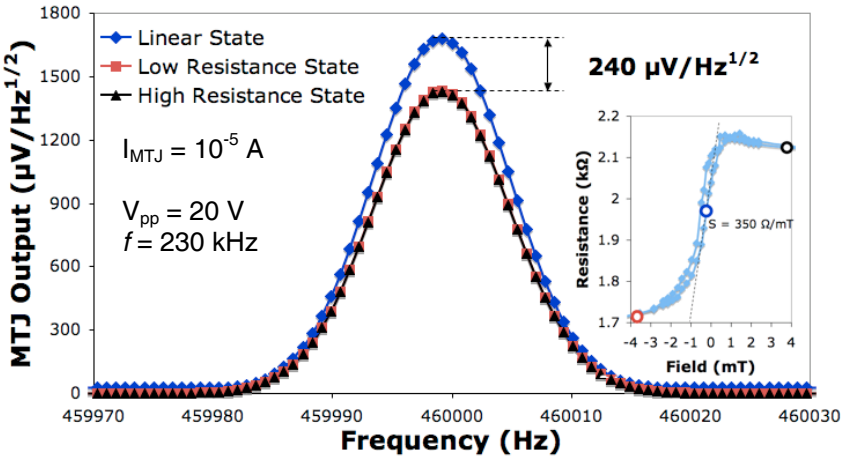

Figure 2

References:

[1] A. Guedes, S.B. Patil, S. Cardoso, V. Chu, J. P. Conde, P. P. Freitas, Jour. Appl. Phys. (*in press*) 2008.

Synthesis of nano-structured copolymeric hydrogels based on *N*-Isopropyl acrylamide (NIPA) by Microemulsion Polymerization

L.G. Guerrero[1], X. Hervías[1], S. Nuño-Donlucas[2], L.C. Cesteros[1], L. Sanz[1], I. Katime[1]

1) Grupo de Nuevos Materiales y Espectroscopia Supramolecular. Facultad de Ciencia y Tecnología. Universidad del País Vasco (UPV/EHU). Campus de Lejona, Apartado. 644 Bilbao, España. E-mail: issa.katime@ehu.es
2) Universidad de Guadalajara. Departamento de Ingeniería Química. CUCEI. Guadalajara (Jalisco, México).

A new nano-sized material has been developed by the copolymerization of *N*-isopropyl acrylamide (NIPA) with modified monomers. One of the most remarkable methods to obtain nanoparticles is the microemulsion polymerization [1]. This feature has not been exploited at all due to the microemulsion polymerization can be also applied to obtain nanohydrogels [2]. Depending on its design, water/oil/surfactant systems present one, two or three phases when they are in equilibrium; one of which contains the quasi-totality amount of the surfactant [3]. The development of Hydrophilic-Liphophilic Balance systems (HLB) has simplified and systematized the selection of an optimal surfactant for specific applications in emulsions and microemulsions [4]. Undoubtedly, the complexity of the nano-science implies the use of new chemical structuration and functionalization techniques that exploit the properties of nanoparticles that let them express in selective manner specific qualities [5]. In this regard, the polymer science is the nearest to allow selective chemical structure due to the polymers are complex materials that have a wide variety of properties that can be changed before, during and after their issuance [6]. Hydrogels based on NIPA show temperature sensitivity due to the Lower Critical Solution Temperature of the NIPA that is located near of 32°C. The importance of the obtantion of nanometric hydrogels is related to administration of medicines; particularly to combat cancer and other industrial diseases. It is also another diverse applications such as tissues, cosmetics, paints, construction, packaged foods, etc. [7]. The nano-sized materials were characterized by DSC, FTIR, QLS and SEM.

References:

[1] Antonietti M., Lohmann S. and Van Niel C., **Macromulecules**, Vol. 25, (1992), 1139-1143.
[2] Katime I., Katime O. and Katime D. **"Los materiales inteligentes de este Milenio: los hidrogeles polímeros"**. Servicio Editorial de la Universidad del País Vasco. Bilbao 2004
[3] A. Chiach, and A. Poniewierski, **Journal of Chemistry and Physics**, Vol. 11, (1994), 8315-8320.
[4] Bancroft W.O., **J. Phys. Chem**., **17**, 514 (1913).
[5] Anderson B. C. and Mallapragada S. K., **Biomaterials**, Vol. 23, (2002), 4345-4352.
[6] Funke W., Okay O. and Joos-Müller B., **Advanced Polymer Science**, Vol. 136 (1998), 139.
[7] Maitra A. N., Mitra S. and Sahni M. **Indian Patent Application.** (1999) 1000/cal/99

Figures:

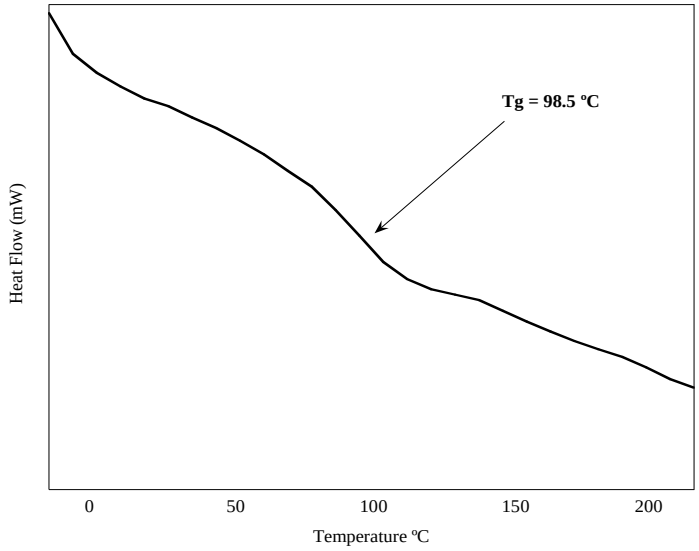

Figure 1. DSC calorimetric curve of NIPA based hydrogels.

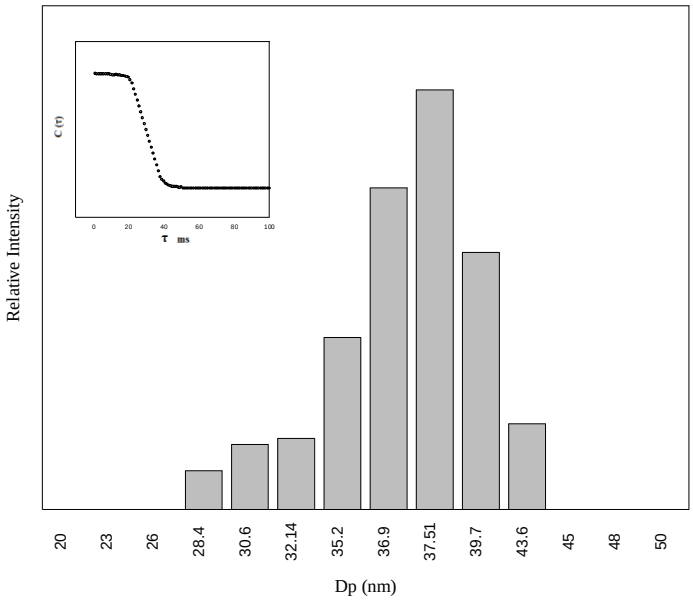

Figure 2. Particle size distribution of the NIPA based hydrogels measure by QLS.

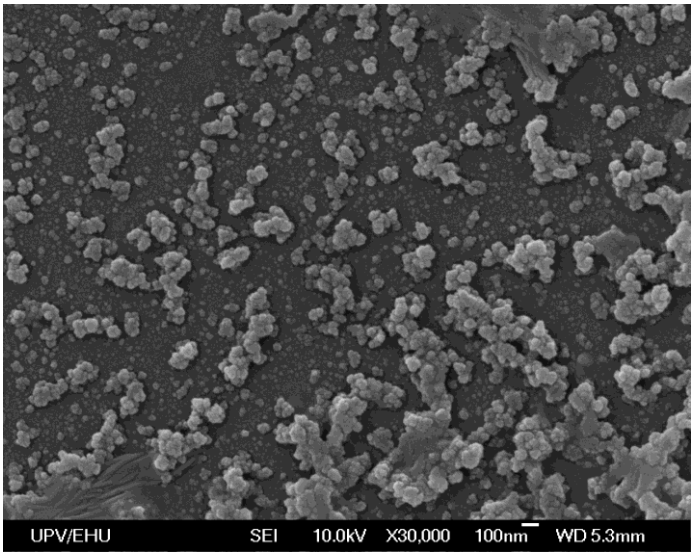

Figure 3. SEM micrography of the NIPA based hydrogels.

ENHANCED CONTROL OF POROSITY IN ELECTROSPUN NANOFIBER MESHES

Ana C. Guimarães [1,2], Albino Martins [1,2], Rui L. Reis [1,2], Nuno M. Neves [1,2]
[1] 3B's Research Group - Biomaterials, Biodegradables and Biomimetics, Department of Polymer Engineering, University of Minho, Campus de Gualtar, 4710-057 Braga, Portugal; [2] IBB - Institute for Biotechnology and Bioengineering, PT Associated Laboratory, Braga, Portugal.
anaguimaraes@dep.uminho.pt

Electrospinning has gained popularity as a simple and versatile technique to produce synthetic polymeric ultrafine fibers. This technique allows the production of non-woven meshes with fiber diameters in the nanometer range, which results in a high surface area-to-volume ratio and high porosity. Additionaly, these nanofiber meshes can mimic the extracellular matrix of human tissues and, therefore, can be used as scaffolds for Tissue Engineering (TE) applications. However, electrospun nanofibers meshes have an important drawback for this type of application. The obtained pore size is tipically too small to allow cell penetration into the inner regions of the nanofibrous scaffold. To overcome this problem, PCL and PEO solutions were electrospun simultaneously to obtain a dual composition nanofiber mesh. Then, a selective dissolution of PEO nanofibers was performed.
These structures were characterized in terms of morphology, mechanical properties and cellular response. PCL nanofiber meshes with comparable volume of material were used as control. The dual composition electrospun nanofiber meshes showed an increased porosity when compared with PCL meshes. The biologic assays were conducted with human osteoblast-like cells (Saos-2 cell line). By SEM and confocal microscopy, it was shown that the cells can penetrate into the nanofibrous structure, forming a fully cellularized construct appropriated for TE applications.

Figures:

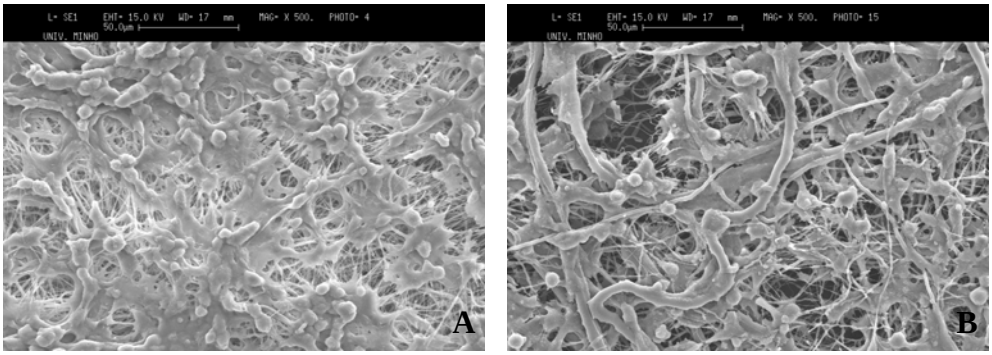

Fig. 1 - SEM micrographs of electrospun nanofiber meshes after 1 day of culture with Saos-2 (original magnification of 500x). (**A**) As electrospun mesh of PCL and (**B**) dual composition electrospun nanofiber mesh of PCL and PEO after dissolution of PEO in water.

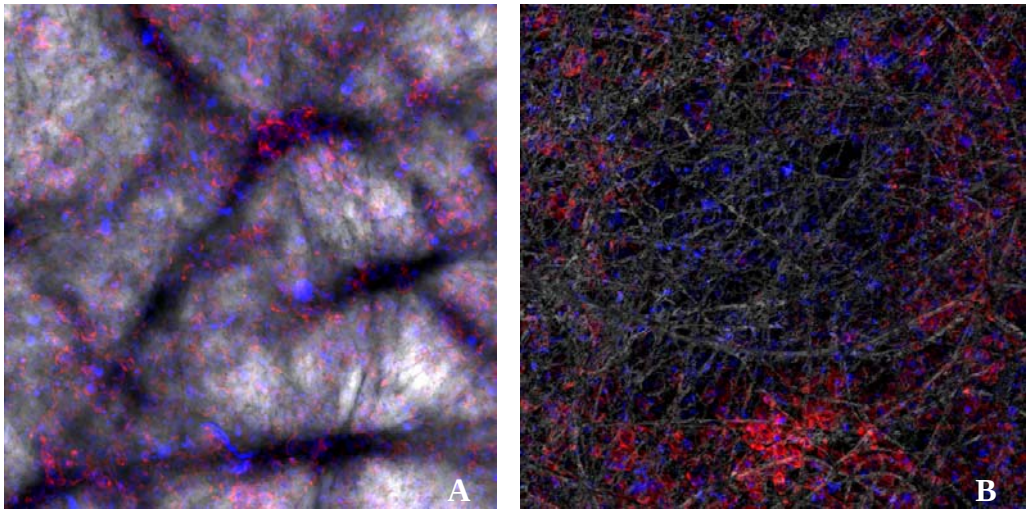

Fig. 2 - Confocal microscopy images of electrosupun nanofiber meshes after 5 days of culture with Saos-2. (**A**) As electrospun mesh of PCL and (**B**) dual composition electrospun nanofiber mesh of PCL and PEO after dissolution of PEO in water (10x objective and digital magnification of 2x).

BIOLOGICAL CHARACTERIZATION OF Ti-Si-C-N-O NANOCOATINGS FOR PROSTHETIC DEVICES

Mariana Henriques[1], *Sandra Carvalho*[2], *Paula Regina Souza*[1], *Maria Susano*[1], *Rosário Oliveira*[1]

[1]*IBB-Institute for Biotechnology and Bioengineering Centre for Biological Engineering Universidade do Minho,Braga, Portugal*
[2] *Dept. Física, Universidade do Minho, Guimarães, Portugal*
mcrh@deb.uminho.pt

Implant-associated infections can cause serious complications including osteomyelitis and soft tissue damage, which can lead to implant rejection. These infections are often related to biofilm formation by pathogenic microrganisms of the human flora, as *Staphylococcus epidermidis* [1]. The production of the so-called multifunctional-coated materials is of major interest in the development of more resistant and long-lasting implants. These coatings must possess high adhesion/cohesion, improved mechanical and tribological properties but also antimicrobial activity and no citotoxicity. Thus, the purpose of this work is to determine the biological properties of implant materials coated with Ti-Si-C-O-N. In this sense, biological properties include microbial and mammalian cell interactions.

The Ti-Si-C-ON films were deposited by reactive dc magnetron sputtering in a Ar + (N_2 + O_2) atmosphere. Two opposed high purity Ti targets (20x10 cm^2) were used. One with C pieces (TiC target) and the other with Si pieces (TiSi target) embedded in its erosion zone. The Ar, N_2 and O_2 flows were kept constant at 60, 2.5 and 1 sccm. The samples were deposited by changing the substrate bias voltage between 0 and -100V. The current density applied to the TiC target was 5 mA/cm^2 and that to the TiSi target was 6 mA/cm^2.

The topography of the films was studied by Atomic Force Microscope (AFM).

Biofilms of *Staphylococcus epidermidis* 9142 were formed, on 6 well plates containing the coated samples, for 48h at 37ºC and 100 rpm. Total biofilm biomass was determined by staining samples with crystal violet, according to Henriques et al. [2].

Cytotoxicity was determined on fibroblasts 3T3 (CCL-163). The coated samples were immersed in each well, of a 6-well plate, containing a confluent monolayer of fibroblasts and a plastic holder, and incubated at 37ºC in 5% CO_2 for 24 h. Cell death was determined using Celltiler 96®AQueous One Solution Cell Proliferation Assay (MTS).

Regarding the effect of the applied voltage on surface roughness, a continuous smoothing of the surface is observed, since the Rms decreases from 9 to 4.5 and to 3.4 nm for substrate bias voltage of 0, -50 and -100V, respectively. The ion bombardment plays a main role on this evolution. The high-enough ion flux and subsequently higher surface mobility enables the atoms to avoid the direct sticking on the top of the columns and to diffuse efficiently over the surface filling the voids between them.

Considering biofilm formation (Figure 1a) it is possible to notice that S. epidermidis colonizes all the samples. However, the sample deposited with a substrate bias voltage of -50V is more prone to microbial colonization. Thus, there is no direct correlation between the ability of biofilm development and substrate bias voltage or sample roughness.

Concerning cytotoxicity (Figure 1b), it can be observed that all samples promote a cellular death lower than 25%. Moreover, the sample developed without substrate bias voltage causes significantly less cell death than the others.

Regarding biofilm formation, bias conditions of 0 and -100 were the most appropriate for a coating development. However, cytotoxicity assays show that the sample developed grown with bias voltage of -100 causes significantly higher cellular activity loss.

It can be concluded that Ti-Si-C-N-O nanocoatings developed at specific conditions (bias voltage) can achieve appropriate biological properties for indwelling prosthetic devices.

References:

[1] Cerca N et al. Research in Microbiology, **156** (2005) 650.
[2] Henriques M, Azeredo J, Oliveira R., British Journal of Biomedical Sciences, **63** (2006) 5.

Figures:

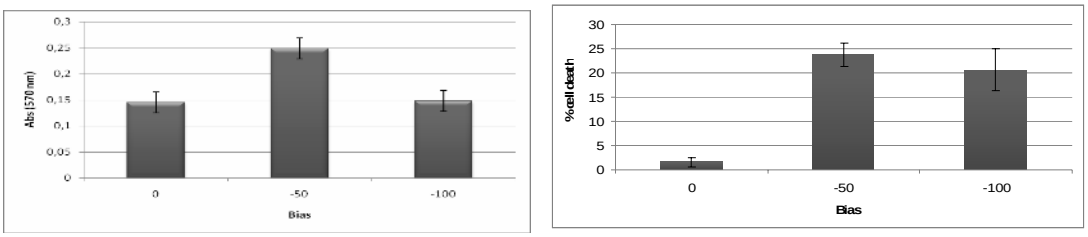

(a) (b)

Figure 1 – Samples biological properties. (a) Crystal violet absorbance (at 570 nm) of biofilms formed by *Staphylococcus epidermidis* 1942 on coated samples. (b) Percentage of fibroblasts 3T3 (CCL-163) death after contact with coated samples.

Study of drug release on smart nano-sized hydrogels based on *N*-isopropyl acrylamide by High Performance Liquid Chromatography

X. Hervías[1], L.G. Guerrero[1], S. Nuño-Donlucas[2], L.C. Cesteros[1], L. Sanz[1], I. Katime[1]

1) Grupo de Nuevos Materiales y Espectroscopia Supramolecular. Facultad de Ciencia y Tecnología. Universidad del País Vasco (UPV/EHU). Campus de Lejona, Apartado. 644 Bilbao, España. E-mail: issa.katime@ehu.es
2) Universidad de Guadalajara. Departamento de Ingeniería Química. CUCEI. Guadalajara (Jalisco, México).

A novel method to measure the drug release of 5-Florouracil (5-FU) on smart nano-sized hydrogels based on *N*-isopropyl acrylamide has been developed using a High Performance Liquid Chromatography (HPLC) technique. The employ of polymeric materials such a hydrogels in drug release, generates o lot of possibilities in specific drug delivery systems [1]. The release of the active agent may be constant over a long period, it may be cyclic over a long period, or it may be triggered by the environment or other external events [2]. The nanoparticles were synthesized by inverse microemulsion polymerization using a method previously reported [3]. The release speed of a drug is virtually controlled by the polymer properties and some factors such the pH of the release medium [4]. The behaviour of this nanoparticles show a selective swelling-collapse response to external pH changes [5]. It is known that the incorporation of pH sensitive groups into polymer grid, can modify the original behaviour of this macromolecules [6] changing the pH response value. The use of these materials is an important application in delivery and administration of drugs due to incorporation of polymeric systems advantages [7]. Nanohydrogels were charged with 5-FU by the dispersion of the nanoparticles in a phosphate buffer solution (pH 7.4) in which 5-FU was previously added. Purification process of the charged nanohydrogels was carried out by washing the samples with ultra purified water. The HPLC equipment was conditioned using KH_2PO_4 0.01 M as a mobile phase and the optimal flow rate for the system was obtained in 1 mL/min, the wavelength UV detector was located at 254 nm. The 5-FU concentration released by the nanogels was calculated after calibrating equipment with 5-FU standards by integrating the peak area in each case. UV-visible spectroscopic experiments were performed to corroborate the kinetic curve obtained by HPLC. These experiments were carried out using a peristaltic pump coupled with a Peltier Power Supplied Thermocell to keep constant the flow rate and the concentration gradient. The measurements made by UV-visible spectroscopy confirm the values obtained by HPLC.

References:

[1] Katime, I., Katime, O. and Katime, D. **"Los materials inteligentes de este Milenio: los hidrogeles polímeros"**. Universidad del País Vasco. Bilbao 2004
[2] Brannon-Peppas L., **Medical Plastics and Biomaterials Magazine** (1997)
[3] Katime I., Guerrero L.G., Cesteros L.C. and Nuño Donlucas S. **IV World Congress on Biomimetics, Artificial Muscles and Nano-Bio 2007**. Pag. 43.
[4] Sáez V., Hernáez E. and Sanz Angulo L., **Revista Iberoamericana de Polímeros,** Vol. 5 (2004), 55-70.
[5] Heller J., Pangburn S.H., and Penhale D.W.H., **Controlled-Release Technology, Fharmaceutical Applications**, ACS Symposium Series, (1987) pp 172–187,
[6] Vert M., Li S., and Garreau H., **Journal of Controlled Release**, Vol. 16 (1991), 15–26.
[7] Buckpitt A.R., Boyd M.R., **Analytical Biochemistry,** Vol. 106, 432-437.

Figures:

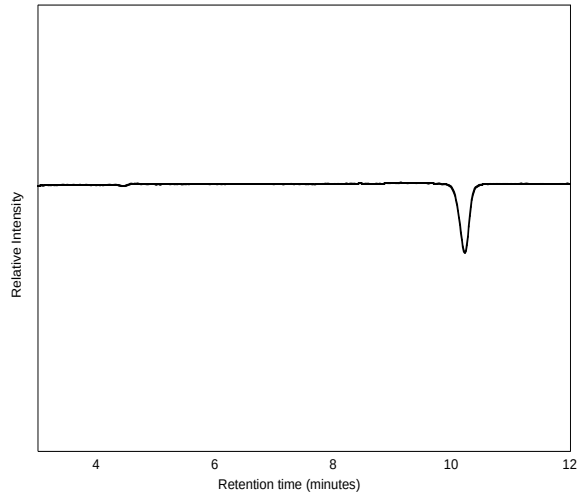

Figure 1. HPLC measurement of the drug release in smart nanohydrogels at pH 7.4.

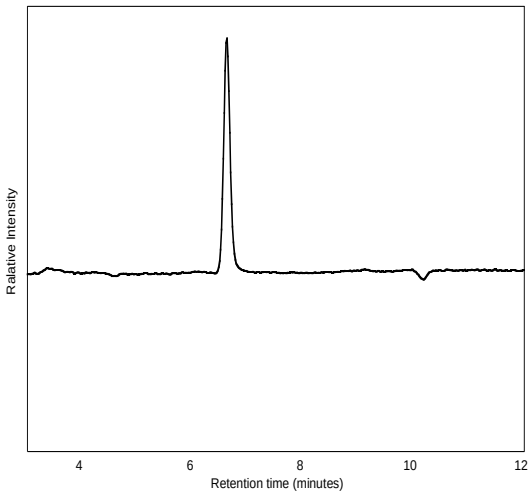

Figure 2. HPLC measurement of the drug release in smart nanohydrogels at pH 4.0.

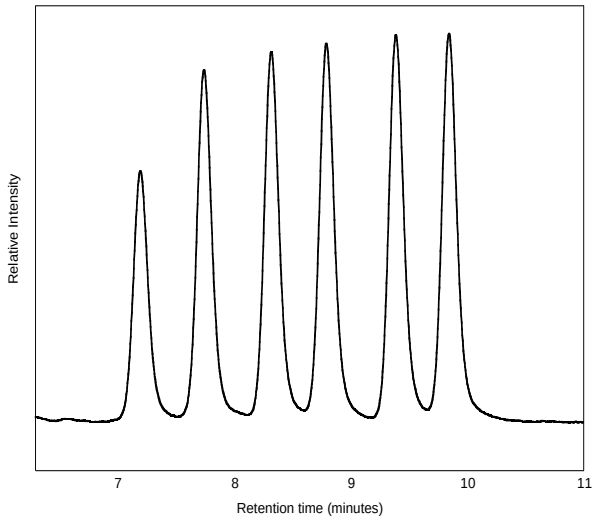

Figure 3. Drug release kinetics in smart nanohydrogels charged with 5-FU at pH 4.0.

Enzymatic Synthesis of Amorphous Calcium Phosphate-Chitosan Nanocomposites and its Processing into Hierarchical Structures

Mª Luisa Ferrer, Mª Jesus Hortigüela, M. C. Gutierrez, I. Aranaz, F. del Monte
Instituto de Ciencia de Materiales de Madrid, Campus de Cantoblanco 28049
mferrer@icmm.csic.es

The requirements for the production of suitable supports for the growth of cells and tissues involve the use of biocompatible and/or biodegradable materials and the processing of the components into a porous matrix of adequate morphology. The use of organic and inorganic materials has been widely explored, but lately, the use of organic-inorganic composite materials is attracting even increased attention. Controlling the length scale at the organic-inorganic interface within the nanometer range produces a wealth of both novel structural features and enhanced properties arising from the synergistic interaction of the individual constituents; i.e., consequence of the strong mechanical interface between mineral substrate and polymer matrix [1]. Biomineralization offers the opportunity to produce highly organized nanocomposite structures, controlling specific architectures over extended length scales for a wide range of compositions [2]. Here in, we have applied an enzymatically assisted route (e.g., the urease assisted hydrolysis of urea) for the preparation of nanocomposites. The base generated by urea hydrolysis promoted both CHI gelation and calcium phosphate precipitation at biological temperatures (~37 ºC) [3]. Macroporous hierarchical structures were thereafter obtained by a cryogenic process (named ISISA, ice segregation induced self-assembly) that simply consist on the unidirectional freezing (at -196 ºC) of the hydrogel nanocomposite [4, 5]. Upon freezing, the ice formation (hexagonal form) causes every solute originally dissolved/dispersed in the hydrogel to be segregated from the ice phase. After freeze-drying, the resulting hierarchical structures consists on well aligned micrometer-sized pores in the freezing direction corresponding to the empty areas where ice crystals originally resided, being the macrostructure supported by the matter (e.g., calcium phosphate nanoparticles dispersed within CHI matrix) accumulated between adjacent ice crystals [6].

References:

1] (a) Mann, S. *Angew. Chem. Int. Ed., 39*, (2000) 3392-406. (b) Sanchez, C.; Arribart, H.; Giraud-Guille, M. M. *Nat. Mater., 4*, (2005)277.

[2] (a) Sanchez, C.; Julián, B.; Belleville, P.; Popall, M. *J. Mater. Chem. 15 (*2003), , 3559-3592. (b) Tai, K.; Ulm, F.-J.; Ortiz, C. *Nano Lett. (6)*,2006, 2520-2525.

[3] (a) Sondi, I.; Matijević, E. J. Coll. Inter. Sci. 238, (2001), 208-214. (c) Chenite, A.; Gori, S.; Shive, M.; Desrosiers, E.; Buschmann, M. D. *Carbohyd. Polym. 64, (* 2006), 419-424.

[4] For a recent review see: Gutierrez, M. C.; Ferrer, M. L.; del Monte, F. *Chem. Mater. 20,(4), (*2008), 634-648.

[5] See also: (a) Mukai, S. R.; Nishihara, H.; Tamon, H. *Chem. Commun.* 874, (2004). (b) Gutierrez, M. C.; Hortigüela, M. J.; Amarilla, J. M.; Jimenez, R.; *Ferrer, M. L.*; del Monte, F. *J. Phys. Chem. C*, *111*, (2007) 5557, and references there in. (c) Gutierrez, M. C.; Garcia-Carvajal, Z.; Hortigüela, M. J.; Yuste, L.; Rojo, F.; *Ferrer, M. L.*; del Monte, F. *J. Mater.*

Chem. 17(29), (2007), 2992-2995. (d) Gutierrez, M. C.; Garcia-Carvajal, Z.; Yuste, L.; Rojo, F.; *Ferrer, M. L.*; del Monte, F. *Adv. Funct. Mater.* 2007 (DOI: 10.1002/adfm200700093) (e) Abarrategui, A.; Gutierrez, M. C.; Moreno-Vicente, C.; Hortigüela, M. J.; Ramos, V.; López-Lacomba, J. L.; *Ferrer, M. L.*; del Monte, F. *Biomaterials 29, (*2008), 94-102.

[6] Gutierrez, M. C.; Jobbagy, M.; *Ferrer, M. L.;* del Monte, F. *Chem. Mater.,20 (* 2008), 11-13.

Figures:

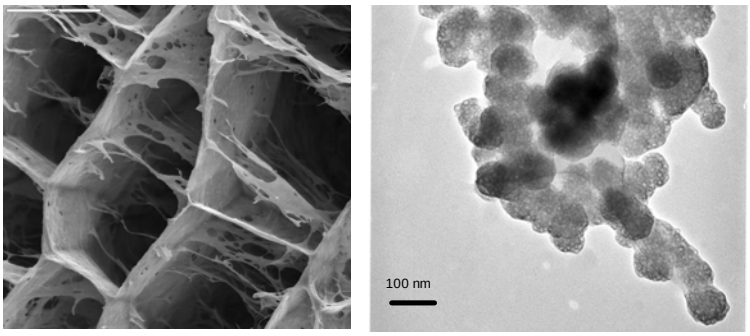

Figure 1: SEM micrograph of hierarchically structured amorphous calcium phosphate-chitosan nanocomposites (left, bar is 50 μm). TEM micrograph of amorphous calcium phosphate aggregates entrapped within the chitosan network gel (right, bar is 100 nm).

SOL–GEL DERIVED BIOCOMPATIBLE GLASSES TOWARDS BONE IMPLANT INTEGRATION

Graham Hungerford[1,2], Pedro Martins[1], Mariana Amaro[1], Carlos M. Costa[1], Senen Lanceros Mendez[1], M. Isabel Ferreira[1], Emma Cowan[3] and A. Sheila Holmes-Smith[3]

[1]*Centro de Física, Universidade do Minho, 4710-057 Braga, Portugal*
[2]*Physics Department, King's College London, Strand, London WC2S 2LS, UK*
[3]*Department of Biological and Biomedical Sciences, School of Life Sciences,Glasgow Caledonian University, Glasgow, G4 0BA, UK*

(graham@fisica.uminho.pt)

Over the last decade progress has been reported on the development of novel biocompatible glasses for medical applications, namely in the field of bone implants[1]. Most preparation methods, based upon the synthesis of hydroxyapatite[2], demand annealing at very high temperatures, thus precluding the addition of additives that enhance osseointegration, such as collagen and polysaccharides.

This work reports on the preparation of samples containing calcium carbonate and calcium phosphate, by the sol-gel technique[3] at temperatures well bellow 100º C. These samples display interesting morphological and mechanical properties, such as porosity, Young modulus and compressive strength regarding integration with bone tissue. The control over pore size was also achieved. Each sample was examined by X-ray diffractometry (XRD) and scanning electron microscopy (SEM). The chemical composition of the samples was confirmed by EDX/EMA/XPS. Moreover, incorporation *ab initio* of the solvatrochromic dye Nile red reported on local environments that may determine, to a large extent, the mechanism(s) of interaction between these glasses and *in vivo* systems. Finally, biocompatibility was examined through sample immersion in a simulated body fluid.

References

1. Höland, W., Biocompatible and bioactive glass-ceramics – state of the art and new directions. *J. Non-Crystal. Sol*., **219** (1997) 192-197.
2. Suominen, E., Aho, A.J., Vedel, E., Kangasniemi, I., Uusipaikka, E. and Yli-Urpo, A., Subchondral bone and cartilage repair with bioactive glasses, hydroxyapatite, and hydroxyapatite-glass composite. *J. Biomed Mat. Res*., **32** (1996), 543-551.
3. Hungerford, G., Amaro, M., Martins, P., Ferreira, M.I., Uttamlal, M. and Holmes-Smith, A.S., Effect of polymer strengtheners on the local environment of biocompatible glass as probed by fluorescence. *J. Fluoresc.*, **18** (2008) 297-303.

TRUE VARIABLE FIELD MAGNETIC FORCE MICROSCOPY FOR NANOSTRUCTURES CHARACTERIZATION

Miriam Jaafar[1], *Julio Gómez*[2], *Manuel Vázquez*[1], *Agustina Asenjo*[1]
[1]Instituto de Ciencia de Materiales de Madrid, CSIC, 28049 Madrid
[2]Dpto. Física de la Materia Condensada, UAM, 28049 Madrid

m_jaafar@icmm.csic.es

Spin structures of nanoscale magnetic elements are the subject of increasing scientific effort. As the confinement of spins, imposed by geometrical restrictions, makes these structures comparable in size to some intrinsic characteristic length of the magnet new properties emerge. Part of this effort is devoted to the development of new techniques with suitable resolution and sensitivity to characterize nano-objets. Particularly interesting and hard to achieve is a direct study of their magnetization reversal process [1, 2]. In this respect, Magnetic Force Microscopy (MFM) is an advanced technique for domain observation, which can become a powerful "local" technique to study the switching process at the nanometer scale when an in situ magnetic field is applied. Moreover, since atomic force microscopy based techniques enables the simultaneous observation of magnetic domains and surface topography of the same area, the quantitative analysis of these reversal processes reveals the interplay between both structure and magnetic properties.

A new variable external field magnetic force microscope (VF-MFM) is here introduced [3]. The most outstanding feature of the system is its capability to perform stable images under a variable external magnetic field that can be applied both in-plane (up to 0.15 T) and out-of-plane directions (up to 0.2 T). The main advantage of the so-called Variable Field Magnetic Force Microscope (VFMFM) is its mechanical stability under variable external magnetic field applied both in-plane and out-of plane directions. This microscope has been used to characterize different magnetic nanostructures.

The application of a magnetic field during the MFM operation can be used to modify the magnetic state of the tip as well as the magnetic state of the sample. While the effect of the magnetic field depends on the relationship between the maximum applied field and the coercivity of the sample, the magnetization of the tip and /or the magnetization of the sample can be switched by choosing a suitable magnetic field.

Furthermore, the evolution of the MFM signal versus the external magnetic field [4, 5, 6] allows us to achieve the hysteresis loop of nanoelements. The results obtained for an array of Ni nanowires embedded in AAM (Anodic Alumina Membrane) are shown in figure 1. In addition to the standard MFM images, we have performed the so-called "3Dmodes" [7] measurements. This new imaging mode is achievable thanks to the above mentioned mechanical stability that allows the observation of spin dynamic at the nanoscale. This new method has been used to obtain the hysteresis loop of the MFM probes [8] (see figure 2).

References:

[1] Choe S B, Acremann Y, Scholl A , Bauer A , Doran A, Stohr J and Padmore H A Science **304** (2004) 420-422.
[2] Yamada K, Kasai S, Nakatani Y, Kobayashi K, Kohno H, Thiaville A and Ono T Nature Materials **6** (2007) 270 - 273
[3] M Jaafar, J Gómez-Herrero, A Gil, P Ares, M Vázquez and A Asenjo, submitted to Nanotechnology
[4] Endo Y , Fujimoto H, Kawamura Y, Nakatani R and Yamamoto M J. Magn. Magn. Mat. **310** (2007)2436
[5] Asenjo A, Jaafar M, Navas D and Vázquez M J. Appl. Phys. **100** (2006) 023909
[6] Escrig J, Altbir D, Jaafar M, Navas D, Asenjo A and Vázquez M Phys. Rev. B **75** (2007), 184429
[7] Gómez-Navarro C, Gil A, Álvarez M, De Pablo P J, Moreno-Herrero F, Horcas I, Fernández R, Colchero J, Gómez-Herrero J and Baró A. M Nanotechnology **13** (2002) 314

[8] Jaafar M, Asenjo A and Vázquez M 2008 IEEE Nano in press

Figures:

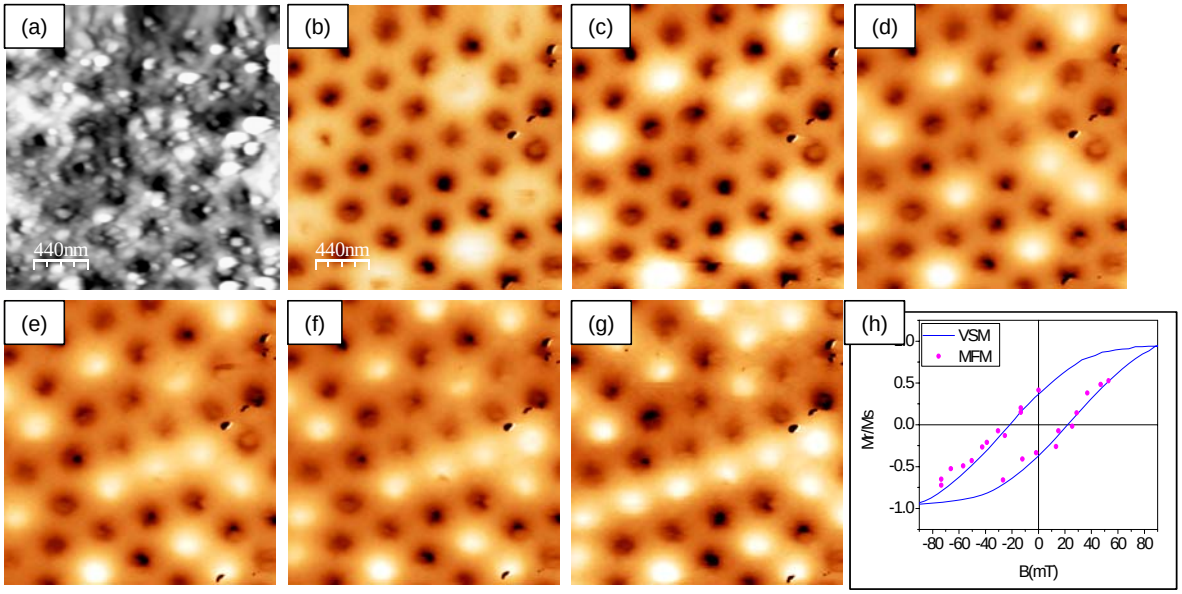

Figure 1 (a) AFM images at 60 mT of an array of Ni nanowires embedded in alumina membrane.(b) MFM images for 6 different magnetic fields 60 mT, (c) 40 mT, (d) 15 mT, (e) 0 mT, (f) -15 mT, (g)-25.5 mT. The MFM contrast (frequency shift) of the images is around 40Hz.(h) Hysteresis loop of the array measured by VSM and VF-MFM

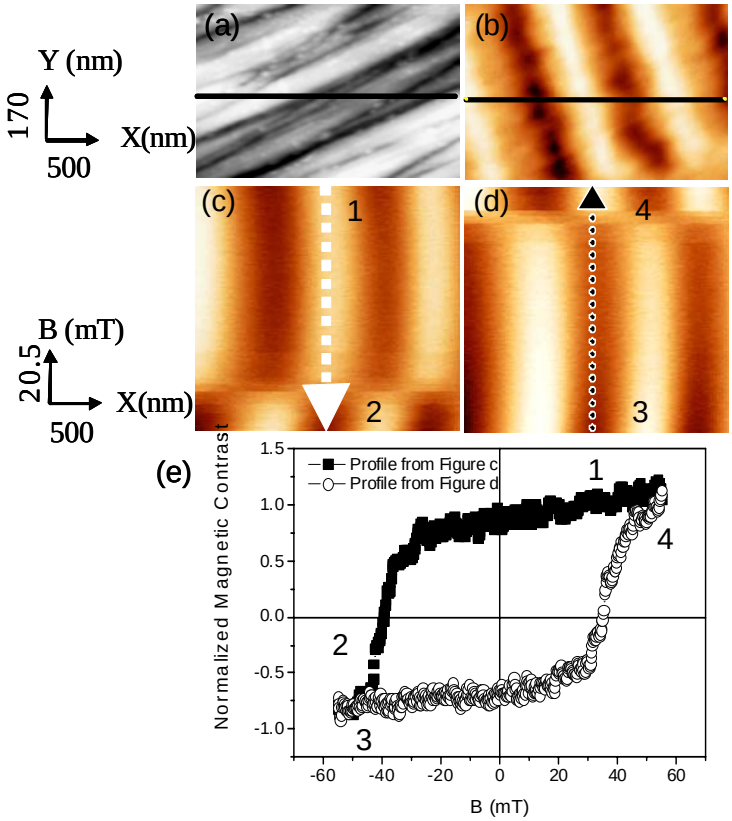

Figure 2 (a) AFM topography of a commercial hard disk (b) MFM image obtained in the same area (c) (d)"3dmode" images where the horizontal x direction (in nm) is the frequency shift (magnetic signal) for different out-of-plane magnetic fields (vertical direction in mT), the field is increased along the arrows directions (e) Hysteresis loop of the MFM probe obtained from the marked lines in (c) and (d)

ELECTRICAL CHARACTERISTICS OF GRAPHENE BASED TRANSISTORS

David Jiménez

Departament d'Enginyeria Electrònica, Escola Tècnica Superior d'Enginyeria, Universitat Autònoma de Barcelona, 08193-Bellaterra, Barcelona, Spain
(*) david.jimenez@uab.es

Graphene has recently emerged as a potential candidate material for nanoelectronics due to its electronic properties[1]. Geometrically is a monolayer of carbon atoms tightly packed into a 2D honeycomb lattice known to be a zero-gap material that could be fabricated using mechanical exfoliation[2] and epitaxial growth[3]. Interestingly, graphene could be patterned in nano-ribbons, using planar technologies as electron beam lithography and etching[3-4], having properties theoretically predicted to range from metallic to semiconducting depending on their width and edges[5]. This band-gap tuning capability and the possibility of large-scale integration using planar technologies open a route towards an all-graphene electronic nanodevices and circuits. Notably, recent studies[2] reported mobilities for electrons and holes in graphene of the order of 10^4 $cm^2/V{\cdot}s$. However, mobility for GNRs is expected to have smaller values than graphene, with an inverse dependence with the band gap[6], but conclusive experimental studies still lack. At this early state of development of GNR technology it seems timely to develop models of building blocks helping to conduct experiments in the same line as previously reported for carbon nanotube based devices[7-8]. This work presents an easy to implement model for analyze or design the current-voltage (I-V) characteristics of GNR-FETs in connection with physical parameters, such as GNR width (W) and gate insulator thickness (t_{ins}), and electrical parameters, such as SB height (φ_{SB}). The proposed approach prevents the computational burden that self-consistency implies by using a closed-form electrostatic potential from Laplace's equation. This simplification yields accurate results compared with self-consistent results from NEGF method[9] in the relevant limit dominated by the GNR quantum capacitance (C_{GNR}). Note that it appears to be the interesting case for advanced applications because the ability of the gate to control the potential in the channel is maximized. The presented model is intended to assist at the design stage as well as for quantitative understanding of experiments involving GNR-FETs.

References:

[1]A. K. Geim et al., Nature Materials **6**, 183 (2007).
[2]K. S. Novoselov, and A. A. Firsov, Science **306**, 666 (2004).
[3]C. Berger et al., Science **312**, 1191 (2006).
[4]P. Avouris et al., Nature Nanotech. **2**, 605 (2007).
[5]K. Nakada et al., Phys. Rev. B **54**, 17954 (1996).
[6]B. Obradovic et al., Appl. Phys. Lett. **88**, 142102 (2006).
[7]D. Jiménez et al., Nanotechnology **18**, 025201 (2007).
[8]G. Fedorov et al., Nano Lett. **7**, 960 (2007).
[9]Y. Ouyang et al., IEEE Trans Electron Devices **54**, 2223 (2007).

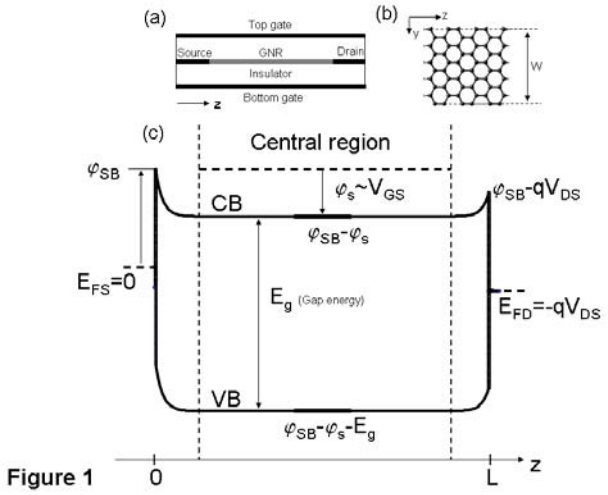

Fig.1: *Geometry and band diagram of the GNR-FET: (a) cross-section, (b) top view of the armchair shaped edge GNR forming the channel, and (c) sketch of the spatial band diagram along the transport direction.*

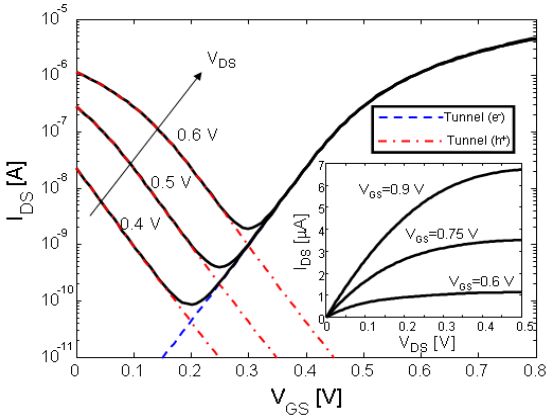

Fig.2: *Transfer and output characteristics (inset) for the nominal GNR-FET. Decomposition of the total current in electron and hole tunneling contributions are shown.*

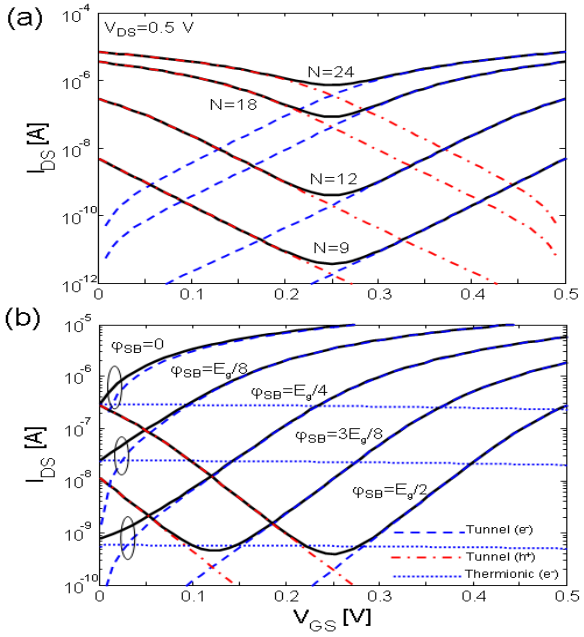

Fig.3: Influence of the GNR width (a) and SB height (b) in the transfer characteristics.

EXPERIMENTAL EVIDENCE OF THE EXISTENCE IN SOLUTION OF ORGANIZATIONS OF ZnO NANOPARTICLES SYNTHESIZED BY ORGANOMETALLIC METHOD USING DYNAMIC LIGHT SCATERRING

Myrtil L Kahn, Carole Pagès, André Maisonnat, and Bruno Chaudret

Laboratoire de Chimie de Coordination, UPR8241 CNRS, 205 route de Narbonne, 31077 Toulouse Cedex, France.

Corresponding author: Myrtil L Kahn, Fax 0033561333179, email: myrtil.kahn@lcc-toulouse.fr

Zinc oxide is a material of particular interest because it possesses unique optical and electronic properties. It is a wide-band-gap semiconductor (3.37 eV) that is also luminescent and emerged as a good candidate for many applications. As a result ZnO stimulates research in a wide range of domains. For example, thin films of ZnO were reported to display good conductivity and high transparency in the visible region and have been envisaged as transparent electrodes for solar cells[1a] as well as gas sensors,[1b] and recently, ultraviolet lasing effect has been observed at room temperature using ZnO nanowires.[1c] These fascinating examples are based on the control of both the physical and chemical properties of the nanoparticles. Besides, it is well known that these properties depend on the synthetic method used and as a consequence, applications of nanomaterials are directly linked to the successful control of the synthetic process.

We recently developed a novel organometallic synthetic method for the preparation of crystalline ZnO nanoparticles of controlled size and shape.[2] Tendency of the nanoobjects to self-organize onto the T.E.M. grid is observed.

This contribution concerns the field of the fundamental understanding of the self-assembly of nanoparticles to form superlattices in solution. We demonstrate the existence of superlattices of nanoparticles in solution and that this formation is indeed a thermodynamic process. We also pointed out the important role of weak interactions (Van der Walls, dipolar and hydrogen bounding) for the stabilization of the superlattices.

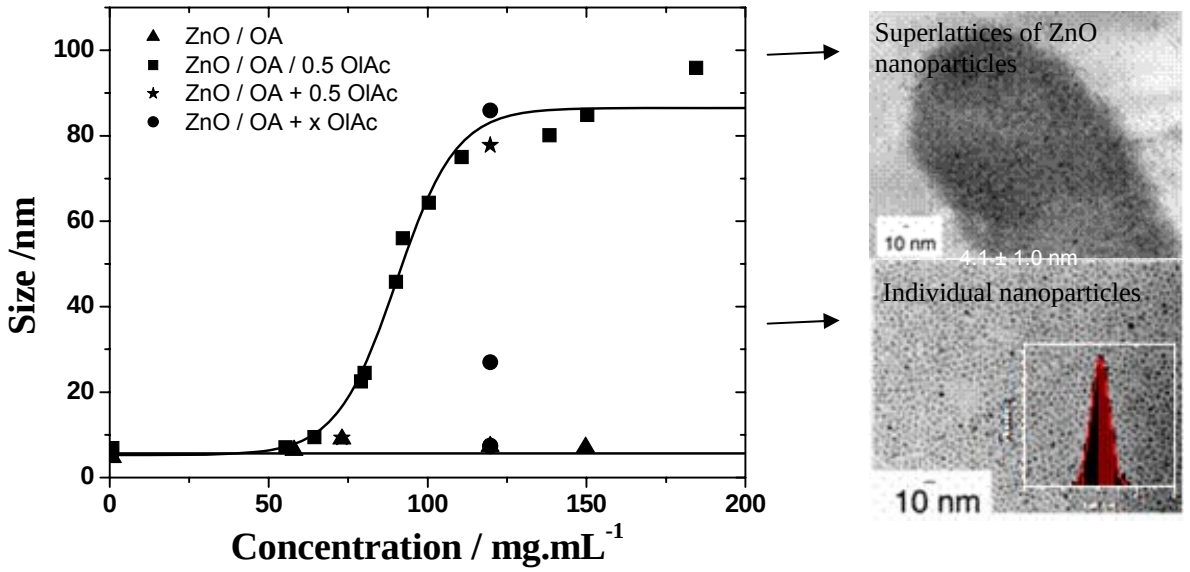

Figure 1: Variation of the size of the diffusive objects as a function of the concentration of the colloidal ZnO solutions. ▲: Colloidal solution of OA-stabilized ZnO nanoparticles; ■: Colloidal solution of OA/OlAc-stabilized ZnO nanoparticles; ●: Colloidal solution of OA-stabilized ZnO nanoparticles with a step by step addition of OlAc; ★: Colloidal solution of OA-stabilized ZnO nanoparticles with 0.5 eq of OlAc for two different concentrations.

References:

[1] a- K. Westermark, H. Rensmo, H. Siegbahn, K. Keis, A. Hagfeldt, L. Ojamae, P. Persson, J. Phys. Chem. B 2002, 106, 10108; b- J. A. Rodriguez, T. Jirsak, J. Dvorak, S. Sambasivan, D. Fischer, J. Phys. Chem. B 2000, 104, 319; c- Mao, H. Feick, H. Yan, Y. Wu, H. Kind, E. Weber, R. Russo, P. Yang, Science 2001, 292, 1897.

[2] a- M. Monge, M. L. Kahn, A. Maisonnat, B. Chaudret, Angew. Chem. Int. Ed., 2003, 42(43), 5321. b M. L. Kahn; M. Monge; A. Maisonnat; B. Chaudret, French Patent CNRS, Fr 03-042825, 2003, PCT procedure under progress; c- M. L. Kahn, M. Monge, V. Collière, F. Senocq, A. Maisonnat, B. Chaudret, *Advanced Functional Materials* 2005, 15, 458

SYNTHESIS AND CHARACTERIZATION OF SILICA MICROCAPSULES CONTAINING ORGANIC COMPOUNDS OF DIFFERENT VISCOSITY

Idurre Kaltzakorta, Edurne Erkizia
Labein-Tecnalia, Calle Geldo, Edificio 700, Parque Tecnológico de Bizkaia, Derio 48160, BIZKAIA-SPAIN
ikaltzakorta@labein.es

Because of its importance in different areas of industry such as agriculture, pharmaceutics medicine and cosmetics there is an extensive research going on the field of encapsulation[1] where organic as well as inorganic capsules of different sizes have been prepared and investigated.[1,2] Inorganic capsules offer some advantages comparing to the organic shells. They have very good stability at high temperatures as well as against chemicals, they show higher mechanical strength and not swelling in organic solvents compared to most organic and polymeric shells.[2,3]

In the current study silica microcapsules with diameters in 0.1~100µm range containing organic compounds of different viscosities were synthesized following a core/shell based *in situ* microencapsulation method via a sol-gel route[1]. The viscosity of the organic compounds encapsulated in the current study ranged between 3 cP to 6000 cP and in all cases, even in the highest viscosity one, microcapsules containing the organic material have been obtained. It has been observed that the viscosity of the compound encapsulated has an effect in the type of shell obtained.

References:

[1] B.Y. Ahn, S.I. Seok, I.C. Baek, S.I: Hong, Chem. Commun., **2** (2006) 189-190 and references therein.
[2] M.S. Kim, B.Y. Ahn, S.I. Seok, J. So-Gel Sci. Tech.., **27** (2003) 335-361.
[3] B.Y. Ahn, S.I. Seok, I.C. Baek, Mat. Sci. & Eng. C., doi:10.1016/j.msec.2007.11.001 Available online

Nanoscale Characterization of Ferroelectric Materials via Piezoresponse Force Microscopy

A. L. Kholkin, I. K. Bdikin, D. K. Kiselev, Jingsong Liu, M. Machado, V. S. Bystrov, I. Delgadillo
Department of Ceramics and Glass Engineering & CICECO, University of Aveiro, 3810-193 Aveiro, Portugal
kholkin@ua.pt

Coupling between electrical and mechanical phenomena is very often in nature. Apparently, it underpins the functionality of materials and systems as diversified as ferroelectrics and multiferroics to electroactive molecules to biological materials. In ferroelectrics, electromechanical behavior is directly linked to polarization order parameter and hence can be used to study phenomena ranging from polarization reversal mechanisms, domain wall pinning, cross-coupled phenomena in multiferroics, to direct imaging of electron-lattice coupling. It may be said that electromechanical coupling is also a key component of many electrochemical transformations, in which changes in oxidation state are associated with the variation in molecular shape and bond geometry. Electromechanical energy conversion is an integral part of processes such as triboelectricity, cavitation, and sonoluminescence. It will not be an exaggeration to say that electromechanics, along with mechanics and transport, is one of the fundamental phenomena in nature. Therefore, it forms a basis for numerous device applications, and is thus directly relevant to virtually all existing and emerging aspects of materials and nanoscience.

Recent years showed significant growth of interest towards nanoscale electromechanical phenomena originating independently in ferroelectric MEMS, biological, nano- and material science, and organic chemistry communities. The interest is stimulated both by development of nanoscience and necessity for efficient electromechanical motion and transformation at the nanoscale, and also recent emergence of scanning probe microscopy techniques capable of addressing electromechanical phenomena at a local level. As a relevant comparison, nanoscale properties are often accessible as a result of evolutionary development from macroscopic probes (e.g. interferometry or Berlincourt meter) to nanoscale, and corresponding macroscopic properties have been studied systematically since the dawn of industrial revolution. Electromechanical properties described by antisymmetric tensors averaged out in macroscopic systems and corresponding coupling coefficients are typically small (~100 pm/V), necessitating precise measurement tools even for macroscopic samples. These two factors resulted in limited quantitative and reproducible macroscopic studies of electromechanics even in single crystals and ceramics, recognized as important for applications (piezotransducers, SAW, sonar, ultrasonic imaging devices). Nanoscale offers a set of novel electromechanical phenomena induced by symmetry breaking at low dimensionality and by unique combination of high electric field and charge in nanovolumes that can lead to anomalous polarization reversal [1].

Ferroelectric materials are being intensively investigated due to their outstanding characteristics useful for various microelectronic devices ranging from nonvolatile ferroelectric random access (FeRAMs) memories to microelectromechanical systems (MEMS). For these applications, the nanoscale properties of ferroelectrics are of crucial importance. Since the feature size of potential devices is currently approaching to the submicron dimensions, local characterization techniques are becoming indispensable to meet the requirements of microelectronic industry. Local properties are expected to deviate from macroscopic ones due to confinement effects, lack of sufficient nucleation, and surface phenomena [2]. Piezoresponse Force Microscopy (PFM) has recently proved its usefulness for high-resolution domain imaging and local electromechanical characterization of ferroelectric materials [3].

In this presentation, the overview of the state-of-art in local ferroelectric characterization via PFM in several piezoelectric important materials (PZT, SBT, PZN-PT) will be given [4]. Local polarization switching and hysteresis [5], cross-sectional domain analysis [6] and polarization patterning [7] will be, in particular, addressed with special emphasis on the effect of PFM instrumentation on the measured properties. Based on these observations, the mechanism of local polarization reversal via PFM tip will be delineated. In the second part of the talk, the nanoscale properties of relaxor ferroelectrics will be shortly addressed. In these materials, the remanent polarization is absent at the macroscopic level due to strong disorder of ferroelectrically active ions. It will be shown that on the nanoscale the properties of relaxors are different due to symmetry breaking [8] and the material typically exhibit a clear piezoelectric contrast with the domain correlation length of the order of tens nm. Long-range order can be induced by applying small dc voltages to the tip [9]. The results confirm great potential of PFM for studying polar structures in ferroelectric and related materials.

References:

[1] A. L. Kholkin, I. K. Bdikin, V. V. Shvartsman, N. A. Pertsev, *Nanotechnology* **18** (2007) p. 095502.
[2] A. Gruverman and A. Kholkin, Rep. Progr. Phys. **69** (2006), pp.1-32.
[3] A. L. Kholkin, S. V. Kalinin, A. Roelofs and A. Gruverman in *"Scanning Probe Microscopy: Electrical and Electromechanical Phenomena at the Nanoscale"*, Eds. S. Kalinin, A. Gruverman, Springer (2007), V. 1, pp. 173-214.
[4] A. L. Kholkin, I. K. Bdikin, D. A. Kiselev, V. V. Shvartsman and S.-H. Kim, *J. of Electroceramics* **19** (2007), pp. 81-94.
[5] I. K. Bdilin, A. L. Kholkin, S. V. Kalinin and A. Morozovska, Appl. Phys. Lett. (submitted).
[6] J. S. Liu, H. Z. Zeng and A. L. Kholkin, *J. Phys. D: Appl. Phys.* **40** (2007), pp. 7053-7056.
[7] V. S. Bystrov, I. K. Bdikin, D. A. Kiselev, S. Yudin, V. M. Fridkin and A L Kholkin, *J. Phys. D*. **40** (2007, pp. 4571-4577.
[8] V. V. Shvartsman and A. L. Kholkin, *J. Appl. Phys.* **101** (2007), p. 064108.
[9] D. A. Kiselev, I. K. Bdikin, E. K. Selezneva, K. Bormanis, A. Sternberg and A. L. Kholkin, *J. Phys. D.* **40** (2007), pp. 7109-7112.

Figures:

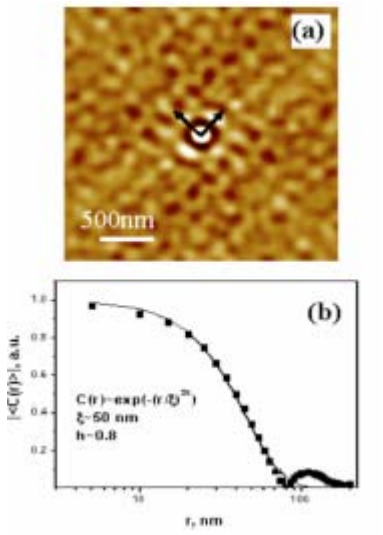

Fig. 1. Local ordering of nanodomains on the surface of disordered PLZT ceramics (a) and corresponding autocorrelation function (b).

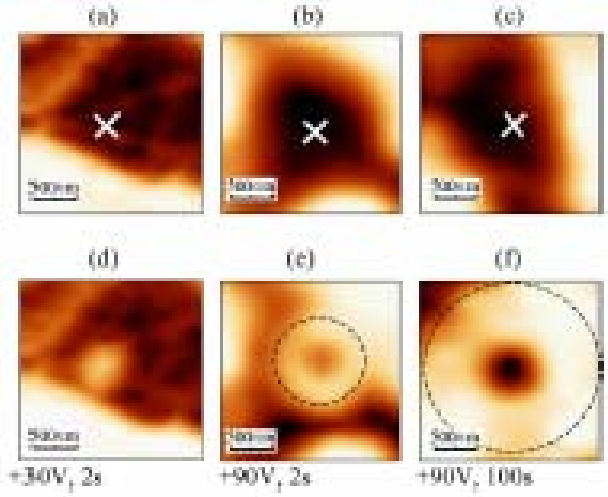

Fig. 2. Inverse polarization in PZN-PT [1]

SCANNING NANO-METROLOGY OF ULTRA THIN FILMS

V.Khosla, I.Hermann, N.Gitis, M.Vinogradov
CETR, 1715 Dell Avenue, Campbell, CA, USA
info@cetr.com

Traditional techniques of tribological and mechanical characterization of coatings are limited to friction, wear and scratch tests on a micro-level with balls or pins having much larger sizes, and loads-displacements much larger, than the film thickness. Lately-popular nano-indentation allows for testing of thinner films, but its pressure distribution is concentrated under (in the front of) the indenter and thus makes it vulnerable to substrate effects for ultra-thin films, while ultra-shallow depths would require unachievable-yet resolution of tip and system calibration. Common AFM-based techniques use smaller tips and displacements, but limited to nano-dimensional and topographic characterization of surfaces.

Moreover to detect the nano-non-homogeneities, a high-resolution surface mapping is required. Use of traditional nano-indentation for surface mapping is limited by the duration of a required series of numerous indents and their spacial resolution (the minimum space between indents is typically three times the diameter of the tip, or over 100 nm, to avoid the effect of the preceding indent). This makes nano-indentation unsuitable for studies of local nano-defects, or non-homogeneity

To overcome the shortcoming of traditional nano indentor a novel new tool, nano analyzer, was developed. It measures scratch-hardness of ultra shallow films where the pressure distribution (still in the front of the indenter) in the same surface layer where the indenter is sliding. As post-scratch detection of the shallow nano-scratches is challenging, it utilizes the same tip for both scratching and nano-imaging for nano-scratch-hardness testing of ultra-thin films. And to detect homogeneity of films the tool uses technique of nano-mapping, where a diamond nano-tip is vibrating in a tapping mode, frequency and phase of its vibrations are monitored and analyzed, and simultaneous topographical and stiffness (Young's modulus) maps of surface are produced with nano-resolution in both vertical and horizontal directions (Figure 1). Thus a novel new technique nano-analyzer enables effective quantitative tribo-mechanical characterization of ultra-thin films.

Examples of the nano-analysis of various thin hard films are discussed in detail (Figure 4). The paper also discusses mechanical property analysis of bump like structures under different loading conditions (figure 2,3). The tool is used to indent a bump and then do non destructive nano mapping of cracks Young's modulus. This paper compares touches on the fundamental constraints of the current techniques, and throws light on new technologies.

REFERENCES

1. D. Tabor (1996). Indentation hardness: Fifty years on. - Philosophical Magazine A, V. 74, No 5, pp. 1207-1212.
2. Nano and Micro Indentation and Scratch Tests of Mechanical Properties of Metals Dr. Norm Gitis, Dr. Ilja Hermann, Dr. Suresh Kuiry and Vishal Khosla

Figures

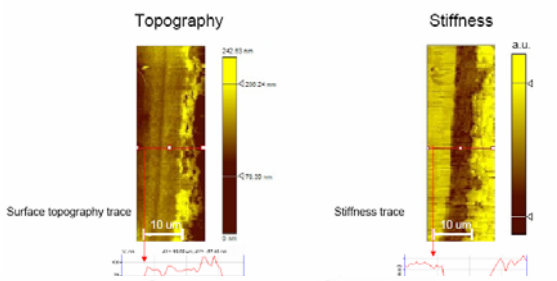

Figure 1. Topographical and stiffness map by Nano-analyzer NA-1

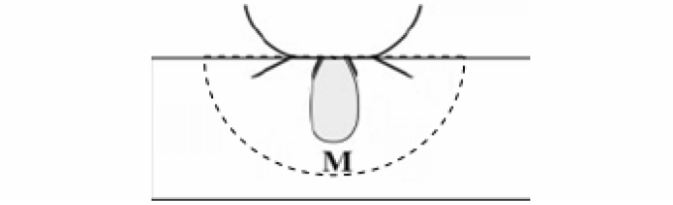

Figure 2. Cracks propagation mechanism when indenting on top of a bump

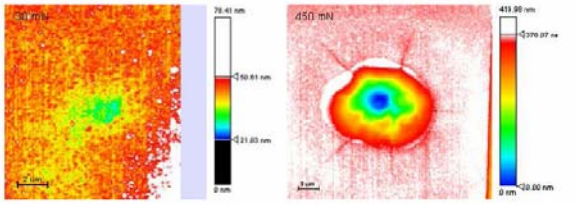

Figure 3. Results obtained after indenting a bump. Mechanism shown at different load with modulus mapping of the surface after the indent.

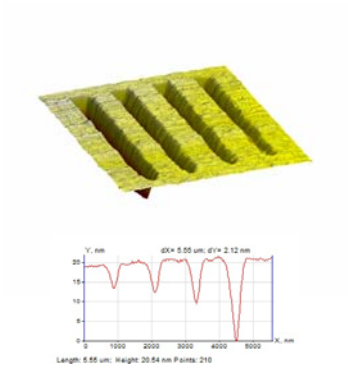

Figure 4 Ultra Shallow scratches in order of nm to find the scratch hardness of the low k materials

ANODIC ALUMINUM OXIDE-BASED CAPACITIVE HUMIDITY SENSOR INTEGRATED WITH MICRO-HEATER

Young Deuk Kim, Bong Bu Jung, Hun Kee Lee, Kun Hong Lee, Hyun Chul Park
Mechanical Engineering, Pohang University of Science and Technology,
Dept. of Mechanical Engineering, Pohang University of Science and Technology, San31, Hyoja-Dong, Nam-Gu, Pohang, Gyeongbuk, 790-784, Korea (south),
Pohang, Korea (south)
E-mail: ydk@postech.ac.kr

AAO(Anodic Aluminum Oxide) film is fabricated as a sensing material of capacitive humidity sensors. Because AAO films have a lot of nano-size pores, many water vapors can be absorbed. The size of a pore diameter is 80nm. Rectangular spiral-shaped type and interdigitated type are designed and fabricated as electrode types. A micro heater is also integrated because condensed water vapors and contaminants should be evaporated. Using heater, we can improve linearity and reliability and we can reduce hysteresis largely.

As a porous layer thickness increases, a sensitivity become higher. That means a thick porous layer can absorb more water vapors. But a response time also increases as a porous layer thickness increases. A sensitivity of rectangular spiral-shaped type is higher than that of interdigitated type. And a response time of rectangular spiral-shaped type is faster than that of interdigitated type. But a hysteresis is independent of electrode type.

The experiment using heater shows a good linearity with a small hysteresis for the relative humidity. The condition is the interdigitated type with a 50 porous layer under the electric power of 7v(749mW) . Under this condition, we don't need a additional linear modification.

References:

[1] L. H. Mai et al., Sensors and Actuators B 66(2000), 63p
[2] C. Dai, Sensors and Actuators B 122(2007), 375p
[3] R.K. Nahar, Sensors and Actuators B 63(2000), 49p

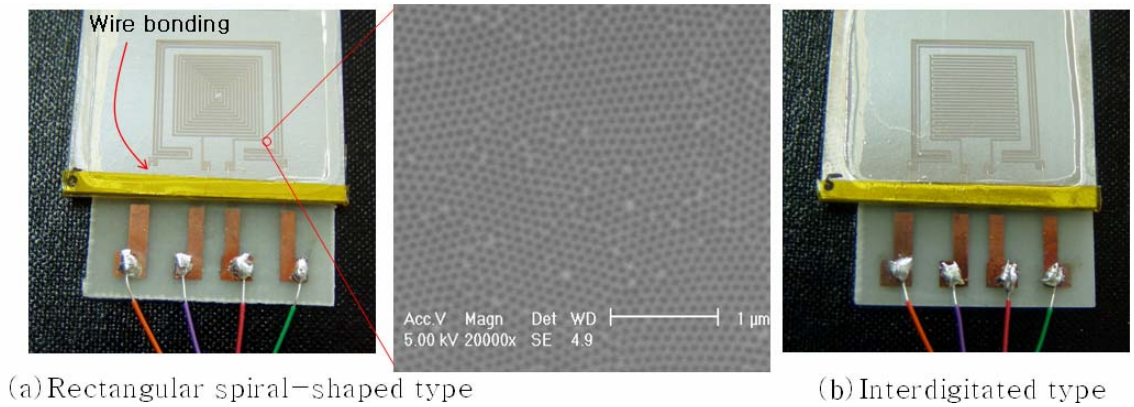

Fig.1. Humidity sensor device.

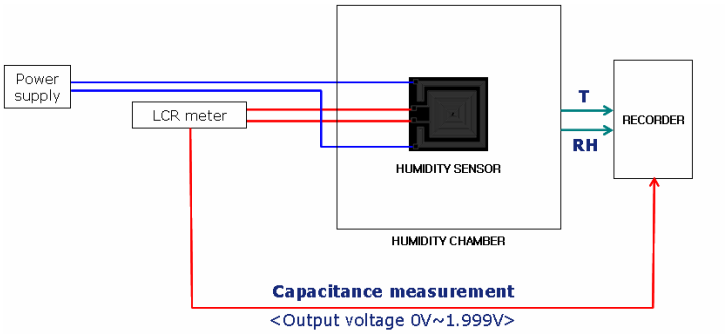

Fig.2. Experiment constitution.

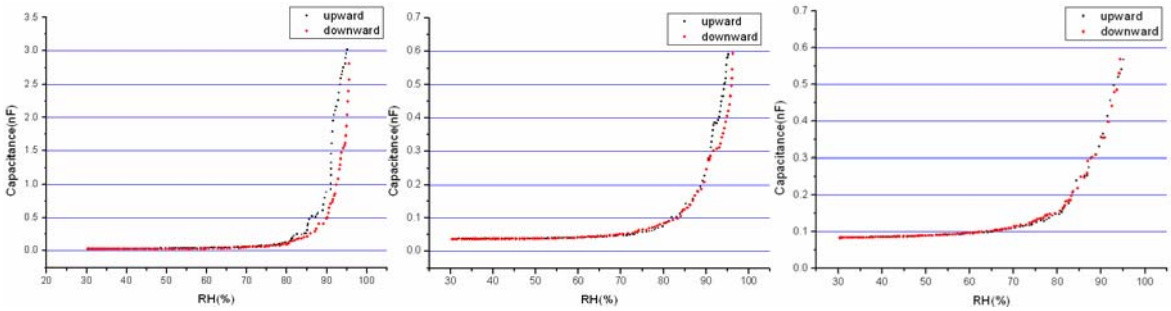

(a) (b) (c)

Fig.3. Capacitance characteristic of rectangular spiral-shaped type : with 50 porous layer(a); with 30 porous layer(b); and with 10 porous layer(c).

Parameter \ Electrode type	Rectangular spiral-shaped type	Interdigitated type
Sensitivity	10674.4%	9230.4%
Response time	30m 32s	31m 28s
Hysteresis	From 80%RH	From 80%RH

Table 1. Performance parameters of sensors with a 50 porous layer

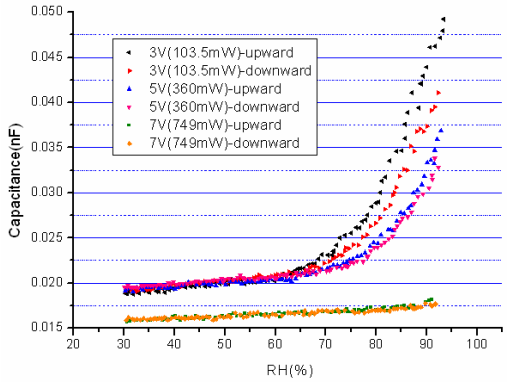

Fig.4. Capacitance characteristic of inter-digitated type with 50 porous layer under different electric power conditions

NANOSCALE PROPERTIES OF RELAXOR CERAMICS VIA SCANNING PROBE MICROSCOPY

Dmitry Kiselev, Igor Bdikin, Andrei Kholkin
Department of Ceramics and Glass Engineering, CICECO,
University of Aveiro, 3810-193 Aveiro, Portugal

Marija Kosec
Jozef Stefan Institute, University of Ljubljana, Ljubljana, Slovenia.

dmitry@ua.pt

Relaxor ferroelectrics (with smeared phase transitions) are highly inhomogeneous systems [1]. These materials are characterized by anomalies of the susceptibilities over an extremely wide range of temperatures. The unique properties of relaxor ferroelectrics offer strong possibilities for their practical application [2]. Effects of La impurities on the microstructural and property changes have recently been reported for $Pb_{1-3/2x}La_x(Zr_{1-y}Ti_y)O_3$ with Zr/Ti ratios of 65/35. Increasing La impurity content was found to induce a common sequence of domain like states in the rhombohedral ferroelectric *x*/65/35 compositional sequence including: normal nm-sized domains, tweed like precursors, and polar nanodomains (or clusters).

In this work we present the experimental SPM study of the geometry of the nanoscale domain structure in classical lead zirconate-titanate relaxor ceramics (PLZT x/65/35) with La concentration 8 and 9.5%. Domain images were obtained by the SPM method using a commercial atomic force microscope (Multimode, Nanoscope IIIA, Digital Instruments). The SPM method is based on the detection of thickness oscillations of ferroelectric materials under an ac voltage applied between the SPM tip and the bottom electrode in a conventional contact mode [3]. The amplitude of the measured vibration is proportional to the effective longitudinal piezoelectric coefficient, while its phase depends on the orientation of the out-of-plane component of the polarization vector.

Figure 1 show topography and piezoresponse images of PLZT ceramics at room temperature. Figures 1 (*b,d*) is domain structures of the PLZT ceramics using the SPM in piezoresponse mode, which clearly reveals fingerprint patterns related to domains with antiparallel polarization [4]. These stripes show a pronounced contrast and different contrast in the different areas (A, B, C and D) appearing in Fig. 1 (*b,d*) due to different crystallographic orientations of the individual grains. The bend and split of the domain marked by arrows at the grain boundary regions (shown arrows) may be attributed to the existence of inhomogeneous lattice distortions or spatial defects which destroyed the continuity of ferroelectric domains and minimized the elastic energy and depolarization fields at the grain boundaries. We believe that the observed contrast is due to the agglomerates of polar clusters. Since random fields and mechanical stresses play important roles in the formation of these agglomerates, they are expected to obey the fractal laws even in the presence of the stabilizing effect of the surface.

In the same time, the size and shape of these polar nanoregions seem random at first sight. For the quantitative data treatment we used a correlation function technique, which has been successfully used for topographic data analysis [5, 6]. The fitting gave the values of correlation length for PLZT 8/65/35 of about 160 nm and for 9.5/65/35 ~ 120 nm, respectively.

The degree of fractal branching of domain structure typically changes at the grain boundary. Two types of grain boundary have been found: with correlation and without correlation in domain structures of the neighbored grains. Continuous fractal branching from one grain to another present only for linear character of domain structure. For non correlation

domain structures in neighbored grains its character has more degree of fractal branching, especially near the grain boundary.

It is thus can be concluded that the PLZT ceramics with high concentration of La (≥8 at. %) preserve the domain contrast at the nanoscale, even if the macroscopic properties do not exhibit any ferroelectricity. Random network of maze nanopolar patterns is a direct consequence of La-induced disorder and have to be investigated as a function of temperature in order to observe the freezing of polar nanoclusters. These measurements are currently underway. It is proved that the PFM technique is well suited for the inspection of polar mesoscopic structures on the surface of relaxor ferroelectrics.

References:

[1] G. A. Smolenskii and A. I. Agranovskaya, Fiz. Tverd. Tela (Leningrad) **1** (10), 1563 1959.
[2] L. E. Cross *Ferroelectrics* **151**, 305, 1994.
[3] A. Kholkin, S.V. Kalinin, A. Roelofs, A. Gruverman, "Review of Ferroelectric Domain Imaging by Piezoelectric Force Microscopy", in "Scanning Probe Microscopy: Electrical And Electromechanical Phenomena at the Nanoscale", ed. by S. Kalinin and A. Gruverman, Springer, 2006.
[4] Q.R. Yin et al. *Appl. Phys. A* **78**, 699, 2004.
[5] R. C. Munoz et al. *Phys.Rev. B* **62**, 4686, 2000.
[6] D.A. Kiselev et al. *J. Phys. D: Appl. Phys.* **40**, 7109, 2007.

Figures:

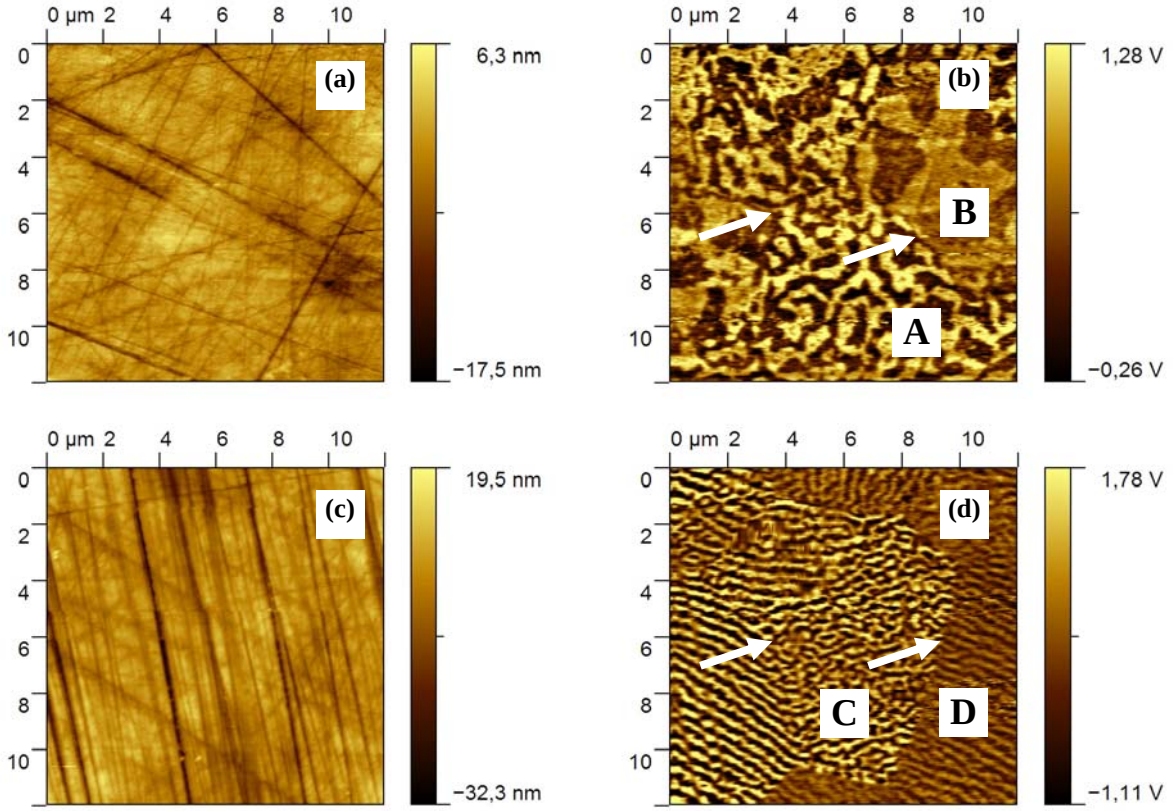

Figure 1. Topography (a, c) and piezoresponse images (b, d) of ceramics PLZT with concentrations La 8 and 9.5 %, respectively.

OPTO-MAGNETIC DETECTION OF DIMER FORMATION OF SUPERPARAMAGNETIC FE_3O_4 NANOPARTICLES IN LIQUIDS. APPLICATION TO A MOLECULAR RECOGNITION TRANSDUCER.

Mariana Köber, Mónica Luna, Fernando Briones
Instituto de Microelectrónica de Madrid, c/ Isaac Newton 8, E-28760 Tres Cantos, Spain
briones@imm.cnm.csic.es

Fe_3O_4 superparamagnetic nanoparticles with a diameter below 10nm are of large interest for biosensors, medical diagnosis and NMR imaging techniques [1,2].

In the proposed biosensor biofunctionalized superparamagnetic nanoparticles [3] are to be used as ultra-sensitive molecular imaging nanoprobes for the detection of targeted biological objects. The detection mechanism is optical, employing a polarized light source which passes through the solution containing the nanoparticles. If dimers are present (which will be caused by molecular recognition) the application of a magnetic field orthogonal to the direction of light propagation will lead to a well defined axis of optical anisotropy in the solution, in turn leading to a difference in light intensity of the passed polarized light with changing applied magnetic field. The magnetic field can be pulsed or rotating.

Present work is concerned with preliminary studies employing superparamagnetic but not biofunctionalized Fe_3O_4 nanoparticles. The response signal for a rotating as well as pulsed magnetic field is analyzed, varying input parameters such as the strength and frequency of the magnetic field as well as the concentration of the nanoparticles in solution. Other parameters that can be used to detect molecular recognition are the phase lag between the magnetic field and the signal as well as the Brownian relaxation time of the particles when switching off the magnetic field. From the Brownian relaxation time, for example, one can extract the hydrodynamic diameter of the particle, knowing the viscosity of the solution [4]. Figure 1 shows the signal evolution for a pulsed magnetic field of 2.5 kA/m. An exponential fit to the relaxation signal yields the characteristic relaxation time from which the hydrodynamic diameter of the particles can be extracted (Figure 2).

References:

[1] E. Katz and I. Willner, Angew. Chem. Int. Ed., **43** (2004) 6042.
[2] Q.A. Pankhurst, J. Connolly, S.K. Jones and J. Dobson, J. Phys. D: Appl. Phys., **36** (2003) R167
[3] J.M. de la Fuente, S. Penadés, Biochimica et Biophysica Acta **1760** (2006), 636
[4] E. Romanus, C. Groß, G. Glöckl, P. Weber, W. Weitschies, J. Magn. Magn. Mater., **252** (2002) 384

Figures:

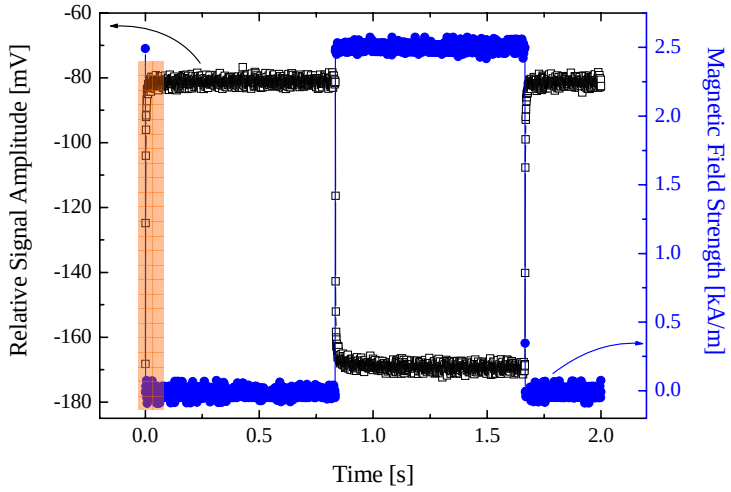

Figure 1 Signal evolution for a pulsed magnetic field of 2.5 kA/m. When the magnetic field is switched off the particles relax (marked region).

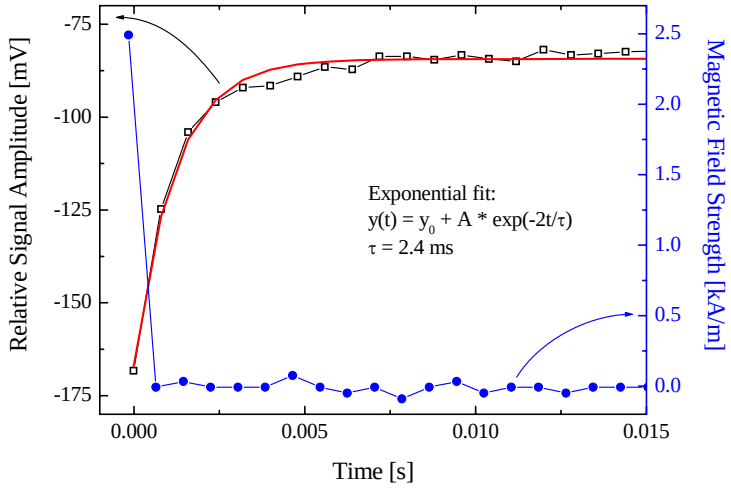

Figure 2 Exponential fit to the relaxation signal yields the characteristic relaxation time of the nanoparticles which can be translated into their hydrodynamic radius.

SURFACE-ENHANCED FLUORESCENCE AND RAMAN SCATTERING STUDY OF ANTITUMORAL DRUG HYPERICIN: AN EFFECT OF AGGREGATION AND SELF-SPACING DEPENDING ON pH

Gejza Lajos [1], D. Jancura [1], P. Miskovsky [1,3], J. V. García-Ramos [2], S. Sanchez-Cortes[2]

1 Division of Biophysics, Safarik University, Jesenna 5, 041 54 Kosice, Slovakia
2 lnstituto de Estructura de la Materia, CSIC, Serrano 121, 28006 Madrid, Spain
3 International Laser Centre, Ilkovicova 3, 812 19 Bratislava, Slovakia
gejza.lajos@upjs.sk

Surface-enhanced Raman scattering (SERS) represented a great advance in the field of Raman spectroscopy. SERS is based on the huge enhancement of Raman emission of certain molecules when they are placed in the proximities of certain rough metal surfaces. (1,2) This technique can be successfully applied in the study of poor soluble compounds in water, since very low concentrations are required. The main advantage of the SERS is the fluorescence quenching occurring on the metal surface (3). The fluorescence quenching occurring on metal nanoparticles (NPs) is attributed to charge-transfer phenomena taking place between the adsorbate and the metal. However, at a proper distance from the surface (more than 50Å) the emission of fluorophore can be enhanced by metal surface, and this phenomenon is called SEF (Surface-enhanced fluorescence) or MEF (metal-enhanced fluorescence)(4). The fluorescence emission of fluorophores is markedly enhanced at distances between 70 and 100Å (4). If the distance from the surface is not too far, a combined SERS+SEF spectrum can be registered, thus providing information from the vibrational and electronic processes occurring in the adsorbed species. In order to place the fluorophore at a proper distance from the metal one must functionalize the metal surface with a spacer. This was accomplished by covering the NPs with spacers such as fatty acids (5,6), or proteins (7). In this work we demonstrate that intense SEF spectra can be obtained by self-spacing when using fluorophores able to aggregate at certain conditions. This is the case of many anthraquinone antitumoral drugs such as hypericin (3, 8). In this case, intense SERS and SEF spectra can be obtained and can be used to understand the aggregation processes taking place in these important molecules.

In this work we show the SEF and SERS combined spectra of HYP and the dependence on the pH, when adsorbed on colloidal silver and aqeuous solution at different pH. This is also the first step in the application of SEF-SERS study of anthraquinone drugs interacting with biomolecules.

References:

[1] Moskovits, M. Rev. Mod. Phys, **57**, 1985,783
[2] Wokaun, A. Mol. phys, **56**, 1985, 1
[3] D. Jancura, S. Sanchez-Cortes, E. Kočišová, A. Tinti, P. Miškovský and A. Bertoluzza; Biospectroscopy Vol. **1**, No. 4, 1995, 265-275
[4] Lakowicz, JR, Geddes, CD, Gryczynski, I, et al. J. Fluorescence **14** (4): 2004, 425-441,
[5] C. J. L. Constantino and R. F. Aroca; J. Raman Spectrosc. **31**, 2000, 887–890
[6] C.J.L. Constantino, R.F. Aroca, C.R. Mendonc¸, S.V. Mello D.T. Balogh, O.N. Oliveira Jr.; Spectrochimica Acta Part A **57** 2001 281–289
[7] Badri P. Maliwal, Joanna Malicka, Ignacy Gryczynski, Zygmunt Gryczynski, Joseph R. Lakowicz; Biopolymers (Biospectroscopy), Vol. **70**, 2003, 585–594
[8] P. Miškovský, L. Chinsky, G. V. Wheeler and P. Y. Turpin; Journal of Biomolecular Structure and Dynamics Vol. **13**, No. 3, 1995, 547-552,

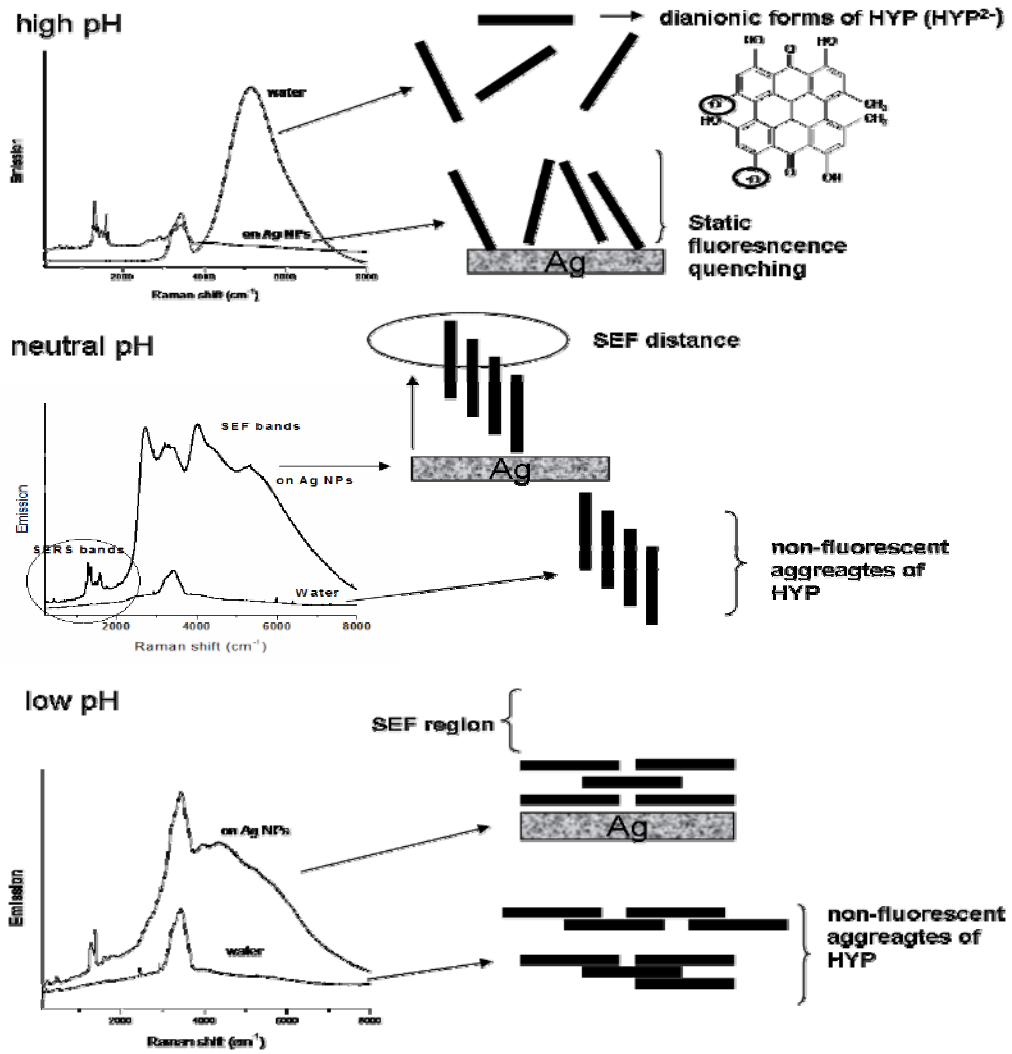

Figure: *Schematic explanation of state of Hyp in water and colloid at different pH*

Poster

SNOM study of periodically poled ferroelectric domains in $LiNbO_3$, $LiTaO_3$ and $Ba_2NaNb_5O_{15}$ crystals

Jorge Lamela[1], Eugenio Cantelar[1], Daniel Jaque[1], Ginés Lifante[1], Fernando Cusso[1], Francisco Jaque[1], Shi-Ning Zhu[2], Alexander Kaminskii[3]
[1]Departamento de Física de Materiales, C-IV, Universidad Autónoma de Madrid, 28049, Madrid, Spain
[2]National Laboratory of Solid State Microstructures, Nanjing University, China
[3]Institute of Crystallography, Russian Academy of Sciences, Moscow 119333, Russia
jorge.lamela@uam.es

The feasibility of forming periodic ferroelectric domain structures in ferroelectric crystals as: $LiNbO_3$, $LiTaO_3$ and $Ba_2NaNb_5O_{15}$, has extended the range of application of these materials in the photonic field. In fact, it has been demonstrated the ability, using these ferroelectric periodic structures, to manufacture different non-linear optical devices as: optical super-lattices (OSLs), second harmonic generation (SHG), and difference frequency generation (DFG), as well as in new fields like squeezed light generation for optical communication and information processing [1,2].

These periodic ferroelectric structures can be achieved using different procedures: during the crystal growth by the "off centre Czochraski technique" (OCCT), applying an external electric field (EF) or by electron beam injection method (EBI).

The aim of this work is to study, in periodically poled $LiNbO_3$ (CT), $LiTaO_3$ (EF) and $Ba_2NaNb_5O_{15}$ (CT) crystals, new phenomena arising from the interaction between laser propagating beams and refractive index singularities associated with the ferroelectric domains. For this purpose scanning near-field optical microscopy (SNOM) technique has been used [3]. The SNOM study has been combined with far field light diffraction experiments.

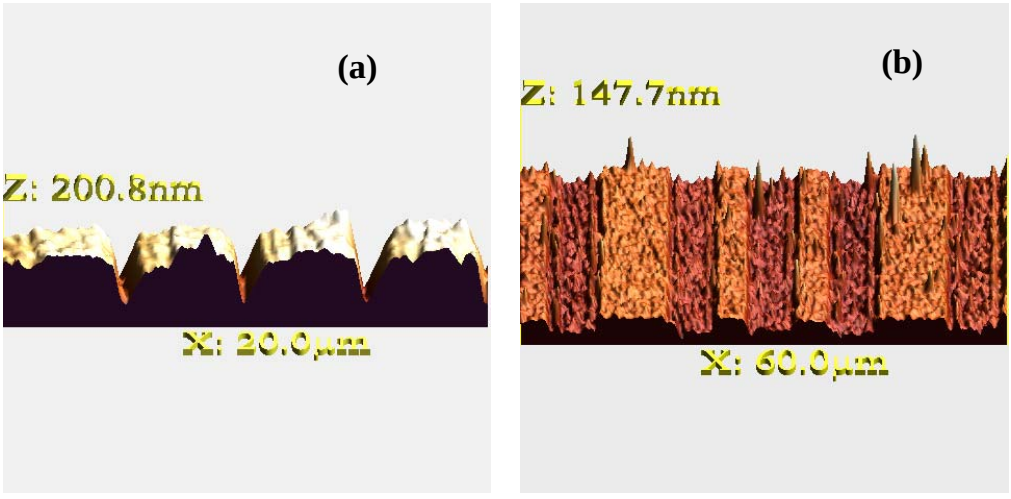

Figure 1. AFM images of (a) Er-Yb doped $LiNbO_3$ and (b) $LiTaO_3$ periodically poled crystals.

In order to know the structure of these domains, images using atomic force microscopy (AFM) in etched samples were obtained. As an example, Figure 1a shows the 3D topographic image obtained in periodically poled Er-Yb doped $LiNbO_3$ (OCCT) sample. As it can be observed, the etching gives place to a series of depressions or walls in the negative ferroelectric domains faces with a periodicity of ~ 6 μm. Figure 1b shows the 3D AFM image of an etched $LiTaO_3$ (EF) sample. In this case the etching reveals the ferroelectric domain structure produced by applying an external electric field pulse using a specific electrode configuration typical for SHG applications. [4]

Figure 2a shows the SNOM image observed using the reflection mode in Er-Yb doped $LiNbO_3$ crystals grown by OCCT. The SNOM image presents an unexpected high optical contrast with a periodicity of ~6 μm, according with Figure 1a. Figure 2b shows the SNOM image obtained using the reflection mode in $Ba_2NaNb_5O_{15}$ (OCCT) crystal. The back scattering light intensity shows a very high optical contrast with a periodicity of ~4.5 μm which corresponds to the ferroelectric domains structure created during growth.

High optical contrast with periodicities consistent with the ferroelectric domain structures using the SNOM transmission and collection modes were also observed. The largest optical contrast values, close to 80%, were obtained by the collection method in $Ba_2NaNb_5O_{15}$ [5,6].

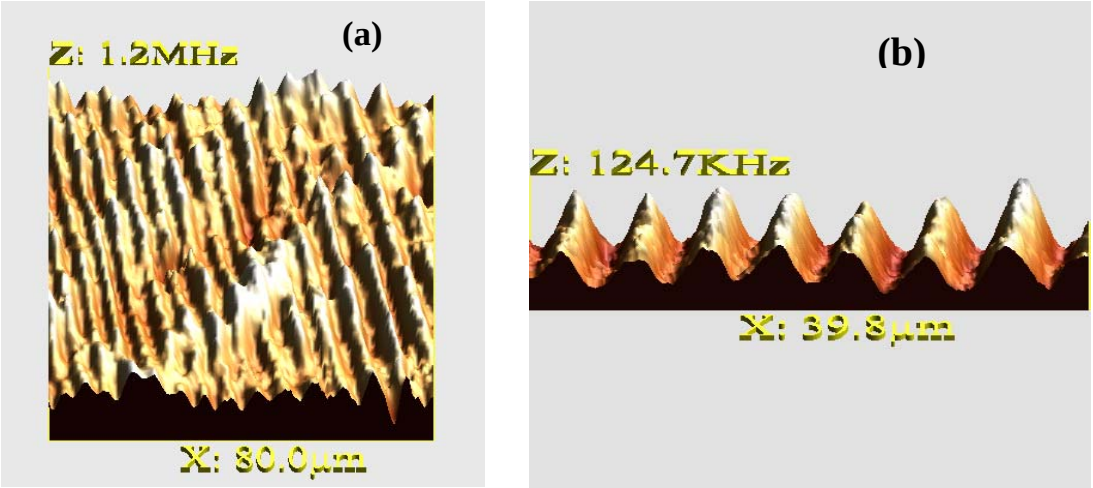

Figure2. SNOM images of (a) Er-Yb doped $LiNbO_3$ and (b)$Ba_2NaNb_5O_{15}$.

The unexpected large optical contrast observed in the three systems is explained, by means of a beam simulation method, considering that the ferroelectric domains operate as a periodic array of planar waveguides or optical superlattice.

References

[1] K. Nakamura, H. Ando, and H. Shimizu, Appl. Phys. Lett. **50**, 1413 (1987)

[2] P. Xu, S. N. Zhu, X. Q. Yu, S. H. Ji, Z. D. Gao, G. Zhao, Y. Y. Zhu and N. B. Ming, Phys. Rev. B **72**, 064307 (2005)

[3] E. Betzing, J.K. Trautman, Science **257**, 189, (1992)

[4] Z. D. Xie, G. Zhao, P. Xu, Z. D. Gao, and S. N. Zhu, "Study of optical elastic scattering in a quasiperiodically poled LiTaO3 crystal", J. Appl. Phys. **101**, 056104 (2007).

[5] Lamela, A. Ródenas, G. Lifante, D. Jaque, F. Jaque, and A.A. Kaminskii, Laser Phys. Lett. **1-5**, 10.1002/lap 200710133 (2008)

[6] J. Lamela, F. Jaque, E. Cantelar, D. Jaque, A.A. Kaminskii and G. Lifante, Optical and Quantum electronics (in press) (2008)

Py ANTIDOT THIN FILMS: A TRANSPORT AND MAGNETIC CHARACTERIZATION AS A FUNCTION OF TEMPERATURE

D. C. LEITAO[1], C. T. SOUSA[1] J. VENTURA[1], F. CARPINTEIRO[1], K.R.PIROTA[2], M.VAZQUEZ [2], J. B. SOUSA[1], J. P. ARAÚJO[1]

[1] IFIMUP, Rua do Campo Alegre 687, 4169-007 Porto

[2] Instituto de Ciencia de Materiales de Madrid, CSIC, 28049 Madrid, Spain

dleitao@fc.up.ptl

Nanopatterned media, and in particular arrays of magnetic dots and antidots, have gained increased attention in the last years. Antidots are particularly interesting because, since there is no isolated magnetic volume, the superparamagnetic limit below which thermal fluctuations erase the average magnetization [1], does not occur. In this way, they are strong candidates to be used as ultra-high density recording media. However, to achieve the desired submicron features, expensive, time consuming lithographic techniques, like e-beam or focused ion beam lithographies are usually required. An alternative route to obtain antidots is the use of easily fabricated nanoporous alumina as templates for the subsequent growth of a thin magnetic layer on top [1]. These templates present enormous advantages such as the possibility to build a net of aligned and ordered nanostructures and the ability to control their dimensions as desired.

Nanoporous alumina films were obtained by electrochemical oxidation of high-purity (>99.997%) aluminum foils. Prior to anodization, samples were cleaned in acetone and degreased in etanol. For surface improvement, samples were also electropolished at 20V for 3min in an Etanol (75%) : Perchloric Acid (25%) solution. With this procedure a mirror surface was obtained, setting the necessary conditions for a well organized porous structure to be obtained. In this work, the first anodizations were performed at a constant voltage of 40 V for 2 hours, with a 0.3 M oxalic acid solution (used as electrolyte) at a temperature between 2-6ºC. Afterwards, the resulting porous-oxide layer was then etched in 0.5 M Phosphoric Acid : 0.2 M Chromic Acid mixture at 60ºC for 2 hours. A standard two-step anodization procedure, first introduced by Masuda [2], is used in order to achieve some organization of the pore structure. So, a second anodization of the aluminum, using the engraved hole structure as *pre-pattern*, was then carried out using the same conditions as the first one. These anodization conditions resulted in nanoporous alumina substrates with average pore diameter of approximately 35 nm and separation of about 100 nm.

Permalloy thin films were then deposited on top of nanoporous alumina substrates with an Ion Beam Deposition (IBD) system. This system presents a base pressure less than 10^{-7} Torr. The Py films were deposited using a flow of Ar atoms in the deposition gun of 5.5 sccm, giving a work pressure in the chamber of about $2x10^{-4}$ Torr during the deposition process.A beam voltage of 1000V was applied giving a beam current of about 10.0 mA. With these condition a deposition rate of 0.35 A/s for Py target was obtained. A magnetic field of 250 Oe was applied to the substrate, during the deposition, in order to induce an uniaxial anisotropy. The morphology of the nanoporous alumina films and Permalloy thin films on the alumina -templates was characterized using FEI Quanta 400FEG SEM.

Thus the size of the magnetic antidots is related to the stability of the written bits, we have fabricated antidots of various sizes, but keeping the same density controlling the thicknesses of the deposited Permalloy films (3 nm to 100 nm). We were able to established a quasi-linear dependence of the pore diameter on the film thickness: for low thicknesses, the magnetic film starts by retaining the shape and size of the underneath nanopores, but, with increasing thickness, the size of the holes is reduced, until they close and a continuous film is formed.

As expected, antidot matrices exhibit properties very different from those of continuous films. The holes introduce shape anisotropies and act as major nucleation sites for magnetic domains. Other important consequence of the presence of these holes are the changes in the macroscopic magnetic properties such as magnetic anisotropy, coercive field and magnetoresistance. We will also present a detailed study of temperature dependence of electrical resistivity and magnetoresistance as a function of pore diameter.

References:

[1] Z. L. Xiao et al., *Appl. Phys. Lett.*, **81,** (2002) pp. 2869-2871.
[2] H. Masuda et al. , *Science*, **268**, (1995) pp. 1466-1468.

Figures:

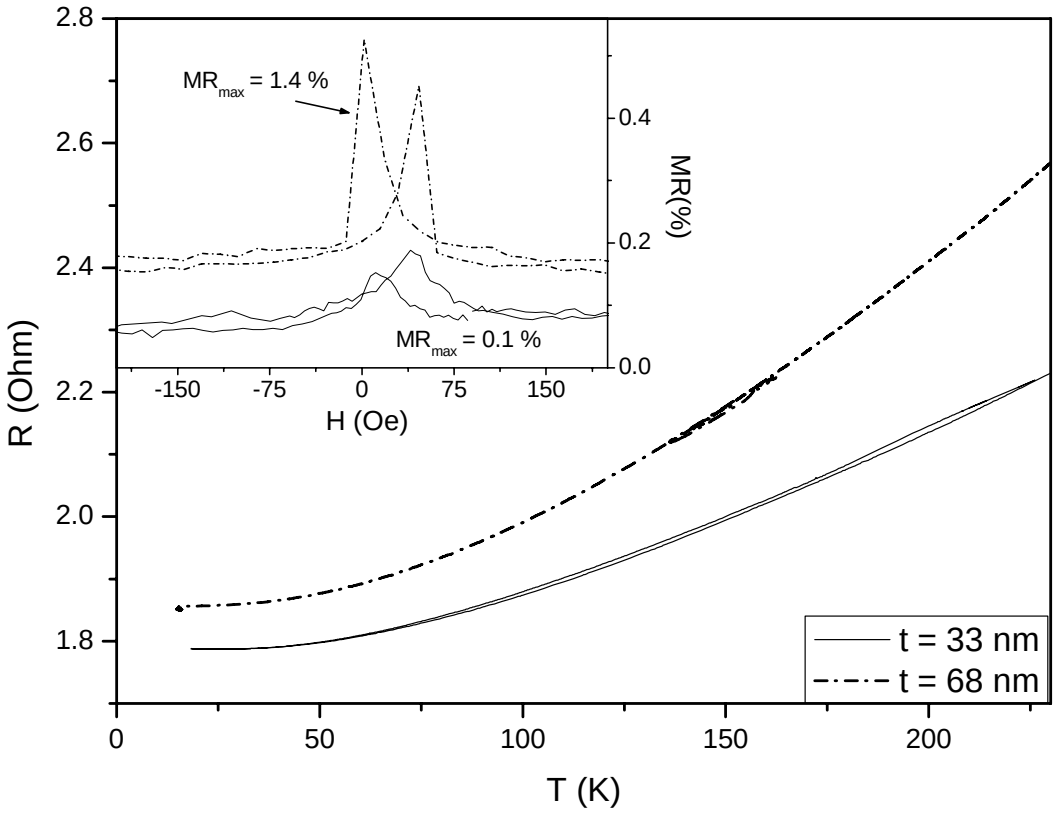

Fig. 1: R(T) for Py (33nm) and Py (68nm) over nanoporous alumina. Inset: MR(T=100K) for the same samples.

Electrochemical immunosensing of folic acid based on improved nanostructured transducer

A. Lermo[1], S. Fabiano[2], S Hernández[2], R. Galve[3], M.-P. Marco[3], S. Alegret[1], M.I. Pividori[1]*
[1] Grup de Sensors & Biosensors, Unitat de Química Analítica, Universitat Autònoma de Barcelona Edifici Cn. Campus UAB, 08193, Bellaterra, Barcelona, Spain
[2] Laboratorio de Sensores y Biosensores, Química Analítica I, Facultad de Bioquímica y Ciencias Biológicas, Universidad Nacional del Litoral, Santa Fe, Argentina
[3] Applied Molecular Receptors Group (AMRg), IIQAB-CSIC, 08034 Barcelona, Catalonia, Spain
**AnaIsabel.Lermo@uab.es*

Enzyme-linked immunosorbent assays (ELISAs) today represent an important percentage of the tests performed in clinical diagnostics or quality control of foods and pharmaceuticals. For some substances they represent the most reliable quantification method [1-4]. Furthermore such tests represent a good alternative to microbiological tests, which often take days to perform and do not always show high specificity, and are often used as a complementary method to HPLC [5].

Recent advances allow the immunoassays to be performed on magnetic beads as a support. The magnetic beads are known to be a powerful and versatile tool in a variety of analytical and biotechnology applications. The use of non-porous magnetic beads greatly improves the performance of the immunological reaction, due to: (i) an increase in the surface area, as well as (ii) the fast assay kinetics achieved because the beads are in suspension and the analytical target does not have to migrate very far. According to their properties as well as the improved washing and separation steps, the matrix effect is minimized despite this increased surface area. Additionally, the magnetic beads can be easy magnetically manipulated by using permanent magnets or electromagnets. Therefore, the analysis of samples performed on magnetic beads can be easily achieved without any pre-enrichment, purification or pre-treatment steps, which are normally necessary for standard methods [6-8]. All these advantageous properties of magnetic beads are improved when they are nano-sized.

Most immunoassays are designed for the quantification of proteins or peptides. However, small organic molecules can also be quantified by the same technique. Hormones, antibiotics, small peptides, amino acids or vitamins are popular targets for such tests. However, the assays have to be designed in the competitive or inhibition mode rather than a sandwich-type mode, as most of these small molecules have only one functional site, which can be recognized by an antibody. Folic acid, a water-soluble compound of the vitamin B group, is added to many food products to prevent folate deficiency in individuals [9]. Supplementation with folic acid is particularly important with pregnant women, as insufficient folic acid can cause neural tube defects in the developing foetus. Moreover, folate deficiency is the most common cause of anaemia after iron deficiency [10].

In this work, we present the development of a novel magneto-ELISA with optical detection for the quantification of folic acid. The immunological reaction for this strategy detection was performed on nanostructured magnetic beads and is based on a direct competitive assay using a tracer with HRP peroxidase for the enzymatic labelling. The magnetic nanobeads are then attached to improved nanostructured magnetic transducer for the electrochemical detection, based on bamboo structured CNT.

Moreover, we present preliminary results of a novel electrochemical immunosensing strategy based on magneto sensors for folic acid detection in milk. This strategy combines the

advantages taken from immunochemical assays, nano-sized magnetic beads separation and electrochemical transduction based on bamboo structured CNT.

Future work will be focused on the application of this method for the detection of folic acid on food, and clinical samples, with the electrochemical immunosensing strategy.

References:

[1] D. Hoegger, P. Morier, C. Vollet, D. Heini, F. Reymond, J.S. Rossier, Anal. Bioanal. Chem. (2007) 387:c267–275.

[2] Zh. V. Samsonova, O. S. Shchelokova, N. L. Ivanova, M. Yu. Rubtsova, and A. M. Egorov, Enzyme-Linked Immunosorbent Assay of Ampicillin in Milk, Applied Biochemistry and Microbiology, Vol. 41, No. 6, (2005), pp. 589–595.

[3] K N Woodward, ANTIBIOTICS AND DRUGS: Uses in Food Production, (1993), 249-254, Encyclopaedia of Food Science, Food Technology and Nutrition, Academic Press.

[4] A A Bergwerff and J Schloesser, ANTIBIOTICS AND DRUGS: Residue determination, (1993), 254-261, Encyclopaedia of Food Science, Food Technology and Nutrition, Academic Press.

[5] C J Bates, FOLIC ACID: Properties and Determination, (2004), 2559-2564, Encyclopedia of Dairy Sciences, Elsevier.

[6] E. Zacco, J. Adrian, R. Galve, M.-P. Marco, S. Alegret, M.I. Pividori, Electrochemical magneto immunosensing of antibiotic residues in milk, Biosensors and Bioelectronics 22 (2007) 2184–2191.

[7] E. Zacco, M.I. Pividori, S. Alegret, Electrochemical biosensing based on universal affinity biocomposite platforms, Biosensors and Bioelectronics 21 (2006) 1291–1301.

[8] M.I. Pividori, A. Lermo, E. Zacco, S. Hernández, S. Fabiano, S. Alegret, Bioaffinity platforms based on carbon-polymer biocomposites for electrochemical biosensing, Thin Solid Films (2007), in press.

[9] J. Hughes, J. Buttriss, An update of folates and folic acid: Contribution of MAFF-founded research, Nutrition Bulletin, (2000), 25, 113-124.

[10] J.M. Scott, P. Browne, Megaloblastic anemia, (2005), 109-117, Encyclopedia of Dairy Sciences, Elsevier.

ELECTROCHEMICAL BIOSENSING IN FOOD FOR PATHOGENIC BACTERIA BASED ON NANOSTRUCTURED TRANSDUCERS

Susana Liébana, ***Anabel Lermo, Salvador Alegret, Isabel Pividori***
Grup de Sensors & Biosensors, Unitat de Química Analítica, Universitat Autònoma de Barcelona Edifici Cn. Campus UAB, 08193, Bellaterra, Barcelona, SPAIN
Susana.Liebana@uab.cat

The control of food quality has become of growing interest for both consumer and food industry since the increasing incidence of food poisoning is a significant public health concern for customers worldwide [1]. While additives were at one time a major concern, nowadays microbiological issues are the greatest. Among food pathogens, *Salmonella enteritidis* has been the source –in the last decade– of many outbreaks, while *Salmonella typhimurium* and other antibiotic-resistant salmonellae have also recently become a concern [2].

Many factors have contributed to recent food emergencies, such as the increasingly complexity of the food production chain because of mass production. Food regulatory agencies have thus established control programs in order to avoid food pathogens from entering the food supply. One of the most effective ways for the food sector to protect public health is to base their food management programs on Hazard Analysis and Critical Control Point (HACCP). Biosensing devices can be considered as ideal tools to be implemented in HACCP programs, for being used as an ‘alarm' to rapidly detect the risk of contamination by food pathogens in a rapid, inexpensive and sensitive manner and in a wide variety of food matrixes [3,4]. An ideal biosensing device for the rapid detection of microorganisms should be fully automated, inexpensive and routinely used both ‘in field’ and the laboratory.

Electrochemically based transduction devices are robust, user-friendly, portable, sensitive, and cost-effective analytical systems which can operate in turbid media such as food matrixes. Electrochemical biosensors devices thus, offer considerable promise to obtain the risk of contamination by food pathogens in a faster, simpler and cheaper manner compared to traditional methods.

Rigid conducting composites represent a simple method for the immobilization of nanostructure materials for biosensing proposes, ranged from high molecular weight biological molecules, metal nanoparticles, or carbon nanotubes.

Carbon composites result from the combination of carbon with one or more dissimilar materials. Each individual component maintains its original characteristics while giving the composite distinctive chemical, mechanical and physical properties. The capability of integrating various materials (such as metal nanoparticles as well as CNT), is one of their main advantages. Some components incorporated within the composite result in enhanced sensitivity, such as bamboo-structured CNT. The best composite compounds to be used as electrochemical transducer for biosensors will give the resulting material improved chemical, physical and mechanical properties. As such, it is possible to choose between different binders and polymeric matrices in order to obtain a better signal-to-noise ratio, a lower nonspecific adsorption, and improved electrochemical properties (electron transfer rate and electrocatalytic behavior). These materials can just be prepared through ‘dry chemistry’ using procedures that can be easily transferred to mass fabrication of thick film devices.

The development of magnetic beads based separations has also brought unique opportunities for biological detection strategies. DNA, cells, antibodies, and enzymes, can be selectively bound to the magnetic beads and then separated from its matrix by using a magnetic field.

Magnetic beads have been recently used in new strategies for electrochemical biosensing [5,6].

In this work, a novel strategy for electrochemical biosensing of food pathogenic bacteria using nanostructured electrochemical magneto electrode is reported.

In this approach, the bacteria are attached to magnetic nanoestructured beads by immunological reaction with specific antibody for *Salmonella*. Further reaction with a second enzyme-conjugated antibody is performed. The magnetic nanobeads are then attached to improved nanostructured magnetic transducer for the electrochemical detection, based on bamboo structured CNT.

The features of this new approach are compared with classical cultured methods as well as PCR strategies and other electrochemical detection methods based on classical micro-sized magnetic beads and conventional non-nanostructured transducers.

References:

[1] D. Roberts, in: B. Caballero, L. Trugo and P.M. Finglas (Eds.), Encyclopedia of Food Science and Nutrition, Academic Press, 2003, pp. 2654.
[2] C. Wray, in: B. Caballero, L. Trugo and P.M. Finglas (Eds.), Encyclopedia of Food Science and Nutrition, Academic Press, 2003, pp. 5074.
[3] L.D. Mello, L.T. Kubota, Food Chemistry 77 (2002) 237.
[4] P. Leonard, P. Hearty, J. Brennan, L. Dunne, J. Quinn, T. Chakraborty, R. O'Kennedy, Enzyme and Microbial Technology 32 (2003) 3.
[5] E. Zacco, J. Adrian, R. Galve, M.-P. Marco, S. Alegret, M. I. Pividori, Biosensors and Bioelectronics 22, (2007) 2184-2191.
[5] A. Lermo, S. CAmpoy, J. Barbé, S. HErnández, S. Alegret, M. I. Pividori, Biosensors and Bioelectronics 22, (2007) 2010-2017.

"TUNING THE EXPRESSION OF SUPRAMOLECULAR CHIRALITY BY MOLECULAR FOOTPRINT ENGINEERING ON METAL SURFACES"

M. Lingenfelder[*], G. Tomba[°], S. Haq[§], G. Costantini[*], Y. Wang[*], A. De Vita[°], R. Raval[§] and K. Kern[*].

[*]*Max-Planck-Institute for Solid State Research, Heisenbergstr. 1 D-70569 Stuttgart, Germany*
[°]*Physics Department, King's College London, Strand, London WC2R 2LS, United Kingdom*
[§]*The Surface Science Research Centre*
The University of Liverpool,
Liverpool L69 3BX, United Kingdom.
m.lingenfelder@fkf.mpg.de

The emergence of homochirality in biomolecular systems is one of the most intriguing open questions of Nature. The self-assembly and amplification of chiral subunits into higher-order species is crucial in understanding the development of homochirality in biological function. On the other hand, a practical perspective of molecular chirality arises from the fact that the two mirror images of a chiral molecule can have vastly different physiological impacts when ingested by living organisms [1]. As a consequence, there is a strong industrial need to produce and separate single enantiomers (i.e., *Chirotechnology*).

Unraveling the basics mechanisms of chiral recognition, templation and enantioselectivity is then crucial for the development of more effective separation methods and reactions used to achieve enantiopurity. Amino acids and peptides appear as good candidates for the creation of enantioselective surfaces, since they present a variety of functional groups that can be chosen to achieve specific reactions.

Although the enantioselectivity of metal surfaces templated with organic modifiers has been demonstrated by a couple of experiments over the past years [2], the requirements for the design of enantioselective surfaces are not yet clear. In particular, local characterization of the supramolecular structures formed by the chiral modifiers and systematic studies on the effects of specific molecular adsorption and 'chiral footprints' [1] of the same molecule on the templating effect are very rarely found in literature [3]. One proposition is that for a surface to show enantioselectivity, the template molecule should be rigidly bonded to the surface in order to prevent azimuthal rotation of the chiral center [4]. This lack of freedom would allow the adsorption mode of the chirally modified organic reactant to be more strictly controlled, enabling the enantioselective response to survive under a variety of conditions [5]. More recent studies on amino acids seem to support this hypothesis, suggesting that two anchoring adsorption points are needed for chiral templating to work [3].

To get an insight into the basic requirements for bestowing chirality to achiral metal surfaces, we have studied the chiral templation of the amino acid L-Phe (Figure1.1a, 1.2) on the Cu (110) substrate. As a first step, information on the local level was obtained by Scanning Tunneling Microscopy (STM). Reflection-Absorption Infrared Spectroscopy (RAIRS) and Temperature Programmed Desorption (TPD) have been combined to determine the chemical states, orientations, molecular arrangements and bonding interactions of the molecules at the Cu surface. The interpretation of the adsorption geometries was aided by molecular dynamics simulations. The studies show that L-Phe is present on different chemical states going from acidic to zwitterionic to anionic depending on the adsorption temperature in the 85 K-400 K range. We concentrate on the phase at 400 K to discuss the interplay of inherent molecular chirality and the expression of chiral motifs induced by the preferential adsorption geometry of two anchoring points to the surface in terms of conformational flexibility and optimized molecule-surface interactions (*footprint chirality*).

[1] the adsorption geometry determined by the preferential interaction of specific functional groups in close proximity to the surface

Moreover, we study the effect of a third anchoring point molecule-surface by comparative adsorption of different isomers of L-Tyr (Figure 1.1b, 1.3) on Cu(110). Our results show that preventing the conformational flexibility for rotation of the functional groups around the chiral center is crucial for the expression of only one chiral footprint on the surface. This is likely to play an important role for potential enantioselective reaction paths on the templated surface.

We have recently demonstrated that chiral recognition of adsorbed dipeptides takes place via an induced-fit mechanism [6,7]. Moreover, we can now show that conformational rigidity is a key parameter for the expression of footprint homochirality on metal surfaces and that this parameter can be tuned by the appropriate choice of the amino acid residue [8].

References:

[1] Dekker, *Dekker Encyclopedia of Nanoscience and Nanotechnology* ,VCH, Eds. James A.Schwartz-Christian Contescu-Karol Putyera, (2004).
[2] S. M. Barlow *et al.*, Surface Science 590, **243** (2005) 0039-6028.
[3] Z. Ma and F. Zaera, Surface Science Reports **61** (2006) 229.
[4] D. Stacchiola *et al.*, Journal of Physical Chemistry B **109** (2005) 851.
[5] E. M. Marti, S. M. Barlow, S. Haq, and R. Raval, Surface Science 501, **191** (2002) 0039-6028.
[6] M. Lingenfelder, G. Tomba, G. Costantini, L. Colombi Ciacchi, A. De Vita, and K. Kern, Angew. Chem. Int. Ed. **18** (2007) 951.
[7] G. Tomba, M. Lingenfelder, G. Costantini, K. Kern, F. Klappenberger, J.V. Barth, L. Colombi Ciacchi, and A. De Vita, J. Phys. Chem. A **111** (2007) 12589.
[8] M. Lingenfelder, G. Tomba, S. Haq, G. Costantini, Y. Wang, R. Raval, A. De Vita and K. Kern, *in preparation*.

Figures:

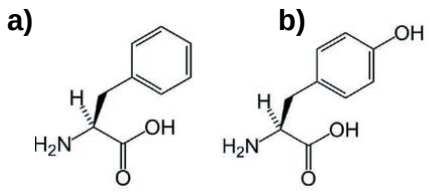

Figure 1.1 a) squematic drawing of L-Phe .b) squematic drawing of L-Tyr

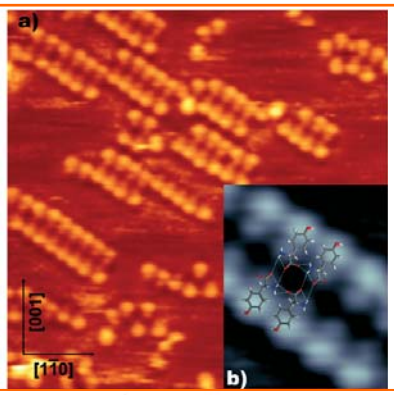

Figure 1.3
a) Supramolecular chains of L-Tyr on Cu(110).b) HR STM image

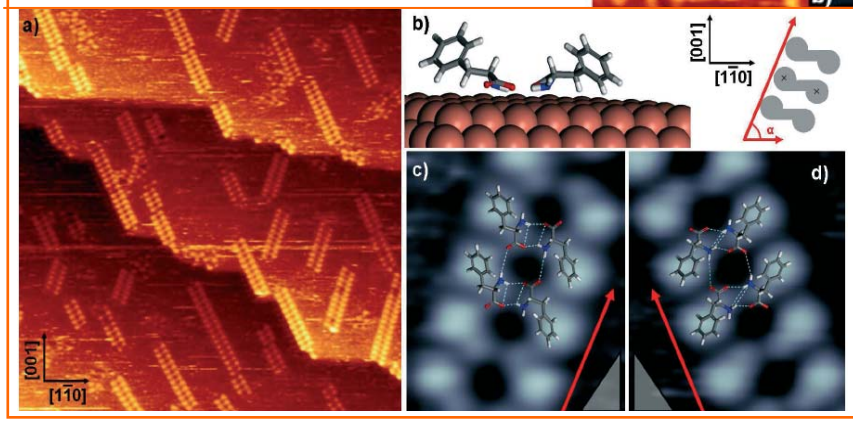

Figure 1.2 Supramolecular chains of L-Phe on Cu(110) . a) STM image c),d) HR STM (4x3 nm) of the different adsorption motifs and superimposed schematic model. b) lateral view of the model proposed in c). The triangles indicate mirror-imaged footprints.

NANOPARTICLES IN $YBa_2Cu_3O_{7-\delta}$ SUPERCONDUCTING THIN FILMS.

S.Ricart, A. Llordes, F.Martínez-Julián, F. Sandiumenge A.Pomar , T.Puig, X.Obradors
Institut de Ciència de Materials de Barcelona (CSIC), Campus UAB, 08193 Bellaterra, (España).
ricart@icmab.es

There is a large number of functional materials were the possibility to have a high contact surface between two dissimilar materials by means of a nanometric structure, give them a high added value. Nanoparticles are considered as essential materials in nanotechnology. Physical and chemical properties of nanoparticles can be varied by changing its size and morphology .In particular, the use of metallic nanoparticles approach has been applied to nanocomposite superconducting layers having high critical currents.

The present communication deals with the preparation of nanocomposite superconducting layers by Chemical Solution Deposition (CSD) using the Metal Organic Decomposition approach (MOD).

The final goal will be the prevention of vortex motion produced when an electrical current is applied to a superconducting material situated in a magnetic field. Vortex motion produces dissipation and, as a consequence a reduction of the critical current density.

The presence of non superconducting nanosized defects in the superconducting layers prevents this loss of energy by pinning the vortices. There is a close relationship between the composition and shape of these nanometric structures and their effectiveness in pinning the vortices and, hence, enhancing the properties of the superconducting material.

There are very few procedures described for the preparation of these nanocomposite materials and, mainly, the first approaches have been recently achieved by physical methods such as Pulsed Laser Deposition (PLD). [2] .

In this communication we present a new approach based in an “all chemical” process using the methodologies for the preparation the superconductor solution precursors. The goal of the present work is to obtain a nanocomposite thin film containing previously or simultaneously synthesized nanoparticles of a non-superconducting second phase (BZO[3], Au, Ag, CeO_2) in the YBCO matrix using the Metal Organic Decomposition. The general principle of the MOD process is the decomposition of metal organic precursors at 310ºC to obtain a mixture of fluorides, oxides and oxifluorides which are subsequently thermally treated at 795-810ºC to obtain the desired superconductor oxide phase.

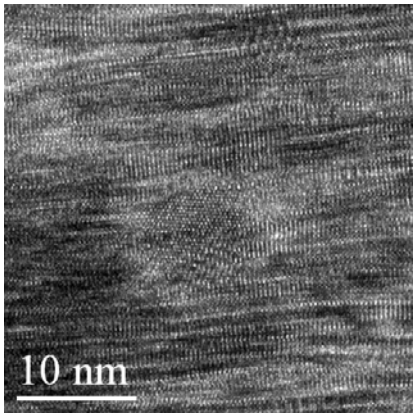

Figure 1. SEM image of a YBCO/BZO (7%) superconducting layer

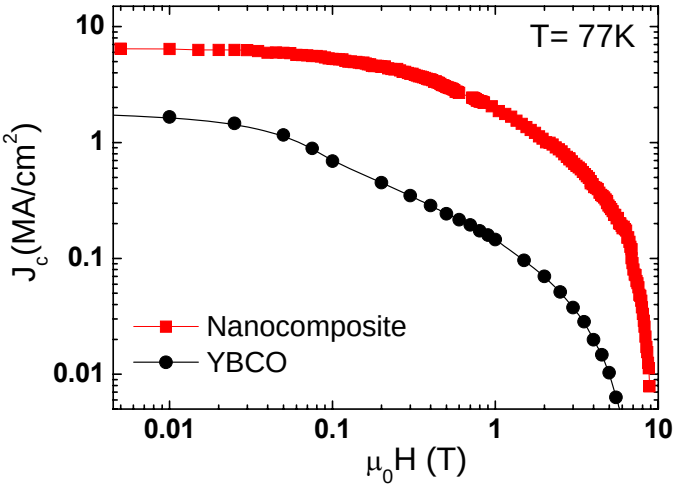

Figure2. Effect of the presence of BZO nanoparticles in the magnetic field dependence..

We have succeeded in growing nanocomposites with BZO nanoparticles. We present here the results obtained using different approaches to YBCO films with other metallic nanoparticles and the effect of their presence in the critical current density at high magnetic films.

Referencias:

[1] X.Obradors et al, *Supercond. Sci. Technol.*, **2004**, *17*, 1055.

[2] J. L. MacManus-Driscoll et al, *Nature Mat.*, **2004**, *3*, 439.

[3] J. Gutierrez et al. *Nature Mat.*, **2007**, *6*, 367.

Spin Dependent Injection Model for Monte Carlo Device Simulation

H. López, X. Oriols, J. Suñé and X. Cartoixà
Universitat Autònoma de Barcelona, 08192 Bellaterra, Spain
e-mail: Hender.Lopez@campus.uab.cat

Nowadays, there is great interest in the study and development of semiconductor devices based on the manipulation and control of the electron spin (Spintronics [1]). These devices must have an efficient spin-polarized electron injection at room temperature so that they can be used in practical applications. Ferromagnetic-metal/semiconductor structures are a possibility to achieve this goal [2]. On the other hand, the Monte Carlo method for the study of electronic transport in semiconductor devices is a widely used technique [3]. In this work we present a spin dependent injection model suitable for use with Monte Carlo (MC) simulators.

The electrical spin injection from ferromagnetic contacts can be thought of in terms of a spin-dependent contact resistance [4]. Physically, this is typically achieved by means of a tunnel barrier between the contact and the semiconductor. In our model, two spin states are considered ($\uparrow$ and $\downarrow$) and they are injected in a previously chosen proportion $F = n_\uparrow/n_\downarrow$. A two terminal ballistic device is simulated (see Fig. 1), in which electrons are injected from both terminals (c = source s or drain d) and tunneling probabilities are defined ($P_c^\uparrow$ and $P_c^\downarrow$). The injection rates are calculated following the work of Oriols *et al.* [5]. When an electron is to be injected, a random number r uniformly distributed between zero and one is generated and if $r < P$ the carrier is successfully injected. A similar procedure is done when a carrier reaches a contact from the device region. Simulations were done using an ensemble Monte Carlo code coupled to a 3D Poisson solver, where carriers move ballistically inside the device according to the semiclassical equations of motion.

As expected, the current grows with the value of P (Fig. 2), indicating a decrease of the contact resistance. In order to evaluate the accuracy of the algorithm used, resistances were calculated by a linear fit to the I-V curves, finding good agreement with the expected [6] $(1 - P)/P$ behavior (Fig. 3). The method presented here reproduces the fundamental physics of a spin dependent resistance and can easily be adapted to standard Monte Carlo codes.

References

[1] I. Zutic *et al.*, Rev. Mod. Phys., **76** (2004) 323.

[2] K. H. Ploog, J. Appl. Phys., **91** (2002) 7256.

[3] C. Jacoboni and L. Reggiani, Rev. Mod. Phys., **55** (1983) 645.

[4] I. Rashba, Phys. Rev. B **62**, (2000) R16267.

[5] X. Oriols *et al.*, Solid State Electronics **51**, (2007) 306.

[6] S. Datta, Electronic Transport in Mesoscopic Systems, (1997), Cambridge University Press.

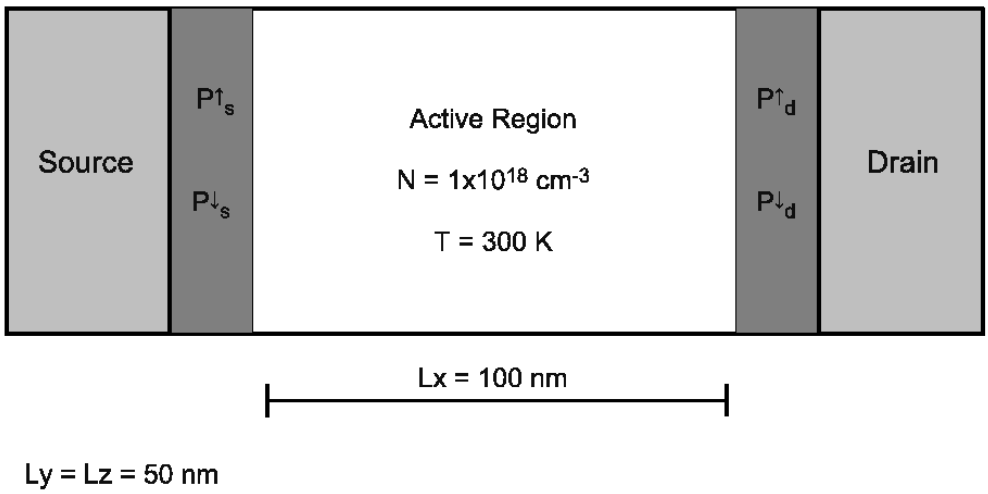

Figure 1: Schematic representation of the device structure under investigation

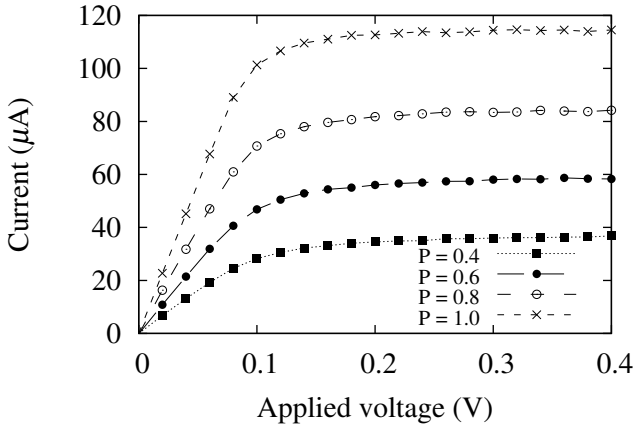

Figure 2: I-V curves for different values of Tunnel Probabilities (P) using $F = 1$

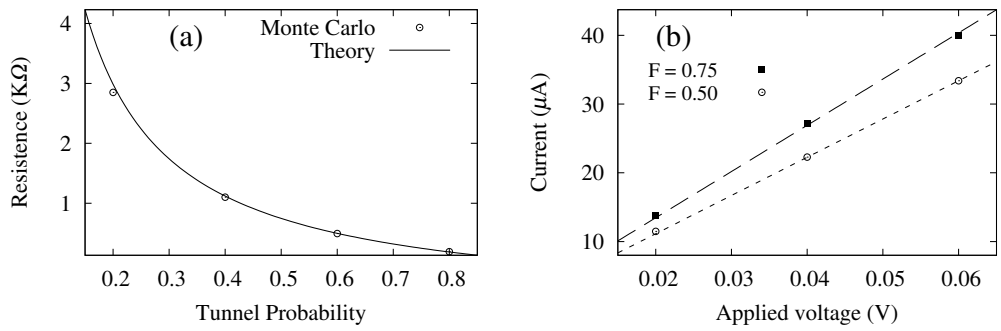

Figure 3: (a) Resistance Values as a function of the Tunnel Probability using $F = 1$. Points=This Work. Line= 746 (1-P)/P Ω. (b) I-V curves for two different fractions F of spin injected compared to $I = V[F/(R_i + 2R_\uparrow) + (1 - F)/(R_i + 2R_\downarrow)]$ where R_i is the resistence for $P = 1$ and $R_{\uparrow/\downarrow}$ the resistence of the channel for the state up or down.

A SERS STUDY OF CHARGE-TRANSFER PROCESSES IN THE RAMAN SPECTRUM OF THE BENZOATE ANION ADSORBED ON SILVER NANOSTRUCTURES

M.R. López-Ramírez, J.L. Castro, J.F. Arenas and J.C. Otero
Department of Physical Chemistry, Faculty of Science,
University of Málaga, E-29071-Málaga, Spain
mrlopez@uma.es

Much is now known about the properties of the ground electronic states of molecules adsorbed on solid surfaces, due, in large part, to the tremendous power of both, the experimental and theoretical approach to modern surface science. However we know considerably less about the properties of the excited electronic states of adsorbed species and the way in which they interact with the substrate due to the relatively scarce number of techniques available to probe such states.

Molecules adsorbed on some metal surfaces such as silver, copper and gold, can exhibit enormous enhanced Raman scattering, and such technique has become known as surface-enhanced Raman scattering (SERS) [1–3]. The SERS effect has historically been associated with substrate roughness on two characteristic length scales. Surface roughness on the 10 to 100 nm length scale supports the electromagnetic resonances which are the dominant mechanism of enhancement. These electromagnetic resonances can increase the scattered intensity by ca. 10^4 to 10^7. A second mechanism often thought to require atomic scale roughness, is referred to as the chemical enhancement mechanism. This second mechanism involves the creation of new electronic excited states which result from adsorbate–substrate chemical interactions. It is estimated that the chemical mechanism can enhance the scattering cross-section by a factor of ca. 10 to 10^2. Estimations have been made of the magnitude of the chemical mechanism in the presence of the electromagnetic one in silver island films in ultra-high vacuum (UHV) [4]. These two mechanisms operate simultaneously making it difficult to isolate the role and magnitude of each one.

The chemical mechanism of SERS is a process analogous to molecular resonance Raman scattering except that the resonances involved are not intramolecular in origin [3-5]. They are charge transfer resonances in which a photoinduced charge hopping between the adsorbate and the substrate occurs. The general consensus had been that atomic scale roughness is required to couple electronically the adsorbate states to the substrate states in such a manner as to produce charge-transfer excitations and Raman enhancement [1,2]. It has been proven to be very difficult to study the chemical enhancement mechanism selectively for two reasons. First, such mechanism contributes a small fraction to the total enhancement. Second, almost any experimental parameter which can be varied to probe a system will have an influence via both mechanisms, making the separation of effects difficult, if not impossible. For this reason, there has been considerable effort to understand the effect in detail [6,7].

The main aim of this work is to contribute to the knowledge of role of charge transfer excited states within a CT-SERS process by studying aromatic molecules such as benzoic acid. The SERS analysis of the benzoate anion is carried out using the proposed methodology in previous works [6,7] focused on the detection of charge transfer resonance processes. It is necessary the use of ab initio calculations to get complementary information about electronic properties of the excited states.

The analysis of the SERS spectra of benzoate anion on the basis of the CT mechanism takes account for the experimental evidences. It is able to explain not only the enhancement of several SERS bands but also why some specific modes are the strongest ones at negative electrode potentials. In addition, we have been able to extract information on the two lowest CT excited electronic states which are very close in energy as happens in the radical anions of aromatic molecules similar to benzene.

References:

[1] M. Moskovits, Rev. Mod. Phys. **57** (1985) 783.
[2] B. Pettinger, in: J. Lipkowski, P.N. Ross (Eds.), Adsorption of Molecules at Metal Electrodes, VCH, New York, 1992, p. 285.
[3] A. Campion, P. Kambhampati, Chem. Soc. Rev. **27** (1998) 241.
[4] I. Mrozek, A. Otto, J. Electron Spectrosc. Relat. Phenom. **54** (1990) 895.
[5] J.R. Lombardi, R.L. Birke, T. Lu, J. Xu, J. Chem. Phys. **84** (1986) 4174.
[6] J.F. Arenas, I. Lopez Tocon, J.C. Otero, J.I. Marcos, J. Phys. Chem. **100** (1996) 9254.
[7] J.F. Arenas, M.S.Wooley, J.C. Otero, J.I. Marcos, J. Phys. Chem. **100** (1996) 3199.

Figures:

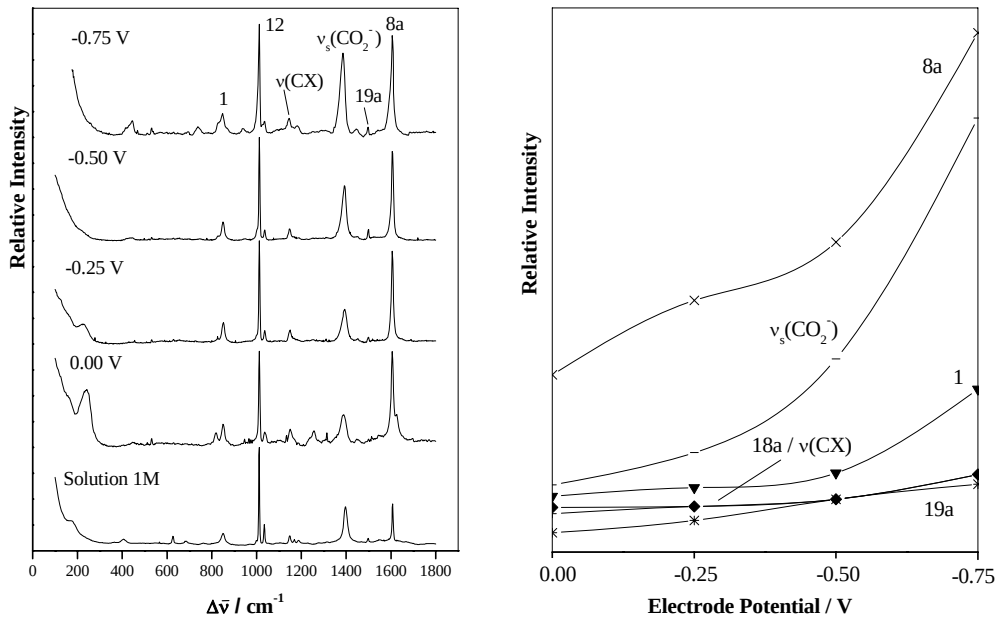

(I) **(II)**

Figure 1. (I) Raman spectra of an aqueous solution and SERS of sodium benzoate on recorded silver at different electrode potential. (II) Relative intensities of the strongest bands recorded in the SERS of sodium benzoate referred to that of mode 2; ν (CH).

Acknowledgements:

This research has been supported by the Spanish Ministerio de Educación y Ciencia (Project Number NAN2004-09312-C03 and CTQ2006-02330) and Junta de Andalucía (Project Number FQM-01895).

Influence of stress and size over the magnetic response of nickel nanowires

Román López-Ruiz, Fernando Luis and Juan Bartolomé

Instituto de Ciencia de Materiales de Aragón, CSIC - Universidad de Zaragoza, Departamento de Física de la Materia Condensada, Pedro Cerbuna 12, 50009 Zaragoza Spain

rlruiz@unizar.es

Nickel nanowires were prepared using electrochemical methods. Porous alumina membrane is used as a template to grow nanowires [Fig. 1]. Different synthesis parameters, such as anodization voltage, anodization time, plating time or temperature determine the morphology and size of our nanowires. This enables us to independently control the size and aspect ratio of the nanowires [Fig. 2].

The magnetic response does not show any evidence of a superparamagnetic blocking, which confers to the material an important application in data storage devices [1]. At room temperature, hysteresis is determined by shape anisotropy [2]. Room temperature coercive field values lower than the predicted in the Stoner-Wohlfarth "in unison" model were measured. The magnetic response of wires with varying aspect ratios shows evidences from particle-to-wire crossover above an aspect ratio Length/Diameter ≈ 4.6. The coercive field for nanowires shows an agreement with "nucleation and propagation" fanning reversal mode for diameters lower than 43 nm (a mode usually neglected) [3]. For larger diameters, the "curling" reversal mode is in qualitatively agreement with our experimental data [Fig. 3].

Below room temperature, a thermally-induced magnetoelastic anisotropy competes with the shape anisotropy. Compression stress due to different thermal expansion coefficients of aluminium [4] and nickel gives rise to a thermally-induced magnetoelastic effect that reduces the coercivity. The latter behavior is shown only if aluminium is not removed from the samples. Otherwise, we obtain the monotonic decrease of coercive field with increasing temperatute that is expected for a thermally activated magnetization switching process. Our work, therefore, puts a end to the controversial question [5] about the origin of this effect. The influence of the stress on the coercive field depends on the aspect ratio of the samples.

Above room temperature, in a range of temperatures not covered until now, the aluminium expansion produces a tensile stress that is the responsible of a coercive field maximum at room temperature. The Curie temperature T_C progressively decreases with decreasing wire diameter [6] [Fig. 4]. In agreement with models, this reduction of the T_C is due to finite-size effects. The T_C extrapolated to infnite diameter shows a decrease of about 3 K with respect the bulk value [7]. This suggest that stresses, whose presence and influence on the magnetic properties have been put into evidence by hysteresis experiments, also modify T_C. This effect is not present for nickel nanowires embedded in mica, where stresses are very weak [8].

References:

[1] H. He and N. J. Nongjian, Encyclopedia of Nanoscience and nanotechnology, **X** (2003) 1
[2] P. M. Paulus, F. Luis, M. Kroll, G. Schmid and L. J. de Jongh, Journal of Magnetism and Magnetic Materials, **224** (2001) 180.
[3] E. H. Frei, S. Shtrikman and D. Treves, Physical Review **106** (1957) 446.
[4] A. Kumar, S. Fahler, H. Schlorb, K. Leistner and L. Schultz, Physical Review B, **73** (2006) 064421
[5] M. Vazquez, K. Pirota, J. Torrejon, D. Navas and M. Hernandez-Velez, Journal of Magnetism and Magnetic Materials, **14** (2005) 715.
[6] D. P. Landau, Physical Review B, **14** (1976) 255.
[7] L. Patrick, Physical Review, **93** (1954) 384.
[8] L. Sun, P. C. Searson and C. L. Chien, Physical Review B **61** (2000) R6463.

Figures:

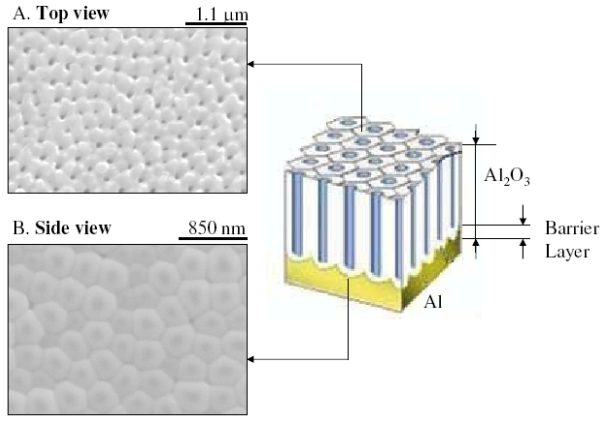

Fig. 1. Schematic drawing of the nanoporous alumina structure as obtained as a result of anodic oxidation. Example of the top view (A) and the side view after aluminium removal (B) of a sample synthesized at 160 V during 2 hours in H_3PO_4 1%.

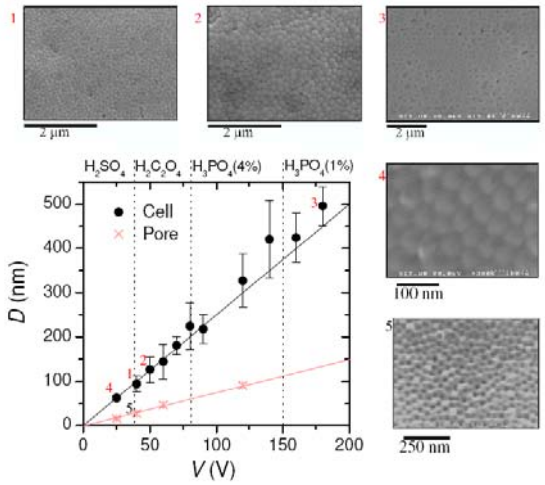

Fig. 2.. Voltage influence on cell and pore diameter. Temperatures and electrolytes used are described in table 2.2 and marked in superior scale. For all samples: t_1 =30 min and t_2 =120 min. Black and red lines are linear fits for cell and pore diameters respectively.

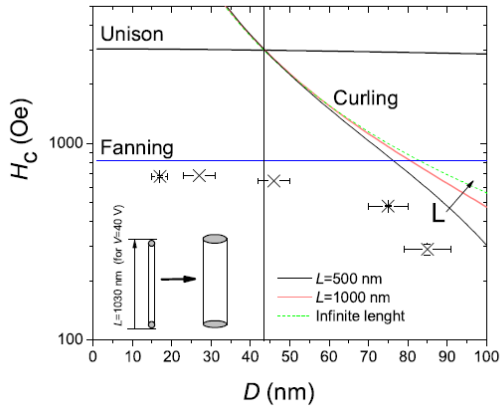

Fig. 3. Coercivity evolution for samples with different diameter. Nucleation field predictions for the diverse reversal modes in samples with a finite length of 1000 nm (length that correspond with sample prepared at 40 V and filled during 10 min) are shown. The vertical line signals the critical diameter D_{cr}. The different curves for curling correspond to wires with various lengths.

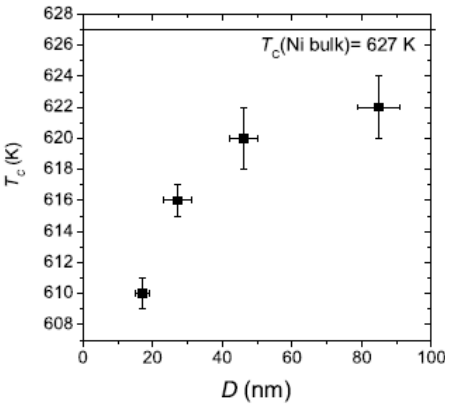

Fig. 4. Curie temperature evolution for samples with different nanowire diameters.

INTEGRATED PLATFORM FOR STEM CELLS SEPARATION/COUNTING

J.Loureiro, S.Cardoso,C.L.Silva,J.M.Cabral,P.P.Freitas
INESC-MN, Rua Alves Redol, Lisboa, Portugal
jloureiro@inesc-mn.pt

Hematopoietic stem/progenitor cells (HSC) have vast potential for use in medical applications (such as bone marrow transplantations) and the separation of these cells from blood has an important role in the stem cells research [1]. However, the most usual techniques, (MACS™) and (FACS), have some drawbacks like being cell-loosing or very time-consuming.
This works is in the area of nanobioengineering, combining a cross-disciplinary approach of nanotechnology, bioseparation engineering and hematology with a common goal: the separation, purification and monitoring of HSC *in vitro*.
Until now a device based on magnetophoresis has been developed using microfluidics and in-situ magnetic fields (up to 6kA/m), generated by metallic lines, in order to separate stem cells from blood in a more efficient and easy way [2], [3], [4], [5]. In the same device Spin Valve sensors are used to measure the efficiency of the separation (by counting the cells as they are separated).
The geometry of the separator makes it possible to change only the path of specific stem cells, that are magnetically labeled with 50nm magnetic beads functionalized with monoclonal antibodies (MAbs), instead of separating all the magnetic elements in the fluid (which is vital to keep count of the stem cells).
The fluidic system consists in 2 micro-channels (150µm wide, 14µm thick and 40µm apart) joined over several gaps of 2.5mm and disposed in an "H"-type geometry (fig.1 and fig.2). The laminar flow is generated in the y-direction along both channels, from the inlet to the outlet. The fluidic system is bonded to the separator platform which consists in two successive lines (7um wide and 500nm thick), deviated from the y-direction by an angle of 5 degrees, starting in one channel and ending in the other one. At the end of each metallic line there are 3 SV in each channel to count the cells that have been separated and those that might fail to be separated [6],[7].
To prove the concept and test the design, preliminary tests were made passing 2um magnetic particles through the channels. These particles (χ=0.22 and ρ=1.1x10^3 kg/m^3) feel a magnetic force of 9.5pN, when passing over the metallic lines (due to a magnetic field of 6kA/m and a gradient of 2.2x10^6 kA/m, when applying 100mA), which force them to be deviated in the x-direction. With velocities flow rates around 30nL/min, particles were observed to follow the line path, moving from the beginning of the line (in the first channel) until the end of it (in the second channel) (fig.3). When any particle fail to feel the first line (due to agglomeration for e.g.) it can be separated when passing over the next line. These measurements were made for a concentration of 1x10^5 particles/µl to make the optical inspection easier. The real experiment will be made with human hematopoietic stem/progenitor cells ($CD34^+$ enriched cells), from umbilical cord blood samples.

References:

[1] - "Ex-vivo expansion of hematopoietic stem cells in bioreactors", Cabral, J.M. (2001) Biotechnology Letters *23*, 741-751.
[2] – "Flow through, Immunomagnetic Cell Separation", J.J.Chalmers, M.Zborowski, L.Sun and L.Moore, in Biotechnol. Prog. 1998, 14, 141-148
[3]– "Separations based on magnetophoretic mobility", M. Zborowski, L.Moore, P.Stephen Williams and J.J.Chalmers, in Separation Science and Technology, vol.37, No.16, pp.3611-3633, 2002

[4] – "Continuous sorting of magnetic cells via on-chip free-flow magnetophoresis", N.Pamme and C.Wilhelm, Lab-Chip, 2006, 6, 974-980

[5] – "Analytical model for the magnetic field and force in a magnetophoretic microsystem", E.P.Furlani and Y.Sahoo, in J.Phys. D: Appl. Phys. 39 (2006) 1724-1732

[6]- "Flow Velocity Measurement In Microchannels Using Magnetoresistive Chips", H.A. Ferreira, D. L. Graham, P. Parracho, V. Soares, and P.P.Freitas, IEEE Trans Magn., vol.40, pp. 2652-2654, July 2004.

[7]- "Magnetoresistive sensors", P.P Freitas, R.Ferreira, S.Cardoso and F.Cardoso, in J.Phys.: Condens. Matter 19, N16 (23 April 2007), 165221 (21pp)

Figures:

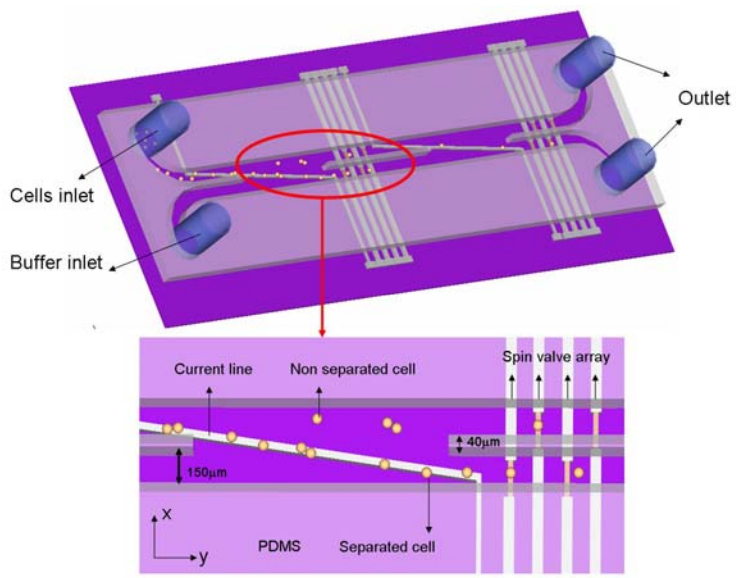

Fig1: "H-type" fluidic platform, allowing stem cells to be separated from one channel to the other due to the magnetic field created by the oblique current lines. Each channel has spin valves at the end to count the cells

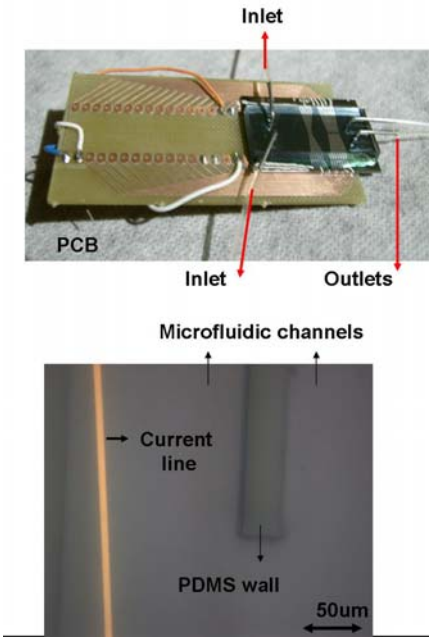

Fig2: Real chip mounted on a PCB to allow electrical measurements (top); Microscope image of the microfluidic system showing the current line near the gap between both channels

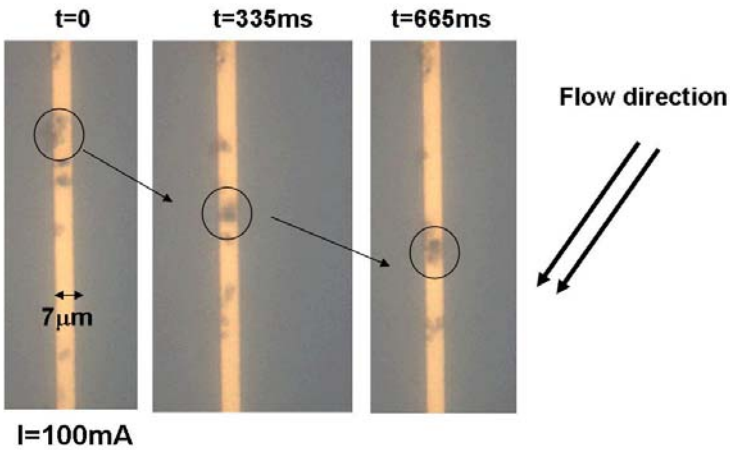

Fig3: Time evolution of the 2µm particles position due to the fluid velocity and the magnetic field created by the current line (when applying 100mA) during the separation. These particles were moving over the line with a velocity around 75µm/s.

PURE COPPER DEFORMED BY EQUAL-CHANNEL ANGULAR PRESSING (ECAP)

Nayar, Lugo[*]; Núria, Llorca[**]; José, M. Cabrera[*,*]**
[*]Department of Materials Science and Metallurgical Engineering ETSEIB, Polytechnic University of Catalonia.
Av Diagonal 647, 08023 Barcelona, Spain.
nayar.lugo@upc.edu, jose.maria.cabrera@upc.edu
[**]Department of Materials Science and Metallurgical Engineering, University of Barcelona. C/ Martí i Franqués 1-11, 08028 Barcelona, Spain.
nullorca@ub.edu
[***]CTM Technical Centre, Av. Bases de Manresa 1, 08242, Manresa, Spain.

ABSTRACT- Severe Plastic Deformation processes (SPD) have acquired a grate importance in the last decades in the production of nanostructured materials. Different processes have been developed by several research groups around the world and interesting results have been reported in the bibliography [1-5]. However, one of most attractive SPD processes is the Equal-Channel Angular Pressing (ECAP, see fig.1) because bulk materials with excellent mechanical properties and homogeneous deformation are produced by this technique. The aim of the present work is to study several aspects related to the microstructure obtained due to the ECAP process following a particular and most effective route (Route Bc) on pure copper samples and their influence on mechanical properties. Starting 99,98% pure Cu samples with an average grain size of ~60 μm (fig. 2) were processed at room temperature by Equal-Channel Angular Pressing (ECAP) introducing severe plastic deformation. The microstructure and properties survey was carried out by microscopy and mechanical characterization. A significant decrease in grain size was observed by transmission electron microscopy resulting after 8 passes through the die, in grain sizes in the order of 250nm (fig. 3). Tensile and microhardness tests were carried out on the deformed material in order to correlate microstructure and mechanical properties. From the first passage through the ECAP die, an increase in mechanical properties was reported with a gradual small increase for the subsequent ECAP passes (table 1). The mechanism for the process has been studied and several steps can be related starting from deformation, dislocation motion, cells/subgrain generation (LAGB), and stabilisation as (HAGB).

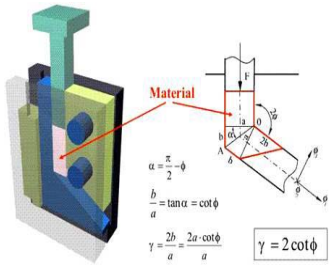

Fig. 1 Test system of the equal-channel angular pressing.

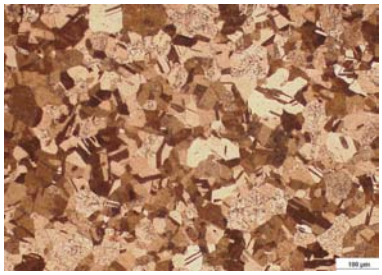

Fig. 2 Microstructure of pure copper after annealing at 600ºC for 2 hours.

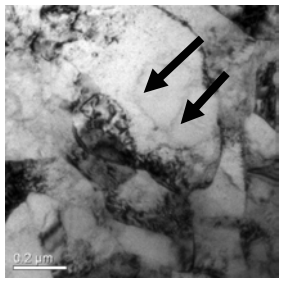

Fig. 3 TEM image of a processed sample (ECAP) after 8 passes.

Table 1: Material Characterisation and properties

Sample	Grain Size (µm)	Hardness HV	Dislocation density ρ (m^{-2})	YS(MPa)	UTS(MPa)	%RA*
Annealed	65	70 ± 2	1.00E+14	200	275	95
1 pass	15	139 ± 5	3.45E+14	337	411	90
2 passes	0.99	150 ± 5	4.02E+14	415	429	91
3 passes	0.37	151 ± 3	4.89E+14	424	458	87
4 passes	0.34	152 ± 4	6.89E+14	448	469	86
5 passes	0.3	153 ± 3	8.12E+14	441	460	89
6 passes	0.31	156 ± 2	7.36E+14	459	480	85
7 passes	0.34	158 ± 2	6.32E+14	447	468	88
8 passes	0.25	157 ± 1	4.09E+14	477	498	88

***% Reduction of Area**

ACKNOWLEDGEMENTS.-
Thanks are given to the Ministry of Science and Technology of Spain to support the project DPI2005-09324-C02-01/02. NL thanks the scholarship (BES-2003-2754) granted by the Ministry of Science and Technology of Spain.

REFERENCES.-

[1]V.M. Segal, V.I. Reznikov, A.E. Drobyshevskiy,V.I. Kopylov. 1981. Russian Metall.1, pp 99-105.
[2]R.Z. Valiev, N.A. Krasilinikov, N.K. Tsenev. 1991. Mat. Sci. Eng. A 137, pp 35-40.
M. Furukawa, Z. Horita, N. Nemoto, T.G. Langdon J. 2001.Materials Science.36, pp 2835-2843.
[3]Y. Iwahashi, J. Wang, Z. Horita, M. Nemoto, T.G. Langdon. 1996. Scripta Mater.35, pp143-146.
[4] N. A. Smirnova, V. I. Levit, V. I. Pilyugin, R. I.. Kuznetsov, L. S. Davydova and V. A. Sazonova: Fiz. Met. Metalloved., 61 (1986) 1170-1177.
[5] G. Sakai, Z. Horita, T.G. Langdon, Mat. Sci. Eng. A 393 (2005) 344-351.
[6] K. Nakashima, Z. Horita, M. Nemoto, T.G. Langdon, Acta Mater.; 46 (1998) 1589-1599..
[7] Y. Iwahashi, Z. Horita, M. Nemoto, T.G. Langdon, Acta Mater.; 46 (1998) 3317-3331.
[8] B.L. Li, N. Shigeiri, N. Tsuji, and Y. Minamino, Materials Science Forum 503-504 (2006) 615-620.

Poster

NANO-SIZED MGO-BASED MAGNETIC TUNNEL JUNCTIONS FABRICATED BY E-BEAM LITHOGRAPHY COMBINED WITH CHEMICAL-MECHANICAL POLISHING

Rita Macedo, R.Ferreira, P.Wisniowski S.Cardoso, P.P Freitas
INESC-MN, Rua Alves Redol nº9 1000-29, Lisbon, Portugal
rmacedo@inesc-mn.pt

In this work a new nanofabrication method was used to integrate nano-sized (down to 48x180nm^2) MgO-based magnetic tunnel junctions (MTJs) in to complete current-perpendicular-to-plane (CPP) devices.

This alternative fabrication process combines micro and nano direct-write lithography techniques. The active elements are defined by electron beam and patterned by ion milling, while bottom and top electrodes are defined by conventional laser lithography. Chemical Mechanical Polishing (CMP) of SiO_2 passivation/planarization film allows contact to the top electrode of the buried pillar [2]. The TMR is calculated as $(R_{high}-R_{low})/R_{low}$, where R_{low} is the low resistance state, and R_{high} is the high resistance state.

The samples presented in this abstract show the successful working and reproducibility of this process. The sucture of the samples presented are:

- Samples 1/2/3 (from IBD):

Ta(50)/Ru(200)/Ta(50)/MnIr(150)/CoFe(20/30/20)/Ru(8)/CoFeB(40)/MgO(7/7/10)/CoFeB(30/20/30)/Ru(30)/Ta(100)

- Samples 4/5 (from PVD):

Ta(50)/Ru(180)/Ta(30)/PtMn(160)/CoFe(20/24)/Ru(9/9.6)/CoFeB(30)/MgO(11/7)/CoFeB(30/15.5)/Ru(50)/Ta(50)

The device resistance is plotted vs 1/Area for samples 1, 2, 3 and 4 in Figure 1, exhibiting the expected linear dependence. From this figure the RA characteristic of each sample can be extracted: $RA_{SAMPLE\ 1} \sim 0.8\ \Omega.\mu m^2$, $RA_{SAMPLE\ 2} \sim 1\ \Omega.\mu m^2$ and $RA_{SAMPLE\ 3} \sim 15\ \Omega.\mu m^2$ $RA_{SAMPLE\ 4} \sim 50\ \Omega.\mu m^2$. These MTJs, as a current-perpendicular-to-plane device, show a constant (controlled by the MgO barrier). In figure 2 is summarized the dependence of the tunnel magnetoresistance (TMR) on the RA product [3]. A decrease of TMR is observed for samples with thinner MgO, so that the TMR values of the samples with 0.7 and 0.75 nm thick MgO range from 20-50%. For a sample deposited by PVD with a MgO barrier of 1.1 A can reach TMR values of 200%. For the low resistance devices (from sample 1) current induced switching was measured. Figure 3 shows the transfer curve obtained under an external applied magnetic field (TMR 25% RA=0.82 $\Omega.\mu m^2$). Spin transfer was demonstrated (under a constant +35 Oe bias field), at critical current of $2.6x10^7$ A/cm^2, with the same resistance change (25%)

References:

[1] European Patent EP1212777 "Ion Beam vacuum sputtering apparatus and method", M.Davis, G.Proudfoot and D.Pearson (2001)
[2] R. J. Macedo, J. Sampaio, J.Loureiro, P.Wisniowski, S. Cardoso and P. P. Freitas, IEEE Trans.Nanotech. (submitted 2007)
[3] S.Cardoso, R.Macedo, R.Ferreira, A.Augusto, P.Wisniowski and P.P.Freitas, J.Appl.Phys. (in print)

Figures:

Figure 1: Resistance versus 1/A for samples 1, 2, 3 and 4. the insets shows SEM pictures of selected junctions areas.

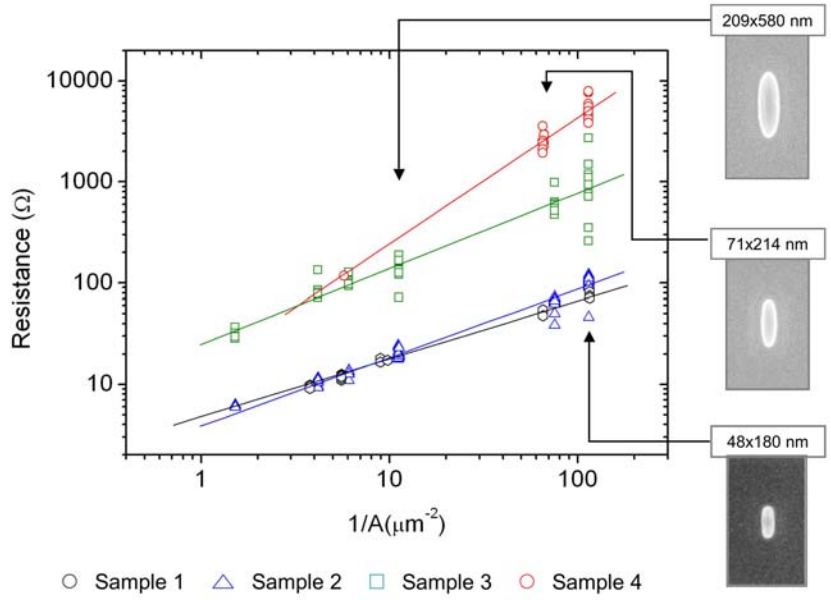

Figure 2: TMR an RA product as a function of MgO barrier thickness**.**

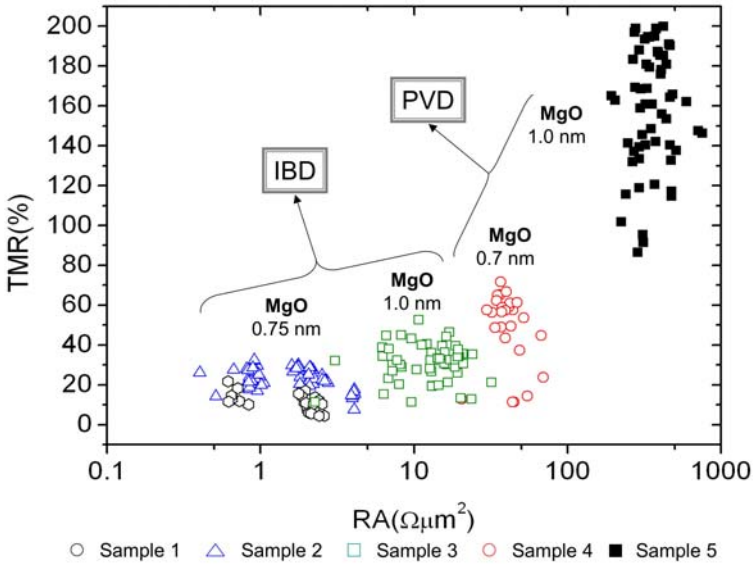

Figure 3: Right:Sample transfer curve.Left: spin transfer switching of the same MTJ element.

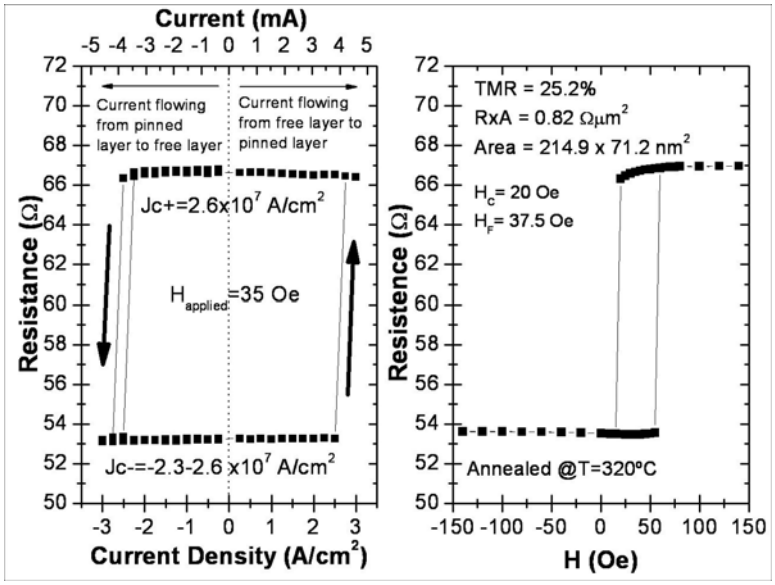

LIQUID-PHASE HYDROGENATION OF UNSATURATED ALDEHYDES: ENHANCING SELECTIVITY OF MWCNT CATALYSTS BY THERMAL ACTIVATION

Bruno F. Machado[1], Helder T. Gomes[1,2], Philippe Serp[3], Philippe Kalck[3], Joaquim L. Faria[1]
[1]Laboratório de Catálise e Materiais, Laboratório Associado LSRE/LCM, Departamento de Engenharia Química, Faculdade de Engenharia, Universidade do Porto, Portugal
[2]Departamento de Tecnologia Química e Biológica, Escola Superior de Tecnologia e de Gestão, Instituto Politécnico de Bragança, Portugal
[3]Laboratoire de Chimie de Coordination UPR CNRS 8241, composante ENSIACET, Toulouse University, France
bmachado@fe.up.pt

Introduction

In a recent review, the importance of carbon nanomaterials as catalytic supports, namely of nanotubes (single- and multi-walled) and nanofibers, was explored [1]. An interesting application of these materials as supports is the preparation of noble metal catalysts for the selective hydrogenation of α,β-unsaturated aldehydes, valuable intermediates in the industrial preparation of fine chemicals. Allylic alcohols, for example, are obtained by the reduction of the carbonyl group and are used in the production of perfumes, flavoring additives, pharmaceuticals and agrochemicals. Selectivity towards unsaturated alcohols is limited by kinetic and thermodynamic reasons but can be improved by creating proper conditions. One of the most important factors is the nature of the active metal phase in the catalyst. Ir and Os are considered to be rather selective while Pt, Ru and Co are only moderately selective [2]. The way these and other metals are dispersed over the surface of the support can also influence the performance of the catalyst. Liquid-phase oxidation with nitric acid is a common technique used to enhance metal dispersion by introducing high amounts of oxygenated surface groups which act as anchoring sites for the metal phase. Some of these remaining groups are often found to negatively influence the catalytic properties of the system. They can be removed by high temperature thermal treatments, which normally affect the dispersion of the metal phase, thus leading to a loss of performance. However, in this study we found the opposite effect for our carbon nanotubes supported catalysts used in the liquid-phase hydrogenation of cinnamaldehyde.

Experimental

Multi-walled carbon nanotubes (MWCNT) were prepared by chemical vapor deposition of ethylene using Fe/Al_2O_3 as catalyst following a procedure described elsewhere [3]. Monometallic catalysts supported on MWCNT oxidized with nitric acid, containing 1 wt. % Pt or Ir were prepared using the wet impregnation technique and characterized by N_2 adsorption isotherms, transmission electron microscopy (TEM), thermogravimetric analysis (TGA) and temperature programmed desorption (TPD). After calcination and reduction, the catalysts were used in the liquid-phase hydrogenation of cinnamaldehyde. The reaction was carried out in a 100 mL stainless steel reactor at 363 K and 10 bar total pressure. Products were analyzed by gas chromatography (DANI-1000, with a column WCOT Fused Silica 30 m, 0.32 mm i.d., coated with CP-Sil 8 CB low bleed/MS 1μm film).

Results and discussion

Following nitric acid oxidation, carbon materials often contain different types and amounts of surface groups, namely carboxylic acid and anhydride, lactone and carbonyl/quinone [4]. According to a technique developed in our group [4] it is possible to identify these oxygenated surface groups by deconvolution of the TPD spectra. These TPD spectra indicate that a post-reduction treatment (PRT) performed at 973 K reduces the concentration of the

oxygenated surface groups. After this treatment only traces of carbonyl/quinone groups (detected in CO desorption spectra) remain on the surface. Metal particle size is an important parameter that could be seriously compromised by this high temperature treatment but H_2 chemisorption measurements corroborated by TEM rule out any significant metal sintering effect. The thermal stability exhibited by the catalysts is based on a strong covalent bond between the carboxylic groups in the oxidized surface and the metal precursor. The PRT had a pronounced effect on both activity and selectivity towards the desired cinnamyl alcohol (COL). According to Toebes *et al.* [5] the adsorption of cinnamaldehyde molecule over Pt/GNF catalysts is conditioned by the amount of oxygen groups present at the support surface and their removal allows the molecule to strongly adsorb over the non-polar support, yielding hidrocinnamaldehyde (HCAL). This explanation is not in line with our observed results, where a Pt/MWCNT catalyst showed an 8 fold increase on selectivity towards COL (conversion of 79%) after the 973 K treatment (Figure 1). Similar results were observed with an iridium catalyst supported in the same MWCNT.

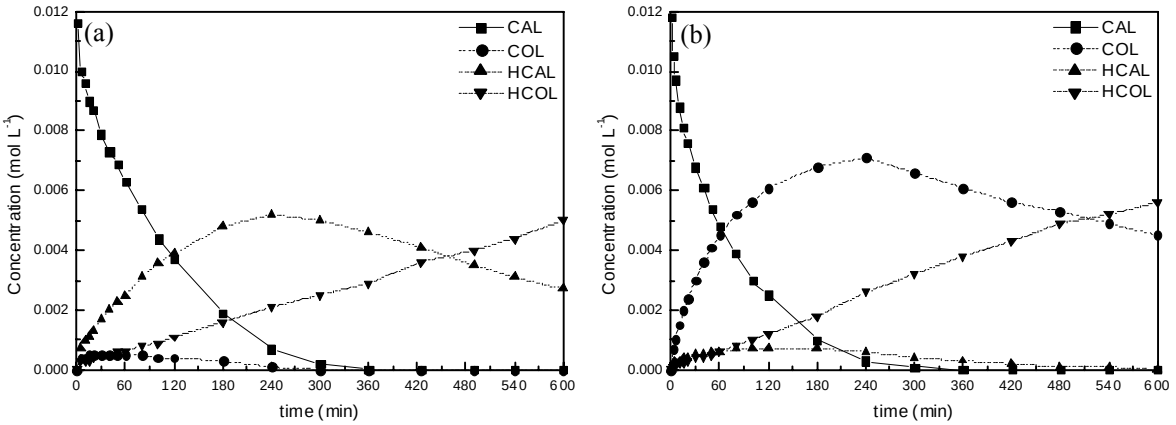

Figure 1 Effect of post-reduction treatment on the conversion and selectivity towards unsaturated alcohol with a 1 wt. % platinum catalyst supported on MWCNT: (a) before PRT; (b) after PRT.

Conclusions

The activation step produces a positive effect on selectivity and enhances the catalytic activity by a factor of 2. Platinum and iridium catalysts proved to be equally selective towards the unsaturated cinnamyl alcohol. Variance with the results in Pt/GNF may result from different orientation of the graphitic planes in both carbon materials, as well as different interaction of the metal phase with the support.

Acknowledgements

BFM acknowledges FCT the PhD grant SFRH/BD/16565/2004. This work was supported by FCT, POCTI/FEDER (project POCTI/1181) and POCI/FEDER (POCI/EQU/58252/2004).

References

[1] P. Serp, M. Corrias, P. Kalck, Applied Catalysis A: General, **253** (2003) 337.
[2] P. Gallezot, D. Richard, Catalysis Reviews-Science and Engineering, **40** (1998) 81.
[3] A. Morançais, B. Caussat, Y. Kihn, P. Kalck, D. Plee, P. Gaillard, D. Bernard, P. Serp, Carbon, **45** (2007) 624.
[4] J.L. Figueiredo, M.F.R. Pereira, M.M.A. Freitas, J.J.M. Órfão, Carbon, **37** (1999) 1379.
[5] M.L. Toebes, T.A. Nijhuis, J. Hájek, J.H. Bitter, A.J. van Dillen, D.Y. Murzin, K.P. de Jong, Chemical Engineering Science, **60** (2005) 5682.

Direct Numerical Simulation of Carbon Nanofibre Composites Under Shear Flow

João M. Maia, Mikio Yamanoi
I3N-Institute for Nanostructures, Nanomodeling and Nanofabrication
Department of Polymer Engineering, University of Minho
4800-058 Guimarães, Portugal
jmaia@dep.uminho.pt ; yamanoi@dep.uminho.pt

The mechanical and transport properties of carbon nanofibres, CNF, in combination with their low production costs make them a promising material for use in polymer composites. However, the level of these properties is largely dependent on the fibres' dispersion state and aspect ratio, which, in turn, depend on the processing history of the composites. Due to strong Van der Waals interactions, CNFs tend to agglomerate, reducing their effectiveness in polymer composites. Applied shear during processing can break up the agglomerates and disperse the CNFs, but excessive shear can lead to fibre breakage, which negatively affects final properties. It is therefore crucial to 'tailor' the level of shear to obtain good dispersion, without fibre length reduction.

The current work studies the effect of simple shear flows (dominant in typical polymer processes) on the dispersion state of CNF composites and consists in a direct simulation method based on the Particle Simulation Method developed by Yamamoto et al. to analyze fiber dispersed systems. In the present work fibers are modelled as a series of connected spheres, with stretching force, torsion and bending torques being considered. Also studied is the effect of van der Waals interactions on the state of aggregation of the nanofibres. In addition our code allows the simulation of the effects of both near-field and far-field hydrodynamic interactions with relatively short computational times.

The method is a very powerful one, currently allowing the semi-quantitative prediction of the dynamics of the fibre suspensions as well as the correct prediction of the kinematics, including some previously unexplained orientation effects observed experimentally.

Modelling of the Optical Spectra of CVD-deposited Silicon Films For Solar Cell Applications

E. Malainho, M. I. Vasilevskiy, J. P. Alpuim, S.A. Filonovich
Centre of Physics, University of Minho, 4710 - 057 Braga, Portugal
id1960@alunos.uminho.pt

In contrast with crystalline solids, the quasimomentum conservation is relaxed for amorphous semiconductors, leading to a substantial difference in their optical properties. The Tauc model [1] was developed for the description of the optical properties of such systems, based on the following assumptions: (i) parabolic shape of the density of states (DOS) in the valence and conduction bands, (ii) relaxation of the *k* selection rule for optical transitions, and (iii) the energy-independent transition matrix element. This model enables one to estimate the optical band gap (E_g) of amorphous materials using the so called Tauc plot, $(\alpha E)^{1/2}$ versus E (α is the absorption coefficient and E the photon energy).

However, despite the Tauc model's simplicity, for materials presenting oscillatory transmittance spectra, the linear fit to the spectral region above the gap is not obvious, bringing a significant uncertainty into the evaluation of E_g. Silicon films with sub-500 nm thickness, deposited on glass substrates for solar cells applications using Chemical Vapour Deposition (CVD), are within such group. Taking this fact into account, the present work has been developed with the scope of modelling the samples' transmittance spectra and the evaluation of E_g of the hydrogenated amorphous silicon (a-Si:H).

First, we introduced some modifications in the traditional Tauc model by taking into account the absorption tail below the gap, produced by the fluctuations of the band edges. We used the approach [2] usually taken for heavily doped crystalline semiconductors with direct band gap, although the energy scale of the tail cannot be obtained theoretically and has to be considered as a fitting parameter in our case. By constructing the imaginary part of the dielectric function ($\hat{\varepsilon}$) of the amorphous silicon from the tail-added joint DOS, the real part of $\hat{\varepsilon}$ was obtained using the Kramers-Krönig relation. Given this, the optical transmittance and reflectance spectra were calculated using the standard approach for multilayer structures taking into account all the multiple reflections at the interfaces.

We have achieved a good agreement between the theoretical and the experimental transmittance spectra. This has enabled us to determine self-consistently the band gap values for a-Si:H films grown in different conditions. The results show that E_g is influenced by the percentage of hydrogen added during the film deposition, since E_g increases with the hydrogen concentration.

References:

[1] Morigaki, K., Physics of Amorphous Semiconductors, Imperial College Press and World Scientific Publishing, (1999).
[2] Shklovskii, B. I., Efros, A. L., Electronic Properties of Doped Semiconductors, Springer, (1984).

Electronic properties of finite single wall carbon nanotubes bonded to $Al_{13}H$ cluster

A. Mañanes[1], F. Duque[1], M. J. López[2] and J. A. Alonso[2]
[1]Departamento de Física Moderna, Universidad de Cantabria, 39005 Santander, Spain
[2]Departamento de Física Teórica, Atómica y Óptica, Universidad de Valladolid, 47011 Valladolid, Spain
angel.mananes@unican.es

We analyze the equilibrium geometries and the electronic properties of finite pieces of single walled carbon nanotubes SWNT when they interact with clusters of metallic elements. We have chosen the magic cluster $Al_{13}H$ which, due to its high stability, could be synthesized and manipulated to modify the properties of electronic nanodevices based on carbon nanotubes.

It is well established that the presence of clusters of metallic elements on SWNTs can produce novel electronic properties as it has been shown in detailed experimental analysis of the interaction between those clusters and SWNTs [1]. Furthermore, recent calculations [2] indicate that the aluminium cluster Al_{13} adsorbed on the walls of SWNTs can appreciably modify the electrical conductance of the system when a molecular species is adsorbed on the active sites of the nanocluster, a modification which is ruled by the charge transfer upon the adsorption of the molecule.

Our calculations are performed within density functional theory using the ADF 2007.01 code. Both LDA and GGA approximations for the exchange correlation energy are considered. We have first analyzed the interaction of the cluster with a graphene sheet to fix the equilibrium distance, 5.38 Å, which we have used as approximate radius for the carbon nanotubes in order to optimize the interaction between the cluster and the nanotube when the cluster is inside the SWNT. Two different finite nanotubes are considered: The armchair (8,8) and the zigzag (14,0), which are simulated using $C_{176}H_{32}$ and $C_{168}H_{28}$ respectively, with the correct symmetry in which the H atoms saturate the dangling bonds of the carbon atoms at the edges. We have calculated, both in LDA and GGA –using revPBE functional- , the binding energy of the cluster to the nanotubes as a function of the distance between their centres. Only the LDA calculations produce a reasonable binding, of around 0.5 eV, and equilibrium distance.

For the equilibrium geometries of the cluster-nanotube system, we have compared the electronic densities of states with those of the clean nanotubes. For example, we present in Figure 1 the electronic DOS of the clean finite (14,0) zigzag nanotube with indication in (a) of the wave functions of the HOMO and LUMO. These states, and others close to them, are edge states located at the boundary zigzag carbon atoms. In Fig. 1(b) the DOS corresponds only to those states which are distributed over the whole nanotube and it is compared with the corresponding to a π-electron tight-binding model. The comparison indicates that the calculated DOS retains certain properties of the infinite tube, in spite of the effects associated with the finite size which show up as more important for the (14,0) zigzag nanotube .

Figure 2 gives the evolution of the energies of the frontier orbitals for the cluster interacting with the (8,8) nanotube in the LDA calculation. The presence of the aggregate induces a large increment in the number of electronic states under the HOMO level with respect to the situation for the clean finite nanotube; the wave functions of these new states are located at the cluster with a very small hybridization with the states at the nanotube. As is indicated in Fig. 2, there is a very small electronic gap in the global system; furthermore the LUMO state results distributed both in the cluster and in the nanotube. The charge transfer obtained, calculated as the Hirshfeld charge, is 0.1 electrons from the SWNT to the cluster, a result that is analogous to previous estimations [2].

References:

[1] Q. Zhao, M. Buongiorno Nardelli, W. Lu, and J. Bernholc, Nano Lett., **5** (2005) 847. T. W. Odom, J-L Huang, Ch. L. Cheung, and Ch. M. Lieber, Science **290** (2000) 1549-1552.
[2] B.-K. Kim, N. Park, P. S. Na, H-M So, J-J Kim, H. Kim, K-J Kong, H. Chang, B-H Ryu, Y. Choi, and J-O Lee, Nanotech., **17** (2006) 496.

Figures:

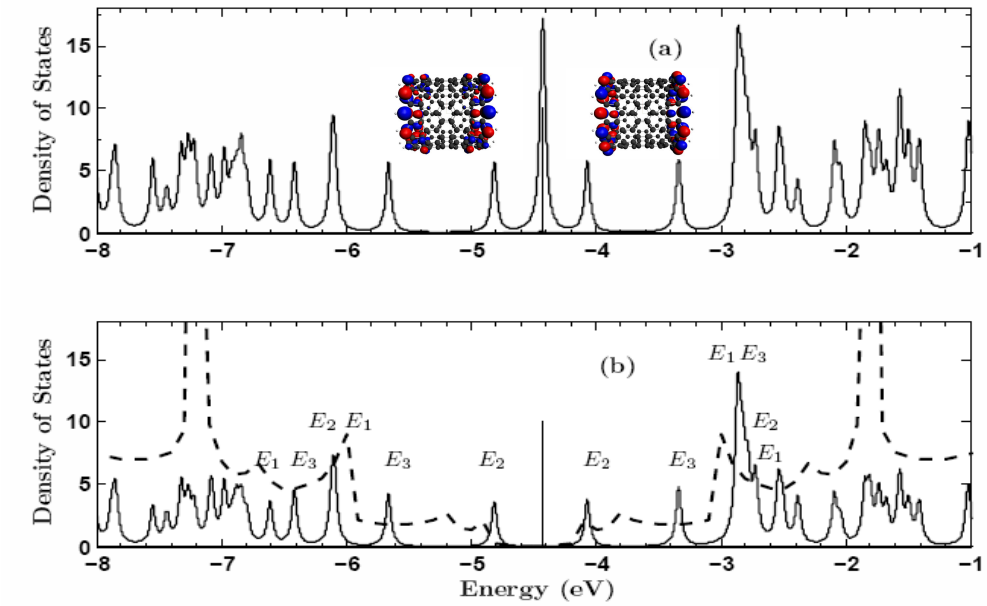

Fig. 1.- Electronic DOS for a finite zigzag (14,0) $C_{168}H_{28}$ SWNT. The total DOS is given in panel (a), where the degenerated HOMO and LUMO are indicated by a vertical line. The insets give the wave functions of the HOMO (left) and the LUMO (right). The DOS obtained by excluding the contributions of the two more external carbon rings are given in panel (b). The dashed curve gives the DOS of a p-tight binding model for an infinite nanotube. The labels in (b) correspond to the D_7 symmetry of the system.

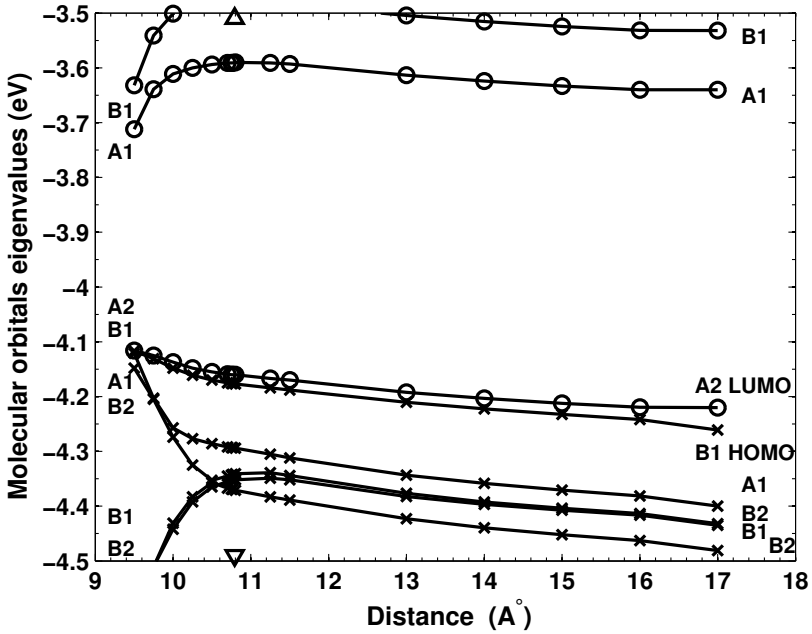

Fig. 2.- LDA eigenvalues of the frontier molecular orbitals as a function of the distance between the cluster and the (8,8) finite nanotube. The labels of the orbitals correspond to the global C_{2V} symmetry of the system. The small triangles indicate the equilibrium distance.

ELECTROCHEMICAL GENOSENSORS LABELLED WITH CdS QDs

Sergio Marín Mancebo[1,2], *Maria Teresa Castañeda*[1,2], *Salvador Alegret*[2], *Arben Merkoçi*[1]
[1] *Institut Català de Nanotecnologia,* [2]*Grup de Sensors i Biosensors,*
Universitat Autònoma de Barcelona
Barcelona, Catalonia, Spain
Sergio.marin@uab.cat

The enormous information generated in the Human Genome Project has prompted of DNA sensors and high-density DNA arrays.
Nevertheless the biological researches as well as other application fields need a broader range of more reliable, more robust labels so as to enable high-throughput bioanalysis and determination of multiple-molecule types presents in a sample. The existing labelling techniques have several drawbacks; the markers used have short life-time and have a limited number of combinations that practically can be used for simultaneous analysis of various analytes.
It is possible to "bare-code" DNA and proteins, using metal nanoparticles like quantum dots (QD). The basic concept relies on finding a way to develop a large number of smart nanostructures with different electrochemical properties that have molecular-recognition abilities and built-in codes for rapid target identification.
Nanoparticles-based materials offer excellent prospects for DNA analysis, owing to their many attractive properties [1] .An electrochemical genomagnetic hybridization assay has been developed to take advantage of an efficient magnetic separation/mixing process. It represented on example of coupling a magnetic isolation with electrochemical detection of DNA hybridization. The new protocol employs linked sandwich solution hybridization, with a magnetic-particle labeled probe hybridizing to biotinylated DNA prove that captures a streptavidin. A simple method use the detection DNA is based on screen-printed electrodes and handheld potentiostatic device. The detection is based on the stripping of electrochemical reduced cadmium at hybridization solution by using the square wave voltammetry.

References:

[1] Arben Merkoçi, Sergio Marín, María Teresa Castañeda, Martin Pumera, Josep Ros, Salvador Alegret, Nanotechnology, **17** (2006) 2553-2559

PRELIMINARY STUDIES CONCERNING THE RHEOLOGICAL STABILITY OF CERTAIN PHARMACEUTICAL FORMULATIONS WITH CONTROLLED ACTION IN THE FIELD OF NANOMEDICINE

RODICA SIRBU*, MARIS MARIA* , DAN ARTENIE MARIS*, MINODORA LECA, ANAMARIA BECHIR*, EMILIA MIHAELA CADAR*****

**"Ovidius" University of Constanta, Faculty of Pharmacy, Romania*
*** University of Bucharest Romania****
30 - School of Constanta, Romania

Nanomedicine is a field which requires elaborated studies with a view to explaining, understanding and treating multiple diseases widely spread among humans.

The fundamental substance of the gum chorion, by its chemical composition and the polymerization degree of its macro-molecules favour cellular movement and the distribution of biologically active substances. This important characteristic of the fundamental gum substance allows us to use collagen gels mixed with active ingredients in the extracts from marine algae in innovative parodonthal biotherapy.

In order to obtain therapeutic effects at nanostructure level, it is important to know the rheological characteristics of the relevant mixtures of collagen gels and extracts from marine algae selected for use, [1,2,3].

In this survey we have studied mixtures made of non-denatured fibrillar collagen hydrogels where different concentrations of marine algae have been incorporated.

The gels studied are shown in table 1

Table 1. Collagen gels without/with prepared extracts from algae,

Alga extract	The gel's aspect	No. Samples
Without alga extract	Colourless, clear Colourless, clear Colourless, barely opalescent	SAMPLE 1 SAMPLE 2 SAMPLE 3
Brown alga CYSTOSEIRA BARBATA	Opalescent, yellowish green More opalescent, brownish yellow	SAMPLE 1 SAMPLE 2
Green alga ULVAE LACTUCA	Clear, barely green Barely opaque, barely green	SAMPLE 1 SAMPLE 2
Red alga CERAMIUM RUBRUM	Barely opalescent, yellowish green A degree more opalescent, brownish yellow	SAMPLE 1 SAMPLE 2

Gels in table 1 have been subjected to the rheological measurements at 25 ± 0.1^0C, after at least 15 minutes of thermostatic treatment at the above-mentioned temperature. To this effect, we have used a rotation viscosimeter Haake VT 550 with coaxial cylinders, which is capable of developing a shearing speed, $\dot{\gamma}$, with values between 0.6 and $3.0.10^4$ s^{-1}, of measuring shearing tensions, τ, with values between 1 and 10^5 Pa and, depending on the sensors system used, of measuring apparent viscosities, η^*, between 1 and 10^9 mPa.s.

Based on the data obtained for the shearing tensions, we have traced the rheograms – the diagrams for shearing tensions depending on the shearing speed values – from which we have calculated the apparent viscosities as ratios between shearing tension and speed values, which have been figured in relation to the shearing speed values, with a view to levelling dependency.

Table 2. Characteristics of 0.6 % collagen gels which contain extract of CYSTOSEIRA BARBATA

Extract content in gel, % (g/100g gel)	Viscosity at zero shearing speed, mPa.s	Rheological behaviour
5	2084,97	Pseudoplastic
10	2813,94	Pseudoplastic

Table 3. Characteristics of 0.6 % collagen gels which contain extract of ULVAE LACTUCA

Extract content in gel, % (g/100g gel)	Viscosity at zero shearing speed, mPa.s	Rheological behaviour
5	3248,96	Pseudoplastic
10	2978,05	Pseudoplastic

Table 4. Characteristics of 0.6 % collagen gels which contain extract of CERAMIUM RUBRUM

Extract content in gel, % (g/100g gel)	Viscosity at zero shearing speed, mPa.s	Rheological behaviour/Remarks
5	2386,59	Pseudoplastic
10	3065,66 2656,64	Pseudoplastic, with all points Value without the final point

The rheograms have shown the type of rheological behaviour for each gel. Tables 2, 3 and 4 show the characteristics of 0.6% collagen gels, with the selected marine algae types.

Based on the studies performed, we can reach certain conclusions as to the stability of mixtures in time, as well as certain associations concerning the possibility to transfer active ingredients to the affected tissues.

References

[1] M.-T. Sheu, J.-C. Huang, G.-C. Yeh and H.-O Ho, Biomaterials **22**, 1713 (2001).
[2]J. B. Parks, Biomaterials: Principle and Applications, CRC Press, Boca Raton, 2002.
[3 S. Yunoki, T. Suzuki and M. Takai, J. Biosci. Bioeng. **96**, 575 (2003).

IN SITU DIFFRACTION STUDY OF HIGH-PRESSURE TRANSFORMATION OF C_{60} TO DISORDERED sp^2-CARBON

L.Marques * , M. Mezouar# and J-L. Hodeau§*
**Departamento de Física and Ciceco, Universidade de Aveiro 3810-193, Portugal*
 # E.S.R.F., 38043 Grenoble, France
§ Institut Néel C.N.R.S., 38043 Grenoble, France
lmarques@ua.pt

C_{60}-2DR polymer amorphisation under high pressure has been studied by in situ diffraction techniques employing the Paris-Edinburgh press. The initial interest of this study was to find structural signatures of the so-called magnetic carbon phase, which would be formed by the C_{60}-2DR polymer phase close to the molecular collapse. Evolution of the transformation process was followed by 2D angular-dispersive diffraction. The recorded diffraction patterns show that the C_{60} polymer phase gradually amorphises into a disordered sp^2-carbon phase. Changes in the diffraction pattern of the 2DR C_{60} polymer during the amorphisation transition, which would be indicative of the magnetic phase, were not perceived. This must be confirmed by detailed data analysis, under way.
Samples quenched at different levels of transformation were recovered in order to perform x-ray diffraction and complementary magnetization measurements. Diffraction patterns of the partial amorphised samples show that both the amorphous sp^2 carbon and the 2DR C_{60} polymer are highly oriented. This indicates an orientational relationship between the parent polymeric structure and the amorphous transformed structure: the graphitic planes and C_{60} polymerized planes have a precise orientational relationship typical of martensitic transformations. Therefore C_{60} molecules amorphise in a way that does not involve the complete collapse of the cage structure, in contrast to what one would expect. More experimental data is needed to obtain the full orientational relationship between parent, 2DR C_{60}, and transformed, sp^2 carbon, structures.

Carbon nanotubes growth from L-type and AlPO4-5 zeolites by thermal chemical vapour deposition

I. Martín [a], *G. Rius* [a], *P. Atienzar* [b], *L. Teruel* [b], *N. Mestres* [c], *F. Pérez-Murano* [a], *H. García* [b], *P. Godignon* [a], *A. Corma* [b], *E. Lora-Tamayo* [a]

[a] *Centro Nacional de Microelectrónica (CNM-IMB, CSIC), Campus UAB, Bellaterra, SPAIN.*
[b] *Instituto de Tecnología Química (ITQ), Av. de los naranjos s/n, Valencia, SPAIN.*
[c] *Instituto de Ciencia de Materiales de Barcelona (ICMAB),Campus UAB, Bellaterra, SPAIN.*
inigo.martin@cnm.es

The use of Carbon Nanotubes (CNTs) is considered as one of the most promising alternatives for the fabrication of nanoelectronic devices. However, there are two main technological difficulties that need to be solved: control over the chirality of the nanotubes and their placement at desired positions in a determined direction on the substrate.

The first approach for controlling the CNTs structure consists in obtaining narrow distributions in diameter of the nanotubes. For this aim, it is necessary to control the size of the catalyst particle. However, although patterned growth of CNTs can be afforded through Chemical Vapour Deposition (CVD) growth by a selective deposition of catalyst, the nanotube growth direction cannot be controlled in batch synthesis.

Zeolites are crystalline microporous materials that have ordered and oriented pores of less than 2 nm in diameter [1]. These materials are an option for CNTs controlled growth as their pores can be used as a container for catalyst and as a guide for CNT growth.

We have studied growth of CNTs by CVD when placing the catalyst inside L-type (Fig.1 (a)) and AlPO4-5 (Fig.1 (b)) zeolites. The pore diameter is 0.71 nm and 0.73 nm for the L-type and the AlPO4-5 zeolites respectively. Fe/Co was used as catalyst in both types of zeolites. Fe/Co particles, up to 2.5% of the total mass, were introduced in the pores of the L-type zeolites. In the case of AlPO4-5 zeolites, 1% of the atoms forming the structure were substituted by catalyst ones. Zeolites were then dispersed in ethanol and the solution was spin coated on Si substrates. Growth of CNTs was performed in a Rapid Thermal CVD system where temperature ramps up to 30ºC/s can be applied. Process temperature was maintained in each experiment at 800ºC. CH_4 was injected as the carbon containing gas, and H_2 as the supporting gas that activates the formation of the CNTs.

SEM images and Raman spectra in Fig.2 and Fig.3 demonstrate growth of CNTs from L-type and AlPO4-5 zeolites. In the case of L-type zeolites, either small densities of SWCNTs (Fig.2 (a)) or high densities of CNTs (Fig.2 (b)) have been obtained. E-beam etching of the zeolite (inset in Fig.2 (a)) has demonstrated SWCNTs grow from inside the zeolites. In the case of AlPO4-5 zeolites, although there is no SEM evidence of CNTs growth (Fig.3 (a)), Raman spectra (Fig.3 (b)), which is in accordance with ref. [2,3], confirms growth of 0.420 nm and 0.397 nm in diameter SWCNTs.

In conclusion, we have been able to grow SWCNTs in the porous of L-type and AlPO4-5 zeolites, as the first step for the batch synthesis of oriented nanotubes at wafer scale. In parallel, the fabrication of specific surface patterns for selective and oriented deposition of L-type zeolites on the substrate is being examined. When zeolites deposition parameters will be optimized, we will be able to control the location, direction and the density of CNT growth on a substrate.

References:

[1] Ch. Baerlocher, W.M. Meier and D.H. Olson, "Atlas of Zeolite Framework Types", 5th ed., Elsevier: Amsterdam, 2001.
[2] Yu, G.J., et al., Diamond and Related Materials, **15** (2006), 1261.
[3] Zhai, J.P., et al., Carbon, **44** (2006), 1151.

Figures:

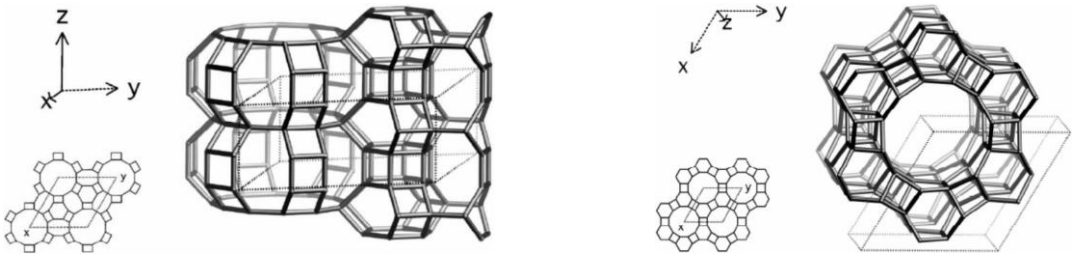

(a) **(b)**

Fig. 1: Frameworks viewed normal to [001] and projection down [001] on the bottom left corner for L type zeolites in (a) and AlPO-5 type zeolites in (b). [1]

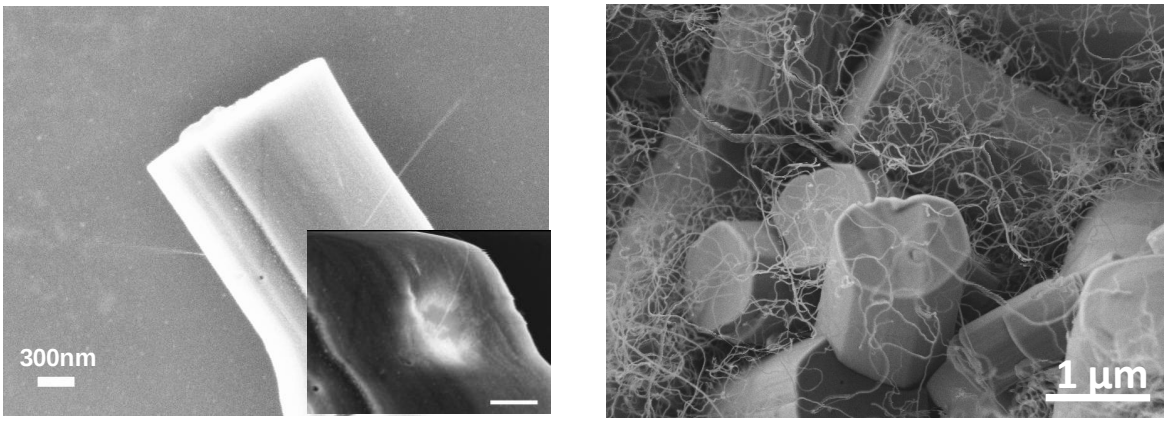

(a) **(b)**

Fig.2: SEM images of CNT growth from L-type zeolites. In (a), growth of small density of SWCNTs. An E-beam etching of the zeolite demonstrates CNTs grow from inside the pores. In (b), high density of CNT growth.

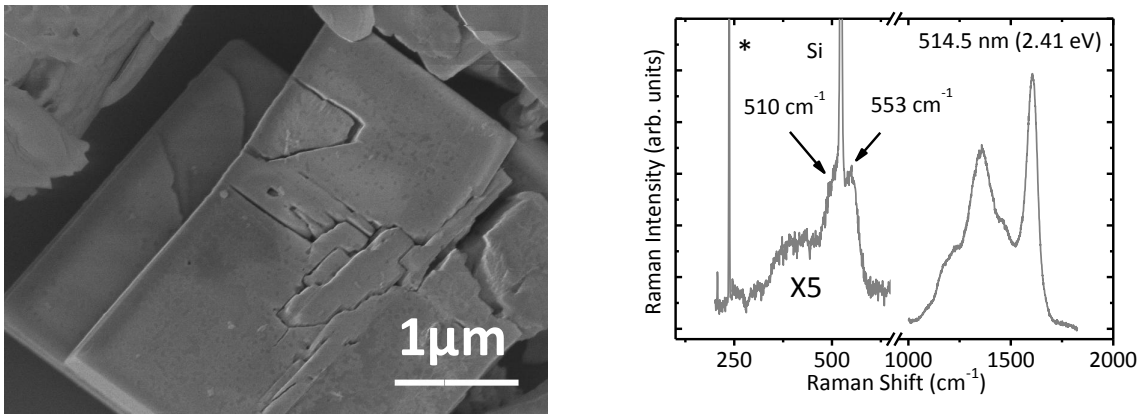

(a) **(b)**

Fig.3: SEM image (a) and Raman spectra (b) of AlPO4-5 zeolites after CVD process. Peaks in the Raman spectra at 510 cm^{-1} and 553 cm^{-1} indicate growth of 0.420 nm and 0.397 nm in diameter SWCNTs.

NANOBIOSENSOR FOR GLUCOSE BASED ON CHEMICALLY MODIFIED GLUCOSE OXIDASE LABELLED TO MAGNETIC NANOPARTICLES.

Natalia Martínez de Baroja[1,2], Pilar Faustino[1,2], Valeria Grazú[2], Susana de Marcos[1,2],Jesús M. de la Fuente[2] and Javier Galbán[1,2]

[1)]GBA (Analytical Biosensors Group), Analytical Chemistry Department, Faculty of Sciences, University of Zaragoza (Spain). [2)]INA (Institute of Nanoscience of Aragon) University of Zaragoza (Spain).

natmtz@unizar.es

In recent years our research group has used the spectroscopic properties of chemically modified enzymes with fluorophores (figure 1), in order to develop analytical methodology for the design and construction of autotransducer biosensors that could be used *in vivo.* The best results were obtained with the fluorescein derivative fluorescein-5(6)-carboxamido-caproic acid N-hydroxy-succinimide ester (FS), which produces changes in fluorescence, at wavelengths of the FS, which are proportional to the concentration of the corresponding substrate (analyte) and the system is reversible. In previous work, the research group has developed an enzymatic biosensors of chemically modified Glucose Oxidase (GOx-FS) immobilised on polyacrylamide [1].

Nanoparticles, can be channelled in a biological fluid, directed by the action of an external magnet to low tissue thickness and be maintained in these areas, without causing any deterioration in the body, so they could be used as a basis of a subcutaneous support for non-invasive nanobiosensors. In this work we are presenting the first results obtained using GOx-FS linked to magnetic nanoparticles (figure 2).

Magnetite magnetic nanoparticles were synthesized according to the Tago [2] protocol. Previous to enzyme immobilisation, the magnetic nanoparticles were functionalised with DMSA (dimercapto succinic acid) in order to keep them in solution.

The immobilisation of GOx-FS to nanoparticles (Np) was conducting by the –COOH terminal groups of the DMSA and $–NH_2$ groups of the enzyme. There were studied two different alternatives: a) protecting the –SH terminal groups of DMSA with 2-PDS in order to avoid competitive reaction, and b) without protection of the –SH groups. Best results were obtained by protecting the –SH groups and direct reaction of Np and GOx-FS at pH 5. After 5 minutes of reaction about 100% of GOx-FS was labelled to Np and the enzyme activity remaining at about 100%. It was also observed a change on fluorescence signal of GOx-FS-Np according to glucose concentration. A theory justifying the two different GOx-FS-Np immobilization procedures have been developed and it is being experimentally demonstrated. Simulation studies for “in vivo” determination of glucose are being carried out.

Acknowledgements. This work was supported by the Ministry of Education and Science (MEC) of Spain within the project CONSOLIDER-INGENIO 2010 **NANOBIOMED**, and by the University of Zaragoza within the project UZ2007-CIE-11 which is gratefully acknowledged. JMF thanks ARAID for financial support.

References:

[1] V Sanz, J Galbán, S de Marcos and JR Castillo, Talanta, **60** (2003), 415.
[2] T. Tago, et al, J. Am. Chem. Soc., **85**, (2002) 2188.

Figure 1: Change on fluorescence signal of GOX-FS (6.5 UI / ml) according to glucose concentration. Blue line: 1000 µg / ml and red line: 250 µg / ml.

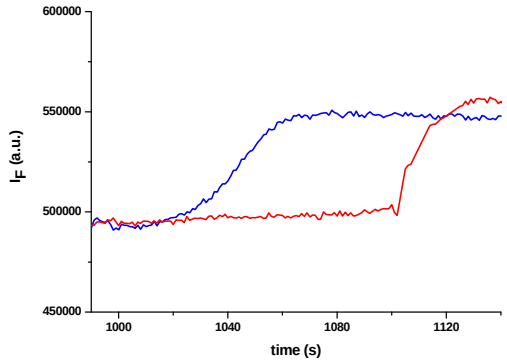

Figure 2: Change on fluorescence signal of GOX-FS-Np (6.5 UI / ml) according to glucose concentration. Blue line: 1000 µg / ml and red line: 250 µg / ml.

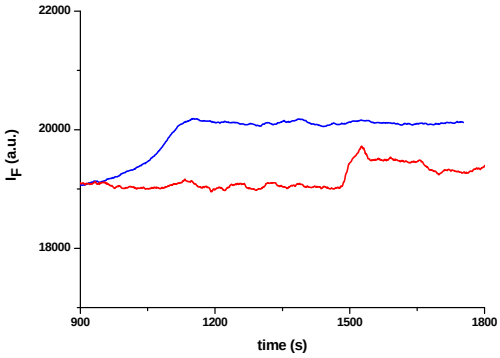

Size-dependent magnetic properties of magnetoferritin

Mª José Martínez[a], *C. Carbonera*[a], *R. de Miguel*[b], *M. Martínez-Júlvez*[b], *A. Lostao*[b], *C. Piquer*[a], *C. Gómez-Moreno*[b], *J. Bartolomé*[a], *and F. Luis*[a]

[a]*Instituto de Ciencia de Materiales de Aragón, CSIC-Universidad de Zaragoza, 50009 Zaragoza, Spain*

[b]*Instituto de Nanociencia de Aragón (Zaragoza Univ.) and Dep. de Bioquímica (Zaragoza Univ.), c/Cerbuna 12, 50009 Zaragoza, Spain.*

fluis@unizar.es

Ferritin is the iron storage protein of living beings from bacteria to mammals [1]. In its natural form, each ferritin molecule stores about 4500 Fe atoms in a weakly magnetic nanoparticle of ferrihydrite. In 1991, it was shown that the cavity of the apo-ferritin, i.e. the empty form of the protein, can be used as a confined reaction vessel to synthesize nanoparticles of maghemite (magnetoferritin) [2]. Since then, other oxides, like Co_3O_4 and also metals like Cu, Pd, Ni, Cr, Co, CoPt, etc, have been prepared [3]. In this contribution, we report a detailed experimental study of the structure, morphology and magnetic properties of magnetoferritin. By controlling the amount of iron added to an aqueous solution of apo-ferritin, it is possible to control the particle's average diameter D from 2 nm up to more than 6 nm (Fig. 1). Chemical analysis, X-ray diffraction, and Mössbauer spectroscopy data are compatible with the formation of maghemite γ-Fe_2O_3. TEM images (see Fig. 2), suggest that the nanoparticles grow from the protein's wall towards the centre of the cavity, and only tend to become spherical when the molecule becomes nearly full. The magnetic susceptibility shows the typical superparamagnetic behaviour (Fig. 3) with a magnetic freezing below a blocking temperature T_b that increases with the average particle's size. From the combined analysis of the susceptibility curves and the magnetization isotherms, we have extracted the distribution of magnetic moments. The comparison of these data with the distribution of sizes obtained from TEM (inset of Fig. 1) reveals the existence of a large disorder in the inner magnetic structure of the particles. This disorder, which becomes larger with decreasing size, leads to a smaller magnetic moment than what would be expected for a perfect alignment of spins. A scaling analysis of the ac susceptibility similar to that described in [4] enables us to extract the magnetic anisotropy constant K. It is found to be much larger than the anisotropy ($\approx 4.7\times10^4$ erg/cm^3) of bulk maghemite and to increase with decreasing D. These results indicate that the magnetic properties of magnetoferritin are largely influenced by the surface. This influence is probably enhanced in the present case by the special mechanism of particle growth. Indeed, for low iron contents, the nanoparticles have a very large surface to volume ratio and probably a considerable degree of structural disorder as well. The enhanced anisotropy is probably due

to the existence of low-symmetry surface atomic sites. This interpretation is confirmed by the observation of a component in the Mössbauer spectra associated with a very large quadrupolar splitting $\Delta E_Q \approx 0.96$ mm/s, whose intensity increases with decreasing size.

References:

[1] G. C. Ford *et al*., Philos. Trans. R. Soc. London Ser. B **304**, 551 (1984); E. P. Bauminger and I. Nowik, Hyperfine Interactions **50**, 489 (1989).

[2] F. C. Meldrun, B. R. Heywood, and S. Mann, Science **257**, 522 (1992); K. K. W. Wong, T. Douglas, S. Gider, D. D. Awschalom, and S. Mann, Chem. Mater. **1998**, 279.

[3] B. Warne et al., IEEE Trans. Magn. **36** (5), 3009 (2000); M. Okuda, K. Iwahori, I. Yamashita, H. Yoshimura, Biotechnology and Bioengineering **84** (2), 187 (2003); T. Ueno et al., Ang. Chem.-Int. Ed. **43** (19): 2527, (2004); N. Gálvez, P. Sánchez, J. M. Domínguez-Vera, Dalton Transactions **15**, 2492 (2005); N. Gálvez *et al*., J. Mater. Chem. **16**, 2757 (2006); R. Tsukamoto, K. Iwahori, M. Muraoka, I. Yamashita, Bull. Chem. Soc. Jpn **78**, 2075 (2005).

[4] F. Luis *et al*., Phys Rev. B **65**, 094409 (2002).

Figures:

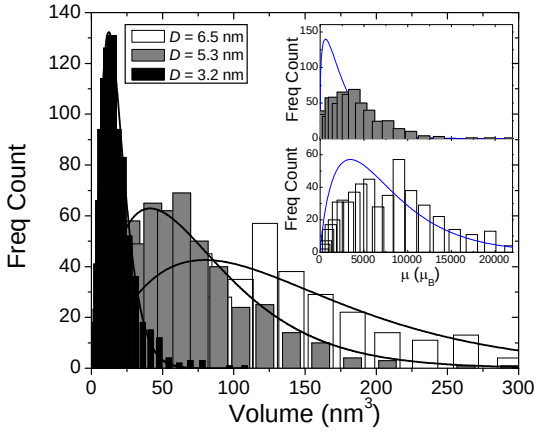

Figure 1: Distribution of particle sizes of three magnetoferritin samples. The inset compares two of these distributions with the corresponding distributions of magnetic moments obtained from the magnetic measurements (solid lines).

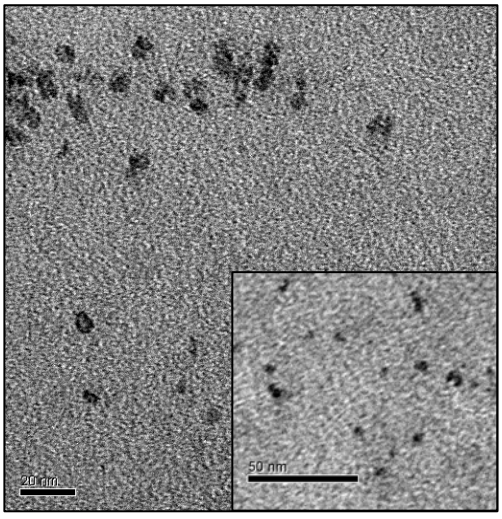

Figure 2: TEM image of a magnetoferritin sample with D = 6.5 nm. The inset shows the typical shape of the nanoparticles of the sample with D = 3.2 nm.

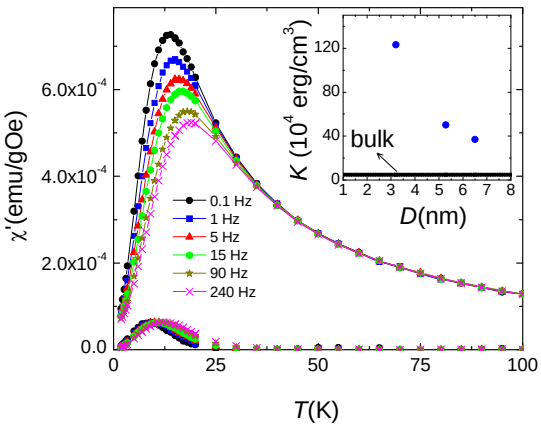

Figure 3: Ac susceptibility data of the D = 3.2 nm magnetoferritin nanoparticles. The inset shows the magnetic anisotropy constant of magnetoferritin as a function of the average particle's size

ELECTROCHEMICAL SYNTHESIS OF MAGNETITE NANOPARTICLES COATED OF METHYLENE BLUE

M. Martinez[1], D. Reyman[1], L. Cabrera[1,2] and P. Herrasti[1]
[1]Universidad Autónoma de Madrid, Cantoblanco s/n, Madrid 28049, Spain
[22]IIC, Universidad de Guanajuato, Cerro de la Venada s/n 36040, Guanajuato, México
dolores.reyman@uam.es

Methylene blue is a photosensitizer used in photodynamic therapy because this drug can generate singlet oxygen [1]. This very aggressive chemical species will very rapidly react with any nearby biomolecules which can irreversibly damage the treated tissues. On the other hand, these nanoparticles could also be used as magnetic resonance imaging contrast agent for tumour detection or for hyperthermia therapy [2]. The result is a single particle platform that combines therapy and diagnostic possibilities at the same time.

Our proposal is to oxidize electrochemically Fe to form magnetite nanoparticles in the presence of ammonium surfactants and methylene blue. The nanoparticles generated are coated by these compounds where the surfactants prevents them from aggregating, methylene blue confers them with fluorescent properties

The system consists of a two neck electrochemical cell where two Fe electrodes of purity 99.5% were placed. These two electrodes must be at a distance of approximately 1 cm. One of the electrodes was used as a sacrificial anode and was subjected to a current of 100 mA/cm^2; its oxidation resulted in the formation of magnetite [3].

The generated material was characterized by characterized by microscopy (TEM and fluorescence confocal) and spectroscopic techniques (X-ray diffraction, Raman, UV-Vis, and FT-IR).

The results show that when the reaction takes place only in the presence of surfactant the average size of nanoparticles is about 30 nm; when the concentration of surfactant is lower, and the concentration of methylene blue is increased, nanoparticles size increases, to values of about 70 nm. When only methylene blue is used as the electrolyte, there is no formation of nanoparticles. This is due to the polymerization of methylene blue on the surface of the Fe, preventing further oxidation of the metal. The nanoparticles formed in the presence of methylene blue were fluorescent when tested by a confocal microscopy. X-ray spectra of these material indicated the presence only of magnetite and no impurities was observed. The analyses by UV-visible and FT-IR spectroscopy confirmed the presence of methylene blue in the generated nanoparticles.

References:

[1] Tada, DB; Vono, LLR; Duarte, EL, et al., Langmuier, **23** (2007) 8194
[2] Xiao, GN; Man, SQ, Chem. Physcs. Letts. **447** (2007)

[3] Cabrera, L; Gutiérrez, S; Menéndez, N; Morales, MP; Herrasti, P, Electrochim. Acta., **53** (2008) 3436

Aknowlegments

The authors acknowledge the Spanish M.E.C. (CTQ2005-04469/BQU) and the Comunidad de Madrid project S-0505/MAT/019, as well as Nanospain2008 Conference for the assistantship granted to the author.

ORDERED STRUCTURES IN POLYMER MELTS

José A. Martins, Weidong Zhang
Departamento de Engenharia de Polímeros, Universidade do Minho, Campus de Azurém
4800-058 Guimarães, Portugal
CICECO, Universidade de Aveiro, 3810-193 Aveiro, Portugal.
jamartins@dep.uminho.pt

Nanoconfined macromolecules interact with their confinement when the confinement dimension is comparable to the chain's radius of gyration and to its contour length. Examples of these effects are the T_g depression of polystyrene thin films with a thickness lower than 600 Å [1], the change of the spherulitic morphology when the film thickness is $d > 2\ R_g$ (radius of gyration), to a dense-branch morphology and dendrites when $R_g < d < 2\ R_g$, and an "islands" structure when $d < R_g$ [2]. Also, the channels' dimension affects the flow of macromolecules. Recent microfluidic and nanofluidic experiments have clearly demonstrated these effects.

A physical understanding, at a molecular scale, of nanoconfinement effects requires knowledge of polymer melt morphology, its change with flow fields and the effect of this morphology on the solidification process. This implies understanding the effects that topological constraints, called entanglements, have on the melt morphology. In this work it shown that ordered structures exist in polymer melts, both quiescent and sheared, and that the effect assigned to topological constraints should be assigned instead to local ordered regions. These regions are, in fact, the precursor structures for crystallization of semicrystaline polymers and they also affect the solidification of amorphous polymer determining the nature of the glass transition [3].

The demonstration that topological constraints do have any effect on the flow behaviour and properties of long chain macromolecules is based on the evaluation of the different factors contributing to the flow activation energy. It was shown that the contributions to this energy are the local and correlated conformational energy jumps and an additional contribution resulting from the interaction potential energy between adjacent chain segments. It was shown that crossing of chains or their partial looping have a negligible contribution to the flow activation energy because the interaction potential energy of these constraints is similar to the thermal energy at the melt temperature. The Kuhn monomer friction coefficient was evaluated from first principles and, contrary to common assumptions, it was also shown it does not play any role in the flow behaviour of macromolecules. To do this evaluation it was considered that, at a molecular scale, the friction results from the drag between adjacent chains segments, and that to slide adjacent and parallel chain segments they must gain energy enough to surmount first their interaction energy and to change further their conformational states. The monomeric friction coefficient is then defined as the product of the ratio between the interaction energy of the segments and their interacting area by their relaxation time, which depends on two energy barriers: an energy barrier for local and correlated conformational transitions and an additional energy barrier resulting from the van der Waals interactions between adjacent chains segments. Evaluations for the monomeric friction coefficient based on the above reasoning agree with previous evaluations for this relaxation time based on the relaxation spectrum and on the relationship between different relaxation times.

Table I illustrates the evaluations mentioned above. Information for flow activation energy and reptation time was obtained from ref. [4]. Figure 1 indicates the variation of the difference between the flow activation energy and the energy barrier for local and correlated

conformational transitions and a function of temperature and length of the ordered structures. The length of ordered structures increases with the temperature decrease. The predicted value at the glass transition temperature is 630 Å, which agrees with the predicted growing length scale with the approach of glass transition, which is around 5 to 20 molecular diameters [5].

Similar information is obtained for semicrystalline polymers. It is indicated in Fig. 2. Ordered regions at the molten state have dimensions around 40 Å. They are the precursor structures for crystallization. Their length increases with the lowering of temperature reaching a value around 50 Å (below the typical lamellar thickness) at the crystallization temperature. During shear these structures are aligned with the flow direction. The maximum alignment is reached at steady state. The strain need to reach this state decreases with temperature, confirming the predictions of Figs. 1 and 2 [4]. Crystallization of melts sheared up to steady state saturates [4]. They have lower number of constraints than unsheared melts (around 2/3) [4]. This result demonstrates a flaw on existing theories for the flow of polymer melts [4]. All models, except those based on the slip-link concept, assume a constant number of topological constraints.

References:

[1] C. J. Ellison, J. M. Torkelson, Nature Materials, **2** (2003) 695.
[2] Q. Congde *et al.*, Acta Polymerica Sinica, **8** (2006) 964.
[3] J. A. Martins, Etanglements – the Ether of Polymer Physics, submitted.
[4] J. A. Martins, W. Zhang, A. M. Brito, Macromolecules **39** (2006) 7626.
[5] L. Berthier *et al.*, Science **310** (2005) 1797.

Acknowledgments: The author acknowledges the Portuguese Foundation for the Science and Technology under the framework of POCTI and FEDER programs for funding the projects POCTI/CTM/46280/2002, PTDC/CTM/68614/2006 and BPD/5517/2001.

Table I. Energy barriers, interaction potential energy, friction coefficient and different relaxation times for linear chains of PS. To agree with literature information, all temperature dependent values were evaluated at 463.15 K. For PS at 443 K, the value evaluated for ζ_o is 9.52 x 10^{-9} kg/s and literature values range from 1.56 x 10^{-8} to 3.02 x 10^{-8} kg/s.

	PS
M_w (kg/mol)	271.0
M_w/M_n	2.0
E_{flow} (kJ/mol)	95.5
$\Delta E_{cf.}$ (kJ/mol)	70.0
L_{ring} (Å)	39.1
n_{mon}	15
W_{ring} (kJ/mol)	-0.89
l_k (Å)	18
W_{lk} (kJ/mol)	-0.80
$\zeta_{o,lit}$ (kg/s)	1.12 x 10^{-10}
ζ_o (kg/s)	4.04 x 10^{-9}
τ_k (s)	1.01 x 10^{-5}
l_{or} (Å)	550
W_{or} (kJ/mol)	25.1
τ_{rept} (s)	0.57

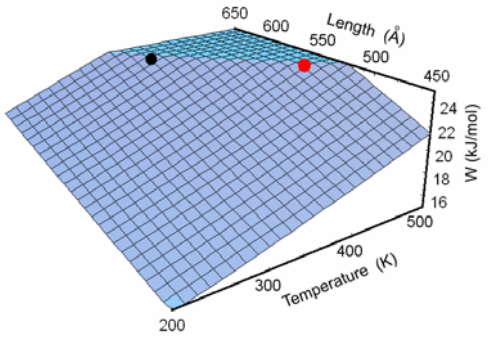

Fig. 1. Variation of the interaction potential energy of local ordered regions in the melt for linear polystyrene as function of temperature and length. At 463.15 K their length is 550Å (red circle). At the typical glass transition temperature of PS (363.15 K) their dimension is 630 Å (black circle).

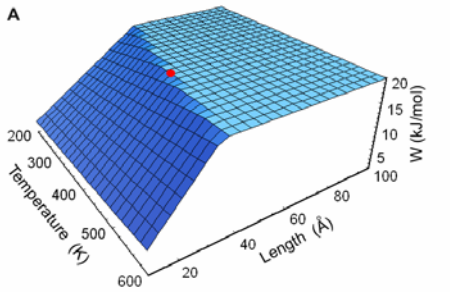

Fig. 2. Variation of the interaction potential energy of local ordered regions in the melt for linear polyethylene as function of temperature and length. After cooling from the molten state PE crystallizes at around 393 K (red circle).

ELECTROSPUN NANOFIBROUS STRUCTURES AS SCAFFOLDS FOR CONNECTIVE TISSUES REGENERATION

Albino Martins[1,2,], José V. Araújo[1,2], Marta Alves da Silva[1,2], Elisabete D. Pinho[1,2], Alexandra P. Marques[1,2], Rui L. Reis[1,2], Nuno M. Neves[1,2].*

*[1]3B's Research Group – Biomaterials, Biodegradables and Biomimetics, University of Minho, Campus de Gualtar, 4710-057 Braga, Portugal; [2]IBB - Institute for Biotechnology and Bioengineering, Braga, Portugal. *e-mail: amartins@dep.uminho.pt*

Fibrous structures mimicking the natural extracellular matrix (ECM) morphology are considered promising scaffolds for Tissue Engineering (TE). Electrospinning has emerged as a very promising technology enabling to produce synthetic polymeric ultrafine fibers. These fibers in mesh, have diameters in the submicron range which results in a high surface area-to-volume ratio and high porosity. The meshes have a typically random distribution or, in some special cases, some preferential directions of alignment.

Aiming at obtain nanofiber meshes with different topographies (texture, alignment and porosity), a synthetic biodegradable polymer (polycaprolactone, PCL) was electrospun using specially-designed conductive static collectors. Scanning electron microscopy (SEM) analysis showed a random distribution of nanofibers, when a flattened collector was used. This is expected owing to the chaotic motion of polymeric jets of solution during the electrospinning process (Figure 1 A). However, when a metallic wire net was used as collector, it was possible to observe two distinct areas of nanofibers deposition (Figure 1 B). The fibers appeared parallely aligned and collapsed at the wire locations, where the electric field is more intense (Figure 1 C). In the spaces between the wires, the nanofibers deposition occurred more randomly, with diameters varying between 560 nm and 1,5 μm (Figure 1 D). Inversely, random collapsed fibers were present in protuberances (Figure 1 E) and aligned nanofibers deposition occurred in the spacing between protuberances (Figure 1 F) of a corrugated tube, presenting diameters between 200 nm and 1.2 μm. The former two nanofibrous structures presented distinctive properties in the same mesh, constituting the so called patterned nanofiber meshes.

The electrospun nanofibrous structures can be explored in diverse areas of tissue engineering, including the field of vascular regeneration. We considered an approach to controlled fabrication of biodegradable vascular substitutes by means of electrospinning technique. The procedure consisted of using a circular mandrel (4 mm diameter) as collector, rotating at 600 rpm. The electrospun fibrous scaffolds were manufactured with a length of approximately 15 cm and cut in pieces of 3 cm (Figure 1 G). In SEM micrographs was possible to observe a certain degree of nanofiber alignment induced by the rotating collector.

Despite the alterations in nanofiber mesh topography presented previously, we were also able to produce nanofibrous structures with control over the fiber composition. Thus, a polymeric solution of Polyvinylpirrolidone (PVP) and Tetraisopropanolato de Titânio ($Ti(O_iPr)_4$) was prepared and electrospun using a coaxial double capillary system as spinneret. By SEM analysis of the transversal section of PVP/Ti(OiPr)4 nanofiber mesh it was possible to observe that nanofibers were hollow with an external diameter ~1,2 μm and an internal diameter of 650 nm. These nanofibers can be used as a drug delivery system with fine tuned control over the release kinetics, depending on the polymer wall thickness.

Different cell types, such as fibroblasts (L929 cell line), osteoblasts (SaOs-2 cell line) and human bone marrow-derived stromal cells (hBMSCs), were seeded onto patterned nanofiber meshes. The aim was to study the relevance of the patterned nanofiber meshes for tissue engineering applications. SEM micrographs from the *in vitro* studies indicated that the different cells preferred to adhere to randomly distributed nanofibers. Fibroblasts and

hBMSCs also adhered and proliferate parallel to the aligned nanofibers of the patterned nanofiber meshes (Figure 2). hBMSCs were also induced to differentiate into the osteogenic pathway. Results supported that patterned nanofiber meshes are promising scaffolds for bone tissue engineering applications using hBMSCs as cell source.

Novel electrospun nanofiber meshes coated with biomimetic calcium phosphate (BCP) were also developed (Figure 3 B), mimicking the extracellular microenvironment found in the bone structure. The influence of the BCP on the viability, adhesion and proliferation of human osteoblast-like cells was assessed. It was shown that nanofiber meshes coated with a BCP not only support but also enhance the proliferation of osteoblasts for longer culture periods (Figure 3 D). The results suggested a high potential use of this Ca-P coated PCL nanofiber mats as components of polymeric scaffolds suitable for bone regeneration approaches.

Figures:

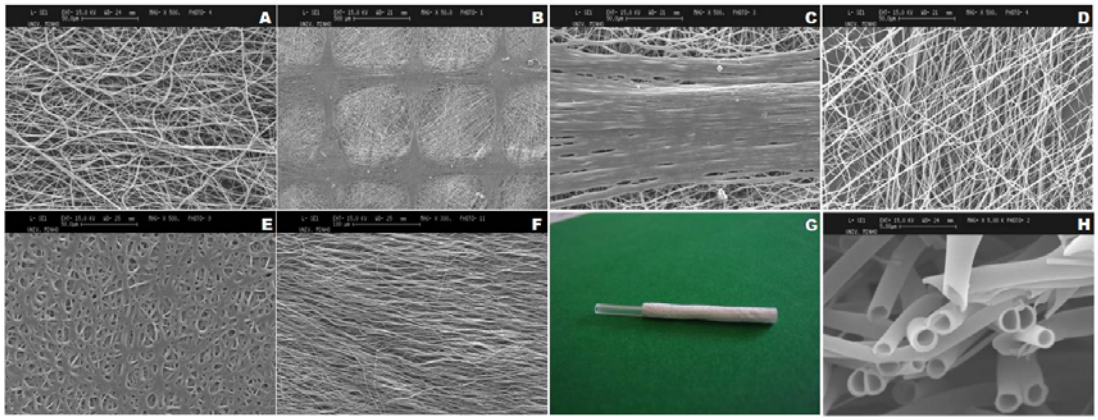

Figure 1 - SEM micrographs of random (**A**) and pattern PCL nanofiber meshs (**B-F**) composed by areas of randomly aligned nanofibers (**D** and **E**) and regions of parallely aligned fibers (**C** and **F**). Photograph of a electrospun vascular nanofibrous scaffold with 3 cm and an internal diameter around 4 mm (**G**). SEM micrographs of a transversal section of hollow PVP/$Ti(OiPr)_4$ nanofibers in a mesh (**H**).

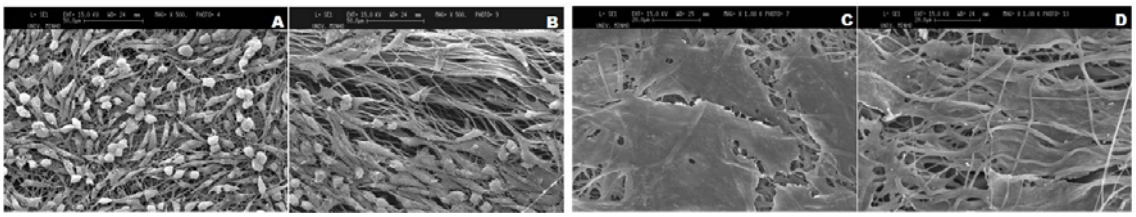

Figure 2 - Direct contact tests were performed fibroblasts (**A** and **B**) and human bone marrow-derived stromal cells (**C** and **D**). Phenotypic alterations of cells, reacting to areas of randomly alignment(**A** and **C**) and parallely aligned fibers (**B** and **D**) of pattern meshes.

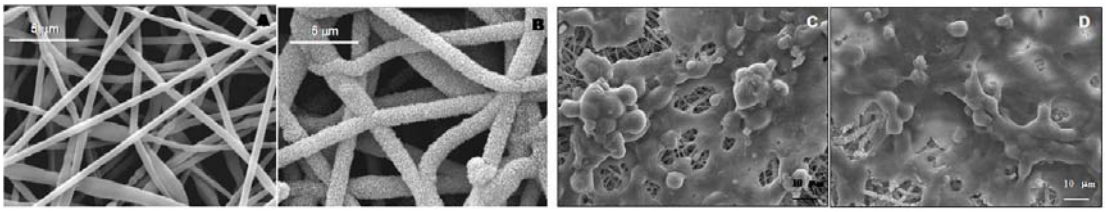

Figure 3 - PCL nanofibre mesh (**A**) with a biomimetic calcium phosphate (BCP) layer (**B**). Direct cell contact studies with osteoblast-like cells on PCL (**C**) and PCL-BCP nanofiber meshes (**D**).

HYDROPHOBIC-HYDROPHILIC PROPERTIES OF TITANIUM DIOXIDE THIN FILMS

A. J. Martins[a], V. Teixeira[a] , J. Carneiro[a], J. H. O. Nascimento[b], J. Neves[b], M. Ribeiro[c], A. Vieira[c]

[a] *Physics Department, University of Minho, Campus Gualtar, 4710-057 Braga, Portugal*
[b] *Textil Engineering Department, University of Minho,* Campus de Azurém, 4800-058 Guimarães, Portugal
[c] *CeNTI, Centre for Nanotechnology and Smart Materials*, 4760-034 Vila Nova de Famalicão, Portugal

e-mai address: anajoaom@gmail.com , vasco@fisica.uminho.pt

Abstract

The self-cleaning of super-hydrophobic micro- to nano-structured surfaces was first observed to be a property of some plants (e.g. leaves of Lotus). Researchers try to copy nature but with synthetic surfaces. Hydrophobic-hydrophilic properties and photocatalytic behavior of nanoscale materials and nanocoatings is receiving growing interest in nanoscience and technology research, given the foreseeable introduction of commercial products into markets. For example recent studies have shown that it is possible to disinfect air by photocatalytic techniques similar to those proven successful in killing microorganisms in water. Nanocomposite and nanostrucutured thin films can be tailored in order to show easy-release, hydrophobic and anti-microbial properties, particularly of interest for technological applications where nanocoatings are applied on plastics, glass, fiberglass and technical textiles products.

Titanium dioxide is among the few semiconductors that have good chemical/photochemical stabilities and high oxidation power. However, its relatively high band gap makes it only effective when exposed under UV light. It has been found that the addition of some metals to TiO_2 and/or plasma treatment during film growth can improve the photocatalytic activity by UV irradiation and extend its use in the visible region of the electromagnetic spectrum.

In this work, transparent photocatalytic titanium dioxide (TiO_2) thin films were deposited onto microscope glass slides, polycarbonate substrates and textile surfaces by means of the DC reactive magnetron sputtering method using Ar and O_2 as working gases. The film surface morphology and roughness were characterized by atomic force microscopy (AFM). The contact angle and surface energy were measured in order to study the hydrophobic-hydrophilic properties of undoped and undoped titanium dioxide nanocoatings. Fe-doped and Nd-doped TiO_2 films were also prepared to study the effects on the photocatalytic activity of the TiO_2 thin films. The influence of total sputtering pressures and iron doping concentrations on the surface properties of the TiO_2 thin films were investigated.

QUANTUM DOTS/POLYMER-NANOCOMPOSITES FOR LUMINESCENT OPTICAL FIBER PROBES

Manuel A. Martins [a*], *P. A. S. Jorge* [b], *César Maule*[b, c], *Tito Trindade* [a]

a) Department of Chemistry, CICECO, University of Aveiro, 3810-193 Aveiro, Portugal
b) Optoelectronics Unit, INESC Porto, Rua do Campo Alegre, 687, 4169 007 Porto, Portugal
c) Departamento de Física da Faculdade de Ciências da Universidade do Porto.

** mamartins@ua.pt*

The remote detection and monitoring of biochemical parameters have an increasing importance for a wide range of applications and industries. The combination of integrated optics and optical fiber technologies with luminescence based sensors, has successfully addressed the trend to miniaturization and demand for increasing sensibility and selectivity standards, particularly in environmental and biomedical applications. Some examples are already commercially available (e.g. oxygen and pH sensors). However, these sensors still show some limitations. The leaching and photo-bleaching of the sensing dyes are the most common problems. Furthermore, the majority of the luminescence based sensors show a strong dependence between temperature and luminescence intensity as well as the excited state lifetimes. The introduction of luminescent semiconductor nanocrystals (quantum dots: QDs) as sensing probes, can potentially solve some of these limitations [1,2].

QDs show improved properties when compared to conventional organic dyes, such as: narrow emission, broad absorption bands, high quantum yields, increased photostability and the ability to tune their properties by changing the nanocrystals size and/or composition. Colloidal suspensions of QDs can be prepared with a variety of emission wavelengths (from 350 to 2000 nm), and can be immobilized in a variety of matrices. The immobilization of QDs in polymeric matrices is particularly interesting, namely because the optical behavior of the final nanocomposites seems to depend on the type of polymer used. For example, we have shown that highly luminescent nanocomposites can be obtained with QDs immobilized in poly(butyl acrylate) (PBA) [3].

Here we wish to report our preliminary results on the use of CdSe/ZnS QDs-PBA nanocomposites as luminescent sensors in optical fiber sensing systems. Organically capped core/shell CdSe/ZnS QDs were first prepared using chemical reactions in high boiling point and coordinating solvents. These QDs were then used as the starting materials to produce QDs-PBA nanocomposites by *in situ* miniemulsion polymerization of butylacrylate.[3] Fiber probes were prepared using silica optical fibers with core/cladding diameters of 550/600 μm respectively. The fiber tips were slowly dipped in 50% HF prior to coating. By this method the cladding was removed and tapered probes were obtained with increased excitation/collection efficiency. The nanocomposites were then attached at the surface of the fiber tapers by dip/coating using a latex suspension, and then followed by drying with an air flow.

Using the setup in Figure 1, the coated fibers were excited with a blue laser diode (473 nm) and the luminescence response was recorded using a CCD spectrometer. It was observed that the fibers were uniformly coated with a polymer film displaying strong luminescence. The behavior of the luminescent probes was then tested under different working conditions. Here preliminary results will be shown demonstrating the suitability of the nanocomposite to be used as a self-referenced temperature fiber probe (Figure 2). When used in combination with other sensitive dyes these fiber probes will enable temperature independent measurement of a diversity of analytes. Results showing the influence of pH in the luminescent signals will also be presented.

In addition, we will show that the nanocomposite materials after acid hydrolysis can be enriched in functional groups at the surfaces, thus providing potential for biofunctionalization procedures. This is an important feature since it can open the way to the detection of a wide variety of analytes at the tip of an optical fiber, including biological material, enabling the fabrication of advanced analytical tools.

References:

[1] P. A. S. Jorge, C. Maule, A. J. Silva, R. Benrashid, J. L. Santos, F. Farahi, Analytica Chimica Acta **606** (2008) 223–229.
[2] P. A. S. Jorge, M. A. Martins, T. Trindade, J. L. Santos, F. Farahi, Sensors, **7**, (2007), 3489-3534.
[3] M. Peres., L. C. Costa, A. Neves, M. J. Soares, T. Monteiro, A. C. C. Esteves, A. Barros-Timmons, T. Trindade, A. Kholkin, E. Alves, Nanotechnology **16** (2005) 1969–1973.
[4] A. C. C. Esteves, A. Barros-Timmons, T. Monteiro and T. Trindade, Journal of Nanoscience and Nanotechnology, **5,** (2005) 766-771.

Figures:

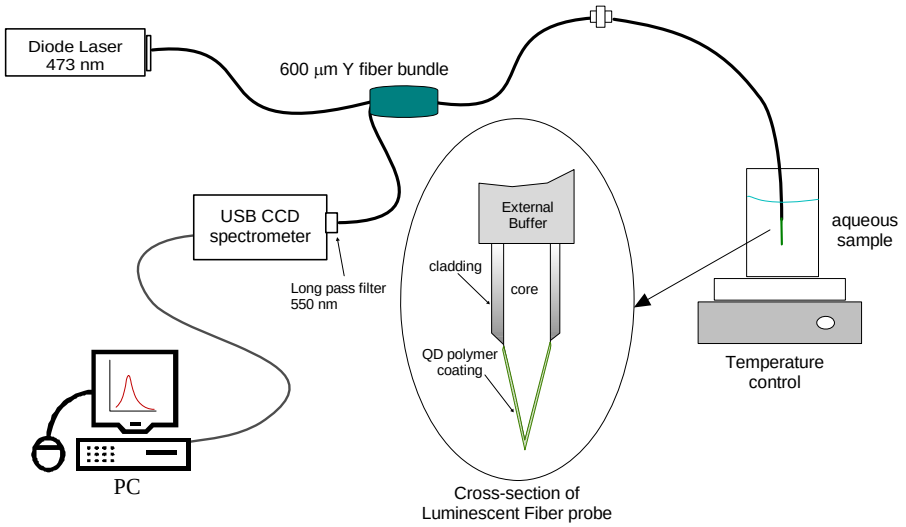

Figure 1: Experimental set-up for characterization of the luminescent fiber probes.

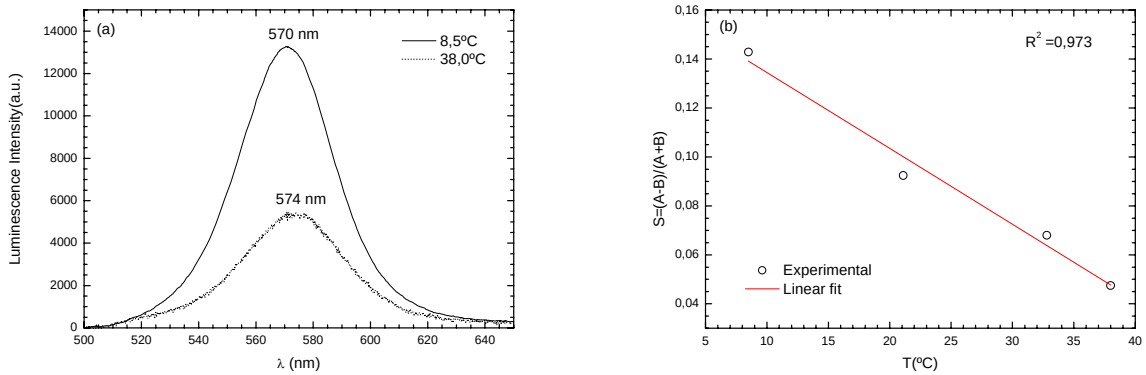

Figure 2: (a) Spectral response to temperature of immobilized QD. As temperature increases luminescence is quenched and emission peak is red shifted (b) Application of a ratiometric scheme allows obtaining a self-referenced output with linear dependence on temperature.

Manuel Martins acknowledges FCT for a PhD Grant (SFRH/BD/29475/2006). César Maule acknowledges the support from the Marie Curie Early stage research training network, funded by European Commission under the contract MEST-CT-2005-020353. Funding provided by FCT and FEDER (project PTDC/QUI/67712/2006).

BIOLOGICAL DETECTION LIMIT OF A GMR-BASED BIOCHIP FOR PATHOGENIC ANALYSIS

V. C. Martins[1,2], F. A. Cardoso[1], S. Cardoso[1], L. P. Fonseca[2], P. P. Freitas[1]
1 - Instituto de Engenharia de Sistemas e Computadores - Microsistemas e Nanotecnologias (INESC-MN), R. Alves Redol, 9-1º, 1000-029 Lisbon, Portugal, 2 - Center for Biological and Chemical Engineering (CEBQ), Instituto Superior Técnico, Av. Rovisco Pais, 1049-001 Lisbon, Portugal.

Abstract

INESC-MN and its collaborators are pursuing the development of an integrated platform where the magnetic sensing unit, the biochemical interface (functionalized organic/inorganic surface), the macro/micro-fluidic system (sample preparation, cell concentrator, fluid transport), and the electronic data read-out and automation are combined in an easy-to-use and portable platform [1-3]. This contribution presents the latest achievements on the biochemical sector. A particular application is being targeted on the evaluation of microbiological quality of water for human consumption through the detection of waterborn pathogen microorganism. Two different strategies of biomolecular recognition events, involving DNA oligonucleotide sequences and antibodies as recognition agents, are under development for the quantitative determination of *Escherichia coli* and *Salmonella sp.* as model microorganisms in water samples. The biological detection limit of the device was assessed using 20mer single stranded DNA probes encoding to the genomic region of the 16S ribosomal sub-unit of *E. coli*.

The device consists in 24 U-shaped (2.5 x 80 μm^2) spin-valve sensors array of multi-layer structure Ta 15Å/NiFe 30Å/ CoFe 25Å/ Cu 21Å/ CoFe 25Å + oxid./ MnIr 80Å/ Ta 20Å/ TiW(N) 150 Å, fully passivated with 300 nm oxide layer. Additionally, a 200 Å gold thin-film was RF sputtered and gold pads of 43 x 13 μm^2 were defined precisely on top of sensor sites (Fig. 2). After a meticulous cleaning step, thiol-modified DNA oligos were directly attached to the gold surface and further used as biorecognition probes. Hybridized target molecules were labeled with 250 nm diameter magnetic particles (Micromod, Germany) through a biotin-streptavidin binding system. During the experiment 16 sensors were sequentially monitored in real-time applying 1 mA bias current through each sensor and recording an ac voltage change with a lock-in amplifier technique. An in-plane ac excitation field of 13.5 Oe rms at 31 Hz plus a dc field of 30 Oe were applied to magnetize the nanoparticles and to center the sensor transfer curve in the operating region.

Complementary target DNA solutions at different concentration, ranging from 1 μM down to 1 pM, were measured through the detection of nano-sized magnetic labels, originating average voltage signals of 500 μV down to 77 μV, respectively. The background noise associated to a measurement when no target DNA is present in the hybridization solution is 29 ± 13 μV. Moreover, in the presence of a non-complementary target (70% mismatch) at 1 μM the sensor detection signal is around 43 ± 30 μV (Fig. 1).

[1] Graham, D. L., Ferreira, H. A., Freitas, P. P., Magnetoresistive-based biosensors and biochips, *Trends Biotechnol* 2004**,** 22, 455-462.

[2] Ferreira, H. A., Cardoso, F. A., Ferreira, R., Cardoso, S., Freitas, P. P., Magnetoresistive DNA chips based on ac field focusing of magnetic labels, *J. Appl. Phys.* 2006, **99**, 08P105.
[3] Cardoso, F. A.; Germano, J.; Ferreira, R.; Cardoso, S.; Martins, V. C.; Freitas, P. P.; Piedade, M. S., Sousa, L., Detection of 130 nm magnetic particles by a portable electronic platform using spin valves and magnetic tunnel junctions sensors, *J. Appl. Phys.* 2007, in press.

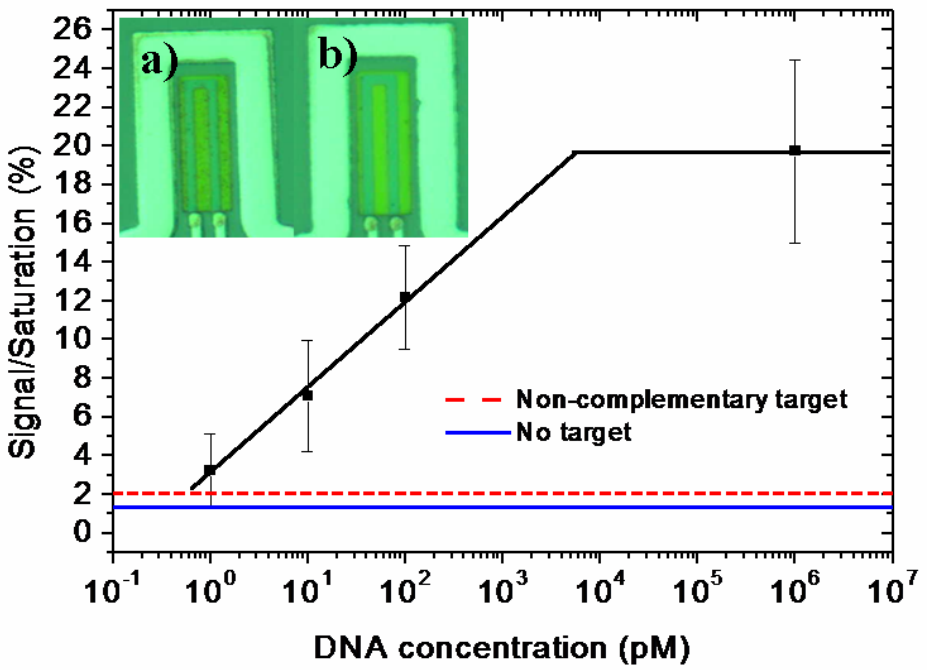

Fig. 1: Biological detection limit for single stranded DNA sequences encoding for the genomic region of the 16S ribosomal sub-unit of *E. coli*. Optical microscope picture at 800x magnification, from individual sensors corresponding to a) 1 μM target and b) no target assay.

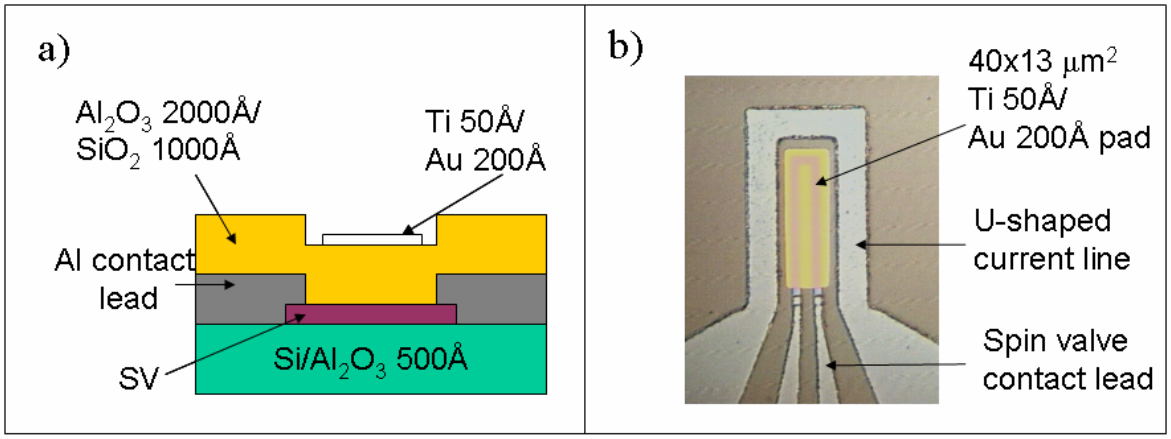

Fig. 2: Cross (a) and top view (b) of a spin valve chip sensing site showing the sensor, focusing current line, passivation layers and gold pad.

PARTICLE FORMATION BY SUPERCRITICAL FLUID-ASSISTED PROCESSES

L. Padrela, M. Rodrigues, A. Almeida[a], *H. A. Matos, E. Gomes de Azevedo*

Department of Chemical and Biological Engineering
Instituto Superior Técnico, Av. Rovisco Pais , Lisboa, PORTUGAL
Contact e-mail: egazevedo@ist.utl.pt
and
[a] Research Institute for Medicines and Pharmaceutical Sciences (*i*Med.UL), Faculdade de Farmácia
Universidade de Lisboa, Av. Prof. Gama Pinto, Lisboa, PORTUGAL

Recent developments in biotechnology forecast a new generation of therapeutics. Yet, the increasing specificity of emerging drug candidates and its susceptibility to the classical administration routes raise new challenges to the Galenic pharmacology.

The pulmonary route is becoming an attractive alternative for the delivery of pharmaceutics[1], especially macromolecules like peptides, and proteins. However, it requires exquisite particles with specifications hard to achieve by most of the established technologies. Therefore, particle engineering using appropriate processes and excipients is required to produce particles of optimal size, morphology, and surface properties that would enhance drug target efficiency[2]. As a consequence, the preparation of drug micro and -nanoparticles with a controlled particle size distribution has become an important focus for the development of pharmaceutical delivery formulations[3].

Supercritical fluid-assisted technologies allow the generation of particles that are difficult or even impossible to obtain by traditional techniques such as milling, crystallization and spray drying which don't provide an efficient control of the particle size (a broad particle size distribution is normally obtained).

A novel method to produce fine dry powders (e.g. proteins, polymers, composites, cocrystals), making use of the properties of supercritical fluids, has been developed at IST. It consists of a concerted precipitation by two distinct mechanisms, the anti-solvent crystallization and the atomization and spray drying (A-SAIS process). Our results show that bioavailability issues can be overcome by accurate control of the particulate products properties, such as the crystalline form, morphology, size distribution, and the excipients composition and layering. Depending of the leading mechanism (atomization or anti-solvent) the morphology will vary from spheres to fibers (figure 1).

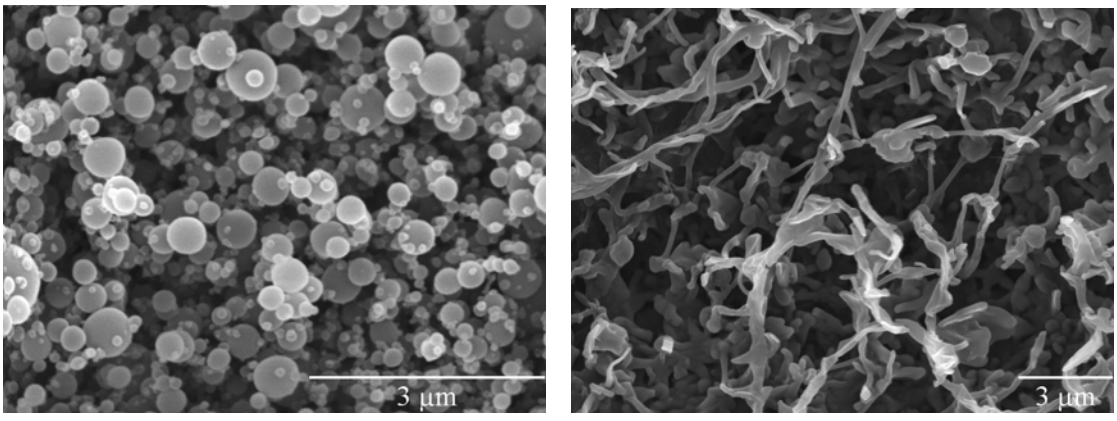

Figure 1 – Scanning Electron Microscopy images of lysozyme particles processed by the A-SAIS process: (a) spheres, and (b) fibers

The knowledge of the production process variables for the two precipitation mechanisms is the key to determine the precipitation sequence of drugs and excipients and then the degree of microencapsulation.

References

[1] Porta, Giovanna D., Vittori, Carlo D., Reverchon, E., AAPS PharmSciTech, **Supercritical Assisted Atomization: A Novel Technology for Microparticles Preparation of an Asthma-controlling Drug,** Volume 6, Number 3 (2005), E421-E428

[2] Rodrigues, M., Peiriço, N., Matos, H., Gomes de Azevedo, E., Lobato, M.R., Almeida, A.J., Journal of Supercritical Fluids, **Microcomposites theophylline/hydrogenated palm oil from a PGSS process for controlled drug delivery systems**, Volume 29, Issues 1-2 (2004), pp175–184.

[3] Reverchon, E., Adami, R., Journal of Supercritical Fluids, **Review, Nanomaterials and Supercritical Fluids**, Volume 37, Issue 1 (2006), pp 1-22

Gold Anisotropic Nanoparticles: Synthesis and Characterization

Adelaide Miranda[a], Patrícia A. Carvalho[b], Eulália Pereira[a], Baltazar de Castro[a]

[a]REQUIMTE - Departamento de Química,Faculdade de Ciências,Universidade do Porto, Rua do Campo Alegre, 687, 4169-007 Porto, Portugal
[b]Departamento de Engenharia de Materiais, Instituto Superior Técnico, Av. Rovisco Pais, 1049-001 Lisboa, Portugal
E-mail: mariaadelaidemiranda@gmail.com

The development of new synthetic methods to prepare nanoparticles with different morphological characteristics is critical for the successful application of nanotechnology. We are specially interested in new synthetic and functionalization methods for metal nanoparticles for developing biochemical sensors.

Gold nanotriangles were obtained by the photocatalytic reduction of hydrogen tetrachloroaurate (III) by triethanolamine using Sn (IV) meso-tetra(N-Methyl-4pyridyl)porphine tetratosylate chloride as the photocatalyst, and CTAB as the capping agent, in aqueous medium (pH = 6.5-8.0). pH and the concentration of CTAB and SntMepyP have a strong influence on the morphology of the nanoparticles. These factors were optimized for the preparation of nanotriangles with length ≈130 nm and 15-19 nm height. The combination of TEM, AFM and electron diffraction analysis allowed a thorough investigation of the nanotriangles morphology, resulting in further insight on the dependence of morphology on growth conditions, as well as the mechanisms of crystal growth.

Acknowledgements
Financial support from Fundação para a Ciência e a Tecnologia through project POCTI/QUI/45145/2002. Adelaide Miranda thanks FCT for a Ph.D. grant (SFRH/BD/17566/2004).

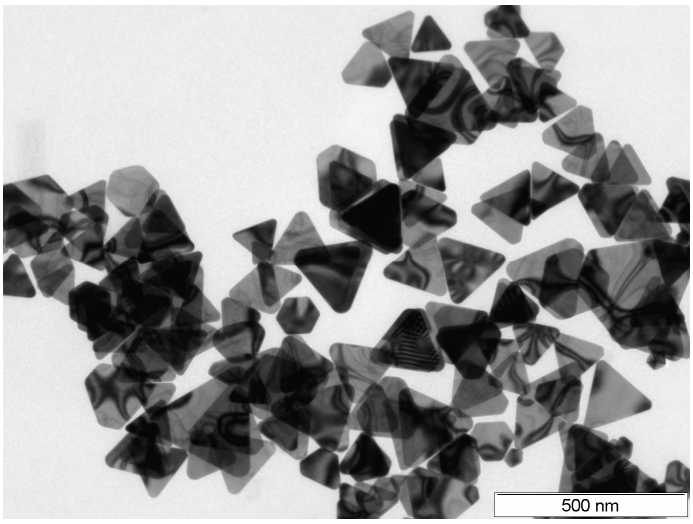

Fig. 1: Gold nanotriangles obtained in optimal conditions.

AB INITIO STUDIES OF DIRECT PROPENE EPOXIDATION AT OXIDE-SUPPORTED GOLD CLUSTERS AND NANOPARTICLES

Luis M. Molina, María J. López and Julio A. Alonso

Departamento de Física Teórica, Atómica y Óptica,
Universidad de Valladolid, 47011 Valladolid (Spain)
lmolina@fta.uva.es

Gold nanocatalysts have recently attracted a great deal of interest due to their novel applications, one of the most interesting ones being the direct formation of propene oxide (C3H6O) from propene, oxygen and hydrogen at TiO2-supported gold nanoparticles. When these particles have a diameter of around 3-4 nm, they become active and extremely selective [1]; such selectivity is extremely sensitive to the degree of dispersion of the catalysts, and particles only slightly smaller (~2 nm) mainly produce propane. The reasons for such complex behaviour, as well as the detailed reaction mechanisms that take place, are to a large extent unknown. In this presentation, we will report the results obtained in an extensive ab initio DFT study of the reaction at the Au/TiO2 interfacial region, since recent experimental results by Nijhuis *et al.* [2] suggest that the active reaction sites are located there.

Figure 1 shows the base model system built for the simulations, where a thin Au rod is placed on top of the anatase-TiO2(101) surface. Then, the main stages of the epoxidation reaction were simulated, starting with the dissociation of H2, coadsorption of O2 at a partially hydroxylated surface, and the interaction of propene with the catalyst in the presence of various co-adsorbates. The results are in agreement with the experimental findings by Nijhuis et al., which suggest an easy formation of a strongly bound propene oxide species at the Au/TiO2 interface. We find an easy reaction of propene with co-adsorbed peroxo (-OOH) species, leading to formation of metallocycle-like propene oxides species at the TiO2 substrate in the neighbourhood of the Au nanoparticle, which catalyzes the reaction. Finally, preliminary results from simulations of the analogous process at similar catalysts (with gold supported at a different oxide material) will be presented, showing that the activity of gold for propene epoxidation is not specific to a particular oxide.

References:

[1] A. K. Sinha, S. Seelan, S. Tsubota and M. Haruta, Topics in Catal., **29** (2004) 95.

[2] T. A. Nijhuis, T. Visser and B. M. Weckhuysen, Angew. Chem. Int. Ed., **44** (2005) 1115.

Figures:

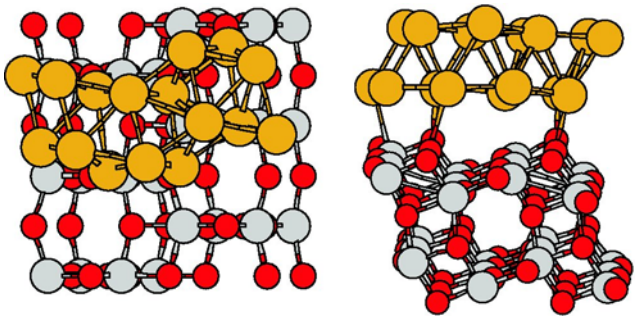

Figure 1: Model of the Au/TiO2 perimeter interface for propene epoxidation catalysts

SILVER NANOPARTICLES AND GOLD METALLODENDRIMERS: FROM MOLECULAR PRECURSORS TO NANOMATERIALS

Eduardo J. Fernández,[a] Jorge García-Barrasa,[a] Antonio Laguna,[b] José M. López de Luzuriaga,[a] Miguel Monge,[a] M. Elena Olmos,[a] Eva Sánchez-Forcada,[a] and Carmen Torres[c]

[a]Departamento de Química. Universidad de La Rioja. Grupo de Síntesis Química de La Rioja, UA-CSIC. Madre de Dios 51. E-26006 Logroño (Spain)
[b]Departamento de Química Inorgánica. Instituto de Ciencias de Materiales de Aragón. Universidad de Zaragoza-CSIC. E-50009 Zaragoza (Spain)
[c]Departamento de Agricultura y Alimentación. Universidad de La Rioja. Madre de Dios 51. E-26006 Logroño (Spain)
miguel.monge@unirioja.es

The increased interest in the synthesis of new metal-based nanomaterials stems from the fact that new electronic, optical or magnetic properties can be reached at this length scale. These properties can be tuned depending on the size and the shape of the new nanomaterials. By the use of our experience in gold and silver organometallic and coordination chemistry we have carried out the synthesis of metal nanoparticles and nanometer sized metallodendrimers through chemical methods.

The first research line makes use of the organometallic silver precursor $[Ag(C_6F_5)]$ that under mild conditions and in the presence of stabilizers, permits the synthesis of small size silver nanoparticles. This *organometallic method* leads to Ag nanoparticles stabilized in different substrates such as organic ligands (amines), polymers (PVP, cellulose acetate) or inorganic SiO_2 (see Figure 1). Moreover, alkylamine capped silver nanoparticles (ca. 10 nm) display high antimicrobial activity against some representative microorganisms.[1]

We have also focused on the synthesis and study of a series of gold metallodendrimers. These new materials are based on PPI or PAMAM dendrimers functionalized with peripheral PPh_2 groups what permits the coordination of Au(I) fragments. Depending on the dendrimer generation it is possible to design new complexes from the molecular level to the nanoscale. For example, when the periphery of the dendrimer is grafted with Au(I)-thiolate units luminescent metallodendrimers can be obtained (see Figure 2).[2]

References:

[1] E. J. Fernández, C. Torres, J. M. López de Luzuriaga, M. Monge, J. García-Barrasa, Spanish Patent P200700456, 2007.

[2] E. J. Fernández, A. Laguna, J. M. López de Luzuriaga, M. Monge, M. Montiel, M. E. Olmos, R. C. Puelles, E. Sánchez-Forcada, Eur. J. Inorg. Chem. (2007) 4001-4005.

Figures:

Figure 1. Transmission electron micrographs (a and c) of different magnifications and, particle size distribution (b) of HDA capped Ag nanoparticles.

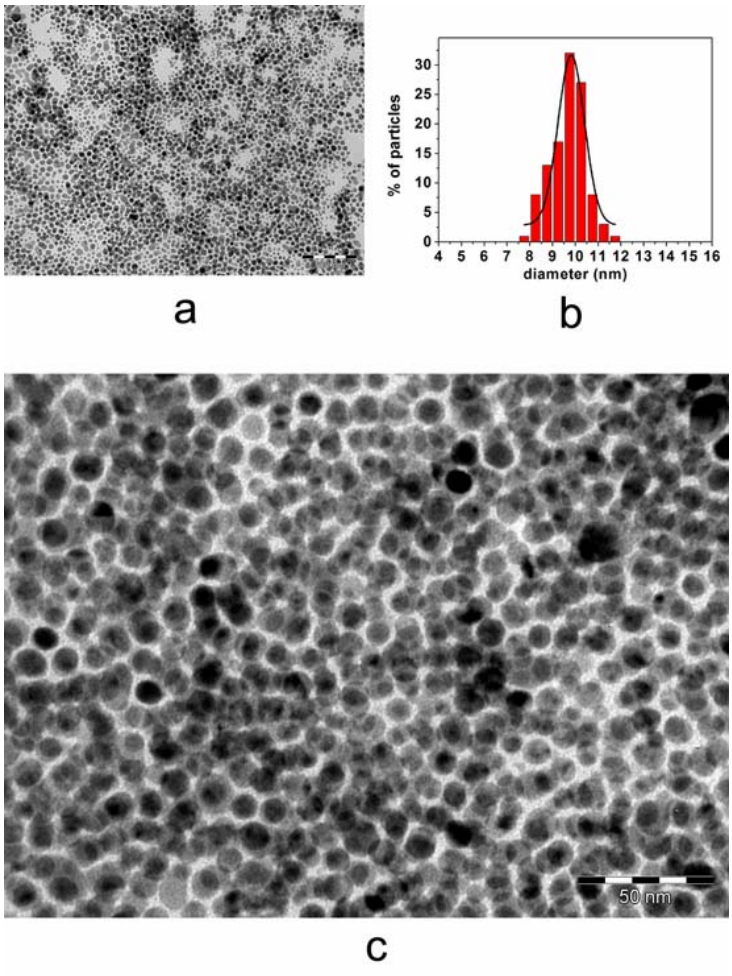

Figure 2. Octanuclear phoshine thiolate gold dendrimers with different 4-substituted benzenethiolates and emission spectra in solid state at 77 K.

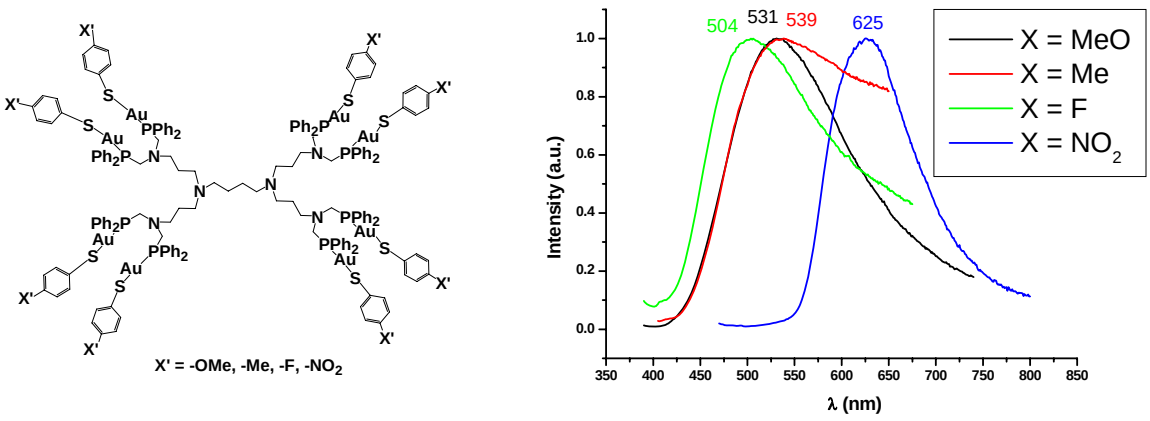

A 3D TYPE I COLLAGEN / HYDROXYAPATITE NANOPARTICLES COMPOSITE FOR BONE REGENERATION

A.Y. Pataquiva Mateus [1,2], M.P. Ferraz[1,3], E.J. Herrero[4], F.J. Monteiro[1,2]
[1] INEB— Instituto de Engenharia Biomédica, Laboratório de Biomateriais, Rua do Campo Alegre, 823, 4150-180 Porto, Portugal.
[2] Universidade do Porto, Faculdade de Engenharia, Departamento de Engenharia Metalúrgica e Materiais, Rua Dr. Roberto Frias, s/n 4200-465 Porto, Portugal.
[3]Universidade Fernando Pessoa, Praça 9 de Abril 349, 4249-004 Porto, Portugal.
[4] Hospital Universitario Puerta de Hierro, Unidad de Biomateriales, Servicio de Cirugía Experimental, San Martín Porres 2, 28035 Madrid, Spain.

Introduction

Collagen (COL) is the major structural protein of connective tissue such as skin, bone, cartilage, tendons and ligaments.COL is present in 19 varieties in the human body. It constitutes about one-third of the total body protein in mammals. Because of its biological properties and easy availability, COL type I is widely used as a biomaterial, on multiple physical forms such as sponges, films and membranes, wire, fabrics. Among relevant properties of COL are low immune response, low toxicity, the ability to promote cellular growth and attachment, homeostasis and the ability of COL solution to reconstitute *in vitro* the microfibrillar structure found in natural tissues [1].

Synthetic hydroxyapatite (HA) has excellent biocompatibility and bioactivity due to its chemical and structural resemblance to mineral bone and tooth. It has been clinically used as sintered bulk ceramic, porous structures, granules and coatings. Nano-sized HA formulations, with properties closer to those of living bone, are presently being studied, as HA particles size is a relevant factor for i*n vitro* cell activity, and is a parameter of great importance for injectability and handling. Desired characteristics of synthesised HA are fine and uniform particle size, in the nanometre range, phase homogeneity and minimized degree of particle agglomeration. Although many chemical processing routes have been employed to prepare fine HA powders, in this work chemical precipitation has been chosen as it is the most commonly used alternative [2].

Materials and Methods

Solutions of calcium hydroxide (Ca(OH)2) and ortho-phosphoric acid (H3PO4, 85%), both of analytical grade, were used as reactants for the preparation of HA nanoparticles. Firstly, 1L of an aqueous suspension of H3PO4 (0.6M) was slowly added drop by drop to 1L of an aqueous suspension of Ca(OH)2 (1M) with addition of sodium dodecylsulphate (10g) while vigorously stirring for 2h at room temperature. Concentrated NaOH was added until a final pH of 10.5 was reached. The white and opaque solution obtained was washed using de-ionized water and was dried at 80°C for 24 h.

Type I Collagen was obtained from the tail tendons of young *Wistar* rats. After washing in 1% (w/v) NaCl solution, the tendons were dissolved in 0.5M acetic acid for 3-4 days at 4ºC. After adding pepsin (0.5mg/ml) in 0.5M acetic acid was incubated for 24h and with a subsequently centrifugation at 5000rpm for 1h at 4ºC. Solid NaCl was added to the pepsin-soluble portion to a final concentration of 1M. After centrifugation and re-suspension in acetic acid the solution was dialyze against 0.5M acetic acid at 4ºC to remove salt [3]. Fig 1 shows an interconnective macroporous sponge obtained from a collagen solution lyophilised for 48h.

The solution of COL/nanoHA was prepared adding 0.5 – 5% w/w nanoHA on a collagen solution and put in moulds after constant agitation avoiding the materials separation. Solution was frozen at -80ºC for 24h and follow was lyophilized for 48h.

Results

Samples were taken for SEM observation, after gold sputtering at an accelerating voltage of 10 kV. Preliminary observations presented sponges of COL/HA, with controlled pore size and fully interconnective macroporosity, well distributed through out the all sponge, with particles both integrating the pores walls, but also with many aggregates being present at the surface. This structure is now being fully physically characterized

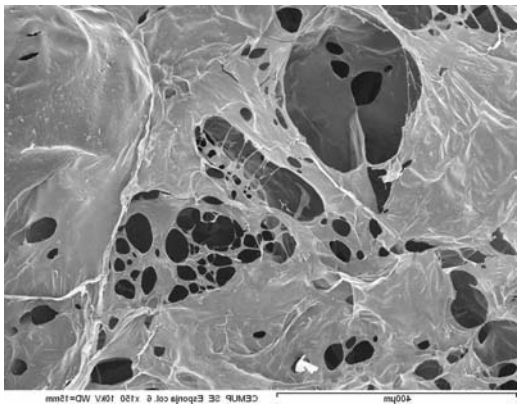

Fig. 1: Scanning electron micrograph of COL/HA sponge (x150)

Composite materials of COL and nano-sized HA

The use of collagen type I and nano-particulate HA for the generation of new bone substitutes is a promising approach for the generation of new bone substitutes to mimic structural and morphological features of natural bone, and to obtain materials with improved mechanical and biological properties.

In this context we prepared composite materials from collagen and nano-sized HA, described above. SEM and TEM results of the composites show morphological characteristics that suggest a potential use as bone tissue engineering soft scaffolds, due to the presence of collagen, as an attractive cell scaffold, and of nanoHA generating multiple binding sites for adhesion of several macromolecules of interest.

References

1) Sionkowska, A. Polymer Degradation and Stability. 68 (2000) 147-151.
2) Jarcho, M., Clinical Orthopeadics Related Research. 157 **(**1981) 259-278.
3) Rainey, J., Wen, C., Goh, C. Matrix Biology. 21 (2002) 647-660.

ACKNOWLEDGMENTS

Alis Pataquiva Mateus is grateful to FCT for awarding her a PhD scholarship SFRH/BD/16616/2004. This work was performed under contracts POCTI/SAU/BMA/56061/2004 and CRUP – Acções Integradas Luso – Espanholas 34/06, 2006.

INFLUENCE OF SURFACE COATING IN THE INTERACTION OF MAGNETITE NANOPARTICLES WITH TUMORAL HeLa CELLS

Angeles Villanueva [1], Magdalena Cañete[1], María del Puerto Morales[2], A. G. Roca[2], C. J. Serna[2] and Rodolfo Miranda[3,4]
[1]Departamento de Biología, Universidad Autónoma de Madrid,
[2] Instituto de Ciencias de Materiales de Madrid –CSIC,
[3]Departamento de Física de la Materia Condensada, Universidad Autónoma de Madrid.
Instituto Madrileño de Estudios Avanzados en Nanociencia (IMDEA-Nanociencia)
Cantoblanco. 28049 Madrid. Spain.
angeles.villanueva@uam.es

In the last few years magnetic nanoparticles are being intensively studied as contrast reagents for imaging with NMR techniques and active vectors for cancer therapy by hyperthermia [1]. In the latter case, their selective interaction with tumour cells is essential for an efficient treatment. We describe here the incorporation of nanoparticles into HeLa cells depending on their surface functionalization and their interference with the cell division processes.

Nanoparticles of magnetite with an average size of 10 nm have been prepared by coprecipitaton and surface-coated with dextran (no surface charge), dextran amine (positive surface charge) or heparin (negative surface charge). HeLa tumour cells have been cultivated in a standard medium with magnetite nanoparticles at different concentrations ranging from 0.05 to 0.5 mg/ml, for times going from 6 to 24 h. Particles with positive surface charge penetrate efficiently the cells by endocytosis (they are detected inside the cells already after 1 hour and even for the smallest concentration of nanoparticles), accumulate inside the cells in large amounts and remain there for long time (days). Figure 1 shows the incorporation of magnetite nanoparticles covered with dextran amine after 24hours in a concentration of 0.5 mg/ml.

Contrary to this observation, magnetite nanoparticles functionalized with heparin (i.e. with negative surface charge) do not penetrate efficiently into the cells, and those covered with dextran (i.e. without surface charge) are not visualized at all inside the cells.

We have also visualized the possible alterations in the microtubules structure during mitosis produced by the presence of nanoparticles with different surface functionalization. Figure 2 shows that nanoparticles with positive surface charge do not interfere with the microtubules structure neither during the interphase nor during the cell division, in spite of the remarkable accumulation of nanoparticles inside the cells.

Magnetite nanoparticles functionalized with heparine (i.e. with negative surface charge), which are internalized in the cells in a much smaller amount that those positively charged, are able to block the cell division in the metaphase. This originates multipolar mitotic structures and other damages that cannot be repaired by the cell and induce the apoptosis. Accordingly, 25% of the cells die after being cultivated for 24 hours with a concentration of nanoparticles of 0.5 mg/ml.

In summary, magnetite nanoparticles whose surface is functionalized with positive charge are internalized in HeLa cells in large amounts, but do not induce cytotoxicity, nor do they jeopardize the viability of cell division. They are good candidates to form magnetic cationic liposomes by embedding magnetic nanoparticles in positively charged lipid

This work has been financially supported by the Comunidad de Madrid and the MEC through projects NANOMAGNET and CONSOLIDER in Molecular Nanoscience, respectively.

References:

[1] P. Tartaj et al, J. Phys. D: Appl. Phys. 36 (2003) R182

Figures:

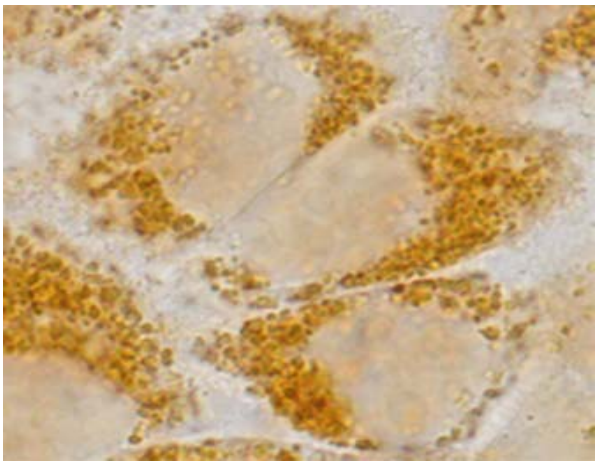

Figure 1: Optical microscopy (bright field) image of HeLa cells incubated with DX-covered magnetite nanoparticles at a concentration of 0.5 mg/ml during 24 hours

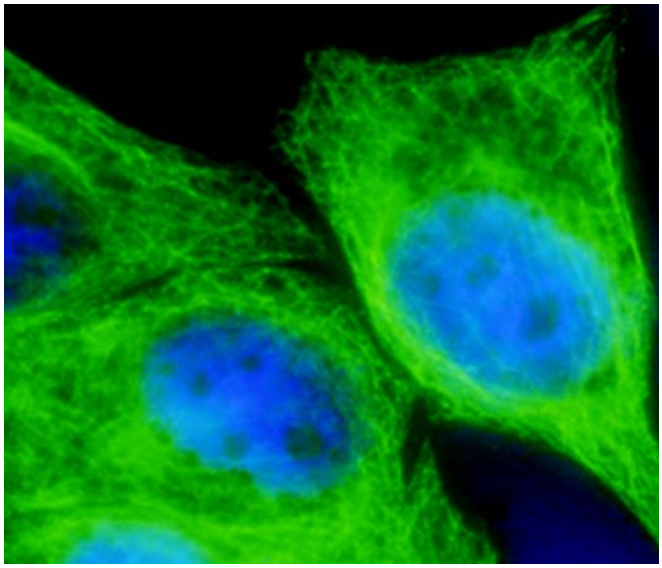

Figure 2: Fluorescence microscopy image of HeLa cells incubated with DX-covered magnetite nanoparticles at a concentration of 0.5 mg/ml during 24 hours.

Reversible Bipolar Resistive Switching $La_{1-x}Sr_xMnO_{3-\delta}$ thin films by C-SFM

C.Moreno [a], C.Munuera [a], A.Ruyter [b], N. Casañ [a], T.Puig [a], X.Obradors [a] and C. Ocal [a]

[a] Institut de Ciéncia de Materials de Barcelona , CSIC, 08193 Bellaterra, Spain
[b] LEMA-Universitè de Tours, CNRS-CEA UMR 6157, Parc de Grandmont, 37000, TOURS, France

cmoreno@icmab.es

Colossal magnetoresistance (CMR) materials have been suggested to be excellent candidates for advanced non-volatile memory devices based on its ability to switch its resistance into two different states. The origin of this phenomenon is still controversial and further investigation of the relationship of the nanostructure and electrical properties at the nanoscale is worthwhile.

We report here SFM results, including local current sensing (C-SFM) measurements on $La_{0.7}Sr_{0.3}MnO_3$ (LSMO) thin films grown by a chemical solution deposition (CSD) process on a $SrTiO_3$ substrate. These films have been developed through a new process leading to epitaxial La_2O_3 nanodots at the surface.

The SFM topographic images allow identifying the interfacial nanodot shape and distribution and the C-SFM permit to observe the insulating character of the nanodots, while the LSMO films display an homogeneous metallic character.

The LSMO film surface can be switched between a conductive ON state and a non-conductive OFF state by the application of an appropriate bias voltage. These results suggest that the LSMO thin films can be suitable especially for a mobile storage application, because of advantages such as a low-cost, ultrahigh density storage, and a low power consumption.

The figure illustrates the reversible switching process by a *writing and erasing* procedure performed at 5% relative humidity (RH). (a) Topographic images of two different areas of the sample surface which, as commented above, consists of a continuous metallic LSMO layer with insulating La_2O_3 islands on its top. (b) *Left column*: **reading process**. Current images taken at a low negative tip voltage over a large to observe the changes induced in a smaller region, (contained and centered in the shown images) after sweeping at three increasing positive tip voltages. *Right column*: **erasing process.** Current images taken at successively larger negative voltages (from top to bottom) until the metallic character of the previously modified region is recovered.

References:

[1] Szot et al. *phys. stat. sol. (RRL)* ***1****, No. 2, R86–R88 (2007)*

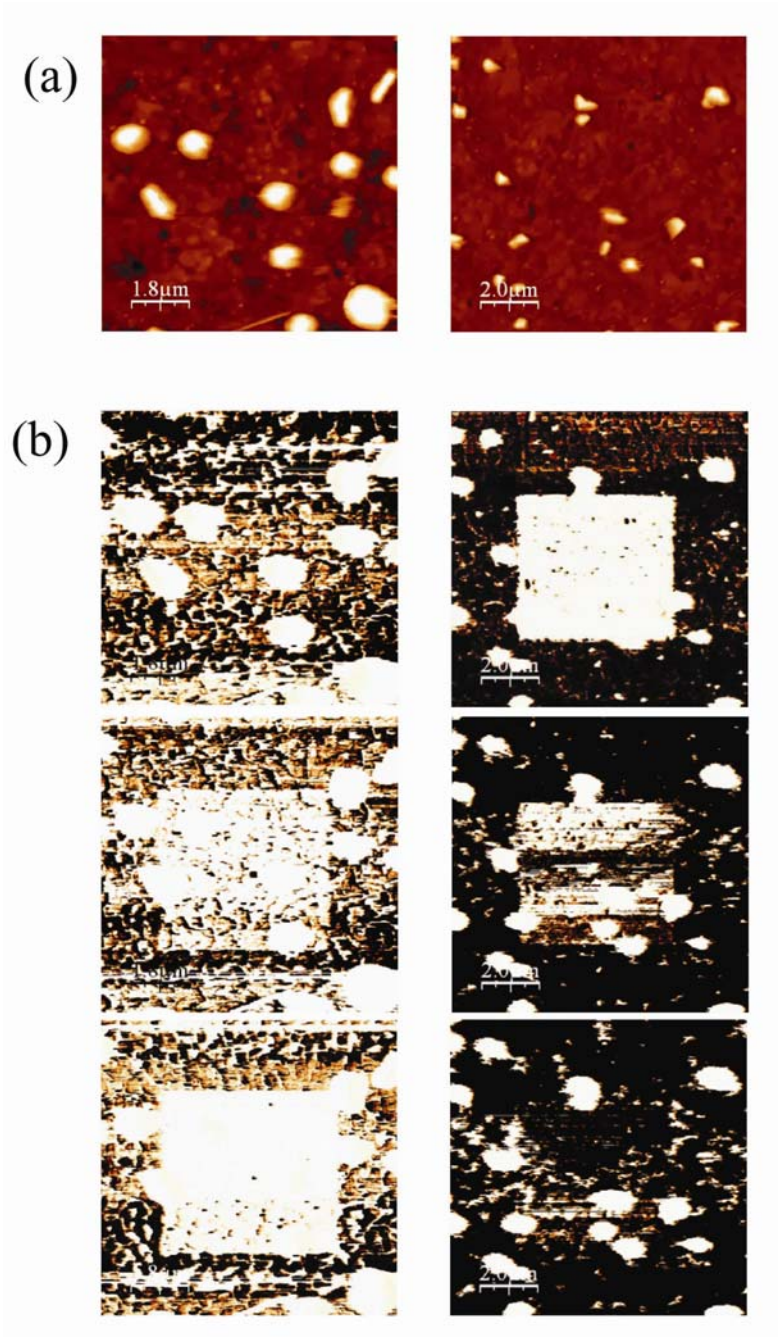
(a)
1.8μm
2.0μm
(b)

Cell response against water stable magnetic nanoparticles obtained by thermal decomposition procedure

María Moros, Beatriz Pelaz, Carlos Cuestas, Valeria Grazú, Jesús M. de la Fuente.
Instituto Universitario de Investigación en Nanociencia de Aragón (INA), Cerbuna 12, 50009-Zaragoza, Spain
mamoros@unizar.es

Magnetic nanoparticles offer a wide range of new opportunities including the quality improvement of contrast agents for MRI, hyperthermic treatment, and site-specific drug delivery. All these biological applications of these nanoparticles require the fulfilment of several features: high magnetization values, size smaller than 20 nm, narrow particle size distribution, simple biofunctionalization and a special surface coating to prevent nanoparticles aggregation, opsonization and toxicity effects [1, 2]. Very recently, Sun and co-workers [3, 4] had markedly improved the synthesis of monodispersed magnetite particles with size around 4 nm by thermal decomposition of iron (III) acetylacetonate in phenyl ether in the presence of oleic acid and oleylamine. As these nanoparticles are coated with a hydrophobic organic layer, they are only soluble in hexane and other non-polar or weakly polar organic solvent. However, these nanoparticles must be transfer to water to be used for biological applications. In this sense, we report here the optimization of two new procedures to prepare magnetite nanoparticles with an average size of 6 nm, a narrow size distribution and high stability in water and physiological media.

The first procedure is based in a previously reported strategy [5], which takes advantage of the hydrophobic surfactant layer of these nanoparticles to introduce an amphiphilic polymer shell. The hydrophobic nature of our nanoparticles can interact with the hydrophobic portion of this polymer. Water solubility of the nanomaterials will be ensured by the hydrophilic portion of the attached polymer. We have optimized the procedure with a different polymer (poly[maleic anhydride alt-1-octadecene]) which has a higher molecular weight than the one previously reported. Beyond the different evaluated parameters, the hydrolysis of the anhydride groups of the polymer resulted the key step for a fully solubilization of nanoparticles in aqueous media with any loss. The second procedure consists in the coating of the magnetic core with a thin gold shell following the procedure described by Wang and co-workers [6]. Then pegylated linkers modified with a thiol moiety [7] were used to drive nanoparticles into water. The water dispersed iron oxide nanocrystals obtained by both procedures were very stable in water and physiological buffers. In both cases, the presence of the outer shells was confirmed by TGA and the characterization was completed with transmission electron microscopy (TEM) and dynamic light scattering.

The influence of these nanoparticles on Hella cell line and human fibroblasts was assessed in vitro in terms of citotoxicity, morphology and cytoeskeleton organization. Standard cell viability assays (MTT and Trypan blue exclusion) demonstrated that cells incubated with all the synthesized nanoparticles remained more than 90% viable after 24 hours of incubation at concentration as high as 1 mg/ml. No difference was observed between the nanoparticles with pegylated linkers and without them, although at high concentrations (i.e 3mg/mL) nanoparticles with PEG resulted more stable. Nanoparticles conjugated with Rhodamine entered the cell, where they concentrated close to the nucleus; these data suggest some type of endocytic

internalization. To evaluate the non-specific proteins binding capacity of the synthesized nanoparticles, we used serum albumin (the most abundant blood protein) as a model. Little amount of BSA was found in nanoparticles, both with pegylated linkers and without them. This result suggests that nanoparticles will achieve long blood circulation half-lives as the removal of particle from circulation by the mononuclear phagocyte system (MPS) begins with the adsorption of plasma proteins.

Acknowledgments: This work has been funded by CONSOLIDER CSD2006-12 project. JS thanks "Ramon y Cajal" program (MEC) for financial support. JMF thanks ARAID for financial support.

References:

[1] Berry, C. C., and Curtis, A. S .G. J. *Phys. D: Appl. Phys.* 2003, 36, R198-R206.
[2] Gupta, A. K., and Gupta, M. *Biomaterials* 2005, 26, 3995-4021.
[3] Sun, S., and Zeng, H. *J. Am. Chem. Soc.* 2002, 124, 8204-8205.
[4] Sun, S., Zeng, H., Robinson, D. B., Raoux, S., Rice, P. M., Wang, S. X., and Li, G. *J. Am. Chem. Soc.* 2004, 126, 273-279.
[5] Pellegrino, T., Manna, L., Kudera, S., Liedl, T., Kokysh, D., Rogach, A. L., Keller, S., Rädler, J., Natile, G., and Parak, W. J. *Nanoletters* 2004, 4(4), 703-707.
[6] Wang, L., Luo, J., Fan, Q., Suzuki, M., Suzuki, I. S., Engelhard, M. H., Lin, Y., Kim, N., Wang, J. Q., and Zhong, C-J. *J. Phys. Chem B* 2005, 109, 21593-21601.
[7] Houseman, B.T., Mrksich, M. *J. Org. Chem.* 1998, 63, 7552-7555.

PHOTOLUMINESCENT DI-UREASIL HYBRIDS CONTAINING CdSe/ZnS QUANTUM DOTS

Márcia C. Neves[1], Manuel A. Martins[1], Paula C. R. Soares-Santos[1], Protima Rauwel[2], Rute A.S. Ferreira[3], Teresa Monteiro[3], Luís D. Carlos[3] and Tito Trindade[1]
[1] *Dep. of Chemistry, CICECO, University of Aveiro, 3810-193 Aveiro, Portugal*
[2] *Dep. of Ceramic and Glass Eng., CICECO, University of Aveiro, 3810-193 Aveiro, Portugal*
[3] *Dep. of Physics, CICECO, University of Aveiro, 3810-193 Aveiro, Portugal*
mcneves@ua.pt

Introduction

In recent years, there has been a growing interest in the synthesis of inorganic-organic functional materials exhibiting novel optical properties. A common procedure involves the association of already made inorganic nanostructures with an organic matrix, which is usually a polymer and that can be generated *in situ* by chemical means but maintaining the chemical integrity of the other component. The main advantage in using *in situ* methods is the often improved microstructure homogeneity of the materials, with important consequences in terms of their performance for example in optical devices and sensors. Using this strategy, a number of polymer nanocomposites have been reported in the literature [2].

Ureasilicate derivatives, often referred as di-ureasils, form a class of hybrid materials whose properties in terms of homogeneity are relevant for their optical performance, for example as a transparent host material in luminescent displays and integrated optical devices. The synthesis and optical properties of QDs, in particular for II/VI semiconductors, have been fully documented during the last decades and several reviews on the subject can be found in the literature [3]. An effective way to achieve highly photoluminescent CdSe QDs has been the passivation of surface defects either using organic capping agents or, more efficiently, to fabricate core/shell nanostructures in which the shell is made of a wide band-gap semiconductor [4]. As a result, radiative decay through emission of photons is a likely event in surface modified CdSe QDs, at room temperature, comparatively to bulk CdSe.

Chemical synthesis of d-U(600)CdSe and d-U(600)(CdSe/ZnS) hybrid materials

Several nanocomposites consisting on di-ureasil matrices doped with organically capped CdSe QDs have been prepared in this work. Despite the optical homogeneity of the CdSe/di-ureasil nanocomposites obtained, preliminary experiments performed on these nanocomposites also showed a low PL emission at room temperature. In principle, this reflects the properties of the individual QDs, since previous reports have shown that highly photoluminescent CdSe QDs need surface passivation with a wide band gap semiconductor (e.g. ZnS). We anticipate that this type of coating might have also a protective role in relation to detrimental effects on the CdSe QDs surfaces during the synthesis of the di-ureasil nanocomposites. In order to coat the CdSe QDs (prepared by Peng *et al* method [5]) with a ZnS phase we have developed in our laboratory a new strategy that is now described here. This involves in a first step the reaction of $Zn(S_2CNEt_2)2$ and thylenediamine (en), and then the thermolysis of the resulting complex $[Zn(en)_3(S_2CNEt_2)_2]$ in OL in the presence of CdSe QDs.

Photoluminescence of the as prepared hybrid materials

In preparing the di-ureasil nanocomposites, the primary effect of using coated CdSe QDs with ZnS was the bright luminescence observed in final transparent materials (figure 1), at least

when compared to their analogues using non-capped CdSe QDs. The lack of understanding on surface phenomena underlying the interaction between the di-ureasil matrices and the CdSe QDs led us to carry out a comparative study on the PL behaviour of the di-ureasil hybrids containing the as prepared CdSe QDs and those containing CdSe QDs which have been previously coated with ZnS.

Conclusions

The chemical synthesis of transparent, flexible and photoluminescent di-ureasil based nanocomposites was achieved by a sol-gel method, in the presence of CdSe and ZnS coated CdSe QDs (Fig. 1) [6]. For the latter a new and alternative process has been investigated, which involves the coating of previously prepared CdSe QDs with ZnS shells derived from an ligand mixed amine-alkyldithiocarbamate Zn(II) complex. The incorporation of such CdSe/ZnS QDs into the d-U(600) di-ureasil hybrid host result in final nanocomposites with emission quantum yields up to 0.11, displaying a huge increase (between 3 and 6 orders of magnitude) in the lifetime of the QDs, relatively to the isolated QDs, induced by d-U(600)-to-CdSe/ZnS QDs energy transfer active channels. Further work is at the moment in progress in our laboratory, including the development of nanocomposites whose photoluminescence can be tuned using distinct particle size distributions. This may be expressed in the future development of new functional nanomaterials which can be processed using already established sol-gel methodologies.

References:

[1] Sanchez C, Soler-Illia GJAA, Ribot F, Lalot T, Mayer CR, Cabuil V, *Chem. Mater.* **13 (**2001) 3061
[2] Kickelbick G, *Prog. Polym. Sci*,. **28 (**2003) 83
[3] Bawendi MG, Steigerwald ML, Brus LE, *Annu. Rev. Phys. Chem.* **41 (**1990) 477
[4] Dabbousi BO, Rodriguez-Viejo J, Mikulec FV, Heine JR, Mattoussi H, Ober R, Jensen KF, Bawendi MG, *J. Phys. Chem. B* **101 (**1997) 9463
[5] Peng ZA, Peng X, *J. Am. Chem. Soc.* **123 (**2001) 183
[6] Neves MC, Martins MA, Soares-Santos PCR, Rauwel P, Ferreira RAS, Monteiro T, Carlos LD, Trindade T, *Nanotechnology*, **19** (2008) 155601

.

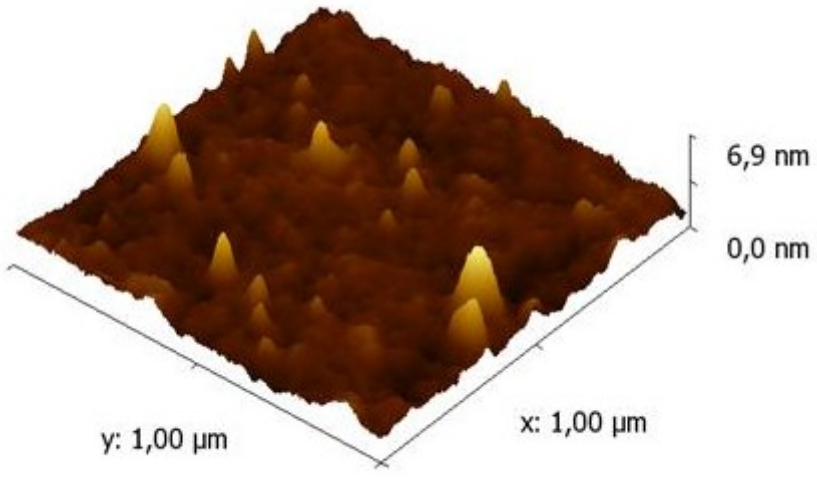

Figure 1: AFM image of a dU(600) di-ureasil hybrid containing CdSe/ZnS QDs

Exploration of laser induced gratings coupled to surface plasmon polaritons

Manfred Niehus
DEETC/ISEL, R. Conselheiro Emídio Navarro 1, Lisboa, Portugal
mniehus@deetc.isel.ipl.pt

Since the discovery of the extraordinary transmission enhancement through subwavelength hole arrays [1] the interest in surface plasmon polaritons has been on the rise, not just due to the astonishingly complex nature of single and coupled electronic, photonic and plasmonic modes and resonances in hybrid metal/dielectric structures on the nanometerscale [2], but also as it allows to engineer plasmonic metamaterials on the nanoscale [3]. Astonishing plasmon-correlated benchmark achievements include the transmission of entangled photons [4], enhanced LED emission [5] or the demonstration of TeraHertz radiation [6].

It is well known since the 1980ies [7] that the coupling between photons and surface plasmon polaritons has to be accomplished through a special coupling in order to assure wavevector conservation, or through Kretschmann configuration, or through a periodic lattice with a constant near to the wavelength of light.

The study of laser induced gratings has been established at about the same time [8]. It allowed to impose a grating period length scale onto a sample and to study its decay by time. Plenty of diffusion processes have been measured that way. Besides the optical detection techniques (with all over limited detection efficiency), electrical detection schemes were developed for the steady-state [9] and time-induced measurements [10].

The use of coherent frequency-shifted laser beams in grating experiments (photomixing) leads to moving photo-carrier gratings and represents an important technique for the generation of TeraHertz radiation [11].

To our knowledge, the surface plasmon polariton coupling of laser induced gratings was not yet explored . We will present in this contribution the outline of our experiments on highly doped semiconductors, the theoretical simulations, and the preliminary experimental results, and discuss them in the light of recent literature concerning the mode formation in one-dimensional gratings.

References:

[1] T.W.Ebbesen, H.J.Lezec, H.F.Ghaemi, T.Thio, and P.A.Wolff, Nature (London), 391, 667 (1998).
[2] L.Martin-Moreno, F.J.Garcia-Vidal, H.J.Lezec, K.M.Pellerin, T.Thio, J.B.Pendry, and T.W.Ebbesen, Phys.Rev.Lett. 86, 1114 (2001).
[3]W.A.Murray and W.L.Barnes, Adv. Mater. 3771, 19 (2007).
[4] E. Altewischer, M.P. van Exter, and J.P. Woerdman, Nature **418**, 304-306 (2002).
[5] J.Vuckovic, M.Loncar, and A.Scherer, IEEE J.Quant.Electr. 36, 1131 (2000).
[6] G.Rivas, J.A.Sanchez-Gil, M.Kuttge, P.H.Bolivar, and H.Kurz, Phys.Rev.B 74, 245324 (2006).
[7] H.Raether, Surface Plasmons on Smooth and Rough Surfaces and on Gratings, Springer, Berlin, 1988
[8] Eichler, P.Günter and D.Pohl, Laser-induced Dynamic Gratings, Springer, Berlin, 1986.
[9] D.Ritter, E.Zeldov, and K.Weiser, Appl.Phys.Lett. 65, 884 (1994).
[10] F.Wang and R.Schwarz, Appl.Phys.Lett. 65, 884 (1994).
[11] M.Tani, P.Gu, M.Hyodo, K.Sakai, and T.Hidaka, Optical and Quantum Electronics 32, 503 (2000).

EU(III)- BASED ORGANIC/INORGANIC LAMELLAR HYBRIDS SELF-DIRECTED ASSEMBLED

Sónia Nobre [1,2*], *Rute A. Sá Ferreira* [1], *Carlos Brites* [1], *Carole Carcel* [2], *Michel W. C. Man* [2], *Joël J.E. Moreau* [2], *Luís D. Carlos* [1]

[1]*University of Aveiro, Physics Department, CICECO, 3810-193 Aveiro, Portugal*
[2]*Ecole Nationale Supérieure de Chimie de Montpellier, Laboratoire Hétérochimie Moléculaire et Macromoléculaire (UMR-CNRS 5076) - 8, rue de l'école normale, 34296 Montpellier CEDEX 05, France*

snobre@ua.pt

Self-assembly of synthetic soft-matter components - such as polymers, liquid crystals, surfactants, colloids, and organic/inorganic hybrids - results in regular hierarchically organized structures. The importance of combining sol-gel methods and self-assembly routes to synthesize hierarchically structured organic/inorganic materials, has been highlighted recently.[1,2] Moreover, the recent advances in the structuring of sol-gel derived bridged silsesquioxanes represented an important breakthrough in the field of hierarchically organized hybrid materials. [3]

Since the beginning of the twentieth century, the radiative transitions of lanthanide ions have received academic and industrial attention. Moreover, the technological applications of lanthanide luminescence encompass not only fluorescent tubes and colour televisions, but also immunoassays, optical amplifiers and light-emitting diodes (LEDs).[4] The Eu^{3+} ion, in addition, is also considered the best choice to act as a probe to investigate the local structure around optically active ions in condensed matter. This is due to its relatively simple energy level diagram and the sensitivity of the energy positions and the intensity of its electronic transitions with the symmetry of the lanthanide local site.[5]

Here, we report on the structural and photoluminescence features of Eu(III)-modified bridged silsesquioxanes. The organic/inorganic precursor molecule - $(EtO)_3Si(CH_2)_3NH(C=O)NH-(CH_2)_{12}-NH(C=O)NH(CH_2)_3Si(OEt)_3$ -is formed of siliceous domains covalently bonded to an alkylene chain with 12 repeat units through urea functional groups. Sol-gel reactions using an acid catalyst, large excess of water and $EuCl_3$ gave rise to the formation of crystalline Eu(III)-based lamellar hybrids through a self-organization process. Three different Eu^{3+}-based hybrids were prepared. The hybrids were studied by X-ray diffraction (XRD), small angle diffraction (SAXS), scanning electronic (SEM) and atomic force microscopy (AFM), Fourier transform absorption mid-infrared (FT-IR), Fourier transform Raman and photoluminescence spectroscopies, ^{29}Si and ^{13}C solid state nuclear magnetic resonance,

The hybrids are the first lamellar organic/inorganic luminescent hybrids incorporating trivalent europium, figure 1 shows a SEM picture of one of the hybrids prepared. The emission spectra of these hybrids, figure 2, are composed of a broad band (380-560 nm), ascribed to electron-hole recombination's occurring within the urea cross-linkages and the siliceous nanodomains [2], and a series of straight lines, ascribed to Eu^{3+} intra-$4f^6$ transitions between the $^5D_0$ first excited state and the $^7F_{0-4}$ levels of the ground multiplet. Based on the photoluminescence features of the hybrids we were able to calculate the quantum efficiency and the number of water molecules coordinated to the Eu^{3+} ion.

References:

[1] K. Vallé, P. Belleville, F. Pereira, C. Sanchez, Nature Mater. **5**, (2006) 107
[2] L. D. Carlos, V.de Zea Bermudez, V. S. Amaral, S. C. Nunes, N. J. O. Silva, R. A. Sá Ferreira, J. Rocha, C. V. Santilli, D. Ostrovskii, Adv. Mater. **19**, (2007) 341.
[3] J. J. E. Moreau, L. Vellutini, M. Wong Chi Man, C. Bied, J.-L. Bantignies, P. Dieudonné, and J.-L. Sauvajol, Self-Organized Hybrid Silica with Long-Range Ordered Lamellar Structure, J. Am. Chem. Soc. **123,** (2001) 7957-7958.
[4] M. Bredol, U. Kynast, C. Ronda, *Adv. Mater.* **3**, 1991, 361.
[5] L. D Carlos, Y. Messaddeq, H. F. Brito, R. A. S. Ferreira, V.de Zea Bermudez, S. J. L.Ribeiro, S. J., *Ad*V. *Mater.* **12**, 2000 **,** 594.

Figures:

Figure 1 – SEM image of the Eu@L12-1 hybrid.

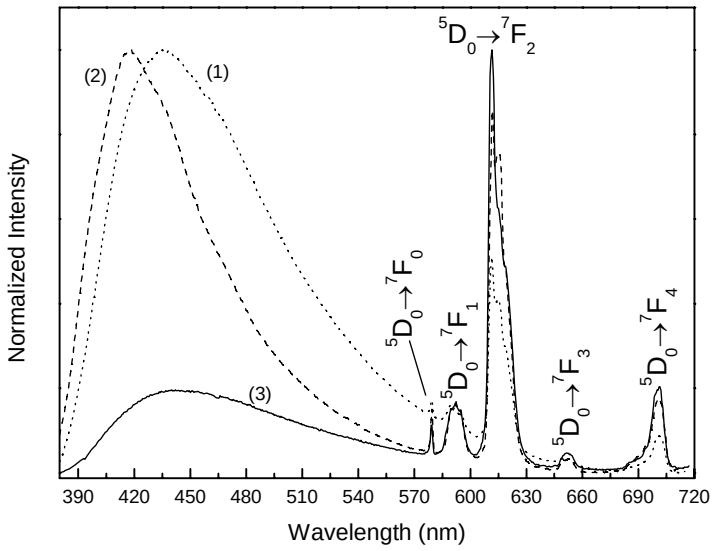

Figure 2 Emission spectra of the lamellar hybrids incorporating three different Eu3+ concentrations (1) 1.01%-Eu@L12 (2) 1.87%-Eu@L12 and (2) 15.0%-Eu@L12.

Rheological studies on polymeric nanoparticle dispersions stabilized by a polyfructose-derivative surfactant

Marc Obiols-Rabasa[1], Jordi Esquena[1,], Conxita Solans[1], Jérémie Nestor[1], Bart Levecke[2], Karl Booten[2], Tharwat F. Tadros[3]*

[1] *CSIC - Institut d'Investigacions Químiques i Ambientals de Barcelona (IIQAB), CIBER-BBN, Jordi Girona 18-26, 08034 Barcelona, Spain*

[2] *Orafti, Bio Based Chemicals, Aandorenstraat 1, B-3300 Tienen, Belgium*

[3] *89 Nash Grove Lane, Wokingham, Berkshire, RG40 4HE, UK*

* *jemqci@iiqab.csic.es*

The preparation of stable concentrated dispersions of latex particles is a very important subject due to technological interest in many applications. In this context, nonionic graft copolymer surfactants are commonly used because of their adsorption onto the particles forming strong steric barriers, highly insensitive to both temperature and electrolyte. We have studied a graft copolymer surfactant, consisting of an inulin (polyfructose) backbone on which several alkyl groups are randomly grafted [1]. The alkyl groups provide the anchor points for attachment at the solid/liquid interface, leaving the polyfructose loops in contact to the external aqueous solution. Previous results showed that particles covered by this surfactant possess very good stability at high electrolyte concentration [2, 3]. Colloidal dispersions stabilized by this inulin-derivative surfactant remain with no flocculation at high electrolyte (Na_2SO_4) concentration such as 1.5 mol.dm^{-3} [3] (Figure 1).

In the present work, a rheological behaviour study of polystyrene (PS) latex particles sterically stabilized with the polyfructose-derivative surfactant was carried out. The results of steady-state shear stress as a function of shear rate showed that could be used for determining the adsorbed layer thickness of the hydrophobically modified inulin polymeric surfactant. The surfactant layer thickness was determined by comparison of experimental data with the Dougherty-Krieger theoretical curve, which describes the relative viscosity as a function of the volume fraction assuming hard sphere systems [4]. The results proved that a graft copolymer layer was adsorbed onto the polystyrene particles reducing the maximum volume fraction from $\phi = 0.6$ assuming randomly packed hard spheres down to $\phi = 0.505$ (Figure 2). From these measurements, an adsorbed graft polymeric surfactant layer thickness of approximately 9.6 ± 2 nm was calculated. Moreover, viscoelastic measurements showed a change from mainly viscous to predominantly elastic response at low effective volume fraction, $\phi_{eff} = 0.24$. The latter indicates strong hydration of the polyfructose loops and tail, providing very strong steric repulsion, which indicates that soft interactions are present between the particles containing adsorbed surfactant.

The results of the layer thickness determination by rheology were consistent with those obtained in previous layer thickness determination studies carried out by means of Dinamic Light Scattering (DLS) [2] and Atomic Force Microscopy (AFM) [5]. Studies by DLS were carried out by post-adding the polymeric surfactant to a surfactant-free PS dispersion. The results showed an adsorbed layer thickness of approximately 10 nm. AFM measurements were carried out by means of a modified

atomic force microscope apparatus [6]. The steric repulsions between two layers of the polymeric surfactant adsorbed onto a hydrophobic sphere and a plate were measured. The results showed that high steric repulsion was present even at high electrolyte concentration when approaching the two adsorbed layers. From these measurements, an adsorbed surfactant layer thickness of 9 nm approximately was obtained, confirming the rheological determinations.

References:

[1] Stevens, C.V., Meriggi, A., Peristeropoulou, M., Christov, P.P., Booten, K., Levecke, B., Vandamme, A., Pittevils, N., Tadros, Th.F., Biomacromolecules **2**, 2001, 1256-1259
[2] Esquena, J., Dominguez, F.J., Solans, C., Levecke, B., Booten, K., Tadros, Th.F., Langmuir **25**, 2003, 10463
[3] Nestor, J., Esquena, J., Solans, C., Levecke, B., Booten, K., Tadros, Th.F., Langmuir **21**, 2005, 4837-4841
[4] Tadros, Th.F., Adv. Colloid Interface Sci. **108-109**, 2004, 227-258
[5] Nestor, J., Esquena, J., Solans, C., Luckham, P.F., Musoke, M., Levecke, B., Booten, K., Tadros, Th.F., J. Colloid Interface Sci. **311**, 2007, 430-437
[6] Braithwaite, G.J.C., Howe, A., Luckham, P.F., Langmuir **12**, 1996, 4224

Figures:

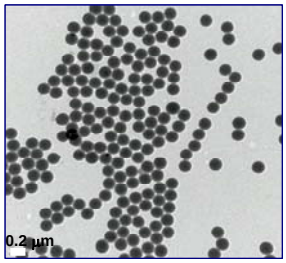

Figure 1. Polystyrene latex particles obtained by Transmision Electron Microscopy (TEM)

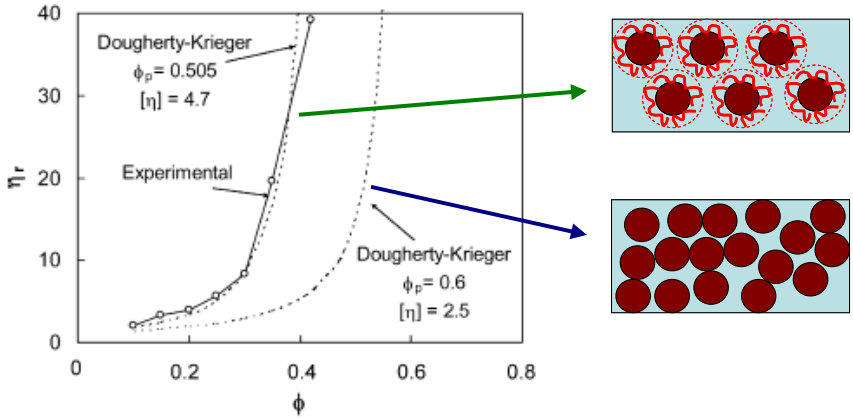

Figure 2. Relative viscosity as a function of particle volume fraction

SILVER NANOWIRES: PHOTOCATALYTIC SYNTHESIS AND CHARACTERIZATION

Inês Osório[a] , *Adelaide Miranda*[a], *Patrícia A. Carvalho*[b], *Eulália Pereira*[a]

[a]*REQUIMTE - Departamento de Química,Faculdade de Ciências,Universidade do Porto, Rua do Campo Alegre, 687, 4169-007 Porto, Portugal*
[b]*Departamento de Engenharia de Materiais, Instituto Superior Técnico,Av. Rovisco Pais, 1049-001 Lisboa, Portugal*

E-mail: efpereir@fc.up.pt

One of the greatest challenges of nanotechnology is the preparation of anisotropic nanoparticles with controlled size and shape. In particular, Ag nanowires have been the focus of much attention due to not only to the fundamental interest in studying the physical properties of such 1D nanoparticles, but also due to its possible applications in the construction of electronic, optoelectronic, electrochemical, and electromechanical nanodevices. There are several reports on wet chemical procedures for the preparation of Ag nanowires, but the mechanism of formation of these nanostructures is still a matter of debate. In order to get a better insight onto the factors governing anistropic growth of Ag nanoparticles, we have studied the formation of Ag nanowires using a novel photocatalytic reducing method and citrate as the capping agent. Citrate is known to promote the formation of anisotropic Ag nanoparticles,[1] but the results reported so far show that the morphology and size of the nanoparticles obtained are strongly dependent not only on the capping effect, but also on the kinetics of the reducing reaction.[2,3] The present approach was selected since it allows the independent study of the influence of the reduction kinetics and the capping effect on the formation of Ag nanowires.

Silver nanowires were obtained by the photocatalytic reduction of silver nitrate, using a Sn(IV) porphyrin as the phtocatalyst, and triethanolamine (TEA) as electron donor, in the presence of sodium citrate (NaCit), by a method adapted from the literature.[4]
The formation of Ag nanowires was detected after only 2 minutes of irradiation by the change in the colour of the solution to red-brown, due to the appearance of a plasmon band around 600 nm (Figure 1), and was confirmed by TEM (Figure 2). The nanowires obtained are not stable in solution, and after 4 min start to undergo a morphological transition to spherical nanoparticles, with a change of colour of the solution from red-brown to green. This morphological transition is faster in the presence of a strong capping agent (11-mercapto-undecanoic acid), a strong reducing agent ($NaBH_4$), and when the reaction is carried out anaerobically, indicating that the morphological transition probably involves oxidative etching and agglomeration/aggregation of nanoparticles.

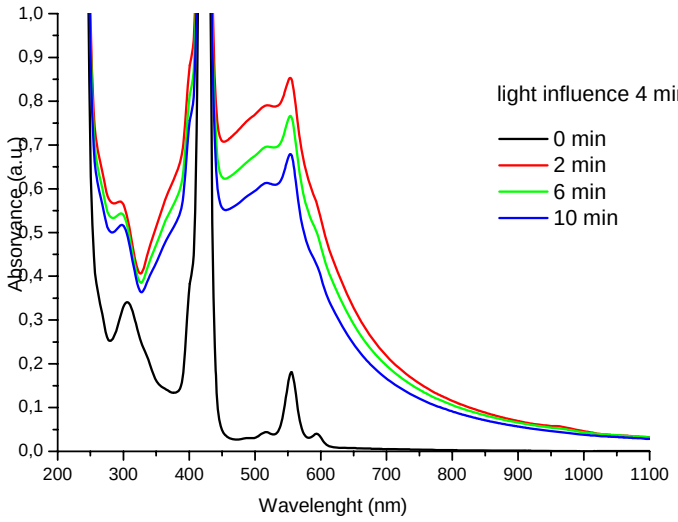

Figure 1: UV/vis spectra of the silver nanoparticles obtained by the photocatalytic method in the presence of citrate as a capping agent.

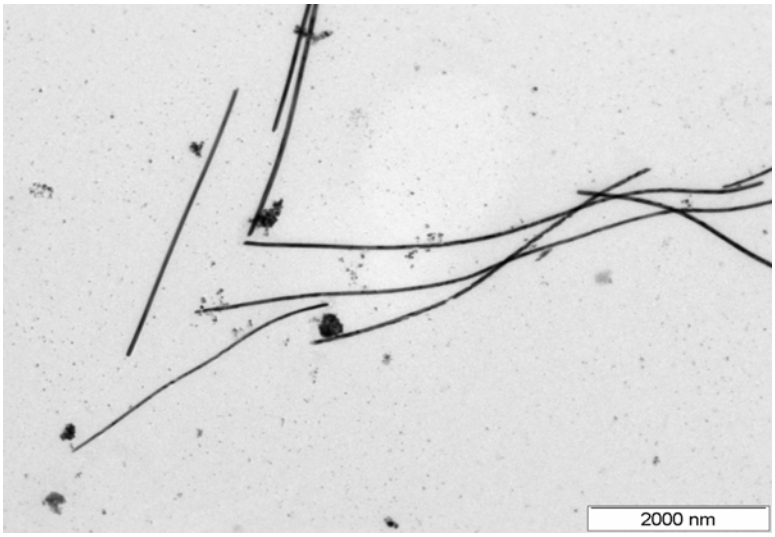

Figure 2: TEM image of the silver nanoparticles obtained after 4 minutes of irradiation.

(1) Zhang, S. H.; Jiang, Z. Y.; Xie, Z. X.; Xu, X.; Huang, R. B.; Zheng, L. S. *J. Phys. Chem. B* **2005**, *109*, 9416-9421.
(2) Pillai, Z. S.; Kamat, P. V. *J. Phys. Chem. B* **2004**, *108*, 945-951.
(3) Henglein, A.; Giersig, M. *J. Phys. Chem. B* **1999**, *103*, 9533-9539.
(4) Song, Y. J.; Yang, Y.; Medforth, C. J.; Pereira, E.; Singh, A. K.; Xu, H. F.; Jiang, Y. B.; Brinker, C. J.; van Swol, F.; Shelnutt, J. A. *J. Am. Chem. Soc.* **2004**, *126*, 635-645.

Acknowledgments: Fundação para a Ciência e a Tecnologia (FCT), Portugal, through project PTDC/QUI/64484/2006; A. Miranda thanks FCT for PhD fellowship SFRH/BD/18630/2004.

1D ZnO Chains as the Spinal Cord of Adsorbed Metalloporphyrin Nanotubes Linked by Water Ligands

Marta Trelka[1], Christian Urban[1], Celia Rogero[2], Eva Mateo[2], Paula de Mendoza[3], Wang Yang[4], Iñaki Silanes[5], Manuel Alcamí[4], Andrés Arnau[5], José Ángel Martín Gago[2,6], Fernando Martín[4], Antonio Echavarren[3], José María Gallego[6], Roberto Otero[1] & Rodolfo Miranda[1,7]

[1] *Dep. de Física de la Materia Condensada & Instituto Nicolás Cabrera, Universidad Autónoma de Madrid, Campus de Cantpoblanco, 28049 Madrid, Spain*
[2] *Centro de Astrobiología (CSIC-INTA), 28850 Madrid, Spain*
[3] *Institut Català d'Investigació Química, 43007 - Tarragona, Spain*
[4] *Dep. de Química, Universidad Autónoma de Madrid, Campus de Cantpoblanco, 28049 Madrid, Spain*
[5] *Donostia International Physics Center (DIPC) and Departamento de Fisica de Materiales and Unidad de Fisica de Materiales, E- 20018 San Sebastian, Spain*
[6] *Instituto de Ciencia de Materiales de Madrid - CSIC, 28049 Madrid, Spain*
[7] *Instituto Madrileño de Estudios Avanzados en Nanociencia (IMDEA-Nanociencia), Madrid 28049, Spain*
roberto.otero@uam.es

Zinc oxide is a technologically attractive material due to its unique piezoelectric and optoelectronic properties. In recent years a very intense activity has been directed towards the fabrication of ZnO nanowires for applications such as room-temperature, ultra-violet lasing, field-effect transistors, chemical and biochemical sensors, etc. The growth of such nanowires is usually carried out by vapour-liquid-solid method, in which liquid droplets of surfactant direct the growth of the ZnO nanowire. The width of the resulting nanowire is thus determined by the size of the surfactant droplets, usually no smaller than 50 nm [1].

On the other hand, it is well known that 1D structures made out of face-to-face stacked metallomacrocycles can be stabilized by ligand coordination between the metal centres. For example, Ru and Os porphyrins can form long 1D, conductive polymers in which pyrazine ligands bridge the metal centres in neighbouring porphyrins. The resulting structure can thus be regarded as a nanotube in which an organic outer scaffolding protects an inner, strictly 1D metal-ligand spinal cord [2].

In this work we describe the formation of long 1D ZnO chains as spinal cords of self-assembled Zn-porphyrin nanotubes created by deposition of aquo(tetramesitylporphyrinato)zinc(II) (H_2O-ZnTMP)) on noble-metal surfaces. Our low-temperature Scanning Tunnelling Microscopy (STM) experiments reveal that the deposition of H_2O-ZnTMP on Au(111) and Cu(100) leads to the formation of long 1D tube-like structures, which are not found upon deposition of the metal-free H_2TMP. Moreover, the nanotubes are also disrupted upon annealing to temperatures in which the H_2O ligands detach from the Zn atoms, as monitored by X-Ray Photoemission Spectroscopy (XPS). Density Functional Theory (DFT) calculations also support this view, yielding binding energies of about 0.7 eV per monomer due to the presence of the water links, whereas in the absence of water ligands the attractive interaction energy between the ZnTMP units is negligible.

This work demonstrates that coordination bonds can be preserved upon sublimation and surface adsorption, opening new ways to steer the coordinative co-polymerization of adsorbed species by deposition of supramolecular units that already contain some of the coordination bonds to be found in the desired final product. We have shown that this method can be used to grow 1D metalloporphyrin coordination copolymers with a ZnO spinal cord with potential applications in molecular optoelectronic devices such as optoelectronic gates.

References:

[1] Z. L- Wang, J. Phys.: Condens. Matter, **16** (2004) R829.
[1] J. P. Collman, J. T. McDevitt, G. T. Yee, et al., Proc. Natl. Acad. Sci. USA, **83** (1986) 4581.

Figures:

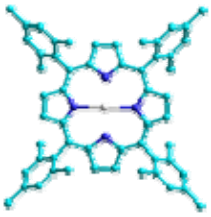

Figure 1. Stick-and-ball model of the Zn porphyrin used in this study.

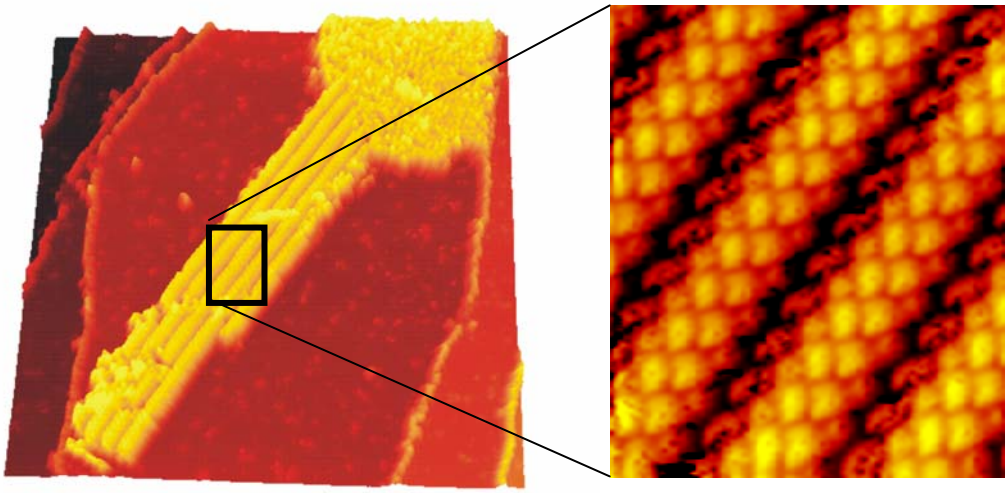

Figure 2. 98.4 × 98.4 nm2 STM image of long tubes coexisting with disorder after depositing ZnTMP on Cu(100) and a zoom-in showing the spiral shape of the tubes

Figure 3. 21 × 25 nm2 STM image showing individual flat lying ZnTMP molecules on Cu(100) after annealing the tubes to 500 K.

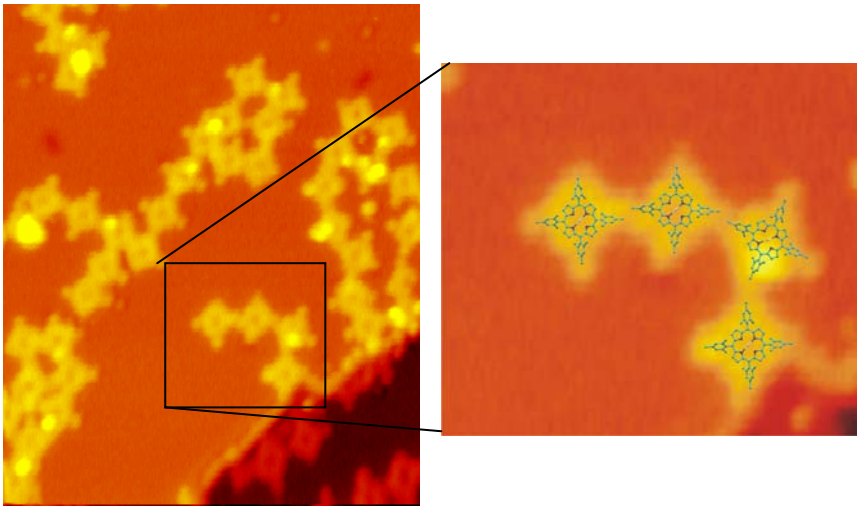

Amperometric (bio)sensors based on carbon nanotubes

M. Pacios, L. Cyganek, M. del Valle, M.J. Esplandiu
Departament de Quimica, Universitat Autònoma de Barcelona
Edifici C7 nord, 08193 Bellaterra, SPAIN.
merce.pacios@uab.cat

Carbon nanotubes CNTs are attractive electrode materials due to their good electrical conductivity and mechanical strength, as well as being relatively chemically inert in most electrolyte solutions, where they still retain a high surface activity and a wide operational potential window. However, the proper construction and orientation of the carbon nanotube electrode is critical for its electrochemical properties; high density of open ends (similar to a graphite edge-plane electrode) can give fast electron transfer response but they only constitute a very small portion of the CNT surface exposed to the solution [1]. Side-walls and amorphous carbon-covered surface dominate on the overall surface area causing slower electron transfer kinetics. Moreover and from the point of view of the amperometric biosensing, the establishment of a fast electron transfer between the active site of a redox biomolecule and the electrochemical transducer is one of the topics that has taken considerable attention in order to design biosensors with progressing sensitive characteristics [2,3].

Accordingly, our purpose is to highlight the transducer and biosensor performance of different electrode systems and configurations based on carbon nanotubes and compare with graphite composites and highly oriented pyrolytic graphite. Specifically, the (bio)sensor behavior of the different carbon configurations functionalized with redox proteins (catalase and myoglobin) will be evaluated. Such proteins exhibit high sensitivity to oxygen and peroxide and are capable to catalyze the reduction of such species, which hold promise as oxygen and peroxide sensors [4]. Figure 1 shows a scheme of the different carbon systems that have been evaluated together with their respective images taken by Scanning Electron Microscopy (SEM). Our results confirmed that carbon nanotube electrodes constitute optimal environments for the direct electron transfer of such redox proteins. Additionally, we found that electrodes based on vertically aligned carbon nanotubes provide the highest electron transfer kinetics to the oxygen or peroxide reduction, the fastest sensor response and the highest signal/noise relation which has allowed the detection of very low analyte concentrations.

References:

[1] C.E. Banks, T.J. Davies, G.G. Wildgoose, R.G. Compton, Chem. Commun. (2005) 829.
[2] J. Li, A. Cassell, L. Delzeit, J. Han, M. Meyyappan, J. Phys. Chem. B, **106** (2002) 9299.
[3] L.Y. Heng, A. Chou, J. Yu, Y. Chen, J.J. Gooding, Electrochem. Comm., **7** (2005) 1457.
[4] A.F. Nassar, Z. Zhang, N. Hu, J. Rusling, T. Kumosinski, J. Phys. Chem. B, **101** (1997) 2224.

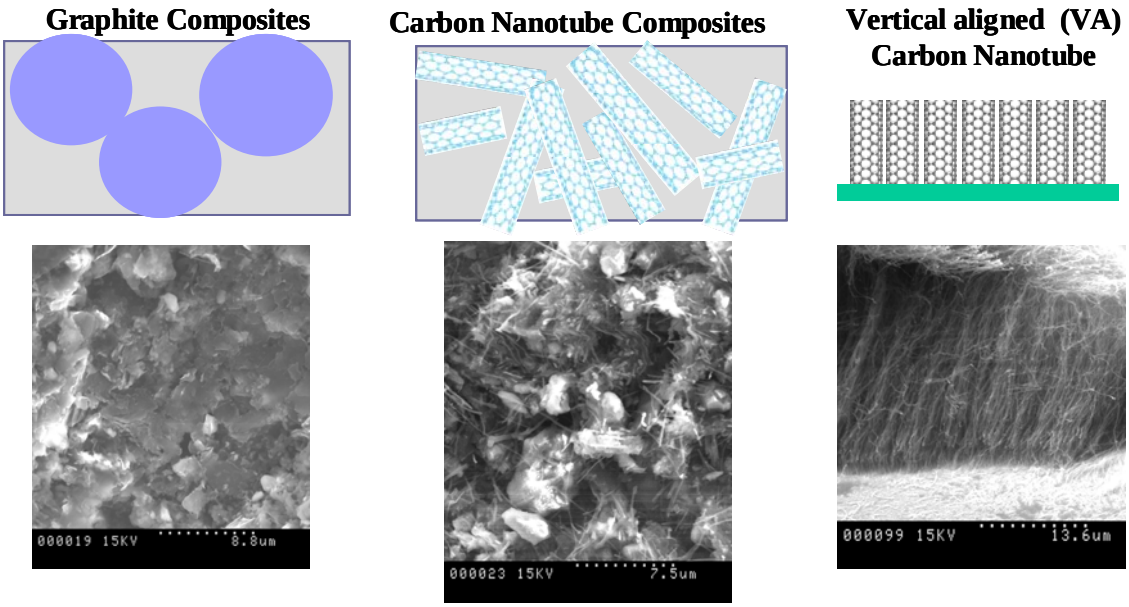

Figure 1. Scheme of the different carbon electrodes under study together with their respective SEM images.

PARTICLE FORMATION BY SUPERCRITICAL FLUID-ASSISTED PROCESSES

L. Padrela, M. Rodrigues, A. Almeida[a], *H. A. Matos, E. Gomes de Azevedo*

Department of Chemical and Biological Engineering
Instituto Superior Técnico, Av. Rovisco Pais , Lisboa, PORTUGAL
Contact e-mail: egazevedo@ist.utl.pt
and
[a] Research Institute for Medicines and Pharmaceutical Sciences (*i*Med.UL), Faculdade de Farmácia
Universidade de Lisboa, Av. Prof. Gama Pinto, Lisboa, PORTUGAL

Recent developments in biotechnology forecast a new generation of therapeutics. Yet, the increasing specificity of emerging drug candidates and its susceptibility to the classical administration routes raise new challenges to the Galenic pharmacology.

The pulmonary route is becoming an attractive alternative for the delivery of pharmaceutics[1], especially macromolecules like peptides, and proteins. However, it requires exquisite particles with specifications hard to achieve by most of the established technologies. Therefore, particle engineering using appropriate processes and excipients is required to produce particles of optimal size, morphology, and surface properties that would enhance drug target efficiency[2]. As a consequence, the preparation of drug micro and -nanoparticles with a controlled particle size distribution has become an important focus for the development of pharmaceutical delivery formulations[3].

Supercritical fluid-assisted technologies allow the generation of particles that are difficult or even impossible to obtain by traditional techniques such as milling, crystallization and spray drying which don't provide an efficient control of the particle size (a broad particle size distribution is normally obtained).

A novel method to produce fine dry powders (e.g. proteins, polymers, composites, cocrystals), making use of the properties of supercritical fluids, has been developed at IST. It consists of a concerted precipitation by two distinct mechanisms, the anti-solvent crystallization and the atomization and spray drying (A-SAIS process). Our results show that bioavailability issues can be overcome by accurate control of the particulate products properties, such as the crystalline form, morphology, size distribution, and the excipients composition and layering. Depending of the leading mechanism (atomization or anti-solvent) the morphology will vary from spheres to fibers (figure 1).

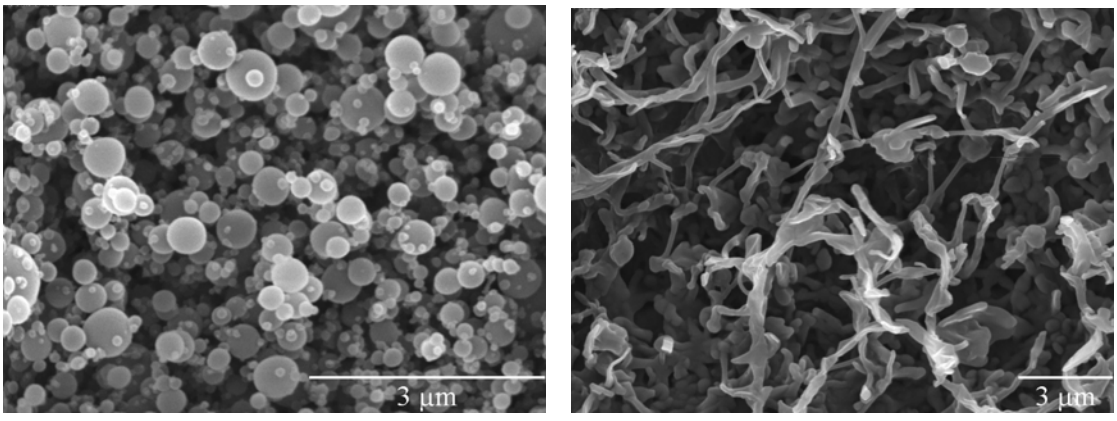

Figure 1 – Scanning Electron Microscopy images of lysozyme particles processed by the A-SAIS process: (a) spheres, and (b) fibers

The knowledge of the production process variables for the two precipitation mechanisms is the key to determine the precipitation sequence of drugs and excipients and then the degree of microencapsulation.

References

[1] Porta, Giovanna D., Vittori, Carlo D., Reverchon, E., AAPS PharmSciTech, **Supercritical Assisted Atomization: A Novel Technology for Microparticles Preparation of an Asthma-controlling Drug,** Volume 6, Number 3 (2005), E421-E428

[2] Rodrigues, M., Peiriço, N., Matos, H., Gomes de Azevedo, E., Lobato, M.R., Almeida, A.J., Journal of Supercritical Fluids, **Microcomposites theophylline/hydrogenated palm oil from a PGSS process for controlled drug delivery systems**, Volume 29, Issues 1-2 (2004), pp175–184.

[3] Reverchon, E., Adami, R., Journal of Supercritical Fluids, **Review, Nanomaterials and Supercritical Fluids**, Volume 37, Issue 1 (2006), pp 1-22

Poster

CHEMICAL FUNCTIONALISATION OF CARBON NANOTUBES FOR THE DISPERSION IN POLYMER MATRICES

Maria da Conceição Paiva[1], Maria Fernanda Proença[2], Carlos J. R. Silva[2], Rui F. Araújo[2], Rui M. Novais[1]

[1]Institute for Polymers and Composites, Department of Polymer Engineering, University of Minho, Campus of Azurém, 4800-058 Guimarães, Portugal

[2]Department of Chemistry, University of Minho, 4710-057 Braga, Portugal

mcpaiva@dep.uminho.pt

Carbon nanotubes (CNT) and nanofibres (CNF) exhibit unique mechanical, electric and thermal properties [1-2]. Their physical form is not convenient for most applications, demanding their combination with a matrix material. The preparation of a composite requires an efficient dispersion of the reinforcing phase and its good interaction with the matrix. However, the chemical inertness and low surface energy of the graphitic structure of the CNT and CNF makes this process difficult. Thus, the surface modification of CNT and CNF, aiming at the improvement of their interaction with other materials, is becoming an area of increasing importance. This modification can be achieved by attaching functional groups to the CNT/CNF surface [3-4] that will interact strongly with the matrix material, thus originating composites with exceptional structural properties at low reinforcement loads [5,6].

Most functionalization methods involve strong acid treatment of the CNT/CNF, producing extensive nanotube breakage. A class of functionalisation reactions that does not involve acid treatment is the direct addition to the π-electrons of the CNT/CNF [7,8]. These chemical reactions are less aggressive to the CNT/CNF in the sense that they do not induce high nanotube breakage, maintaining the CNT aspect ratio almost unchanged relative to the non-functionalised CNT.

The present work reports the functionalisation of CNT and CNF using two different methods. The first method is based on a Diels-Alder addition reaction (DA) of 1,3-butadiene to the CNT surface, as described in a previous work [9]. The other method is based on the addition of 1,3-dipoles to the CNT surface, generated by condensation of an α-amino acid and an aldehyde [8,10], as represented in Scheme 1.

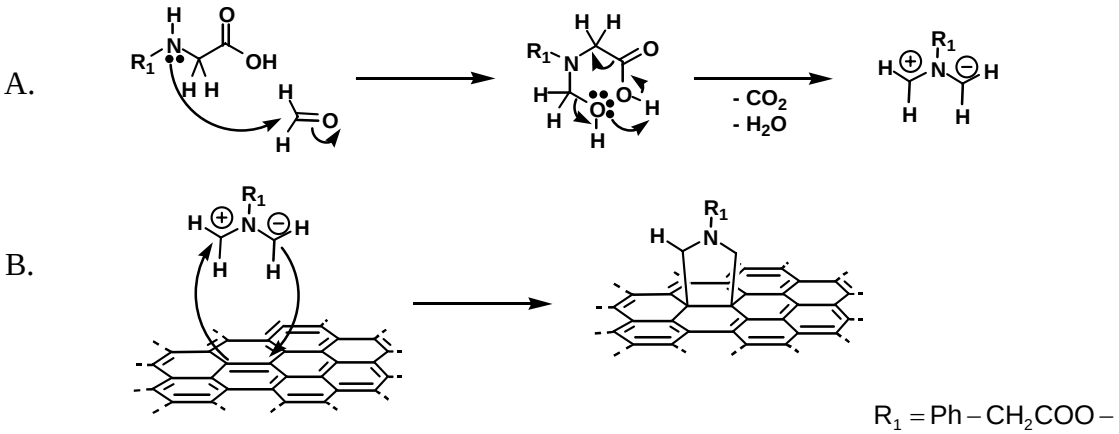

Scheme 1. A. Formation of the 1,3-dipole; B. Addition of the 1,3-dipole to the graphite surface.

The characterisation of the CNT and CNF functionalisation was done by thermogravimetric analysis (TGA), X-ray photoelectron spectroscopy (XPS) and electron microscopy. For the CNT and CNF an increase in weight loss was observed after functionalization, measured by TGA under a constant flow of N_2, as shown in Table 1. The XPS spectra confirmed the

presence of the amine at the surface of the nanofibres functionalized by the 1,3-dipolar cycloaddition reaction. Transmission electron micrographs of the non functionalised and functionalised CNFs are shown in Figure 1. The CNF functionalised by the DA addition of butadiene, under high butadiene concentration, show a layer of a polymeric product formed at the CNF surface (Figure 1 b). The extension of this layer may be controlled by the reaction conditions.

Table 1. TGA weight loss for CNF functionalized in different conditions.

CNF treatment	Weight loss (%) ± Stand. Dev.
Untreated	2.3 ± 1.2
DA reaction	11.2 ± 2.5
1,3-dipolar cycloaddition reaction	16.7 ± 2.3

Figure 1. TEM micrographs of CNFs: a) non-functionalised, b) functionalised by Diels-Alder addition.

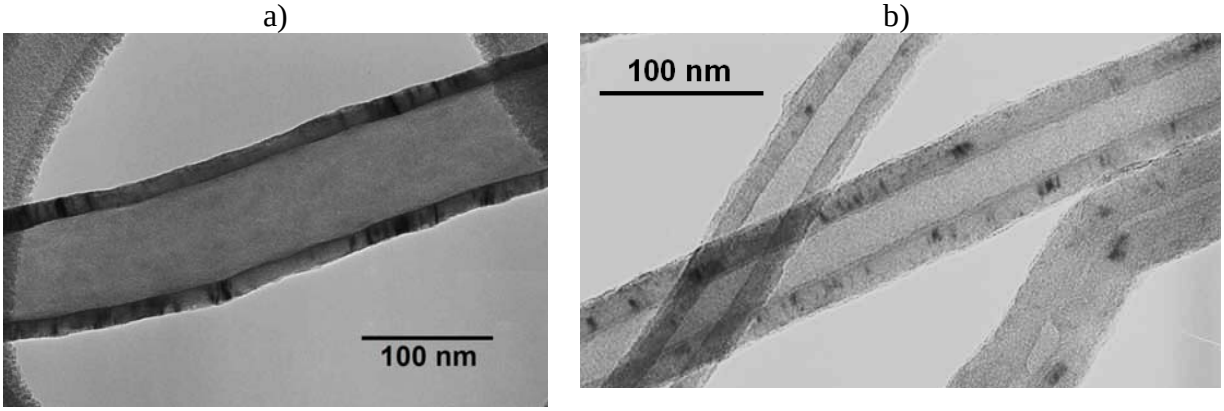

Composites were prepared by mixing the CNF with polymer matrices using melt blending techniques. The analyses of the cross-sections of the composites formed showed that the distribution of the CNF through the polymer matrix was good for the non-functionalised and functionalised CNF in both matrices. The functionalised fibres were well wet by the matrix polymer, while the non-functionalised CNF showed poor wetting by the matrix.

Acknowledgments: The authors acknowledge the financial support from FCT (Portuguese Foundation for Science and Technology) through the project POCI/QUI/59835/2004.

References:

[1] Baughman R H, Zakhidov A A, de Heer W A, Science, 297 (2002) 787-792.
[2] Mamalis A G, Vogtländer L O G, Markopoulos A, Precision Eng, 28 (2004) 16-30.
[3] Bahr J L, Tour J M, J Mater Chem, 12 (2002) 1952-1958.
[4] Tasis D, Tagmatarchis N, Georgakilas V, Prato M, Chem Eur J, 9 (2003) 4000-4008.
[5] Thostenson E T, Li C, Chou T-W, Compos Sci Tech, 65 (2005) 491-516.
[6] Paiva M C, Zhou B, Fernando K A S, Lin Y, Kennedy J M and Sun Y-P, Carbon, 42 (2004) 2849-2854.
[7] K. Balasubramanian and M. Burghard, Small, 1, 2 (2005), 180 –192.
[8] V. Georgakilas, K. Kordatos, M. Prato, D. M. Guldi, M. Holzinger and A. Hirsch, J. Am. Chem. Soc, 124, 5 (2002), 760-761.
[9] F. M. Fernandes, R. Araújo, M. F. Proença, C. J. R. Silva, M. C. Paiva, Journal of Nanoscience and Nanotechnology, 7 (2007) 3514-3518.
[10] Rui Araújo, M. C. Paiva , M. F. Proença, Carlos J. R. Silva, Composites Science and Technology, 67 (2007) 806-810.

MOLECULAR DYNAMICS SIMULATIONS OF PORPHYRIN-DENDRIMER SYSTEMS: TOWARDS MODELLING ELECTRON-TRANSFER IN SOLUTION

Pedro M. R. Paulo, José N. C. Lopes and Sílvia M. B. Costa

Centro de Química Estrutural – Complexo I, Instituto Superior Técnico, Av. Rovisco Pais, 1049-001 Lisboa, Portugal

pedro.m.paulo@ist.utl.pt

Organic dendrimers are highly regular and branched polymers that assume a globular shape in solution with dimensions of some nanometers. Since its discovery more than two decades ago, dendrimers have become a very important building block in supramolecular chemistry and nanoscience. The set of potential applications for these molecules encompass a variety of areas, namely, biology (as mimetic systems of enzymes or redox proteins), medicine (in drug delivery, gene therapy and biochemical sensors) and optoelectronics (for transduction of signals or light-harvesting devices).

In previous studies we focused on the non-covalent interactions of a cationic porphyrin (TMPyP) with negatively charged poly(amido)amine dendrimers (PAMAM) in aqueous solution.[1] TMPyP experiences a strong fluorescence quenching effect upon association with PAMAM dendrimers. This effect was attributed to a photoinduced electron-transfer reaction from the tertiary amine groups of the dendrimer to the excited-state porphyrin. The fluorescence decays of the porphyrin-dendrimer ionic complex are multi-exponential and can be fitted with a dispersive kinetics model that considers a statistic distribution of quenching rates, $k^{i}_{ET}(x)$. This distribution of rates was explained assuming a distribution of donor-acceptor distances that arise from the conformational flexibility of PAMAM dendrimers.[1]

In the present contribution we further explore this issue using Molecular Dynamics simulations. We employed a model based on OPLS/AMBER force field, which was developed for half-generation PAMAM dendrimers.[2] Initially we performed simulations without explicit solvent to achieve simulation times of about one nanosecond. From these trajectories, we could assess different geometries of the porphyrin-dendrimer complex (see figure 1) and retrieve distributions of donor-acceptor distances from the positions of the dendrimer tertiary amines relative to the porphyrin sitting on its *surface*. We have also performed simulations in the presence of explicit solvent (figure 2) and, using a procedure developed by Schulten and co-workers,[3] we were able to estimate the reorganization energy of the medium for different donor-acceptor pairs. The values obtained show a linear dependence with the inverse of the donor-acceptor distance, which is reminiscent of Marcus expression for two charged spheres in a dielectric continuum. Combining the results from the simulations with and without explicit solvent, we have calculated distributions of electron-transfer rates for two simulated configurations of the porphyrin-dendrimer pair using semi-classical Marcus theory of Electron-Transfer. The results obtained from the simulations will be discussed from a critical perspective and, whenever possible, compared to the experimental results.

References:

[1] P.M.R. Paulo, S.M.B. Costa, J. Phys. Chem. B, **109** (2005) 13928.

[2] P.M.R. Paulo, J.N. Canongia Lopes, S.M.B. Costa, J. Phys. Chem. B, **111** (2007) 10651.

[3] M. Nonella, K. Schulten, J. Phys. Chem., **95** (1991) 2059.

Figures:

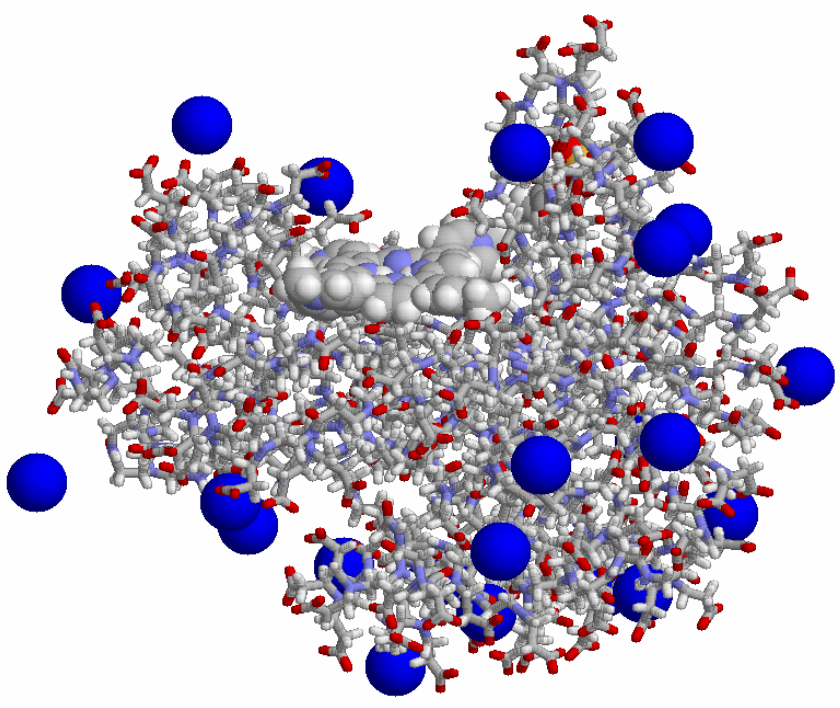

Figure 1 – Snapshot of simulated system without explicit solvent: porphyrin (spacefill) and PAMAM dendrimer (sticks) with sodium counterions (blue spheres).

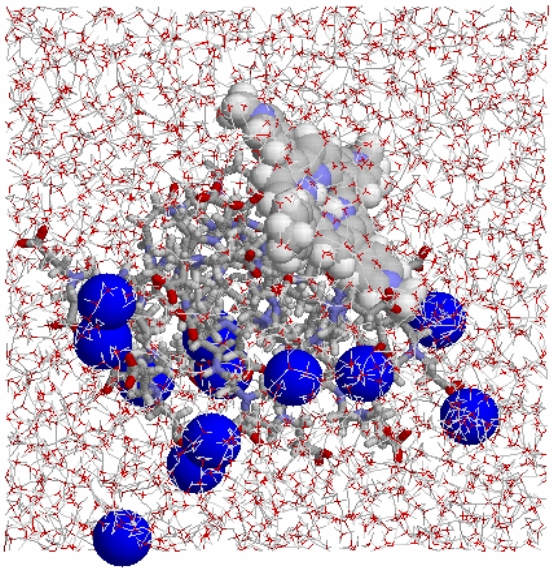

Figure 2 – Snapshot of simulated system with explicit solvent: same representation choice as in figure 1, but with water represented in wireframe.

INDIVIDUAL DETECTION OF GOLD NANOPARTICLES IN LIQUID USING PHOTOTHERMAL CORRELATION SPECTROSCOPY

Pedro M. R. Paulo,[1,*] Alexander Gaiduk,[1] Florian Kulzer,[2,†] Michel Orrit,[1] Thomas Schmidt,[3] and Herman P. Spaink[2]

[1] *Molecular Nano-Optics and Spins (MoNOS), Leiden Institute of Physics, Leiden University*
[2] *Molecular Cell Biology, Institute of Biology, Leiden University*
[3] *Department of Biophysics, Leiden Institute of Physics, Leiden University*
* current address: *Centro de Química Estrutural – Complexo I, Instituto Superior Técnico, Av. Rovisco Pais, 1049-001 Lisboa, Portugal*
[†] current address: *ICFO – Institut de Ciències Fotòniques, Mediterranean Technology Park, 08860 Castelldefels (Barcelona), Spain*

pedro.m.paulo@ist.utl.pt

Gold nanoparticles are often employed as labels for biological systems or as functionalized units for biochemical sensors. Compared to other labels, such as fluorescent molecules and semiconductor nanocrystals, they have the advantage of not suffering from photobleaching or photoblinking. However, the photoluminescence quantum yield of gold nanoparticles is very low (10^{-4} to 10^{-5}) and, thus, it is very difficult to apply single molecule fluorescence techniques for their detection. Photothermal detection provides an interesting alternative for the investigation of single non-luminescent nano-objects. In photothermal detection scheme, the sample is irradiated with a field resonant with the optical absorption spectrum of the nano-object. The photon energy absorbed is dissipated as heat into the environment generating a gradient of temperature around the particle that acts as a thermal lens. This effect is probed by another (non-resonant) field, which is scattered by the local changes in index of refraction.

By combining photothermal microscopy with a heterodyne detection scheme we achieve single-particle sensitivity for sizes down to a diameter of 20 nm. This size limit could be improved by using high numerical aperture optics, but for applications in high-throughput screening the enlarged detection volume used in the present work (approx. 200 fl) is preferable at the expense of better detection efficiency. We present illustrative results of Photothermal Correlation Spectroscopy for free gold nanoparticles in aqueous dispersions and in water-glycerol mixtures. The characteristic diffusion times retrieved from the correlation curves are in the order of tens of milliseconds for 80 nm particles in water and correspond to an average temperature increase of some tens of Kelvin. Increasing the power of the heating laser beam decreases the particle diffusion times, as expected. In back-scattering mode, the photothermal signal shows fast fluctuations arising from an interference effect between the backscattered and reference fields, which introduce a short component in the correlation function. This additional component is eliminated in forward-scattering mode and the signal to noise ratio also increases because the strength of the detected field is better suited to the detector employed. Changing to forward configuration allowed us to detect smaller-sized particles.

The results obtained with Photothermal Correlation Spectroscopy will be discussed in comparison with the more widely known technique of Fluorescence Correlation Spectroscopy (FCS), focusing on the difference between the physical nature of measured signals and its consequences for the respective correlation functions.

Figures:

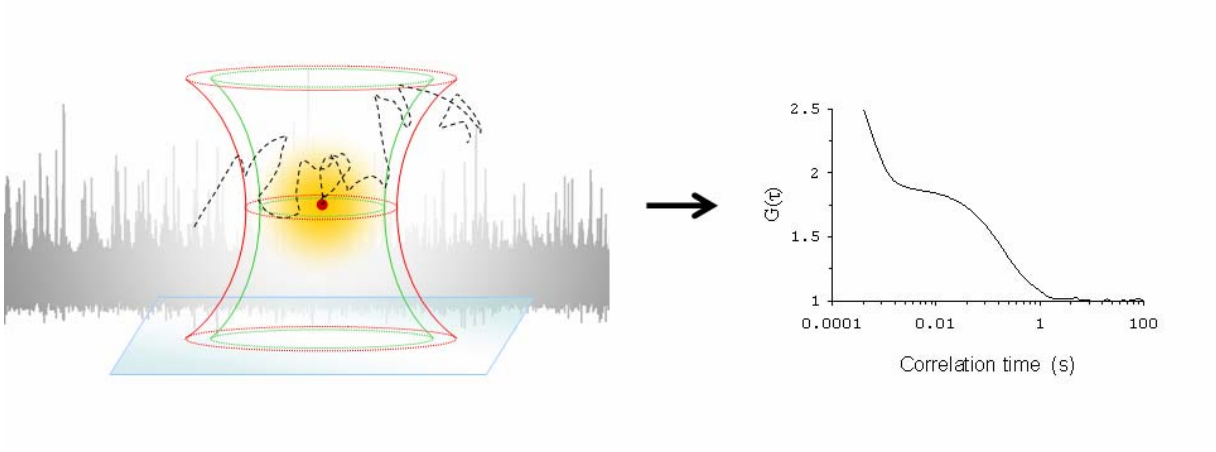

Figure 1 – Graphical abstract.

Protein nanoparticles for molecular therapy: Molecular construction of SIVp17/HIV1p6 nanoparticles and assembly in animal cell cultures

Luísa Pedro, Sandra S. Soares, Guilherme N.M. Ferreira
IBB-Institute for Biotechnology and Bioengineering
Centre for Molecular and Structural Biomedicine
University of Algarve, Campus Gambelas, 8005-139 Faro, Portugal
lpedro@ualg.pt

Protein nanoparticles, such as Virus-like particles (VLPs), are becoming promising agents to delivery molecular therapy agents. A nanoparticle was constructed by fusion of the SIV (Simian Immunodeficiency Virus) p17 matrix protein with the HIV-1 (Human Immunodeficiency Virus Type 1) p6 protein with the goal transport of therapeutically agents to specifically targeted cells [1]. We have previously shown that the chimeric p17/p6 protein assembles from 293T cells as fully membrane encapsulated particle with 80 nm and an average of 7700 protein subunits. The intent of this construction is to enable particle engineering based on molecular assembly strategies in order to incorporate selected targeting motifs and particular therapeutic agents. The particles are assembled in animal cell culture upon transiently transfecting the cells with three different vectors one of which encodes the main structural protein of the nanoparticles - the fusion protein p17/p6. The affinity recognition of p6 protein with specific motives included in HIV-1 Vpr protein is then explored to enable the incorporation into the assembling nanoparticles of specific biomolecules linked to such motives. This is demonstrated by construction a fusion protein containing Vpr and EGFP. Co-transfecting animal cells with this vector and the vector encoding p17/p6 results in the assembly of nanoparticles associated with EGFP which is inside the assembled nanoparticles.
This communication addresses the steps involved in the molecular construction, assembly and characterization of such nanoparticles as well as the attempts to their optimization in animal cell cultures.

References:

[1] Costa, M.J.L., Pedro, L., Matos, A.P.A., Aires-Barros, M.R., Belo, J.A., Gonçalves, J., Ferreira, G.N.M., Biotechnol. Appl. Biochem., 48 (2007), 35.

Acknowledgments:

The authors thank to Portuguese Foundation for Science and Technology (FCT) the financial support through the research project POCI/BIO/62476/2004 and the grants SFRH/BD/36674/2007 and SFRH/BPD/30290/2006.

Tailoring mechanical properties at the nanoscale: the dependence of Young's modulus of nanowires on the shape and axial orientation.

S. Peláez, P. A. Serena*
Consejo Superior de Investigaciones Científicas
Instituto de Ciencia de Materiales de Madrid
c/Sor Juana Inés de la Cruz 3, Cantoblanco 28049-Madrid
**email: spelaez@icmm.csic.es*

Nanotechnology covers a broad variety of basic and applied studies aiming at the control of different properties at the nanometer level for their use in promising applications. In particular, metallic nanowires are very interesting systems for the basic point of view as well as within the context of future nanoelectronics and sensors industry [1]. The mechanical behaviour of metallic nanowires under stress has been intensively studied in order to understand their deformation and fracture mechanisms [2-5]. More recently, several studies have focussed on the dependence of the elastic constants on the nanowire size [6], neglecting the role of the orientation and shape of the nanowire. In this work we present the dependence of the Young's modulus of Al and Ni nanowires on three different parameters: cross-section shape and size, as well as the nanowire crystallographic orientation.

We have studied the tensile stress of Al and Ni nanowires by intensive computer simulations. The Embedded Atom Method (EAM) interatomic potential [8,9] is used to describe the energetic of the nanowires. Periodic boundary conditions are used to simulate infinite nanowires. For each nanowire under study we have carried out a conjugate gradients minimization of the cohesive energy in order to obtain its optimal relaxed structure. We have already used this methodology for calculating edge energies [10]. From this equilibrium condition we contract or stretch the nanowire by imposing compressive and tension loads (see Figure 1a and 1b). The nanowire atomic positions are optimized again for the stressed situation, and from these optimized coordinates the local (microscopic) stress as well as the total energy are calculated. From the total energy *versus* strain curve we determine the Young's modulus.

We have considered nine different sets (or families) of crystalline FCC nanowires. Each family is characterised by a particular cross sectional shape (rectangular, hexagonal or octagonal) and its main axis orientation (parallel to the [100], [110] or [111] crystallographic direction). For each family several nanowires of different size (cross sectional area) have been taken into consideration in order to describe size effects.

We present results on the distribution of the stress inside the nanowire. We show that surfaces, and specially edges, accumulate a high tensile stress when compared with bulk regions. Young's modulus tends to the expected bulk limit value in the corresponding direction when the nanowire cross-section area increases. However interesting size effects are observed for thinner nanowires. Young's modulus of [100]-oriented nanowires becomes smaller than the limit bulk value as thinner nanowires are considered (see Figure 2). However, for [110]- and [111]-oriented nanowires the Young's modulus grows for decreasing nanowires diameters. This general trend is slightly dependent on the kind of cross-section shape. This trend agrees with that observed for thin slabs.

The change of the elastic constants when modifying the nanowire radius opens a way to tailor mechanical properties of future nanoscale devices.

REFERENCES:
[1] N. Agraït, A. Levy-Yeyati and J.-M. van Ruitenbeek, Phys. Rep. **277**, 81 (2002).
[2] Referencias a Landman (articulos seminales)
[3] I.-L. Chang, and Y.-C. Chen, Nanotech. **18** 315701 (2007).
[4] A. Hasmy, E. Medina, and P. A. Serena, Phys. Rev. Lett. **86** 5574 (2001).
[5] P. García-Mochales, S.Peláez, P. A. Serena, E. Medina, and A. Hasmy, Appl. Phys. A **81** 1545 (2005).
[6] J. Diao, K. Gall, M. L. Dunn, J. Mech. Phys. Sol. **52** 1935 (2004).
[7] C. Q. Chen, Y. Shi, Y. S. Zhang, J. Zhu, and Y. J. Yan, Phys. Rev. Lett. **96**, 075505 (2006).
[8] M. S. Daw and M. I. Baskes, Phys. Rev. Lett. **50**, 1285 (1982); S. M. Foiles, Phys. Rev. B **22**, 2409 (1985).
[9] Y. Mishin, D. Farkas, M. J. Mehl, and D. A. Papaconstantopoulos, Phys. Rev. B **59**, 2292 (1999).
[10] S. Peláez and P. A. Serena, Surf. Sci. **601** 4163 (2007).

FIGURES:

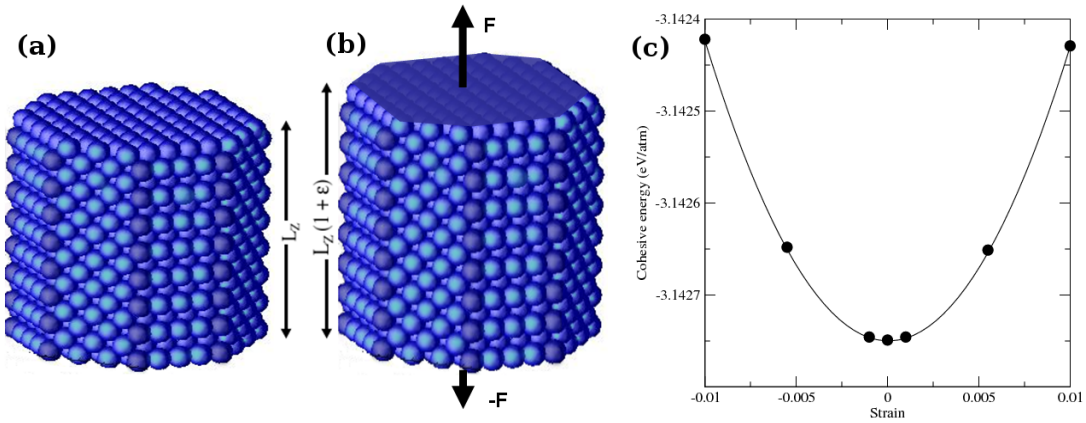

Fig 1. Schematic view of an octogonal nanowire along the [100] crystallographic orientation. Left: original configuration. Right: a strain ε is applied.

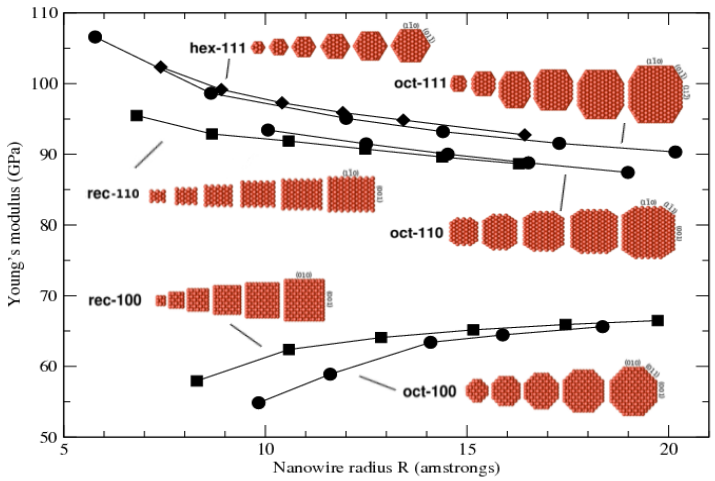

Fig 2. Young's moduli for several families of Al nanowires. Expected

A Comparison of Zeolites and Polymers used as sensitive layers in microcantilever-based gas sensors

I. Pellejero[1], A. Rabal[1],M.A. Urbiztondo[1], M.Villarroya [1], J.Sesé [1], M.P.Pina [1], J.Santamaría[1], S. Tétin[2], I. Dufour[2], C. Pellet[2]

[1]Instituto Universitario de Investigación de Nanociencia de Aragón (INA), Pedro Cerbuna 12, Zaragoza 50009, Spain . [2] University of Bordeaux, IMS Laboratory, 351 cours de la Libération, 33405 Talence Cedex, France

ismapel@unizar.es

Zeolites as sensing layer

The specificity, adsorption and catalytic properties of zeolites, besides the possibility of its pores to host different ions, atoms, molecules and clusters have opened up numerous opportunities of zeolites as advanced nanomaterials, applied in micro-sensor, micro-separators and micro-reactors.

There are several examples where zeolites have been used as a sensitive layer over a cantilever to detect humidity [1] and certain gases like Freon [2]. In this work the use of other zeolitic materials more selective to a specific analyte has been proposed. To obtain this selective material, cation exchanges have been carried on. Increased selectivity to polar molecules using Co-Beta, zeolite with BEA structure exchanged with cobalt, has been verified [3] and it is used as a sensitive layer in this research. This type of zeolite accommodates hydrophilic molecules and big sized molecules in its nanostructure due to its excellent properties of pore size and polar behavior (specific sensors to detect explosive materials, nitrotoluene for instance).

The resonance frequency of microcantilevers is measured and the adsorbed mass of the sensed-gas is then calculated. The cantilevers are fabricated using SOI silicon wafers and Deep Reactive Ion Etching (DRIE) by IMS Laboratory [4]. Zeolites are directly deposited on the surface of the cantilever. An electromagnetic actuation is used to excite the movement and the deflection is measured with integrated piezo-resistive circuit.

In this work, a comparison of zeolites and polymers as sensing layers has been studied. Moreover the selectivity of Co-Beta zeolite to ethanol and nitrotoluene has been performed.

Zeolite versus polymers

Adsorption of ethanol has been tested using different sensing coating layers on the same type of cantilever based sensors. Table 1 summarizes the characteristics of these devices. In particular three standard classical polymers have been tested: PEUT, PECH and PIB. The results obtained with the sensitive layer of Co-Beta zeolites are shown as well.

When ethanol is sensed, the sensitivity normalized to the mass of sensing layer is for zeolite at least 3 times higher (in some cases more than 30 times) than polymers. In figure 1, the variation of the adsorbed ethanol per amount of sensitive layer is shown. Zeolite sensitivity is up to 25 times higher than the values obtained with PEUT polymer. The response time of the sensor was similar when zeolite was used as the sensitive layer instead of a polymer.

To analyze the versatiliy of zeolites as sensing layer, the selectivity of this material to detect nitro-derivates (explosives) has been studied. Adsorption measurements for ethanol and nitrotoluene have been carried out with a sensitive coating of 4.38 µg of zeolite Co-Beta, Figure 2 shows the obtained adsorption curves. In these results the sensitivity ratio obtained of nitrotoluene/etanol is 80, showing that zeolite Co-Beta has good selectivity for nitrotoluen.

Zeolites are shown to be good candidates as sensitive layers for gas detection. When compared to polymers, they offer better stability to vibrations and temperature, thus

increasing the sensor lifetime. They will permit to locally heat the sensor allowing a quick absorption-desorption cycle. Therefore a very fast and re-usable sensor is obtained. Further more it has been shown that the normalized sensitivity is higher compared with several polymers. Finally, their specific selectivity is demonstrated and found to be good candidates as sensing material for explosives detection.

References:

[1] L. Sandella, G. Binder, T. Mezzacasa, J. Gobrecht, R. Berger, et al., ¨Combination of single cristal zeolites and microfabrication: two applications towards zeolite nanodevices,¨ Microporous and Mesoporous Materials **21**, 1998, pp. 403-409.

[2] J. Zhow, P. Li, S. Zhang, Long S., Y. Huang, P. Yang, and M. Bao, ¨Zeolite-modified microcantilever gas sensor for indoor air quality control,¨ Sensors and Actuators B **94**, 2003, pp. 337-342.

[3] D. Vassena, A. Kogelbauer, and R. Prins, ¨Potential routes for the nitration of toluene and nitrotoluene with solid acids,¨ Catalysis Today **60** 2000, pp. 275–287

[4] L. Fadel, F. Lochon, I. Dufour, and O. Français, ¨Chemical sensing: millimeter size resonant microcantilever Performance,¨ Journal of Micromechanics and Microengineering, **Vol 14**, 2004, pp. S23-S30.

Figures:

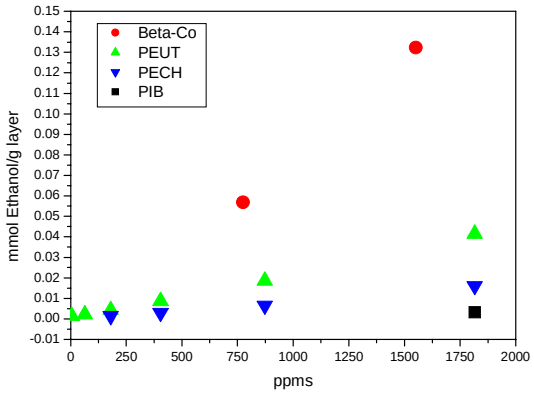

Figure 1: Comparison of ethanol adsorption in the four sensors.

Table 1. Characteristics and properties of cantilevers and layers in ethanol atmosphere.

	Sensor A	**Sensor B**	**Sensor C**	**Sensor D**
Layer	PEUT	PECH	PIB	Beta-Co
Layer-mass	36.5µg	43.5µg	25.3µg	4.38µg
Resonance Frequency.	3061.7Hz	3099.5Hz	4786.2Hz	20289Hz
Quality factor	938	756	1027	375
Sensitivity [mHz/ppm]	0.144	0.026	0.011	0.343
Detection limit	95ppm	147ppm	526ppm	116ppm

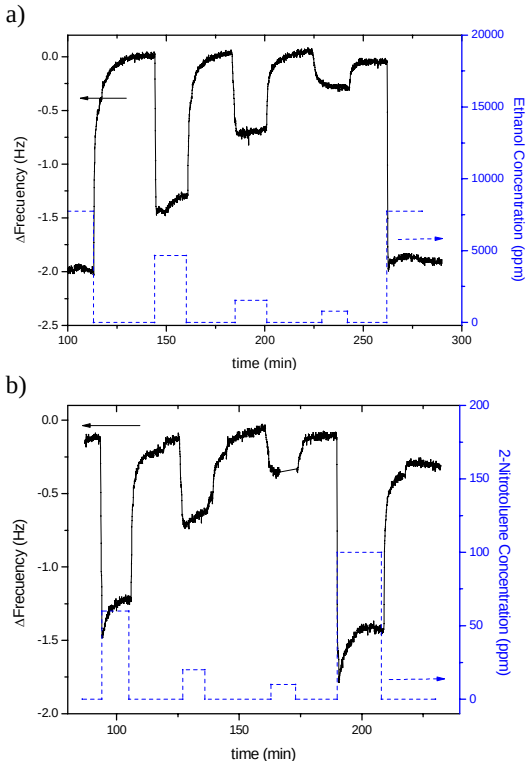

Figure 2. Response of the silicon microcantilever with 4.38 µg Co-Beta. a) Between 7000 ppm and 700 ppm of ethanol. b) Between 100 ppm and 10 ppm of 2-nitrotoluene

BOTTOM-UP APPROACH TO NANOGRAPHENES VIA ARYNES

D. Peña, C. Romero, J. Caeiro, A. Criado, A. E. Díaz, D. Pérez, E. Guitián
Departamento de Química Orgánica, Universidad de Santiago de Compostela
15782-Santiago de Compostela, Spain
godpena@usc.es

In recent years, graphenes have attracted huge attention because of their unique structures and properties.[1] These carbon-based materials have great potential as the basis of optical and electronic devices. Graphenes are normally prepared from graphite in a *top-down* approach based on exfoliation of graphite under harsh conditions. As a result, mixtures of carbon-based materials with different sizes and structural defects are usually obtained. One of the biggest challenges to be addressed in order to integrate graphenes into high performance electronic devices is to avoid the structural *inhomogeneity* implicit with their current syntheses.

In this communication we present our efforts to synthesize well-defined nanographenes using controlled *bottom-up* approaches under mild reaction conditions. These synthetic methodologies allow preparing these carbon-based materials in the same way as nanosized polycyclic aromatic hydrocarbons (PAHs).[2] These approaches minimize difficulties associated with processing, manipulation and characterization of graphene derivatives. In particular, our approach is based on the palladium-catalyzed [2+2+2] cycloaddition of arynes.[3] Figure 1 shows some examples of nanographenes that can be obtained using this methodology.

References:

[1] Novoselov, K. S.; Geim, A. K.; Morozov, S. V.; Jiang, D.; Zhang, Y.; Dubonos, S. V.; Grigorieva, I. V.; Firsov, A. A. *Science*, **306** (2004) 666.
[2] Wu, J.; Pisula, W.; Müllen, K. *Chemical Reviews*, **107** (2007) 718.
[3] Romero, C.; Peña, D.; Pérez, D.; Guitián, E. *Chemistry - A European Journal*, **12** (2006) 5677.

Figure 1: Typical nanographenes obtained in our lab by palladium-catalyzed [2+2+2] cycloaddition of arynes (**1-3**). Compounds **4** and **5** are under preparation using the same methodology.

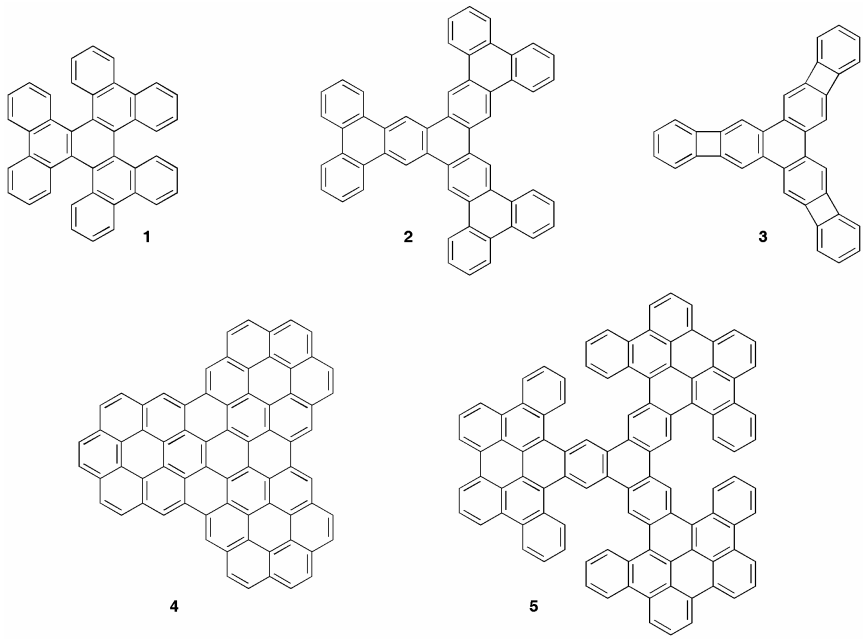

HEAT GENERATION IN TUNNEL JUNCTIONS FOR CURRENT-WRITTEN PINNED LAYER SWITCHING

A.M. Pereira[1,a], J. Ventura, J. M. Teixeira[1], J. P. Araujo[1], F. Carpinteiro[1], J. B.Sousa[1]; b, Y. Liu[2], Z. Zhang[2] and P. P. Freitas[2]
[1]*IFIMUP, Rua do Campo Alegre, 687, 4169-007, Por*to, Portugal
[2]INESC-MN, Rua Alves Redol, 9-1, 1000-029 Lisbon, Portugal
ampereira@fc.up.pt

Tunnel junctions (TJ) consisting of two ferromagnetic (FM) layers separated by an insulator (I) [1] show enormous potential for a multiplicity of applications such as read head [2], strain [3], current, position and speed [4] sensors or even to detect magnetically tagged biological specimens [5].

However, probably the most sought after application is high performance, low cost, non-volatile magnetic random access memories (MRAMs) [6]. In a tunnel junction, the magnetization of one of the FM layers (pinned layer) is fixed by an underlying antiferromagnetic (AFM) layer. The magnetization of the other FM layer (free layer) reverses almost freely when a small magnetic field is applied. Due to spin dependent tunneling one obtains two distinct resistance (R) states (the 0 and 1 bits of a magnetic memory) corresponding to pinned and free layer magnetizations parallel (low R) or antiparallel (high R). Consequently, the standard way to switch between R-states in MRAMs is to use magnetic fields generated by current lines. However, the undesirable switching of half selected bits is still a concern for actual MRAM submicron devices. Furthermore, as the size of a memory cell decreases, the magnetic field needed to induce switching greatly increases. To overcome such limitations, a thermally-induced pinned layer switching mechanism was proposed [7, 8]. In fact, when a sufficiently high electrical current flows through the insulating barrier, local temperatures inside the tunnel junction can increase above the blocking temperature of the AFM layer (T_B ~ 500 K). One is then able to switch the magnetization of the pinned layer with a small magnetic field H and, upon cooling (under H), a new exchange-bias pinning direction is impressed.

Switching of the magnetic state of the TJ (from parallel to antiparallel or vice-versa) is thenpossible. Here we demonstrate the current-driven pinned layer switching effect in thin magnetic tunnel junctions (MnIr/CoFe/AlOx/CoFe/NiFe) with T_B = 520 K [9] using a current density j = 0.75x106 A/cm^2. However, numerical results on heat generation in tunnel junctions show that heating is small when such current densities are applied. In fact, only much larger current densities (~15x106 A/cm^2) lead to heating above the blocking temperature of the AFM layer. One concludes that the experimental observation of thermally driven pinned layer reversal is due to localized heating in nanoconstrictions that concentrate most of the electrical current leading to high local current densities. Thus, to enhance device performance, the insulating barrier of the tunnel junction should have nanometric inhomogeneities where the local barrier thickness is smaller than average. Such hot-spots lead to a confinement of the electrical current and to an increase of local current densities.

Furthermore, one shows that both heating and cooling (above and below T_B respectively) occur over very small time scales (≤ ns), making current-written pinned layer switching a competitive mechanism for technological implementation.

References:

[1] J. S. Moodera, L. R. Kinder, T. M. Wong and R. Meservey, Phys. Rev. Lett. 74, 3273 (1995).
[2] D. Song, J. Nowak, R. Larson, P. Kolbo and R.Chellew, IEEE Trans. Magn. 36, 2545 (2000).

[3] M. Lohndorf, T. Duenas, M. Tewes, E. Quandt, M. Ruhrig and J. Wecker, Appl. Phys. Lett. 81, 313 (2002).
[4] P. P. Freitas, F. Silva, N. J. Oliveira, L. V. Melo, L. Costa and N. Almeida, Sensors and Actuators A 81, 2 (2000).
[5] H. A. Ferreira, D. L. Graham, P. P. Freitas and J. M. S. Cabral, J. Appl. Phys. 93, 7281 (2003).
[6] B. N. Engel, N. D. Rizzo, J. Janesky, J. M. Slaughter, R. Dave, M. DeHerrera, M. Durlam and S.Tehrani, €IEEE Trans. Nanotechnol. 1, 32 (2002).
[7] J. Zhang and P. P. Freitas, Appl. Phys. Lett. 84, 945 (2004).
[8] I. L. Prejbeanu, W. Kula, K. Ounadjela, R. C. Sousa, O. Redon, B. Dieny and J. P. Nozieres, IEEE Trans. Magn. 40, 2625 (2004).

NANOSTRUCTURATED BIOSENSORS FOR THE ANALYSIS OF PHENOLIC COMPOUNDS

Briza Pérez[1,2], Humberto Takeda[3], Adriano Ambrosi[1], Orlando Fatibello[3], Salvador Alegret[2], Arben Merkoçi[1,2]

[1] Nanobioelectronics & Biosensors Group, Institut Català de Nanotecnologia, Campus UAB, 08193 Bellaterra, Barcelona, Catalonia, Spain.
[2] Grup de Sensors & Biosensors, Departament de Química, Universitat Autònoma de Barcelona, 08193 Bellaterra, Catalonia, Spain.
[3] Centro de Ciências Exatas e de Tecnologia, Departament de Química, Universidade Federal de São Carlos - UFSCAR, Sao Carlos, Brasil.

E-mail: *brizaries_77@yahoo.com.mx*

Biosensors represent an interesting alternative for the detection of phenolic compounds. Many different approaches can be found in the literature including carbon-paste biosensors [1], graphite composite electrodes [2], conducting polymer modified electrodes [3], and silica sol–gel composite films [4]. Some of these methods are relatively complicated, require the use of several reagents and often the biosensor produced presents stability problems. For that reason new alternative biosensor designs for phenolic compounds are being developed and investigated by our research group. These are based on screen-printed carbon electrodes modified with carbon nanotube and Au electrodes modified with conducting polymer nanolayers.

The use of carbon nanotubes (CNT) has become relevant due to their excellent conductivity including the improvement of electron transfer between the enzymes and the electrode surfaces [5]. CNT works as electron mediators and at the same time provides a very good matrix for enzyme immobilization [6]. On the other hand, the biosensors based on nanostructured layers [7] have demonstrated to be simple in preparation, allowing the easy electrostatic attractions of biomolecules and offering a great promise for developing amperometric biosensors.

Some preliminary results related to the detection of phenolic compounds achieved using different platforms based on either conducting nanolayers or carbon nanotubes structures including enzymes will be shown. The Layer-by-Layer (LbL) technique used to modify the Au electrode with ultra-thin conducting films (i.e. polyaniline) seemed to result the most interesting approach in relation to the preparation of tyrosinase-based biosensors for the analysis of phenolic compounds.

Acknowledgement. This work has been done under the WARMER research project, FP6-034472.

References

[1] A. Merkoci, M. Pumera, X. Llopis, B. Pérez, M. del Valle, S. Alegret, Trends in Anal. Chem. **24**, (2005), 9.

[2] B. Pérez, M. Pumera, M. del Valle, A. Merkoçi, and S. Alegret, J. Nanosci. Nanotech. **5**, (2005), 10.
[3] O. Adeyoju, E.J. Iwuoka, M.R. Smyth, D. Leech, Analyst, **121** (1996), 1885.
[4] J. Li, L.S. Chia, N.K. Goh, S.N. Tan, Anal. Chim. Acta, (1998), 203.
[5] A. Merkoci, Microchim. Acta, **152,** (2006), 157.
[6] B. Pérez, J. Sola, S. Alegret, A. Merkoçi, Electroanalysis, (2007), accepted.
[7] Decher, G.; Hong, J. D.; Macromol. Chem. Macromol Symp., **46** (1991), 321.

NANOPARTICLES IN AGRICULTURE: DEVELOPMENT OF SMART DELIVERY SYSTEMS FOR PLANT RESEARCH

A. Pérez-de-Luque[1,], D. Rubiales[1], C.I. Marquina[2], M.R. Ibarra[2,3], J. M. de la Fuente[3]*
[1]CSIC, Instituto de Agricultura Sostenible, Alameda del Obispo s/n, Apdo. 4084, E-14080 Córdoba, Spain; [2]CSIC-Unversidad de Zaragoza, Instituto de Ciencia de Materiales de Aragón-Departamento de Física de la Materia Condensada, Pedro Cerbuna 12, 50009-Zaragoza, Spain; [3]Instituto de Nanociencia de Aragón, Universidad de Zaragoza, Edificio Interfacultativo II, Pedro Cerbuna 12, 50009-Zaragoza Spain
[*]Corresponding author: bb2pelua@uco.es

One of the most interesting biological applications of nanotechnology is the development of smart delivery systems for local drug delivery. It can be done through the use of nanoparticles incorporated into the blood which travel to specific sites to deliver their chemical load. In this way, it is possible to avoid collateral damage in patients and reduce the amount of active substance for treatments [1].

These techniques have a great potential for application in agriculture. For example, they can be used for the development of insecticides, fungicides, herbicides or fertilizers. In fact, this is really being done by the most important corporations in this field like BASF and Syngenta, and countries like USA and Israel [2]. A more in depth study of these technologies in agronomical sciences would allow their use in crop protection and/or studies of plant-pathogen interactions, opening new gates to face researches still under speculation or belonging to science fiction. The idea presented in this work is to give a step forward to adapt the technology of nanoparticles for systemic translocation in plants [3], allowing the transportation of substances to specific sites, studying the movement of solutes through the plant and the study of the plant-pathogen interaction. The application of this technology for treatment of plants with chemicals acting by contact (fungicides, insecticides, herbicides, etc.) seems to be immediate, but it is more complex for substances which must be translocated whithin the plant to reach the action point. If it is possible to get a distribution of the nanoparticles through the plant vascular system, and guide them to specific areas, they could be used for phytosanitary treatments with a minimum active substance amount, reducing the risks for environmental contamination and the presence of chemicals in the plant for further commercialization. In addition, this system could be used to unload chemicals or substances (plant hormones, elicitors, nucleic acids, etc.) into localized areas of the plant tissues, to carry on several studies at the physiological, biochemical and genetic levels.

For example, nanoparticles could be designed to target specific phytopathogens like fungi, viruses, bacteria or parasitic plants. In some cases, phytopathogens develop inside plant tissues (vascular pathogens [4, 5]) or under earth in the roots (root parasitic plants [6]), and fighting against them is very difficult because they remain undetected until the first disease symptoms appear. And then it is too late to treat the crops. But if nanoparticles can travel through the plant and target those phytopathogens releasing their chemical load at such point, many crops and trees diseases would be easier to control.

In addition, nanoparticles can be used to genetically transform plants in a more controlled way compared to the biolistic method. Following this approach, some works are being developed by USA research groups, as recently reported in Nature Nanotechnology [7].

References:

[1] Fernández-Pacheco R, Marquina C, Valdivia JG, Gutiérrez M, Romero MS, Cornudella R, Laborda A, Vitoria A, Higuera T, García A, García de Jalón JA, Ibarra MR, Journal of Magnetism and Magnetic Materials **311** (2007) 318-322.
[2] BASF, Nanotechnology at BASF. A great future for tiny particles, (2004), URL: http://www.corporate.basf.com/en/innovationen/felder/nanotechnologie/nanotech.htm?id=V00-EnACn72xfbcp2l1
[3] González-Melendi P, Fernández-Pacheco R, Coronado MJ, Corredor E, Testillano PS, Risueño MC, Marquina C, Ibarra MR, Rubiales D, Pérez-de-Luque A, Annals of Botany, **101** (2008) 187-195.
[4] Beckman CH, Roberts EM, Advances in Botanical Research, **21** (1995) 35-76.
[5] European and Mediterranean Plant Protection Organization, EPPO Bulletin, **34** (2004) 201-207.
[6] Joel DM, Hershenhorn J, Eizenberg H, Aly R, Ejeta G, Rich PJ, Ransom JK, Sauerborn J, Rubiales, Horticultural Reviews, **33** (2007) 267-349.
[7] Torney F, Trewyn BG, Lin VSY, Wang K, Nature Nanotechnology, **2** (2007) 295-300.

Characterization of MWCNT/PS/antibody membrane prepared by phase inversion method for biosensing applications

Sandra Pérez [a], *Samuel Sánchez* [a], *Mònica Roldán* [b], *Esteve Fàbregas* [a],
[a]*Sensors and Biosensors Group, Chem. Dept.,* [b] Microscopy Facility, *Universitat Autònoma de Barcelona, Spain*
Sandra.perezra@campus.uab.es

Recent advances in nanoscience greatly influence in the field of electrochemical biosensors during the past years. This has carried an important development of new bio-compatible and highly conductive materials for biosensing applications.

The combination of multi-walled carbon nanotubes (MWCNT) as transducer with polysulfone (PSf) polymer offers unique properties for the easy incorporation of biological moieties providing a composite with high electrochemical response to corresponding analytes. The phase inversion method has been used in recent years for the immobilization of enzymes, proteins and antibodies into polymers [1]. Some of them have been used for their application in biosensors field.

For the design of bio-sensors, the crucial step is the immobilization of biological reagent into/onto the electrode surface, in this case the immuno-reagent. In the phase inversion technique, a thin film of polymer solution is deposited on an inert substrate and then immersed into a coagulant bath containing a non-solvent with respect to the polymer, rapid exchange of the solvent by non-solvent results in diffusion-induced phase separation and membrane formation [2,3]. With this method, biomolecules are easily incorporated and exhibit long-time resistance into the matrix.

Confocal Scanning Laser Microscopy (CSLM) is a rapidly advancing imaging technique which obtains high-resolution images of membranes at successive depths, therefore offers a three-dimensional view of membrane [4]. This technique allows working in two modes. In the reflective mode, CSLM has been mostly applied examine non-biological substrates and polymers and in the fluorescence mode CSLM has been used to analyze antibody localization using labeled antibodies.

In this work, we applied CSLM as a new nondestructive method to characterize the membrane and to study the immobilization of the antibodies in order to cast it onto screen-printed electrodes.

Other techniques as X-Ray Powder Diffraction, Scanning Electron Microscope (SEM) or Infrared Spectroscopy have completed the study of characterization of this composite membrane. Amperometric and voltammetric characterization is also made for the biosensing application.

References:

[1] Zhang,M., Gorski, W., J Am Chem Soc, **127** (2005) 2058-2059.
[2] Mulder,M., Kluwer Academia Publishers,(2000)
[3] Sánchez, S., Fàbregas, E., Biosens.Bioelectron., **22(6)** (2007) 965-972.
[4] Charcosset, C., Cherfi, A., Bernengo, J-C.,Chemical Engineering Science, **55** (2005) 5351-5358.

Figures:

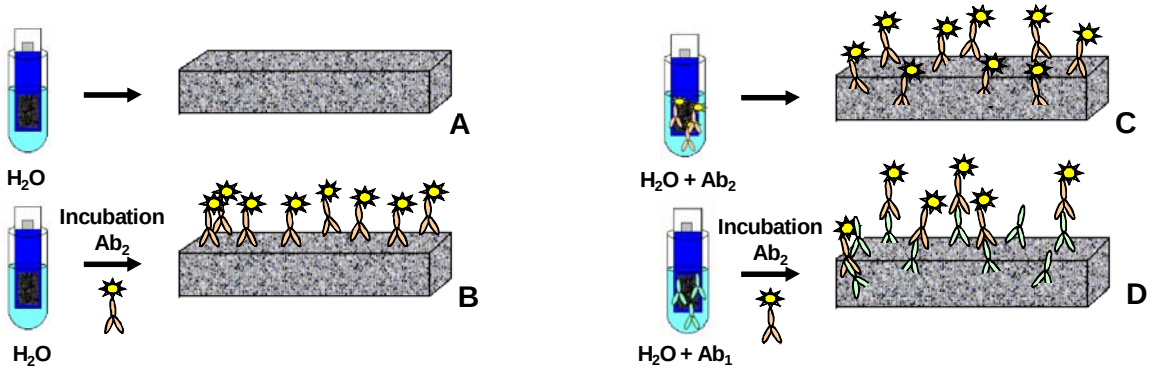

Fig.1 A) PSf/ CNT membrane prepared by phase inversion in H_2O. B) Sample of unspecific adsortion by incubation with AntiRIgG-Alexa568. C) AntiRIgG-Alexa568 introduced by phase inversion. D) RIgG introduced by phase inversion and incubated later with AntiRIgG-Alexa568

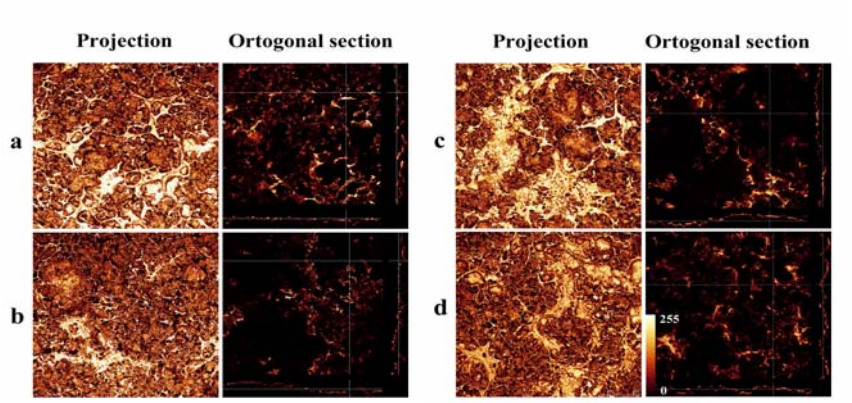

Fig.2 Membrane projection and ortogonal section of the different types of samples

AFM CHARACTERIZATION OF SUPPORTED PLANAR BILAYERS OF THE INNER MEMBRANE OF *ESCHERICHIA COLI*

Laura Picas[1], *M. Teresa Montero*[1,±], *Antoni Morros*[2,¥], *Gerard Oncins*[3], *Jordi Hernández-Borrell*[1,±,*]

[1]*Departament de Fisicoquímica, Facultat de Farmàcia UB, 08028-Barcelona.* [2]*Unitat de Biofísica, Departament de Bioquímica i Biología Molecular, Facultat de Medicina, UAB, 08193-Bellaterra (Barcelona), Spain.*[3] *Serveis Científico Tècnics UB, 08028-Barcelona, Spain. Contact@E-mail: jordihernandezborrellb.edu*

One of the most intriguing questions underway in present membrane biology research is the understanding of the interactions between phospholipids and transmembrane proteins (TMPs). Among TMPs, lactose permease (Lac Y) of *E. coli* is considered as a paradigm for the secondary transport[1]. Although the energetic behind the conformational changes underwent by TMPs, i.e. during lactose-H^+ cotransport[2], is not totally understood, it is conceivable that the work required to induce a transition between two states may arise from changes in the lateral pressure exerted by the phospholipids onto protein surface[3,4] . Hence, phospholipids species closest to the protein should have the adequate physicochemical properties, compressibility and fluidity among them, to adapt to transversal domains of TMPs[5,6]. On the other hand, the natural occurring phospholipids in biological membranes belong to the heteroacid type, with one acyl chain saturated at the *sn*-1 and the other one unsaturated at the *sn*-2 position linked to the glycerol backbone[7]. These phospholipids, 16-18 C long, are in fluid phase in physiological conditions and are highly compressible. Such is the case with 1-palmitoyl-2-oleoyl-*sn*-glycero-3-phosphoethanolamine (POPE) the most abundant phospholipid of the inner membrane of *Escherichia coli*. In regard to the interplay with membrane phospholipids it has been demonstrated that LacY is dependent on phosphatidylethanolamine (PE) presence for *in vivo* function and also for its correct folding [8,9]. Actually, LacY has been reconstituted in a functional state only in phospholipid matrices with high levels of PE, either in the native *E. coli* polar phospholipid membrane extracts [10,11] or in binary mixtures of phosphatidylgycerol (PG) and phosphatidylethanolamine (PE)[12,13]. For this reason, it is reasonable to assume that PE should be part of the neighboring phospholipids that surround the protein, namely the annular region. On the other hand, physical properties of POPE, as its condensation in monolayers[4] at the air water interface and its prone-non bilayer tendency, should play a definite role in providing the adequate lateral surface pressure and membrane curvature for functional packing of the protein[4,6].

The aim of the present work is to study by means of AFM how POPE asymmetric bilayer deposited on mica respond to temperature. In suspension, POPE shows two well characterized thermal transitions: (i) the solid-crystalline (L_β) to the liquid-crystalline (L_α) at ~24 ºC, also known as the gel to liquid phase transition temperature (T_m); and (ii) the lamellar to inverted hexagonal (H_{II}) phase transition at elevated temperatures, ~80 ºC (T_H)[14].

[±] Members of the Institut de Nanociència i Nanotecnologia de la Universitat de Barcelona (IN^{2}UB) and [¥]Centre d'Estudis en Biofísica (CEB) de la UAB.

* Corresponding author: jordihernandezborrell@ub.edu

The thermal behavior and the existence of a single or double transition temperature are of interest to unveil the nature of the POPE phase transitions in supported planar bilayers. In the present work, we applied force spectroscopy (FS) to study the load needed to puncture a POPE bilayer as a function of the temperature. This range of temperatures comprises the transition from L_β to L_α and L_α to H_{II} phases in bilayers.

References:

[1] Guan, L. and Kaback, R., *Annu. Rev. Biophys. Struct*. **2006**.
[2] Yin, Y.; Jensen, M.O.; Tajkhordish, E.; Schulten, K. *Biophys., J.* **2006**.
[3] Cantor, R.S., *J. Phys. Chem.B.* **1997**.
[4] Domènech, Ò.; Ignès, J.; Montero, M.T., Hernández-Borrell, J., *.Phys.Chem.B*.**2007**.
[5] Bezrukov, S. M., *Curr. Opin Coll. & Interface Sci*. **2000**.
[6] Van den Brink, E.; Killian, J. A.;de Kruijff, B. Biochim. Biophys. Acta **2004**.
[7] Dowhan, W. *Annu. Rev. Biochem*. **1997**.
[8] Bogdanov, M, Sun J, Kaback H R, Dowhan W., *J Biol Chem.* **1996**.
[9] Bogdanov, M, Dowhan W., *J Biol Chem.* **1995**.
[10] Vitanen, P., Newman, M. J., Foster, D. L., Wilson; T. H., Kaback, H. R, *Methods Enzymol.*, **1986**.
[11] Consler, T. G, Persson, B. L., Jung, H. Zen, K. H. Jung, K. Prive G. G., Verner, G. E. and Kaback, H.R., *Proc. Natl. Acad. Sci*. USA, **1993**.
[12] Le Coutre, J., Narasimham, L. R., Patel, C. K. N, and, H. R Kaback, *Proc. Natl. Acad. Sci.* USA, **1997.**
[13] Zhao; M., Zen; K. C., Hernández-Borrell, J.; Altenback, C.; Hubbell; W. L, Kaback, H. R. *Biochemistry*, **1999**.
[14] Epand, R.M.; Bottega,R. *Biochim. Biophys. Acta* **1988**.

Figures:

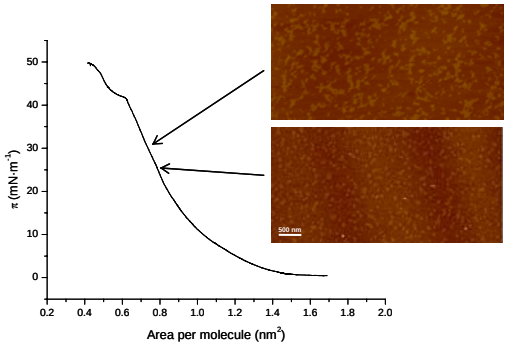

Figure 1. AFM images of POPE monolayers acquired in air

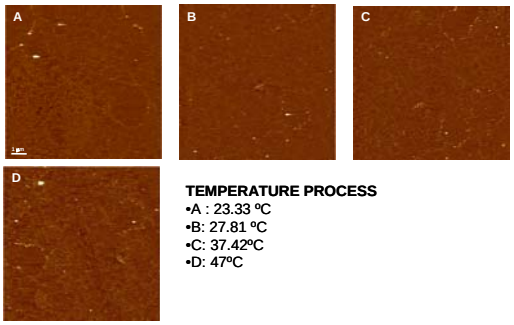

Figure 2. AFM images of asymmetric POPE bilayers acquired in liquid at different temperatures.

SiO_2/Ag thin films with "smart" topography

A.P.Piedade, M.T.Vieira
ICEMS, Department of Mechanical Engineering Rua Luís Reis Silva, 3030-788 Coimbra, Portugal
ana.piedade@dem.uc.pt

Synthesis of nanostructures have triggered continuous interest in the nanoscience field for their potential application such as catalysts and bioadsorption materials[1]. Among these systems the possibility of obtaining nano- microporous surfaces with various ordered structures and pore sizes has increased the interest in the field owing to a better control over the particle's size and location[2].

In this work thin films of silica containing nanoclusters of silver have been deposited by magnetron co-sputtering. The thin films were characterised as-deposited and the mean size of the clusters was estimated by HRTEM (Figure 1 and 2). The kinetic of silver release was evaluated subsequently after being removed from the system. This procedure opens a new application as an antibacterial surface. Further to the possible use as biomaterial, the films were re-characterised with particular emphasis in the surface morphology of the surface before and after the silver removal. This procedure gives a new path for the development of nanocomposites thin films with "smart" topography.

References:

[1] Y.Chen, H.Kim, Mater Lett, **61** (2007) 5040.
[2] L.Armelao, G. Bottaro, R.Campostrini, S.Gialanella, M.Ischia, F.Poli, E.Tondello, Nanotechnology, 18 (2007) 155606.

Figures:

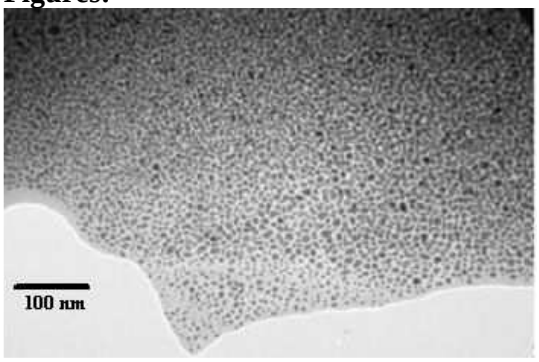

Figure 1- TEM image of the nanocomposite Ag/SiO_2 thin film.

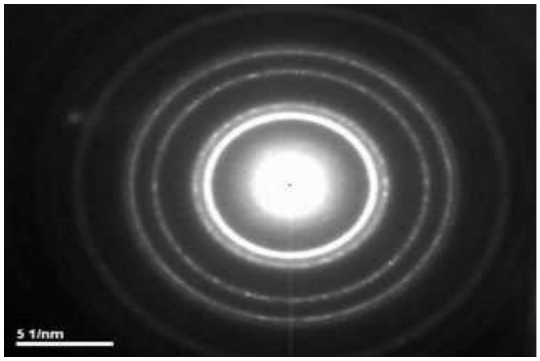

Figure 2 – Electron Diffraction Pattern

BIODEGRADABLE POLYMERIC MICROFIBRES REINFORCED WITH NANOFIBRES FOR BIOMEDICAL APPLICATIONS

*E.D. Pinho[1, 2, *], A. Martins[1, 2], J.V. Araújo[1, 2], R.L. Reis[1, 2], N.M. Neves[1, 2]*

*[1]3B's Research Group – Biomaterials, Biodegradables and Biomimetics, Department of Polymer Engineering, University of Minho, Campus de Gualtar, 4710-057 Braga, Portugal; [2]IBB – Institute for Biotechnology and Bioengineering, PT Government Associated Laboratory, Braga, Portugal. * epinho@dep.uminho.pt*

In the biomaterials field, nanofibre based structures and its composites are promising materials to produce scaffolds. The enhanced physicochemical properties and its structure being similar to the architecture of the extracellular matrix (ECM) may solve the major challenge of tissue engineering, which is obtaining the appropriate scaffold [1].

The main purpose of this work was to develop a novel composite structure which combines polymeric microfibres reinforced by nanofibres. This combination was obtained by melting extrusion of a synthetic biodegradable polymer, poly(butylene succinate) (PBS) (99,95% wt), reinforced with chitosan nanofibre meshes (0.05% wt). The chitosan meshes, composed by randomly aligned nanofibres, were produced by electrospinning technique (Figure 1a)). Longitudinal and cross sections of reinforced microfibres were observed by scanning electron microscopy (Figure 1b)).

The tensile mechanical properties revealed that the introduction of the reinforcement into the microfibres increased the tensile modulus to 553.2 ± 48.4 MPa. This improvement is around 70%, considering that the tensile modulus of microfibres without nanofibre reinforcement was 327.8 ± 35.3 MPa (Figure 2 and Table1).

The various structures were subjected to swelling and degradation tests upon immersion in an isotonic saline solution at 37ºC. The presence of chitosan nanofibres in the microfibres also enhanced the water uptake in up to 10% (Figure 3), caused by the higher hydrophilicity of the chitosan nanofibre meshes.

The combination of good mechanical properties and enhanced degradability of the developed structures is believed to have great potential for the production of 3D fiber mesh scaffolds, to be applied in the field of Tissue Engineering and Regenerative Medicine.

References:

[1] Lutolf, M.P., Hubbell, J.A., "Synthetic biomaterials as instructive extracellular microenvironments for morphogenesis in tissue engineering", Nature Biotechnology, **23**, 2005, 47-55.

Figures:

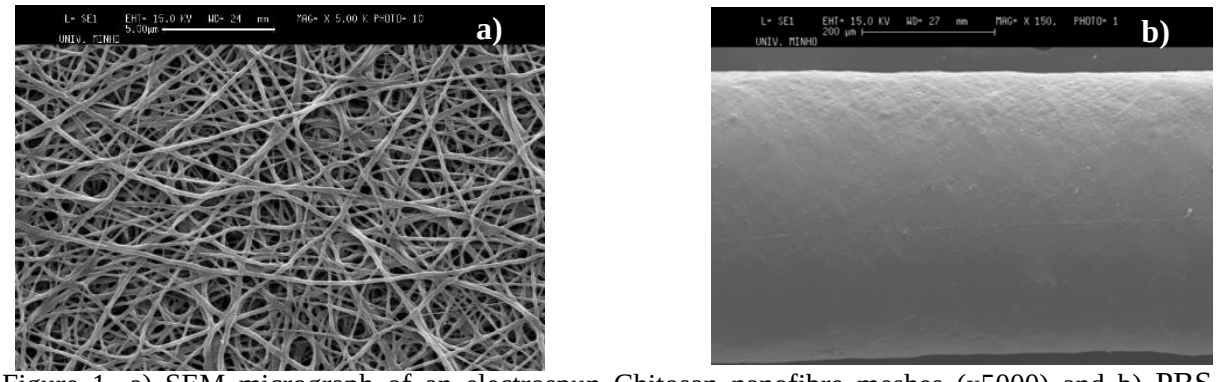

Figure 1- a) SEM micrograph of an electrospun Chitosan nanofibre meshes (x5000) and b) PBS microfibre (x150)

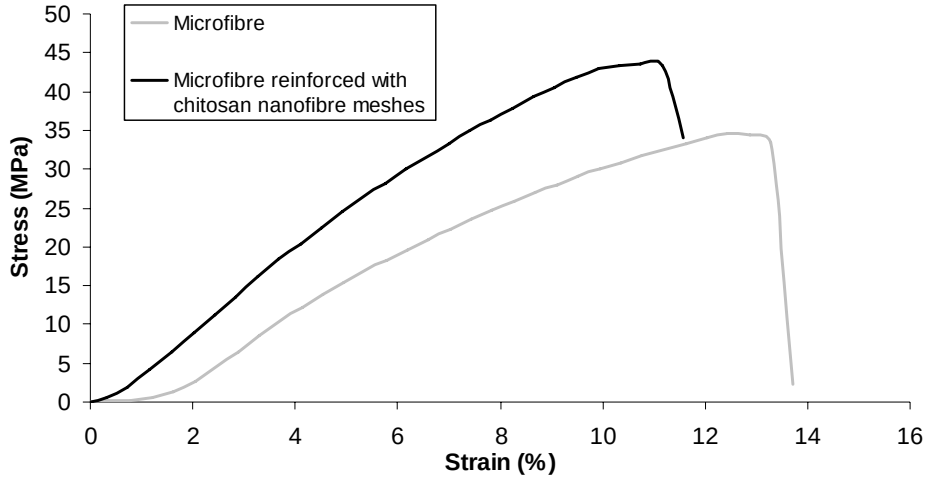

Figure 2 - Tensile stress-strain of chitosan microfibres with and without chitosan nanofibre meshes reinforcements.

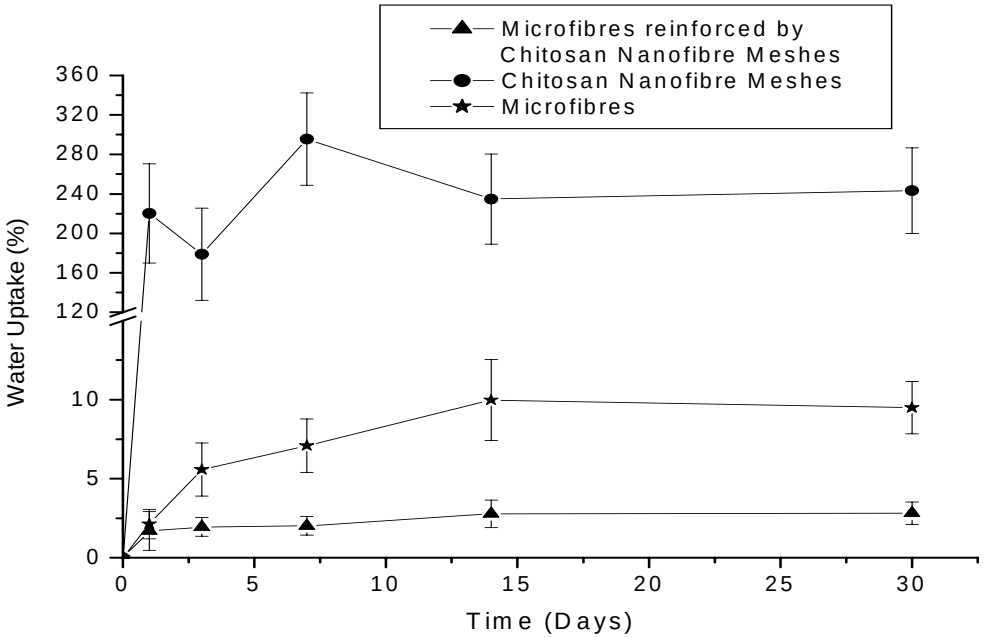

Figure 3 - Water uptake of the microfibres reinforced by chitosan nanofibre meshes, chitosan nanofibre meshes and microfibres, during the periods of immersion in isotonic saline solution.

Table 1 - Tensile properties of microfibres with and without chitosan nanofibres reinforcement.

Materials	Tensile Stress (MPa)	Tensile Modulus (MPa)	Tensile Strain (%)
Microfibres	30.6 ± 7.2	327.8 ± 35.3	11.6 ± 2.3
Microfibres reinforced with chitosan nanofibre meshes	35.4 ± 6.4	553.2 ± 48.4	10.7 ± 0.9

HYBRID NANOPARTICLES FOR MRI AND PHOTOLUMINESCENCE IMAGING APPLICATIONS IN CELLS TRACKING

Sonia Pinho,[a b] Stéphane Mornet,[a] Emeline Julie Ribot [c] Pierre Voisin,[c] Anne-Karine Bouzier-Sore,[c] João Rocha-[b], Luis Carlos, [b] Marie-Hélène Delville,[a]

[a] Bordeaux Institute of Condensed Matter Chemistry, UPR CNRS 9048 / University of Sciences and Technology of Bordeaux, 87 avenue du Dr Albert Schweitzer, 33608 Pessac, France.

[b] Departments of Chemistry and Physics, CICECO, University of Aveiro, 3810-193 Aveiro, Portugal

[c] Résonance Magnétique des Systèmes Biologiques, UMR CNRS 5536, 146 rue Léo Saignat, F-33076 Bordeaux cedex France,

Molecular complex type contrast agents (CA) which are used for in vivo MRI measurements have a full body distribution decreasing its concentration within the vicinity of a targeted site. This requires the injection of very high CA amounts. Our goal is to synthesize new MRI contrast agents containing inorganic nanoparticles able to complex lanthanide chelates. This has the following advantages: (i) locally increases the CA concentration, and (ii) significantly increases the degree of contrast in T1, as shown by preliminary tests.[1] (iii) affords bifunctional nanoparticles (contrast and optical).[2]

Our aim is to combine in the same particle, contrast, optical and targeting agents, in order to have a strong potential of specific recognition of certain tissues or organs. Tissues specificity will improve the clinical diagnosis and decrease the used CA amounts, because the contrast agent may concentrate close to the target. The chemical nature of the nanoparticles we are looking at is multiple: silica SiO_2, γ-Fe_2O_3@SiO_2 core-shell particles and silica shell. Lanthanide chelates (for their paramagnetism or photoluminescence properties) are grafted on these particles and we study the properties especially in the interactions between the iron oxide T2 and Ln T1 contrast agents. The final aim is to introduce these nanoparticles in living cells and follow their behaviour.

References:

[1] Voisin, Pierre; Ribot, Emeline Julie; Miraux, Sylvain; Bouzier-Sore, Anne-Karine; Lahitte, Jean-Francois; Bouchaud, Veronique; Mornet, Stephane; Thiaudiere, Eric; Franconi, Jean-Michel; Raison, Lydia; Labrugere, Christine; Delville, Marie-Helene. Bioconjugate Chemistry **18(4)** (2007), 1053-1063.

[2] Yu, Shi-Yong; Zhang, Hong-Jie; Yu, Jiang-Bo; Wang, Cheng; Sun, Li-Ning; Shi, Wei-Dong. Langmuir **23** (2007), 7836-7840

Nanostructured Materials from Non-Aqueous Sol-Gel Approaches: Optical, Magnetic and Gas Sensing Properties

Nicola Pinna
Department of Chemistry and CICECO, University of Aveiro, 3810-193 Aveiro
pinna@ua.pt

Non-aqueous sol-gel routes are elegant approaches for the synthesis of nanomaterials[1]. Here, it will be shown that these approaches were successfully used for the formation of high quality pure inorganic nanocrystals [1] and ordered hybrid organic-inorganic materials [2]. Especially, the chemical mechanisms taking place during the metal oxide formation greatly influence the morphology, assembly and the final properties.

The peculiar structure and the formation mechanism of organic-inorganic hybrid materials and inorganic nanoparticles doped with magnetic ions will be detailed and correlated to their properties [3]. Especially, the optical properties of lanthanide doped hybrid materials strongly depend on the organic moieties forming the hybrid mesostructure [2].

Pure semi-conducting metal oxide nanoparticles synthesized in non-aqueous media without the need of surfactants are good candidates for resistive gas sensor devices due to their nanometric size, good crystallinity and high purity [4]. Selected examples of gas sensor fabricated with porous thick layers made of nanoparticles will be presented.

References:

[1] N. Pinna, M. Niederberger, *Angew. Chem. Intl. Ed.* **2008**, in print
[2] N. Pinna, *J. Mater. Chem.* **2007**, 17, 2769
[3] G. Clavel, M. Willinger, D. Zitoun, N. Pinna, *Adv. Funct. Mater*. **2007**, 17, 3159
[4] G. Neri, N. Pinna, *Resistive chemical sensors from metal oxides nanocrystals synthesized in organic solvents*, in Nanomaterials: New Research Developments, Nova Science Publishers, **2008**, in print.

Figures:

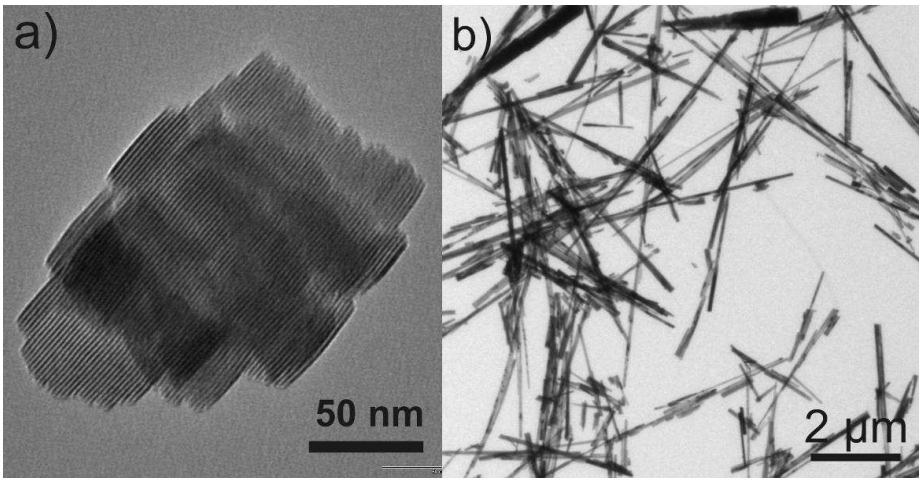

Fig. 1: TEM overview images of the a) neodymium oxide – benzoate hybrid nanostructure, b) Cobalt doped zinc oxide nanowires

Poster

Ge NANOCRYSTALS EMBEDDED IN ALUMINA FOR NON VOLATILE MEMORY APPLICATIONS

S. R. C. Pinto, A. G. Rolo*, A. Chahboun*, ** and M. J. M. Gomes**

** Physics Department, University of Minho, 4710 – 057 Braga, Portugal*
*** Physics Department, Dhar Mehraz Sciences Faculty, BP 1796, Fès, Morocco*
sarapinto@fisica.uminho.pt

Dielectric layers with embedded semiconductor nanocrystals (NCs) are widely studied, in order to overcome difficulties of non-volatile memory devices connected with technology scale-down, and to develop Si-based light emitting diodes (LEDs). In fact, a lot of research has been dedicated to study the quantum-confined electronic states in low dimension structures of group IV indirect-gap semiconductors such as Silicon (Si) and Germanium (Ge). Artificially controlled processes and the natural formation of quantum dots (QDs) of these materials would open new possibilities for the application of these materials in novel integrated optoelectronics and microelectronics devices.

Although related metal–insulator–semiconductor (MIS) structures can be prepared on any semiconductor substrate, silicon-based structures are the most important ones for the technological development. The most common structure used for both memory and LED purposes is the metal or poly-Si/SiO_x/Si structure with Si NCs embedded in the SiO_x layer [1]. However, alumina or stacked dielectrics are also used as dielectric matrix and Ge and SiGe nanocrystals are also often formed inside these matrices. Constant shrinking of the thickness of gate dielectrics to below 2-3 nm has led to a search for alternative materials, whose dielectric constant is higher than that of SiO_2, but whose other properties remain similar to SiO_2, which is the case of Al_2O_3. A dielectric constant (ε_{Al2O3} = 9) more than twice that of SiO_2 (ε_{SiO2}=3.9), a band gap of 9eV, good mechanical properties and high temperature resistance, makes Al_2O_3 a good candidate to replace SiO_2 as a gate dielectric material and an ideal material for Si processing conditions.

Several techniques are being used to fabricate Ge NCs, such as RF co-sputtering, ion implantation, evaporation–condensation, electron beam evaporation, chemical vapour deposition, and pulsed laser deposition. In this work Ge NCs embedded in alumina thin films were deposited over Silicon (111) substrates using RF magnetron co-sputtering technique. Annealing was performed in order to improve the cristallinity of the Ge phase in the films and achieve control over the NCs size [2]

Ge NCs of suitable size and good crystalline quality were obtained by different techniques, including X-ray diffraction (XRD) (Fig. 1, inset), Raman spectroscopy (Fig. 1) and high resolution transmission electron microscopy (HRTEM) (Fig. 2a). The NCs size was estimated from Raman spectra using Fauchet and Campbell model [3] and from X-ray diffraction using Debye-Scherrer equation [4]. Statistical average diameters were obtained from HRTEM pictures.

A good agreement between the three techniques for the size estimation was observed for smallest NCs. However, for larger NCs (> 20 nm) there is a discrepancy between XRD and Raman results. For this sample the LO Raman peak presents a blue shift relative Ge bulk and X-ray peaks are shifted for higher angles relative to the Ge diamond structure. A possible explanation for this shift is the compressive stress exerted on Ge NCs by the Al_2O_3 matrix [5, 6]. Further detailed studies are in course in order to clarify both confinement and stress effects.

References:

[1] Zs.J. Horváth, *Current Applied Physics* 6 (2006) 145–148
[2] P. Caldelas et al, in press in Journal Nanoscience and Nanotechnology.
[3] I. H. Campbell, F. M. Fauchet, Solid State Commun. 58, (1986) 739
[4] E. Lifshin, X-Ray Characterisation of Materials, Wiley-VCH, New York, (1999) p.37
[5] I. D. Sharp et al, Journal. Applied Physics 100, (2006) 114317, and references there in.
[6] O. Conde et al, Journal of Crystal Growth 247 (2003) 371-380

Figures:

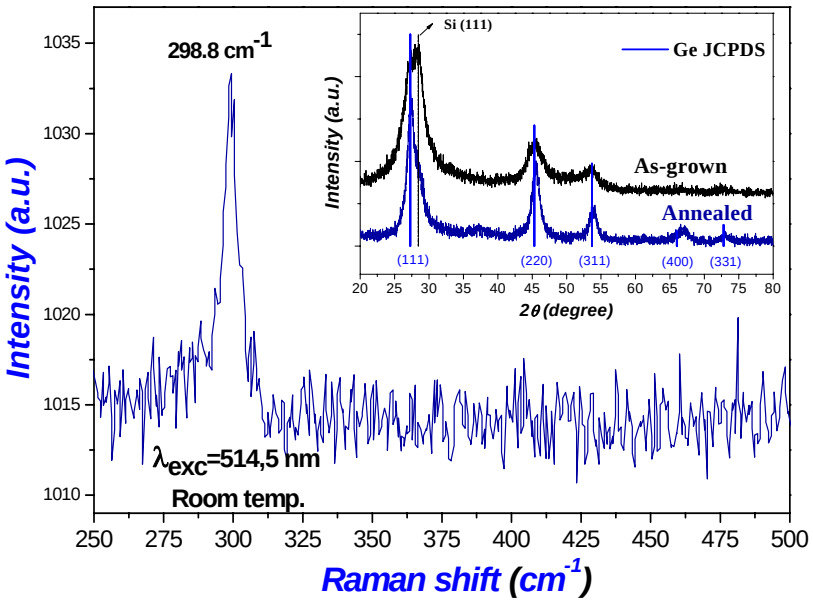

Fig 1: Raman spectrum of one annealed Ge/Al_2O_3 film (800ºC/1hour/4.6E^{-3} mbar air pressure). The LO peak is red shifted relatively to Ge bulk. Inset: XRD spectrum, clearly revealing (220), (311) and (400) reflections corresponding to peaks from Ge diamond structure. The average NC's size increased from approximately 3.4 (as-grown) up to 7.3 nm (annealed).

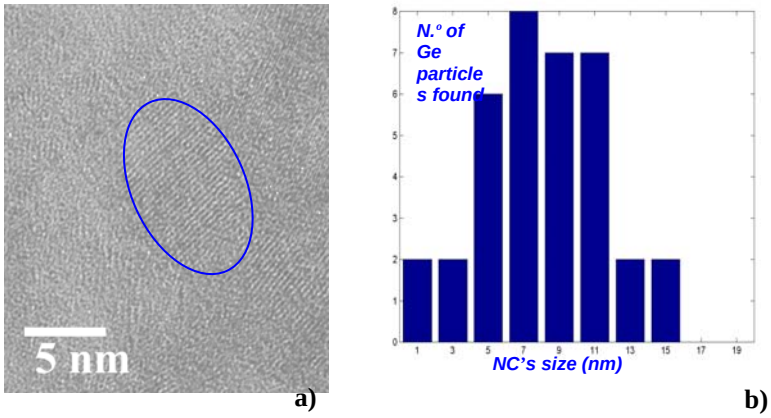

a) b)

Fig.2 – a) A cross section high-resolution TEM micrograph of the Ge/Al_2O_3 annealed film from Fig.1; The lattice fringes from Ge NC's are visible; **b)** Ge NC's size distribution calculated for this sample was 8 ± 3 nm, in agreement with the estimation made using Debey-Scherrer formula on XRD spectrum of Fig.1.

Acknowledgements
This work has been partially supported by the European Commission through project called SEMINANO under the contract NMP4-CT-2004- 505285, by FCT-Fundação para a Ciência e a Tecnologia-Portugal, and by the "Programa Operacional Ciência e Inovação 2010-POCI 2010" co-financed by FEDER (Fundo Comunitário Europeu) throught the Project POCTI/FIS/56930/2004. SRCP thanks FCT for the financial support (grant SFRH/BD/29657/2006).

CHITOSAN NANOPARTICLES FOR THE DELIVERY OF GENES TOWARD TISSUE REGENERATION

Liliana R Pires, Hugo Oliveira, Mário A Barbosa, Ana Paula Pêgo
INEB – Instituto de Engenharia Biomédica, Divisão de Biomateriais,
Rua do Campo Alegre, 823, Porto, Portugal
lipires@ineb.up.pt

Chitosan is a natural polysaccharide that due to its biocompability and low toxicity has been studied for numerous biomedical applications. Chitosan has positive charge in low acidity solutions, being able to produce nanocomplexes with DNA upon electrostatic interaction. Consequently, chitosan has been proposed as a gene delivery vector.

Growth factors play a key role in tissue regeneration. The delivery of these proteins *in loci* has been proposed as a mean to promote or modulate regeneration. Due to the above-mentioned properties, chitosan could be a promising candidate as a vector to mediate the deliver of genes encoding for growth factors, however these vectors were found to have limited gene delivery efficiency in comparison to other polycationic systems.

One of the major barriers described for gene delivery mediated by these systems is the particle escape from the endosomal pathway upon endocytosis. In this work, the incorporation of imidazole units in the chitosan backbone was performed in order to increase the buffering capacity of the polymer in the physiological pH range (7.4-5) and ultimately improve particles escape from the endosome, leading to an efficient gene expression. Chitosan with three different degrees of substitution were prepared. The modified polymers (CHimi) maintain the ability to condense DNA in particles of mean size of approximately 200nm (Zetasizer nano ZS, Malvern). The transfection activity mediated by CHimi polymers was investigated in 293T cells, using pCMV-Sport βGal as reporter gene. The results show that the introduction of imidazole moieties into chitosan backbone leads to a higher transfection activity, in comparison with the starting material. Transfection was found to be dependent on the degree of substitution of the polymer and on the N/P (amino groups of the polymer / phosphate groups of DNA) molar ratio of the complexes.

A gene delivery vector to be applied in a regenerative medicine scenario should guarantee non-toxicity, as well as controlled gene expression during the healing time period. Prospecting this application, the gene expression kinetics and the transfected cell viability were assessed up to 7 days after the transfection. CHimi-based vectors promote a sustained gene expression during this period without altering the viability of the cells.

The present results show that CHimi-based vectors are promising candidates as gene vehicles for regenerative medicine applications, what is currently under investigation.

Acknowledgments:
This project was carried out under the Portuguese Foundation for Science and Technology (FCT) contract POCI/SAU-BMA/58170/2004. H Oliveira acknowledges FCT for his PhD scholarship SFRH/BD/22090/2005.

Hard wear resistant coatings with nanoscale gradient refractive index

Tomas Polcar[1,4], Tomas Kubart[2], Eva Malainho[3], Nuno Parreira[4], Mikhail Vasilevskiy[3], Albano Cavaleiro[4]

1 Czech Technical University, Prague, Czech Republic 2 The Angstrom Laboratory, Uppsala University, Sweden 3 Department of Physics University of Minho, Portugal 4 SEG-CEMUC - Department of Mechanical Engineering University of Coimbra, Portugal

tomas.polcar@dem.uc.pt

Many functionalities of decorative and optical thin films are often hindered by their insufficient mechanical properties and low resistance to wear damage. Therefore, the research in the area of coloured hard coatings has attracted broad attention due to their application possibilities in many domains. However, presently the used nitride or carbonitride coatings exhibit only limited colour spectrum. Consequently, oxide[1,2] and oxynitride[3-6] materials with high hardness, chemical stability, resistance to the oxidation and colour degradation, and tuneable optical properties are assumed to be one of the best candidates for future protective optical films.

In this study, we present a new design for deposition of decorative tungsten oxide coatings based on magnetron sputtering from a tungsten target with reactive gas pulsing. The injection of the reactive gas produces gradient films with an increasing oxygen content from pure tungsten to tungsten trioxide. Thus, such coatings present a gradient concentration profile, which, as shown in this study, is related to their apparent colour. To investigate and understand the color properties of the deposited gradient coating, a dynamic sputtering model was developed together with an optical model based on the transfer matrix formalism. It will be shown that the controlled injection of the reactive gas could lead to any desired apparent color.

With our optical model, we could adjust a few parameters (one or two) of the most influencing coating's sub-layer, in order to obtain a determined position and magnitude for the reflectance maximum. This would allow for optimizing the composition profile of the gradient coating, in order to obtain a desired colour on demand. On the other hand, the dynamic sputtering model will be used to find whether realistic settings of sputtering parameters (i.e. parameters of the gas flow and sputtering power) could be found to achieve such colour. Obviously, the presented process is very versatile and can be used virtually for all sputtered metals in oxygen atmosphere provided the optical properties of their oxides are known, and can be extended to two reactive gases pulsing processes using oxygen and nitride or carbon-based gases. Recent results of the optical properties of the Nb-O-N[7] and Ta-O-N[8] systems deposited with constant nitrogen flow and pulsed oxygen clearly demonstrate the potential of our proposed control of nanoscale gradient layer. Moreover, magnetron sputtering with reactive gas pulsing can be used as well to deposit multi-cycled coatings without metal layer. The optical properties of such film would be driven by synergetic effect of the gradient refractive indices and optical active multilayered structure.

[1] Klingshirn, C., Chemphyschem 8, 782-803 (2007)
[2] Niklasson, G.A., Granqvist, C.G., J. Mater. Chem. 17, 127-156 (2007)

[3] Mohamed, S.H., et al., J. Phys. D Appl. Phys. 40, 7057-7062 (2007)
[4] Peng, X. et al., J Vac. Sci. Technol. A 25, 1078-1083 (2007)
[5] Fenker, M.,et al., Surf. Coat. Technol. 200, 1356-1360 (2005)
[6] Carvalho, P., et al. J. Appl. Phys. 98, 023715 (2005)
[7] Fenker, M. et al., , Surf. Coat Technol. 2007, doi:10.1016/j.surfcoat.2007.08.007
[8] Le Dreo, et al., Thin Solid Films 515, 952-956 (2006)

Figures:

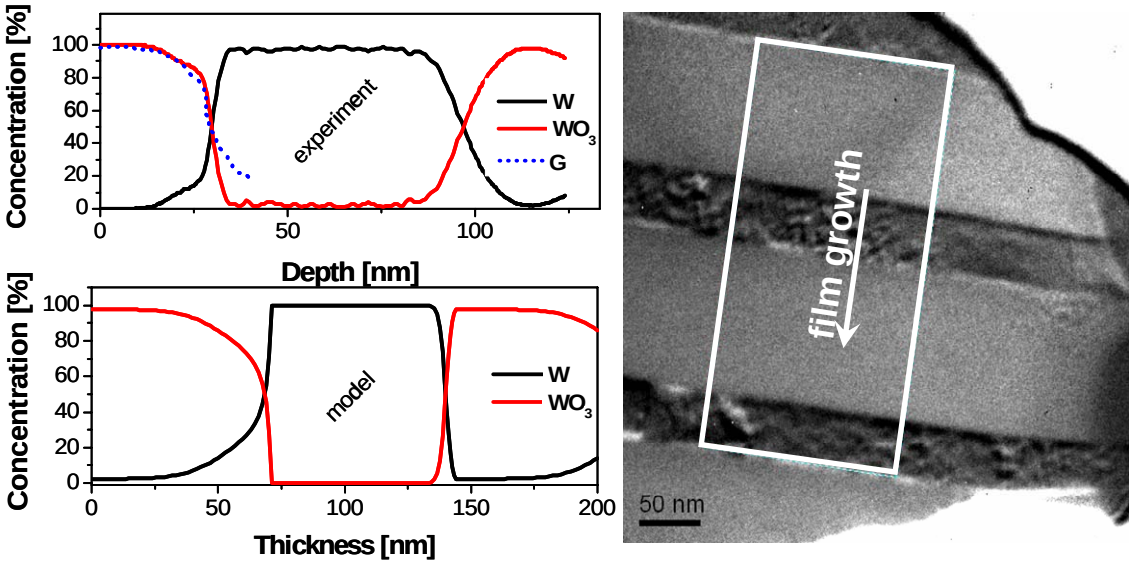

Comparison of the measured and simulated depth profile of gradient WO coating

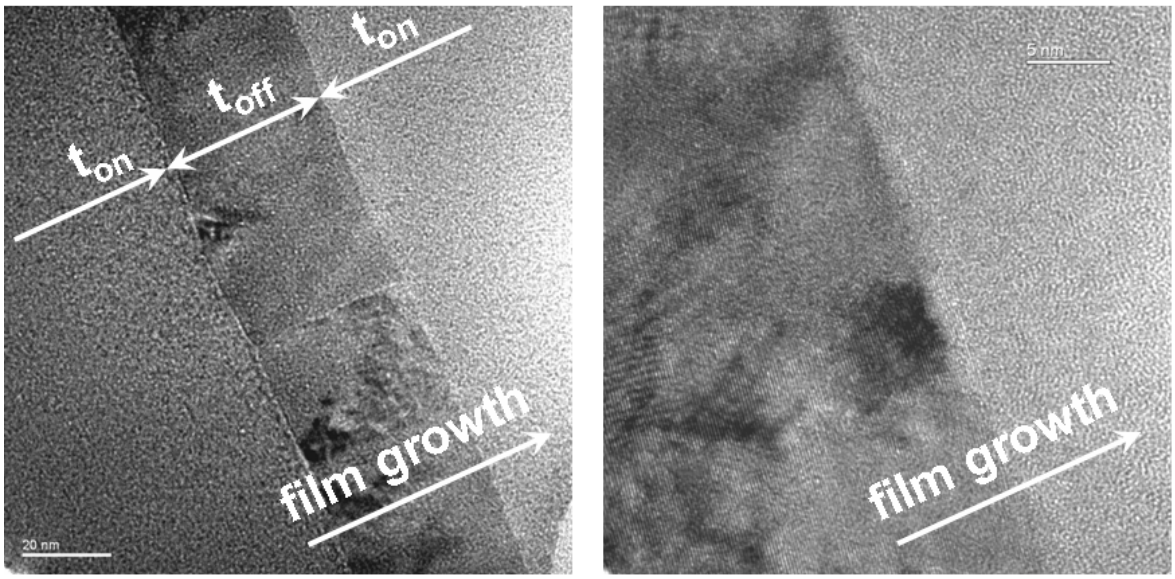

TEM (left) and HR-TEM (right) image of the gradient layer

RELAXATION AND DECOHERENCE IN TWO-ELECTRON SILICON QUANTUM DOTS

M. Prada[1,2], R. H. Blick[2], and R. Joynt[1]
[1]Physics Dpt, University of Wisconsin-Madison, 1150 University Ave., WI 53705, USA.
[2]Electric and Computer Engineering, University of Wisconsin-Madison,
1415 Engineering Drive, Madison WI 53705, USA.
prada@wisc.edu

Recent experiments demonstrate the presence of long-lived spin states in silicon quantum dots [1]. Understanding the processes that relax spins can point to strategies for minimizing relaxation and coherence times, thereby improving coherent control of quantum systems. In the case of electron spins embedded in semiconductor nanostructures, the relaxation properties are strongly affected by the regime of operation. Thus it is important to identify the dominant sources of fluctuations in these systems, the mechanisms by which they couple to the spins, and to analyze the non-equilibrium decay laws in different regimes of external fields. In this work, we investigate the singlet-triplet relaxation process of a two electron silicon quantum dot with circular symmetry. We use second order perturbation theory to compute the phonon-assisted relaxation rates for different fields and level separation.

In the absence of a perpendicular magnetic field, we find that spin-orbit coupling is *not* a source of singlet-triplet relaxation, and a direct singlet-triplet transition is forbidden by energy and spin conservation. Relaxation in this regime occurs mainly via virtual states[2] (see inset of Fig. 1) and is due to nuclear hyperfine coupling. Fig. 1 shows the relaxation time as a function of level separation to the virtual state, J.

In the presence of an external magnetic field perpendicular to the plane of the dot, the spin-orbit coupling opens a new channel for relaxation (see Fig. 2). We find a strong anisotropy for different field directions: parallel magnetic field can increase substantially the relaxation time due to Zeeman splitting, as it can be seen in Fig. 3.a, but when the magnetic field is applied perpendicular to the plane, the enhancement of the spin-orbit effect shortens the relaxation time, as shown in Fig. 3.b. We find the relaxation to be orders of magnitude longer than for GaAs quantum dots [3], due to weaker hyperfine and spin-orbit effects.

Hyperfine coupling also causes decoherence in Si double quantum dots, for which we find coherence times of hundreds of μs for natural silicon, orders of magnitude larger than for GaAs.

References:

[1] N. Shaji, C. B. Simmons, M. Thalakulam, L. J. Klein, H. Qin, H. Luo, D. E. Savage, M. G. Lagally, A. J. Rimberg, R. Joynt, M. Friesen, R. H. Blick, S. N. Coppersmith, and M. A. Eriksson, preprint at hhttp://aps.arxiv.org/abs/0708.0794i (2007).
[2] S. I. Erlingsson, Y. V. Nazarov, and V. L. Falko, *Phys. Rev. Lett.* **94**, 196802 (2005).
[3] R. Hanson et al., *Phys. Rev. B* **64**, 195306 (2001).

Figures:

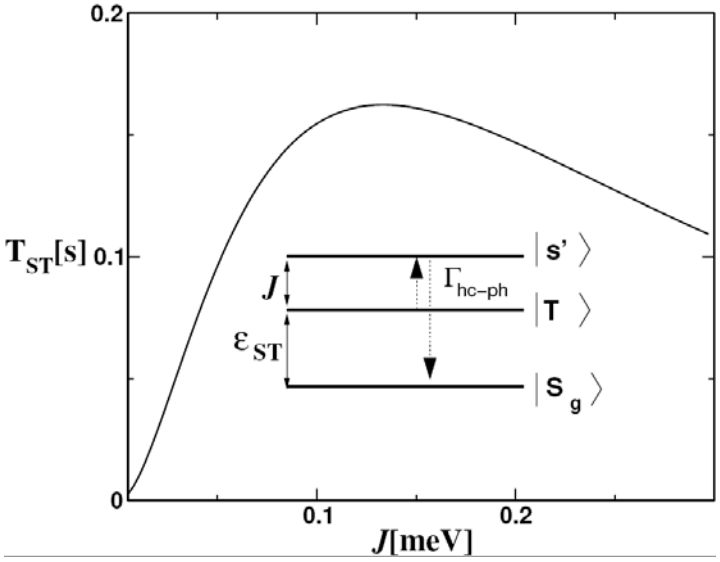

***Fig.1**: T_{ST} as a function of J for the process depicted in the inset: when levels |T⟩ and |s'⟩ are close in energy (J→0), the singlet-triplet transition is dominated by hyperfine coupling (fast). As the energy levels split, the process is dominated by phonon emission. The electron-phonon coupling is provided by a deformation potential, and no piezo-phonon is considered in a centrosymmetric material as silicon.*

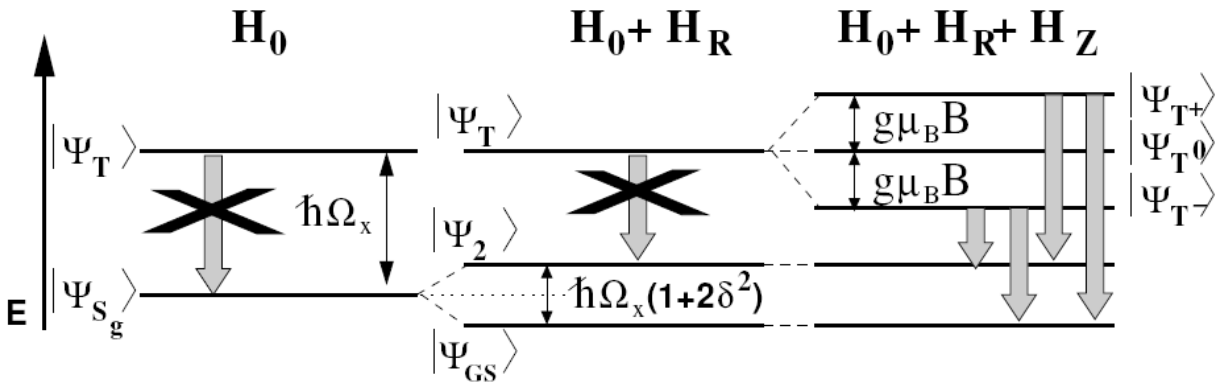

***Fig. 2**: Level scheme for a doubly-occupied Si quantum dot. With the confinement potential H_0, the orbital causes a splitting between the singlet ground state and the triplet, which splits from the excited singlet, |s'⟩(not included) due to exchange interaction. Singlet-triplet transitions are forbidden due to spin conservation. Under the presence of spin-orbit interaction, H_{SO}, the singlet splits in two, whereas the triplet remains degenerated, and thus, the ST transitions forbidden. A magnetic field splits the three triplets by Zeeman interaction, H_Z, allowing ST transitions to occur (vertical wide arrows).*

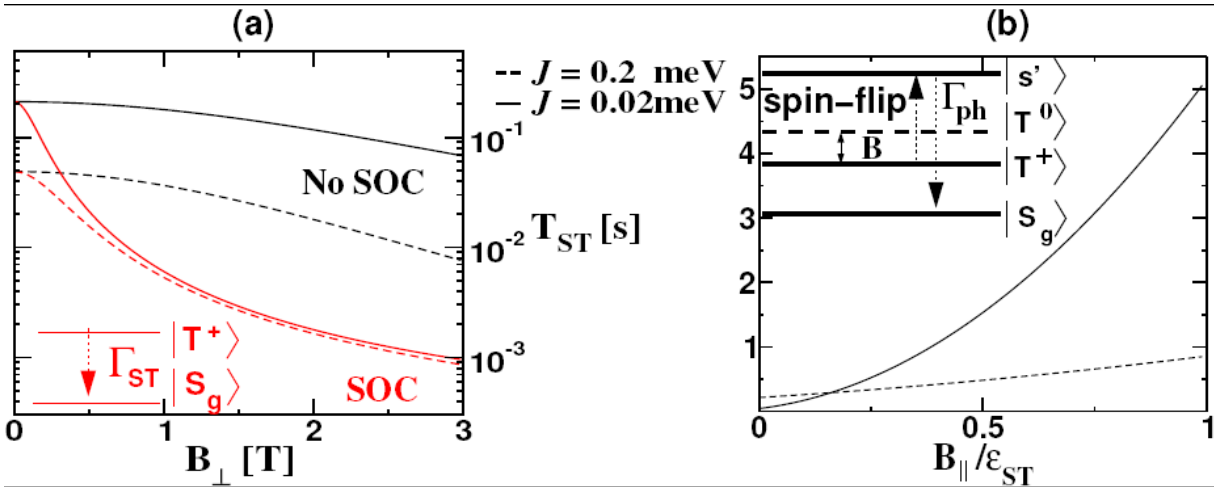

***Fig. 3**: (Color online) T_{ST} as a function of magnetic fields for two values of J. The solid lines correspond to a plausible value of J=0.02meV, and the broken lines to J=0.2meV, for comparison (a) as a function of $B_\perp$, including Rashba (red) and without Rashba (black), and (b) as a function of $B_{||}$. The behavior is strongly anisotropic, showing a monotonic increase of the relaxation time with of $B_{||}$, due to increase in level separation, and decrease with $B_\perp$, due to shrink in effective size of the QD and therefore, lower number of effective ^{29}Si nuclei available for flip-flop processes.*

EMRP RESEARCH PROJECT: TRACEABLE CHARACTERIZATION OF NANOPARTICLES

Emilio Prieto
Centro Español de Metrología (CEM), Alfar, 2, Tres Cantos, 28760 Madrid, Spain
eprieto@cem.mityc.es

Nanoparticles are already in use today in different products (e.g. paints, lotions, protective clothes, etc) and there is public discussion on possible hazardous effects of nanoparticles which has to be addressed by standardisation, control, legislation and, therefore, metrology. Effective control of nanoparticles requires measurement, classification and secure handling/manufacturing. High-resolution microscopy techniques for individual nanoparticle characterization exist (SEM, AFM UV optical), but they require standardisation and the resolution needs to be further developed (e.g. smaller wavelength, fs microscopy) and face serious sampling issues to ensure correct analysis. Other, integral metrology techniques also exist: PCS, scattering methods, etc. However, high quality, well defined nanoparticle standards from different materials are lacking. If available, these would help to better cross-correlate the results of local and integral methods and this would allow to achieve the 1 nm accuracy target.

Manufacturing of nano-materials with novel functionalities such as nanotubes and fullerenes requires metrological support through traceable characterisation. In addition well documented concerns about the health risks of nanoparticles, such as combustion, exist. Thus metrological research towards traceable measurements of toxicity, shape, size, size distribution, chemical identity of nanoparticles, etc., will play a key role in the near future.

A fundamental issue for nanoparticles compared to micron size powder is sampling and preparation methods. The consortium previous experience in the field will help to identify high quality particle size standards, suitable for traceable calibration. An important aspect of this project is to determine long-term stability and humidity dependence of the measurements. The partners will develop validated methods for sampling and agree international methods for the characterisation of the nanoparticles measuring instruments.

The analysis of the light scattered by a particle is a powerful method for detecting its shape and size. New optical methods will be investigated and developed to measure complex-shaped particles, highly concentrated dispersions, and push the resolution limit of existing instruments.

The consortium will investigate the use of different materials (metallic, ceramic, polymer) as possible new reference materials to complement the existing types (spherical polystyrol spheres). An important improvement on the state of the art is focused on the comparison between high resolution (SFM, STEM, etc.) and integral (SAXS, optical scatterometry) techniques on different types of nanoparticles. The methods used will range from synchrotron based SAXS for size and size distribution of nanoparticles to dynamic light scattering or AFM measurement.

Shape measurements for sub 100 nm nanoparticles are a real issue for nanoparticle characterization and their applications. An entire work package is dedicated to this important issue. At the end of the project, partners will have introduced a new set of parameters describing non-spherical particles for standard measurements and internationally agreed definitions for characterisation of shape and surface of nanoparticles.

Besides management (WP1) and dissemination (WP6), the project is divided into the following WPs:

WP2: Sample preparation. This is the first important step for comparable results. The sample preparation has to maintain the original size and distribution, together with sufficient stability over time.

WP3: Aerosol measurement. Development of nanoparticle (NP) generation and measurement methods for number concentration, size and shape. A Single Charge Aerosol Reference Instrument (SCAR) will be constructed to realize a validated traceable measurement standard for the number concentration of nanoparticles (NP) for characterisation of commercial NP measuring instruments. An analysis method based on light scattered by a NP will be developed and compared against SCAR.

WP4: Size distribution measurement on spherical nanoparticles. Focused on the comparative measurement of nearly spherical nanoparticles with ensemble (SAXS, DLS, etc.) and single particle orientated methods (SFM, SEM/STEM, etc.) and the cross-check of the obtained results.

WP5: Size and shape measurement on high aspect ratio nanoparticles. Standardized definition for high aspect ratio (1:3) nanoparticles and nanotubes and issues related to shape measurement for nanoparticles.

Participants:

National Physical Laboratory, NPL, UK (Coordinator)
Czech Metrological Institute, CMI, CZ
Centre for Metrology and Accreditation, MIKES, FI
Physikalisch-Technische Bundesanstalt, PTB, DE
Istituto Nazionale di Ricerca Metrologica, INRIM, IT
Centro Español de Metrología, CEM, ES
Federal Office of Metrology, METAS, CH
Institutul National de Metrologie, INM, RO
Tampere University of Technology, TUT, FI (co-funding partner)

References:

[1] H.-U. Danzebrink, L. Koenders, G. Wilkening, A. Yacoot and H. Kunzmann: *Advances in Scanning Force Microscopy for Dimensional Metrology*, CIRP Annals – Manufact. Techn., Volume **55**, Issue **2** (2006) 841-878.

[2] V. Korpelainen et al., Calibration of a commercial AFM: traceability for a coordinate system, Meas. Sci. Techn., **18** (2007) 395-403.

[3] H. Keskinen et al., Preparation of ZrO2 Fine Particles by CVD Process, Jour. of Mat. Sci. Let. **39** (2004) 4923-4929.

[4] H. Keskinen et al., Generation of Silver/Palladium Nanoparticles by Liquid Flame Spray, Jour. of Mat. Res. **19** (2004) 1544-1550.

[5] J. Ristimäki et al., On-line measurement of size distribution and effective density of submicron aerosol particles, J. Aerosol Sci. **33** (2002) 1541-1557.

[6] F. Meli, Particle diameter calibration by means of a metrology AFM, Proc. of the 1st euspen Topical Conference on Fabrication and Metrology in Nanotechnology, L. De Chiffre and K. Carneiro (Eds.), Vol. **1**, May 2000, Copenhagen, p.45-51.

[7] F. Meli, Lateral and vertical diameter measurements on polymer particles with a metrology AFM, Nanoscale Calibration Standards and Methods, G. Wilkening and L. Koenders (Eds), 2005, Wiley-VCH Verlag, Weinheim, 361-374.

[8] J. Schlatter, LAPAZ: a laser particle counter as a primary number concentration standard, European Aerosol Conference, September 2004, Budapest, Proc., 901-902.

EMRP RESEARCH PROJECT: NEW TRACEABILITY ROUTES FOR NANOMETROLOGY

Emilio Prieto
Centro Español de Metrología (CEM), Alfar, 2, Tres Cantos, 28760 Madrid, Spain
eprieto@cem.mityc.es

Through the iMERA European project the metrology community and its stakeholders identified the major challenges for European metrology for the coming years, focusing particularly on those challenges best addressed collaboratively. Following a road-mapping exercise these challenges were captured in the European Metrology Research Programme (EMRP) (www.emrp.eu).

The aim of the Joint Research Project (JRP) "Nanotrace" here presented is National Metrology Institutes to collaborate in finding and testing new interferometric techniques to allow traceability of sensors and actuators at the nanoscale with a target accuracy better than 10 pm on a 10 to 100 um scale.

In the last two decades the invention and the development of scanning probe microscopy (SPM) has revolutionized the microscopic world science: scanning tunnel microscopy, atomic force microscopy and optical probe microscopy made possible observations and measurements with a resolution unthinkable before. The sub atomic resolution has made possible to observe the shape of molecules, the arrangement of atoms on a crystal, to study chemical reactions to the atomic level. The common principle of the SPMs, a probe tip scanning the surface in a 3 coordinate cartesian system, allows the realization of SPMs with integrated metrology system to obtain traceable measurements. Most NMIs have their own metrological SPM equipped with high resolution optical interferometer. The weak point is that the resolution of the SPMs is at least one order of magnitude smaller than the accuracy of the best interferometer available today.

There is no doubt that today the interferometer is the best choice for length measurement traceability: in fact interferometric measurement is based on the wavelength of a stabilized laser source which in turn is directly linked to the definition of the metre through frequency measurement. In its classic use (length measurements from millimetres to kilometres) the uncertainty of interferometric measurements is mainly limited by the knowledge of air refractive index and by laser frequency stability. When used for measurements down to the nanometre level, the interferometer fringe (being hundreds of nanometers long) must be subdivided in small equal parts. This measurement (which in fact is a phase measurement) is not straightforward.

To improve the resolution/accuracy of optical interferometers beyond the state of the art, allowing traceability of measurements at the nanoscale is the goal of this JRP. The target accuracy of 10 pm will allow to fill the gap existing between the resolution of existing measurement devices and the accuracy of the present metrology systems.

One of the possible traceability routes at the nanoscale is the use of crystalline surfaces and artificial arrangements of single atoms and nanotubes as standards for calibration or as base for new sensors. After some discussion it came out that, though the research in this field is proceeding fast, it is sill to young to be competitive with interferometers in the next future. Rather, it is believed that the realization of more accurate interferometer will accelerate the development of this promising research field.

Besides management (WP1) and dissemination (WP6), the project is divided into the following WPs:

WP2: Development of new interferometric techniques to minimize measurement uncertainty at the nanoscale.

WP3: Realization of a transfer standard with extreme metrological capabilities to allow the comparison between the interferometers that cannot be moved from a laboratory to another. Two ways will be investigated: a calibrated piezo-capacitive actuator, a compact interferometer or a combination of the two.

WP4: X-ray interferometer set-up to allow its use for the characterization of the interferometers developed in WP2.

WP5: Comparison (directly for transportable interferometers or indirectly by means of the transportable standard developed in WP3 for non transportable ones) with the X-ray interferometer developed in WP4, allowing a reliable evaluation of the results.

Participants:

Istituto Nazionale di Ricerca Metrologica, INRIM, Italy (Coordinator).
Bundesamt für Eich- und Vermessungswesen, BEV, Austria
Czech Metrology Institute, CMI, Czech Republic
Centre for Metrology and Accreditation, MIKES, Finland
National Physical Laboratory, NPL, United Kingdom
Physikalisch-Technische Bundesanstalt, PTB, Germany
Tubitak Ulusal Metroloji Enstitüsü, UME, Turkey

References:

[1] P. Heydemann, Appl. Opt. **20**(19) (1981) 3382.

[2] A. E. Rosenbluth and N. Bobroff, Optical sources of non-linearity in heterodyne interferometers, Prec. Eng. **12**(1) (1990) 7-11.

[3] A. Sacconi, G.B. Picotto and W. Pasin, The IMGC calibration setup for microdisplacement actuators, IEEE Trans. Instrum. Meas. **48**(2) (1999) 483-487.

[4] M. Tanaka, T. Yamagami, and K. Nakayama, Linear interpolation of periodic error in a heterodyne laser interferometer at subnanometer levels, IEEE Trans. Instrum. Meas. **38**(2) (1989) 552-554.

[5] W. Hou and G. Wilkening, Investigation and compensation of the nonlinearity of heterodyne interferometers, Prec. Eng. **14**(2) (1992) 91-98.

[6] J. M. De Freitas, Analysis of laser source birefringence and dichroism on non linearity in heterodyne interferometry, Meas. Sci. Technol. **8** (1997) 1356-1359.

[7] C. Wu, J. Lawall, and R.D. Deslattes, Heterodyne interferometry with subatomic periodic nonlinearity, Appl. Opt. **38**(19) (1999) 4089-4094.

[8] V.G. Badami and S. R. Patterson, A frequency domain method for the measurement of nonlinearity in heterodyne interferometry, Prec. Eng. **24** (2000) 41-49.

[9] S. Cosijns, H. Haitjema, and P. Schellekens, The influence of polarization states on non-linearities in laser interferometry, Proc. of the 3rd EUSPEN Conference, Vol. **2** (2002) 593-596.

[10] TaeBong Eom et al., A simple method for the compensation of the non-linearity in the heterodyne interferometer, Meas. Sci. Technol. **13** (2002) 222-225.

[11] G. Dai et al., Meas. Sci. Technol. **15** (2004) 444-450 .

[12] H. Haitjema, S. Cosijns, N. Roset and M. Jansen, Improving a commercially available heterodyne laser interferometer to sub-nm uncertainty, Proc. SPIE Vol. **5190** (2003) 347.

[13] G.B. Picotto, Interferometric calibration of microdisplacement actuators, Proc. SPIE Vol. **5190** (2003) 355-360.

NANO-TiO_2 PHOTOCATALYTIC DEGRADATION OF PCB WASTE OILS

J. Fermoso[a], O. Prieto[a], O. Pérez[a] and R. Irusta[a,b]

[a] FUNDACIÓN CARTIF
Technology Park of Boecillo, Boecillo, Valladolid, Spain (olgpri@cartif.es)
[b] Department of Chemical Engineering and Environmental Technology. School of Industrial Engineering. University of Valladolid.
(rubiru@eis.uva.es)

Introduction

Photocatalytic technology is becoming more and more attractive to industry today because global environmental pollution has come to be recognized as a serious problem that needs to be addressed immediately [1]. Nanostructured titanium dioxide (TiO_2) is the most attractive semiconductor used currently, having high photocatalytic efficiency, stability against photocorrosion and chemicals, insolubility in water, low toxicity, and low cost. Its band gap energy of 3.2 eV leads to photoexcitation requiring wavelengths less than ca. 385 nm, corresponding to a near-UV irradiation. Aroclor® 1254 was one of the most commonly used industrial PCB fluids. There are 37 congeners (each at greater than 0.5% by weight) that can be found in this Aroclor®. Congener 138 (2,2,3,4,4,5-hexachlorobiphenyl) is one of the major congeners that accounts for 9.1% of the total mass of Aroclor® 1254.

In this study, a photocatalytic degradation method was developed for polychlorobiphenyl (PCB) from insulating waste oil transformers.

Experimental

The transformer oil employed in the experiments was supplied by Management Waste Company S.A. located in Oviedo (Spain). This is a viscous fluid with a yellowish colour.
We carry out a previous study centered on the determination a rapid method for extraction and quantification of PCBs in transformer oil and the dissolution of these into water to carry out a photocatalytic degradation. The extraction method is based in the U. S. Patent [2], that provides a rapid and easily determining the concentration of PCBs in a given sample of dielectric fluid. This is accomplished by first extracting the PCBs from transformer fluid with polyethylene glycol, subsequently extracting the PCBs from the polyethylene glycol solution by cyclohexane extraction, and thereafter analyzing the PCB-cyclohexane extract by gas chromatography-electron capture (CG/ECD) to determine its PCB concentration. In this study, the concentration of PCBs in transformer oil fluid was 115,5 ppm.

To prepare aqueous solutions of PCBs, a suitable amount of dissolution of PCBs in cyclohexane was evaporated over pyrex glass balls. Then, PCBs were redissolved with methanol (20 % v/v) and distilled water.

The study of photodegradation of PCBs in water was carried out using the Taguchi's Parameter Design method. This methodology is useful to minimize process sensitivity to debilitating sources of variation. Robust Design allows understanding and exploiting interactions between controllable parameters and uncontrollable "noise" ones.

Figure 1. Experimental Facilities

The experimentation were carry out using 1g/L of nano-TiO_2 (P25 Degussa, 20 nm and 50 m^2/g) in a closed reactor that is illuminated with a UV radiation, that shown in figure 1.

Among the different process influential factors (temperature, nano-TiO_2, O_2, H_2O_2 and PCBs concentrations, pH and UV radiation intensity); H_2O_2 concentration, pH and PCBs concentration were chosen as control factors (F) based on references, previous studies and experience of the research group. Control factors chosen and their levels are given in Table 1. The orthogonal array (OA) L4 shown in table 2 was selected to carry out the experimental plan [3].

Table 1. Levels of Control Factors

Level	pH	[H_2O_2]	[PCBs]
1	Acid	0.05 M	100 ml
2	~ 7	0.1 M	200 ml

Table 2. L4 Orthogonal Array

Run n#	pH	[H_2O_2]	[PCBs]
#1	1	1	1
#2	1	2	2
#3	2	1	2
#4	2	2	1

The illuminated suspensions were extracted by liquid-liquid extraction (LLE) to determine the PCBs. We carry out the extraction following the modified method described in *UNE-EN-ISO 6468* [4]. So, 5 ml of heptane are added at 5 ml of aqueous samples by shaking (20 s by handing and following 20 min on sonication). Finally, the samples are centrifuged and analyzed by CG/ECD.

References:

[1] O. Prieto, J.Fermoso, Y. Nuñez, J.L. del Valle and R. Irusta. Solar Energy 79 (2005) 376-383.

[2] Pytlewski et al. U.S.Patent 4.430.208. "Method for the solvent extraction of polychlorinated biphenyls". (1984)

[3] Wu, Y. and Wu A. 1992. Diseño robusto utilizando Métodos Taguchi. (Madrid Ed. Díaz de Santos, S.A.

[4] *UNE-EN ISO 6468 (ISO 6468:1996).* Calidad de agua. Determinación de ciertos insecticidas organoclorados, bifenilos policlorados y clorobencenos. Método por cromatografía de gases con extracción líquido-líquido.

Acknowledgements

Financial support by A520/2007/2-07.1 (MMA) is acknowledged.

ORDERED ASSEMBLY OF OXIDE NANOTUBES IN A POROUS ALUMINA MEMBRANE

M.P. Proenca, C.T. Sousa, A.M.L. Lopes, D.C. Leitao, J. Ventura, J.B. Sousa, J.P. Araujo
Dep. Física and IFMUP, Rua do Campo Alegre 687, 4169-007 Porto, Portugal
mippro@gmail.com

Nanoporous alumina membranes are an easy-made product that has attracted much interest in these last years. They can be used as templates for well ordered growth of nanowires, nanotubes, nanorods and nanodots, thus providing a wide range of applications in areas such as medicine [1] (biosensors, photocatalysts), electronics (ultrahigh-density magnetic memories, optoelectronic devices), energy storage (solar cells).

In this work we used nanoporous alumina membranes to produce two types of oxide nanotubes: silica (SiO2) [2] and perovskite manganites (CaMnO3) [3], via the sol-gel template method. These templates can be easily fabricated using adequate anodization conditions and the pore size and interpore distance easily varied. Furthermore, their use for growth of nanotubes has enormous advantages: the possibility to build a net of aligned and ordered nanostructures, the chance to fill or functionalize their inner side without affecting their outer surface and the ability to control the dimensions required. Using this method, not only can we control the length of the nanotubes, but we can also control their diameter and thickness, allowing us to vary these characteristics along their surface.

We will present an optimization study of the sol-gel template method using nanoporous alumina membranes allowing to achieve high quality oxide nanotubes and nanowires of SiO2 and CaMnO3, varying template characteristics such as pore and interpore sizes, as well as sol-gel parameters such as temperature, concentration, viscosity and deposition time. The developed methods can be adequately applied to other oxides.

References:

[1] S.J.Son, X.Bai and S.B.Lee, Drug Discov. Today, **12** (2007) 650.
[2] D.T.Mitchell, S.B.Lee, L.Trofin, N.Li, T.K.Nevanen, H.Soderlund and C.R.Martin, J. Am. Chem. Soc., **124** (2002) 11864.
[3] P.Levy, A.G.Leyva, H.E.Troiani and R.D.Sánchez, Appl. Phys. Lett., **83** (2003) 5247.

Figures:

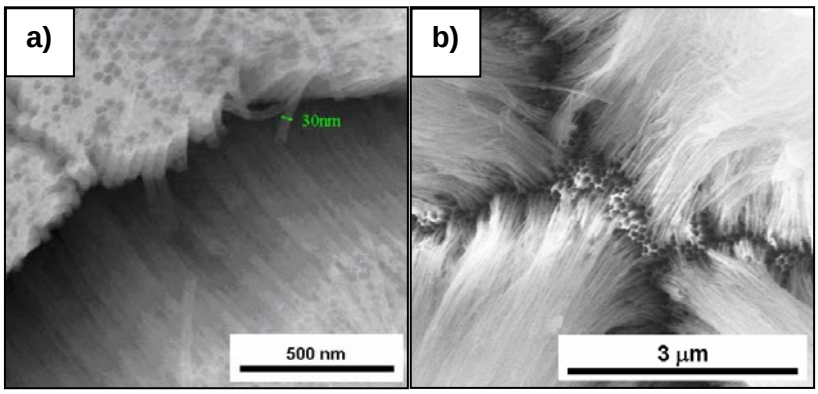

SEM images of silica (a) and manganite (b) nanotubes obtained by the sol-gel template method.

BIOFUNCTIONALITATION OF MAGNETIC NANOPARTICLES FOR INMUNOMAGNETIC BIOSENSORS

S. Puertas, V. Grazú, M. Moros, M. Arruebo, J.M. de Teresa, J. Sesé, C. Marquina, R. Ibarra, J.M. de la Fuente

Universidad de Zaragoza, Instituto de Nanociencia de Aragón (INA)
C/Pedro Cerbuna 12,50009,Zaragoza, Spain
selmer@unizar.es

Lateral-flow biosensors are well known strategies for the detection of specific analytes. One of the most common lateral flow biosensor is the pregnancy test. Lateral-flow assays consist of a nitrocellulose membrane with micrometric pores allowing the flow of liquid via capillarity. In this support, a biological recognition agent is previously deposited in the test line and traps the targeted analyte if present in the flowing liquid. The biological recognition events are labelled with colloidal particles giving identifiable colour the test line when the test is positive. The test is considered positive when the amount of analyte is large enough so that the labelling colloidal particles can be detected by eye view. However, this kind of tests does not allow the quantification of the analyte.

For the last 30 years, there is a growing interest in the use of magnetic nanoparticles for application in quantitative and highly-sensitive biosensors. The use of them as labels of the biological recognition events and their detection by means of some magnetic methods makes one way to realize quantitative high-sensitive lateral-flow assays.

We present here different approaches for the functionalization of magnetic nanoparticles with specific antibodies for their use in immunomagnetic biosensors based on lateral-flow assays. Our analyte model is the human chorionic gonadotropin hormone (hCG) produced during pregnancy. Different types of commercial available magnetic nanoparticles with a mean diameter around 200 nm have been chosen. Depending on the strategy used, we can get a perfect control in the presentation of the antibody (IgG anti-hCG) on the surface of the nanoparticles. The sensitivity of the biosensor has been increased by one order of magnitude when the antibodies are right oriented on the nanoparticle. With these results, we show the importance of the antibodies immobilization for the right molecular recognition in biosensing assays.

Acknowledgments: This work has been funded by CONSOLIDER CSD2006-12 project. JS thanks “Ramon y Cajal” program (MEC) for financial support. JMF thanks ARAID for financial support.

References:

[1] De Teresa J.M., Grazú V., Moros M., et al. Biosensors and Bioelectronics.Submitted
[2] Fuentes M., Mateo C., Guisán J.M., Fernández-Lafuente R., 2005. Biosensors and Bioelectronics 20, 1380-1387.
[3] Turkova J., 1999. J. Chromatogr. B 722,11-31.

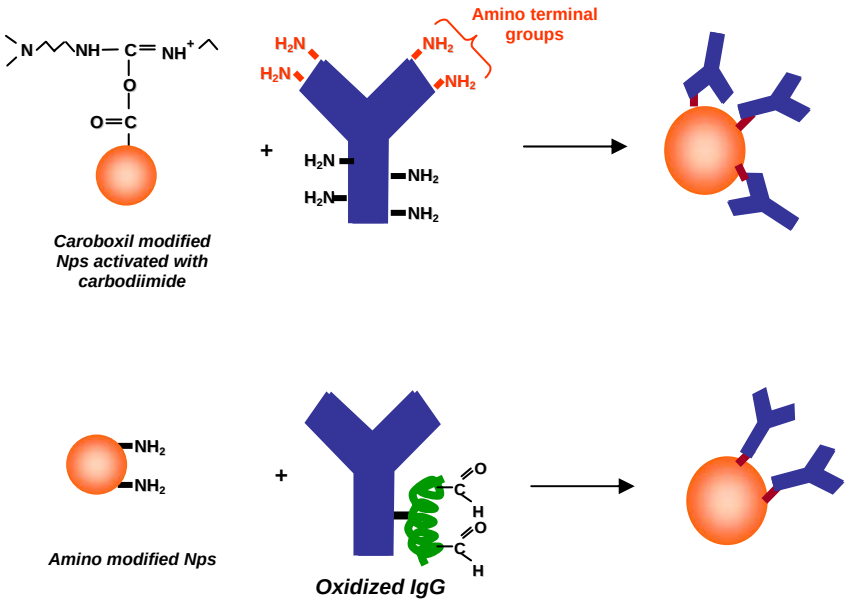

Figure 1. Inmobilization strategies.

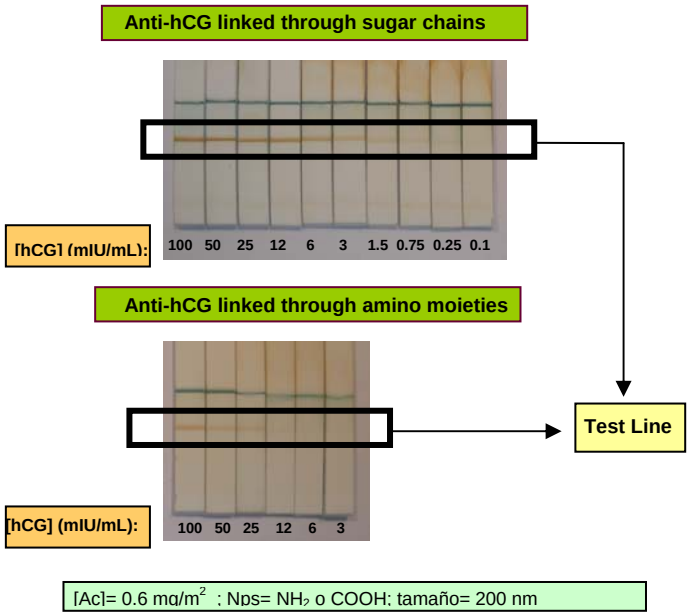

Figure 2. Lateral-flow assay results using different antibodies immobilization strategies.

Sonochemical formation of gold nuclei on magnetite nanoparticles and growth to a core-shell system

Pedro Quaresma[a,e]*, *Ricardo Franco*[b], *Patrícia Carvalho*[c], *João Pedro Araujo*[d], *Pedro Baptista*[e] *and Eulália Pereira*[a]

a REQUIMTE/Faculdade de Ciências, Universidade do Porto, R. Campo Alegre 687, 4169-007 Porto, Portugal
b REQUIMTE/Departamento de Química, CQFB, FCT-UNL, 2829-516 Caparica, Portugal
c Departamento de Engenharia de Materiais, IST, Av. Rovisco Pais 1049-100 Lisboa, Portugal
d IFIMUP, R. Campo Alegre, 678, 4169-007 Porto, Portugal
e CIGMH/Departamento de Ciências da Vida, FCT-UNL, 2829-516 Caparica, Portugal
* Corresponding author: pedro.quaresma@fc.up.pt

Magnetic nanoparticles for selective capture of biomolecules in complex mixtures is gaining momentum in bionanotechnology by providing significant advantages over traditional methods of separation[1]. A magnetite-gold core-shell structure would grant researchers with an integrated detection and "gene fishing" platform by means of the detection properties of gold nanoparticle systems combined with a magnetic component[2, 3].

An ultrasound mediated procedure was employed for *in-situ* formation of gold nuclei on the surface of magnetite nanoparticles. The growth of the gold nuclei on the magnetite to a gold shell layer was achieved by an iterative addition of gold precursor and reducing agent. The growth of the gold layer was followed by T.E.M., UV-Vis and EDS. Several parameters, such as gold precursor concentration, reductant concentration, rate of reagents addition and initial nanoparticle concentration were analysed. Also, different chemical reductants were evaluated for their ability to produce a complete gold shell.

References:

1. Ito, A.; Shinkai, M.; Honda, H.; Kobayashi, T., Medical application of functionalized magnetic nanoparticles. *Journal of Bioscience and Bioengineering* **2005,** 100, (1), 1-11.

2. Wang, L. Y.; Luo, J.; Fan, Q.; Suzuki, M.; Suzuki, I. S.; Engelhard, M. H.; Lin, Y. H.; Kim, N.; Wang, J. Q.; Zhong, C. J., Monodispersed core-shell Fe3O4@Au nanoparticles. *Journal of Physical Chemistry B* **2005,** 109, (46), 21593-21601.

3. Xu, C.; Xie, J.; Ho, D.; Wang, C.; Kohler, N.; Walsh, E. G.; Morgan, J. R.; Chin, Y. E.; Sun, S., Au-Fe3O4 dumbbell nanoparticles as dual-functional probes. *Angewandte Chemie-International Edition* **2008,** 47, (1), 173-176.

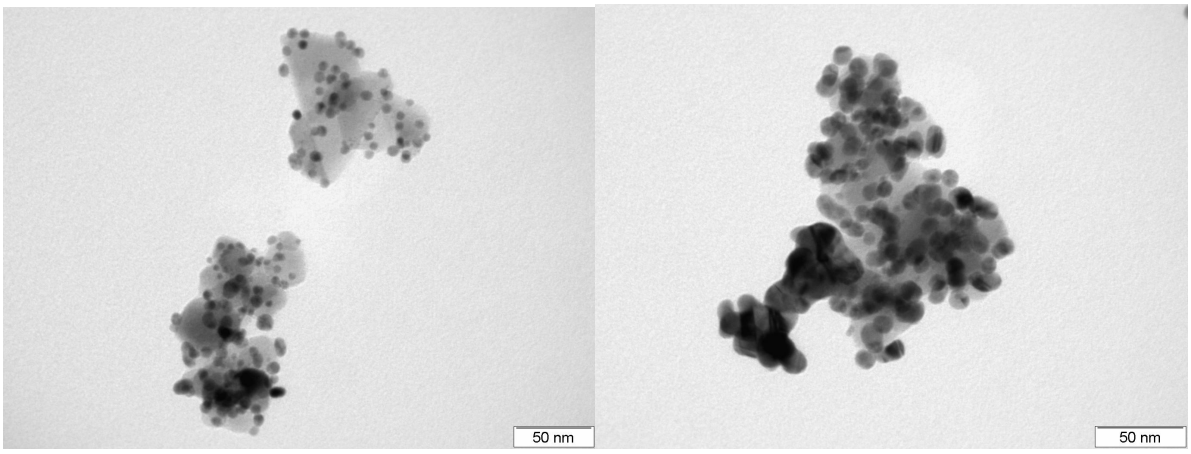

Figure 1- Left: nanoparticles obtained by ultrasound mediated procedure; right: nanoparticles obtained by further addition of gold precursor and reductant.

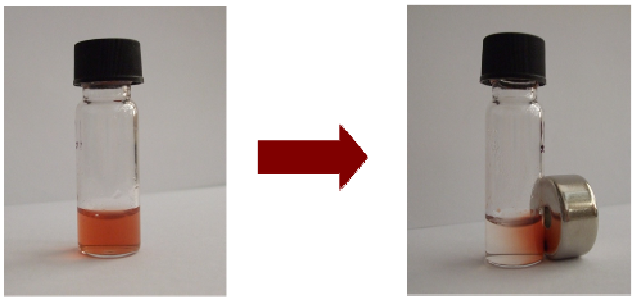

Figure 2 – Magnetic separation of magnetite-gold nanoparticles with a permanent magnet.

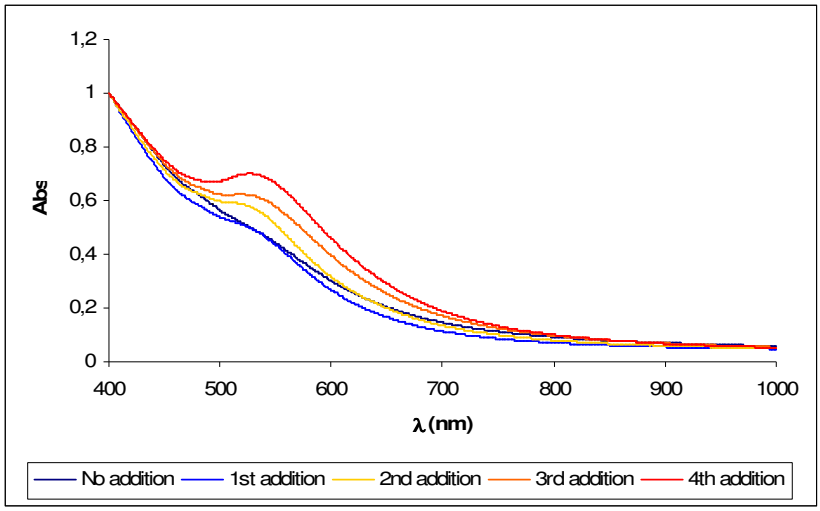

Figure 3 – UV-Vis spectra showing the growth of the gold surface plasmon band through the iterative addition of gold precursor and reducing agent.

Acknowledgments

The authors would like to thank FCT (Fundação para Ciência e Tecnologia) through projects PTDC/BIO/66514/2006; PTDC/QUI/64484/2006 and PTDC/SAU-BEB/66511/2006, and SFRH/BD/28209/2006 to Pedro Quaresma.

TUNABLE HYDROTHERMAL SYNTHESIS OF $BAMNO_3$ NANOCRYSTALS

Ana Querejeta[1], *Marina Parras*[1], *Aurea Varela*[1], *Jose González-Calbet*[1], *Francisco del Monte*[2], *Mª Mar García Hernández*[2]
[1]*Universidad Complutense de Madrid, Facultad de Ciencias Químicas, Ciudad Universitaria, 28040, Madrid, Spain*
[2]*Instituto de Ciencia de Materiales de Madrid, Consejo Superior de Investigaciones Científicas, Cantoblanco, 28049, Madrid, Spain*
jgcalbet@quim.ucm.es

Although synthesis of nanooxides has been attempted by many different and innovative chemical approaches, further research is still needed to develop inexpensive and mass-production methods capable to provide pure products and thus make nanocrystals' technological applications viable.

Hydrothermal synthesis matches these requirements. Under hydrothermal conditions, where an aqueous reaction mixture is heated above 100 ºC in a sealed reaction container, density, ionic product, viscosity and dielectric constant of water change dramatically as a consequence of the autogenous pressure, creating a medium suitable for crystallization reactions that would not occur under conventional conditions[1]. As a relevant factor, the hydrothermal synthesis of multinary oxides is specially accessible in comparison with other approaches, due to the high solubility and mobility of species under these conditions.

Manganese oxides perovskites ($A_{1-x}A'_xMn_{1-y}M_yO_{3-\delta}$) or manganites exhibit a rich variety of structures (from one-dimensional to three-dimensional)[2] and outstanding properties, such as colossal magnetoresistance (CMR)[3-4], high permittivity[5], multifferroic behaviour[6-7], etc…As it is well-known, nanocrystals' properties strongly depend on their shape and dimensions. Nanomanganites have been prepared by hydrothermal route[8-12], but no precise control over the size and shape has been achieved. As a result, further research on hydrothermal reaction conditions is still required.

Herein, we report on the hydrothermal synthesis of single-cristalline nanoparticles of $BaMnO_3$. The particle size distribution of the resulting nanoparticles is found to be centered at 20-40 nm. Such a good control of the particle size and distribution is obtained by fine tune of reaction medium alkalinity and concentrations of the precursor metallic salts. We also evaluate the relevance of temperature, time and pressure on the final structural properties of the resulting products. The nanocrystals are thoroughly characterized by means of power X-ray diffraction (XRD), dynamic light scattering (DLS), transmission electron microscopy (TEM), high resolution transmission electron microscopy (HRTEM), electron diffraction (ED) and energy-dispersive X-ray analysis (EDAX). The magnetic behavior of the nanoparticles is finally discussed.

References:

[1] Rabenau A. *Angew. Chem. Int. Ed. Engl*.,1985, 24, 1026-1040.
[2] R. H. Mitchell. *Perovskites Modern and Ancient*. Ed. Almaz Press Inc., Canada 2002.
[3] Jin, S.; Tiefel, T. H.; McCormack, M.; Fastnacht, R. A.; Ramesh, R.; Chen, L. H. *Science* 1994, 264, 413.
[4] vonHelmolt, R.; Wecker, J.; Holzapefel, B.; Schultz, L.; Samwer, K. *Phys. Rev. Lett*. 1993, 71, 2331.
[5] Keith G. M.; Kirk C. A.; Sarma K.; Alford N. M.; Cussen E. J.; Rosseinsky M. J., Sinclair D. C., *Chem. Mate*r. 2004., 16, 2007.
[6] Hill, N. A.; Rabe, K. M. *Phys. Rev. B* 1999, 59, 8759.
[7] Sharan, A.; Lettieri, J.; Jia, Y.; Tian, W.; Pan, X.; Schlom, D. G.; Gopalan, V. *Phys. Rev. B* 2004, 69, 214109.
[8] Urban J. J.; Ouyang L.; Jo M.; Wang K. S.; Park H. *Nano Lett.* 2004, 4, 8, 1547.
[9] Zhu D.; Zhu H.; Zhang Y. *Appl. Phys. Lett*. 2002, 80, 9, 1634.
[10] Spooren J.; Walton R. I. *J. Solid State Chem*. 2005, 178, 1683.
[11] Spooren J.; Walton R. I.; Millange F. *J. Mater. Chem*. 2005, 15, 1542.
[12] Chai P.; Liu X.; Wang Z.; Lu M.; Cao X.; Meng *J. Cryst.Growth Design*, 2007, 7, 12, 2568.

Figures:

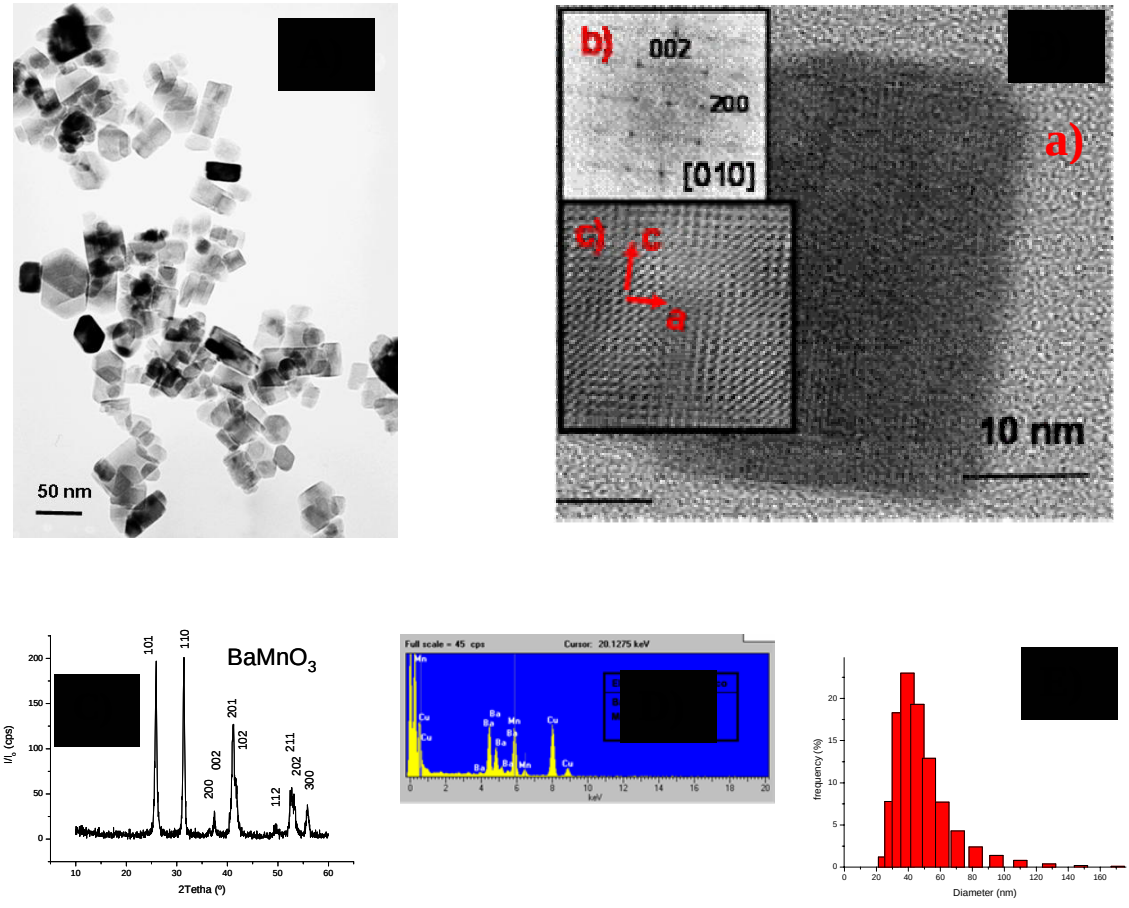

Figure 1. $BaMnO_3$ nanoparticles synthesized by hydrothermal method in alkali medium: A) TEM image; B) a) HRTEM image, b) Fourier transformed, c) filtered HRTEM image; C) DRX pattern; D) EDAX analysis; E) DLS size distribution.

Optical characterization of up-conversion properties of fluorescent $NaYF_4$:Er,Yb nanocrystals

M. Quintanilla[1], N.O. Núñez[2], E. Cantelar[1], M. Ocaña[2] and F. Cussó[1]
[1] Depto. Física de Materiales, C-IV, Universidad Autónoma de Madrid, Spain
[2]Instituto de Ciencia de Materiales, CSIC, Isla de la Cartuja, Sevilla, Spain
marta.quintanilla@uam.es

Fluorides doped with rare earth (RE) ions have been used in a wide range of photonic applications along the last decades. At present, the importance of nanoscale optically functional materials to be used as medical and biological tags has increased the potentiality of fluorides. To exploit those possibilities new methods to obtain several nanostructures based on fluorides are being developed, and several doping possibilities are being tried to obtain visible emissions using biologically innocuous excitation [1,2]. Recently, a novel synthesis method, providing a straightforward and versatile procedure for the synthesis of uniform lanthanide fluoride nanophosphors has been proposed [3].

In the present work, a detailed optical characterization of the Er^{3+}/Yb^{3+} co-doped $NaYF_4$ nanophosphors so synthesised is reported. The dominant Er^{3+} up-converted emission bands have been investigated by exciting the Yb^{3+} ions at around 980 nm.

The RE-doped fluoride nanoparticles were prepared by a homogeneous precipitation reaction in ethylene glycol solutions containing the rare earth precursors and NaF as a source for both, fluoride and sodium ions [3]. In order to investigate the effects of the doping level on the optical properties of the nanophosphors, the Yb^{3+} content was varied in the range 10-20% molar while the Er^{3+} concentration was kept constant (2% molar).

The morphology of the nanoparticles was examined by transmission electron microscopy using a TEM Philips 200CM system. Qualitative composition of the particles was assessed by energy dispersive X-ray analysis using an EDX system (Philips DX4) coupled to an electron microscope. The optical characterization has been performed using a JENOPTIK laser diode source to excite the Yb^{3+} ions with different excitation powers. The visible Er^{3+} luminescence was dispersed by using an ARC Spectrapro 500-I monochromator and then detected with a photomultiplier tube.

In Figure 1 a TEM image of the Er^{3+}/Yb^{3+}-doped nanophosphors can be seen, illustrating the morphology and uniformity of the obtained nanocrystals.

Figure 2 shows the visible emission in the wavelength range 400 nm < λ < 750 nm, arising from Er^{3+} ions after Yb^{3+} excitation at λ = 980 nm. These results demonstrate that effective co-doping has been achieved, providing the adequate conditions for effective energy transfer between Yb^{3+} and Er^{3+} ions. It is also apparent that the emission spectra strongly depend on the excitation power, as it is expected from the spectroscopic properties of Er^{3+}/Yb^{3+} activated materials [4].

References:

[1] L. Wang and Y. Li, Chem. Mater. **19** (2007), 727.
[2] G.S. Yi, G.M. Chow, Adv. Funct. Mater. **16** (2006), 2324.
[3] N.O. Núñez, H. Míguez and M. Ocaña, (submitted)
[4] E. Cantelar and F. Cussó, J. Lumin. **102-103** (2003), 525

Figures:

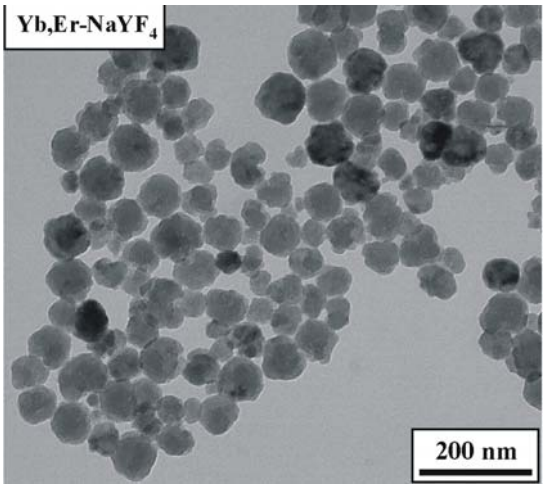

Figure 1. TEM image of the Er^{3+}/Yb^{3+}-doped nanophosphors.

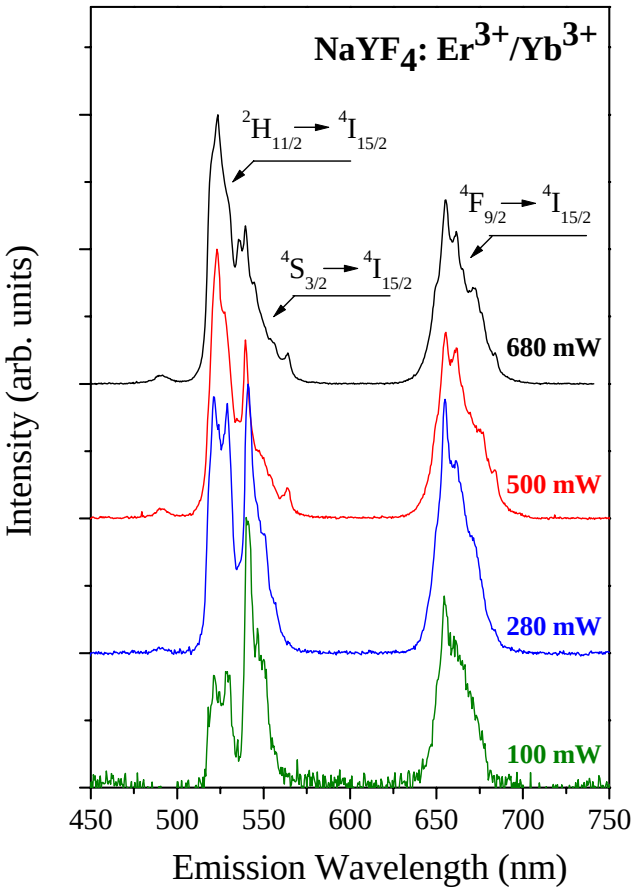

Figure 2. Emission spectra of [Er^{3+}] = 2 mol% and [Yb^{3+}] = 10 mol% codoped samples. The different spectra were measured by pumping at 980 nm with different excitation powers.

ELECTRIC ALIGNMENT OF MICROTUBULES ON A MICROFABRICATED SURFACE: MICRON-LEVEL CONTROL

Ruben Ramalho[a,b,*], *Helena Soares*[a,c], *Susana Cardoso*[b,e], *Luís V. Melo*[b,d]
[a]*Instituto Gulbenkian de Ciência, R. da Quinta Grande 6, Oeiras, Portugal*
[b]*Instituto Superior Técnico, Av. Rovisco Pais, Lisboa, Portugal*
[c]*Escola Superior de Tecnologia de Saúde de Lisboa, Lisboa, Portugal*
[d]*IN, Lisboa, Portugal*
[e]*INESC-MN, R. Alves Redol 9, Lisboa, Portugal*
*rubendrr@igc.gulbenkian.pt

Microtubules are hollow tubes 25 nm in diameter (for 13-protofilament microtubules) whose walls are assembled from parallel α-β-tubulin dimers, making them polar. This structure is capable of providing mechanical support to a cell, while being dynamic enough for quick remodeling (as when forming the mitotic spindle during cell division). In addition, microtubules function as tracks for motor proteins (e.g. dyneins and kinesins), which usually have a preferential sense of movement according to the microtubule's polarity.

We propose to use localized electric fields to induce the alignment (due to their electric dipole) of microtubules on a surface with high precision. This would enable the use of microtubules as interfaces of nanoengineered devices with biomolecules or whole cellular organelles. It would at the very least allow close control of motor protein movements.

We have already demonstrated the viability of this approach with the alignment of a bulk sample of surface-adsorbed microtubules by a high electric field. For that purpose, microtubules were allowed to adsorb to a poly-l-lysine coated glass coverslip while being exposed to a 400 $kV.m^{-1}$ electric field. When dried and imaged with AFM in air, the resulting samples showed preferential alignment of the microtubules parallel to the applied electric field [1].

To expand on these results, we resorted to standard microfabrication technology to manufacture a chip with integrated capacitor arrays. This is designed to obtain much finer control of the alignment, while still applying to a large (8x8 mm^2) area. Specifically, the chip includes structures for bulk parallel alignment and also for alignment along a curved pattern in a non-uniform field.

In preliminary experiments, microtubules were adsorbed to the chip's surface, silicon dioxide coated with poly-l-lysine, under a maximum electric field of 900 $kV.m^{-1}$ (5V over the minimum distance of 5 μm) and imaged in air by AFM. A clear alignment of microtubule bundles was observed along curved field lines in the non-uniform field experiment.

We are presently optimizing the sample preparation method and the device itself.

References:

[1] Ramalho RR, Soares H, Melo LV, Mat. Sci. Eng. 27 (2007): 1207-1210

ORIGIN OF THE RESPONSE OF NANOMECHANICAL RESONATORS TO BACTERIA ADSORPTION

Daniel Ramos, Javier Tamayo, Johann Mertens, Montserrat Calleja
BioNanoMechanics Laboratory, National Centre for Microelectronics, IMM-CNM, CSIC
Isaac Newton 8
(PTM), Tres Cantos, Madrid 28760, Spain
dramos@imm.cnm.csic.es

By performing experiments of adsorption of the bacteria *Escherichia coli* on singly clamped microcantilevers, we demonstrate that the effect of the added mass is not the only and may not be the main origin of the response of these sensors. The experiments show that the magnitude and sign of resonance frequency shift both depend critically on the distribution of the adsorbed bacterial cells on the cantilever. We relate this behavior to the added mass that shifts the resonance to lower frequencies and the higher effective flexural rigidity of the cantilever due to the bacteria stiffness that shifts the resonance to higher frequencies. Both effects can be uncoupled by positioning the cells where each effect dominates, near the free cantilever end for measuring the added mass or near the clamping for measuring the increase of flexural rigidity.

We propose a model that accounts for the mechanical properties of the attached bacteria that increase the stiffness of the cantilever. We model our cantilever as an Euler-Bernoulli beam, in which both the mass per unit length and the flexural rigidity are dependent on the longitudinal position

To calculate the resonance frequency we have applied Rayleigh's approximation. This method deduces the resonance frequencies by performing an energy-work balance and assuming that the eigenmode shapes are not substantially changed by the adsorbed bacteria resonance frequency is calculated as

$$\omega_n^2 = \frac{\int_0^L D(x)\left(\frac{\partial^2 u_n(x)}{\partial x^2}\right)^2 dx}{\rho WT\int_0^L \left(1+\frac{\rho_a}{\rho}\frac{T_a(x)}{T}\right)u_n^2(x)dx}$$

We have applied this equation to estimate the first mode resonance frequency shift due to the increase of mass and flexural rigidity induced by the deposited bacteria. We model the adsorbed bacteria as a homogeneous and uniform disk with a diameter of 100 μm that contains 4200 bacteria cells. The bacterium mass is 665 fg, and the biolayer height is 840 nm, smaller than the bacterium height of about 1 μm, to reflect that the adsorbed bacteria are not densely packed in the experiments. Young's modulus of 1.3 GPa was chosen in order to mimic the experimental results. This value is similar to those obtained by atomic force microscopy measurements in dried bacteria. The second figure shows the calculated frequency shift versus the adsorption position along the cantilever due to the added mass (dashed line), the change of flexural rigidity (dashed line), and both effects (solid line). The experimental values of the resonance frequency shift obtained from the cantilevers shown in the first figure are also included (symbols). The theory shows a good agreement with the experimental data indicating the consistency of the presented model. The added mass of the adsorbed bacteria produces a negative resonance frequency shift whose magnitude varies from approximately null for the adsorption near the clamping to maximal for the adsorption

In conclusion, we have demonstrated that the response of nanomechanical resonators to bacteria adsorption does not only depend on the added mass, but also on the stiffness of the bacterial cells. Both effects can be uncoupled by positioning the bacterial cells where each effect dominates, near the free cantilever end for measuring the added mass or near the clamping for measuring the increase of flexural rigidity. Both geometries allow sensitive bacteria detection of about 0.1 Hz per bacterium. This sensitivity can be easily enhanced by at least one order of magnitude by using higher vibration modes or by scaling down the cantilever size. The results of this work can be generalized to the adsorption of any molecule. In addition, the effect of the mechanical properties of the adsorbed molecules will become increasingly important as the size of the resonators is decreased towards the nanoscale.

References:

D. Ramos, J. Tamayo, J. Mertens, M. Calleja and A. Zaballos, J. Appl. Phys. **100**, 106105 (2006)
D. Ramos, J. Tamayo, J. Mertens and M. Calleja, Appl. Phys. Lett. **89**, 224104 (2006).

Figures:

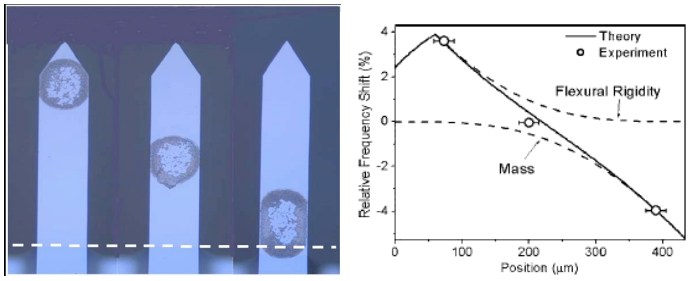

Ti/Al and Ni/Al Nanomultilayer Films – A Comparative Study

A.S. Ramos[1], M.T. Vieira[1], J. Morgiel[2], J. Grzonka[2]
[1]ICEMS, Departamento de Engenharia Mecânica, Faculdade de Ciências e Tecnologia, Universidade de Coimbra, R. Luís Reis Santos, 3030-788 Coimbra, Portugal
[2]Institute of Metallurgy and Materials Science, Polish Academy of Sciences, Reymonta 25, 30-059 Cracow, Poland
sofia.ramos@dem.uc.pt

Advanced Ti and Ni aluminides are potential candidates for practical applications, as bulk or thin films. Among the stable compounds of the Ti-Al and Ni-Al systems, the TiAl, NiAl and Ni_3Al intermetallics are the most promising for high-temperature applications [1,2]. These aluminides could be formed by thermal annealing of alternate layers of Ti (or Ni) and Al that exothermically react. These metals have medium / high energy of mixing and when in adiabatic conditions the reaction is self propagating [3]. Therefore, Ti/Al and Ni/Al reactive multilayers show potential for joining applications, in particular for small components.
In this work, Ti/Al and Ni/Al multilayer films with equiatomic overall chemical composition and different nanometric periods were studied. The nanomultilayers were deposited by magnetron sputtering onto stainless steel and glass substrates. The as-deposited films were analysed by electron probe microanalysis and X-ray diffraction (XRD), while the structural evolution with temperature was followed by differential scanning calorimetry and XRD in a hot stage. The coatings nanostructure was characterised using scanning – transmission High Angle Angular Dark Field (HAADF) as well as high resolution transmission electron microscopy (HRTEM) imaging. The thin foils for these observations were cut using Ga+ focused ion beam (FIB).
In both systems the as-deposited films are constituted by Ti- (Ni-) and Al-rich solid solutions that evolve towards the equilibrium phase γ-TiAl (B2-NiAl) upon thermal annealing. The presence of reaction products that might be formed during the deposition process was not detected even for the Ni/Al films that react at low temperatures. In fact, the structural evolution of the Ni/Al nanomultilayer films towards equilibrium occurs at rather low temperature comparing with the Ti-Al system where no phase transitions occur up to 450-550ºC depending on the modulation period [4]. Nevertheless, in both cases, for short periods (below 20 nm) the equilibrium phases are directly achieved upon annealing, while for periods between 30 and 140 nm trialuminide phases such as $TiAl_3$, $NiAl_3$ and Ni_2Al_3 are formed at intermediate temperatures. The nanostructural characterisation of the nanomultilayer films by TEM reveals well-defined layered structures along their entire thickness and without disruptions, whatever the period. In the STEM image of figure 1 it is possible to observe the layered structure of a Ti/Al film with 20 nm period from the bottom up to the surface. The TEM images also reveal columnar growth morphology typical of thin films deposited under conditions of low adatom mobility (figure 2). The Ti- (Ni-) and Al-rich layers are perfectly identified although there is always some Ti (Ni) in the Al layers and *vice-versa*. The matching between the different layers is very good and semi-coherent interfaces could be observed by HRTEM.

References:

[1] Y-W. Kim, JOM, **46** (1994) 30.
[2] D. B. Miracle, Acta Metall. Mater., **41** (1993) 646.
[3] T. P. Weihs, "Self-propagating reactions in multilayer materials" in Handbook of Thin Films Process Technology edited D. A. Glocker and S. I. Shah, Institute of Physics Publishing, Bristol (1998), Part F.
[4] A. S. Ramos and M. T. Vieira, Surf. Coat. Technol., **200** (2005) 326.

Figures:

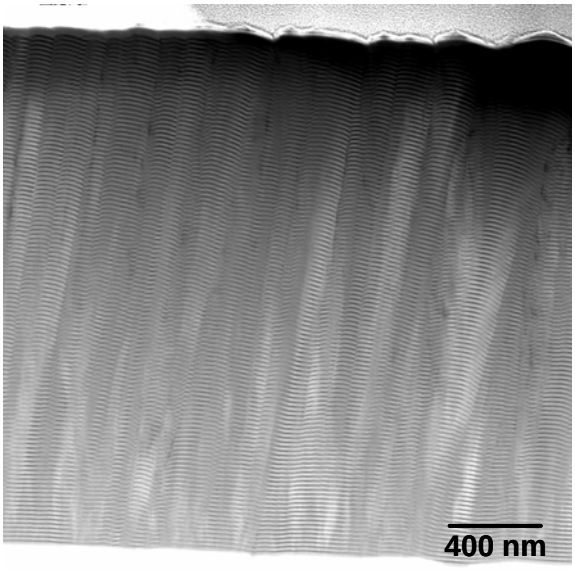

Figure 1 – STEM cross-sectional image of a Ti/Al multilayer thin film with Λ=20 nm.

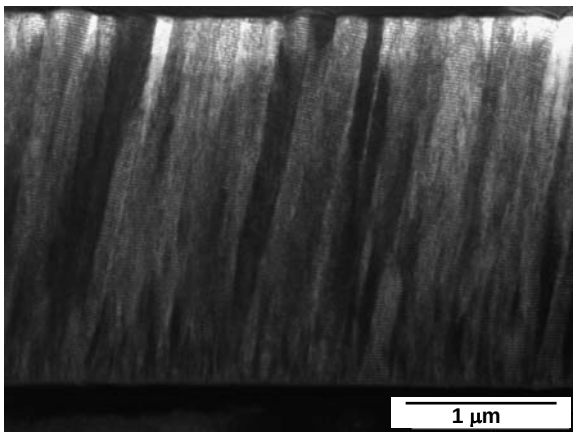

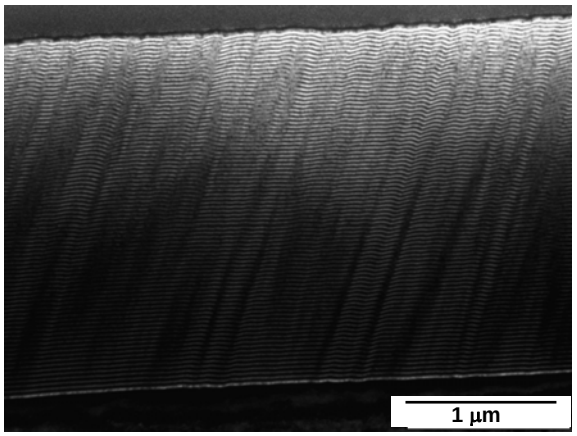

Figure 2 – TEM cross-sectional images of Ti/Al and Ni/Al multilayer thin films

Poster

NON-AQUEOUS SOL-GEL ROUTES APPLIED TO ATOMIC LAYER DEPOSITION

E. Rauwel[1], G. Clavel[1], M.-G. Willinger[1], P. Rauwel[2], F. Ducroquet[3], N. Pinna[1]
1 - Department of Chemistry and CICECO, University of Aveiro, 3810-193 Aveiro
2 - Department of Ceramics and CICECO, University of Aveiro, 3810-193 Aveiro
3 - Minatec-IMEP, 3 Parvis Louis Néel, BP 257, 38016 Grenoble

Usually traditional Atomic Layer Deposition (ALD) processes use aqueous sol-gel routes for oxide thin film growth. Typically, transition metal precursors (halides, alkoxide or amide) are reacted with an oxidizing agent (e.g. water, radical oxygen or ozone). More specifically the reaction of such metal complexes with water leads, upon hydrolysis and condensation, to the formation of a metal oxide thin film. The films grown by this traditional way are amorphous; hence a post-synthetic heat treatment is generally required to induce the desired crystallization in order to improve the quality of the film. They also contain large amounts of undesired impurities ranging from unreacted carbon species to halides. Furthermore, as water is a strong oxidizing agent at the typical ALD range of deposition temperatures (200-400 ºC) some substrates (e.g. Silicon) are rapidly oxidized. In fact, metal oxide thin films grown on silicon always present a non-negligibly thick oxidized interface layer (silica or silicates) in between the silicon and the deposited metal oxide which usually hinders microelectronic applications.

Many solutions are presently proposed to overcome these problems, like using new metal organic precursors [1,2] or by the utilization of plasma during the deposition process.

Recently various non-aqueous sol-gel routes were proposed for the formation of metal oxide nanoparticles [3,4] and hybrid materials [5] in solution. They proved to be powerful alternatives, especially because they have the capacity to overcome the main drawbacks of traditional sol-gel routes. However, only a few non-aqueous routes were applied to ALD. The most successful were the ones reported on the reaction of metal alkoxides with metal halides [6] and the formation of silica and silicates [7, 8].

In this work we present a novel non-aqueous approach applied to ALD [9] leading to the formation of high quality metal oxide thin films. Moreover, this approach demonstrates a real ability to reduce the oxide interlayer in the case of deposition on silicon substrates. This process enables to grow metal oxides coating at temperatures as low as 50 °C on various supports including monocrystalline substrates, carbon nanotubes, organic fibers, etc. The characterization of these films will be presented together with their possible formation mechanism.

References:

[1] A. C. Jones, et al. *Chem. Vap. Dep.* **2006**, 12, 83.
[2] J. Niinistö, et al. *Chem. Mater.* **2007**, 19, 3319.
[3] N. Pinna, M. Niederberger, *Angew. Chem. Int. Ed.* **2008**, DOI: 10.1002/anie.200704541
[4] M. Niederberger, G. Garnweitner, N. Pinna, G. Neri, Prog. Solid State Chem. **2005**, 33, 59.
[5] N. Pinna, J. Mater. Chem. **2007**, 17, 2769.
[6] M. Ritala, K. Kukli, A. Rahtu, P. I. Raisanen, M. Leskela, T. Sajavaara, J. Keinonen, *Science* **2000**, 288, 319.
[7] R. G. Gordon, J. Becker, D. Hausmann, S. Suh, *Chem. Mater.* **2001**, 13, 2463.
[8] D. Hausmann, J. Becker, S. L. Wang, R. G. Gordon, *Science* **2002**, 298, 402.
[9] E. Rauwel, G. Clavel, M.-G. Willinger, P. Rauwel, N. Pinna, *Angew. Chem. Int. Ed.* **2008**, DOI: 10.1002/anie.200705550

INFLUENCE OF THE MOLECULAR ARCHITECTURE ON THE SELF-ASSEMBLY OF PH- AND TEMPERATURE SENSITIVE ELASTIN-LIKE BLOCK-COPOLYMERS.

Javier Reguera, Artur Ribeiro, F. Javier Arias, J. Carlos Rodríguez-Cabello
Grupo Bioforge, Universidad de Valladolid, Centro de I+D, Paseo de Belén 1, 47005, Valladolid, Spain
jreguera@bioforge.uva.es *http://www.bioforge.uva.es*

Elastin-like polymers (ELPs) are a surprising kind of elastic biopolymers [1]. The best known model ELP is the polymer $(VPGVG)_n$ where V stands for L-Valine, G for Glycine, and P for L-Proline. This polymer exhibit some interesting features that make it an excellent candidate for some top nano(bio)tecnological applications. Among their main features are: their mechanical properties showing an almost ideal elasticity, although there are some derivatives can show a more thermoplastic behaviour; their extreme biocompatibility showing excellent results in all the tests made on these polymers; and an acute self-assembly and *smart* nature. This last feature is produced in a mechanism called the Inverse Temperature Transition (ITT), by which, in aqueous medium, there is a reversible phase transition when the temperature goes above a certain temperature (T_t). In this transition, the polymer changes from a soluble state to a segregated state with an acute increase in the solvent-polymer interaction parameter. Together with this phase transition there is dehydration and an increase in the conformational order adopting a regular non-random structure called β-spiral. With that conformational change there is a self-assemble of filaments of three β-spirals that finally gather to form nano- and micro-particles. The T_t depends on the polarity of the polymer chain so with the change of certain functional amino acids (with two states of polarity) in some of the monomers of the model polymer, different ELPs have been synthesized to exhibit a *smart* nature to different stimuli such as pH, electromagnetic waves, redox potential, etc [1].

Another characteristic of this kind of protein-based polymers is that, taking the advantage that they are made from amino acids, it is possible to produce then as recombinant proteins in genetically modified organisms such as bacteria, yeast or plants. This allows the synthesis and bioproduction of monodisperse and more complex polymers with an absolute control in the amino acid sequence and molecular weight, together with an increase in yield with respect to the chemically synthesized polymers. Another advantage of this method of production is that it is independent of petroleum, it uses water as solvent in all the process of production and the resultant polymer is completely biodegradable so they can be considered as environmentally friendly [2].

Two different ELPs have been designed and selected for the purpose of this work. The first one is $[(VPGVG)_2\text{-}(VPGEG)\text{-}(VPGVG)_2]_n$ where E stands for L-Glutamate. This polypeptide exhibits the same properties than the model polymer $(VPGVG)_n$ and in addition a pH-sensitive nature produced for the change in polarity in the protonation-deprotonation of the Glutamate-γ-carboxyl group under changes in the pH [3]. Together with this pH sensitive nature a self-assembly characteristic has been observed when this polymer is deposited on an hydrophobic substrate given rise to the formation of nanopores [4]; The second one is the more apolar polypentapeptide $(VPAVG)_m$ where A stands for L-Alanine. This polymer shows a dissimilar behaviour than the general ELPs. It shows, among other differences, different mechanical properties, or thermo-sensitive behaviour with a higher enthalpy of transition and a clear hysteresis in its heating-cooling cycle [5, 6].

Based in these two different ELPs a set of monodisperse ABA and AB block-copolymers have been synthesized with different precisely controlled block lengths, being A the Glutamate-containing aforementioned block and B the Alanine-containing block.

Depending on the temperature and the pH, different states of block-solvent interactions parameter will give rise to different states of aggregation and structures. Different series of measurements have been made for these di- and tri-block copolymers for different block lengths and different pHs. The results show the formation of different structures, with not-completely independent transitions between the different blocks transitions showing behaviour not only depending on the polarity of the bocks but also on the molecular architecture.

This work was supported by the "Junta de Castilla y León" (VA002/02), by the MCYT (MAT2003-01205 and MAT2004-03484-C02-01) and by the Marie Curie RTN Biopolysurf (MRTN-CN-2004-005516)

References:

[1] J.C. Rodríguez-Cabello, J. Reguera, A. Girotti, M. Alonso, A. M. Testera, Progress in Polymer Science **30** (2005) 1119-1145.
[2] J.C. Rodríguez-Cabello, J. Reguera, A. Girotti, F.J. Arias, M. Alonso. Advances in Polymer Science **200** (2006) 119-167.
[3] A. Girotti, J. Reguera, F.J. Arias, M. Alonso, A. M. Testera, J.C. Rodríguez-Cabello, Macromolecules **37** (2004), 3396-3400.
[4] J. Reguera, A. Fahmi, P. Moriarty, A. Girotti , J.C. Rodríguez-Cabello. J. Am. Chem. Soc., **126** (2004) 13212-13213.
[5] J. Reguera, J.M. Lagaron, M. Alonso, V. Reboto, B. Calvo, J.C. Rodríguez-Cabello, Macromolecules **36** (2003) 8470-8476.
[6] R. Herrero-Vanrell , A.C. Rincón, M. Alonso, V. Reboto, I.T. Molina-Martinez, J.C. Rodríguez-Cabello. J. Control Release 102 (2005), 113–122.

Figures:

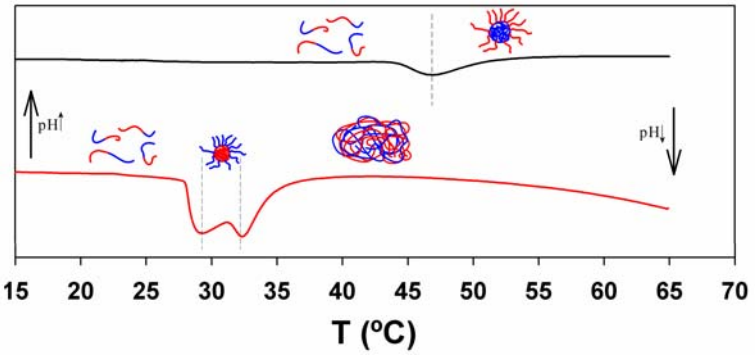

Figure 1: Scheme of the aggregation of the block-copolymers **[(VPGVG)$_2$-(VPGEG)-(VPGVG)$_2$]$_{10}$-[VPAVG]$_{40}$-[(VPGVG)$_2$-(VPGEG)-(VPGVG)$_2$]$_{50}$** on heating.

PRODUCTION AND CHARACTERIZATION OF NANOSTRUCTURED BIOSENSORS

Ana Rei[1], M. Isabel Ferreira[1], Graham Hungerford[1,2]

[1]Centro de Física, Universidade do Minho, 4710-057 Braga, Portugal
[2]Physics Department, King's College London, Strand, London WC2S 2LS, UK
(e-mail anarei@fisica.uminho.pt)

Sol-gel derived materials [1] have attracted great research interest in recent times. Their high porosity and good optical transparency has enabled the incorporation of light addressable entities, such as fluorescent probes. Moreover, the incorporation of biologically important molecules has developed into an active field of investigation [2]. Incorporation of the biomolecules associated with a fluorescent dye allows in situ studies on the conformation and molecular dynamics of the entrapped biomolecules and biomolecule–host interactions. These are important factors to be examined in the production of biosensors.

The present work describes novel techniques of silica matrix modification to provide amenable conditions to protein incorporation. Activity measurements confirmed the capability of the modification techniques in preserving the activity of the proteins tested in the present study. The fluorescent dyes *DASPMI* and *Nile red* were successfully used to study the viscosity and polarity of local environments present within sol-gel derived media [3], thus helping to elucidate conformation and molecular dynamics of the protein and its interaction with the host matrix. The results show that this methodology proved very adept, in that it was possible to discriminate the impact of conformation changes on the activity of proteins from the accessibility of reactants constrained by the host morphology.

1. Hench, L.L. and West, J.K., The sol-gel process. *Chem. Rev.*, 1992, 90, 33-72.
2. Livage, J., Coradin, T. and Roux, C., Encapsulation of biomolecules in silica gels. *J. Phys.:Condens. Matter*, 2001, 13, R673-R691.
3. Viseu, T.M.R., Hungerford, G., Coelho A.F. and Ferreira, M.I.C., Dye-host interactions for local effects recognition in homogeneous and nanostructured media. *J. Phys. Chem. B*. 2003, 107, 13300-13312.

PROTEIN PATTERNING BY THERMAL NANOIMPRINT LITHOGRAPHY ON FUNCTIONALIZED POLYMERS

A. Retolaza[a], S. Merino[*,a], V. Trabadelo[a,d], P. Heredia[b], C. Morales[b], J.A. Alduncín[c], D. Mecerreyes[c], H. Schift[d], C. Padeste[d]

[a]Fundación Tekniker. 20600 Eibar. Guipuzkoa. Spain.

[b] Gaiker. Parque Tecnológico, 48170 Zamudio. Bizkaia. Spain.

[c] CIDETEC, Centre for Electrochemical Tech., 20009 Donostia. Guipuzkoa. Spain.

[d]PSI, Paul Scherrer Institut, 5232 Villigen, Switzerland

[*]Corresponding author: smerino@tekniker.es

The ability to immobilize proteins on sub-micro to nanometric sized areas has become a major challenge for the development of bioengineered surfaces. The ongoing technological advances are partially driven by the aim for broadening the understanding of a variety of surface mediated biological recognition events. Many applications of patterned biomolecules can be enhanced by improving the resolution of the protein features. Smaller feature sizes enable, for example, the fabrication of high density protein arrays for biosensors or proteomic screening, or facilitate studies of cellular interactions with small precisely located clusters of extracellular matrix proteins. A major advantage of nanoimprint lithography (NIL) is that the feature size can be reduced to the nanoscale to create high density arrays, or to control placement of individual proteins, while still retaining high throughput and reproducibility. Most previous work in protein patterning by NIL relied on combining NIL and molecular self assembly by lift-off [1], NIL and lift-off with fluorinated mono and trichlorosilanes [2] or NIL and thin passivating layer of CFx [3]. All these processes use a sacrificial imprinted polymer and a treatment with aminosilanes so as to bind the biotin and get the hydrophilic/hydrophobic chemical contrast on the substrate surface before putting on the streptavidin (SAV). The work presented relies on two types of functionalized polymers: a new biofunctionalized polymethacrylate copolymer with 80% benzyl methacrylate and 20% succinimydil methacrylate, which shows a great affinity to SAV and it allows to bind the protein directly on the imprinted polymer; and polystyrene (PS) with amino groups incorporated via an NH_3/N_2 plasma treatment [4], which can bind directly biotin without the need of any aminosilane.

The imprintings on the functionalized polymethacrylate were carried out using a stamp with five different grating periods ranging from 3.3 to 11.3 μm, 20 mm long and 270 nm in depth. The polymer was imprinted at 160 ºC applying 20 kN force on 4"wafer and demolded at 35 ºC. The stamp used for the PS consisted of a 10 μm period orthogonal array with 5 μm square 700 nm high pillars. The polymer was imprinted at 180 ºC applying 15 kN on 4"wafer and demolded at 80 ºC. From this point on the experimental procedure was different depending on the polymer, as it is shown in figure 1.

In the first approach an antiadhesive coating was applied to the polymer by evaporation of tridecafluoro-(1,1,2,2)-tetrahydrooctyl-trichlorosilane (F_{13}-TCS). Prior to the fluorescence detection, and in order to study the affinity between the functionalized polymer, the antiadhesive layer coating and SAV, blank small samples coated with the polymer and antiadhesive layer were analysed by ELISA technique. Different SAV-HRP concentrations (0-10 μg/ml) were solved in different buffer solutions at different pHs together with 0.01 mg/ml of BSA. The samples were oxidised under tetramethylbenzidina substrate and the colour change was detected at 450 nm. It led to know that if BSA was added to SAV solutions solved in Carbonate-Bicarbonate buffer it avoided unspecific binding and the selectivity between functionalized polymer and F_{13}-TCS was maximum. Once the process conditions were optimized, a fluorescence labelled SAV (Tetramethyl rhodamine, Molecular Probes) was incubated on the samples.

In the second approach, the ammonia plasma treatment for the PS was performed for 1 min at 20 W in a PECVD PlasmaLab 80 Plus. The NH_3 and N_2 flows were 40 sccm and 100 sccm respectively. Then the biotin and subsequent SAV incubations were carried out. In this case no blocking agents (F_{13}-TCS or BSA) were used to avoid the unspecific binding of the SAV. A fluorescence labelled SAV (Alexa-fluor® 488 conjugated, Molecular Probes) was put on the samples. The specimens after immobilization of SAV were assessed using a fluorescence microscope (Zeiss, Axioimager) equipped with a monochrome CCD camera (Zeiss, AxioCam MRm). Figure 2 includes two representative fluorescence images that show the high affinity of SAV to the imprinted functionalized polymers. The work carried out can be easily extended to patterned surfaces under 100 nm and it will allow patterning any biotinylated protein bonded to SAV in an easier way than described previously while keeping the suitability for high throughput protein patterning.

[1] D. Falconnet, D. Pasqui, S. Park, R. Eckert, H. Schift, J. Gobrech, R. Barbucci, M. Textor. Nanoletters **4 (10)** (2004) 1909.
[2] S. Park, S. Saxer, C. Padeste, H.H. Solak, J. Gobrecht, H. Schift. Microelectronic Engineering **78-79** (2005) 682.
[3] J.D. Hoff, L.J. Cheng, E. Meyhofer, L.J. Guo, A.J. Hunt. Nanoletters **4 (5)** (2004) 853.
[4] J. Lub, F.C.B.M. van Vroonhoven, E. Bruninx, A. Benninghoven. Polymer **30** (1989) 40-44.

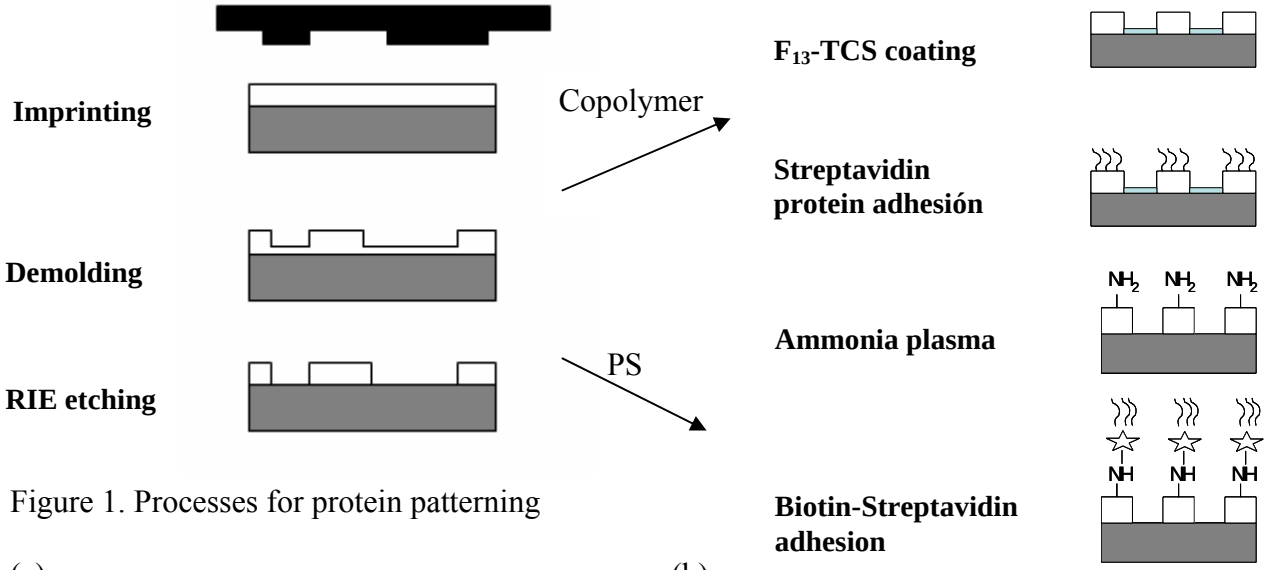

Figure 1. Processes for protein patterning

(a) (b)

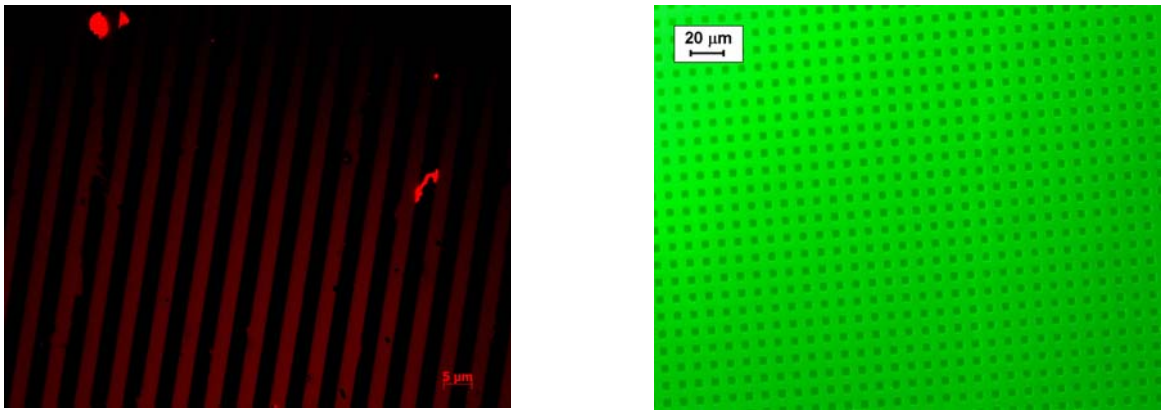

Figure 2. Fluorescence images for (a) first approach (3.3 µm lines) and (b) second approach (10 µm period orthogonal array with 5 µm square holes).

Bacterial cellulose based OLED´s

Legnani, C.[(1)], Vilani, C. [(1)], V.L. Calil[(1, 3)], Barud, H. S.[(2)], Quirino, W. G. [(1)], Achete, C. A.[(1,4)], Messaddeq, Y.[(2)], Ribeiro, S. J. L.[(2)], Cremona, M.[(1,3)]

1. CeDO - Centro de Dispositivos Orgânicos, Dimat – Divisão de Metrologia de Materiais, Inmetro, Duque de Caxias, 25250 – 020 – RJ, Brazil

2. Institute of Chemistry, São Paulo State University- UNESP, CP 355 Araraquara, 14801-970 – SP, Brazil

3. LOEM – Laboratório de Optoeletrônica Molecular, PUC-Rio, Rio de Janeiro, 22453 – 970 – RJ, Brazil

4. COPPE – Programa de Engenharia Metalúrgica e de Materiais, UFRJ, Rio de Janeiro, 22452-970, RJ, Brazil

sidney@iq.unesp.br

Bacterial cellulose (BC) membranes produced by gram-negative, acetic acid bacteria (*Gluconacetobacter xylinus*), were used as flexible substrates for the fabrication of Organic Light Emitting Diodes (OLED). In order to achieve the necessary conductive properties indium tin oxide (ITO) thin films were deposited onto the membrane at room temperature using radio frequency (r.f.) magnetron sputtering with an r.f. power of 30 W, at pressure of 8 mPa in Ar atmosphere without any subsequent thermal treatment. Visible light transmittance of about 40% was observed. Resistivity, mobility and carrier concentration of deposited ITO films were $4{,}90 \times 10^{-4}$ Ohm cm, 8,08 cm^2/V-s and $-1{,}5 \times 10^{21}$ cm^{-3}, respectively, comparable with commercial ITO substrates. In order to demonstrate the feasibility of devices based on BC membranes three OLEDs with different substrates were produced: 1- a reference one with commercial ITO on glass. 2- A second one with a SiO_2 thin film interlayer between the BC membrane and the ITO layer and 3- a third one just with ITO deposited directly on the BC membrane. The

observed OLED luminance ratio was: 1; 0,5; 0,25 respectively, with 1200 cd/m^2 as the value for the reference OLED. Figure 1 shows the Current density (J) and Power vs applied voltage (V) characteristics for BC substrate device. Figure 2 shows AFM images of the native BC membrane and the ITO/SiO_2/BC substrate. These preliminary results show clearly that the functionalized biopolymer, biodegradable, biocompatible bacterial cellulose membranes can be successfully used as substrate in flexible organic optoelectronic devices.

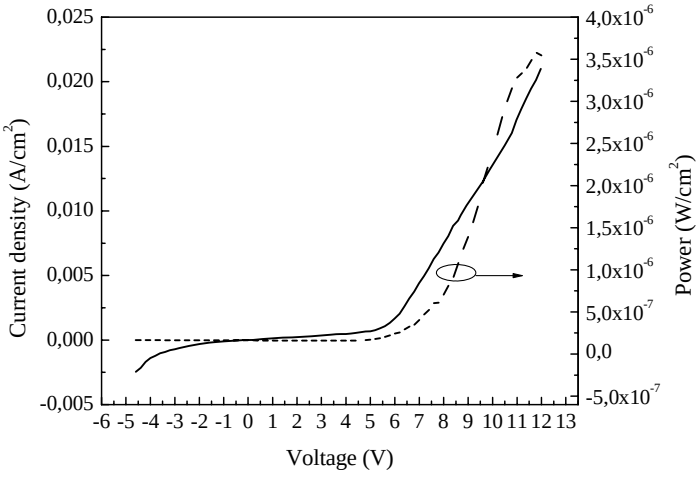

Figure 1- Current density (J) and Power vs applied voltage (V) characteristics for BC substrate device.

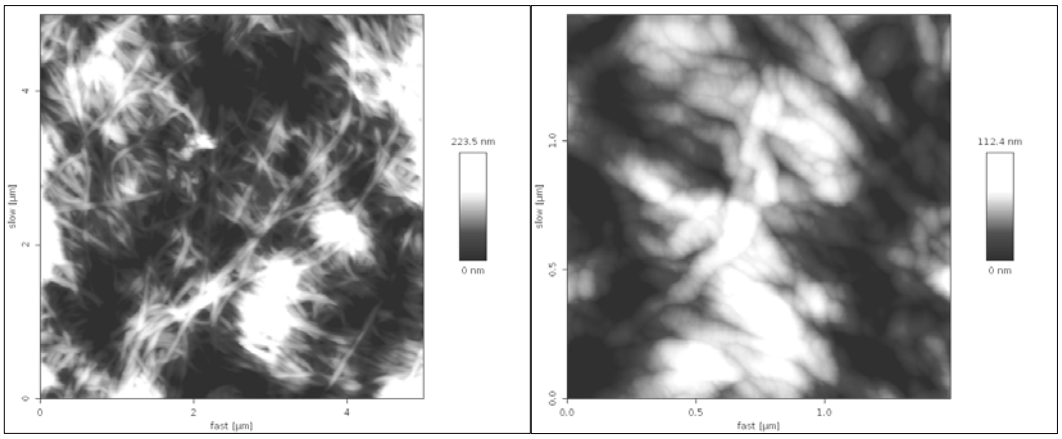

Figure 2- Left- AFM image of native BC membrane showing the microfibrils network Right- AFM image of the ITO/SiO_2/BC membrane showing ITO crystallites.

Nanomechanical resonators integrated on CMOS defined by electron beam lithography

G. Rius, J. Arcamone, J. Llobet, X. Borrisé, F. Pérez-Murano
IMB-CNM-CSIC, Campus UAB, 08193 Bellaterra, Spain
gemma.rius@cnm.es

Nanoelectromechanical devices (NEMS) can be used as high sensitivity mass sensors by detecting the change of resonance frequency when a small quantity of mass is deposited. A specific type of NEMS mass sensor is based on electrostatic actuation of a submicronic cantilever and capacitive detection of its oscillation [1] The mechanical structures are combined with CMOS circuits, so that the circuitry is responsible of readout of the resonator motion by avoiding parasitic capacitances. Direct connection of the mechanical element with the circuit allows optimal signal transduction. In this way, the mass resolution of the device is highly improved.

We present a fabrication process based on electron beam lithography (EBL). It consists of the combination of CNM CMOS circuit technology with the definition of the nanomechanical structure as a post process, as shown in Figure 1. The use of EBL presents the advantages of assumable cost, high resolution and it is adapted to pattern surface with any topography. In this case, the definition of the cantilever after being completed the fabrication of the CMOS circuits give additional flexibility to the design either for the selection of materials and processing at chip level.

Details of the fabrication of integrated cantilevers on CMOS as a post-process module can be found in [2] and are represented in Figure 2. A dedicated area, the integration area, is used for the monolithical integration of the resonator. The layers that constitute the CMOS circuit are used to define the structure. Hence, one of the polySi layers (0.6 µm thick) acts as the structural layer, whereas the field oxide layer (1 µm thick) is used as a sacrificial layer for the release of the structure. After the CMOS circuit fabrication, openings in the pasivation layer are done in the integration areas and the wafers are diced. A PMMA layer is spin coated on the chip for the EBL step. One of the crucial aspects of the fabrication concerns to EBL, where low electron beam energy (3 keV) is used in order to avoid damage of the circuit. A thin layer of Al (32 nm) is deposited after resist development and the resist lift off is done. RIE is used to transfer the Al pattern to the polySi layer and the structures are released by wet etching. In order to protect the circuits during the SiO_2 etching, a negative photoresist mask, patterned by UVL is employed.

Several examples of device fabrication and operation are presented in figure 3. In particular, a system of two cantilevers (lateral motion) has been used for differential measurements of Pt mass deposition in the attogram range [3] (Figure 3, left). Vertical motion plates have been used to monitor the evaporation rate of femtoliter droplets of glycerol [4] (Figure 3, center). In addition, a novel concept of cantilever actuation is presented, using the charging effects induced by electron beam (Figure 3, right).

This work is partially founded by FP7 EU Project Charpan.

References:

[1] J. Verd et al, Journal of Microelectromechanical Systems 14 (3), 508-519 (2005)
[2] S. Ghatnekar-Nilsson et al, Nanotechnology 16 (1), 98-102 (2005)
[3] J. Arcamone et al, IOP Journal of Physics: Conference Series (Accepted)
[4] J. Arcamone et al, Journal Physical Chemistry B111 (45), 13020-13027 (2007)

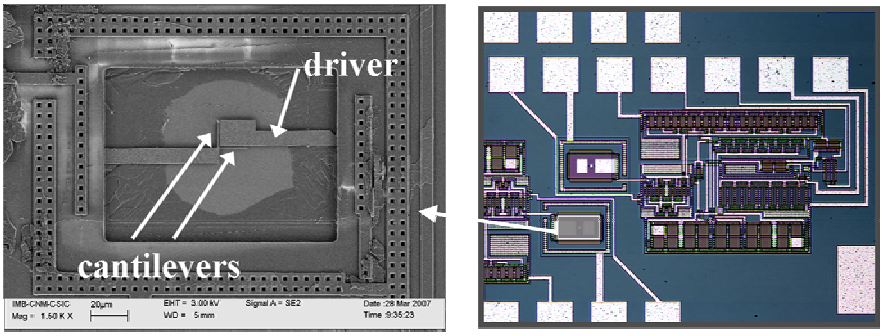

Figure 1 Nanoresonator is monolithically integrated into the CMOS circuitry. Direct connection allows optimization of electrical signal.

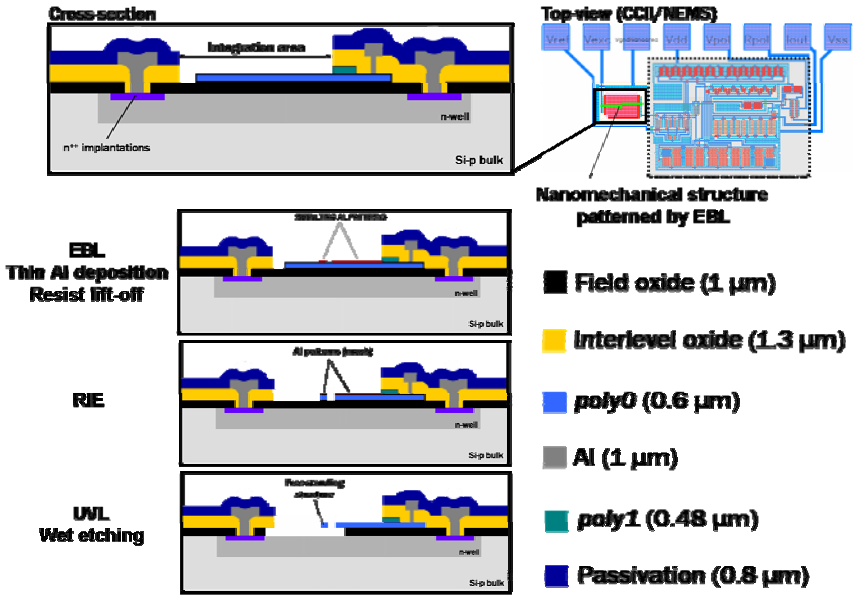

Figure 2 Sequence of fabrication of the resonating structures as a post process after CMOS fabrication. It is based on EBL, thin metal layer and resist lift off, RIE and wet etching.

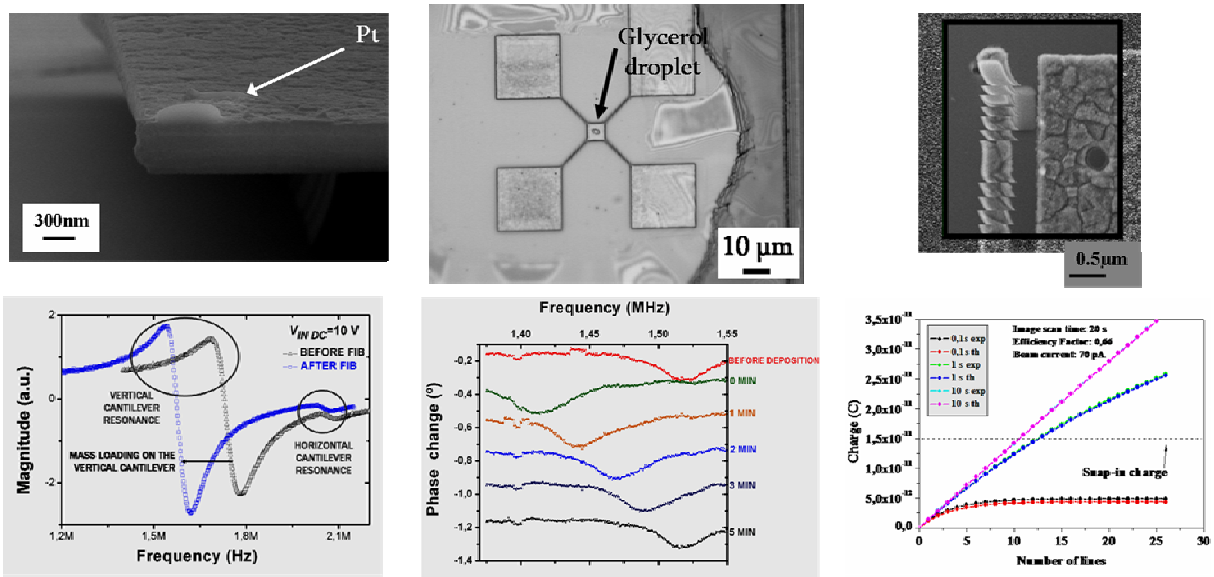

Figure 3 Three examples of applications using nanomechanical structures integrated on CMOS circuits. (Left) Mass sensing in the attogram range [3]. (Center) Monitoring of the evaporation rate of glycerol droplets [4]. (Right) Novel concept of actuation based on electron beam.

Tunable Fabry-Perot Optical Filter with a Resonant Cavity Based on a Piezoelectric Polymer

B. Silva, J.G. Rocha*, A. J. Ferreira**, S.Lanceros-Mendez** and G.Minas**
**Universidade do Minho, Dept. de Electrónica Industrial, 4800-058 Guimarães, Portugal*
***Universidade do Minho, Dept de Física, Campus de Gualtar, 4710-057 Braga, Portugal*

gerardo@dei.uminho.pt

This article describes a tunable Fabry-Perot optical filter with its resonant cavity based on a piezoelectric polymer, for application in the biochemical analysis of biologic fluids. The filter is composed by two thin-films of silver -mirrors- located parallel one to the other and separated by a nanometer size thin polymer film of poly(vinilidene fluoride), PVDF, in its β-phase. When applying an electrical voltage to the mirrors, the thickness of the polymer changes, changing the distance between the mirrors and thus modifying the response of the filter. The lack of parallelism in conventional Fabry-Perot filters is solved with this approach, once the changes in polymer, reflecting variations at a molecular level, are uniform in the whole area. Therefore, this filter provides the selection of a wide range of wavelengths allowing the use of a conventional white light as source, and avoiding the use of monochromatic sources that increase substantially the price of the analysis devices and consequently the cost of the analysis.

The analysis of biological fluids has shown to be a very important factor in the detection and/or treatment of illnesses. For that reason, it is usual a doctor to prescribe, periodically, clinical analysis to the patients for routine diagnosis. Normally the analyses are performed in central laboratories dislocated from the doctor's office, being their results available only some hours or even days later. Due to this situation, the doctor cannot make a reliable diagnosis to the patient in useful time and, moreover, the analysis system becomes expensive and uncomfortable [1, 2]. In order to avoid the drawbacks existing in conventional analysis devices, it has been developed small portable and easy of use devices that provide higher comfort to the patient.

The filter that is presented here constitutes one of the three parts of a clinical analysis microlaboratory, whose working principle is based on the spectrophotometric analysis of biological fluids for measuring the concentration of several biomolecules that are present in those fluids. Each biomolecule presents a maximum value of absorbance when excited by a light at a specific wavelength. The concentration of each biomolecule in the biological fluid is directly related with the value of the absorbance [3, 4].

The referred microlaboratory is composed by three parts. The first one is a microchannel system in which the samples and reagents are placed, and includes microreservoirs where each sample is tested (Fig. 1a). The second part contains optical detectors and their readout electronics, which are usually manufactured in CMOS (Fig. 1b). The third part contains the optical filtering system, which selects the wavelength that corresponds to the biomolecule into analysis (Fig. 1c). The tunable optical filter presented in this article has the main goal of simplifying the third part of the microlaboratory, replacing the array of non-tunable optical filters already implemented by our group (Fig.1c) [5].

The fabrication of the filter is based on thermal evaporation and spin coating techniques. In a first step, a silver mirror was deposited on a glass substrate, whose only function here is to

serve as physical support to the filter. In the next step a nonometer size thin polymer film was spin-coated on top of the silver thin-film already deposited and poled. Finally, the second thin-film of silver was deposited on the polymer film. Fig. 2 shows a picture of the filter.

Acknowledgements:

Work supported by the Portuguese Science Foundation (grant PTDC/BIO/70017/2006).

References:

[1] S. K. Strasinger and M. S. Di Lorenzo, *Urianalysis and Body Fluids*, 4th ed., F. A. Davis Company, Philadelphia, PA. 2001.
[2] C. Pinheiro, J. G. Rocha, L. M. Gonçalves, S. Lanceros-Mendez and G. Minas, *A tunable Fabry-Perot optical filter for application in biochemical analysis of human´s fluids*, in ISIE IEEE, Montréal, Québec, Canada, pp. 2778-2783, July 9-12, 2006.
[3] *Biochemical and Organic Reagents*, Sigma, 2002.
[4] G. Minas, R. F. Wolffenbuttel and J. H. Correia, *A Lab-on-a-Chip for Spectrophotometric Analysis of Biological Fluids*. In Lab-on-a-Chip, The Royal Society of Chemistry, **5**, (2005), pp. 1303-1309.
[5] G. Minas, R. F. Wolffenbuttel and J. H. Correia, *An array of highly selective Fabry-Perot optical-channels for biological fluids analysis by optical absorption using white light source for illumination*. In Journal of Optics A, IOP, **8** (2006), pp. 272-278.

Figures:

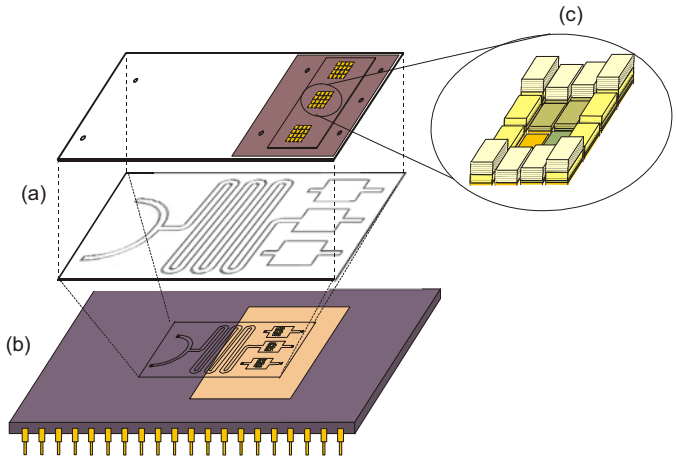

Fig.1: Schematic representation of the lab-on-a-chip structure; a) microchannel system, b) optical detectors and their readout electronics; c) optical filter array.

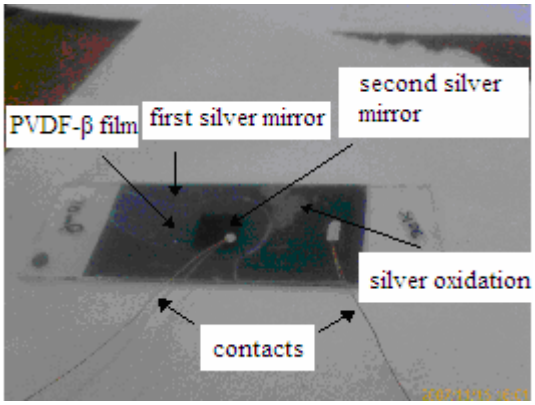

Fig.2: Tunable Fabry-Perot Optical filter prototype.

Peptide Encapsulation in Polyelectrolyte Nanocapsules

Sandra Rocha, Maria do Carmo Pereira, Manuel Coelho
LEPAE, Chemical Engineering Department, Faculty of Engineering, University of Porto, Rua Dr. Roberto Frias, 4200-465 Porto, Portugal
sandra.rocha@fe.up.pt

This work focuses on the design of novel delivery systems for beta-breaker peptides based on nanostructures. The peptide to be delivered is a short sequence homologous to the central region of amyloid beta-peptide, with proline incorporated (iAβ1 peptide). This sequence inhibits the aggregation of amyloid beta-peptide, which is alleged to be a cause of Alzheimer's disease.[1] Polyelectrolyte multilayer capsules are used to increase the peptide plasma residence time and therapeutic index.

The nanocapsules were prepared using the layer by layer self-assembly (LBL) technique.[2] The oppositely charged polyelectrolytes poly(allylamine hydrochloride) (PAH) and sodium poly(styrene sulfonate) (PSS) or poly(L-glutamic acid) and poly(L-lysine) (PLL) were assembled on polystyrene cores. After the assembly of the desired number of layers the template was decomposed with tetrahydrofurane producing a hollow capsule. The nanocapsules were characterized by Laser Scanning Confocal Microscopy (LSCM) and Dynamic Light Scattering (DLS). Nanocapsules constituted by 12 PAH/PSS layers with diameters of 1 μm were used to encapsulate FITC-labeled iAβ1 peptide at acidic pH. LSCM images show that the capsule interior remained fluorescent after washing (Figure 1).

The nanocapsules containing iAβ1 peptide were added to neuroblastoma cell cultures. LSCM images depict nanocapsules internalized by neuroblastoma cells after 3 hours incubation time.

References:

[1] Soto C., et al. Biochem. Biophys. Res. Commun., **226** (1996) 672.
[2] Donath E., et al. Angew. Chem. Int. Ed**. 37** (1998) 2202.

Figures:

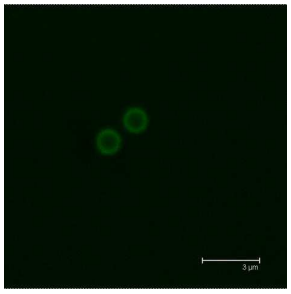

Figure 1. Confocal micrograph showing FITC-labeled peptide (MW 500–700) encapsulated in $(PAH/PSS)_6$ capsules. The scale bar is 3 μm.

ZEOLITE-BASED MICROREACTORS

Y.Rodas, V. Sebastián, O. de la Iglesia, S. Irusta, R. Mallada, J. Santamaría.
Department of Chemical and Enviroment Engineering, University of Zaragoza, Zaragoza (Spaint)
yrodas@unizar.esl

In recent years, microstructured reactors have become one of the most active research areas in catalysis and reaction engineering, as witnessed by several review papers on this subject [1-4]. Microstructured reactors are three-dimensional structures with inner dimensions in the range of 10 to 100 microns [3]. The main feature of microreactors is their high surface area to volume ratio, with values between 1,000 to 50,000 $m^2.m^{-3}$, while those of traditional reactors are about 100 $m^2.m^{-3}$, reaching values of 1,000 $m^2.m^{-3}$ (but only in rare cases).

In Figure 1 can be seen a typical microreactors.

These properties of the microreactors enhance mass and heat transfer and the outcome are higher selectivity, yield, and product quality, besides of higher safety conditions than conventional reactors.

Catalytic activity has been introduced into microreactors by loading noble metals (e.g. Pt, Pd) or mixtures of metals or metal oxides, normally as a washcoat with a suitable support on the microchannels. In this respect, zeolites are specially interesting candidates as catalyst supports, on account of their ability to grow as films on a variety of surfaces. Figure 2 shows seed of zeolites coated the microchannels.

In addition, the ion exchange capacity and the microporous structure of zeolites facilitate a homogeneous distribution of metal active sites. Despite of these properties, there are relatively few publications related to zeolite catalyst in microreactors.

References:

[1] A. Gavriilidis, P. Angeli, E. Cao, K.K. Yeong, Y.S.S. Wan, Chem. Eng. Res. And Des. 80 (2002)3.
[2] G. Kolb, V. Hessel, Chem. Eng. J. 98 (2004)1.
[3] K. Jähnisch, V. Hessel, H. Löwe, M. Baerns, Angew. Chem. Int. Edit. 43 (2004) 406.
[4] L. Kiwi-Minsker, A. Renken, Catal. Today 110 (2005)2.

Figures:

Figure 1.- Microreactors

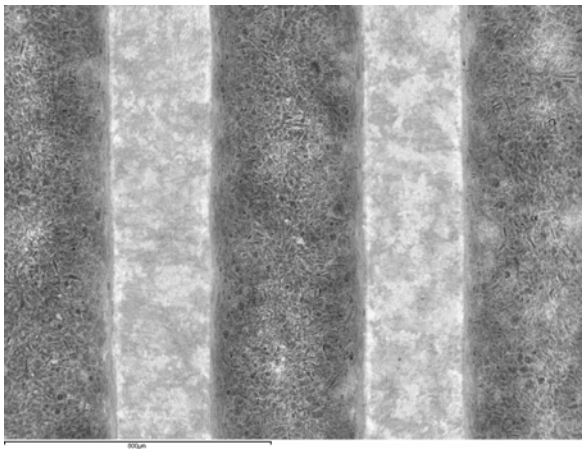

Figure 2,. Microchannels coated with seed of zeolites

QUALITATIVE AND QUANTITATIVE ANALYSIS OF BIORECOGNITION IN PIEZOELECTRIC BIOSENSORS

Rogério M. M. Rodrigues, Luis F.M. Rosa, Guilherme N.M. Ferreira
IBB-Institute for Biotechnology and Bioengineering
Centre for Molecular and Structural Biomedicine
University of Algarve, Campus Gambelas, 8005-139 Faro, Portugal
rogerodrigues@gmail.com

The formation of biomolecular complexes through specific recognition and consequent affinity interaction is an important biochemical process in nature and, among others, includes hybridization of complementary strands of DNA and RNA, antigen–antibody binding, and protein–nucleic acid binding. These processes represent the main source of molecular constructs for the development and design of bioanalytical micro-devices and methodologies. Thus, the detailed study of such devices and methodologies involving such processes, leading ultimately to the quantitative characterization of the involved kinetics, constitutes a major priority in the development of miniaturized devices to detect specific molecules, complex structures or processes.

We use piezoelectric devices to study biorecognition processes in aqueous systems. We demonstrate that these devices operating in liquid environments also sensitively respond to the properties of the solution and films which can easily lead to the misinterpretation of the measured data. We use impedance spectroscopy methods to construct equivalent electric circuits to model the system in order to enable the differentiation of all the contributions to the sensor final signal. We were able to distinguish mass load from acoustic energy viscoelastic losses and detect charge induced parasite/stray capacitive interferences. The quantification of such contributions enables the correction of frequency data measurements and its further use in models to study the biorecognition reaction leading to the determination of more accurate parameters such as kinetic data.

This communications focus the different aspects involved in the development of piezoelectric based biosensors to correctly measure bimolecular binding kinetics as well as to detect biomolecules in biological samples. The quantification of the effect of charged species, density, and viscosity is used to enhance and optimize the sensor signal and performance for binding monitoring and quantification.

We demonstrate the applicability of impedance analysis in quantitatively monitoring the immobilization of alkanethiols onto gold surfaces forming Self Assembling Monolayers, in the detection and quantification of streptavidin binding to biotin and in the development of recombinant antibody-based biosensors to detect HIV-1 virion infectivity factor (Vif). In the last case, the affinities of single chain (4BL) and single domain (VH and VHD) recombinant antibodies generated against HIV-1 Vif were compared. Recombinant antibodies were immobilized onto activated sensors surface and used as biorecognition material. We further demonstrate the potential of these sensors as tools for HIV-1 infection monitoring and follow-up through the successful selective detection of HIV-1 Vif from HEK293 cell culture extracts.

Acknowledgments:
The authors thank to Portuguese Foundation for Science and Technology (FCT) the financial support through the research project POCI/BIO/61912/2004 and the grants SFRH/BD/38136/2007 and SFRH/BD/36294/2007.

MOLECULAR MATERIALS BASED ON ORGANOMETALLIC COMPOUNDS

João Rodrigues, João Figueira, Manuel Jardim, Swarup Maiti*
Centro de Química da Madeira, LQCMM/MMRG, Departamento de Química da Universidade da Madeira, Campus da Penteada, 9000-390 Funchal, PORTUGAL
joaor@uma.pt

In the promising field of molecular electronics[1], polynuclear compounds featuring redox-active organometallic end groups seem especially attractive from various perspectives, in particular for information storage and processing.[2]

The ongoing research at the Molecular Materials Research Group (MMRG), in the field of metallodendrimers and molecular wires, developed in collaboration with other international groups, takes advantage of the use of well known synthetic methodologies for the synthesis of new organic spacers and of the use of transition metal complexes fragments.

Particularly we explore the properties of the nitrile ligand, an isoelectronic group of acetylide, as well as of the acetylide for the preparation of novel metallodendrimers and molecular wires with improved electronic and non linear optical properties.[3]

The prepared metallodendrimers were based on ruthenium and iron complexes having, as organic core, the 1,3,5-tris(4-ethynylbenzonitrile)benzene (an acceptor with an extended π-system and octopolar symmetry), or nitrile-functionalized poly (alkylidene imines) (Fig.1).

Conventional research in the field of molecular wires is focused on the synthesis of π-conjugated oligomers and polymers[4], but these π-systems still suffer from limitations related to the type of elements and molecular motifs that can be incorporated into the wires. In this field, we have under study different organic spacers (*e. g.* 1,4-diethenylbenzene derivatives) as well as metal complexes in view of the preparation of molecular wires with enhanced electronic properties (Fig. 2).

An overview of the most outstanding results will be presented and discussed envisaging the potential application of the novel compounds as nanoelectronic materials.

Acknowledgments:
This work was supported by Fundação para a Ciência e a Tecnologia trough the Research Projects *POCTI/QUI/41814/2001*, *POCTI/CTM/41495/2001 and PTDC/QUI/64202/2006*, by the Ph D grant *SFRH/BD/29325/2006* (JF) and by the NMR and MS Portuguese Networks (*REDE/1517/RMN/2005*, *REDE/1508/REM/2005*). The support from CS Madeira is gratefully acknowledged.

References:

[1] (a) Tour, J. M., *Acc. Chem. Res.*, **33** (2000) 791-803. (b) Caroll, R. L., Gorman, C. B., *Angew. Chem. Int. Ed.*, **41** (2002) 4379-803. (c) Robertson, N., Mc. Gowan, G. A., *Chem. Soc. Rev.*, **32** (2003), 96-103.

[2] (a) Crutchley, R. J., *Adv. Inorg. Chem.*, **41** (1994) 273-325. (b) Schwab, P. F. H., Levin, M. D., Michl, J., *Chem. Rev.*, **99** (1999) 1863-1933. (c) Schwab, P. F. H., Smith, J. R., Michl, J. *Chem. Rev.*, **105** (2005) 1197-1279. (d) Ren, T., *Organometallics*, **24** (2005) 4854-4870.

[3] (a) Dias, A. R., Garcia, M. H., Rodrigues, J. C., Green, M. L. H., Kuebler, S. M., *J. Organomet. Chem.*, **475** (1994) 241-247. (b) Dias, A. R., Garcia, M. H., Rodrigues, J. C., Petersen, J. C., Bjornholm, T., Geisler, J. *J. Mater. Chem. 5* (1995) 1861-1865; (c) Ornelas, C.; Gandum, C.; Mesquita, J.; Rodrigues, J., Garcia, M. H., Lopes, N., Robalo, M. P., Nättinen, K., Rissanen, K. *Inorg. Chim. Acta*, **358** (2005) 2482-2488. (d) Ornelas, C,Vertlib, V., Rodrigues, J., Rissanen, K., *Eur. J. Inorg. Chem.*, **1** (2006) 47-50. (e) Vertlib, V., Figueira, J., Mesquita, J., Rodrigues, J., Nättinen K., Rissanen, K., *Eur. J. Inorg. Chem.*, **13** (2007) 1920 - 1924. (f) Figueira, J., Rodrigues, J., Russo, L., Rissanen, K., *Acta Cryst.*, **C64** (2008) o33-o36. (g) Ornelas, C., Ruiz, J., Rodrigues, J., Astruc, D., *Inorg. Chem.*, 2008, Web Release Date: 21-Mar-2008 (DOI: 10.1021/ic800100k).

[4] For some recent books on the field, see for example: (a) "*Springer Handbook of Nanotechnology*", Edited by Bhushan, B. Springer-Verlag, Berlin, Heidelberg, 2004. (b) "*Molecular Electronics: Commercial Insights, Chemistry, Devices, Architecture and Programming*", Edited by Tour, J. M. World Scientific Publishing, New Jersey, 2003.

Figure 1:

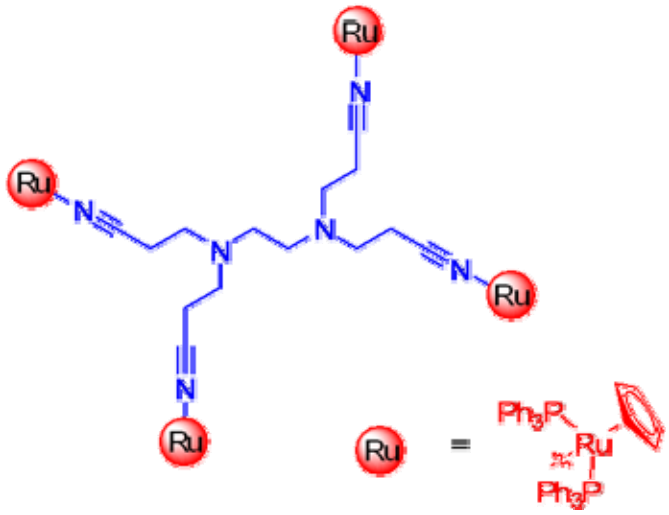

Figure 2:

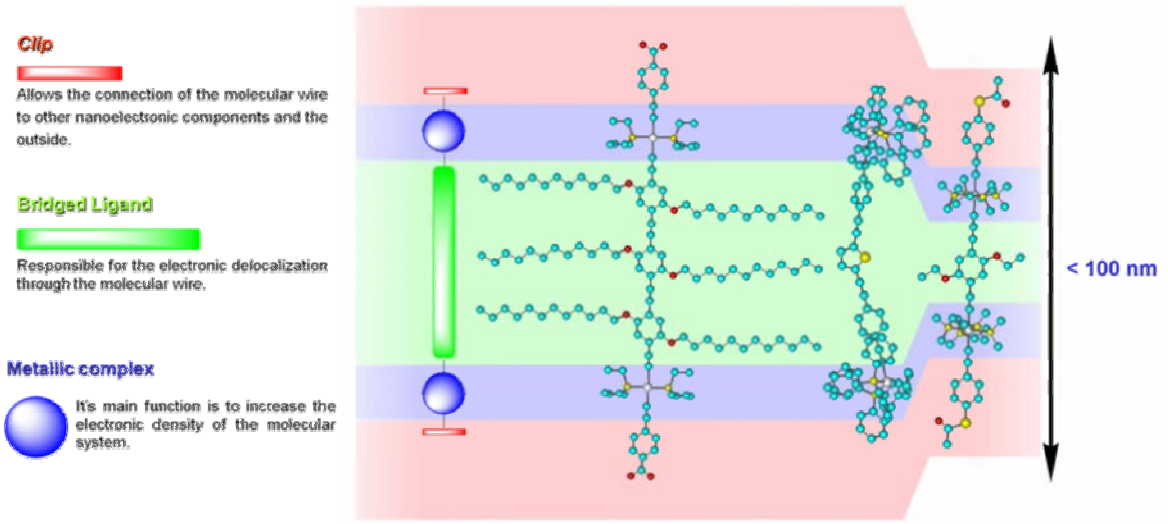

IN-SITU SYNTHESIS OF NANOPARTICLES USING LYOTROPIC LIQUID CRYSTALS AS NANOREACTORS WITH DIFFERENT MORPHOLOGY

Carlos Rodríguez-Abreu[1], *Dharmesh Varade*[2]

[1]*Institut d`Investigacions Químiques i Ambientals de Barcelona (IIQAB/CSIC), Jordi Girona, 18-26, 08034*

[2]*Barcelona, Spain Graduate School of Environment and Information Sciences, Yokohama National University, Tokiwadai 79-7, Hodogaya-ku, Yokohama 240-8501, Japan*

craqci@iiqab.csic.es

Self-assembly of components by non-covalent interactions offers an invaluable tool for the preparation of nanostructures, with the advantage of being an spontaneous process with an inherent low consumption of energy[1]. Although much research has been done on the synthesis of nanoparticles using amphiphilic self-assembling systems, there is still a need of simple, scalable methods for producing three dimensional, ordered arrays of nanoparticles using this route.

Here, we present an study on the synthesis of silver nanoparticles using lyotropic liquid crystals with long range order formed in amphiphilic block copolymers in the presence of block selective solvents. Aqueous solutions of silver salts are solubilized and confined inside the reverse aggregates forming the liquid crystals, having aligned hydrophilic nuclei. The hydrophilic blocks of the copolymer act as reductants so there is no need to add reducing agents to produce metallic silver. Nanoparticle formation was followed by in situ UV-Vis spectroscopy , Small Angle-X-ray Scattering (SAXS), and Transmission Electron Microscopy (TEM), addressing the effect of different parameters such as temperature, salt concentration and liquid crystal morphology (micellar cubic or hexagonal). It was found that relatively uniform silver nanoparticles are formed and grow without disrupting the structure of the liquid crystalline host. Evidence on the presence of sub-nanometer atomic clusters was also found. Due to the high viscosity of the media, it is supposed that the collisions and diffusion of reactants between aggregates is much less than in previously studied systems, such as fluid microemulsions. Possible synthesis mechanisms and applications for material fabrication will also be discussed.

References:

[1] Lazzari, M. ; Rodríguez, C.; Rivas, J.; López-Quintela, A. J. Nanosci. Nanotechno., 6 (2006) 892.

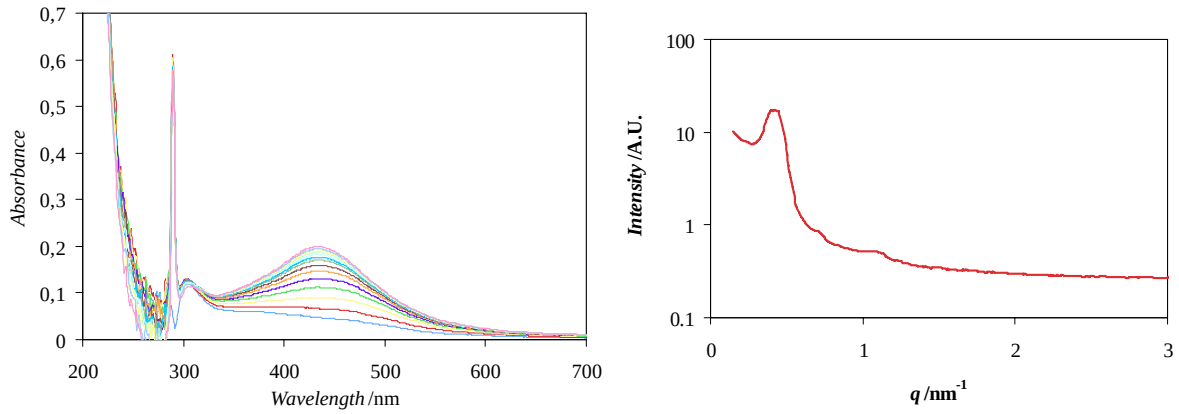

Fig.1 (Left) Time resolved UV spectra during nanoparticle formation inside a reverse micellar cubic liquid crystal (Right) SAXS spectra of the liquid crystal with embedded nanoparticles.

Poster

Modeling and Investigation of the ester cleavage in modern Photoresists materials

Pedro Javier Rodríguez Cantó

1. *Department of physical Chemistry, University of Erlangen, Egerlandstrasse 3, D-91058 Erlangen, Germany*
2. *Nanophotonics Technology Center, Camino de Vera s/n, 46022, Valencia, Spain*

pjrodrig@ntc.upv.es

Chemical amplified resists (CAR´s) are widely used in the semiconductor industry very well since its invention in 1980 in terms of high resolution and sensitivity.
Patterning of CAR´s by means of photolithography requires a heating process of 30 - 120 s with a temperature between 110 and 150 ºC between the exposure and the selective development of the polymer to make the polymer soluble.

This process is as follows (Figure 1): a photosensitive molecule (PAG = photo Acid generator) splits off in a strong acid in the exposed areas of the resist. During the post-bake of the resist film (for temperatures higher than 80 ºC) the proton of this acid can react with the t-butyl group of the polymer (inhibitor) at the ester bridge to form the corresponding acid. Isobutene is released as a byproduct. The proton generated upon exposure remains in the formed carbon acid group of the polymer with the subsequent change of solubility in the developer. Simultaneously, a new proton from a methyl group is produced. The course of this catalytic ester cleavage determines, on the one hand, the activation energy (and activation entropy) of the cleavage and on the other hand the diffusivity of the acid in the resist.

Simulation of these processes is very important for the semiconductor industry to minimize time, expenditure and to provide fast analysis and process optimization. Current models for simulation of CAR's (continuum models) are very fast and are often able to accurately simulate photoresist performance for a variety of process conditions. However, they rely heavily upon extensive calibration to expensive lithography experiments, and thus are limited in their predictive capability. Due to the continuum nature of these simulations, they are also limited in their ability to investigate stochastic phenomena such as feature roughness. For this reason, a kinetic molecular model (Figure 2) is presented in this work in which the inhibitor groups (magenta points) form a close meshed grid. As for, the PAG molecules (blue points) are placed into the grid before forming a wide meshed grid. At the exposed areas this grid changes to a partial grid of acid.

During the bake, the proton does not move independently but coupled to the bulky anion, which leads to a limited proton mobility. This has a big influence on the spatial propagation of the ester cleavage. Through the reorientation of the anion, the catalytic proton can react with the majority of the inhibitor groups placed in its surroundings. In order to cleave other inhibitor groups, the bulky anion has to migrate together with the proton. As a result, „virtual holes“ are created around the original location of the PAG, which locally induces a significant change in the networking and dielectric constant of the polymer and hence in the polymer solubility. From this theoretical approach, it can be concluded, that the inhibitor cleavage in the resist takes place spherically. The correlation of the measured kinetic data with the theoretical approach results from a spherical model.

From this approach the specific model parameter **τ** can be defined as the minimal bake time in which the proton (and its anion) cleaves enough inhibitor groups, so that the resist can be develop in this area. This parameter can easly be determined from special experiments varying the exposure time and the bake step. With this model and suitable experiments, we can discriminate between diffusion and reaction. Important data required for simulation can also be determined.

References:

[1] R. Leuschner, G. Pawlowski, *Handbook of semiconductor technology*, Wiley-VCH, (1998).
[2] D. Matiut, A. Erdmann, B. Tollkühn, A. Semmler, Proc. SPIE, **5039**, (2003), 1132-1141.
[3] X. Shi, J. Vac. Sci. Technol., **B 17(2)**, (1999), 350-354.
[4] S. Robertson, *Resist Models: A practical Guide to timely parameter determination and a review of model deficiencies*, 1st IISB Simulation Workshop, Hersbruck (2003).

Figures 1:

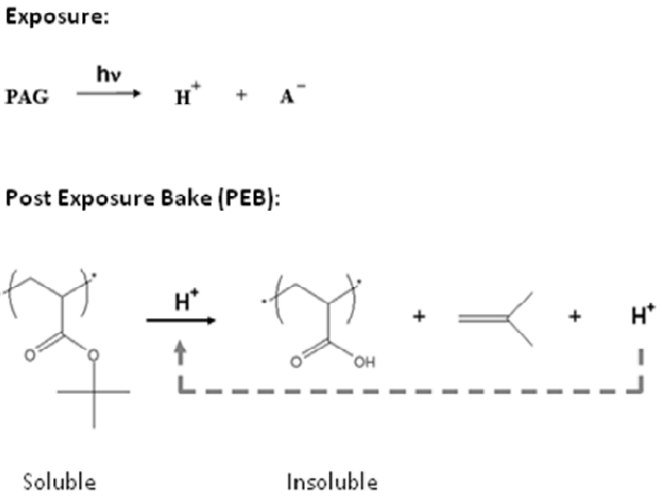

Figure 2:

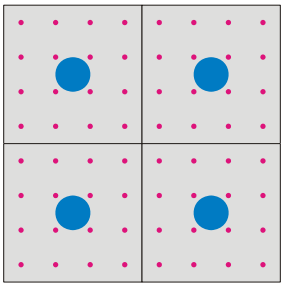

Figure 3:

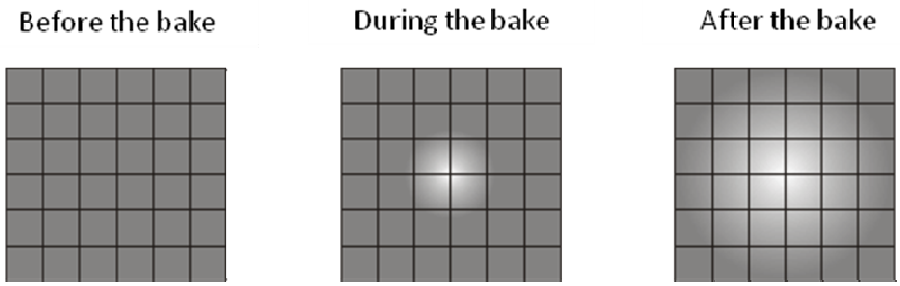

Poster

SYNTHESIS, CHARACTERIZATION AND STABILITY OF CARBOXYLATE-MODIFIED SILVER CLUSTERS POWDERS DISPERSIBLE IN WATER

María J. Rodríguez – Vázquez[1], *Cristina Hoppe*[2] *and M. Arturo López – Quintela*[1]

[1]Laboratory of Magnetism and Nanotechnology, Technological Research Institute. University of Santiago de Compostela, E-15782 Santiago de Compostela, Spain

[2]Institute of Materials Science and Technology (INTEMA), University of Mar del Plata and National Research Council (CONICET), J. B. Justo 4302, 7600 Mar del Plata, Argentina.

mary268@usc.es, qfarturo@usc.es

Water-dispersible carboxylate-modified silver clusters have been synthesized in a single-phase system by reduction of silver nitrate with sodium borohydride in tetrahydrofuran, using several thio-carboxylic acids (mercaptoundecanoic acid, mercaptosuccinic acid, L-glutathione reduced and N-(2-mercaptopropionyl)-glycin) as stabilizing ligands. This method is based on the formation of polymeric precursors, Ag(I)- thiolates, which generate carboxylate-stabilized metal clusters by chemical reduction. Fast precipitation of the reaction products prevented growth and coalescence enabling the synthesis of small silver clusters. The samples were characterized by several techniques, like UV-vis and fluorescence spectroscopies, TEM, X-ray diffraction, light scattering and others. This procedure opens new ways for biological applications of the silver clusters.

Acknowledgments

This work was funded by the Spanish Science and Technology Ministry (National Project MAT2005-07554-C02-01, Strategic Action for Nanoscience and Nanotechnology NAN2004-09133-C03-02, and CONSOLIDER-INGENIO 2010 – NanoBioMed-), as well as the the European Union (Contract No. 037465-FLUOROMAG, EU-FP6 Framework Programme LIFESCIHEALTH-6).

Poster-Flash

INFLUENCE OF THE ALIPHATIC WRAPPING IN THE CRYSTAL STRUCTURE OF BENZENE TRICARBOXAMIDE SUPRAMOLECULAR POLYMERS

Catalina Ruiz-Pérez,[a] Claudio A. Jiménez,[b] Jorge Pasán,[a] Julio B. Belmar,[b] Leandro Ortíz,[b] Oscar Fabelo,[a] Laura Cañadillas-Delgado,[a] Fernando S. Delgado,[a,c] Eliezer Sepúlveda,[a] Mariadel Déniz,[a] Maria Milagros Laz,[d] María Hernández-Molina[d]

[a]Laboratorio de Rayos X y Materiales Moleculares, Departamento de Física Fundamental II, Universidad de La Laguna, 38204 La Laguna, Tenerife, Spain
[b] Departamento de Química Orgánica. Facultad de Ciencias Químicas. Universidad de Concepción. Casilla 160-C, Concepción. Chile.
[c]BM16 – LLS European Synchrotron Radiation Facility, 6 Rue Jules Horowitz - BP 220 38043 Grenoble CEDEX 9, France;
[c]Laboratorio de Rayos X y Materiales Moleculares, Departamento de Edafología y Geología, Facultad de Biología, Universidad de La Laguna, 38204 La Laguna, Tenerife, Spain
caruiz@ull.es

One of the aims of crystal engineering is to establish control over the preparation of crystalline solid materials so that their architecture and properties are, at least to some extent, predictable.[1] From an esthetical and practical point of view, C3-symmetrical molecules are highly attractive building blocks for the formation of supramolecular architectures.[1] Subsequently, a series of the benzene-1,3,5-tricarboxamide derivatives have been studied. Their self-assemble into helical columnar aggregates and the quantitative analysis of the 'majority rules' principle in aggregates of extended discotics were reported.

In particular, trialkyl-substituted benzenetricarboxamides have attracted special attention since they show discotic liquid crystalline phases, being the intermolecular hydrogen bonding assumed to stabilize the columnar order.[1a,1c,2-4] Matsunaga *et al.* had studied these compounds for their thermotropic liquid-crystalline behaviour,[1a,5] while Hanabusa *et al.* had observed that they formed organogels in selected solvents.[1c,6] The efficiency of gel formation was attributed to a combination of intermolecular hydrogen-bonding between N–H and C=O of amides and van der Waals interactions between the alkyl side chain. They conclude that longer and hence, bulky alkyl groups substituted in the benzenetricarboxamide will prevent the molecular packing showed in trimethyl-1,3,5-benzenetricarboxamide (**1**) stabilizing metastable gel-like states.[1c] To demonstrate this assesment we are able to synthesize and crystallize the *tris*(ethyl) (**2**) and *tris*(propyl)benzene-1,3,5-tricarboxamides (**3**).

The crystal structure of *N,N',N''-tris*(2-methoxyethyl)benzene-1,3,5-tricarboxamide (**4**) reported by Lightfoot *et al.*[1e] has been proposed as a model for the aggregation pattern of columnar mesophases. In them the molecules exhibit a columnar arrangement, being the π-stacking of the aromatic cores and the three intermolecular C=O···H–N hydrogen bonds responsible for the linkage of the units along a 2_1 screw axis. The X-ray structure clearly showed the presence of a triple-helical network of hydrogen bonds that resembled the α helix in proteins. The amide moieties were tilted by about 40º with respect to the central benzene core. The inter-ring separation is similar to those inferred for discotic liquid crystalline phases based on aromatic cores.[1e] Thus, he columnar structure can be envisaged as a model for the aggregation pattern for columnar mesophases. However, the crystal structure of the *N,N',N''-tris*(propyl)benzene-1,3,5-tricarboxamide (**3**) shows that other conformations, where the alternation of chirality is not precluded, are possible (see Scheme 1).

Since the benzene-1,3,5-tricarboxamides with substituents longer than butyl are mesogenes,[1a] the drastic change of the hydrogen bonding pattern from **2** to **3** could be the reference mark for the occurrence of these processes. The crystal structures of the ethyl (**2**) and propyl (**3**) *N,N',N''-tris*(alkyl)-benzene-1,3,5-tricarboxamides together with those of already reported methyl- (**1**) and methoxyethyl- (**4**) substituted triamides can offer better clues to the nature of the mesophases[1a] and lyotropism[1c] observed.

This work was supported by University of Concepción (PDI). Funding for this work is also provided by the Ministerio Español de Educación y Ciencia through projects MAT2004-03112, MAT2007-60660 and "Factoría de Cristalización" (Consolider-Ingenio2010, CSD2006-00015). Pre-doctoral fellowships (O. F., L. C.-D., E. S. and M. D.) and a post-doctoral contract (J. P.) is acknowledged.

References:

[1] C_3-symmetrical tricarboxamides: (a) Matsunaga, Y.; Miyajima, N.; Nakayasu, Y.; Sakai, S.; Yonenaga, M. *Bull. Chem. Soc. Jpn.*, **61** (1988) 207. (b) Fan, E.; Yang, J.; Geib, S. J.; Stoner, T. C.; Hopkins, M. D.; Hamilton, A. D. *Chem. Commun.,* (1995) 1251. (c) Hanabusa, K.; Koto, C.; Kimura, M.; Shirai, H.; Kakehi, A. *Chem. Lett.*, **26** (1997) 429. (d) Yasuda, Y.; Iishi, H., Inada, H., Shirota, Y. *Chem. Lett.* **25** (1996) 575. (e) Lightfoot, M. P.; Mair, F. S.; Pritchard, R. G.; Warren, J. E. *Chem. Commun.*, (1999) 1945. (e) Bushey, M. L.; Nguyen, T. Q.; Zhang, W.; Horoszewski, D.; Nuckolls, C. *Angew. Chem. Int. Ed.,* **41** (2002) 2828.

[2] Harada, Y.; Matsunaga, Y. *Bull. Chem. Soc. Jpn.*, **61** (1988) 2139.

[3] Malthéte, J.; Levelut, A. M.; Liébert, L. *Adv. Mater.,* **4** (1992) 37.

[4] Beginn, U. *Prog. Polym. Sci.*, **28** (2003) 1049.

[5] Matsunaga, Y.; Nakayasu, N.; Sakai, S.; Yonenaga, M. *Mol. Cryst. Liq. Cryst.* **141** (1986) 327.

[6] Hanabusa, K.; Kawakami, A.; Kimura, M.; Shirai, H. C*hem. Lett.* (1997) 191.

Figures:

Scheme 1

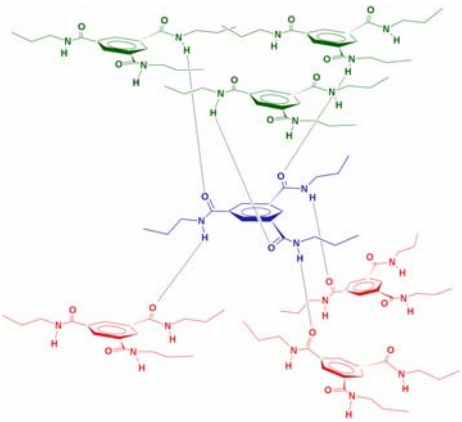

3

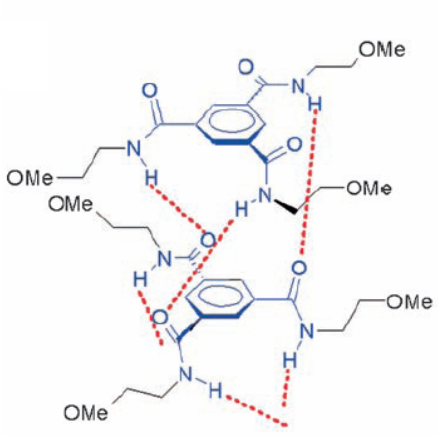

4

SYNTHESIS OF SINGLE-CHAIN POLYMERIC NANOPARTICLES BY A COMBINATION OF RAFT POLYMERIZATION AND "CLICK" CHEMISTRY TECHNIQUES

Alaitz Ruiz de Luzuriaga, Iraida Loinaz, Nerea Ormategui, Ibon Odriozola , Ignacio Garcia, Hans J. Grande, Jose A. Pomposo
New Materials Department, CIDETEC, Parque Tecnológico de San Sebastián, Paseo Miramón 196, E-20009 Donostia-San Sebastián, Spain
E-mail: aruiz@cidetec.es

The synthesis and characterization of polymeric nanoparticles has attracted significant attention in recent years due to new and promising properties of nano-objects compared to bulk materials [1]. A good example is the viscosity drop observed in polystyrene melts upon nanoparticle addition, against classical Einstein´s predictions [2]. In spite of this general interest, synthetic routes to single-chain cross-linked polymeric NPs in the 5 - 20 nm size range are certainly scarce and have severe limitations.

The aim of this work was to design, synthesize and characterize new functional polymeric nanoparticles with improved properties. Hence, RAFT polymerization has been employed for the synthesis of well-defined functional terpolymers and "click" chemistry has been used to promote efficient single-chain intramolecular cycloaddition leading to individual single-chain nanoparticles in high yield [3].

In a first step, a terpolymer of methyl methacrylate, 3-azidopropyl methacrylate and 3-(trimethylsilyl)propyn-1-yl methacrylate has been prepared under reversible addition fragmentation chain transfer (RAFT) conditions.

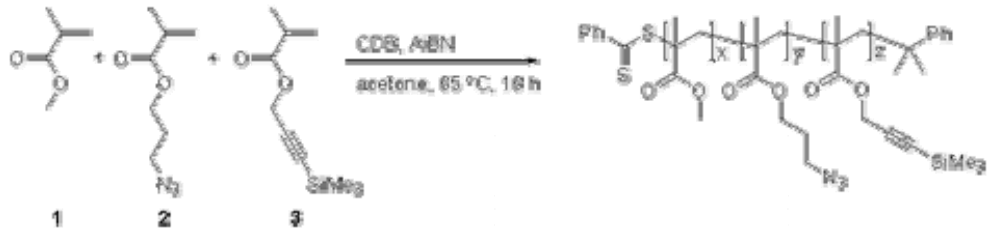

Figure1. Synthesis of poly(methyl methacrylate$_x$–co-3-azidopropyl methacrylate$_y$-co-3-(trimethylsilyl)propyn-1-yl methacrylate$_z$) terpolymers by RAFT polymerization.

In a second step, one-pot deprotection of the propargyl monomer units in the terpolymer has been performed followed by single-chain intramolecular Cu^I-catalyzed azide alkyne 1,3-dipolar ("click") cycloaddition at room temperature using a continuous addition technique.

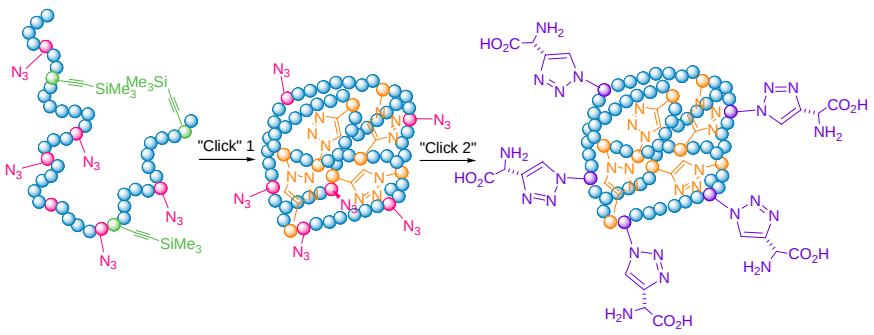

Figure 2. Preparation single-chain cross-linked PMMA NPs and bioconjugated nanoparticles thereof.

As illustrated in Fig. 2, this general method can be easily extended leading to obtain functionalized nanoparticles such as aminoacid-PMMA bioconjugated nanoparticles.

AFM and TEM images of the resulting single-chain polymeric nanoparticles are shown in Figure 3. The average nanoparticle size was determined to be 5 ± 1.5 nm by AFM and 6.5 ± 1.4 nm by TEM.

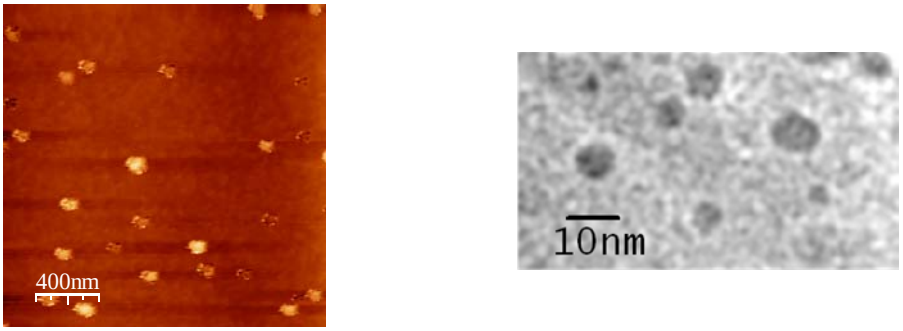

Figure 3. AFM (left) and TEM (right) images of single-chain polymeric nanoparticles synthesized by a combination of RAFT polymerization and "click" chemistry techniques.

References:

[1] A. C. Balazs, T. Emrick and T. P. Russell, "Nanoparticle polymer composites: where two small worlds meet", Science, vol. 314, pp. 1107-1110, 2006.
[2] M. E. Mackay, T. T. Dao, A. Tuteja, D. L. Jo, B. v. Horn, H-C. Kim and C. J. Hawker, "Nanoscale effects leading to non-Einstein-like decrease in viscosity", Nature Materials, vol. 2, 762-766, 2003.
[3] Alaitz Ruiz de Luzuriaga, Nerea Ormategui, Hans J. Grande, Ibon Odriozola, José A. Pomposo and Iraida Loinaz, "Intramolecular click cycloaddition: an efficient route towards bioconjugable polymeric nanoparticles at room temperature", Macromol. Rapid Commun. In press.

ADHESION HYSTERESIS IN DYNAMIC ATOMIC FORCE MICROSCOPY

Enrique Sahagún[2], Mariana Köber[1], Martina Fuss[1], Fernando Briones[1], Mónica Luna[, 1] and Juan José Sáenz[2]*

[1] *Instituto de Microelectrónica de Madrid (IMM-CSIC) Isaac Newton 8, E-28760 Tres Cantos, Madrid, Spain*

[2] *Departamento de Física de la Materia Condensada, Universidad Autónoma de Madrid, E-28049 Madrid, Spain*

enrique.sahagun@uam.es

The effects of adhesion hysteresis in the dynamic-dissipation curves measured in amplitude-modulation atomic force microscopy are discussed. Hysteresis in the interaction forces is shown to modify the dynamics of the cantilever leading to different power dissipation curves in the repulsive and attractive regimes. It is very common to find that dissipated power and dissipated energy are treated as equivalent terms in literature. Experimental results together with numerical simulations show that power dissipation, as measured in force microscopy, is not always proportional to the energy dissipated in the tip-sample interaction process [1].

Most real processes that occur when two materials are brought together involve energy dissipation or hysteretic phenomena. Understanding of the microscopic mechanisms of energy dissipation is then fundamentally relevant for a large variety of basic and applied problems (adhesion, contact formation, friction, wear …) and has motivated extensive theoretical and experimental efforts over a century [2]. The development of the atomic force microscope (AFM) opened a new way to study energy losses at nanometre scales. Phase shift variations, measured by recording the phase lag of the cantilever oscillation relative to the driving signal, are directly linked to energy dissipation processes [3-5]. At fixed feedback amplitude, phase contrast images are proportional to power dissipation maps which can potentially be translated into maps of substrate physicochemical properties [6].

Amplitude-modulation AFM (AM-AFM), often known as tapping mode AFM, has been shown to be a powerful tool for **qualitative** compositional/dissipation mapping. AM-AFM dissipation spectroscopy, based on the analysis of the dissipated power as a function of the cantilever oscillation amplitude, has been proposed as a way to identify specific energy-dissipation processes behind the compositional contrast [6]. However, despite of these important advances, the actual link between power dissipation and nanoscale surface properties is not well understood.

As a general approach, power dissipation in AM-AFM is naturally considered synonymous of energy dissipated per cycle. This energy can then be directly related to specific tip-surface interaction processes, number of chemical bonds, etc. In striking contrast with this apparently natural argument we show that **the dissipated power is not always proportional to the energy dissipated in the tip-sample interaction process**.

In this Letter we present AM-AFM dynamic-dissipation experiments performed on mica samples (at 0 % relative humidity) together with numerical calculations based on a point mass model. An excellent agreement between experiments and calculations is obtained assuming a simple mechanical hysteresis model where the energy dissipated in every contact process is a fixed quantity. Due to the bistable motion of the cantilever [7,8], the dissipated power strongly depends on the AFM operating regime [9]. While in the repulsive (high amplitude) regime power dissipation is constant (as expected from a fixed energy loss per cycle), in the attractive (low amplitude) regime both experimental and calculated power dissipation strongly depend on the cantilever oscillation amplitude.

* Corresponding author: e-mail enrique.sahagun@uam.es, Phone: +34 91 497 4757, Fax: +34 91 497 39 61

References:

[1] M. Köber, E. Sahagun, M. Fuss, F. Briones, M. Luna and J.J. Sáenz (to be published).
[2] Fundamentals of Friction: Macroscopic and Microscopic Processes, Edited by I.L. Singer and H.M. Pollock, NATO ASI Series E: Applied Sciences, Vol. 220 (Kluwer, Dordrecht, 1992).
[3] J.P. Cleveland, B. Anczykowski, A.E. Schmid, and V.B. Elings, Appl. Phys. Lett. 72, 2613 (1998).
[4] J. Tamayo and R. García, Appl. Phys. Lett. 73, 2926 (1998).
[5] P. D. Ashby and C. M. Lieber, J. Am. Chem. Soc. 127, 6814 (2005).
[6] R. Garcia, R. Magerle and R. Pérez, Nature Materials 6, 405 (2007).
[7] P. Gleyzes, P. K. Kuo, and A. C. Boccara, Appl. Phys. Lett. 58, 2989 (1991)
[8] B. Anczykowski, D. Krüger, and H. Fuchs, Phys. Rev. B 53, 15 485 (1996).
[9] E. Sahagún, P. García-Mochales, G.M. Sacha, and J.J. Sáenz, Phys. Rev. Lett. 98, 176106 (2007).

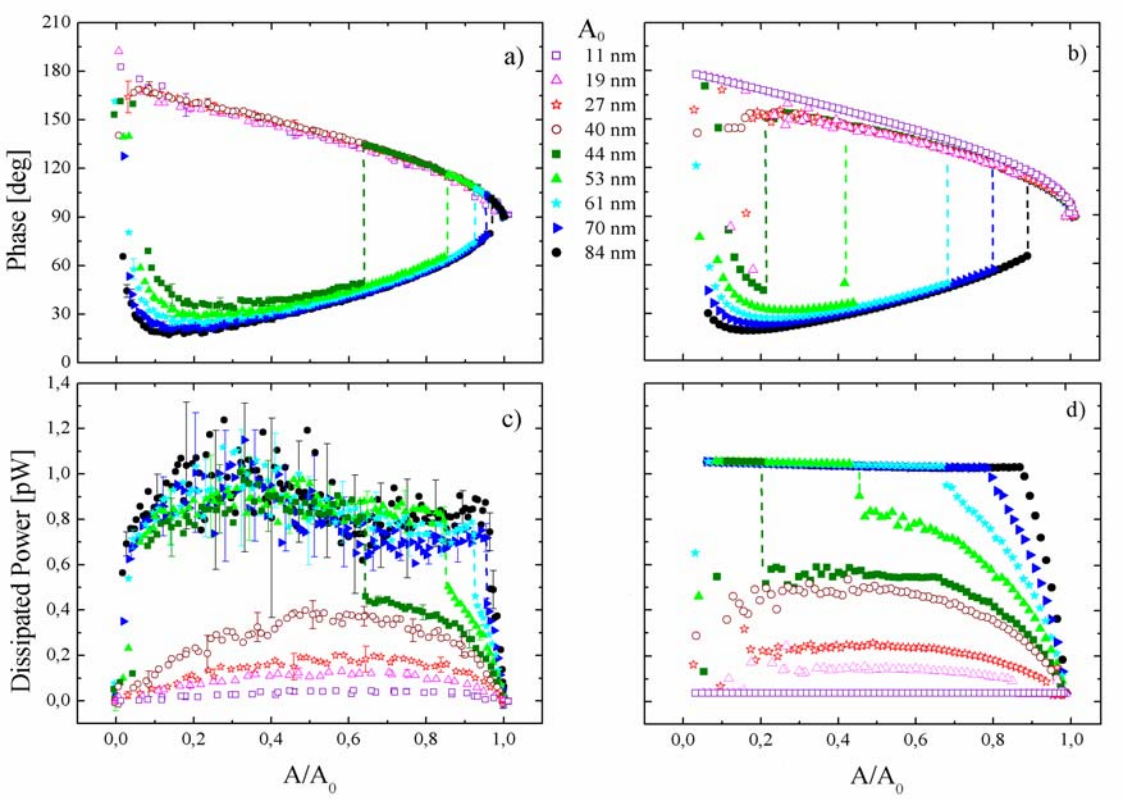

Figure 1a-d: Experimental (1a) and calculated (1b) phase shift and experimental (1c) and theoretical (1d) dissipated power versus the oscillation amplitude obtained as the tip-sample distance is reduced. Symbols correspond to different free oscillation amplitudes A_0. Experimental data were smoothed (average over 10 data points), the standard deviation is shown.

CUSTOMISED NANOCOMPOSITES BASED ON RUBBER MATRICES FOR HIGH DEMAND APPLICATIONS.

CLAUDIO FERNANDEZ, LUIS MARTINEZ DE MORENTIN, MIGUEL SAINZ
FUNDACIÓN L'UREDERRA
Area Industrial Perguita c/A nº 1 Los Arcos 31210 NAVARRA (SPAIN)
claudio.fernadez@lurederra.es

L'Urederra for Technical and Social Development is a non-profit, private Technological Centre created in June 1999 with the objective to perform and promote activities of Research & Technological Development on behalf of the industries and other economical agents within its sphere of influence, followed by implementation of the innovations developed at their production sites. L'Urederra counts with a staff of 30 highly skilled scientists as well as state-of-art facilities to carry out high profile labours in the fields of nanotechnology and advanced materials.

CUSTOMISED NANOCOMPOSITES BASED ON RUBBER MATRICES FOR HIGH DEMAND APPLICATIONS.

Fundación L'Urederra, DPTO. De Investigación y Desarrollo Tecnológico, Area Industrial Perguita c/A nº 1, Los Arcos (Navarra), SPAIN

Università Degli Studi di Milano, Dipartimento di Chimica Organica e Industriale, Via Golgi 19, I -20133 Milano, ITALY
Institute for Engineering of Polymer Materials and Dyes Division of Elastomers and Rubber Technology, Piastow, POLAND
Smithers Rapra Technology Limited, Shawbury Shrewsbury, Shropshire SY4 4NR, UNITED KINGDOM.
Laviosa Chimica Mineraria Spa. Via Leonardo Da Vinci, Livorno, ITALY.
Plasma & Ceramic Technologies Ltd, LTD 34 Miera Str LV-2169 SALASPILS-1, LATVIA

I. INTRODUCTION.

The NANORUB project aims to improve the knowledge and understanding of nanofillers and their application to rubber products facilitating the development of high performance formulations. The project's aim is to demonstrate the opportunity of providing step changes in the performance of elastomeric materials through the incorporation of mineral nanofillers. Target property improvements include notable increase in modulus and tensile strength, gas/liquid transmission rates reduced, and tear strength improved by 20 %. One of the other main goals of this project is to avoid the effect on the vulcanisation processes of commercial nanofillers.

II. EXPERIMENTAL.

1 Organic modification of Montmorillonite

Appropriate amount of montmorillonite is dispersed under vigorous stirring → Exfoliant addition →  → Coupling addition → Reaction mixture was continuously stirred at the appropriate temperature → Drying and filtering process → Final powder. Organically modified montmorillonite completely exfoliated and impregnated with coupling agent. 

2 Production of specific composites

 Organic montmorillonite → Latex addition/ Mixing process →  Nanorubber masterbatches → Formulation/ Addition of additives → Nanorubber material

3 Production/testing of nanorubber prototypes

Nanorubber material → Testing: Mechanical properties, → Manufacture of prototype parts previously selected by end-user → Moulded parts; Conveyor belts; Rubber bearings

III. ORGANIC MODIFIERS (Exfoliants).

•Polvmeric ammonium salts

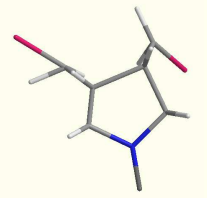

• Low MW polymerizable ammonium salts

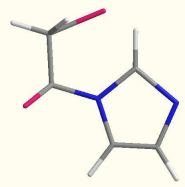

IV. COUPLING AGENTS.

•Purpose-designed silanes

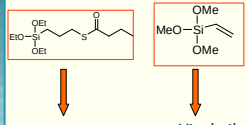

Mercapto functional silane — Vinyl silane

•Functionalised rubber

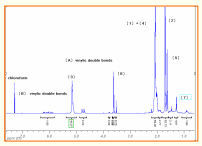

H-NMRspectrum

•Reactive Oligomer

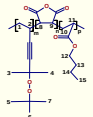

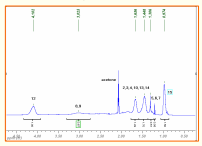

H-NMR spectrum

V. RESULTS.

IR spectra of modified nanoclays

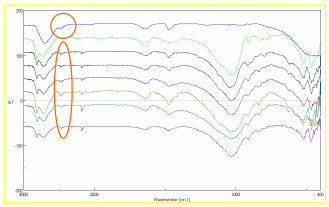

Pristine nanoclay (patron)

Diagnostic peaks marked on the spectra (aliphatic groups) confirm the presence of the modifier in the samples.

XRD Analysis

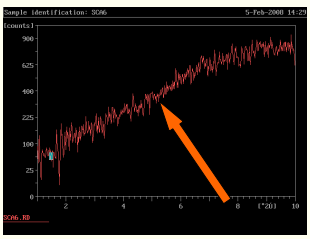

XRD spectrum of modified nanoclay with 15% of polymeric ammonium salt.

NO PEAK!!

COMPLETELY EXFOLIATED STRUCTURE

Mechanical properties of nanorubber material

PROPERTIES	REFERENCE VALUE	TARGET IMPROVEMENT VALUE	REFERENCE FORMULATION MONTMORILLONITE
Hardness *(Shore A)* s. ASTM D 2240	60	60	61-61,5
Tensile strength *(MPa)* s. ASTM D 412	20,6	22-23	21,9
Elongation at break *(%)* s. ASTM D 412	494,7	440-460	531,1
Abrasion resistance *(mm3)* s. ASTM D 2228	163	114-130	139,7
Tear strength *(N/mm)* s. ASTM D 624 (DIEC)	41,5	45,6-49,8	46,5

Nanorubber prototype

Picture below shows one of the parts manufactured by one end-user organisation with the formulation reinforced with organic nanoclay.

VI. CONCLUSIONS

• A new procedure for the organic modification (exfoliation) and impregnation with coupling agents of new nanofillers (montmorillonite) has been developed. New organic treatment achieves the complete exfoliation of the montmorillonite.

• New organic nanoclay developed has been successfully tested into rubber compound increasing mechanical properties and keeping processing conditions, rheological properties and vulcanisation rates.

ACKNOWLEDGEMENTS This work was supported by NANORUB-project, which is co-financed by the Sixth Framework Programme of European Commission (FP6-2003-SME-CRAFT 018003)

NANOSPAIN 2008, Braga (Portugal) April 14-18, 2008

WWW.LUREDERRA.ES
lurederra@lurederra.es

PMMA-Organo Bentonite Nanocomposites from The Exfoliation-Adsorption Technique and Their Characterization by FTIR, XRD, TEM, TSDC and DSC.

Norkis Salazar Serge[1], Nery Suárez[2], José Luis Feijoo[3], María Hernandez[2]
[1]Departamento de Química, [2]Departamento de Física, [3]Departamento de Materiales
Universidad Simón Bolívar, Caracas, Venezuela
nsalazar@usb.ve, nsuarez@usb.ve, jfeijoo@usb.ve, mahernan@usb.ve

This work is related to the preparation of polymer-clay nanocomposites (PCNs) by the exfoliation-adsorption technique, from atactic poly(methyl methacrylate) (PMMA) in solution, using Bentonite (B) as a layered-silicate natural clay. To optimize the intercalation of B with PMMA, it has been organically modified (OB) with a quaternary ammonium salt that helps the interchange of cations, and thus converting its hydrophilic surface to an organophilic one. An investigation of the morphology and molecular motions or dynamics of the net polymer film as well as the PCN final films was performed by X-ray diffraction (XRD), Transmission Electron Microscopy (TEM), Infra-Red Spectroscopy (IR), Thermally Stimulated Depolarization Currents (TSDC), and Differential Scanning Calorimetry (DSC) techniques. One of our interests was to discuss the solvent influence on the polymeric matrix. Herein, comparative studies of the effects of different solvents on the thermal and dielectric properties of the net PMMA films are reported. Four solvents were used to prepare the films, toluene, dichlorometane, tetrahydrofuran and acetone.

Fig. 1 XRD diffraction pattern of B, OB, and PMMA /5%OB

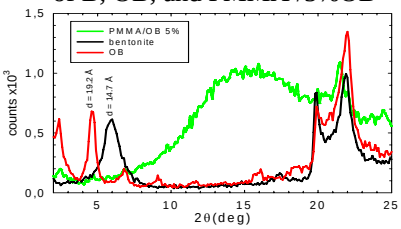

Fig. 2. TEM micrograph of PMMA/2%OB

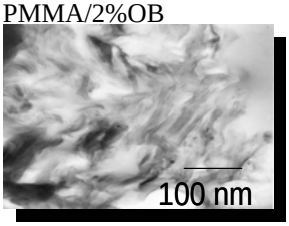

In Figure 1, XRD diffraction patterns(using Cu Kalfa radiation), reports the spacing between ordered layers of clay via the presence of the d_{100} or basal spacing. The original B exhibits a peak associated with a spacing of 14.7 A, whereas the expanded OB shows a value of 19,2 A. The absence of this basal peak suggests a high dispersion of clay platelets (exfoliation) in the PMMA/OB with 5% OB. The broad peak at around $15^{o}=2\theta$ is due to the amorphous hallow of the atactic PMMA nanocomposite. The efficiency of the intercalation can be also check by TEM microphotographs. Figure 2 clearly shows that the OB layers are mainly exfoliated in the PMMA/OB with 2% OB.

Fig. 3 FTIR curves of PMMA/OB PCNs and PMMA/B

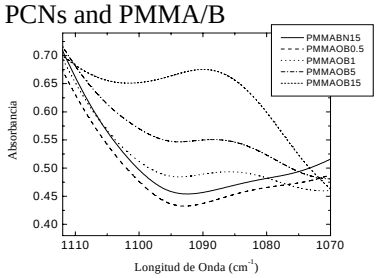

The FTIR spectra of the Si-O stretching region are shown in Figure 3 for PMMA/OB with varying % OB concentration, and PMMA with 15% of natural B. The graph shows the presence of a peak with increasing intensity and slight shift of its maximum towards higher λ^{-1} position as the OB content increases. The absence of this peak in the PMMA/B sample corroborates their previous assignation to Si-O groups [1] interacting with polymer molecules. The significant changes of this peak with the OB content obviously reflect the variation in the distribution of environments of the Si-O bonds, providing also an indication of the increasing overall degree of intercalation/exfoliation.

Figure 4 shows the dielectric spectra of the PMMA films prepared with the different solvents and the compressed molded sample. It displays a series of well established intrinsic relaxation signals [2], i.e., **γ** (methyl groups), **γ´** (adsorbed polar water molecules), β (carboxymethyl side groups flip), β´ (postulated as a main chain rearrangement accompanying the side group flip,

characterized as a rotation around the local chain axis), and long-range conformational change of the polymer backbone. (A) displays the secondary relaxations whose intensity and profile vary with the selected solvent. The glass transition is shown at higher temperaturas (B) as a huge peak, with intensity and temperature position (Tg) variations among the different solvents. The whole spectra of the cast samples exhibit evident intensity atten-uation as compared to the molded film. A lower value of Tg is also a common feature among the cast samples. Comparable Tg trends have been obtained by DSC technique. Traces of the different solvents are expected to reside in relatively strong binding sites [2], e.g., hydrogen bonded to C=O groups. The measured amount of the remanent acetone, dichlorometane, toluene, and tetrahidrofuran solvents, obtained by NMR, is 0.30, 0.40, 9.00, and 14.00% respectively. The samples with higher solvent contents exhibit lower Tg values. The retained solvent molecules, trapped inside the PMMA films, affect the dynamics of the segmental and the localized dielectric relax-axations. This effect differs in function of the nature and the amount of the solvent, and it could be partly explained by acid-base interactions between PMMA and the solvents[3].

Fig. 4 Low temperatura (A), and High temperature (B) TSDC spectra of PMMA molded film and cast films from different solvents.

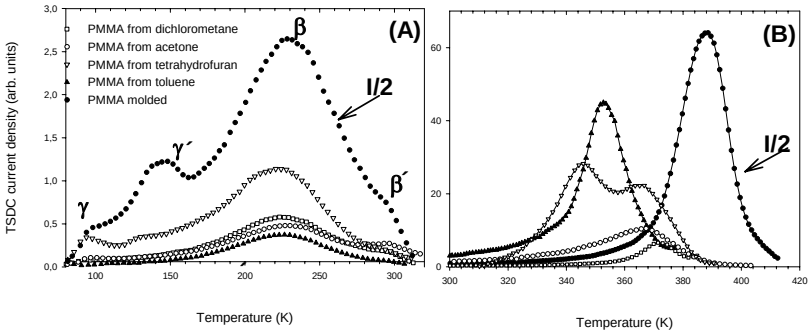

Fig. 5 Low temperatura (A), and High temperature (B) TSDC spectra of PMMA/OB PCNs.

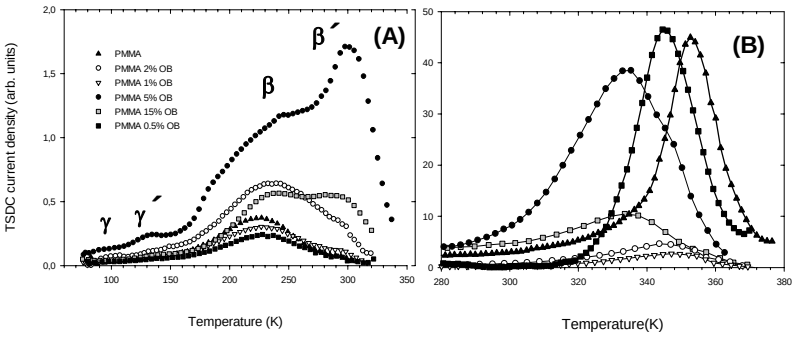

Figure 5 (A) shows that, on increasing the OB content the intensity of the low temperature relax- ations decreases in the sample with 0.5% OB, increases up to 5% OB, and then drops again at 15% OB. A positive high-temperature shift of the low temperature spectra is observed in the samples with 2, 5, and 15% OB. This shift, related with the enhancement of the β´ process, could be explained by the increased exfoliation, as it increases the rotational mobility of the PMMA chains[4]. Figure 5 (B) shows that the temperature position of the dielectric manifestation of the glass transition is a decreasing function of the OB content. Similar Tg decreasing trend was obtained by DSC. This behavior is consistent with previous results[4-5] and have been rationalized assuming that the layered silicates reduce the intermolecular (cooperative) domain size, which increases with the exfoliation. However, as the layered silicate/polymer interactions could restrict segmental mobility, the outcome should be a "tug-of-war", where the influence of these opposite effects must be accounted for.

References:

[1] K. C. Cole, *Macromolecules*, **41(3)** (2008) 834-843.
[2] I. M. Kalogeras, E. R. Neagu, and A. Vassilikou-Dova; *Macromolecules* **37**, (2004)1042-1053.
[3] S. Bistac, J. Schultz, *Mat. Sci. & Eng.*, **31** (1997) 347-350.
[4] R. Davis, A. J. Bur, M. McBrearty, Y. Lee, J. W. Gilman, and P. R. Start; *Polymer* **45**, (2004) 6487-6493.
[5] J. Mijovic, H. Lee, J. Kenny, and J. Mays, *Macromolecules*, **39(6)**, 2006) 2172-2182.

NEW NANOSTRUCTURED MULTICHROMIC MATERIALS FOR ELECTROOPTICAL DEVICES

M. Salsamendi, A. Viñuales, J. Rodriguez, J. A. Pomposo and C. Pozo-Gonzalo

New Materials Department, CIDETEC, Parque Tecnológico de San Sebastián, Paseo Miramón 196, E-20009 Donostia-San Sebastián, Spain
Email: msalsamendi@cidetec.es

Electrochromism has attracted a lot of attention in the past decade due to potential applications of electrochromic materials in smart windows,[1] eye-glasses, rear-view mirrors, displays,[2] and variable optical attenuators.[3 4]

Electrochromism is defined as the property inherent to some materials which can electrochemically switch between different coloured states as a result of a redox reaction. Typical electrochromic behaviour lead to switching between a transparent or bleach state and a coloured state or between two different coloured states.

Many different types of organic and inorganic materials such as inorganic metal oxides, mixed-valence metal complexes, organic small molecules and conducting polymers exhibit electrochromic behaviour. Among the electrochromic materials, conducting polymers have received a great deal of attention due to outstanding electrochromic properties such as switching time, stability, colouration efficiency, or wide range of colours.

Previously, we have studied the electrochemical and electrochromic behaviour of poly(2-(2-thienyl)-1H-pyrrole) (**1**)[5] which showed an interesting orange to black electrochromic behaviour upon oxidation. This work lead us to synthesise new derivatives based on poly(2-(2-thienyl)-1H-pyrrole) bearing substituents with donor and acceptor properties.[6]

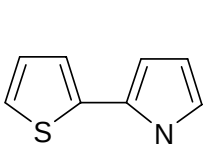

(**1**)

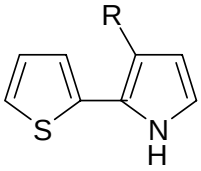

R = Ethyl (**2**)
Propyl (**3**)

In this communication, we report the electrochemical synthesis of copolymers **2** and **3** and their subsequent optical and electrochemical characterisation. Interestingly, the attachment of short alkyl chains lead to new electrochromic properties exhibiting multichromic behaviour with up to five different colours (dark orange, orange-yellowish, brown, blue and blue-greyish) (Figure 1). It is important to remark that although most electroactive polymers have the ability to exhibit two colours, only a few ones show multi-colour states.[7 8]

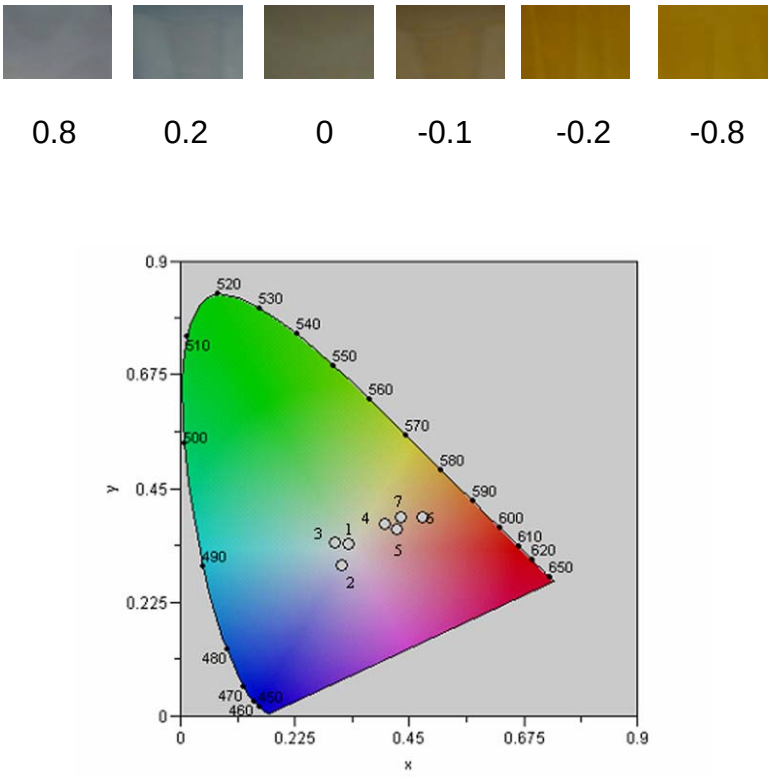

Figure 1: Multichromic behaviour of poly(**2**) films deposited on ITO plastic substrate (top) and CIE chromaticity diagram showing the corresponding (x,y) and (L*a*b*) colour coordinates (bottom). The numbers in the graph correspond to: 1 (as grown, blue - greyish), 2 (+1 V, blue - greyish), 3 (+0.8 V, light blue), 4 (0 V, brown), 5 (-0.1 V, brown), 6 (0.2 V, dark orange) and 7 (-0.8 V, light orange).

References:

[1] G. A. Niklasson, C.G. Granqvist, Journal of Materials Chemistry **12** (2007) 127.
[2] R.J. Mortimor, A.L. Dyer, J.R. Reynolds, Displays **1** (2006) 2.
[3] C. Pozo-Gonzalo, D. Mecerreyes, J.A. Pomposo, M. Salsamendi, R. Marcilla, H.J. Grande, R. Vergaz, D. Barrios, J.M. Sánchez-Pena, Solar Energy Material & solar Cells **92** (2008) 101.
[4] A.L. Dyer, C.R.G. Grenier, J.R. Reynolds, Advanced Functional Materials **9** (2007) 1480.
[5] C. Pozo-Gonzalo, J.A. Pomposo, J.A. Alduncin, M. Salsamendi, A.I. Mikhaleva, L.B Krivdin, B.A. Trofimov, Electrochimica Acta. **14** (2006) 4784.
[6] C. Pozo-Gonzalo, M. Salsamendi, J.A. Pomposo, H.J. Grande, E.Y. Schmidt , Y.Y. Rusakov and B.A. Trofimov, Journal of Materials Chemistry, 2008 (under revision).
[7] S. Varis, M. Ak, IM. Akhmedov, C. Tanyeli, L. Toppare, Journal of Electroanalytical Chemistry **1** (2007) 8.
[8] CL. Gaupp, JR. Reynolds, Macromolecules **17** (2003) 6305.

Poster

DESIGN AND CHARACTERIZATION OF PIEZOELECTRIC MEMS RESONATORS

José Luis Sánchez-Rojas, Jorge Hernando, Maria Jesús Oliver and Javier Vázquez
University of Castilla-La Mancha Spain

In this presentation, our recent results in the simulation, electrical and interferometric characterization of piezoelectric beams will be reviewed. A systematic impedance analysis of the resonance response obtained from ZnO piezoelectric cantilevers, comprising both experimental and simulation work, has been carried out. The approach is based on both impedance and laser Doppler interferometry measurements, and supported by some computational analysis as well. The experimental results obtained by the two different techniques agree reasonably well, as for the location of the resonances in the spectrum is concerned. Although non-fundamental modes are less used in sensing applications, they are emphasized in this work. The characterization of some non-fundamental modes, torsionally shaped, reveals an unexpected behaviour that should be known and understood previously to any gravimetric sensor design using torsional modes. An explanation to this phenomenon, based on the redistribution and cancellation of surface reaction charges, is given in detail and supported by simulation results.

Besides, simulations and measurements of AlN based microstructures will be presented, including devices for the determination of the piezoelectric coefficients.

CHARACTERIZATION AND ENHANCEMENT OF ELECTROCHEMICAL PROPERTIES OF MWCNT/POLYSULFONE COMPOSITE MODIFIED SCREEN-PRINTED ELECTRODES

Samuel Sánchez[a], Maria José Esplandiu[a], Esteve Fàbregas[a], Martin Pumera[b]
[a]Sensors and Biosensors Group, Chem. Dept., Autonomous University of Barcelona, Spain.
[b]ICYS, National Institute of Material Science, Tsukuba, Japan
Samuel.sanchez@uab.es

The Polysulfone(PSf)/Multi-walled Carbon Nanotubes (MWCNT) composites were prepared by the phase inversion method as previously reported [1,2]. Here we describe a profound characterization concerning the composite construction as well as the thermal, electronic, conductive, morphological, physical, chemical and electrochemical properties.

When polymer is mixed up with CNT suspension, a layer of ≈20 nm of polymer coats every single carbon nanotube separately as observed by SEM and TEM. The main difference (vs graphite composites) in the morphology structure relies on the interaction within the polymer matrix: whilst PSf wraps the MWCNTs separately in the PSf/CNT composite, the polymer glue the big graphite particles with a very low uniformity distribution.

Electronic properties of the composite were enhanced as observed by Atomic Force Microscopy. Thermo gravimetric analysis showed that the thermal stability of CNT composite was 8ºC higher than graphite counterparts. Moreover, this nanocomposite was printed onto screen-printed electrodes, showing higher sensibility, lower resistance and electrocatalytic effect when compared with graphite composite modified electrodes. Impedance Spectroscopy was an interesting tool for the electrochemical resistance characterization of the composites deposited onto screen-printed electrodes. The electrochemical detection of some biomarkers as hydrogen peroxide, ascorbic acid and ferricianide was studied.

In this characterization work, we can conclude that the good interaction between the polymer and nanotubes gives some improved characteristics to the composite and therefore it can be also used as electrochemical platform due to its high electron transfer properties.

The electrochemical activation of multiwall carbon nanotubes (MWCNT) (at potentials of 1.5-2.0 V *vs.* Ag/AgCl for 60-360 s) results in significantly increased electrochemical and catalytic properties. This increase is due to introduction of dramatic wall defects exposing edge planes of MWCNT as well as the diminution of the PSf coating as it was observed by high resolution transmission electron microscopy. X-ray photoelectron spectroscopy (XPS), Raman spectroscopy and electrochemical impedance spectroscopy were used to gain deeper understanding the phenomena. XPS revealed that electrochemical activation of carbon nanotubes leads to relative increase of presence of carboxyl groups while relative presence of carbonyl and alcohol/ether groups decreases.

Electrochemical activation of carbon nanotubes was studied in previously [3, 4], but they presented only electrochemical data and it did not bring any spectroscopic insight why such enhancement happens until Pumera investigations [5]. Moreover, we did not find previous work based on the electrochemical activation of carbon nanotube-based composites. This electrochemical activation was applied to a screen-printed electrode used for cyclic voltammetry of important biomakers.

The aim of this article is to demonstrate that electrochemical activation of carbon nanotubes results into introduction of defects to carbon nanotube walls which lead to higher electroactive sites density and consequently to faster observed heterogeneous electron transfer rate k^0_{obs}. We characterize electrochemically activated carbon nanotubes by cyclic voltammetry, electrochemical impedance spectroscopy, Raman spectroscopy, high resolution transmission

electron microscopy, Scanning electron microscopy and X-ray photoelectron spectroscopy to have insight to the mechanism of such activation.

References:

[1] Sanchez, S., Pumera, M., Fabregas, E. Biosens. Bioelectron. 23 (2007) 332.
[2] Sanchez, S., Pumera,M., Cabruja, E., Fabregas, E. Analyst 132 (2007) 142.
[3] Musameh, M., Lawrence, N. S., Wang, J.. Electrochem. Commun. 7 (2005) 14.
[4] Wang, J., Li, M., Shi, Z., Li, N., Gu, Z. Anal. Chem. 74 (2002) 1993.
[5] Pumera, M. Langmuir. (2008). On revision.

Figures:

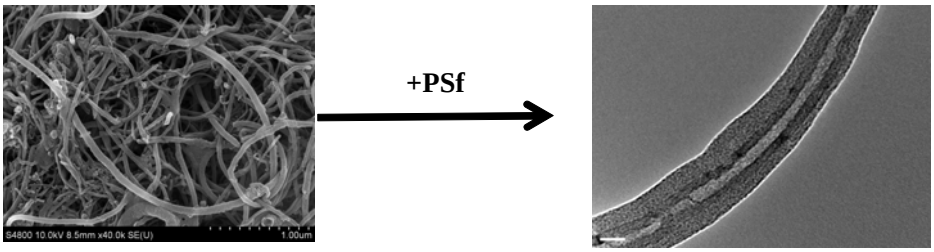

Fig.1. (left) SEM image of CNT powder and (right) TEM of a single CNT with Polysulfone

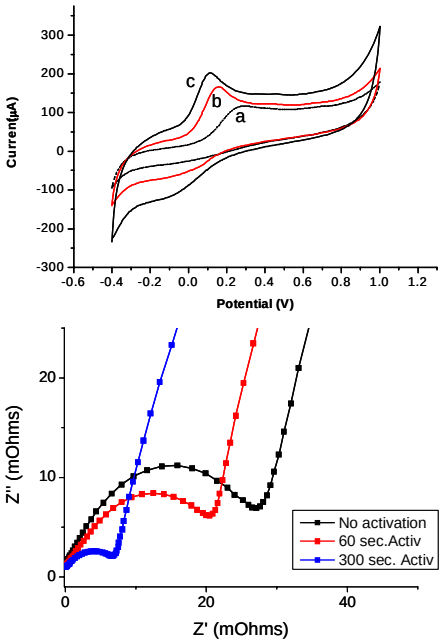

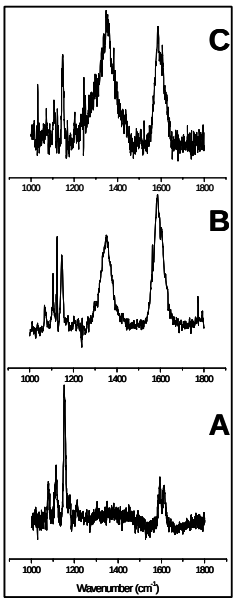

Fig.2. Cyclic voltammograms of ascorbic acid for MWCNT/PSf-modified sensor and Impedance Spectra for ferricianide, a) no activation, b) activation at +1.75 V for 60 sec and c) for 300 sec. Fig.3. Raman spectroscopy of: A) PSf, B) MWCNT/PSf composite and C) MWCNT/PSf composite after activation of 60 s at +1.75 V.

STABILITY OF TRIETHOXYSILANE TERMINATED WATERBORNE POLYURETHANE NANOPARTICLES

H. Sardon[1,2], E. Bourgeat-Lami[2], M. Lansalot[2], L. Irusta[1], M.J. Fernandez-Berridi[1]

1. *DPTO. CIENCIA Y TECNOLOGÍA DE POLÍMEROS, FACULTAD DE QUÍMICA UPV/EHU. 20018-DONOSTIA*
2. *CHIMIE, CATALYSE, POLYMÈRES, PROCÉDÉS (C2P2)-EQUIPE LCPP-UMR5265 CNRS/CPE/UCBL 69616-VILLEURBANNE CEDEX- FRANCE*

hsardon001@ikasle.ehu.es

The water-based systems are gradually dominating most of the coating market as a consequence of their lower toxicity comparing to the organic borne systems. According to this, in the last decades aqueous polyurethanes (PU) [1,2] have grown commercially due to environmental reasons. Polyurethane materials demonstrate a unique combination of performance properties, including excellent abrasion resistance, flexibility, hardness and many other that make then suitable for a lot of useful products including coatings, adhesives and sealants.

Several processes have been developed for the synthesis of polyurethane dispersions. One of the most used is the "acetone process". In that system, the polyurethane is synthesized in a low boiling point solvent (usually acetone). The synthetic procedure is similar to the one used in the traditional formation of polyurethanes, but a part of the chain extender is replaced by a functionalized diol that improves water dispersability. After that, water is added drop wise to the polymeric solution, giving rise to a fine polyurethane dispersion. Finally the acetone is removed by distillation and the aqueous polyurethane dispersion is obtained. Figure 1 shows a scheme of the described process.

Because most commercial aqueous PU-s are linear thermoplastic polymers, the mechanical properties and solvent resistance of these systems is lower than the obtained in crosslinked two pack solvent based PU-s. Many ways of crosslinking waterborne PU-s have been studied. In recent publications [3], PU prepolymer dispersions have been reacted with alkoxisilane containing compounds in order to get a moisture curable PU. These systems display good adhesion to different substrates and improved mechanical properties because of the presence of the inorganic domains. However, the incorporation of the alkoxisilane end groups can reduce the stability of the PU dispersion.

In this work different waterborne polyurethanes were synthesized by means of the acetone process. Isophorone diisocyanate (IPDI), Polyester end capped diol (PBAD), 2,2-bis(hydroxymethyl) propionic acid (DMPA), triethylamine, 1,4-butanediol, sodium hydrogen carbonate ($NaHCO_3$) and a tin catalyst were used for the synthesis of the waterborne polyurethanes.

In addition some of those polymers were reacted with 3- aminopropyltriethoxysilane (APS). The amine group can react with the isocyanate group, giving rise to urea groups. Different reactions were performed using variable amounts of APS. Figure 2 shows the infrared spectra of the obtained polymers.

As can be seen in Figure 2, the modified polymers show a new band (1630 cm^{-1}), attributable to urea groups, whose intensity increases with APS concentration. These results confirm that the APS has been covalently linked to the PU chain.
However, APS ethoxysilane groups are highly reactive and in the presence of water are prone to hydrolyze. Although during the polymerization process in acetone there is not hydrolysis

thanks to the nitrogen inlet, when water is added and the phase inversion starts, the ethoxy groups, coming from the APS, hydrolyze and can condense between them forming a network and making the dispersion less stable.

In order to check the stability of the dispersion, Dinamic light scattering (DLS) measurements were carried out during the phase inversion to monitorize the diameter of the obtained particles (Dp). The obtained results have shown that the addition of APS increases considerably the diameter of the particle and therefore, decreases the dispersion stability.

The authors would like to thank the financial support of the Ministerio de Educación y Ciencia (INTERHYBRID project number MAT2005-08033-C02-01).

References:

[1] A. K. Nanda, D. A. Wicks, Polymer, 47 (2006) 1805-1811.
[2] H. T. Jeon, M. K. Jang, B. K. Kim, K. o Kim, Colloids and Surfaces A: Physicochem. Eng. Aspects, 302 (2007) 559-567.
[3] S. Subramani, J. M. Lee, J. Y. Lee, J. H. Kim, Polym. Adv. Technol, 18 (2007) 601-609.

Figure 1. Scheme of the formation of water borne polyurethane

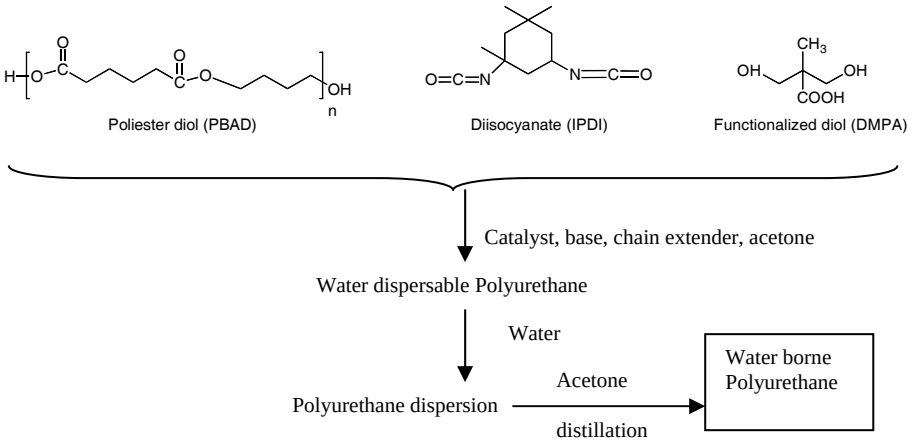

Figure 2. FTIR spectra for different polyurethanes

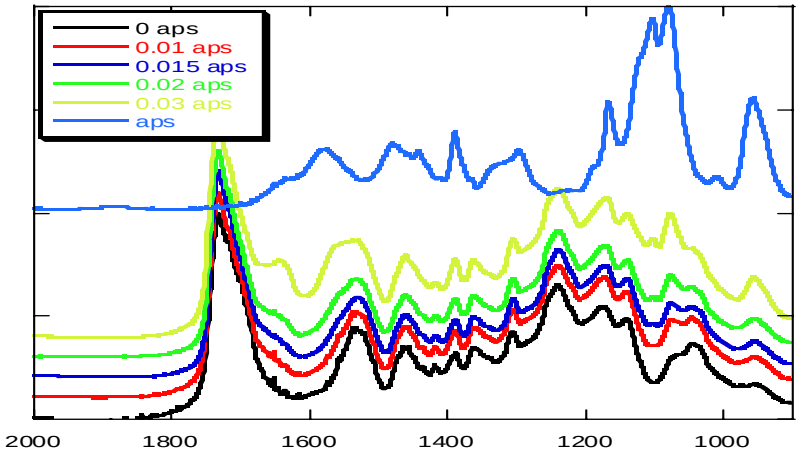

INTERFACE ANALYSIS TECHNIQUES ON NANOSCALE DIMENSION IN FLEXIBLE SOLAR CELLS

Schwarz, R. Ayouchi, C. Casteleiro
Instituto Superior Técnico, Departamento de Física, Av. Rovisco Pais 1, P-1049-001, Lisboa, Portugal
G.M. Junior, M. Ribeiro, P. Alpuim
University of Minho, Department of Physics, P-4800-058 Guimarães, Portugal

Basic idea: This work concerns the study of interface properties in thin film devices on a nanometer depth scale. Several analysis techniques are employed and correlated:

- photocapacitance spectroscopy [1],
- stress measurement at the interface,
- interface recombination by steady-state and transient grating techniques (SSPG, TG),
- photoluminescence (PL), and
- correlation between interface light scattering and the open-circuit voltage V_{oc}.

As a typical example we consider a tandem structure of an amorphous silicon based thin film solar cell consisting of nano-structured ZnO window layer, followed by a p-i-n a-Si:H solar cell deposited at the amorphous-to-microcrystalline transition (polymorphous), and terminating in a hydrogenated microcrystalline silicon bottom p-i-n cell. The three regions are tailored for best performance in the UV, visible, and IR spectral range, respectively. The whole structure is deposited on a flexible polymeric substrate [2].

Techniques: The flexible substrate is critical in two respects: first, the surface roughness of the ZnO contact layer (including ZnO quantum dots as shown in Fig. 1) which is helpful for improving the solar cell efficiency through light scattering may be responsible for creation of detrimental interface trap states. Secondly, a flexible substrate imposes mechanical constraints on the contact layer that may deteriorate the quality of its interface to the semiconductor film. Photocapacitance spectroscopy is sensitive to non-radiative recombination introduced by additional interface states and to the local electric field distribution near the heterostructure interface. Cells will be inserted in a four-point bending jig and their I-V characteristics under fixed illumination will be recorded as a function of the applied bending moment that will induce strain in a controlled manner in the devices. The degradation of solar cell performance, reflected in its V_{oc}, I_{sc} and fill factor values, will be studied as a function of the number of load-unload cycles applied in the four-point bending geometry. Comparison of photocapacitance measurement results performed before and after mechanical stressing of the device will elucidate about the extent of the damage in the interface ZnO/a-Si:H caused by strain [3].

Technology: We have previously used photocapacitance spectroscopy to study the local defect creation in irradiated amorphous silicon-based p-i-n detectors [1]. Here we extend this technique to study thin film solar cells deposited on ZnO-coated flexible substrates (PI and PEN). The p-i-n structures were deposited by RF-PECVD and HW-CVD at particularly low substrate temperature

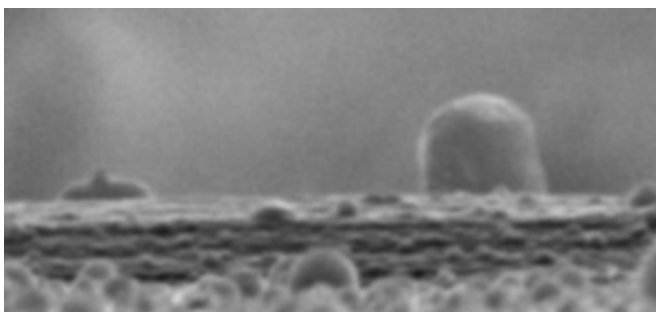

Figure 1: ZnO quantum dot on catalytic Au layer

of 150 ˚C. Hydrogen dilution was varied between 50 and 98 %. One of the contact layers used was polycrystalline ZnO prepared from sintered oxide targets by pulsed laser deposition (PLD). The photocapacitance measurements were done under HeNe laser illumination at a modulation frequency up to 1 MHz, as a function of voltage bias, and under different white light bias conditions. Enhanced recombination is seen by both the reduction of the photocapacitance signal and by faster capacitance decay in pulsed mode. The spatial resolution under focused laser light is limited ultimately by lateral carrier diffusion.

Scientific relevance: The analysis with photocapacitance spectroscopy has several innovative aspects: First, it is an alternative to the usual laser-beam-induced photocurrent measurements (LBIC) to study solar cell quality. Secondly, the technique is sensitive to both interface defects and interface electric field profiles between the ZnO contact layer and the p-i-n solar cell structure. Finally, by scanning a focused laser beam across the cell we obtain a topological image of defect regions of the solar cell.
The 4-point bending technique allows the application of pure bending to the specimen under study, if it is placed between the two inner loading points. It is possible to apply tractile of compressive strain just by placing the device in the convex or concave surface upon bending. The effect on solar cell performance of the cracks that will develop perpendicular to the substrate and through the solar cell thickness under positive strain and the eventual recover of device performance under negative strain will be measured. The combination of this technique with the photocapacitance spectroscopy will allow to assess the relative importance of the mechanically damage in the bulk of the device and in the interface with ZnO.

Conclusions: Spectrally and spatially resolved photocapacitance measurements, stress measurement at heterointerface, the correlation between interface recombination, open-circuit voltage and photoluminescence yield give a comprehensive picture of the interface quality between a conductive transparent oxide layer and a thin film solar cell. As an example we studied a typical solar cell structure composed of ZnO/a-Si:H on polymer substrate. A lateral spatial resolution of a few tens of microns is achieved when scanning across the cell surface. The depth resolution obtained by wavelength selection is of nanometer scale in the interface region.

References:

[1] C. Casteleiro, R. Schwarz, A. Maçarico, J. Martins, M. Vieira, F. Wuensch, M. Kunst, E. Morgado, P. Stallinga, H. Gomes, "*Spatially-Resolved Photocapacitance Measurements to Study Defects in a-Si:H Based p-i-n Particle Detectors*", to be published in Thin Solid Films (2008).

[2] S.A. Filonovich, P. Alpuim, L. Rebouta, J.-E. Bourée, Y. M. Soro, *"Amorphous and nanocrystalline silicon solar sells deposited by HWCVD and rf-PECVD on plastic substrates at 150ºC"*, Journal of Non-Crystalline Solids, in print (2008).

[3] P. Alpuim, S. Lanceros-Mendez, V. Sencadas, M. Andrade, S.A. Filonovich, *"Piezo-Resistive Properties Of Nanocrystalline Silicon Thin Films Deposited On Plastic Substrates By Radio-Frequency And Hot-Wire Chemical Vapor Deposition"*, Thin Solid Films, 515 (19), 7658 (2007).

WATER/L-ALANINE INTERACTIONS: HYDROPHILLICITY VS. HYDROPHOBICITY

Segura, Juan José; Verdaguer, Albert; Fraxedas, Jordi.
Centre d' Investigació en Nanociència i Nanotecnologia (CIN2-CSIC-ICN)
Edifici CM7, campus UAB, 08193, Bellaterra, Spain
juanjo.segura@cin2.es

L-alanine is a non-essential chiral amino acid with a non-reactive hydrophobic methyl group as a side chain. However, it exhibits a relatively high solubility in water which is due to its zwitterionic form. Cleaved (011) and (120) surfaces of single crystals of L-alanine grown from aqueous solutions have been characterized by atomic force microscopy (AFM) at room temperature as a function of the relative humidity (RH). Their behaviour is radically different: while (011) surfaces are highly hydrophilic, (120) surfaces are highly hydrophobic.

The AFM experiments have been performed in a glove box with a 5500 Agilent Technologies AFM (Agilent Technologies, USA) under controlled humidity using microfabricated silicon cantilevers with force constants $k_c \sim 40$ N/m and ultrasharp silicon tips (tip radius R< 10 nm) (NanoAndMore GmbH, Germany). RH inside the box was decreased or increased by flowing dry nitrogen or by bubbling nitrogen through MilliQ water, respectively. The single crystals were cleaved inside the glove box at the lowest achieved RH (< 5%).

Figure 1(a) shows an AFM image in acoustic mode (amplitude) taken immediately after cleavage al low humidity (RH ~ 5%) of a (011) surface. The surface exhibits a combination of well-defined long and shorter straight steps. The measured step height is ≈ 0.5 nm, in agreement with the distance between two adjacent (011) planes (0.52353 nm). The effect of humidity is quite drastic on the (011) surfaces. Already at 20% RH [Fig. 1(b)] important morphological changes can be observed at the surface. Islands with heights of ≈ 0.3 nm are formed on the terraces. As humidity increases the islands grow two-dimensionally and at RH ~ 50% [Fig. 1(c)] the original steps are hardly identified. At this humidity the islands have merged forming terraces with irregular edges covering the entire surface [Fig. 1(d)]. At high humidity (RH>70%) holes appear at the surface indicating large dissolution of the crystal. For higher humidity, tip perturbation of the surface can be observed as a strong dissolution process at the areas where the tip has been scanning.

Freshly cleaved (120) surfaces show well-defined steps along the crystallographic *c*-axis, as shown in Fig. 2(a). The measured step height was found to be ≈ 0.5 nm, again in agreement with the distance between two (120) adjacent planes. Surfaces showing mostly steps in the [001] direction remained unaffected upon exposure to water vapour up to high humidity (RH ~ 75%). At high humidity conditions the scanned regions become perturbed due to the tip but when the surroundings of the observed area are imaged, it is found that they remain essentially unaffected [Figure 2(b)]. The stability of the morphology of the surface is a proof of the hydrophobic nature of the (120) face. A closer look to what happens on the steps growing perpendicularly to the [001] direction reveals some anisotropic degree of hydrophilicity. This is shown in Fig. 2 (c), where we observe that the long step edges remain unperturbed while nanoneedles aligned along

the [001] direction are formed. A further proof that water preferentially interacts in such regions is given by the phase image shown in Fig. 2(d) where a high phase contrast is observed due to water absorption. We also observe the formation of needles on the terraces. Starting from small crystals that deposits on the surface the needles grow in the [001] direction.

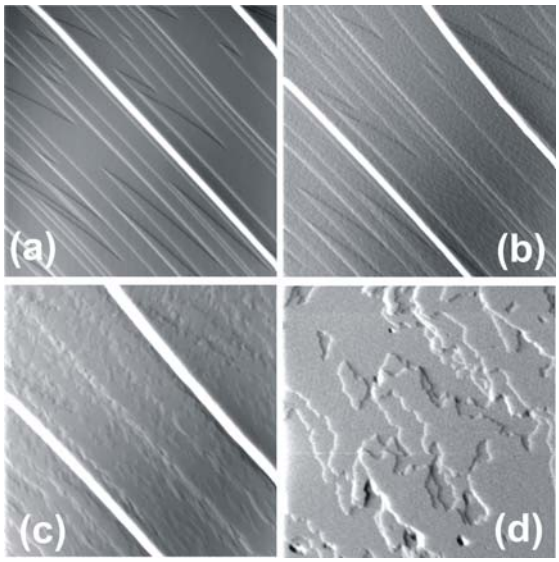

Figure 1: Evolution of amplitude AFM images of a L-Alanine (011) surface as a function of RH: (a) ~ 5%, (b) ~ 20% and (c) ~ 50%. Figure (d) shows a zoom of a surface region taken at RH ~ 50%.

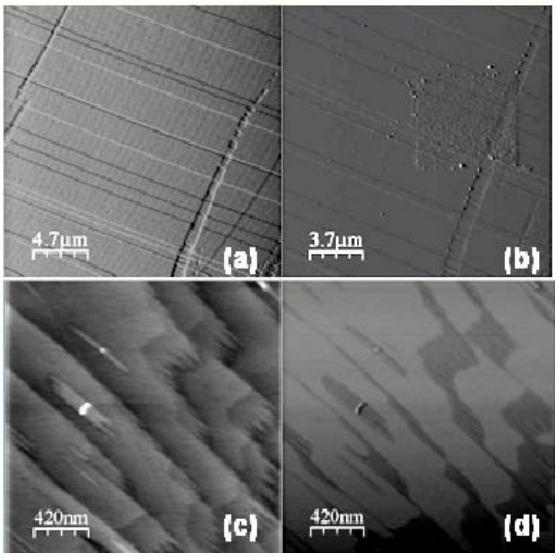

Figure 2: Evolution of AFM images of a L-Alanine (120) surface as a function of RH; (a) ~ 5%, (b) ~ 10% [after exposure at ~75%. The irregular square shows the zone where all the experiment was taken] and (c) ~ 45%. (d) phase image of (c)

PROCESSING AND CHARACTERIZATION OF NANO COMPOSITES OF POLY (VINILIDENE FLUORIDE) DOPED WITH SILVER NANO-PARTICLES

D. Miranda,V. Sencadas*, I. Pastoriza-Santos**, L. M. Liz-Marzán **, S. Lanceros-Mendez**

**University of Minho, Dept. of Physics, 4710-057 Braga, Portugal*

***University of Vigo, Dept. of Chemistry, Campus de Gualtar, 4710-057 Braga, Portugal*

[1]vsencadas@fisica.uminho.pt

In the last decades it has been increasing interest on polymer materials for electronic and other technological applications [1]. One recent area in this field is the inclusion of metallic nanoparticles within dielectric polymers in order to vary and/or tune their optical and dielectric properties [2].

In this work, nano-composites of metallic nanoparticles dispersed in an electroactive polymer matrix have been investigated. The polymer chosen as a matrix is poly (vinilidene fluoride) PVDF, as it shows interesting piezoelectric, pyroelectric and ferroelectric properties [1, 3]. The metallic nanoparticles are silver (Ag) nanospheres stabilized with polyvinylpirrolidone (PVP) [4]. The main objective of this work is the processing of nano-composites of PVDF@Ag with different mass percentages of silver nanoparticles (%Ag) with the polymer both in the non-electroactive α and the electroactive β crystalline phases, respectively. The mass-percentages of nanoparticles were 0,005%, 0,007%, 0,012% and 0,020%. The silver nanoparticles, embedded in DMF show spherical geometry with a diameter of 26 nm. The effect of the silver nano-particles in the macroscopic response on the material was also studied.

The processing conditions have been optimized in order to obtain a better dispersion of nano-particles within the polymer matrix. We used the method of crystallization from solution followed by fusion in order to obtain α-PVDF@Ag. The β-PVDF@Ag samples were obtained by uniaxial stretching of originally α-phase samples [5].

In this study we will focus on the discussion of the processing method of PVDF@Ag and on the influence of the silver nano-particles in the microstructure, the α to β phase transformation, the degree of crystallinity and the resulting influence in the macroscopic optical and dielectric response.

In particular it has been concluded that samples of α–PVDF@Ag grow directly from the melt with a similar spherulitic microstructure than the pure polymer samples (Figure 1).

By mechanical stretching, the α → β phase transition is gradually induced, as it is in pure PVDF. For the nano-composites, the maximum amount of β-phase obtained by stretching ranges from 60 to 71%. These values are lower than the ones obtained for pure PVDF (80%)

Samples of α-PVDF@Ag with 0012% and 0020% show an absorption band in the UV-Visible spectra around 400 nm, related to the surface plasmon resonance –SPR- (Figure 2). The SPR band weakens during the α → β phase transformation due to a decrease of the effective concentration of nano particles with mechanic drawing.

The melting temperature (T_f) and the degree of crystallinity of the PVDF@Ag samples are larger than for pure PVDF, which indicates increased stability of the lamellar structure and that the nano particles might act as nucleating agents for crystallisation.

With increasing mass percentage of Ag nano-particles, the value of the dielectric constant increases, due to the additional polarizability induced by the presence of nano-particles (Figure 3). The dielectric values are larger for the β-PVDF material due to the polar structure of these samples.

References:

[1] H. S. Nalwa, *Journal of Macromolecular Science-Reviews in Macromecular Chemistry and Physics* C13 (4), 341, (1991).
[2] Luis M. Liz-Marzán, *Materialstoday* 26, 31, (2004).
[3] V. Sencadas S. Lanceros-Mendez; R. Gregorio-Filho, submitted to Acta Materialia
[4] P.-Y. Silvert, R. Herrera-Urbina, N. Duvauchelle, V. Vijayakrishnan and K T Elhsissen *J. Mater. Chem.*, 6(4), 573, (1996).
[5] – V. Sencadas S. Lanceros-Mendez; R. Gregorio-Filho; A.S. Pouzada; *Materials Science Forum*, Vol. 514 – 516, 872, (2006).

Figures:

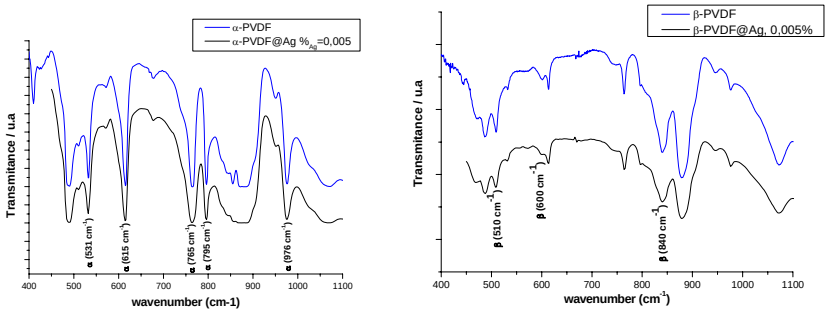

Figure 1: Far infrared spectra of α and β-PVDF and the corresponding nano composites

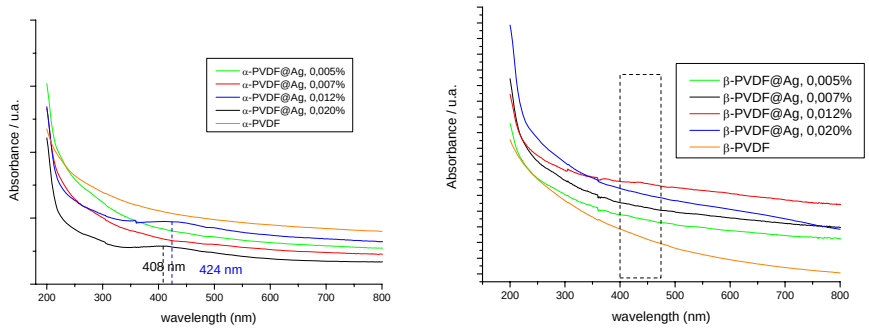

Figure 2: UV-Vis espectra of α and β-PVDF Ag nano composites for several Ag concentrations

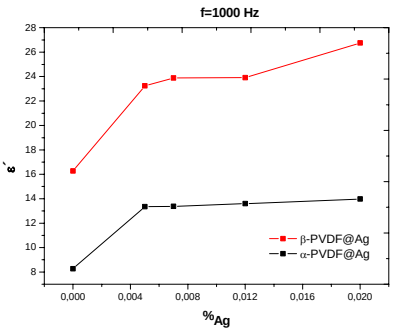

Figure 1: Dielectric constant as a function of Ag concentration for α and β-PVDF Ag nano composites

SURFACE TAILORING OF COIL COATING USING NANOSTRUCTURED FILMS OBTAINED BY PLASMA POLYMERIZATION OF ORGANOSILANES PRECURSORS

R. Serra, M.L. Zheludkevich, M.G.S. Ferreira
Aveiro University, CICECO, Dep. Eng. Cerâmica e do Vidro, 3810-193 Aveiro, Portugal
Contact: rserra@ua.pt

Coil coatings are widely used as corrosion protection systems. They are one of the most advanced techniques to apply continuously an organic coating on a metal sheet during fabrication. The pre-coated material is a product of consistent quality, with excellent formability, durability, corrosion and weathering resistance. It is however lacking of easy-to-clean and anti-scratch properties with controlled optical properties.

The use of plasma polymerization with organosilane precursors was shown to be an effective route to generate films with such properties. Deposition of plasma polymer nanstructured films on top of coil coating systems provide a possible solution to tailor the surface properties of the coil coating.

The present work is devoted to the investigation of this type of films, which were deposited on top of polyurethane coil coating. The effects of utilization of different plasma reactors, composition of precursor mixtures and gas pressure during polymerization on the properties of the obtained plasma polymer films were studied. Also the influence of the plasma polymerization procedure on the coil coating properties was investigated.

TEM and SEM techniques allowed to study the surface morphology and structure of the plasma polymer films formed, Figure 1. The electrochemical properties of the system were also analysed, as exemplified in Figure 2. Film composition was determined by XPS.

The results demonstrate a strong dependence of the plasma film deterioration on the composition of the gas precursor mixture and operating pressure. Decrease of the operating pressure and of the oxygen concentration in the precursor mixture lead to formation of more compact and nanostructered layers that also showed increased stability. The negative impact on the barrier properties of the coil coating is also strongly dependent on the amount of oxygen present during the polymerization procedure.

Optimization of the operating variables leads to decrease the negative influence of the plasma polymerization process on the weathering properties of the system, keeping the additional properties required.

Keywords: plasma polymerization, coil coating, EIS, AFM, TEM,

Figures:

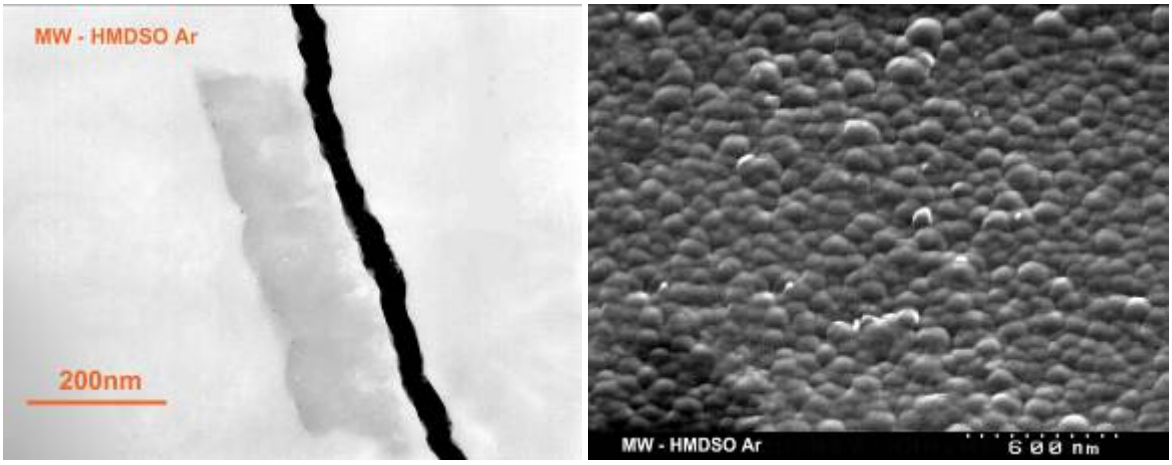

Figure 1 – Nanostructure of the plasma polymer film. Transmission Electronic Microscopy and Scanning Electronic Microscopy techniques.

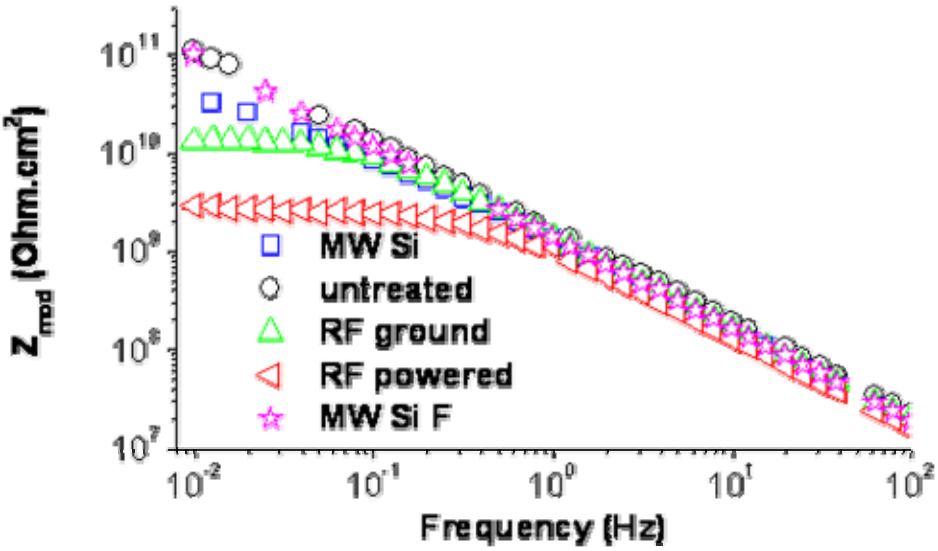

Figure 2 – Influence of different plasma reactors and different precursor mixtures on the barrier properties of the coating system. Electrochemical Impedance measurements.

SYNTHESIS AND CHARACTERIZATION OF ZN NANOFERRITES

I. Sevillano[1], J. Moreno[1], F. Fernandez[2] V. Blanco[3], A. García[1]
[1]Departamento de Ingeniería Eléctrica, EUIT Industrial.
[2]Departamento de Química Industrial y Polímeros, EUIT Industrial,
Universidad Politécnica de Madrid
Ronda de Valencia 3, 28012 Madrid
[3]Departamento de Química Inorgánica, Facultad de Ciencias Químicas
Universidad Complutense
28040 Madrid
e-mail: ignaciobenito.sevillano@upm.es

Fe_2ZnO_4, nanopowders were prepared by hydrotermal method at 160ºC. The structure of magnetic powders were characterized by X-ray diffraction, thermal gravimetric analysis and scanning electron microscopy, while magnetic properties at 300K and 5K were determined by using a SQUID magnetometer working at 100 Oe.

XRD patterns of Fe_2ZnO_4 nanopowder and Fe_2ZnO_4 Franklinite were shown in Fig.1. All the diffraction peaks in the XRD patterns of Fig. 1 can be indexed to face center cubic structure of Iron ferrite, Franklinite, according to JCPDS card No. 22-1012

We can observe for Fe_2ZnO_4 nanopowder low intense and broad diffraction peaks characteristic of low crystallinity and low particule size.

Magnetic characterization of Fe_2ZnO_4 nanopowder obtained by hydrothermal method, Figure 2, shows a characteristic strait hysteresis loop with a saturation magnetic moment of 2 emu at 300K and 8 emu at 5K. These high saturation magnetic moment for this Fe_2ZnO_4 nanopowder are lower than ferromagnetic Franklinite. These results are characteristic of the new superparamagnetic materials.

Fig.3. display the Zero Field Cooling (ZFC) and Field Cooling (FC) curves magnetization measurements of Fe_2ZnO_4 nanopowder shown two broad maximum at temperature as lowest of 21.8K. This may indicate that there are strong interactions between the particles modified by their samall size.

High electric resistivity of ceramic ferrites and straight hysteresis loop are interesting for electric power energy transformation due to low parasitic energy lost specially at high frecuency.

References:

[1] Smit, J., Wijn, H.P.J., Ferrites, Amsterdam, J. Wiley & Sons, (1959), page.136.
[2] R.W. Chantrell, K. O'Grady, in: Applied Magnetism, Kluwer. Academic, The Netherlands, (1994), page 113.
[3] J.L. Dormann, D. Fiorani, Magnetic Properties of Fine Particles, North-Holland, Amsterdam, (1992).
[4] W. Luo, S.R. Nagel, T.F. Rosenbaum, R.E. Rosenwig, Phys.Rev.Lett.67 (1991) 2721.
[5] J.L. Dormann, L. Bessais, D. Fiorani, J. Phys. C 21 (1988) 2015.
[6] Fashen Li, Haibo Wang, Li Wang, Jianbo Wang, Magnetic properties of $MnFe_2O_4$ nanoparticles produced dy a low-temperature solid-state reaction method, Journal of Magnetism and Magnetic Material, 309 (2006), page 295-299.

Figures:

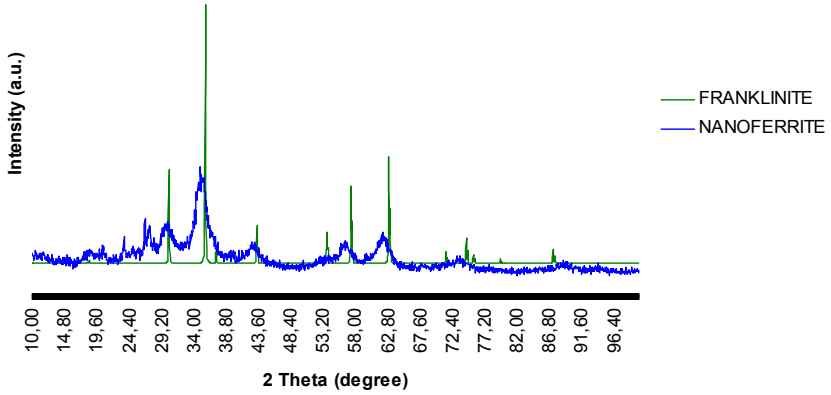

Fig. 1. XRD patterns of Fe_2 ZnO_4 nanopowder and Fe_2 ZnO_4 Franklinite.

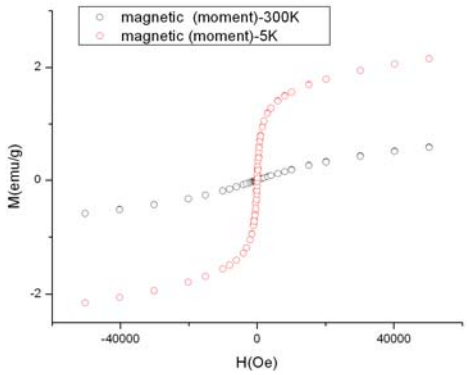

Fig. 2. Magnetic hysteresis loop for of Fe_2ZnO_4 nanopowder at 5K and 300K.

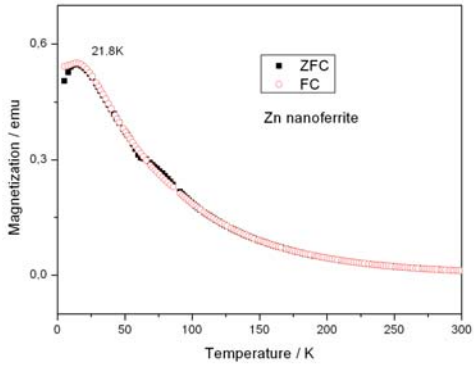

Fig. 3. Zero Field Cooling (ZFC) and Field Cooling (FC) magnetization measurements of Fe_2ZnO_4 nanopowder.

OPTIMIZATION AND CHARACTERIZATION OF AMORPHOUS/NANOCRYSTALLINE BIOSENSORS FOR DNA DETECTION USING GOLD NANOPARTICLES

L. B. Silva[1], P. Baptista[2], H. Águas[1], G. Doria[2], R. Martins[1] and E. Fortunato[1]
[1]CENIMAT/I3N, Materials Science Department, Campus de Caparica, 2829-516 Caparica, Portugal
[2]CIGMH/SABT, Faculdade de Ciências e Tecnologia, Universidade Nova de Lisboa, 2829-516 Caparica, Portugal
Tel: +351212948562; Fax: +351212948558

lbds@fct.unl.pt

Nanotechnology is having a positive impact on nearly every industry, and in particular in healthcare, where it is extending the limits of molecular diagnostics to the nanoscale – Nanodiagnostics. Here we describe an innovative optoelectronic platform for the colorimetric detection of nucleic acids based on oligonucleotide-derivatized gold nanoparticles. The device integrates an amorphous/nanocrystalline biosensor and a light emission source with a gold nanoprobe for specific DNA detection.

The sensor (optical and electrical properties) showed an optimized spectral response at around 527 nm, also the maximum absorbance for the gold-nanoprobes, and SNR in the order of 130 dB for a green (532nm) light source of 5mW. The described system presents several advantages: i) no need to functionalize the glass surface with probe DNA; ii) the sample is directly applied on the back side of the biosensor ensuring maximum photon capture and the possibility of re-use; iii) requires small amount of biological sample.

The described system combines two technologies - gold nanoparticle based DNA detection and optical sensors based on thin film technology - leading to significant cost and time savings in DNA/RNA assays, allowing for molecular diagnostics at point-of-care without compromising specificity and sensitivity.

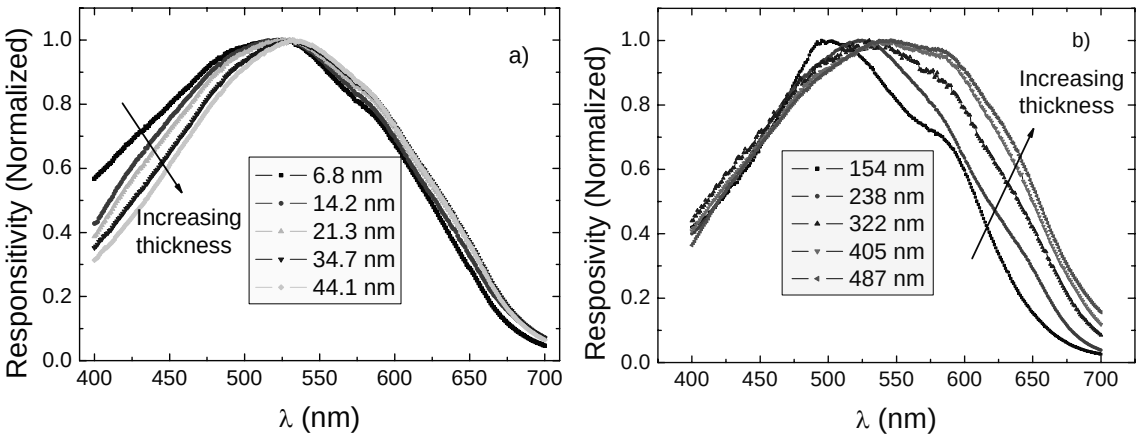

Influence of the thickness on the responsitivity of the sensor for the a) p-layer and b) i-layer.

References

R. Martins, P. Baptista, L. Raniero, G. Doria, L. Silva, R. Franco and E. Fortunato, Appl. Phys. Lett., 90 (2), 023903 (2007)

Patent nº 103561 pending, FCT-UNL, September 2006

MAGNETIC AND STRUCTURAL PROPERTIES OF IRON OXYHYDROXYNITRATE NANOPARTICLES

N. J. O. Silva[1], V. S. Amaral[2], L. D. Carlos[2], Angel Millán[1], Fernando Palacio[1], Benito Rodríguez-González[3], Luis M. Liz-Marzán[3], Thelma Berquó[4], F. Fauth[5], Verónica de Zea Bermudez[6]

[1]Instituto de Ciencia de Materiales de Aragón, CSIC-Universidad de Zaragoza, 50009 Zaragoza, Spain.
[2]Departamento de Física and CICECO, Universidade de Aveiro, 3810-193 Aveiro, Portugal.
[3]Departmento de Quimica Fisica, Universidade de Vigo, 36310 Vigo, Spain.
[4]Institute for Rock Magnetism, University of Minnesota, Minneapolis 55455-0128, USA5.
[5]Labor. Llum Sincrotró, BM16-CRG,c/o ESRF, 6 rue Jules Horowitz, BP220, 38043 Grenoble, France.
[6]Departmento de Química, Universidade de Trás-os-Montes e Alto Douro and CQ-VR, Quinta de Prados,Apartado 1013, 5001-911 Vila Real, Portugal.
nunojoao@unizar.es

Iron oxyhydroxynitrate, with general formula $FeO(OH)_{1-x}$ $(NO_3)_x$ ($0.2<x<0.3$), is an ordered precursor of 6-line ferrihydrite in the process of hydrolysis of an iron nitrate salt in aqueous solution [1]. The iron(III) oxyhydroxynitrate was obtained for the first time in the form of a powder consisting of aggregated nanoparticles after freeze drying a Fe(III) nitrate water solution [1,2]. Here we report magnetic and structural properties on iron(III) oxyhydroxynitrate nanoparticles with different average sizes grown in a organic-inorganic hybrid matrix and compare them to those of other iron oxides. The use of a matrix to grow iron(III) oxyhydroxynitrate allowed to access the magnetic properties of the isolated nanoparticles. The first step of the nanohybrids preparation involves the synthesis of a cross-linked organic-inorganic hybrid precursor, similar to the one used in the synthesis of an undoped matrix, termed di-ureasil [3]. In the second step, a solution of iron(III) nitrate nonahydrate, water and ethanol was added to the non-hydrolyzed hybrid precursor. The resulting mixture was then stirred in a sealed flask for a few minutes at RT. After this, the solution was cast into a mould and transferred to an oven at ca. 40 ºC during 7 days. Samples were obtained after aging for 3 weeks at ca. 80 ºC. Samples were labelled Ih(x), where x is the iron mass concentration.

The powder XRD patterns of the two most concentrated samples of Ih nanohybrids (Fig. 1a) show that iron(III) oxyhydroxynitrate nanoparticles were efficiently stabilized in the matrix. Differences between patterns of iron(III) oxyhydroxynitrate and ferrihydrite are apparent: in the iron(III) oxyhydroxynitrate nanoparticles XRD patterns the relative intensity of the double peak at 60-65 ºC is the opposite of that of ferrihydrite, and the shoulder appearing at 33 ºC in the ferrihydrite nanoparticles is not present in the Ih nanohybrids. TEM images of the Ih(3.8) and Ih(6.5) nanohybrids show the presence of globular-shaped nanoparticles, with diameters of the order of 3 nm. The nanoparticles have nonfacetted and fuzzy edges and the nanoparticles/matrix contrast is low. SAXS patterns of Ih nanohybrids can be modelled as spherical isotropic and diluted Ih nanoparticles dispersed in a homogeneous matrix using GNOM [4]. With this analysis we conclude that the particles size increases with the iron content. The temperature dependence of the dc susceptibility χ shows that the Ih nanoparticles are superparamagnetic (Fig. 1b). The zero-field-cooled curves present a maximum at $T=T_B$ that increases with the iron content (Fig. 1b, inset). This increase agrees qualitatively with the observed size increase, since the anisotropy energy E_a and therefore T_B are expected to be related to size by a positive power. Below $T \approx T_F$, the $M(H,T)$ curves of the Ih nanocomposites

show irreversibility, that depends on the sample temperature and field history. Above $T \approx T_F$, the *M(H,T)* curves of the Ih nanohybrids are reversible, and can be described has having linear and partial saturation components, associated to the antiferromagnetic susceptibility and the uncompensated moment, respectively. For $T > T_B$, a paramagnetic-like doublet in the Mössbauer spectra of the Ih nanohybrids is observed, as expected for unblocked superparamagnetic particles. For temperatures below T_B, the Mössbauer spectrum is magnetically split in a sextet. As observed in the susceptibility, T_B identified with Mössbauer increases with the iron content. In sample Ih(6.5), the magnetic hyperfine field B_{hf} at 4.2 K is similar to that previously found for iron(III) oxyhydroxynitrate powders B_{hf} =450-460 kOe [2]), being lower than that of 6-line ferrihydrite. At the same time, the isome shift *QS* shows some differences when compared to that usually found in 6-line ferrihydrite (-0.06 mm/s), approaching for that fitted for schwertmannite (*QS*=-0.37 mm/s at 4.2 K).

References:

[1] U. Schwertmann, J. Friedl, and H. Stanjek, J. Coll. Interface Sci., **209** (1999) 215.
[2] U. Schwertmann, J. Friedl, and G. Pfab, J. Sol. State Chem., **126** (1996) 336.
[3] V. de Zea Bermudez, L. D. Carlos, and L. Alccer, Chem. Mater., **11** (1999) 569.
[4] D. Svergun, J. Appl. Cryst., **25** (1992) 495.

Figures:

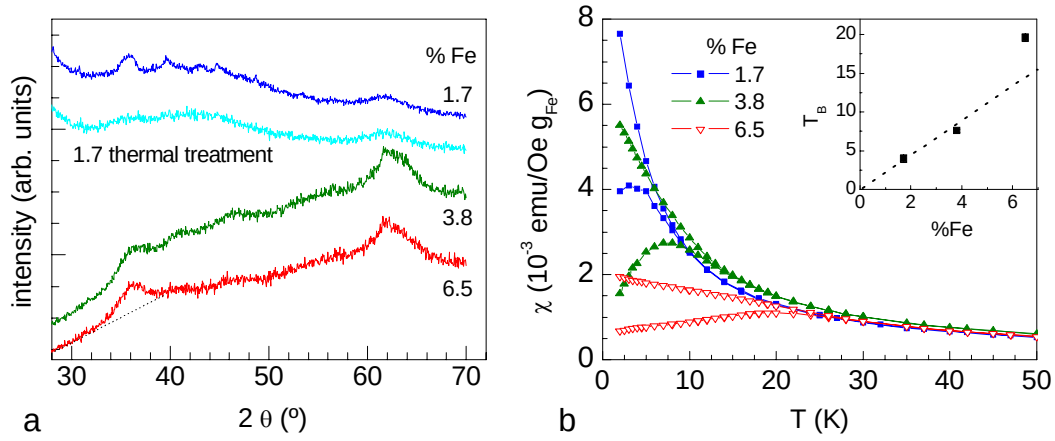

Fig 1. a. X-ray diffraction (XRD) patterns of Ih(x) nanohybrids and sample Ih(1.7) after a thermal treatment; b. dc susceptibility χ of Ih nanohybrids as a function of temperature. Inset shows the dependence of T_B with the iron content.

STUDY CONCERNING THE NANOBIOTECHNOLOGY OF OBTAINING OF COLLAGEN GELS FROM MARINE FISH SKIN AND YOUR RHEOLOGICAL CHARACTERISATION FOR USING IN DENTAL MEDICINE

Rodica Sirbu*, Minodora Leca, Anamaria Bechir*, Maris Maria*, Emilia Mihaela Cadar*****

*"Ovidius" University of Constanta, Faculty of Pharmacy, Romania
** University of Bucharest Romania
*** 30 - School of Constanta, Romania*

Type I fibrillar collagen is a triple-helix structure protein present in the skin and in cartilaginous tissues. The acknowledged disadvantages related to obtaining collagen by extraction from fish skin consist mainly in the persistence of pigments and fish odour, the denaturation temperature values being lower – usually under 30° C – which is a disadvantage concerning their use as bio-nanomaterials. Nonetheless, fish-derived collagens can be widely used due to their indisputable advantages:

- they are easier to extract and they have shown better performance compared to collagens extracted from mammals' skin;
- they bear a relatively low risk of containing unknown pathogens;
- the denatured collagen-based matrixes allow better tissue regeneration compared to the native collagen-based ones [1], and the reticulate matrixes derived from fish collagen are likely to contain partially denatured structures due to the lower denaturation temperature.

Although fish-derived collagen does not form high-viscosity gels, it is extremely convenient for some applications, such as micro-encapsulation or obtaining photosensitive coatings. Films and porous matrixes can be obtained from the collagen-based gels, as well as from those derived from animal skin. They can be successfully used in dental medicine for treating oral diseases – they form bio-absorbable membranes and matrixes and they can incorporate various active ingredients which can be subsequently released in order to obtain the expected therapeutic effects.

Depending on the treatment applied, we can distinguish between four categories of bionanotechnologies used for obtaining collagen from marine fish:

- basic and acid treatments [2];
- acid treatment [3, 4-6];
- enzyme treatment [5, 6];
- combined treatments.

This study aims at presenting the biotechnology used to obtain collagen-based gels from shark (Squalus acanthias) and brill skin, marine fish growing in the Black Sea. Due to the structure of its microfibres, the collagen can be considered a nanomaterial - in order to use collagen-based matrixes as biomaterial, rheological studies will be performed to prove their stability. In order that the triple-helix structure remains stable within these gels at room or human body temperature, they will be stabilized by reticulation.

Reticulation has been performed by using glutaric aldehyde at 4-6^{o}C for different concentrations of collagen derived from the two species of fish.

The rheological behaviour has been determined by using a rheoviscosimeter Haake VT 550 with the following layout: S_3 (MV1) sensors system, d_1 and d_2 measuring ranges, shearing speed range, $\dot{\gamma}$, between 1.17 and 1872 s^{-1}. The measurements have initially

been performed at a 25 ± 0.1^0C temperature, with a thermostatic time of 20 minutes, and then – using ice – at 20 ± 0.1^0C. In order to establish whether the dispersed systems show a time-dependant rheological behaviour or not, measurements have been performed when increasing and decreasing the shearing speed values, which allowed the tracing of the hysteresis loops for the film-forming systems with time-dependant rheological behaviour. The position of the two rheograms in figures 1 and 2 – meant to represent the hysteresis loop – proves that the gels obtained from shark skin (Fig. 1) and brill skin (Fig. 2) have a time-dependant rheological behaviour, namely strongly thixotropic, without structure recuperation at low shearing speed values.
The conclusions we have reached confirm the fact that the gels based on collagen derived from shark and brill skin have an ideal-plastic behaviour, which allows their use for creating different pharmaceutical formulations.

BIBLIOGRAPHY

1. M. Koide, K. Osaki, J. Konishi, K. Oyamada, T. Katakura, A. Takahashi and K. Yoshizato, J. Biomed. Mater. Res. **27**, 79 (1993).
2. T. Nagai and N. Suzuki, Food Chem. **68**, 277 (2000).
3. S. Rama and G. Chandrakasan, J. Biosci. **5**, 147 (1983).
4. S. Kimura, Y. Miyauchi and N. Uchida, Comparative Biochem. Physiol. **99B**, 473 (1991).
5. Y. Nomura, H. Sakai, Y. Iashii and K. Shirai, Biosci., Biotechnol., Biochem. **60**, 2092 (1996).
6. Y-.X. Shen, Z. Wang, Y.-F. Fu and Y. Zhao, IFT Annual Meeting, July 15-20 2005, New Orleans, Louisiana, U. S. A.

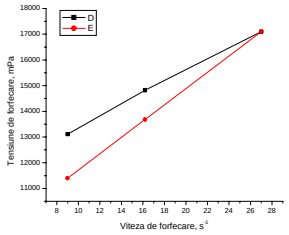

Figure 1. Rheograms obtained when: D – increasing; E – decreasing the shearing speed values

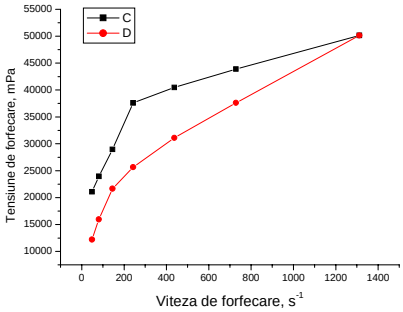

Figure 2. Hysteresis loop obtained for the brill skin-derived gel when:
D – increasing; E – decreasing the shearing speed values

PRODUCTION AND CHARACTERIZATION OF NANOCOMPOSITE AMORPHOUS CARBON THIN FILMS

A. J. Martins, P. Soares, V. Teixeira*, J. Carneiro, F. Cerqueira

Physics Department, University of Minho, Campus de Azurem, 4800-058 Guimaraes, Portugal

*e-mail address: anajoaom@gmail.com pmcsoares@gmail.com vasco@fisica.uminho.pt
Phone: +351 253510400/65; Fax: +351 253510401

Abstract

Carbon based films can combine the properties of solid lubricating graphite structure and hard diamond crystal structure, i.e., high hardness, chemical inertness, high thermal conductivity and optical transparency without the crystalline structure of diamond. Issues of fundamental importance associated with nanocarbon coatings are reducing stress, improving adhesion and compatibility with substrates. In this work new nanocomposite coatings with improved toughness based in nanocrystalline phases of metals and ceramics embedded in amorphous carbon matrix will be developed: nc-MeNxCy/a-C(Me) with Me =Cu, Al, Ti, Si etc.. These novel coating architectures will be adopted with the objective to decrease residual stress, improve adherence and fracture toughness, obtain low friction coefficient and high wear-resistance. The characterisation of the coating's physico-mechanical properties will be presented in order to understand the influence of the deposition parameters and metal content used within the a-C matrix in the coating properties. Film microstructure will be characterized by XRD and Raman Spectroscopy. In order to characterize morphology SEM and AFM will be used. Contact angle and surface energy will be also analysed for different surface layers. Adherence will be studied by scratch test and hardness by Nanoindentation. Residual stresses in the produced coatings will be analysed by bending technique.

Acknowledgements:

To Fundação para a Ciência e Tecnologia by the financial support done through the research project POCTI/CTM/61589/2004: "NANOCARBON-Nanocomposite Metal-Ceramic Amorphous Carbon Thin Coatings"

Targeting Biotech Drugs
Nanosized Lipid Particles versus Drug Nanocrystals

Eliana B. Souto[1,2], *Rainer H. Müller*[2]
[1] *Faculty of Health Sciences, Fernando Pessoa University, Rua Carlos da Maia, 296, 4200-150 Porto, Portugal*
[2] *Department of Pharmaceutical Technology, Biopharmaceutics and NutriCosmetics, Free University of Berlin, Kelchstrasse 31, 12169 Berlin, Germany*
eliana@ufp.pt

Nanotechnology and, in particular, the development of nanosized delivery systems for biotech drugs (namely peptides, proteins and oligonucleotides), is a multidisciplinary field undergoing exponential development in the latest years [1-3]. The rate of these developments has been dictated in parallel by the progress of biotechnology. Biotechnological techniques have expanded the variety of therapeutically active biotech drugs, which are nowadays the molecules of primary interest in the pharmaceutical market. Peptides, proteins and oligonucleotides have been formulated in innovative colloidal delivery systems with the aim to [4-7]: (i) achieve a modified-release profile (controlled, prolonged or targeted depending on the therapeutic needs), (ii) reduce adverse-side effects due to a non-targeted distribution and delivery to the site of action, (iii) increase drug bioavailability, (iv) increase patient compliance to the therapeutics, (v) optimize a more comfortable administration route, as well as to (vi) decrease the cost of the therapeutics if possible [3]. The present review presents the usefulness of nanosized lipid particles and the drug nanocrystal systems to target biotech drugs intended for different administration routes.

Nanosized lipid particles are derived from o/w emulsions by replacing the liquid lipid (oil) by a solid lipid, i.e. a lipid being solid at room and simultaneously at body temperature [2]. In the beginning of the nineties the so-called solid lipid nanoparticles (SLN™) have been developed. Due to their solid matrix, drug release from these particles can be modulated, which could be exploited to optimize the blood profile. The distinct advantage of SLN is that they fulfil the pre-requisites to market a product. The excipients used are of recognized status, i.e. all lipids and surfactants used for oral and parenteral dosage forms can be employed. The excipients are of low costs and large scale production is possible by high pressure homogenization lines, which are already approved for pharmaceutical industry, for example for the production of parenteral emulsions such as Intralipid®. At the turn of the millennium, a second generation of nanosized lipid particles was developed. These are the nanostructured lipid carriers (NLC™), which are prepared not from a solid lipid only but from a blend of a solid lipid with an oil and can be used for the same purposes as SLN. The main advantage of NLC over SLN is the higher loading capacity due to a less organized lipid matrix creating a higher number of voids and vacancies available for drug entrapment/encapsulation.

Another approach to formulate poorly soluble drugs for oral and parenteral administration is the development of drug nanocrystals [2,5]. This alternative can be used for drugs for which the dissolution velocity in water is an absorption/bioavailability limiting step. It is well known that micronization of a drug powder increases its dissolution velocity. For this purposes, drug nanocrystals decrease in size one dimension further by means of a nanonization process. Another interesting feature is the increased saturation solubility of nanonized drugs compared to micronized or larger sized powders. Both increased surface area and increased saturation solubility enhance the dissolution velocity. For some drugs, the drug nanocrystal principle proved to be highly effective. For example, the oral bioavailability of danazol could be improved from 5.1% to 82.3% when replacing the microsuspension by nanosuspension [8].

Precipitated drug particles exhibit very often the tendency to continue crystal growth to the size of micrometer crystals. Depending on the precipitation conditions these particles can be completely amorphous, partially amorphous or completely crystalline. To ensure the long term stability of the crystalline status, the easiest approach is to have particle in the low energy crystalline modification. Amorphous or partially amorphous particles bear the risk re-crystallization of this amorphous fraction followed by decrease in bioavailability. Both problems, avoidance of further crystal growth and uncertainty of crystalline/amorphous state, can be solved by combining the precipitation with a second high energy addition step. The precipitated particle suspension is subsequently homogenized which can basically preserve the size range of the particles obtained after the precipitation step. This annealing process converts all precipitated particles to crystalline material. This removes all concerns about physical stability of amorphous material. The drug nanocrystals possess a definite crystalline state. In comparison to the nanosized lipid particles, drug nanocrystals have the advantage of being easier to produce. Microsuspensions can be transferred to nanosuspensions simply by pearl milling or by high pressure homogenization [2]. On the other hand, both SLN and NLC are composed of a lipid matrix, and lipids are known to promote absorption of some drugs through e.g. oral route [9]. Therefore, another purpose of the present review was to compare the efficiency of nanosized lipid particles versus drug nanocrystals to enhance bioavailability of biotech drugs with practical relevance for potential market products. The various analytical techniques to characterise these colloidal carriers and to predict their long-term stability are also addressed, i.e. means Coulter Counter technology, photon correlation spectroscopy, laser diffractometry, light and electron microscopy and zeta potential measurements. The techniques are critically reviewed regarding advantages and limitations.

The authors present a new approach to formulate biotech compounds using nanosized lipid particles and the drug nanocrystal technology. The applications of such production procedures as feasible approaches systems for nanomedicine are emphasized. Parameters to control the nanosystem composition, its size, shape and functionality are discussed ans the biological effects of well-optimized nanoparticulate systems are also addressed when delivered by different administration routes. The background knowledge of these studies will be of great relevance in the design of safer nanosystems for biotech drugs. Analysis of the theoretical and practical applications of these systems is an important aspect that will enable rapid development in this emerging field of nanotechnology.

References:

[1] Kayser O, Lemke A, Hernandez-Trejo N, Curr Pharm Biotechnol 6 (2005) 3.
[2] Muller RH, Keck CM, J Biotechnol 113 (2004) 151.
[3] Salmaso S, Bersani S, Semenzato A, Caliceti P, J Nanosci Nanotechnol 6 (2006) 2736.
[4] Almeida AJ, Souto E, Adv Drug Deliv Rev 59 (2007) 478.
[5] Muller RH, Runge S, Ravelli V, Mehnert W, Thunemann AF, Souto EB, Int J Pharm 317 (2006) 82.
[6] Muller RH, Runge SA, Ravelli V, Thunemann AF, Mehnert W, Souto EB: Eur J Pharm Biopharm (2008) in press.
[7] Brioschi A, Zenga F, Zara GP, Gasco MR, Ducati A, Mauro A, Neurol Res 29 (2007) 324.
[8] Liversidge G, IIR Drugs Delivery Partnerships™ Meeting, Workshop In; Cologne/Germany. 2003
[9] Charman WN, J Pharm Sci 89 (2000) 967.

NOVEL ANIONOPHORES FOR BIOSENSOR APPLICATIONS CHARACTERISATION OF IMIDAZOLIUM PROTOPHANES AND CYCLOPHANES ON GOLD SURFACES

Christian Sporer [1,2,3], *Lucia Casal*[4], *David Caballero*[2,5], *Abdelhamid Errachid* [1,2], *Ermitas Alcalde*[4], *Josep Samitier*[1,2,3], *Mª. Lluisa Pérez-García*[4]

[1] Centro de Investigación Biomédica en Red en Bioingeniería, Biomateriales y Nanomedicina (CIBER-BBN), España. [2] Grup de Nanobioenginyeria, Institut de Bioenginyeria de Catalunya (IBEC), Josep Samitier 1-5, 08028 Barcelona, España. [3] Departament d'Electrònica, Universitat de Barcelona, c/ Martí i Franquès 1, 08028 Barcelona, España. [4] Departament de Farmacologia i Química Terapèutica, , Facultat de Farmacia i Institut de Nanociència i Nanotecnologia UB (IN2UB) Universidad de Barcelona, Barcelona, España. [5] Parc Científic de Barcelona, c/ Josep Samitier 1-5, 08028 Barcelona, España.

csporer@pcb.ub.es, mlperez@ub.edu

The development of miniaturized sensor devices for the detection and analysis of biologically relevant molecules is a rapidly growing research field with particular importance in many areas of modern life sciences like medicine technology, therapeutics, farmaceutical research and biosciences. In such sensors, one of the fundamental principles of signal generation relies on molecular recognition, where specific interactions between an organic host and a guest molecule are present; DNA sensor arrays or sensors based on antigen /antibody interactions are most prominent examples.[1]

During the last decades a variety of organic host molecules have been described that are also capable to recognize and to interact selectively with small molecules or inorganic ions. Among these, by far more cation host molecules are described than anions receptors.[2]

Recently it has been shown that organic compounds based on positively charged imidazolium molecules can act as efficient host for anions.[3,4] These imidazoliophanes interact reversible with oxoanions or halides and can serve as models for anion recognition. [4]
We have synthesized a series of novel anionophores based on imidazolium protophanes and heterocyclophanes (see figure 1). NMR titration experiments in polar media reveal their good anion recognition capacity and selectivity of the compounds towards phosphate over carboxylates or halides.

Modification of the anionophores with alkylthioether anchor groups allows them to be deposited onto gold surfaces of sensor electrodes.

Here we report on the results of surface deposition of the novel amphiphilic imidazolium heterocyclophanes and protophanes on gold electrodes and their characterization by techniques like Atomic Force Microscopy (AFM), Time-of-Flight Secondary Ion Mass Spectrometry (TOF-SIMS) and Contact angle measurements.

References:

[1] Pochinger-Kuller, U. E., *Chemical Sensors and Biosensors for Medical and Biological Applications*, Wiley VHC, Washington, **1998**.
[2] a) Bianchi, E. Garcia-España and K. Bowman-James (Eds.), *Supramolecular Chemistry of Anions*, Wiley-VCH, New York, 1997. b) F. P. Schmidtchen, M. Berger Chem. Rev. **1997**, 97, 1609-1646
[3] J. Yoon, S. Kyung Kim, N. J. Singh, K. S. Kim *Chem. Soc. Rev.*, **2006**, *35*, 355–360
[4] E. Alcalde, N. Mesquida, L. Pérez-García *Eur. J. Org. Chem.* **2006**, 3988–3996

Figures:

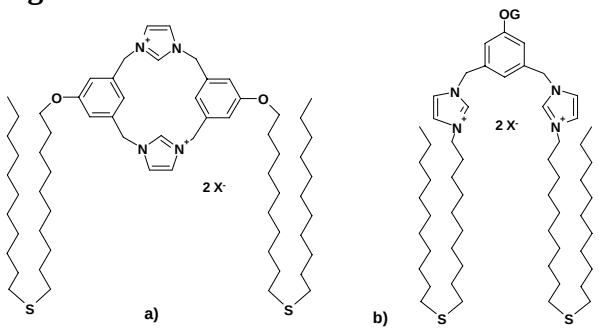

Figure 1: Chemical structure of heterocyclophanes (a) and protophanes (b)

Acknowledgements. This worked has been suported by the Ministerio de Educación y Ciencia (MEC) trough projects TEC2005-07996-C02-02/MIC and CTQ2006-11821/BQU, and the Generalitat de Catalunya 2005SGR00158. L.C. thanks the UB and the MEC for predoctoral grants.

TEM STUDIES OF CRYSTALLINE HYDROXYL AND FLUORO-APATITE IN BONE TISSUES

A. Caraiane[1], V. Ciupina[1], G. Prodan[1], S. Zamfirescu[1], M. Prodan[1], I.M. Stanescu[1], V. Mocanu[1], C. Stefanov[1], E. Vasile[2]

[1] Ovidius University of Constanta, Mamaia Avenue No.124, 900527
[2] Metav CD, Bucharest, C.A. Rosetti No. 31, 020011

We study the presence of apatite on different bone tissues and characterize this material by electron microscopy and additional techniques. First group of tissue was dental tissues, which exhibit a crystalline form of hydroxyl and fluoro-apatite. Electron diffraction and XRD data confirm presence of polycrystalline like material. The morphological characteristics of tissue are investigated by using TEM micrograph and show apatite nanocrystal arranged around osteocyte cell, that are apatite generator in tissue. The dimension of this cell is also investigated. Also the bone tissue is examined. Samples are prepared for TEM by included small piece of material in epoxy resin and cut thin section by means of ultramicrotome equipped with diamond knife. Thickness of ultrathin sections are kept around 50-60nm. The size of sections are keep small, around 500 μm and less, to eliminate the artifact that appear on section due to hardness of material. Structural data was completed by examine the chemical composition by means of EDX technique.

Keywords: TEM, XRD, EDX, apatite, osteocyte

OPTICAL CONDUCTIVITY OF GRAPHENE BEYOND THE DIRAC CONE APPROXIMATION

T. Stauber and N. M. R. Peres
Centro de Física e Departamento de Física, Universidade do Minho, P-4710-057 Braga, Portugal
Contact@E-mail

We calculate the conductivity of a clean graphene sheet at finite temperatures starting from the tight-binding model. We obtain a finite value for the dc-conductivity at zero temperature. For finite temperature, the spontaneous electron-hole creation, responsible for the finite conductivity at zero temperature, is washed out and the dc-conductivity yields zero. Our results are in agreement with calculations based on the field-theoretical model for graphene.

We then compute the optical conductivity of graphene beyond the usual Dirac cone approximation, i.e., we include non-linear corrections to the density of states. The effect of next nearest neighbour hopping is also discussed. We find that the additional terms to the current operator do not contribute to the conductivity and that modifications only enter through the modified energy dispersion.

Using the full conductivity of clean graphene, we determine the transmissivity and reflectivity of light that is scattered from two media with different permittivity and graphene at the interface. Our results are relevant for optical experiments in the visible frequency range.

NANOMECHANICAL DEVICES: ULTRASENSITIVE SENSORS OF MOLECULAR RECOGNITION AND CONFORMATIONAL CHANGES OF BIOMOLECULES.

Javier Tamayo, Johann Mertens, Daniel Ramos, María Arroyo and Montserrat Calleja
Institute of Microelectronics of Madrid (IMM-CNM, CSIC), Isaac Newton 8 (PTM), Tres Cantos, 28760 Madrid, Spain
jtamayo@imm.cnm.csic.es

In the last years, a large variety of ultrasensitive nanomechanical sensors that have been developed and used as biological sensors. The results demonstrate that rapid detection of biomolecules with high sensitivity and specificity without need of sample pre-treatment and labeling with fluorescent dyes. The applications range from protein and DNA detection to detection of single pathogens. This technology has the potential to revolutionize the fields of molecular biology and preventive medicine. However, it is still needed a major multidisciplinary convergence and development of nanofabrication techniques, measurement schemes, theory, large scale integration of nanodevices, optical and electrical components & microfluidics. In addition, all of these high cost developments must lead to a final technology suitable for mass production at low cost. Here, we present results in several of the battle fronts described above faced in collaboration with several multidisciplinary scientific and industrial partners. The results can be split into dynamic and static modes nanomechanical sensors. In the dynamic mode, the nanomechanical structure resonates at its natural frequency, which sensitively changes when the resonator interacts with the biomolecules present in the sample [1,2]. In the static mode, it is monitored the deflection of a cantilever which changes as a consequence of the surface stress originated from molecular adsorption.

Dynamic Nanomechanical Biosensors

In order to develop nanomechanical devices for ultrasensitive pathogen detection, we have measured the effect of the bacteria adsorption on the resonant frequency of microcantilevers as a function of the adsorption position and vibration mode [3,4]. The resonant frequencies were measured from the Brownian fluctuations of the cantilever tip. We found that the sign and amount of the resonant frequency change is determined by the position and extent of the adsorption on the cantilever with regard to the shape of the vibration mode [5,6]. To explain these results, a theoretical one-dimensional model is proposed. We obtain analytical expressions for the resonant frequency that accurately fits the data obtained by the finite element method. More importantly, the theory data shows a good agreement with the experiments. Our results indicate that there exist two opposite mechanisms that can produce a significant resonant frequency shift: the stiffness and the mass of the bacterial cells. The combination of high vibration modes and the confinement of the adsorption to defined regions of the cantilever allow detection of single bacterial cells by only measuring the Brownian fluctuations, i.e., without any use of external energy. These results are relevant in order to obtain reproducible and sensitive nanomechanical sensors. The results of this study have been applied for a new design of arrays of nanomechanical resonators, with a volume of about 10^4 times smaller for ultrasensitive detection of nucleic acids. The fabricated arrays have alternate nanomechanical resonators with different sensitized regions to obtain a double signature of the target based on the mass and stiffness of the molecule. We have been able to detect DNA hybridization at the level of few femtograms in air and without any external excitation, which implies one of the highest sensitivities obtained in these conditions.

Static Nanomechanical Biosensors

We show two relevant applications of nanomechanical biosensors: functional genomics and bionanomachines. In the first case, we show that adsorption of water on highly-packed self-assembled monolayers of single stranded (ss) DNA has an extraordinary effect on the intermolecular interactions. We have followed the process by measuring the nano-scale bending that a silicon microcantilever, on which the ssDNA monolayer is attached, experiences under controlled relative humidity. More importantly, the hydration-induced tension undergoes dramatic changes when the monolayer interacts with either complementary or single mismatched ssDNA targets. The analysis of the results suggests that the tension of the nucleic acid films is mainly governed by the hydration forces originated in the intermolecular channels. The discovered phenomena open the door for the development of a novel label-free DNA biosensor with specificity to single mutations and a sensitivity of at least ten times higher than the label-dependent DNA microarrays [7]. In the second case, bionanomachines such as chaperonines are immobilized on the cantilever. The conformational changes driven by the ATP hydrolysis lead to measurable cantilever fluctuations. This technique can provide new insight about the dynamics of molecular motors that have been elusive so far.

D.R. acknowledges the fellowship funded by the Autonomic Community of Madrid. This research was supported by Spanish Ministry of Science under grant No. TEC2006-10316 and by Autonomic Community of Madrid under grant No. 200550M056.

References:

[1] J. Tamayo, Nature Nanotechnology **2** (2007) 342.
[2] J. Tamayo, M. Calleja, D. Ramos and J. Mertens, Physical Review B **76** (2007) 180201(R).
[3] D.Ramos, J.Tamayo, J. Mertens, M. Calleja and A. Zaballos, Journal of Applied Physics **100** (2006) 106105.
[4] D. Ramos, J. Tamayo, J. Mertens, M. Calleja, L.G. Villanueva and A. Zaballos, Nanotechnology **19** (2008) 035503.
[5] J. Tamayo, D. Ramos, J. Mertens and M. Calleja, Applied Physics Letters **89** (2006) 224104.
[6] H. Craighead, Nature Nanotechnology **2** (2007) 18.
[7] J. Mertens, C. Rogero, M. Calleja, D. Ramos, C. Briones, J.A. Martín-Gago and J. Tamayo, submitted.

Mechanical Properties of Nanocrystalline and Ultrafine Grained Steel Obtained by Mechanical Milling

R. Tejedor[1]; R. Rodríguez-Baracaldo[1,2]; J. A. Benito[3,4]; J. M. Cabrera[1,4]; J. M. Prado[1,4]

1 Department of Materials Science and Metallurgical Engineering, ETSEIB, Universitat Politècnica de Catalunya, Av. Diagonal 647, 08028 Barcelona, Spain
robert.tejedor@upc.edu
2 Departament of Engineering, Universidad Nacional de Colombia, Campus la Nubia, Manizales, Colombia
3 Department of Materials Science and Metallurgical Engineering, EUETIB, Universitat Politècnica de Catalunya, Comte d'Urgell 187, 08036 Barcelona, Spain
4 Centre Tecnològic de Manresa, CTM, Av. Bases de Manresa 1, 08240, Manresa, Spain.

ABSTRACT- The stress-strain response of steel (0.05 and 0.6 wt.% C) obtained by a warm consolidation process from mechanically milled powder has been studied by means of compression tests. The samples were consolidated and subsequently heat treated at different temperatures in order to obtain ferritic grain sizes within the nanocrystalline and ultrafine grained regimes.

INTRODUCTION: In recent years, the mechanical behavior of nanocrystalline (NC) and ultrafine grained (UFG) iron (Khan et al [2000]; Ma et al. [2003]) and steel (Zhao et al [2006]; Murty al. [2006]) has been studied. High strength and low ductility were observed, especially in the NC regime and UFG iron. In the case of UFG steels with medium carbon content (0.45-0.6 wt.%), a small amount of tensile uniform elongation can be achieved.

PROCEDURES, RESULTS AND DISCUSSION: Iron powder of commercial purity was severely deformed in a ball mill for 52 hours together with a small amount (0.8 wt.%) of EBS wax (Benito et al. [2007]). In the case of the 0.05 wt.%C steel specimens, the same iron powder was deformed for 17 hours with no presence of wax. The both kind of powders were first cold compacted at 1300 MPa and subsequently warm consolidated at temperatures between 425ºC and 500 ºC under a pressure of 850 MPa for 1 hour. Subsequent heat treatments were applied in both cases to obtain the desired ferritic grain sizes. All the consolidation and heat treatment temperatures are listed in Table 1 together with the corresponding grain sizes and mechanical properties. In all cases the relative density of samples was above 96%.

In NC samples the ferrite grains were randomly oriented and quite homogeneous in size (Fig. 1A and 1C). In the UFG samples a wider distribution of the ferrite grain size was found, so grains larger than the average were easily observed (Fig. 1B).

The true stress-strain curves obtained by compression test are shown in Fig. 2. The NC 0.6 wt.%C steel samples showed high strength and low ductility as the samples failed with low plastic deformation. However, the NC 0.05 wt.%C steel showed a better response since it was deformed up to a plastic strain of 42%. The samples underwent work hardening up to a strain level of 3.5%. From this point, a slight flow softening appeared until the end of the test. This effect has been related to the beginning of dislocation annihilation in the deformed NC grains (Wei et al [2004]). In the low UFG regime, the steel samples showed an increase in the total plastic strain (80%) although the work hardening capacity was not enhanced. Only when the ferritic grain size was around 1 μm the steel showed large strain hardening.

References:

Benito, J.A., Rodríguez, R., Cabrera, J.M., Prado, 2007, J.M., J. Mat. Sci., 42, 1757.
Khan, A.S., Zhang, H, Takacs, L., 2000, Int. J. of Plas., 16, 1459.
Ma, E., Jia, D., Ramesh, K.T, 2003, Acta Mater. 51, 3495.

Murty, N., Torizuka, S., Muramatsu, E., Nagai, K., 2006, Script. Mater. 55, 751.
Wei, Q., Kecskes, L., Jiao, T., Hartwig, K:T:, Ramesh, K.T., Ma, E:, Acta Mater., 52, 1859.
Zhao, M., Hanamura, T., Qiu, H., Nagai, K., Yang, K., 2006, Script. Mater. 54, 1385.

Figures:

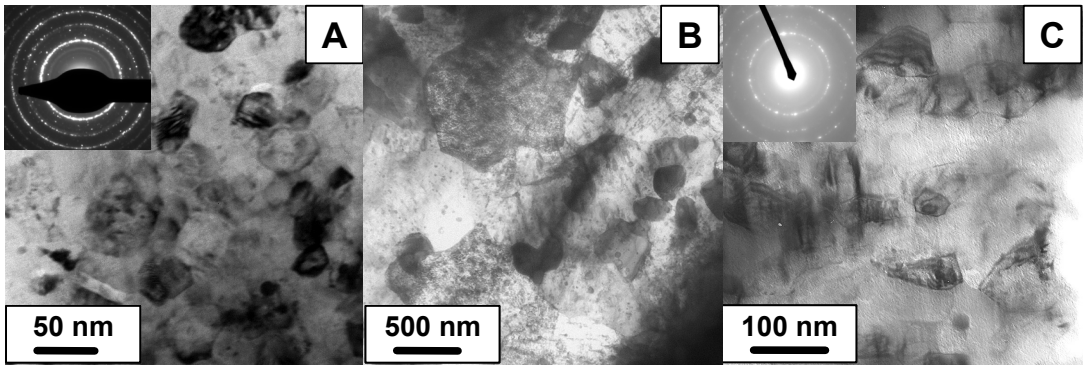

Figure 1. TEM micrographs showing the microstructure of A) 0.6 wt.%C steel with average grain size of 46 nm; B) 0.6 wt.%C steel with average grain size of 1 μm; C) 0.05 wt.%C steel with average grain size of 96 nm.

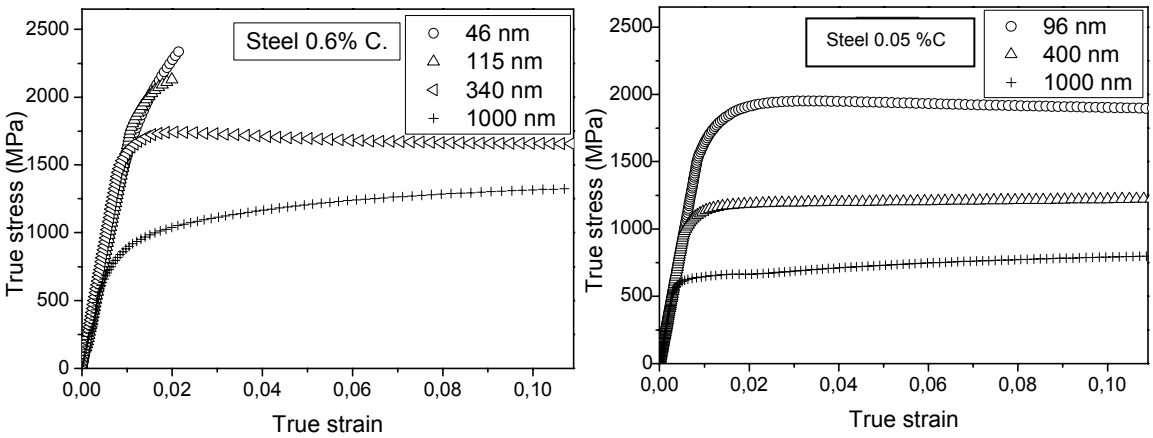

Figure 2. True stress-true strain curves obtained by compression tests for nanocrystalline and ultrafine grained samples.

Table 1: Consolidation and Heat Treating Temperatures, Ferritic Grain Size and Mechanical Properties for the 0.05 and 0.6 %C Steel Samples. WC: Warm Compaction, HT: Heat Treated, Y.S.: Yield Strength, M.S.: Maximum Strength.

Steel	Consolidation Procedure	Average grain size (nm)	$HV_{0.2}$ (GPa)	Y.S (MPa)	M.S (MPa)	Plastic Strain (%)	Strain Hardening (%)
0.6 %C	WC 460 °C	46 ± 21	8.4 ± 0.4	2040	2340	2.35	2.35
0.6 %C	WC 500 °C	115 ± 45	6.4 ± 0.4	1880	2140	2.1	2.1
0.6 %C	WC 500 °C + HT 700°C	340 ± 220	4.7 ± 0.2	1635	1740	80	2.2
0.6 %C	WC 460 °C + HT 775°C	~1000	4.1 ± 0.2	720	1390	80	35.2
0.05 %C	WC 500 °C	96 ± 36	6.0 ± 0.4	1724	1951	42	3.5
0.05 %C	WC 500 °C + HT 700°C	400 ± 215	4.2 ± 0.3	1095	1238	80	22.8
0.05 %C	WC 460 °C + HT 750°C	~1000	2.5 ± 0.2	620	870	80	47.9

POWDER COATINGS: A STUDY OF PROPERTIES BY ADDITION OF NANORESINS.

Ángel Tolosa [1], *Inmaculada Iñigo, Consuelo Moren, Natividad Alcón.*
Asociación Industrial de Óptica, Color e Imagen, AIDO, Parque Tecnológico, C/ Nicolás Copérnico, 7, 46980, Paterna (Valencia), Spain
atolosa@aido.es

Since the past decade until nowadays the interest in the powder coating development has been growing due to some characteristics that make this kind of paint an important alternative to traditional liquid paints.

A powder coating [1] consists in finely ground plastic particles formed from resin, crosslinker (in thermoset powders), pigments and extenders and various flow additives and fillers to achieve specifics properties. When the applied powder is heated, melt to form a continuous film; typically very durable and resistant films. One of most interesting characteristics of powder coating is that they are applied as a dry film, i.e., they contain very little, if any, Volatile Organic Compounds (VOC), so the raw material is literally a powder, mixed, dry extruded and ground into the final material. Then thermoset powder coatings are applied on the substrate by electrostatic or triboelectric spray application and cured by heat.

In this work, the changes of several optical and mechanics properties when we add different percentages of nanoresin to the paint formula have been studied and will be discussed. Nanoresin employed has been silica reinforced solid low molecular weight (type 2.5) epoxy resin. The silica phase consists of surface modified SiO2 nanospheres —average diameter of 20 nm— with a narrow particle size distribution with maximum diameter of 50 nm. Despite the high SiO_2 content (see Table 1), this nanoresin has a low melt viscosity due to the agglomerate-free colloidal dispersion of nanoparticles in the resin.

As nanoresin used is an epoxidic type of resin, we formulated a standard epoxy-polyester hybrid powder coating (50/50) to compare the results obtained with and without nanoresin; the standard epoxy resin employed has the same chemical properties than epoxy nanoresin.

In order to investigate certain optical properties, reflectance and colour measurements [2] were carried out by means of Perkin Elmer Lambda 800 UV-VIS spectrophotometer; and gloss measurements at 20º, 60º and 85º [3]. The mechanical properties evaluated were the flexibility and adhesion [4], [5] and impact resistance [6].

References:

[1] Powder Coater's Manual: http://www.coatings.de/pcmanual/pcmanual.cfm
[2] Commission Interationale de l'Eclaire (CIE), Colorimetry, CIE 15:2004, 3rd edition.
[3] Paints and varnishes: Determination of specular gloss of non metallic paint films at 20 degrees, 60 degrees and 85 degrees, ISO 2813:1994.
[4] Paints and varnishes: Bend test (conical mandrel), ISO 6860:2006.
[5] Paints and varnishes: Cross-cut test, ISO 2409:2007.
[6] Paints and varnishes:Rapid-deformation (impact resistance) tests. Part 1: Falling-weight test, large-area indenter, ISO 6272-1:2002.

The authors thank Ministerio de Industria, Turismo y Comercio of Spain for financial support (PROFIT, nº exp. FIT-020400-2007-21).

Figures:

TABLE 1. Main properties of nanoresin employed in the study.

Property	**Units**	**Typical values**
Base resin		Low molecular weight “type-2,5”epoxy resin
Appearance		Yellowish flakes
SiO2 – content	[wt%]	32
Melt viscosity @150 ºC	[Pas]	50
Softening point	[ºC]	93
Epoxy equivalent weight	[g/eq]	1050

PAMAM DENDRIMERS USED AS VECTORS FOR GENE DELIVERY INTO MESENCHYMAL STEM CELLS

[1]José L. Santos, [1]Elena Oramas, [2,3]Ana Paula Pêgo, [2,3]Pedro L. Granja, [1]Helena Tomás
[1]Centro de Química da Madeira, Dep. Química, Universidade da Madeira, Campus Universitário da Penteada, 9000-390 Funchal, Portugal; [2]INEB – Instituto de Engenharia Biomédica, Divisão de Biomateriais, Rua do Campo Alegre, 823, 4150-180 Porto, Portugal; [3]Universidade do Porto, Faculdade de Engenharia, Dep. Eng. Metalúrgica e Materiais, Rua Dr. Roberto Frias s/n, 4200-465 Porto, Portugal.
lenat@uma.pt

The gene therapy area has expanded its search to find high-efficient and nontoxic nonviral gene delivery vectors. Numerous materials (such as cationic liposomes and polymers) have been studied as potential vectors for gene delivery with varying results. Polyamidoamine (PAMAM) dendrimers with primary amino surface groups were shown to have the inherent ability to associate, condense and efficiently transport DNA into a wide number of cell types[1]. A comparative study with several representative transfection systems (that included branched and linear polyethyleneimines, polyamidoamine and poly(propyleneimine) dendrimers, poly[N-ethyl-4-vinyl pyridinium bromide, as well as copolymers and lipid based reagents) has shown that transfection efficiency strongly varies with the kind of vector molecule used but also with the type of cells (10 different cell lines were tested)[2].

In the present work, our main goal was to perform a systematic evaluation of the transfection efficiency achieved by different generations of PAMAM dendrimers using mesenchymal stem cells (MSCs) due to the relevance of these cells in bone regeneration applications and in tissue engineering. A β-Galactosidase reporter gene system was used and several experimental conditions were assayed.

Since the transfection efficiency obtained was always very low, it was hypothesized that even a low transfection level could however be sufficient for the envisaged application, i.e., to improve the *in vitro* differentiation of MSCs towards the osteoblastic lineage. To confirm this possibility, MSCs were genetically engineered to express the human BMP-2 gene using PAMAM dendrimers. Differentiation of MSCs was studied through the analysis of established markers of the osteoblastic phenotype, including the activity of alkaline phosphatase, secretion of osteocalcin, and deposition of a calcified matrix. Results clearly pointed out that the systems PAMAM dendrimers/hBMP-2 plasmid DNA strongly induced *in vitro* differentiation of MSCs to the osteoblast phenotype suggesting that other low toxic and low efficient nonviral vectors can actually be used with efficacy in orthopaedics, despite their low transfection efficiency.

The Portuguese Foundation for Science and Technology (FCT) is acknowledged for founding through the Project DENDRALGENE - PTDC/SAU-BEB/71161/2006 and J. L. Santos PhD scholarship (SFRH/BD/19450/2004). Authors are also grateful to Prof. Dr. Yasuhiko Tabata for kindly providing the hBMP-2 plasmid DNA.

References:

[1] Guillot-Nieckowski M, Eisler S, Diederich F., New J Chem, **31** (2007) 1111.
[2] Gebhart CL, Kabanov AV., J Control Release, **73** (2001) 401.

Poster

ANALYSIS OF COAGULATION–FRAGMENTATION EQUATIONS: THREE ERAS OF MICELLIZATION

Francisco Torrens, Gloria Castellano
Institut Universitari de Ciència Molecular, Universitat de València, Edifici d'Instituts de Paterna, P. O. Box 22085, 46071, and Instituto Universitario de Medio Ambiente y Ciencias Marinas, Universidad Católica de Valencia San Vicente Mártir, *46003, València, Spain*
francisco.torrens@uv.es

The existence of single-wall carbon nanotubes (SWNTs) in organic solvents in the form of clusters is discussed [1]. A theory is developed based on a *bundlet* model for clusters describing the distribution function of clusters by size [2]. The phenomena have a unified explanation in the bundlet model of a cluster, in accordance with which the free energy of an SWNT involved in a cluster is combined from two components: a volume one, proportional to the number of molecules n in a cluster, and a surface one, proportional to $n^{1/2}$ [3]. The model yields an activation barrier and predicts that pores with a radius below a certain critical value are unstable, while those above this radius will grow indefinitely until the membrane ruptures [4]. During the latter stage of the fusion process, the dynamics were governed by the displacement of the volume of liquid around the fusion site [5]. Based on a simple kinetic model *micellization* of rod-like aggregates occurs in three separated stages [6]. A convenient relation is obtained for $<n>$ at transient stage; at equilibrium another relation determines binding energy a. A relation with surface dilatational viscosity is obtained. The model predicts that pores with a radius below a certain critical value are unstable. The *line graphs* in Figure 1 depict $<k>^2 r_k$ as a function of $x = k/<k>$ for the times $\tau = 0.5\times10^5$, 10^5 and 1.5×10^5. They are nearly superimposed on top of each other. The *heavy dots* correspond to the plateau time $\tau = 20$, so the change in the distribution shape over the whole time span $20 < \tau < 1.5\times10^5$ is not rather great. Figure 2 illustrates the evolution of the size distribution for the rescaled binding energy $\varepsilon = e^{-\alpha}/\rho = 4.54\times10^{-4}$ (corresponding to $\alpha = 10$ and $\rho = 0.1$), where the binding energy of the k cluster $\varepsilon_k = (k-1)\alpha k_B T$, and ρ is the ratio number of particles/number of spaces. It records the time-dependent behaviour of the average cluster size $<k>$. It is a log-log plot of $<k>/e$ *vs.* τ. It reveals an initial rapid growth of $<k>$ to a *plateau value* close to e, roughly located in the interval $10 < \tau < 100$. In the subsequent growth after the plateau, large clusters with $k >> 1$ eventually appear. Figure 2 indicates that by time $\tau = 5\times10^4$, k clusters having $<k> \approx 10$ are prevalent. In the time interval $2\times10^4 < \tau < 5\times10^5$, the log-log plot of $<k>/e$ *vs.* τ is close to a straight line of slope 1/2. This strongly supports the existence of a self-similar stage of the kinetics. Notice that the average cluster size $<k>$ corresponding to the intermediate transient (Figure 2, *dotted line*) approaches the asymptotic value (*straight line* of slope 1/2). Provisional conclusions follow. (1) Based on a simple kinetic model, *micellization* of rod-like aggregates occurs in three separated stages: (a) many clusters of small size are produced while the number of monomers decreases sharply; (b) aggregates are increasing steadily in size, and their distribution approaches a self-similar solution of the diffusion equation; (c) a simple mean-field Fokker–Planck equation describes the third era until the equilibrium distribution is reached. In order to validate the theory by an experiment, it would be important to measure the average cluster size as a function of time. To determine the time scale, one needs a measure of the cluster diffusion coefficient d that was set equal to 1. A convenient relation in dimensional units is $<k> \approx (d\pi t)^{1/2}$. In case the self-size similar distribution is not reached during the intermediate phase, another way to determine d is to study the equilibration era and compare the experimentally obtained size distribution with the numerical solution of the model. At equilibrium, $<k>^2 \approx \rho e^{\alpha}$, and this relation determines the dimensionless binding energy α. (2) Fullerene–SWNT cluster formation suggests that the cluster *sheath* is filled with pores. The *membranous character* of growth process in clusters explains experimental data dispersion. The model yields an activation barrier and predicts that

pores with a radius below a certain critical value are unstable, while those above this radius will grow indefinitely until the membrane ruptures. During the latter stage of fusion the site expansion velocity slowed down by two orders of magnitude. Dynamics were governed by the displacement of the volume of liquid around the fusion site.

References:

[1] F. Torrens and G. Castellano, Comput. Lett., **1** (2005) 331.
[2] F. Torrens and G. Castellano, Curr. Res. Nanotechn., **1** (2007) 1.
[3] F. Torrens and G. Castellano, Microelectron. J., **38** (2007) 1109.
[4] F. Torrens and G. Castellano, J. Comput. Theor. Nanosci., **4** (2007) 588.
[5] F. Torrens and G. Castellano, Nanoscale Res. Lett., (in press).
[6] J.C. Neu, J.A. Cañizo and L.L. Bonilla, Phys. Rev. E, **66** (2002) 61406.

Figures:

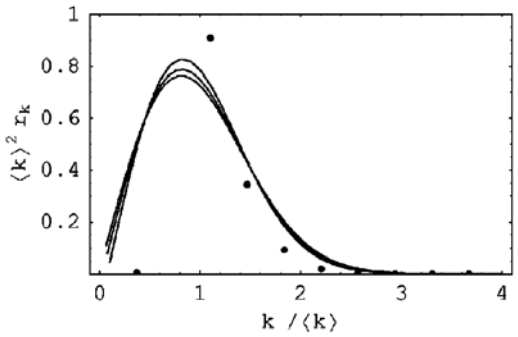

Figure 1. Approximate self-similar behaviour of the size distribution at times $\tau = 50\,000$, 100 000 and 150 000 (*solid lines*). Notice that $\langle k \rangle^2 r_k$ is approximately the same function of $k/\langle k \rangle$ at different times. The dots correspond to $\tau = 20$.

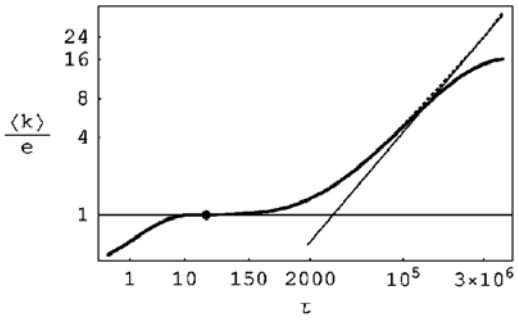

Figure 2. Evolution of the average cluster size $\langle k \rangle / e$ *vs*. the scaled time τ (thick solid line). The dotted line corresponds to the intermediate transient with an initial condition corresponding to the dot. The straight line of slope 1/2 corresponds to the asymptotic self-similar continuum size distribution.

Measurement of Repulsive Casimir Forces Using MEMS Structures

F. Torres, G. Abadal, G. Murillo, J.LL. López, A. Uranga, J. Giner and N. Barniol
Departament Enginyeria Electrònica, ETSE, Universitat Autònoma de Barcelona
Edifici Q, Campus UAB, 08193 Bellaterra, Spain
Francesc.Torres@uab.cat

In 1948, H.B.G. Casimir published a famous article with a simple but profound explanation about retarded Van der Waals interactions [1] as a manifestation of the zero-point energy of a quantized field. In its simplest form, the so-called Casimir effect is the interaction of a pair of neutral, parallel conducting planes due to the disturbance of the vacuum of the electromagnetic field. It is a pure quantum effect, there is no force between the plates (assumed to be neutral), in classical electrodynamics. Casimir was the first that was extracted a finite force between these two neutral plates, an attractive force:

$$F(d) = -\frac{\pi^2}{240}\frac{\hbar c}{d^4}A \qquad (1)$$

where *d* is the distance between plates and *A* is their area. In recent years, this effect has become highly popular both due to theoretical and experimental developments. The Casimir force was measured through different ways, with force pendulum or Atomic Force Microscopy [2, 3]. Theoretically there was an important development on calculus that involves a great spectrum of materials and geometries. The main theoretical results for micro and nanoelectromechanics field was the possibility that Casimir forces could appear as a repulsive forces, both depending on the materials [4] and the geometries [5] involved. As an example, it was proposed the geometry shown in *figure 1* as rectangular cavities made on the MEMS or substrate. The Casimir force appearing in this geometry mix both repulsive and attractive effect and, depending on the relation between dimensions, one feature could be larger than the other one. We can see in *figure 1* that for the rectangular cavity, if $a_1 << a_2 << a_3$, then [5]

$$F_2 = \hbar c\left[\frac{\pi^2 a_3}{720 a_1^3} - \frac{\xi_R(3)}{8\pi}\frac{a_3}{a_2^3} + \frac{\pi}{48 a_2^2}\right] \qquad (2)$$

where ξ_R denotes the Riemann zeta function. The repulsive Casimir forces are an interesting way to avoid the collapse of the structure into the substrate/electrode, which is the most important problem for micro and nanoelectromecanical devices (MEMS/NEMS).
The measurement of Casimir forces become very difficult, not only because of the magnitude of the forces involved (near pN) but, mainly, because of the extreme dependence of this effect on the roughness of the material and on the parallelism between planes. Both effects (an excessive roughness and a slight non-parallelism) diminishes the Casimir forces.
The work presented here is an attempt to measure the repulsive Casimir forces in real MEMS. Our first target is to try to measure the spring softening caused by Casimir forces in a silicon (heavily doped) membrane. This is based on the ACO (Anharmonic Casimir Oscillator) model [6] that predicted a shift of resonant frequencies of a resonator (based on the mass-spring model) due to the presence of Casimir Forces.
In *figure 2* we show the experimental device, with a membrane and a metallic electrode bigger than the membrane, in order to diminish as much as possible the non-parallelism between them. It is crucial that the silicon membrane will be heavily doped, because of the nature of the Casimir effect, based on the fact that the contour conditions must be metallic (or

near metallic) to ensure a good reflectivity of the electromagnetic field. And, also, it is crucial to ensure electric neutrality for the entire device to avoid the presence of electrostatic forces that could screen the Casimir interaction. The membrane, sited into high vacuum, vibrates due to thermal energy (without any other kind of external excitations) in its normal modes, and the ressonances will be measured via optical interferometry. The shift predicted by ACO model are around 2 Hz for resonators of 200 μm^2 of area and 50 nm distance between the electrode and the membrane, and increasing to 60-100 Hz for 700 μm^2 of membrane area.
The work presented here will be done in the framework of the project "fuerzas de Casimir repulsivas, medida y aplicabilidad" (TEC2007-29622-E).

References:

[1] H.B.G. Casimir, Proc. K. Ned. Akad. Wet. **51** (1948) 793.
[2] S.K. Lamoreaux, Physical Review Letters **78** (1997) 5.
[3] U. Mohideen, A. Roy, Physical Review Letters **81** (1998) 4549.
[4] O. Kenneth, I. Klich, A. Mann, M. Revzen, Physical Review Letters **89** (2002) 033001-1.
[5] A. Gusso, A.G.M. Schmidt, Brazilian Journal of Physics **36** (2006) 168.
[6] F.M. Serry, D. Walliser, G. J. Maclay, Journ. Microelectrom. syst. **4** (1995) 193.

Figures:

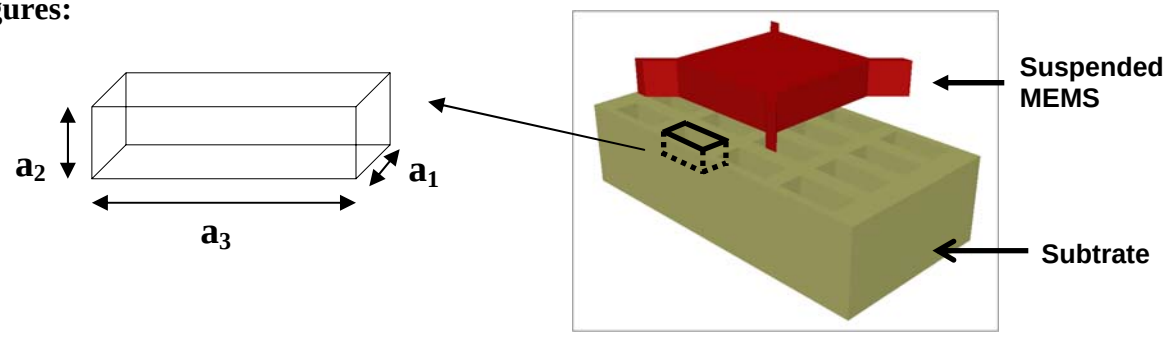

Figure 1: Possible geometry for repulsive Casimir forces

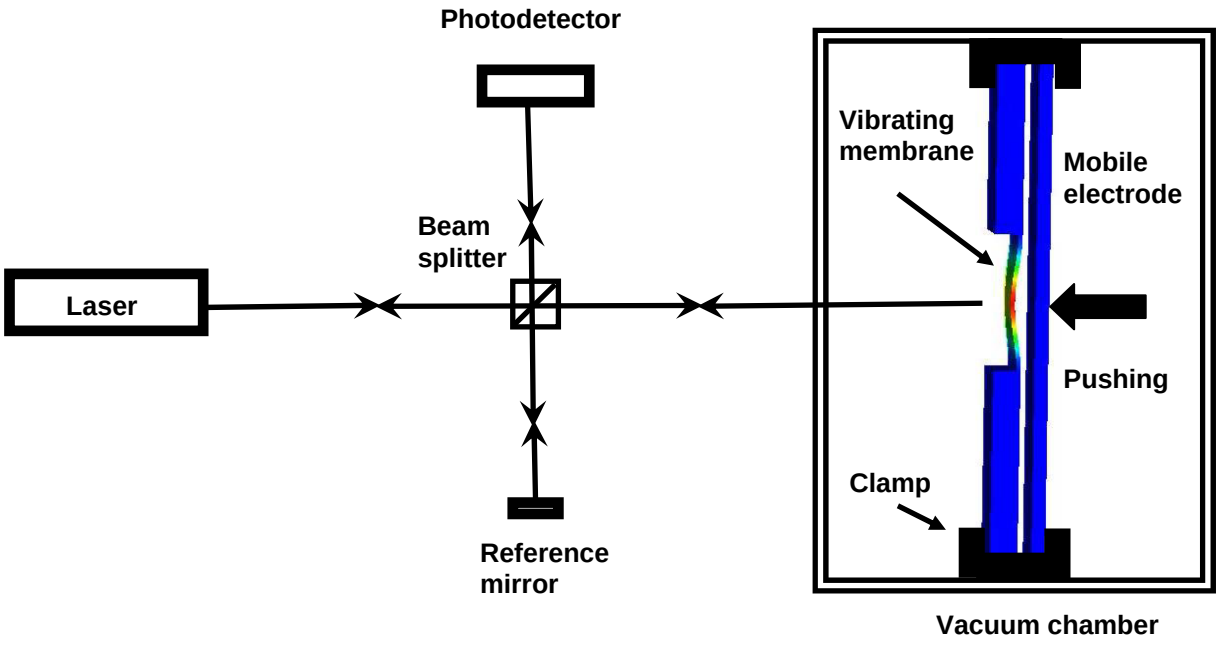

Figure 2: Set up for the measurement of the device based on a silicon membrane

SYNTHESIS OF RUTHENIUM AND PLATINUM NANOPARTICLES STABILIZED BY HEAVILY FLUORINATED COMPOUNDS

Mar Tristany,[a] Bruno Chaudret,[b] Philippe Dieudonné,[c] Yannick Guari,[d] Pierre Lecante,[e] Victor Matsura,[d] Marcial Moreno-Mañas,[a] Karine Philippot,[b] and Roser Pleixats.[a]**

[a]*Department of Chemistry, Universitat Autònoma de Barcelona, Cerdanyola, 08193-Barcelona, Spain*

[b]*Laboratoire de Chimie de Coordination du CNRS, 205 route de Narbonne, 31077-Toulouse, France*

[c]*Laboratoire des Colloïdes, Verres et Nanomatériaux (CNRS, UMR 5587), Université de Montpellier II, 34095-Montpellier, France*

[d]*Laboratoire de Chimie Moléculaire et Organisation du Solide (CNRS, UMR 5637) Université de Montpellier II, 34095-Montpellier, France*

[e]*Centre d'Elaboration des Matériaux et d'Etudes Structurales du CNRS, 29 rue Jeanne Marvig, BP4347, 31055-Toulouse, France*

tristany@lcc-toulouse.fr

During the past decade, metal nanostructures have attracted a considerable interest due to their properties in various areas such as optics, magnetism, catalysis...[1] Many efforts have thus been devoted to their synthesis and characterization and various approaches are now available for their preparation, such as chemical reduction, thermal or sonochemical decomposition, UV photolysis, chemical vapour deposition, electrochemical synthesis and organometallic synthesis.[2] However, since both the physical and the chemical properties of nanostructures are dependent on their morphologies,[3] it is necessary to find synthesis methods allowing a good control of their morphology.

In this field, here we describe our collaborative results on the stabilization of ruthenium(0)[4] and platinum(0)[5] nanoparticles by heavily fluorinated compounds, organized into spherical, rod or wire shaped superstructures (figure 1). Such organization results from the combination of an organometallic route[6] leading to size-controled nanoparticles with the use of heavily fluorinated compounds[7] to self-assemble as stabilizing agents (figure 2).

Several techniques were employed to characterize the nanomaterials obtained including TEM, HTEM, WAXS, SEM-FEG and SAXS which confirmed the nanoparticles organization.

Such fluorinated-ligand-stabilized NPs could find application in fluorous biphase catalysis or in materials chemistry.

References:

[1] *Clusters and Colloids. From Theory to Applications*, ed. G. Schmid, Vch, Weinheim, 1994 and *Nanoparticles. From Theory to Applications*, ed. G. Schmid, Wiley-Vch, Weinheim, 2004; K. J. Klabunde, C. Mohs in *Chemistry of Advanced Materials. An Overview*, ed. L. V. Interrante and M. J. Hampden-Smith, Wiley-Vch, New York, 1998, ch. 7; *Nanoscale Materials in Chemistry*, ed. K.J. Klabunde, Wiley-Interscience, New-York, 2001; *Metal Nanoparticles. Synthesis, Characterization, and Applications*, ed. D. L. Feldheim and C. A. Foss Jr, Marcel Dekker, New York, 2002;

[2] K. Philippot, B. Chaudret, in *Comprehensive Organometallic Chemistry* III, ed. R. H. Crabtree and M. P. Mingos, Elsevier, 2007, vol. 12, ch. 12.03, pp. 71-99.

[3] M.A. El-Sayed, Acc. Chem. Res., **34** (2001) 257-264.

[4] M. Tristany, B. Chaudret, P. Dieudonné, Y. Guari, P. Lecante, V. Matsura, M. Moreno-Mañas, K. Philippot, R. Pleixats, Adv. Funct. Mater., **16** (2006) 2008-2015.

[5] M. Tristany, M. Moreno-Mañas, R. Pleixats, B. Chaudret, K. Philippot, P. Dieudonné, P. Lecante, J. Mat. Chem., **18** (2008) 660-666.

[6] B. Chaudret, *Synthesis and surface reactivity of organometallic nanoparticles* in Topics in Organometallic Chemistry, **16** (2005) 233-259.

[7] A. Schulte, V. M. Hallmark, R. Twieg, K. Song, J. F. Rabolt, Macromolecules **24** (1991) 3901-3905; V. C. R. McLoughlin, J. Thrower, Tetrahedron **25** (1969) 5921; R. J. Twieg, J. F. Rabolt, Macromolecules **21** (1988) 1806-1811; M. Moreno-Mañas, R. Pleixats, S. Villarroya, Synlett (1999) 1996-1998; O. Porcherie, Y. Guari, C. Reyé, New J. Chem. **29** (2005) 538-543.

Figures:

Figure 1. Superstructures of the nanocomposites of ruthenium(0) (left) and platinum(0) (right) nanoparticles embedded into heavily fluorinated compounds.

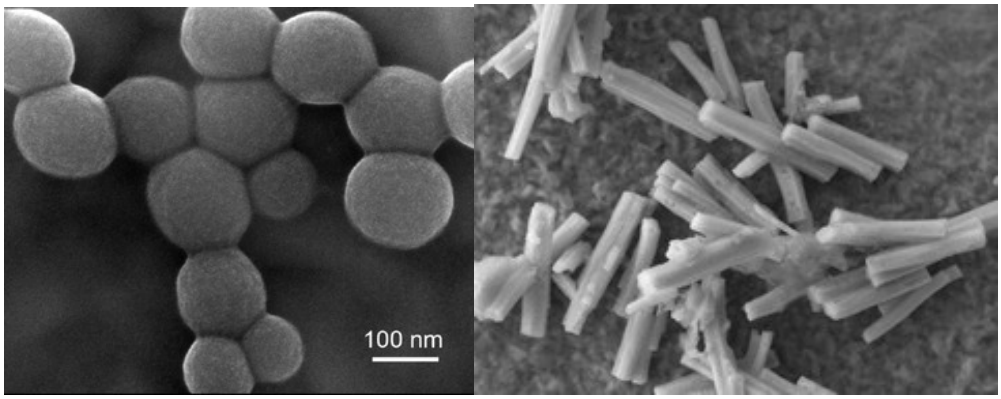

Figure 2 Family of heavily fluorinated compounds used as stabilizing agents for nanoparticles synthesis.

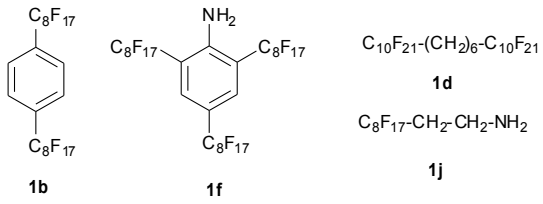

MONTE-CARLO UNCERTAINTY EVALUATION OF TRANSFER STANDARDS FOR ATOMIC FORCE MICROSCOPY

J. L. Valencia, H. González-Jorge, V. Alvarez-Valado, J. Rodríguez and F. Yebra
LOMG, Parque Tecnolóxico de Galicia, San Cibrao das Viñas (Ourense), Spain
jlvalencia@lomg.net

Atomic force microscopes (AFMs) are frequently used to measure surface features and parameters. The traceable calibration of images obtained is a pre-requisite for establishing the uncertainty associated with such a measurement and to be used in quality assurance processes. For this purpose, the typical procedures for the calibration of these instruments use transfer standards, which typically consist on gratings produced using optical lithography with x-y-z dimensions traceable to a national laboratory [1 - 3]. In this way, the traceability chain for AFM instruments is the following: meter – laser interferometry – MAFM (metrologic AFM with displacements measured by means of laser interferometry) – transfer standard – AFM.

In this work, we will estimate the uncertainty of a typical transfer standard for AFM calibration using a Monte-Carlo technique. This procedure appears very useful specially when model equations are complicated and the sensitivity coefficients are difficult to obtain. Uncertainty budget and model equations (xy and z) for the calculations are obtained from bibliographic data [4], where the gratting calibration was made using a MAFM. Next we describe equations, standard uncertainty and type of distribution for each term:

$$L_{xy} = l_{xy}\frac{\lambda}{4n\cos\theta_{xya}\cos\theta_{xym}\cos\theta_{xyt}} + L_{xyAbbe} + L_{xydp} + L_{xymf} \qquad \text{(x-y axis)}$$

$$L_z = l_z\frac{\lambda\cos\theta_{zt}}{4n\cos\theta_{zm}} + L_{zAbbe} + L_{zdp} + L_{zmf} + L_{zct} \qquad \text{(z axis)}$$

where:

l_{xy} is the distance in the *x* or *y* axis (u_{lx} = 6.1·10^{-9} m; u_{ly} = 10^{-8} m; probability distribution: normal).

l_z is the distance in the *z* axis (u_{lz} = 9.2·10^{-10} m; probability distribution: normal)

n is the refractive index (u_n = 7.8·10^{-6}; probability distribution: normal)

λ is the laser wavelength (u_l = 10^{-15} m; probability distribution: normal)

$\cos\theta_a$ is the angle between the measurement axis and the displacement axis ($u_{\cos\theta a}$ = 10^{-10}; probability distribution: rectangular)

$\cos\theta_m$ is the angle between the incident laser beam and the mirror normal ($u_{\cos\theta m}$ = 2·10^{-6}; probability distribution: rectangular)

$\cos\theta_t$ is the tilt angle of the simple relative to the *x* measurement axis ($u_{\cos\theta xt}$ = 1.3·10^{-6}; $u_{\cos\theta yt}$ = 2.6·10^{-6}; $u_{\cos\theta zt}$ = 2.5·10^{-6}; probability distribution: rectangular)

L_{Abbe} is the correction factor of Abbe offset (u_{xLAbbe} = 1.3·10^{-9} m; u_{yLAbbe} = 1.1·10^{-11} m; u_{zLAbbe} = 1.3·10^{-10} m; probability distribution: rectangular)

L_{dp} is the correction factor for the dead path length in the interferometer ($u_{xLdp} = 9 \cdot 10^{-11}$ m; $u_{yLdp} = 1.5 \cdot 10^{-10}$ m; $u_{zLdp} = 1.4 \cdot 10^{-10}$ m; probability distribution: rectangular)

L_{mf} is the correction factor for thermal expansion in the metrology frame ($u_{xLmf} = 1.7 \cdot 10^{-11}$ m; $u_{yLmf} = 2.2 \cdot 10^{-10}$ m; $u_{zLmf} = 1.9 \cdot 10^{-10}$ m; probability distribution: rectangular)

L_{ct} is the correction factor of the cross-talk movement of the AFM tip ($u_{Lct} = 4.3 \cdot 10^{-11}$ m; probability distribution: rectangular)

Monte-Carlo evaluation was performed for 100000 random values generated according the above mentioned input distributions. Output values obtained for the three measurement axes are the following:

$L_x = 189$ nm $U(L_x) = 12$ nm (95 % confidence)

$L_y = 189$ nm $U(L_y) = 20$ nm (95 % confidence)

$L_z = 79.1$ nm $U(L_z) = 1.8$ nm (95 % confidence)

All of them are in agreement with those achieved in the bibliography [4]. This fact demonstrates the good fitting of the output uncertainty to a normal distribution and the accomplishment of the Central Limit Theorem. An example of one output distribution is depicted in Figure 1. The application of Monte-Carlo technique for uncertainty evaluation in nanometrology opens the possibilities to quantify more complicated model equations that can take into account the dimensions of the tip or the Van der Waals forces between tip and sample.

References:

[1] R. Leach, J. Haycocks, K. Jackson, A. Lewis, S. Oldfield, and A. Yacoot, Nanotechnology, **12** (2001) R1-R6.
[2] WGDM-7: Preliminary comparison on nanometrology. Final Report of Nano 4: 1D gratings (2000) 7.
[3] WGDM-7: Preliminary comparison on nanometrology. Final Report of Nano 2: Step height standards (2003) 3.
[4] J. Haycocks and K. Jackson, Precision Engineering, **29** (2005) 168-175.

Figure 1: Uncertainty distribution of L_z obtained using Monte-Carlo evaluation

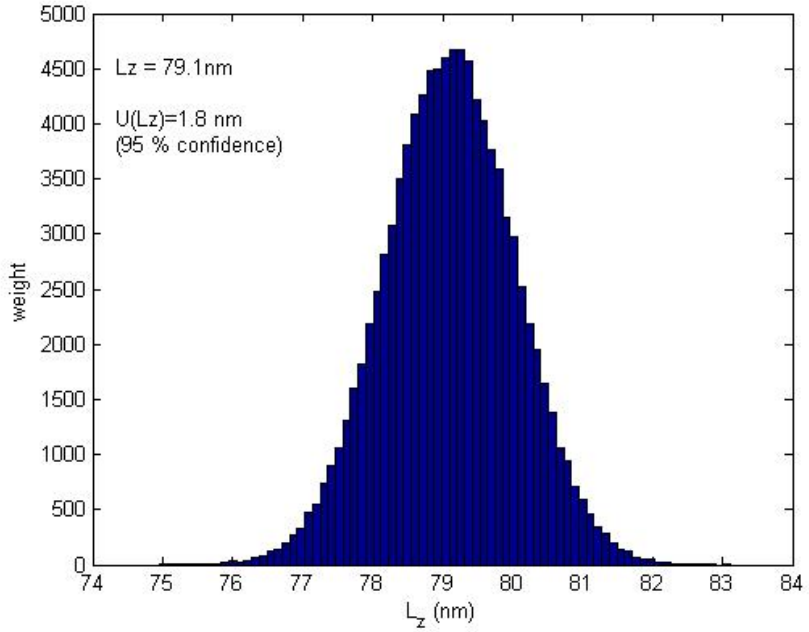

NEW DYE SENSITIZED NANO SEMICONDUCTORS IN WATER PURIFICATION WITH SOLAR LIGHT

H. Cristina Vasconcelos[a]
[a] Departamento de Ciências Tecnológicas e Desenvolvimento, Universidade dos Açores, Rua da Mãe de Deus, 9501-855 Ponta Delgada, S. Miguel, Açores.
hcsv@notes.uac.pt

M. Carmo Barreto[a,b]
[b] Centro de Investigação em Recursos Naturais (CIRN), Universidade dos Açores, Rua da Mãe de Deus, 9501-855 Ponta Delgada, S. Miguel, Açores.
barreto@notes.uac.pt

Nano crystalline semiconductors, such as TiO2 and Fe2O3, with relatively high band gaps, are suitable catalysts for photo-degradation of water contaminants, due to their stability and high oxidizing power. The high band gaps limit their use to UV regions, which is not abundant in sunlight. Therefore, dyes are used to sensitize such semiconductors to visible light.
The dye sensitized semiconductor systems have been effectively investigated by many researchers, and have been used to degrade several water contaminants. Despite this, the modified semiconductors still suffer many disadvantages, such as: technical difficulty of recovery, dyes may be hazardous themselves, limited efficiency of sensitized catalysts to degrade stable contaminants, regeneration of catalysts, and others.
In this work, a new class of photo-catalysts has been developed. Dye modified TiO2 catalysts have been supported onto activated carbon particles to yield AC/TiO2/dye catalytic systems. Two different dyes have been experimented. The new hybrid systems have been employed to catalyze different organic water contaminants using visible and UV regions. The support enhanced the catalyst efficiency, and made it easier to recover after reaction completion.

DEVELOPMENT OF PROTEOLIPOSOMES AS NANOMEDICAL TOOLS TO DELIVER BIOMOLECULES WITH THERAPEUTIC GOALS

Ana Vecino
Universidad del Pais Vasco,Bioquímica y Biología Molecular
Barrio Sarriena s/n Leioa (Vizcaya)
Email: gbbveora@lg.ehu.es

The field of nanobiotechnology deals with the observation of pre-existing cell structures and processes to use them as models for different applications. Within this field, the nanomedicine brings together the utilization of self-assembled structures of biomolecules for therapeutic purposes. In this context, liposomes are thought to mimic cell membranes found in living organisms and have great potential for the efficient and selective drug delivery to target cells. Likewise, bacterial conjugation is a process of much interest as a DNA injection mechanism. Actually, it is a highly efficient and broad host range process during which DNA is transferred from a donor to a recipient bacterium across the envelope of both cells. Conjugative DNA transfer requires three sets of plasmid-encoded proteins called Dtr (DNA transfer and replication), Mpf (mating pair formation) and a coupling protein. Dtr proteins process conjugative DNA through the formation of a nucleoprotein complex, the relaxosome, that cleaves and unwinds DNA in order to form the single DNA to be transferred (T-strand). The relaxosome "moves" to the transport site by means of the coupling protein, where the DNA transport apparatus (Mpf proteins) provides the pore for transport of the T-strand to the recipient cell. Plasmid R388 has the shortest known mobilization region. Only three plasmid-encoded proteins, TrwA, TrwB, and TrwC, together with *oriT*, are involved in R388 mobilization.

TrwB is the coupling protein encoded by the conjugative plasmid R388. It plays an essential role in bacterial conjugation. Its homologues in other conjugative systems include TraD from plasmid F, TraG from RP4 and HP0524 from *Helicobacter pylori*. TrwB is an integral membrane protein consisting of 507 residues, that contains characteristic nucleotide triphosphate-binding domains, reminiscent of those of F_1-ATPase α and β subunits. The protein consists of a large (ca. 440 residues) extramembranous domain, and a transmembrane domain comprising the 70 N-terminal residues that includes two transmembrane helices and a small periplasmic domain in between.We reported the purification of native TrwB in monomeric and hexameric forms, in the presence of β-D-dodecylmaltoside (DDM).

In this project, we hypothesize that proteoliposomes made up of the conjugative protein TrwB reconstituted in liposomes could transport and, subsequently, accurately inject DNA fragments, previously encapsulated inside the liposomes themselves, into target cells. Similarly, to warrant an efficient transfer to the target cells, this nanosystem for the delivery

of DNA fragments would most likely need the incorporation of other protein components, such as proteins of the T4SS secretion system, to the proteoliposome. The ultimate goal of the current project is the development of a nanomedical tool (*i.e.*, proteoliposomes made up of coupling proteins and/or proteins of the T4SS secretion system reconstituted in liposomes, with encapsulated DNA fragments) as a preliminary step to the future development of a nanobiotechnological system to efficiently and selectively deliver biomolecules for therapeutic purposes to target cells inside the human organism.

REFERENCES

- Moncalián, G, Cabezón, E, Alkorta, I, Valle, M, Moro, F, Valpuesta, JM, Goñi, FM, de la Cruz, F. 1999. Characterization of ATP and DNA binding activities of TrwB, the coupling protein essential in plasmid R388 conjugation. *J. Biol. Chem. 274 (51):* 36117-36124

- Hormaeche, I, Alkorta, I, Moro, F, Valpuesta, JM, Goñi, FM, de la Cruz, F. 2002. Purification and properties of TrwB, a hexameric, ATP-binding integral membrane protein essential for R388 plasmid conjugation. *J. Biol. Chem. 277 (48):* 46456-46462

- Hormaeche, I, Iloro, I, Arrondo, JL, Goñi, FM, de la Cruz, F, Alkorta, I. 2004. Role of the transmembrane domain in the stability of TrwB, an integral protein involved in bacterial conjugation. *J. Biol. Chem. 279 (12):* 10955-10961

- Hormaeche, I, Segura, RL, Vecino, AJ, Goñi, FM, de la Cruz, F, Alkorta, I. 2006. The transmembrane domain provides nucleotide binding specificity to the bacterial conjugation protein TrwB. *FEBS Lett. 580:* 3075-3082

Poster

Production of Apatite-like lanthanum silicate thin film electrolytes by oxidation of La-Si sputtered thin films

M.M. Vieira [a*], *J.C. Oliveira* [b], *A.L. Shaula* [b] *and A. Cavaleiro* [b]

[a] *School of Technology and Management of the Polytechnic Institute of Leiria, Morro do Lena – Alto do Vieiro, 2411-901 Leiria – Portugal*

[a] *SEG-CEMUC, Department of Mechanical Engineering, University of Coimbra, Rua Luís Reis Santos, 3030-201 Coimbra, Portugal*

milena.vieira@dem.uc.pt

The development of Intermediate Temperature Solid Oxide Fuel Cells (IT-SOFCs) requires electrolyte materials with ionic conductivity higher than the conventional yttria-stabilised zirconia (YSZ) at moderate temperatures. Lanthanum gallates (LSGM) and ceria-gadolinia (CGO) which are often cited as promising solutions present important drawbacks such as high cost of gallium and chemical instability of lanthanum gallate, and the onset of electronic conductivity in CGO under reducing environments. Recently, lanthanum silicates materials ($La_{9,33}Si_6O_{26}$) with an apatite-like structure have attracted considerable interest as potential low cost electrolyte materials. Some of these materials show conductivities comparable to, or better than, YSZ at 875 K, and are thus potential electrolytes for economic feasible fuel cells. One major drawback of these materials is that they require sintering at very high temperatures (typically >1600°C) to achieve dense materials. Using the sputtering deposition technique to produce the lanthanum silicate electrolyte allow the deposition of dense films at temperatures much lower than their bulk counterpart.

The main objective of this work is the production of apatite-like lanthanum silicates thin films by magnetron sputtering. La-Si films with the appropriate La/Si atomic ratios were deposited by magnetron sputtering from LaSi and Si targets and subsequently oxidized in controlled atmosphere to obtain the targeted lanthanum silicate oxide.

The chemical composition of the coatings was determined by electron probe microanalysis (EPMA). The structure of the coatings was studied by X-ray diffraction (XRD) using a Phillips diffractometer operated in Bragg-Brentano configuration with Co(Kα) radiation. The cross section and surface topography of the La-Si films were examined on a JEOL scanning electron microscope (SEM) equipped with an EDAX energy dispersive spectrometer (EDS). The electrical properties of the films were measured by AC impedance spectroscopy (HP4284A precision LCR meter, 20 Hz – 1 MHz).

Poster

AGE-HARDENING EFFECT ON THE PROPERTIES AND NANOSTRUCTURE OF FUNCTIONALLY GRADED AL ALLOY – SICP COMPOSITES

A.C. Vieira[(1*)], L.A. Rocha[(1)], J.R. Gomes[(1)], A.M.P. Pinto[(1)]

[(1)] *CT2M* – Centre for Mechanics and Materials Technologies (www.ct2m.uminho.pt); Research Group on Functionalized Materials and Surfaces Performance; University of Minho, Mechanical Engineering, Department (DEM)**.** Campus de Azurem, 4800-058 Guimarães, Portugal

**catarina.vieira@engmateriais.eng.uminho.pt*

Abstract

Functionally graded Al/SiC_p composites (FGMMC´S) have shown a great potential for industrial applications in the aerospace and automotive industries [1-3]. The combination of a high wear resistance up to relatively high temperatures and good bulk toughness, provided by the incorporation of the ceramic particles on the superficial region of the component, are the main advantage of these materials. These composite materials are produced by conventional liquid metallurgy processes (stir and centrifugal casting), the properties of the produced components being those resulting from this processing route. It becomes possible to perform post-processing age-hardening heat treatments and combine this capability with adequate castability, by adjusting the chemical composition of the Al-alloy matrix[4]. Age-hardening originates nano-scaled precipitates which can improve the hardness and toughness of the material [5]. An unknown issue is the influence of the presence of the SiC particles, and particularly of the SiC/Al-alloy interface on the precipitation sequence in these materials.

The main aim of this work is to investigate the effect of age-hardening on the properties and nanostructure of functionally graded Al/SiC_p composites. The structures of the materials were studied at the micro and nano-scale by complementary characterization techniques (TEM, AFM and nano-identation).

[1] A. Velhinho - Fundição centrífuga de compósitos de alumínio/SiC com gradiente funcional de propriedades: processamento e caracterização, PhD thesis, UNL, Lisboa 2003.

[2] D.B. Miracle - Metal matrix composites - From science to technological significance, Composites Science and Technology, 65 (2005) 2526–2540.

[3] S. Das - Development of aluminium alloy composites for engineering applications, Transactions of the Indian Institute of Metals, 57 (4), (2004) 325-334.

[4] K. Mahadevan, K. Raghukandan, T. Senthilvelan, B.C. Pai, U.T.S. Pillai - Investigation on the influence of heat-treatment parameters on the hardness of AA6061-SiCp composite - Journal of Materials Processing Technology 171 (2006) 314–318.

[5] A. Abdel Aal - Hard and corrosion resistant nanocomposite coating for Al alloy, Materials Science and Engineering A (2007).

Poster

SYNTHESIS AND FUNCTIONALIZATION OF SILICA NANOPARTICLES WITH HYDROPHILIC OR HYDROPHOBIC GROUPS

Clara Yagüe, Francisco Balas, Silvia Irusta, Manuel Arruebo, Jesús Santamaría
Department of Chemical and Environmental Engineering and Aragon Nanoscience Institute, University of Zaragoza, 50009 Zaragoza, SPAIN
clara.yague@unizar.es

Different organic materials such as polymeric nanoparticles, liposomes, and micelles have been studied as possible vectors for bio-applications. In order to offer an alternative to the biodegradable (i.e., polyesters) and no-biodegradable (i.e., methacrylate) polymeric micro and nanoparticles as carriers, the use of silica has been proposed based on its non-toxicity and biocompatibility, its high chemical and mechanical stability and its hydrophilic character, and porous structure that can, in principle, be tailored to control the diffusion of an adsorbed or encapsulated molecule.

In this work, silica particles functionalized with different organic groups have been synthesized and characterized in order to study their potential application as gene and drug delivery carriers.

First, silica nanoparticles with uniform particle size were synthesized and characterized [1]. A hydrophilic functionalization of the mesopores was obtained by using 3-aminopropyltriethoxysilane (APTES) as source of amino groups. The conjugation was done following a co-condensation method [2]. The content of amino groups was determined by a colorimetric method [3]. The zeta potential of the functionalized nanoparticles was evaluated by using Photon Correlation Spectroscopy (PCS) (Figure 1). Rhodamine B isothyocianate was covalently bonded to the amino functionalized nanoparticles.

The same procedure was used in order to obtain hydrophobically modified silica nanoparticles by using methyltrimethoxysilane (MTMS) (Figure 2). Fourier Transformed Infrared Spectroscopy (FTIR) analysis (Figure 3) was used to corroborate the presence of surface methyl groups as well as the absence of any of the structure directing agent (hexadecyltrimethylammonium bromide, CTAB) used in the synthesis of the mesoporous silica nanoparticles. A catalytic chamber was used to avoid the interferences caused by the hydroxyl groups of water. Adsorption isotherms of rhodamine B on the methyl-functionalized silica nanoparticles were calculated by using spectrophotometry.

The influence of the solvent (methanol and water) was study in the adsorption of rhodamine B on the hydrophobically modified nanoparticles by using a dynamic and a discontinuous system, respectively. No adsorption was observed using methanol as solvent. Indeed, the opposite effect was obtained with water. The dynamic adsorption was tracked by using a UV-Visible spectrophotometer equipped with a photo diode array detector. The advantage of an array is the ability to do side-by-side readings, thus increasing speed.

A complete characterization of all the nanoparticles used in this work was performed by analyzing their particle size and morphology with Photon Correlation Spectroscopy (PCS) and Scanning Electron Microscopy (SEM), respectively. The structural characterization and porosity and surface area was evaluated by using Small Angle X-Ray Scattering (SAXS) and Nitrogen Adsorption Isotherms (BET). Fourier Transformed Infrared Spectroscopy (FTIR) was used to monitor the presence or absence of the functional groups.

References:

[1] Clara Yagüe, María Moros, Valeria Grazú, Manuel Arruebo, Jesús Santamaría, Chemical Engineering Journal, (2007) In press.
[2] Wei Zeng, Xue-Feng Qian, Yan-Bo Zhang, Jie Yin, Zi-Kang Zhu Zeng, Materials Research Bulletin **40** (2005) 766–772.
[3] Ian J. Bruce and Tapas Sen, Langmuir **21** (2005) 7029-7035.

Figures:

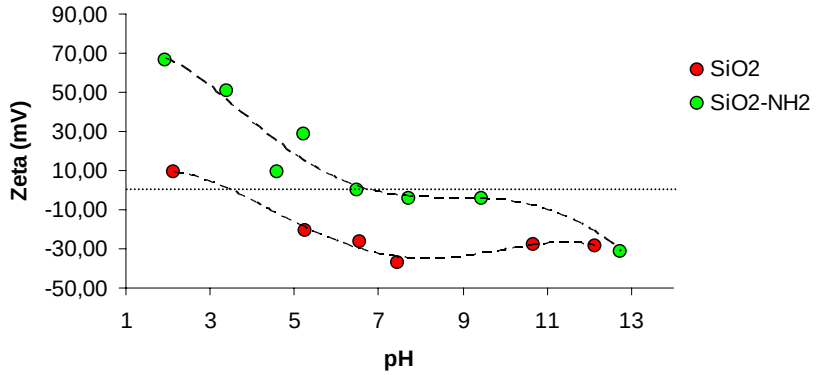

Figure 1. Zeta potential of amino-functionalized silica nanoparticles.

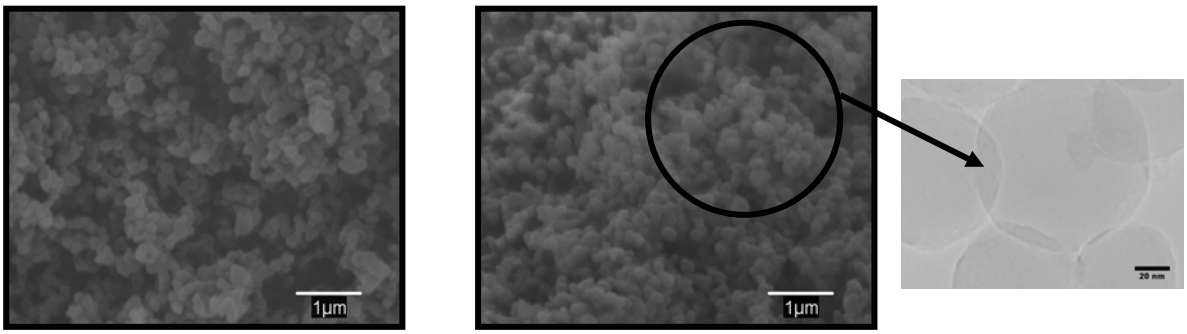

Figure 2. SEM photographs of silica particles hydrophobically modified with methyl groups.

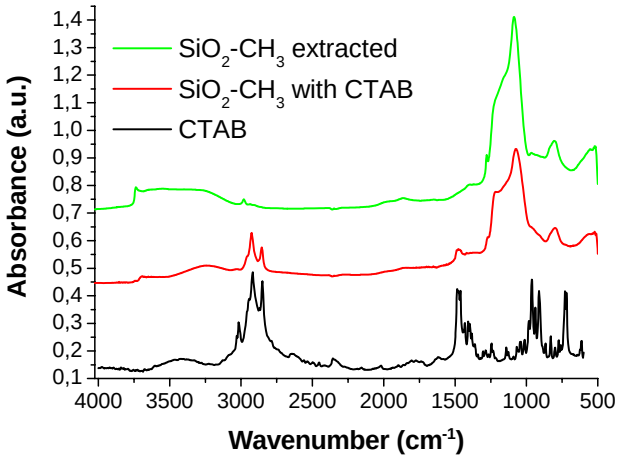

Figure 3. FTIR spectra of modified nanoparticles as-synthesized and after extraction of CTAB.

A STUDY OF THE LOCALIZED CORROSION BEHAVIOR OF METALS BY AFM/SKPFM TECHNIQUE

K.A. Yasakau, M.L. Zheludkevich, M.G.S. Ferreira
University of Aveiro, Dep. Ceramics and Glass Eng., CICECO, 3810-193 Aveiro, Portugal
kyasakau@ua.pt

Atomic Force Microscopy (AFM) allows imaging the topography of different materials with nanometer resolution. However, the classical AFM gives only topographical information, which limits the application of the technique in corrosion research. Introduction of the Scanning Kelvin Probe Force Microscopy (SKPFM) [1] allowed to determine the electrical properties of surface on a sub-micro level with the resolution of a hundred nanometres. The working principle of SKPFM is based on the determination of the Volta potential difference (VPD) (or difference in work function) between the conducting tip and the surface under investigation. The measurements of VPD performed in air can be correlated to the electrochemical corrosion potential of metals [2]. Since the corrosion process involves cathodic zones, which have nobler potential, and anodic zones that are less noble, SKPFM allows determination of the electrochemical nature of such places as it was shown in [3]. However, some factors may influence the Volta potential measurements. For instance, sample preparation procedure, structure and the presence of surface oxide films, layers of the corrosion products and others can significantly alter the experimental results. Nevertheless, understanding the limitations, SKPFM technique becomes a great tool for the characterization of electrochemical properties of metallic surfaces giving important information concerning the mechanisms of corrosion processes on micro- nano-scale.

In the present paper we demonstrate applicability of SKPFM and in-situ AFM techniques to study mechanisms of corrosion and corrosion inhibition processes on aluminum alloys 2024 and 5083. The AFM coupled with SKPFM allowed monitoring the VPD of alloy surface before and after exposure in different corrosion solutions with and without the presence of organic and inorganic inhibitive compounds. Before corrosion VPD map shows an intermetallic with higher VPD (white area across the black line) **Fig. 1(A).** The localised corrosion attack always starts on the border between noble intermetallic that works as an effective cathode and surrounding alloy matrix, which becomes an anode. The VPD increases in the place of cathodic intermetallics and adjacent matrix after corrosion exposure **Fig. 1(B).**

The results showed that the addition of organic inhibitors blocks the corrosion because of specific adsorption on the surface and results in almost unchanged map of VPD between the intermetallic (white area across the black line) and surrounding matrix **Fig. 2**. The use of Ln based inhibitors results in precipitation of insoluble hydroxides in the places with cathodic activity, therefore stopping further corrosion process.

The in-situ AFM experiments allowed calculating kinetics of the localized pitting growth on AA5083 in NaCl solution **Fig. 3**. The influence of NaCl solution concentration on the kinetics of insoluble La hydroxides precipitation is shown for AA2024.

References:

[1] M. Nonnenmacher, M.P. O'Boyle, and H.K. Wickramasinghe, Appl. Phys. Lett., **58** (1991) 2921-2923.
[2] P. Schmutz, G.S. Frankel, J. Electrochem. Soc., **145** (1998) 2285-2295.
[3] P. Schmutz, G.S. Frankel, J. Electrochem. Soc., **145** (1998) 2295-2306.

Figures:

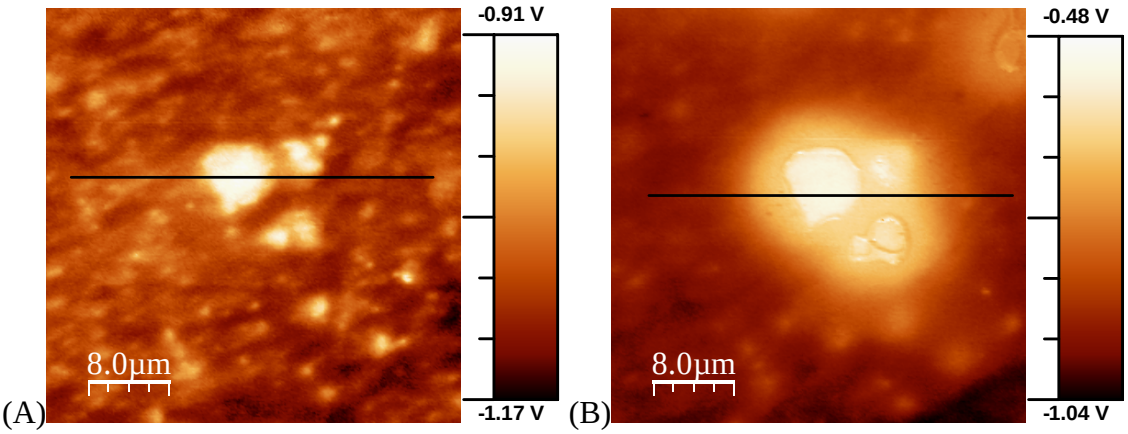

Fig. 1. Evolution of VPD before (A) and after (B) immersion of polished AA2024 in 0.05 M NaCl solution.

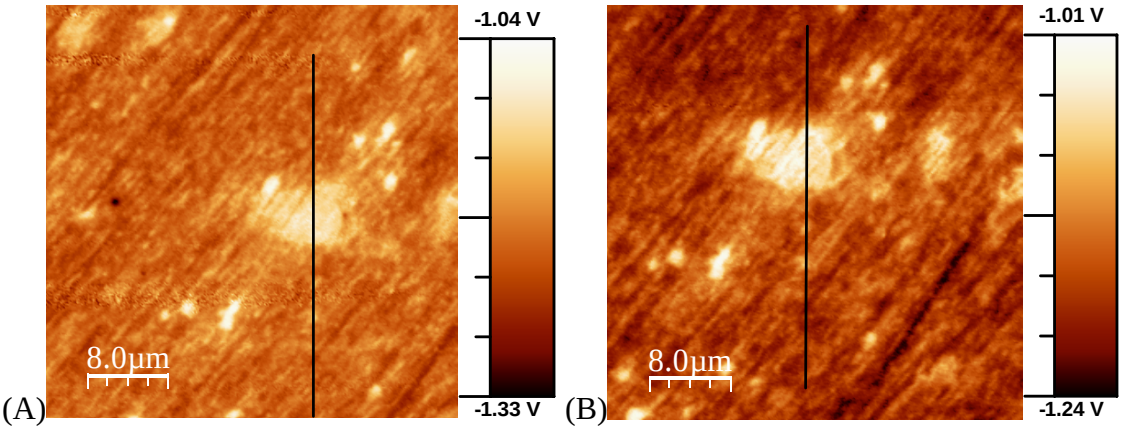

Fig. 2. Evolution of VPD before (A) and after 3h (B) of immersion of polished AA2024 in 0.05 M NaCl solution with organic inhibitor 8Hydroxyquinoline.

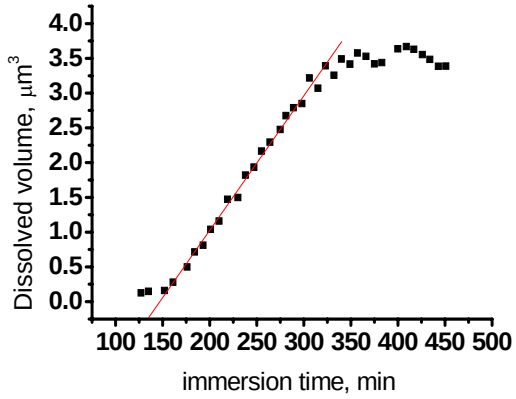

Fig. 3. Kinetics of dissolution of aluminum matrix near Fe-rich intermetallic on AA5083 during immersion in 0.05 M NaCl solution.